

DISCOVERY OF NOVEL NATURAL PRODUCT BASED HIF- 1 α :HIF-1 β INHIBITORS AS POTENTIAL ANTICANCER AGENTS

Yassine Bendiabdellah

A thesis submitted in partial fulfilment of the requirements for the degree of
Doctor of Philosophy



**The School of Pharmacy
University of London**

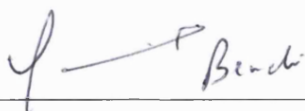
2010

Supervisors:

Dr. Giovanna Zinzalla

Prof. David E. Thurston

This thesis describes research conducted in the School of Pharmacy, University of London between 2006 and 2010 under the supervision of Dr. Giovanna Zinzalla and Prof. David. E. Thurston. I certify that the research described is original and that any parts of the work that have been conducted by collaboration are clearly indicated. I also certify that I have written all the text herein and have clearly indicated by suitable citation any parts of this dissertation that has already appeared in publication.



Signature

04/11/10

Date

ProQuest Number: 10104185

All rights reserved

INFORMATION TO ALL USERS

The quality of this reproduction is dependent upon the quality of the copy submitted.

In the unlikely event that the author did not send a complete manuscript and there are missing pages, these will be noted. Also, if material had to be removed, a note will indicate the deletion.



ProQuest 10104185

Published by ProQuest LLC(2016). Copyright of the Dissertation is held by the Author.

All rights reserved.

This work is protected against unauthorized copying under Title 17, United States Code.
Microform Edition © ProQuest LLC.

ProQuest LLC
789 East Eisenhower Parkway
P.O. Box 1346
Ann Arbor, MI 48106-1346

To Abdesselam and Rachida

Acknowledgement

I would like to thank Professor David Thurston for providing me with the opportunity to work within his research group, and for his continuous guidance, encouragement and scientific insight. In addition, David has been consistently enthusiastic about my career as a pharmacist and as a future teacher and researcher. I would also like to thank Dr Giovanna Zinzalla who has been an exceptional supervisor and has provided me with so much support and advice throughout my PhD studies.

This project is a reflection of a collaborative effort between various members of the Cancer Research UK Protein-Protein Interaction Drug Discovery Research Group. In this regard, I would like to thank all senior scientists and students who have contributed. In particular, I would like to thank Mrs Kazi S. Nahar, Mr Antonio Misale, Dr Dyeison Antonow, Dr Isabel V. Margalef, Dr Khondaker M. Rahman, Mr Chris Chamberlain, Ms Samantha Essex, Mr Jonathan Palmer and Dr Emma Sharp. I must also thank our collaborators at the National Cancer Institute, Professor Giovanni Melillo, Dr. Robert Shoemaker, and Ms Uranchimeg Badarch. I would also like to thank Dr Helene Bertrand and Professor Gerald Blunden for their efforts in proof-reading this thesis and for their priceless guidance and advice.

My parents, Rachida and Abdesselam, were my first and my best teachers, and they have always encouraged me in my pursuits and expressed their pride in my accomplishments. I am grateful to them for their love and support, for their confidence in me, and for the lessons and values they have given me.

I would also like to thank all my friends, in particular those at the School of Pharmacy, who made a tremendous difference to my level of happiness during my studies, although they may not have been aware of it at the time.

My final thanks go to the Algerian Ministry of Higher Education for sponsoring my PhD and for providing me with the opportunity to study in the United Kingdom, and particularly in such a high quality research institution.

Abbreviations

$[\alpha]_D$	Specific rotation
17-AAG	17- <i>N</i> -Allylamino-17-demethoxygeldanamycin
ADME	absorption, distribution, metabolism and excretion
ARNT	Aryl receptor nuclear translocator
Bcl	B-cell lymphoma 2
bHLH	Basic helix loop helix
BINOL	1,1'-Bi-2-naphthol
Bn	Benzyl
Calcd	Calculated
CBP	CREB-binding protein
CBS	Corey-Bakshi-Shibata
COSY	Correlation spectroscopy
DA	Diels-Alder
DCM	Dichloromethane
DFO	Desferroxamine
DMF	Dimethyl formamide
DMSO	Dimethyl sulfoxide
dr	Diastereomeric ratio
DR	Digoxin receptor
EC50	Median effective concentration (required to induce a 50%)
ee	Enantiomeric excess
EGFR	Epidermal growth factor receptor
ELISA	Enzyme-linked immunosorbent assay
EMSA	Electromobility gel shift assay
Eq	Equivalents
ESI	Electrospray ionization
FDA	Food and drug administration
FIH	Factor inhibiting HIF
FP	Fluorescence polarisation
FRET	Fluorescence resonance energy transfer
GA	Geldanamycin
Grb2	Growth factor receptor-bound protein2
HDACI	Histone deacetylase inhibitor
Hdm-2	Human MDM-2
HIF	Hypoxia inducible factor
HOMO	Highest occupied molecular orbital
HPH	Hypoxia prolyl hydroxylase
HPLC	High pressure liquid chromatography
HRMS	High Resolution mass spectrometry
HTS	High throughput screening
Hz	Hertz

IC50	Inhibition constant
IPAS	Inhibitory PAS domain
IPAS	Inhibitory PAS domain
IR	Infrared
<i>J</i>	Coupling constant
LC-MS	Liquid chromatography-mass spectrometry
LUMO	Lowest unoccupied molecular orbital
Mal	Maleimide
MAPK	Mitogen-activated protein kinase
Mdm2	murine double minute
MeOH	Methanol
mmol	Millimoles
Mp	Melting point
MS	Mass spectrometry
mTOR	Mammalian target of rapamycin
MW	Molecular weight
NCI	National Cancer Institute
NMR	Nuclear magnetic resonance
NOESY	Nuclear Overhauser effect spectroscopy
NQ	Naphthoquinone
ODDD	Oxygen-dependent degradation domain
PA	Propionic acid
PAS domain	Per-Arnt-Sim domain
PHD	Prolyl hydroxylase domain
Phe	Phenyl
PI3K	Phosphatidylinositol-3-kinase
PP	Protein-protein
PPI	Protein-protein interactions
ROS	Reactive oxygen species
rt	Room temperature
SAR	Structure activity relationship
SH2	Src homology 2
SIM	Single-minded protein
SOI	Secondary orbital interactions
SPR	surface plasmon resonance
STAT	Signal Transducers and Activators of Transcription protein
TAD	Transactivation domain
TLC	Thin layer chromatography
TOF	Time of Flight
TPT	Topotecan
VEGF	Venous endothelial growth factor
VHL	Von Hippel Lindau
Y	Yield

Abstract

Hypoxia-inducible factor 1 (HIF-1), a heterodimeric protein comprising of the HIF-1 α and β sub-units, is a key regulator of angiogenic and glucose metabolism processes utilised by hypoxic tumour cells for survival and growth. The inhibition of heterodimeric protein-protein interactions (PPIs) such as the HIF-1 α /HIF-1 interaction is a viable approach for novel chemotherapeutic strategies. Using an ELISA-based screen, rolitetracycline was originally identified by the Melillo laboratory (NCI) as a selective inhibitor of the HIF-1 α :HIF-1 β interaction, although this particular lead molecule has very poor cellular penetration properties. The main goal of this project was to synthesise libraries of rolitetracycline mimetics to explore SAR, and to try to obtain more-potent and more-selective analogues that might be progressed into pre-clinical studies.

The design of the first focused library of tetracyclic mimetics involved retention of the core molecular framework and spatial conformation of rolitetracycline, while changing perimeter functional groups. These molecules were synthesized by employing consecutive Diels-Alder cycloadditions and Indium-mediated chemistry. An alternative synthetic approach to other libraries involved asymmetric Diels-Alder cycloadditions employing various chiral catalysts to prepare enantiomerically pure tetracyclic mimetics. BINOL-ate catalysts were found to be the most effective, and a series of novel polyketide heterocyclic frameworks were prepared using highly regio- and diastereoselective one-pot reactions *via* a domino process to produce tetracyclic mimetics containing oxygen and nitrogen heterocycles.

A selection (40 molecules) of the total (54 molecules) synthesized during this project were screened in a luciferase-based plasmid reporter assay using U251-HRE cells that contained a HIF Response Element (HRE) and in U251-pGL3 control cells that lacked a HRE. This identified seven “hit” molecules and distinct structure activity relationships (SARs). The two best “hits”, YB036 and YB039, selectively inhibited HIF-1-dependent luciferase expression with EC₅₀ values of 1.75 μ M and 1.45 μ M, respectively. These molecules were progressed into a screening cascade which showed that they selectively reduced the level of HIF-1 α protein in cells while not affecting the levels of constitutively expressed HIF-1 β . They also selectively inhibited down-stream genes in the HIF-1 signalling pathway such as VEGF. Crucially, YB036 and YB039 had good cellular penetration characteristics compared to rolitetracycline. Although a suitable candidate for progression into pre-clinical studies was not identified during the course of this project, these studies have laid the foundations for further studies in the future that might achieve this goal.

Table of contents

Chapter 1: Protein-protein interaction

1.1	The rationale behind protein-protein interaction (PPI) modulation	2
1.2	Structural features of PPIs	3
1.3	Hot spots and allosteric sites	8
1.4	Strategies to identify small-molecule PPI modulators	10
1.5	Conclusions and future perspectives	19

Chapter 2: Hypoxia inducible factor

2.1	Hypoxia	22
2.2	Hypoxia inducible factor (HIF)	23
2.2.1	HIF1- α and - β subunits: structures and characteristics	23
2.2.2	bHLH/PAS proteins	25
2.2.3	Other HIF- α isoforms	25
2.2.4	HIF-2 α PAS domains	26
2.2.5	Comparison between HIF-1 α and HIF-2 α	27
2.2.6	HIF degradation	28
2.2.7	Alternate mechanisms of HIF regulation	31
2.2.8	HIF Target genes	32
2.2.9	The balance between adaptation and cell death	33
2.3	Modulating HIF-1 signalling pathway for drug discovery	34
2.3.1	Promoting HIF-1 pathway for ischaemic diseases	34
2.3.2	Inhibiting HIF-1 pathway for cancer therapy	35
2.3.3	HIF-1 inhibitors	36
2.4	Conclusion	45

Chapter 3: Diels-Alder reaction

3.1	The Diels Alder reaction	47
3.1.1	Background	47
3.1.2	Dienes and dienophiles	47
3.1.3	Pericyclic, ionic and radical Diels-Alder reactions	48

3.1.4	Regiochemistry	49
3.1.5	Stereoselectivity	52
3.1.6	Multiple Diels-Alder reaction	53
3.1.7	Lewis-acid catalysed Diels-Alder reactions	56
3.1.8	Applications of DA to the total synthesis of natural products	60
3.2	The cross-conjugated trienes	64
3.2.1	3-Methylene-1,4-pentadiene	64
3.2.2	Substituted cross-conjugated trienes	67
3.2.3	Conclusion	69

Chapter 4: Aims and objectives

4.1	Aims and objectives	71
-----	---------------------	----

Chapter 5: Design, synthesis and biological evaluation of novel molecules inhibitors of HIF-1 α : HIF-1 β PPI interactions.

5.1	Tetracycline mimetics	74
5.2	Retrosynthetic analysis of tetracycline mimetics	74
5.3	Synthesis of tetracycline mimetics	75
5.3.1	Synthesis of the cross-conjugated triene building blocks	75
5.3.2	Synthesis of the naphthoquinones	82
5.3.3	Synthesis of the maleimides	83
5.3.4	Synthesis of anthraquinones via DA cycloaddition	83
5.3.5	Synthesis of the pentacyclic compounds via DA reaction	90
5.3.6	Conclusion	97
5.4	Biological evaluation of the tetracyclic mimetics	97
5.4.1	Screening protocol	97
5.4.2	The first-generation library (5.79-5.89 and 5.98-5.109)	100
5.4.3	The second-generation library	110
5.5	Conclusions	118

Chapter 6: One-pot synthesis of fused-tetracyclic scaffolds employing a Lewis acid-catalyzed domino reaction of naphthoquinones

6.1	Introduction	121
6.2	Results and discussion	123
6.3	Conclusions	131

Chapter 7: Development of chiral Bronsted/ Lewis acid-catalysed enantioselective naphthoquinone Diels-Alder cycloaddition

7.1	Introduction	133
7.2	Results and Discussion	137
7.3	Conclusions	144

Chapter 8: Conclusions and future work

8.1	Concluding remarks	146
8.2	Future work	149

Chapter 9: Experimental section

9.1	Synthesis of HIF-1α:HIF-1β PPI inhibitors	153
9.1.1	General Procedure for the Synthesis of Trienes	154
9.1.2	General Procedure for the Synthesis 2-methyl- and 2,3-dimethyl-naphthoquinone	160
9.1.3	General Procedure for the Synthesis of the tricyclic compounds: 1 st Diels-Alders reaction	162
9.1.4	General Procedure for the synthesis of the pentacyclic compounds: 2 nd Diels-Alders reaction	170
9.2	One-pot synthesis of fused-tetracyclic scaffolds employing a Lewis acid-catalyzed domino reaction of naphthoquinones	207
9.2.1	Synthesis of dienes and cross-conjugated trienes	207
9.2.2	Synthesis of the tricyclic scaffolds	219
9.2.3	Synthesis of the tetracyclic scaffolds	226
9.2.4	Synthesis of polycyclic derivatives	234

9.3	Development of chiral Bronsted/ Lewis acid-catalysed enantioselective naphthoquinone Diels-Alder cycloaddition	237
9.3.1	Asymmetric Diels-Alder using Oxazaborolidine derivatives	238
9.3.2	Asymmetric Diels-Alder using Binaphthol derivatives	243
9.3.3	Asymmetric Diels-Alder using thiourea derivatives	245
Chapter 10:	References	247
Chapter 11:	Appendix	
11.1	Enantiomeric Resolution of YB036	266
11.2	U251-HRE 3 rd generation screening assay	270
11.3	Materials and Methods describing the biological screening	271
11.4	Selected NMR spectra	278

CHAPTER 1

Protein Protein Interactions

Contents:

1.1	The rationale behind protein-protein interaction (PPI) modulation	2
1.2	Structural features of PPIs	3
1.3	Hot spots and allosteric sites	8
1.4	Strategies to identify small-molecule PPI modulators	10
1.5	Conclusions and future perspectives	19

1.1 The rationale behind protein-protein interaction (PPI) modulation

The ability of proteins to interact with each other rests at the core of biology. Even though the regulation of cellular processes is mediated predominantly by post-translational alteration of proteins, cellular architecture, information transfer and chemical specificity derive from highly precise recognition events frequently involving the association of two or more proteins. PPIs occur due to the stereochemical interaction between surfaces of homologous or heterologous protein subunits as a result of the association of quaternary structures and macromolecular complexes.¹ Proteins can associate with each other with variable affinities, but never in a disorganised manner.² PPIs play a pivotal role in all aspects of cell biochemistry. Intra-cellular recognition and cell attachment in the extracellular environment is, for example, based upon the interaction of cell surface receptor proteins (e.g. cadherins) with their cell surface partners (e.g. actin). Signal transduction from the cell surface to the nucleus is often achieved through protein-protein associations as well. PPIs also occur during DNA replication, gene regulation, transcription (in which factors, activators and suppressors assemble), protein synthesis and secretion, and programmed cell death.

A number of human diseases associated with abnormal PPIs³ could be due to the loss of an essential interaction or through the irregular formation of a protein complex. Examples can be seen in cervical cancer, leukemia, bacterial infections and neurodegenerative diseases.³ Thus, over the last decade, PPIs have become attractive molecular targets for novel therapies,⁴⁻⁵ and the modulation of PPIs affecting transcription factors that coordinate signalling cascades is of particular importance to the discovery of novel therapeutic agents for cancer therapies.⁶

Molecules that can selectively modulate PPIs involved in the regulation of transcriptional processes also play a pivotal role in chemical biology to progress our understanding of signalling cascades, and for the investigation of upstream activation by other pathways.⁷ In addition, such molecules could provide a better understanding of the interaction between transcription factors and gene expression levels. These studies could help expand the window for therapeutic intervention, especially in the anticancer field.⁸

1.2 Structural features of PPIs

1.2.1. Challenges and misconceptions

Targeting PPI is not clear-cut, and cancer as a target disease is no exception to this. Due to the recent emergence of interest in the field, the challenges relate mostly to the structural features of the protein and the chemistry of the interactions. PPI are not perceived as a simple target compared with, for example, enzymes and G-proteins-coupled receptors. The key challenges that have so far been associated with PPIs are:

- a) *Functionally-undesirable PPI targets*: The design of PPI inducers compared with inhibitors is a challenge. If a mechanism is suppressed in a disease state, restoring it would seem a reasonable strategy in drug discovery. The discovery of activators of PPIs to restore apoptosis is an example of this.
- b) *Large and complex surfaces of interactions*: When the binding surface of interaction between two protein partners is extensive, a small molecule cannot compete. This is the case with β -catenin and Tcf. The structure of β -catenin⁹ does not contain any deep cavities, and its binding partner Tcf wraps around its surface at three points, one of which sits in a pocket of a realistic size which can be a target of small drugs. However, the three contact regions are so widespread that no molecule with a small molecular framework (e.g. 400-600 kDa) would cover the whole area. In addition, other downstream partners of β -catenin, which are tumour growth suppressors, bind to the same regions as Tcf, therefore limiting the selectivity of potential small-drug inhibitors.
- c) *Surfaces with inappropriate shapes*: Ideally, to achieve tight binding of a small molecule to an interaction surface between two proteins, a pocket that the small molecule can occupy with a high degree of affinity is desirable. When it comes to targeting PPIs in cancer cells, these are rarely seen. The oncogenic protein Ras, for example, binds to its downstream partner Raf thus activating this kinase to carry out signalling across cancer cells. This interaction represents a potential therapeutic target. However, because the binding occurs throughout an extensive edge-to-edge β -strand from each protein, an effective disruption by a small molecule seems unfeasible.
- d) *Interactions requiring highly polar ligands*: In order for small molecules to cross cell membranes, they should not be too polar, especially when the target is intracellular. A good example is the growth factor receptor-bound protein2 (Grb2)

Src homology 2 (SH2) domain, a key signal transducer in cancer cells (EGF receptors). The binding site of all SH2 domains contains a phosphorylated tyrosine. The structure of SH2 has been elucidated and shown to exhibit high affinity binding to certain peptide ligands.¹⁰ However, these ligands do not have drug-like properties due to their high polarity, high flexibility and metabolic instability.

Nevertheless, a number of examples have shown that it is possible to overcome these challenges and develop PPI modulators as drugs.¹¹ As these challenges are identified and assessed, useful and novel chemical strategies for the design and identification of small molecule PPI modulators are becoming apparent.

Recently, a review by Nussinov and Keskin highlighted the essential structural requirements for targeting PPIs.¹² In addition, they reinforced the view that proteins are flexible molecules, even though we frequently treat them as being rigid, and that protein surfaces are far from being flat, but filled with pockets, clefts and indentations. The grooves that constitute the surface of proteins in the unbound state are generally filled with water molecules. When the two proteins come in contact, the grooves on one partner protein become occupied by fragments of the other protein. In drug discovery, an effective modulator of a PPI does not necessarily have only to cover the whole surface of the interaction. A small molecule may interact with a limited number of essential amino acids.

The small molecules discovered to date that inhibit PPIs are powerful examples of how PPIs can be tractable therapeutic targets. In particular, in cancer research, two examples of signalling proteins where PPI small molecule inhibitors of signalling pathways are in phase II clinical trials, and these are described below.

1.2.2. Two successful examples of PPI modulators

An important cellular function that has been the target of drug discovery for many years is “programmed cell death”, also known as apoptosis. It is important in cancer cells, as when this function is diminished it leads to survival, proliferation and resistance to chemotherapy. Chemical agents that can promote apoptosis have the potential to treat cancers related to abnormalities in the apoptotic pathway.¹³ In addition, solid tumours often have over-expressed levels of antiapoptotic *bcl-2* genes, which are known to cause

resistance to cytotoxic drugs. That induces apoptosis. Consequently, interest in targeting the Bcl-2 protein has been growing.¹⁴

In cells, pro-apoptotic members, such as Bax and Bak, bind to, and consequently, are inhibited by Bcl-2 and Bcl-XL proteins, thus preventing apoptosis. To date, agents developed to inhibit Bcl-2 expression have shown a lack of specificity, affecting non-cancer cells or have been associated with unacceptable toxicities.¹⁵ More recently, two specific PPI inhibitors of this target have been reported (*Figure 1.1*).¹⁶ ABT-737, from Abbott Laboratories, is the first dual inhibitor of Bcl-2 and Bcl-XL proteins. Its binding to these two proteins inhibits their interaction with pro-apoptotic proteins (Bax and Bak) which trigger apoptosis in cancer cells.¹⁷ This molecule is currently in Phase II clinical trials. However, it exhibits a poor oral bioavailability and consequently a second-generation analogue of ABT-737 was developed. This inhibitor, ABT-263 or NavitoclaxTM, is currently in multiple Phase II clinical trials in small cell lung cancer and haematological malignancies.

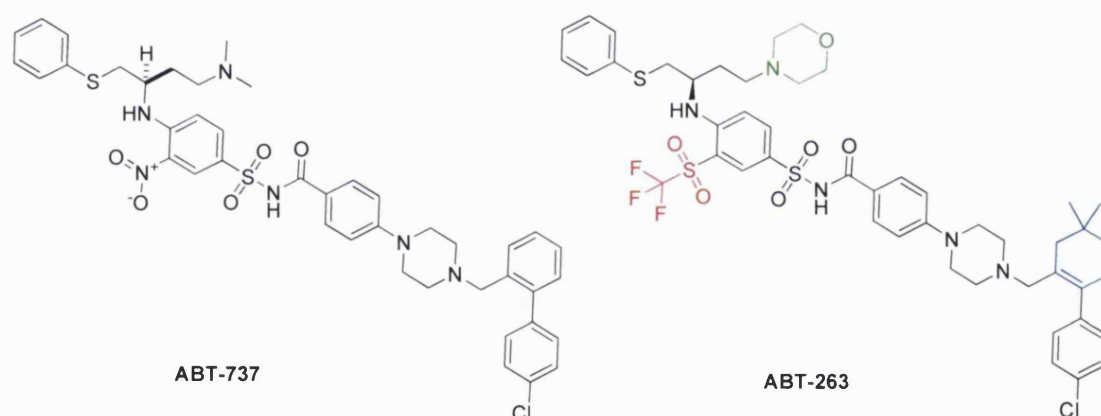


Figure 1.1 | First- and second-generation Bcl-2 inhibitors. The three modifications highlighted in green, red and blue increase the oral bioavailability of ABT-263.

Another cellular oncology target is the tumour suppressor gene *p53*. This gene becomes inactivated by mutations or deletions in the majority of human tumours. Its functions include the activation of cell cycle arrest and apoptosis when DNA damage is detected. If the function of *p53* is restored, it can induce the death of tumour cells. Thus, several anticancer agents have been developed to restore this function. However, to date, none of these agents has shown activity *in vivo*.¹⁸⁻¹⁹ MDM2 (or HDM2 in human) is a gene that is responsible for the reversible deactivation of wild-type *p53* gene with consequences for cell growth and tumourigenesis.²⁰ MDM2 regulates *p53* signalling by binding to *p53* and inhibiting its function and by promoting

its degradation and ubiquitination. MDM2 levels are often high in many human tumours. Disrupting this interaction in order to restore p53 function is thus a valid therapeutic goal. MDM2 interacts with p53 through its N-terminal domain consisting of 120 residues. The binding epitope for p53 has been identified as having 15 amino acids and this polypeptidic sequence could be reproduced and its structure in complex with MDM2 determined. This led to identification of three hydrophobic residues from p53 binding to a sub-pocket in MDM2. At first sight, this sub-pocket was thought to be too small to accommodate a drug-like small molecule. High-throughput screening of a synthetic library identified a number of active inhibitors of the p53-MDM2 interaction. Several classes of small-molecule inhibitors with distinct chemical structures have now been reported to inhibit this PPI.²¹⁻²² The most promising appear to be the tetra-substituted imidazoline (*Figure 1.2-a*, Nutlin-3a) from Hoffman-La Roche²³ and MI-219,²⁴ both of which have progressed into early clinical trials and advanced preclinical studies, respectively. Nutlin-3a has been shown to be efficacious in all xenograft models examined, with average tumour growth inhibition of more than 98% and tumour regressions observed in all models.²³ This molecule was shown to bind by directing its three aromatic substituents into the hydrophobic subpockets.²⁵ A high resolution structure of the complex in which nutlin is shown to inhibit p53-MDM2 has also been obtained (*Figure 1.2-b*).

MI-219 (and more recently MI-319²⁶) is the first example of a small molecule more potent and selective than Nutlin-3a.²¹ It stimulates rapid but transient p53 activation in xenograft tumour tissues, resulting in inhibition of cell proliferation, induction of apoptosis and complete tumour growth inhibition, all consistent with its proposed mechanism of action.

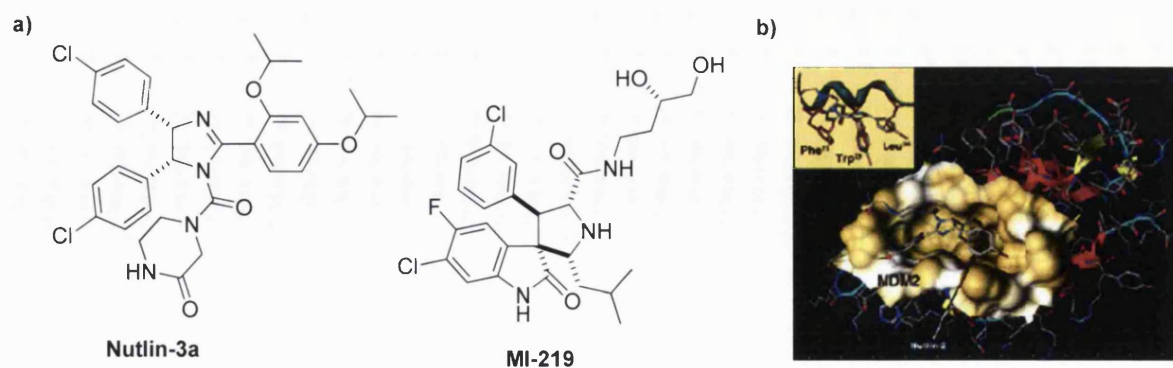


Figure 1.2 | *a)* Most promising p53:MDM2 inhibitors discovered to date. *b)* Example of a binding site for which the high affinity drug-like small molecule (Nutlin) has been shown to bind to and inhibit the MDM2-p53 interaction - *Reproduced from*²⁷

1.2.3. PPI features important for modulation with small molecules

The discovery of novel and efficient PPI modulators requires extensive knowledge of the target being evaluated. In fact, a number of features are common to the majority of protein-protein complexes. The review by Keskin and Nussinov describes in detail the essential aspects driving the preferred types of associations of protein complexes.¹² The main features and challenges crucial to the discovery of novel PPI modulators and the establishment of biophysical and biochemical assays are outlined below:

- PPI are essentially mediated by hydrophobic (Van Der Waal) interactions. Consequently, hydrogen bonds and electrostatic interactions are secondary but important. In drug discovery, the significance of this applies to the physical and chemical properties of the ligand required to ensure optimum complementarity.
- Most PP associations form and dissociate continuously and, therefore, they exist in complex stable or transient dynamic equilibria.²⁸ Computer-based approaches (e.g., virtual screening), allow the design of PPI modulators. If available, either crystallographic or NMR data of the PP complexes are the first step in the design process. In addition, the PPI can be assessed in terms of K_d values, which provides a powerful indication about the strength of these interactions. Optimal K_d values for PPI modulators range from micromolar to picomolar, thus allowing the evaluation of the efficacy of PPI modulators.
- The design of synthetic ligands through either computational techniques or through biochemical and biophysical assays can be performed when the two protein partners are bound to each other or when a chaperone is attached. This is because the protein

domain of the target PPI could become disordered or unfold in the absence of its partner.²⁹

- In some cases, similarities between protein domains that relate to the target PPI could be up to 80-95%.³⁰ In addition, certain proteins may use the same binding sites to attach to different partners through a conformational change. Examples include Elongin B/Elongin C/VHL and Elongin B/Elongin C/SOCS2. Knowledge of this is essential when analysing the binding affinity and selectivity of novel ligands for targeting PPI modulation.

1.3 Hot spots and allosteric sites as targets for small-molecule PPI modulators.

Hot-spots^{12, 31} and allosteric sites³²⁻³³ are the two main sites of interaction of ligands for PPI inhibition. Looking for hotspots and allosteric sites has enabled the discovery of a number of small-molecule PPI inhibitors.

1.3.1 Hot-spots

It has been shown that the stability of a PP complex may be dependent on a small portion of amino acids where most of the binding energy is found.³⁴ This region of the protein is called a hot spot and represents “active site” for the interaction. Binding of a ligand to the hot spot region of a protein competes with the other protein partner, therefore disrupting the PPI (*Figure 1.3*). A small molecule that modulates a PPI could cover an area of approximately 300–1000 Å². The surface area of a hot spot is normally around 600 Å², making it a viable target for the discovery of PPI modulators.

X-ray crystallography and site-directed mutagenesis studies have shown that hot spots are highly complementary to each other, with buried charged residues forming electrostatic bridges and hydrophobic residues on one side associating with complementary residues on the other side. In addition, the association surface tends to be flat, lacking crevices and binding pockets that might provide tight binding sites for small molecules. Another feature of PPIs critical for the design of small molecule inhibitors is that the interaction surface is a result of a considerable degree of flexibility and adaptivity between the two proteins to create a complementary surface. This represents a challenge when carrying out X-Ray crystallography as the active conformation may not always be defined. It can also be difficult to identify the stoichiometry for the interaction of small molecules at the PPIs. This might be especially problematic when the proposed drug is hydrophobic or amphipathic, thus

forming micelles or liposomes. It is also possible that the drug can act as a denaturant or covalent inhibitor in which case the protein function is disrupted but the binding does not happen at the interface. Artefacts can also arise when proteins are being targeted and in the case of PPIs, they are hard to exclude. Determining which protein the inhibitor is bound to, can be hard to predict even though fitting algorithms have been put in place to assess this. Overall, there might be several mechanisms that can lead to the observed inhibition.

It has been estimated that only 9.5% of the interfacial residues in PPIs are within hot-spots.³⁵ Ideally, a database of hot-spots based on nuclear magnetic resonance (NMR), and X-ray crystallography would be beneficial, but to build it would be very expensive and time-consuming. Recently, effort to develop computational strategies to screen PP interfaces with the goal of identifying hot-spots has increased.³⁵⁻³⁶ Docking algorithms could be used to differentiate between these regions, and support the concept of targeting hot-spots using drug design methodologies.³⁷

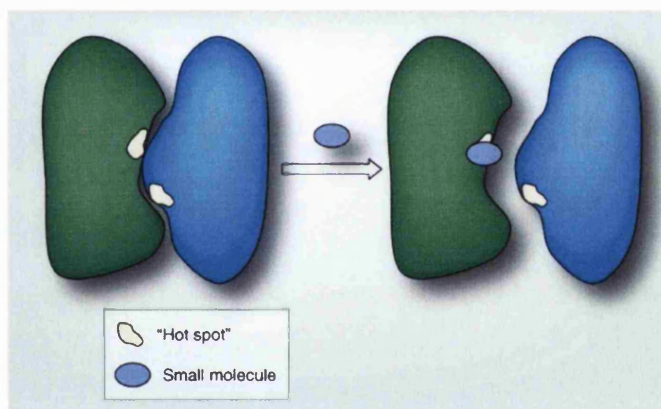


Figure 1.3 | Hot spots as targets for PPI Modulators – *Adapted from Zinzalla and Thurston, 2009.*³⁸

1.3.2 Allosteric sites

Enzymes use allosteric control as a mechanism to regulate their function. It is described as a conformational change at the active site of the enzyme, which is induced when a ligand binds to a different site. With regards to PPI, a ligand that binds to an allosteric site (i.e., positioned offset from the PP interface and not competing with the binding protein partner) could interfere with the main PP interface, and eventually inhibiting it (*Figure 1.4*).

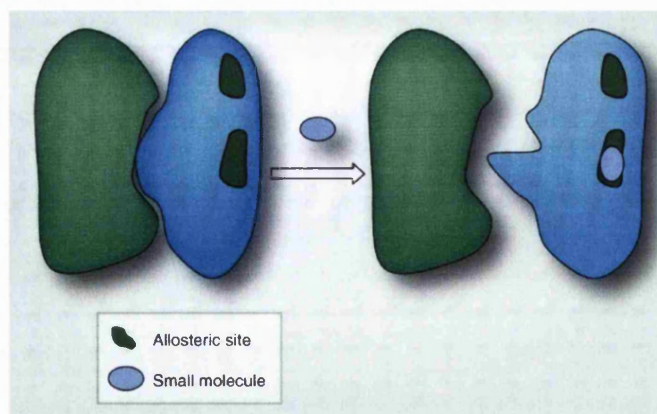


Figure 1.4 | Allosteric regulation of PPI – *Adapted from Zinzalla and Thurston, 2009.*³⁸

A number of advantages exist from modulating PPI through allosteric sites. Compared with hot spots, allosteric regulation of PPI allows a more effective control of these interactions (i.e. saturation and not overdosing), in addition to a higher specificity. These sites may also be less challenging to identify than hot spots due to their pronounced shapes and wide distribution. This approach is now gaining widespread use by a range of techniques including high throughput screening, x-ray crystallography, phage display etc. As a result, more successful examples of allosteric regulation can now be found.³⁹

1.4 Strategies to identify small-molecule PPI modulators: a critical perspective

- Peptides and peptidomimetics.

A different approach to the design of PPI inhibitors is to use the binding locus of one of the two proteins to prepare a short peptide that bears the main residues from the bonding epitope. This route is fast and relatively simple if the structure of the proteins is available. Nevertheless, as the peptides are not drug-like molecules and suffer from poor bioavailability, the challenge lies in designing small molecule peptidomimetics, which has proved successful in many cases.

A first example includes Src-homology 2 (SH2) domains, which are important for signal transduction between cell surface receptors and cytosolic proteins. The SH2 domain within Src-family kinases binds to phosphorylated tyrosine residues found in downstream signalling proteins. One member of the SH2 domains with tyrosine kinase is the protein p56^{lck}, which interacts with T-cell receptors leading to cytokine production and cell proliferation. From a five-negatively charged peptide inhibitor,

Boehringer and coworkers designed a mono-charged peptidomimetic inhibitor which has weaker inhibition ($K_d = 1\mu\text{M}$), but improved cell permeability (**1.1**, *Figure 1.5*).⁴⁰

Another example of a target where peptide mimetics have been employed is the pathogenic factor C5a that mediates a range of immuno-inflammatory diseases (**1.2**, *Figure 1.5*). Site-directed mutagenesis has allowed the development of peptide inhibitors which were optimized by the Finch group to generate cyclic peptide mimetics of the original peptide. The most potent molecule had an $\text{IC}_{50} = 0.3\mu\text{M}$, measured by competitive assay using I^{125} -labeled C5a. Intravenous administration in rat models showed good anti-inflammatory activity.⁴¹

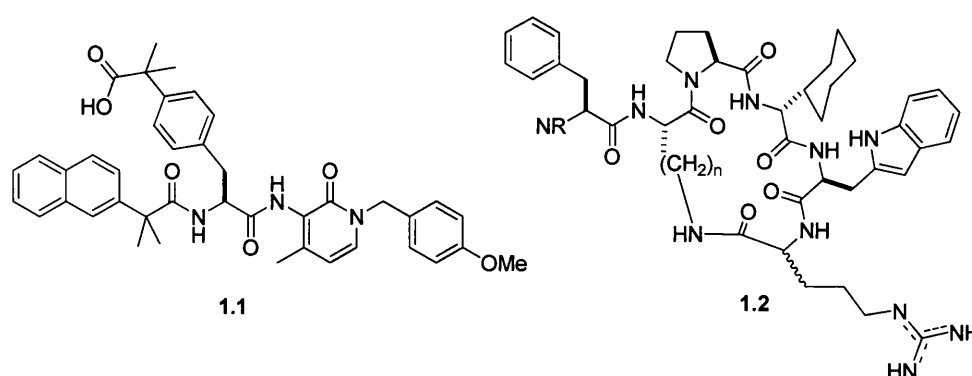


Figure 1.5 | PPI peptidomimetic inhibitors of SH2 domain (**1.1**) and pathogenic factor C5a (**1.2**).

- Natural products: An important source of PPI.

Over the past 30 years, 24 natural products have been approved as drugs.⁴²⁻⁴³ Interestingly, only half of these was shown to fall within Lipinski's Rule of Five.⁴⁴ The other half, that did not pass these rules, still displayed good oral bioavailability. This is a clear indicator that the Rule of Five is not an accurate indicator for oral bioavailability. In addition, Koehn and co-workers observed that a number of natural products falling outside the Rule of Five range have a 50% success rate in being developed as orally administered drugs.⁴⁵

The use of natural products in targeting signal transduction pathways is an important aspect of drug discovery. Natural products are a rich source of novel and diverse molecular frameworks. The synthesis of natural product analogues allows the preparation of a wide range of molecular structures diverting from an initial scaffold providing a greater molecular diversity. New chemical methodologies have arisen in the last 10 years enabling the high-throughput synthesis of libraries using natural products

as starting points.⁴⁶ Natural product-based compounds have the advantage of having their chemical structures biologically pre-validated, promising high specificity and binding affinity to different targets. As a result, natural products are excellent starting points for PPI inhibitors, providing well-defined and validated 3D structures and a basis for specificity and differentiation between closely related proteins.⁴⁷

An example of a PPI inhibitor discovered from natural product sources is rolitetracycline (*Figure 1.6*), an inhibitor of the HIF-1 pathway. This will be presented in further detail in the next chapter.⁴⁸

Another example of a PPI involved in the regulation of the HIF-1 signaling pathway is the complex of HIF-1 α with p300/CBP binding protein, responsible for enhancing HIF-1 transcriptional activity. A HTS of over 600,000 compounds allowed for the identification of chetomin (*Figure 1.6*) as a selective inhibitor of this PPI.⁴⁹ Chetomin was shown to bind to the CH1 domain of p300 causing the disruption of its tertiary structure. Although animal toxicity has limited the further development of chetomin, it still serves as a useful lead structure, and starting point for the design of novel scaffolds.

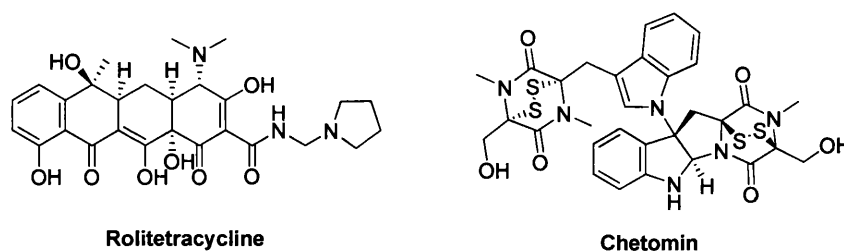


Figure 1.6 | Successful natural product protein–protein interaction inhibitors of the HIF-1 signalling pathway.

- PPI modulators not obeying Lipinski’s rules.

As much as naturally occurring compounds and their analogues appear to be good inhibitors for a number of protein-protein interactions, these do not always obey Lipinski’s rule of five.^{38, 50-51} These compounds could fall outside Lipinski’s ranges even though a good pharmacokinetic ADME (absorption, distribution, metabolism and excretion) profile would be maintained, which still makes them good candidates. This could be supported by the fact that over half of the FDA approved small molecules used orally do not obey Lipinski’s rules. Wilkinson’s group suggested that the current ‘over-emphasis’ on complying with druggability rules should be replaced by a more programmatic and balanced approach to drug discovery.⁵¹ Less defined molecular

targets such as PPIs make it even more challenging to adhere to the rule of five, therefore the focus should be on PPI inhibitors that display promising potency and selectivity, even though their cell membrane penetration would not appear to be fantastic.

Wells and McClendon described a number of protein–protein interaction inhibitors, some in clinical trials, with K_i values of less than 1 μM and molecular masses of 500–900 Da.¹¹ This group predicted from a comparative study that a molecular mass of between 650 and 700 Da would represent a more applicable range for PPI modulators rather than under 500 Da as proposed by the rule of five.

In light of these observations, it would be appropriate to suggest that there is always an interplay between compound binding affinity and properties such as pharmacokinetics, solubility, toxicity and ease of synthesis, which together determine the probability that a compound will succeed as a drug.

- High throughput screening (HTS): a traditional drug discovery approach

The discovery of novel PPI modulators through HTS is highly efficient and more applicable, especially when knowledge about structural features of the target proteins is limited.⁵² In order to perform this type of screening, a number of elements need to be ensured.³⁸ First, compound libraries need to be selected such that a high degree of molecular diversity and complexity, and not only the size, is ensured. This has been supported by the effort of a number of groups to introduce new molecular and skeletal diversity using new synthetic methodologies.^{53–54} Another important element in the development of HTS is selecting the right assay. Competitive binding assays such as FRET and FP, discussed previously, are more commonly used in PPI screening and more amenable to high throughput methods, due to their simplicity and relatively lower cost when compared with other screens such as ELISA. Phenotypic cellular assays are also important for HTS whenever a phenotype is expected to result from a modulation of a PPI. Nevertheless, they still require competitive binding screens to allow the elucidation of their mode of action. Biophysical assays, which use NMR spectroscopy and surface plasmon resonance (SPR), have also been used in HTS. These assays can be more costly as they utilise expensive instrumentation but could be beneficial in the sense that they offer a high sensitivity.

An example of PPI hits that have emerged from HTS follows a recent interest in developing *c-Myc:MAX* protein inhibitors for cancer therapy. This protein dimer, belonging to the basic helix-loop-helix leucine zipper (bHLH-LZ), was shown to mediate cancer growth and thus its inhibition has been validated as a PPI target for cancer therapy.⁵⁵ *InSilico* studies have not yet revealed structural features of the PPI dimerisation domain which brought further the need to undergo HTS. Thus a primary HTS using fluorescence-based assays (FP and FRET) and an ELISA assay have identified a number of hit compounds with IC₅₀ values in the range of 0.5-60 µM (Figure 1.7 shows the top two hits).⁵⁶⁻⁵⁸ The mode of action of these hits is still under investigation but the authors suggest a possible scope for allosteric inhibition by molecule 10058-F4.

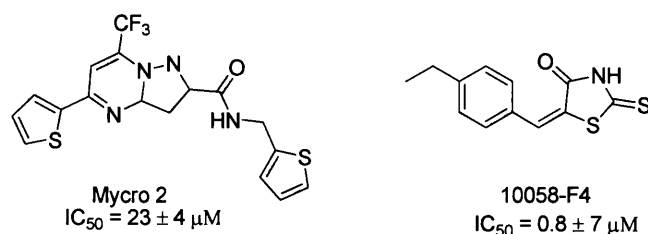


Figure 1.7 | The top two inhibitors of Myc:MAX interaction identified by HTS.

PPIs could be targeted with cell-permeable molecules even when protein surfaces are not fully elucidated. The mode of action of the hits could be investigated *in vitro* and cellular systems (e.g., the yeast two-hybrid system) where they have been shown to be selective for *c-Myc* gene transcription. This has opened the prospect of development of more-potent small-molecule *c-Myc:Max* inhibitors.

- Computational approaches

Virtual screening

Computational screening is a rapid and valuable source of hit generation in the drug discovery process. In PPI, virtual screening has been widely applied, and this can be demonstrated by the work conducted by Wang *et al* to identify inhibitors of Bcl-2 function. A library of 193,383 compounds was screened *in silico* using database docking where each compound is scored for shape complementarity to the Bcl-2 model in different conformations. After further optimization, 28 commercially available compounds were physically screened using a fluorescence polarization assay generating

the compound HA14-1 as the best inhibitor with an $IC_{50} = 9 \mu M$. At $50 \mu M$, this molecule prompted cell death in >90% of cultured human leukemia cells.⁵⁹

Structure-based design

Designing compounds based on the 3D structure of the target protein currently seems one of the most valuable discovery approaches. One method to do so is by selecting a scaffold molecule, normally using software such as CAVEAT,⁶⁰ to which specific side chains are attached in a particular orientation so that they occupy the same region of space as the peptide ligand. Then, these side chains are optimized through synthesis, assays or via combinatorial libraries. This technique was used to design ligands for the somatostatin receptor based on the glucose template. Also, benzene was used as a template for the design of interleukin-1 receptor IL-1 α and IL-1 β inhibitors. Three amino acids Arg-4, Phe-46 and Lys-93 from the binding epitope were replaced by a 1,2,4-trisubstituted benzene which was further optimized to obtain more potent molecules. A considerable advantage of this method is that it takes into account the synthetic accessibility of the designed compounds. On the other hand, this might limit the possibility of having highly potent molecules.

The next example demonstrates how knowledge of the 3D model of a protein-ligand complex was used to discover an inhibitor of the heat shock protein Hsp90. This latter is necessary to ensure the correct folding of certain proteins such as steroid hormone receptors and kinases (e.g. src, raf, Eif-2 α). Thus Hsp90 acts as a chaperone and utilizes co-chaperone p23 protein to release fully functional proteins. This process also requires the hydrolysis of ATP which binds to the N-terminus ATP/ADP binding site on Hsp90. It was shown that ansamycin antibiotics, such as geldanamycin (GA) (*Figure 1.8-a*), bind to Hsp90 and reverse its effect on the folding of v-src, thus presenting a potential target for treatment of cancer.⁶¹ Moreover, 17-allylamino-geldanamycin (17-AAG) (*Figure 1.8-b*), a more potent analogue of GA, has been successful in phase I clinical trials⁶² for treating cancer. In addition to binding to the ATP/ADP site on Hsp90, these natural products are thought to inhibit the interaction between Hsp90 and p23.

The crystal structure of the Hsp90 N-terminal domain associated with GA has helped to identify key structural components responsible for this interaction. These include molecular contact with Asp-93/Ser52, H-bonding with Lys-112/Lys-58 and hydrophobic interactions from six-amino acid side chains. Purine was chosen as a

starting template, mainly for its favourable bioavailability and cell permeability. Employing this template and based on the key interactions, Chiosis and co-workers designed PU3 (*Figure 1.8-c*) which was docked computatively inside the Hsp90 ATP/ADP binding site and was shown to satisfy most of the interactions with the exception of that to Lys-58.⁶³ Inhibition assays showed a good affinity to Hsp90 when compared with 17-AAG. Furthermore, PU3 was proved to lower Her2 levels in MCF7 breast cancer cells and reverse the transformed phenotype of these cells. This molecule represents one of the first successful examples of PPI inhibitors designed de novo based on the knowledge of the crystal structure of the target protein. In addition, it has a low molecular weight and has drug like properties.

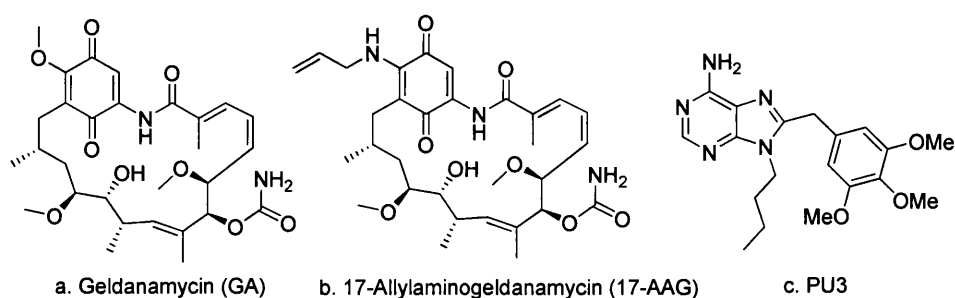


Figure 1.8 | Inhibitors of Hsp90 ATP/ADP binding site.

- Innovative strategies: thinking out of the small molecule box

Cut-down protein frameworks are an emerging useful approach for PPI modulation. These frameworks offer high theoretical ligand binding affinities and lower molecular weight. Furthermore, they allow the attachment of a number of functional groups to preserve and/or enhance the binding activity of the domain. Schepatz and co-workers introduced miniature proteins as a new class of PPI modulators, which was achieved in two steps.⁶⁴ Initially, the binding epitope is identified and the active sequence of amino acids grafted onto an inert stably-folded rigid miniature protein. Next, selected functionalities are introduced to provide chemical diversity, tailoring the conformation and reactivity to prepare a library for ligand identification (*Figure 1.9*).³⁸

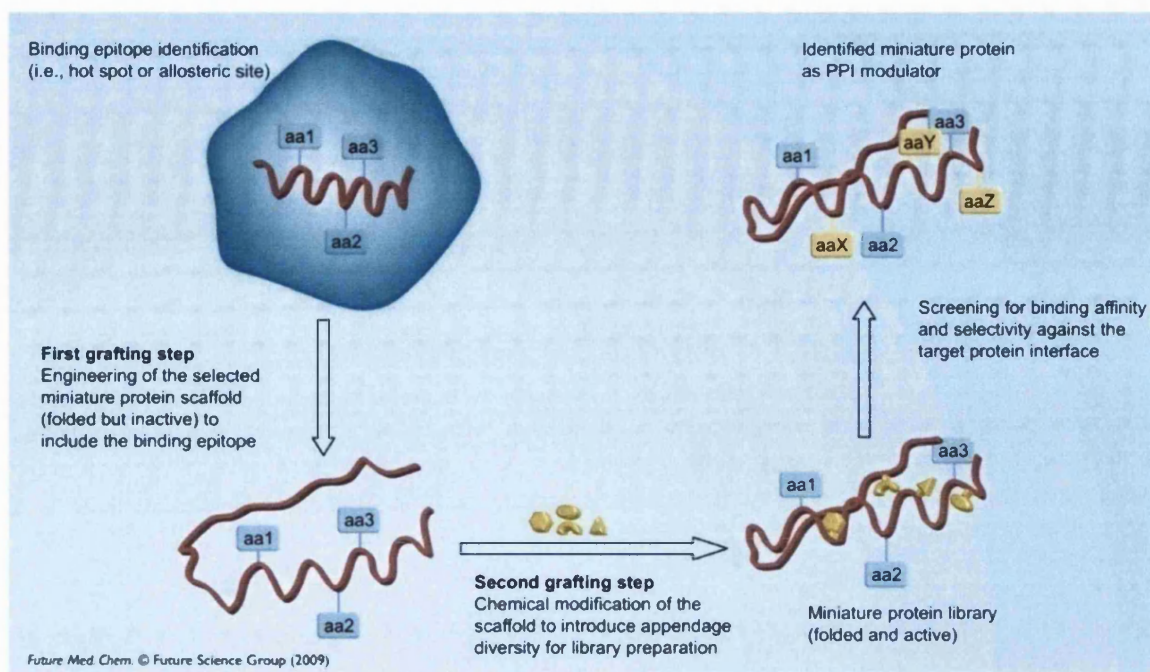


Figure 1.9 | The miniature protein approach of Schepartz and co-workers – Adapted from Zinzalla and Thurston, 2009.³⁸

Applications of this approach to protein targets include Bcl-2,⁶⁵ p53:MDM2,⁶⁶ CBP⁶⁷ etc., by utilizing the small, folded avian pancreatic polypeptide (aPP) as a scaffold. Overall, the use of protein engineering to produce miniature protein frameworks to engineer novel protein-interacting sites is a quickly growing PPI investigation tool. However, a number of challenges still need to be considered, including folding stability, solubility and production yields.³⁸

Hydrocarbon-stapled peptides represent another innovative strategy used in targeting PPIs. It is aimed at stabilising the α -helical conformation of synthetic peptides, which will consequently enhance their binding affinity towards another protein partner. In addition, the induced conformation will increase cell permeability by minimising the exposure of the polar amide backbone to the environment. So far, disulfide and lactam bridge cross-linking has been used, but has been limited due to the lability of these bonds. More recently, Verdine and co-workers reported a novel technique known as ‘peptide stapling’.⁶⁸ They used a ruthenium-catalysed ring-closing alkene metathesis (terminal alkenes of the unnatural amino acids) to stabilize the helix. This results in a significant increase in metabolic stability and cell permeability of these peptides.

The same group has used this approach to the two PP interactions, p53:hDM2⁶⁹ and Bcl-2:Bax/Bad⁷⁰. Transcription factor p53 induces cell cycle arrest and apoptosis in response to DNA damage which protects cells from malignant transformations. hDM2 controls p53 levels through ubiquitilation and its overexpression is the most common defect in human cancers. Co-immunoprecipitation and cell-based experiments have demonstrated that the stapled p53 peptide (through three residues, F19, W23 and L26) binds to and inhibits hDM2 binding thus restoring active p53. This results in tumour cells death.

In summary, metathesis chemistry has enabled the weak disulphide and lactam bridges in constructing stapled α -helical peptides to be overcome. It is likely that these approaches will be widely used in the future for the production of PPI modulators, and for related structural and mechanistic studies.³⁸

Stabilising PPI is another efficient way to modulate signalling pathways in drug discovery. This approach is particularly advantageous and displays potentially favourable thermodynamic aspects of stabilization (i.e., entropy and enthalpy). A number of examples of the stabilization of PPIs has been reported from normal physiological processes and based on the mode of action of some drug molecules. This strategy is potentially useful when targeting transcription factors over-expressed in tumours and the target PPI would result into an induction of the proteolytic degradation of the over-abundant transcription factors.

In the same way as has been previously shown with PPI inhibitors, small molecule PPI inducers could fit into gaps that link PP interfaces thus binding both macromolecules together more tightly. In addition, allosteric stabilization has also been considered, where a small molecule binding at a further site causes a conformational change of the protein at its interface causing an enhanced stabilization. There are two classes of compounds that have been reported to stabilise PPI through direct binding. The first one is bifunctional compounds consisting of domains that can recognize and bind to pockets on the interfaces of both protein partners, which tightens their interaction (*Figure 1.10*).³⁸ Examples of this class include the immunosuppressive macrolide rapamycin which binds to both the receptor protein FKBP12 and to the FKBP12-rapamycin binding (FRB) domain of mTOR, tightening the interaction between these proteins.⁷¹ The second type of stabilizer includes two parts, each interacting with one of the two proteins, and which are joined by a flexible linker (*Figure 1.10*).³⁸ This represents the

vast majority of PPIs as has been shown in the review by Crews and co-workers.⁷² A comprehensive number of bifunctional molecules is presented in this review.

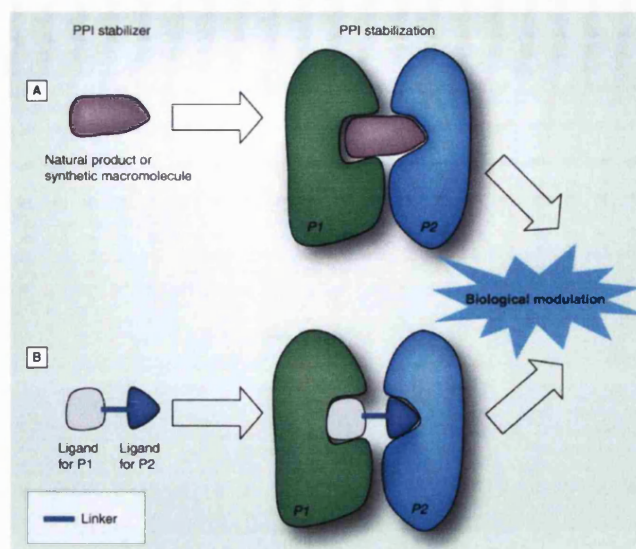


Figure 1.10 | Schematic representation of two classes of direct PPI stabilisers – Adapted from Zinzalla and Thurston, 2009.³⁸

This approach could be faced by a number of challenges. The position, flexibility, length and chemical properties of the linker between the two chemical moieties is critical for both binding affinity and selectivity for the two linked proteins. Another limitation of bifunctional PPI stabilizers is their large molecular size and weight. These drawbacks could, however, be overcome by minimizing ligand and linker size, and by optimizing structure using traditional medicinal chemistry techniques.

1.5 Conclusions and future perspectives

The increasing number of examples of molecules that have been shown to inhibit PPIs is very promising for those who want to pursue this approach in their drug discovery. Various examples, such as the inhibitor of MDM2-p53, clearly demonstrate that these PPI modulators do not need to have high molecular weight (MW) to be effective and potent. It is too early to claim that the challenges that face the discovery of PPI inhibitors have been surmounted. Indeed, in the next few years, emerging techniques are thought to modernize this approach and provide more efficient means for compound library preparation and evaluation. Preparing large libraries through combinatorial synthetic methods for the purpose of screening can now be achieved. Moreover, applying mass spectrometry, nuclear magnetic resonance (NMR) and nanotechnology in

high throughput screening (HTS) have enhanced the screening output in PPI drug discovery.

Currently, there are no general or typical approaches that will reliably lead to the discovery of effective PPI inhibitors, and until a guideline is set, the researchers need to rely on combinations of screening and structure-based design to identify hits. Knowledge of the 3D structure of the protein-ligand will help to optimize these hits. If one is not successful in binding a sufficient proportion of the small molecule into the complementary hydrophobic surface of the protein, allosteric sites may be considered. Understanding of drug discovery through inhibitors of PPIs will certainly evolve over time giving rise to generic structures, for example, that may form the core of PPI inhibitors. More inhibitors are expected to advance through the preclinical and clinical trials in the upcoming years. Perhaps then, the doubts raised about the efficacy of this approach will fade away.

CHAPTER 2

Hypoxia Inducible Factor

Contents:

2.1	Hypoxia	22
2.2	Hypoxia inducible factor (HIF)	23
2.2.1	HIF1- α and - β subunits: structures and characteristics	23
2.2.2	bHLH/PAS proteins	25
2.2.3	Other HIF- α isoforms	25
2.2.4	HIF-2 α PAS domains	26
2.2.5	Comparison between HIF-1 α and HIF-2 α	27
2.2.6	HIF degradation	28
2.2.7	Alternate mechanisms of HIF regulation	31
2.2.8	HIF Target genes	32
2.2.9	The balance between adaptation and cell death	33
2.3	Modulating HIF-1 signalling pathway for drug discovery	34
2.3.1	Promoting HIF-1 pathway for ischaemic diseases	34
2.3.2	Inhibiting HIF-1 pathway for cancer therapy	35
2.3.3	HIF-1 inhibitors	36
2.4	Conclusion	45

HYPOXIA INDUCIBLE FACTOR-1 (HIF1)

2.1 Hypoxia

Hypoxia can be defined as a reduction in the amount of oxygen reaching the tissues of the body due to either normal physiological variations or pathological conditions resulting in a reduced ability of the hypoxic cell to maintain proper energy production. The function of the hypoxic cell becomes disrupted and this can lead to cell death. Physiological variations include embryonic and foetal development through which the development of new cells and organs requires high amounts of oxygen. Moreover, during exercise, the muscle requirements for energy outweigh the oxygen supply leading to a localized hypoxia and the build-up of lactic acid from anaerobic metabolism.

In terms of the pathological states associated with hypoxia, cancer is most notably the main one. Solid tumours have a high number of hypoxic cells and tissues due to the fast cancer cell growth outpacing the angiogenesis and therefore the blood supply. As a result, portions of the tumour become hypoxic or even anoxic. Hypoxic cells are a main feature in the early solid tumour where its diameter does not exceed 3mm. The tumour reacts to hypoxia by seeking other sources of oxygen, e.g. through glycolysis, or through increased angiogenesis. The newly formed blood vessels are unusual, lacking their endothelial lining, anarchic in their distribution and most of them are leaky (*Figure 2.1*). The new vessels also do not reach all tumour cells and oxygen diffusion is limited to the cells nearby the vasculature. Hypoxia, thus, remains a constant feature of solid tumours. This feature is a negative factor in cancer treatment because it lowers the effectiveness of radiotherapy and chemotherapy and also aids malignant progression.

Hypoxia is also present in other pathological conditions such as cardiovascular disease, stroke and chronic pulmonary disease. Ischemic heart disease occurs as a result of atherosclerosis in which the blood vessels are blocked impairing the supply of blood and nutrients to regions of the heart. Stroke can cause cerebral hypoxia because it affects the blood vessels leading to the brain causing localized reduction in oxygen and nutrients. Its impact is very serious leading to irreversible damage to the neurons and thus disability. Chronic obstructive pulmonary disease (COPD) is featured by alveolar

hypoxia and if not treated can be fatal. In these examples, hypoxia results from a disproportion between oxygen supply and energy production.

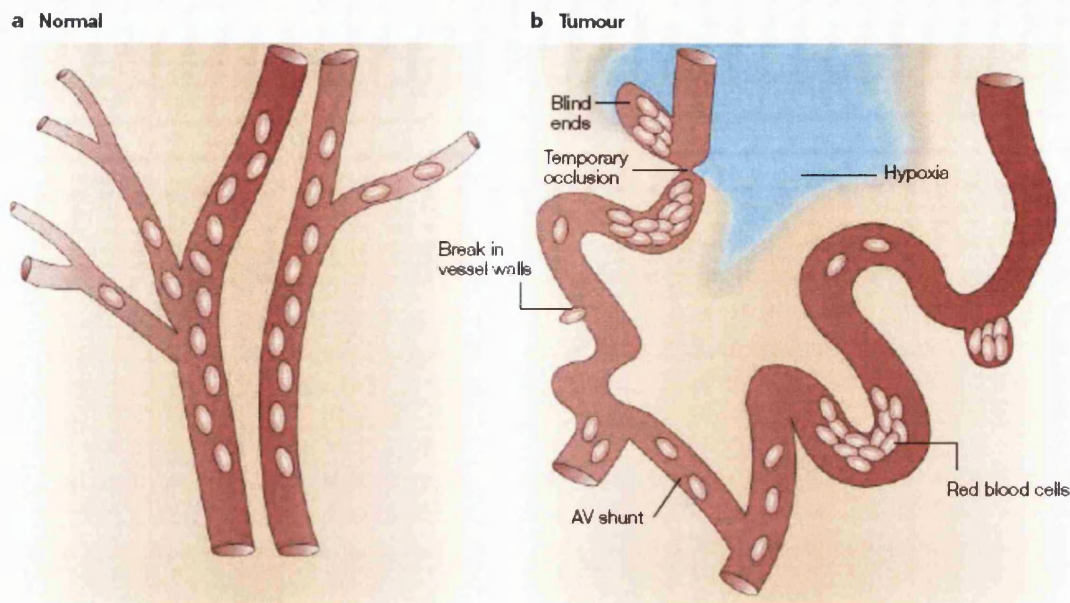


Figure 2.1 | The vascular network of normal tissue versus tumour tissue - *reproduced from Brown, J.M. et al, 2004.*⁷³

2.2 Hypoxia inducible factor (HIF)

2.2.1 HIF1- α and - β subunits: structures and characteristics

When oxygen supply cannot meet the energy demand of the cells, they respond by trying to restore the energy balance and preserve the cell function. A primary adaptive response is the transcriptional regulation of a number of hypoxia-responsive genes. The most prominent and well described mechanism involves the interaction of a family of transcription factors known as hypoxia inducible factors (HIF). Over 70 target genes are directly regulated by HIF and the expression of several hundreds of genes have been shown to be directly or indirectly influenced by HIF.⁷⁴

HIF proteins form heterodimers of two subunits termed α and β . Oxygen levels can affect the protein stability, subcellular localization and transcriptional potency of the HIF- α subunit. This latter quickly accumulates during hypoxia and on re-oxygenation, it rapidly degrades with a half life of less than 5 minutes. On the other hand, the HIF- β subunit, also known as aryl receptor nuclear translocator (ARNT), is constitutively expressed and its activity controlled in an oxygen-independent manner. The alpha class

is composed of HIF-1 α , HIF-2 α and HIF-3 α , which will be discussed in detail later on. HIF-1 β includes ARNT and ARNT2.

The HIF family belongs to a class of transcription factors termed basic helix-loop-helix Per-ARNT-SIM (bHLH/PAS) proteins. Both HIF-1 α and HIF-1 β subunits contain a basic region that contains approximately 15, mostly basic, amino acids which ensure the direct binding of the HIF protein to DNA. The next region contains two amphipathic α -helices separated by a loop, which makes up the main dimerization interface between HIF members. After that, comes the PAS domain the name of which name comes from the first letter of each of the three founding members of the family of proteins i.e. Per-Arnt-Sim. This domain consists of 200-300 amino acids in which there are two loosely conserved, highly hydrophobic regions known as PAS A and PAS B, each comprising about 50 amino acids. These two domains are responsible for the secondary dimerization among family members as well as other roles such as ligand and chaperone (Hsp90) binding in the dioxin receptor (DR) on their hydrophobic core. The HIF-1 α subunit also contains N- and C-terminal transactivation domains better known as N-TAD and C-TAD. These two domains mediate the transcriptional activation and the interaction with activators and are connected by an inhibitory domain. The N-TAD overlaps with the oxygen-dependent degradation domain (ODD) and is concerned with the protein stability. The ODD domain contains a number of prolyl residues which are recognised and hydroxylated by specific prolyl hydroxylase domain (PHD) enzymes under normoxia. As a result, an important negative regulator of HIF-1 α known as von Hippel-Lindau protein (pVHL) binds to this region. This protein, which acts as an E3 ligase, triggers HIF-1 α degradation under normoxia. The C-TAD interacts with co-activators e.g. CBP/P300 regardless of the protein stability (*Figure 2.2*).

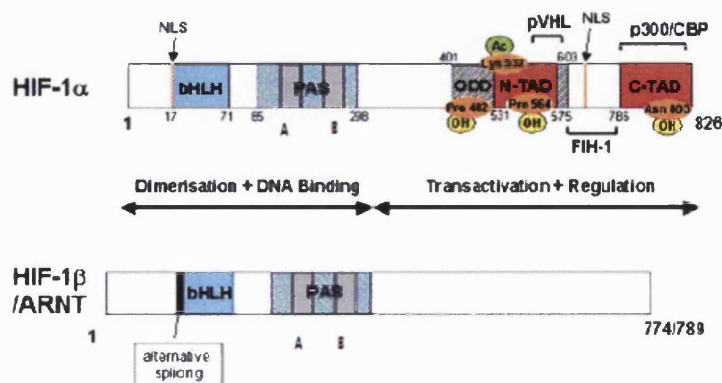


Figure 2.2 | Schematic diagram representing HIF-1 α and HIF-1 β (ARNT) and their functional domains - *adapted from Bardos, J. I. et al; 2004.*⁷⁵

2.2.2 bHLH/PAS proteins

Basic helix–loop–helix (bHLH)/PAS proteins are important in regulating the expression of genes responsible for essential physiological and developmental processes. This family of proteins comprises aryl hydrocarbon (dioxin) receptor (AHR), which modulates transcriptional responses to environmental pollutants, HIF proteins, and single minded proteins (SIM), which control aspects of neural development. The bHLH family of proteins requires dimerization to bind and fully interact with DNA complexes. bHLH/PAS proteins are generally ubiquitous, latent signal-regulated transcription factors and recognize DNA sequences which often differ from the prototypical E-box⁷⁶. Furthermore, they can be divided into two classes: Class I members comprise HIFs, SIMs (SIM1 and SIM2) and AhR and do not dimerize with either themselves or other class I members. Their functional transactivation requires them to dimerize with members from class II i.e. chiefly with ARNT (which can form a homodimer).

2.2.3 Other HIF- α isoforms

The HIF- α family comprises 3 members: HIF-1 α , HIF-2 α –also known as endothelial PAS domain protein 1 or EPAS1 – and HIF-3 α . HIF-2 α shares in total 48% of amino acid sequence identity with HIF-1 α and also contains the pVHL binding domain (ODD region) (*Figure 2.3*). Under hypoxic conditions, HIF-2 α heterodimerizes with ARNT, then binds to the hypoxia response element (HRE) on the DNA. HIF-2 α is expressed in many different human cell lines. However, HIF-1 α seems to be predominant in epithelial cells whereas HIF-2 α is mainly present in endothelial cells, and fibroblasts. More evidence seems to show that HIF-1 α and HIF-2 α may have different functions. Variations of the type of hypoxia or hypoxia mimetic stimulus, cell types or cell populations seem to engender different expression patterns of the two isoforms.

HIF-3 α is highly similar to the other two isoforms with respect to the bHLH and PAS domains. However, it does not contain structures for transactivation found in the C-terminus of HIF-1 α and HIF-2 α – *Figure 2.3*. It also binds to ARNT, under low oxygen concentration, forming a heterodimer, which subsequently binds to the HRE in the DNA. HIF-3 α , on the other hand, suppresses gene expression triggered by other HIFs in the kidney therefore acting as a negative regulator.⁷⁷ HIF-3 α holds many splice variants,

some of which contain the ODD domain also found in the α - and β -isoforms, therefore acting as a VHL substrate. HIF-3 α 2, also called the inhibitory PAS domain protein (IPAS) is a splice variant that acts as a negative regulator of HIF-1 gene expression thus delaying the tumour growth and reducing the vascular density.

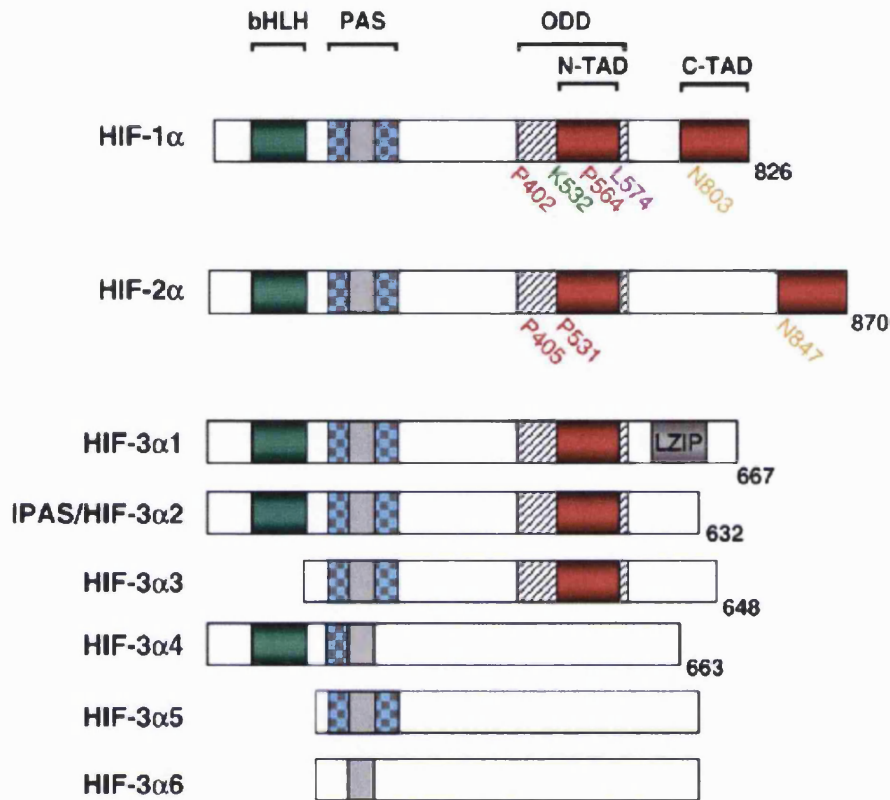


Figure 2.3 | Schematic representation of different HIF- α isoforms showing structural similarities. HIF-3 α splice variants are also shown. LZIP: Leucine zipper - *Reproduced from Bardos, J.I. et al; 2005.*⁷⁷

2.2.4 HIF-2 α PAS domains

Even though many biologically significant PAS domains have been identified, very limited structural information about their interaction is available. Both PAS domains are required for the heterodimerization of HIF-2 α with ARNT, as well as for its biological activity.⁷⁸⁻⁷⁹ Gardner and co-workers used a low-resolution structure of HIF-2 α PAS-B interaction with ARNT PAS-B to demonstrate that these domains interact in an anti-parallel fashion of their solvent-exposed surface of their central β -sheets *in vitro*.⁷⁸ A model that has been proposed to explain the heterodimerization of HIF-2 α /ARNT complex (*Figure 2.4*) supports the anti-parallel binding of the two PAS-B domains. The PAS domains can form a cooperative intermolecular ‘tetramer’ whose interaction converts the relatively weak protein/protein and protein/DNA interactions into a

stronger binding force of a functionally active complex.⁷⁸ However, more needs to be done to understand the PAS interactions and elucidate more reliable models to help the design of PPI modulators.

This β -sheet surface was also shown to be a significant point of interaction between ARNT PAS-B homodimers when not bound to the DNA, and is less important for DNA-bound ARNT homodimers. This could suggest that these domains could play a role in maintaining ARNT homodimers independent of DNA, probably when no heterodimerization partners are present.

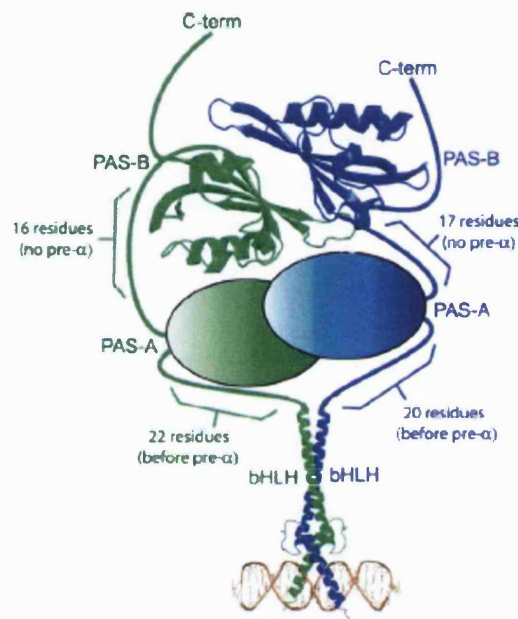


Figure 2.4 | Schematic model showing the interaction of HIF-2 α with ARNT PAS domains as well as the interaction of bHLH with HRE on DNA. In green: HIF-2 α ; blue: ARNT; gold: DNA - reproduced from Bruick, R. K.; 2001.⁸⁰

2.2.5 Comparison between HIF-1 α and HIF-2 α

As mentioned before, HIF-1 α and HIF-2 α have structural similarities, dimerize with the same ARNT, activate gene expression through binding to the HRE domain and are hydroxylated during normoxia by the same enzymes. HIF-1 α is ubiquitously expressed and has been suggested to be the key factor in hypoxic responses. HIF-2 α is also widely expressed, but it can be found in specific cell types, such as vascular endothelial cells, kidney fibroblasts, hepatocytes, glial cells, interstitial cells of the pancreas, Intestinal epithelial cells, neural crest cell derivatives, lung type II pneumocytes, and tumour cells associated with the VHL disease. However, studies on mice have shown that

inactivation of one isoform at a time results in different phenotypes. This could be explained by variations of the cellular distribution as well as the temporal difference in induction time. It was also suggested that this distinctive response could be a result of the activation of different transcriptional targets by each isoform.⁸¹ For example, HIF-1 α appears to be more significant in the expression of glycolytic enzymes with an overall decreased oxidative phosphorylation and increased anaerobic fermentation during normoxia; a characteristic known as the Pasteur Effect⁸². Differences are also noted between the two isoforms in promoting cell proliferation and survival. HIF-2 α tends to promote the growth of undifferentiated stem cells. In clear cell renal carcinoma (CCRC) where the tumour suppressor gene *VHL* is mutated to its inactive form, distinctive differences are observed between the two isoforms. HIF-2 α was shown to express genes responsible for cell survival, such as VEGF and TGF- α , whereas HIF-1 α promotes apoptosis in these cells via expression of BCL2 and BNIP3. Rankin and colleagues demonstrated that HIF-2 α was predominantly or exclusively responsible for *EPO* gene expression in the hepatocytes of mice.⁸¹

Table 2.1 | Summary of HIF-1 α and HIF-2 α target genes analyzed in a study conducted by C-J. Hu *et al.*⁸³

Gene type	Protein
HIF-1 α unique	Hexokinase 2, glucosephosphate isomerase, phosphofructokinase, aldolase A, aldolase C, triosephosphate isomerase, glyceraldehyde-3-phosphate dehydrogenase, PGK-1, PGM-1, enolase 1, LDHA
HIF-1 α and HIF-2 α common	Glucose transporter 1, ADRP, NDRG-1, DMXL-1, IL-6, Carbonic anhydrase XII, filaggrin, ADM, VEGF

2.2.6 HIF degradation

When normal oxygen levels are present in the cell, HIF- α is so rapidly degraded that it is practically unlikely to see any traces of the protein. The instability of the protein is controlled by the ODD domain that overlaps the N-TAD. Under hypoxia however, HIF-1 α and HIF-2 α proteins are stabilized and thus accumulate very rapidly in the cell. It is important to highlight that changes in oxygen chiefly affect the stability of the HIF- α via post-translational modifications such as hydroxylation, ubiquitination, acetylation

and phosphorylation. The oxygenation state of the cell does not significantly affect the transcription and translation of the HIF- α protein. As ARNT is constitutively expressed, neither its stability nor its mRNA expression gets influenced by variations in oxygen levels.

HIF-1 α owes its instability during normoxia to the polyubiquitylation which is followed by proteasomal degradation (*Figure 2.5*). Under hypoxia, the level of polyubiquitylation drops. The von-Hippel-Lindau (VHL) tumour suppressor protein, a component of the E3 ubiquitin-protein ligase complex, contains elongins B and C, Cul2 and Rbx1: essential components for the proteasomal degradation of HIF-1 α and HIF-2 α . The β -domain of VHL binds to the amino acids 557-571 and 380-417 of HIF-1 α and to the amino acids 517-534 and 383-418 in HIF-2 α in normoxia. The α -domain of VHL on the other hand binds elongins. This is followed by a transfer of ubiquitin molecules to a non-specified portion of HIF and thus marking the protein to be destroyed by 26S proteasome. VHL binding to HIF in normoxia is preceded by the irreversible hydroxylation of two proline residues on the HIF located on the ODD domain (P402 and P564 on HIF-1 α ; P405 and P530 on HIF-1 β) which account for the high affinity binding of VHL to HIF under normoxic conditions.⁸⁴ The proteins responsible for this hydroxylation are known as prolyl hydroxylase domains (PHDs) or hypoxia-prolyl hydroxylase (HPH) and have at least three isoforms: PHD1/HPH3, PHD2/HPH2 and PHD3/HPH1. These may have differences in their response, expression patterns and locations within the cells. These enzymes are 2-oxoglutarate-dependent and need oxygen in order to hydroxylate the proline residues. PHDs contain iron bound to two histidine and one aspartic acid residues and di-oxygen when in its ferrous state. One oxygen molecule is passed to the target prolyl residue on the HIF whereas the other one reacts with 2-oxoglutarate to produce succinate and carbon dioxide. Therefore, the PHD/HPH enzymes lose their activity under hypoxia under which HIF proteins are not degraded. It is most probable that PHDs act as direct oxygen sensors thus affecting HIF stability in response to cellular oxygen variations. Interestingly, it was shown that inhibiting HIF-1 α activity also stops its degradation, suggesting that HIF-1 α can upregulate a target enzyme that downregulates it. Since certain PHD/HPHs are target genes of HIF-1, they represent a way through which HIF-1 α self-regulates its expression.⁸⁰

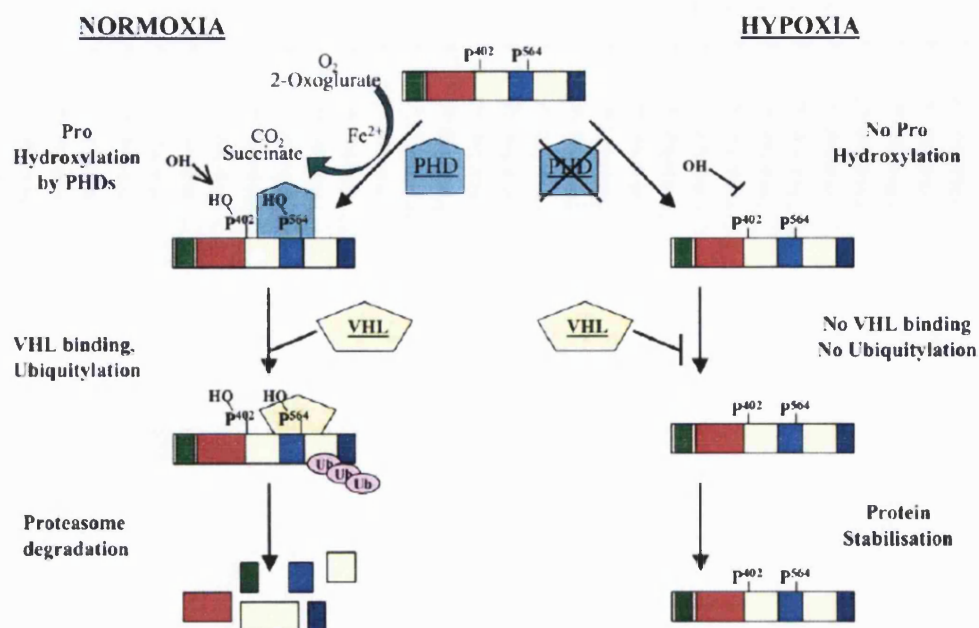


Figure 2.5 | Schematic representation of the oxygen-dependent degradation of HIF-1 α under normoxia and HIF-1 α stabilization under hypoxia - *Reproduced from Card, P. B. et al; 2005.*⁷⁸

After VHL mediated polyubiquitinylation, the second most important mechanism which controls the activity of HIF-1 α is the modulation of transactivation domains N-TAD and C-TAD. In this instance as well, transactivation domains (TADs) are inhibited under normoxia but active under hypoxia. The TADs are essential for binding general co-activators i.e. CBP/p300, SRC-1 and TIF2. The co-activators enable the linkage of HIF protein to the transcriptosome and act as acetyltransferases to achieve chromatin remodeling needed for the transcription. HIF-1 α binding to the CBP/p300 occurs through interaction of C-TAD of HIF with a cysteine/histidine-rich domain (CH1) of p300. This binding is inhibited by p35srj (or cited2), a factor that competes with HIF-1 α for the CH1 binding domain of CBP/p300. Moreover, it was demonstrated that HIF-1 α activates p35srj binding acting as a negative feedback mechanism.

Similar to the previous degradation mechanism, the C-TAD of HIF-1 α is hydroxylated depending on oxygen variations in the cell (*Figure 2.6*). The hydroxylases in this mechanism work only under normoxia and depend on iron and 2-oxoglutarate to function. The hydroxylation affects an asparagine residue (N803 in HIF-1 α and N851 in HIF-1 β) which prevents the association of HIF-1 α and HIF-1 β to the cofactor in normoxia. Thus, hypoxic activation of both HIF-1 α and HIF-2 α involves increased protein stability as well as transcriptional activity, both requiring oxygen-dependent

hydroxylation. The factor inhibiting HIF-1 α (FIH1) is a protein that binds to HIF-1 α and down-regulates its activity. FIH1 also depends on oxygen, iron and 2-oxoglutarate to hydroxylate the asparagine residue responsible for the C-TAD activity on the HIF.

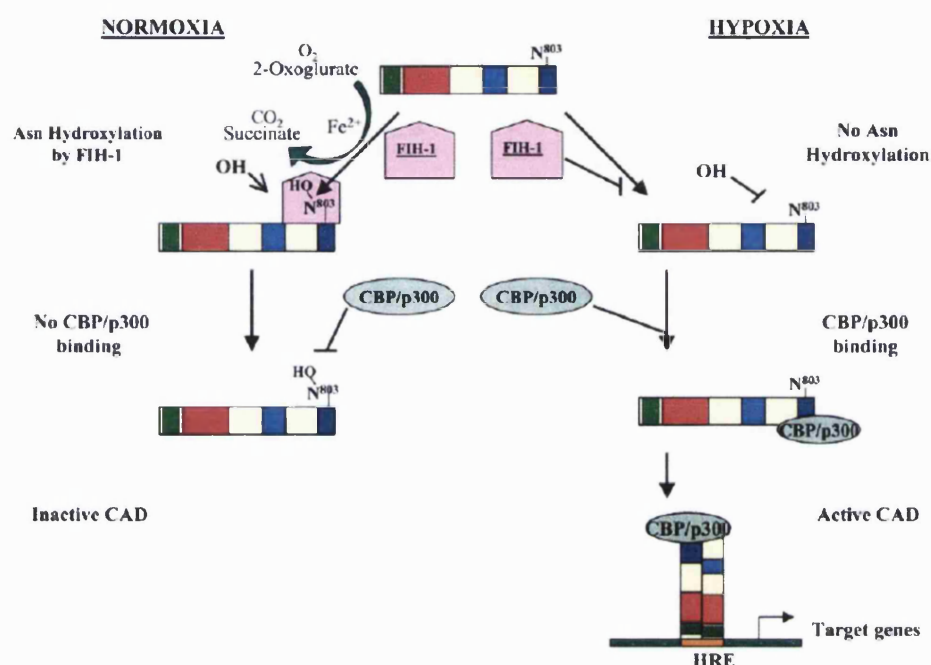


Figure 2.6 | Schematic representation of oxygen regulation of transcriptional activation of HIF-1 α - *Reproduced from Card, P. B. et al; 2005.*⁷⁸

2.2.7 Alternate mechanisms of HIF regulation

HIF-1 α and HIF-2 α are not always degraded under normoxic conditions. Many growth factors and cytokines such as insulin, insulin-like growth factor, transforming-growth factor, platelet-derived growth factor and interleukin-1 β have been shown to stabilize HIF-1 *via* common kinase pathways under normal oxygen levels.⁸⁵ Nitric oxide (NO) has also been shown to act as an activator of HIF-1 α under normoxia although it can also be an inhibitor depending on cell tissues.⁸⁴ Growth factors induce HIF-1 α protein translation and they do so through binding to tyrosine kinase, which then induces phosphatidylinositol-3-kinase (PI3K) and mitogen-activated protein kinase (MAPK) pathways. So, MAPK pathway is responsible for enhancing both HIF protein synthesis and its transcriptional activity.

2.2.8 HIF Target genes

HIF-1 α /ARNT and HIF-2 α /ARNT dimers bind to HRE with the core consensus (A/G)CGTG in the regulatory regions of target genes⁸⁴ to activate their expression. More than 60 recognized HIF-1 α target genes have been identified.⁸⁶ HIF-1 α and -2 α target genes with most relevance to cancer encode for angiogenesis, cell proliferation and survival receptors, glucose transporters and glycolytic enzymes.

- Angiogenesis

Tumours normally have low vasculature or unevenly distributed blood vessels which leaves hypoxic areas where oxygen diffusion cannot reach (*Figure 2.2*). This pathological state triggers angiogenesis through a HIF oxygen-sensing mechanism, which then induces a number of pro-angiogenic genes. Probably the most important one is vascular endothelial growth factor (VEGF), which interacts with its receptor (VEGFR) in endothelial cells. In this way, it recruits endothelial cells in hypoxic areas and stimulates their growth. This leads to an increase in vascular density and thus the oxygen diffusion rate. Other pro-angiogenic targets include inducible nitric oxide synthase, heme oxygenase-1, endothelin-1 and adrenomedullin-1.⁸⁶

- Cell proliferation/survival

HIF-1 induces a number of growth factors that increase cell proliferation and survival. These include insulin-like growth factor-2 (IGF-2) and transforming growth factor- α (TGF- α), which bind to their associated receptors, (IGF1R) and epidermal growth factor receptor (EGFR) respectively, triggering signal transduction pathways which induce HIF-1 expression and promote cell survival. Other target genes, such as PI3K, act as mediators of protein kinases that increase cell proliferation and suppress apoptosis.

- Glucose metabolism

In order to compensate for the energy deficit, hypoxic cells look for other sources of ATP mainly through anaerobic glycolysis. This metabolic route only provides two ATP for each glucose molecule compared with the respiratory cycle (Krebs), which generates 38 ATP. HIF-1 regulates expression of all enzymes in glycolysis in addition to those that mediate cellular glucose uptake, such as (GLUT1) and (GLUT3). This pathway however generates lactate that reduces the cellular pH and limits this source of ATP.

- Erythropoiesis and iron metabolism

HIF-1 increases the expression of transporters of iron to the red blood cells, namely transferrin. HIF-1 also induces the expression of transferrin receptor, which is

responsible for cellular transferrin uptake. Since transferrin can only bind ferric iron, the oxidation of ferrous to ferric iron is mediated by ceruloplasmin or ferroxiadase, another target gene of HIF-1. All these mediators are responsible for haem production.

2.2.9 The balance between adaptation and cell death

Under severe hypoxic conditions, the cell might fail to adapt through the mechanisms discussed above. In these instances, the cell activates a number of apoptotic pathways to eliminate irrecoverably stressed cells.⁷⁴ In this manner, it will increase the chance of survival for neighboring cells by increasing their access to oxygen supply and nutrients. This involves HIF-1 triggered expression of a number of pro-apoptotic proteins such as BCL2 interacting protein 3 (BNIP3) and NIX. HIF activation also helps to stabilize p53 triggering cell-cycle arrest. The factors that determine whether the cell will adapt to hypoxia or commit suicide remain unclear. These are believed to involve a combination of factors including oxygen and key metabolite levels in the cell, the cell metabolic state and the endogenous activity of hydroxylases e.g. PHDs and FIHs. In normoxia, these two enzymes are fully functional and present at their maintenance levels. During mild hypoxic conditions, HIF-1 α is stabilized, probably because PHD is inhibited, but FIH is still capable of hydroxylating the critical asparagine (*Figure 2.7*). It has been hypothesized that HIF-1 α still activates p-300-independent transcription, more probably through genes that prompt the adaptive response. Under severe hypoxic states, PHD and FIH are both inhibited leading to HIF-1 α mediated regulation of all of its target genes, including pro-apoptotic ones.

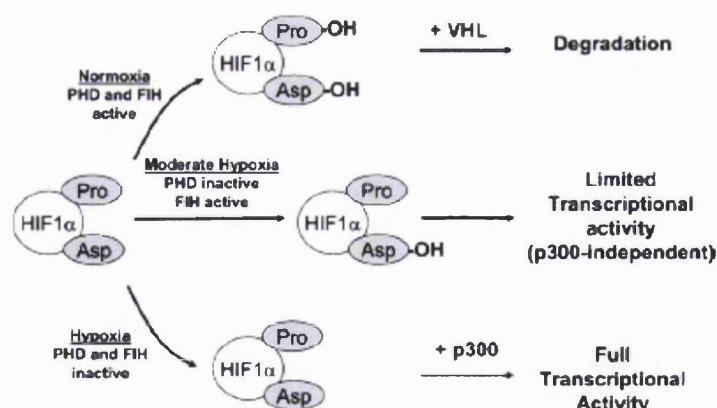


Figure 2.7 | Schematic diagram showing HIF-1 α stability and transcriptional activity under normoxia, moderate hypoxia and severe hypoxia - reproduced from Lee, K *et al*, 2007.⁷⁴

2.3 Modulating HIF-1 signalling pathway for drug discovery.

2.3.1 Promoting HIF-1 pathway for ischaemic diseases.

Activation of the HIF signalling pathway has been shown to be pharmacologically useful in a number of conditions involving a localised hypoxia such as ischemia, heart attack, stroke, wound healing and inflammation.⁸⁷ Furthermore, upregulation of the HIF system could be clinically significant where the use of pharmaceutical agents is preferred to surgery, as in the treatment of critical limb ischemia.

HIF-1 α and HIF-2 α upregulate the expression of several angiogenic factors, such as VEGF, which induces the formation of new blood vessels in the target tissue of the heart and the brain. This leads to an increase in the blood flow, oxygen supply and therefore a reduced ischemic state.⁸⁸ Experiments conducted on mice epidermis showed that HIF-1 α induction promotes hypervascularity without inducing oedema, inflammation or vascular leakage. Induction of angiogenesis through increased HIF-1 expression is particularly attractive as it could permit not just the expression of a single angiogenic factor but of a range of pro-angiogenic factors and their receptors accordingly.⁸⁹ However, pre-clinical studies showed that VEGF-mediated increase of angiogenesis can lead to the formation and evolution of atherosclerotic plaques which cause ischemia and the associated local tissue hypoxia and thereby HIF activation (*Figure 2.8*)⁹⁰. However, the question is still posed as to whether VEGF can balance between angiogenesis and atherosclerosis and the extent of HIF involvement in this process.

Inducers of HIF signalling can act through increasing the stabilization of HIF *via* reducing its degradation which then results in an increased vasculature in the target cell. An example of this includes the macrophage-derived peptide PR39 which has led to an increase in the myocardial blood vessels in mice. Other drugs known to achieve HIF pathway induction include the inhibitors of the VHL-mediated degradation and the prolyl and asparaginyl hydroxylase suppressors.⁹⁰

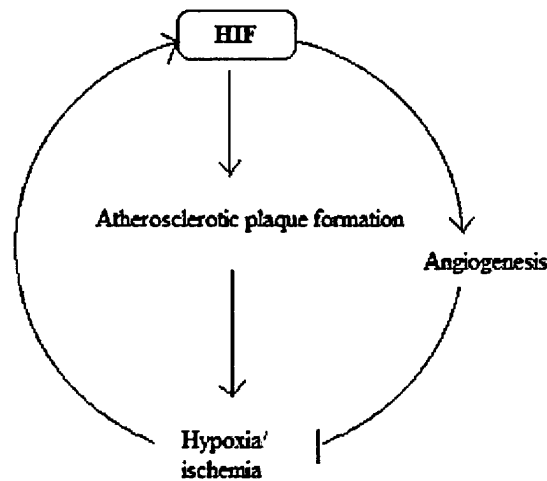


Figure 2.8 | Vicious circle in the ischemic heart showing the effects of HIF activation on promoting / inhibiting ischemia - *adapted from Giaccia, A. et al, 2003.*⁸⁹

2.3.2 Inhibiting HIF-1 pathway for cancer therapy

There has been some early controversy related to the role of HIF-1 α as a therapeutic target. Mostly, this is due to a large number of HIF target genes, the dual action of HIF in inducing cell survival as well as cell death, and the presence of two HIF- α subunits which can have unique roles depending on the type of the tumour.⁹¹ However, tumours might have a much greater need for HIF-1 α , compared with normal cells, and HIF-1 α might be overexpressed due to hypoxia-dependent pathways such as hypoxic stimulus and inhibited proline hydroxylation or hypoxia-independent pathways such as oncogene (Ras, Src) activation, receptor tyrosine kinase stimulus, down-regulation of tumour-repressor genes (VHL, p53), increase in reactive oxygen species (ROS) generation, and glucose deficiency.⁹² Overexpression of both HIF isoforms in tumours is a poor prognostic indication in cancer patients and is associated with poor response to treatment, but it is still questionable whether the HIFs are simply present in tumours as a result of their hypoxic state or if they are active factors in tumour development and invasion. HIF-1 α expression in solid tumours was seen in perinecrotic areas, in stromal inflammatory cells and even in well-oxygenated tumour cells. Experimental animal models using xenografted human tumours reported different results depending on the cell type used, the HIF- α subunit targeted, the site injection in the tumour and the age of the tumour at the time of inhibition.⁹¹ Moreover, studies conducted in cancer patients have been more consistent and confirmed the HIF role in tumour progression.

2.3.3 HIF-1 inhibitors

2.3.3.1 Genetic approaches for HIF-1-targeting anticancer therapy

These approaches target either the expression or the transcriptional activity of HIF-1. One potential therapy that has been shown to suppress the expression of HIF-1 α is through antisense HIF-1 α plasmid, which leads to a reduction in VEGF levels and thereby diminished tumour vasculature.⁹³ Another genetic approach has been to dominant negative isoforms of HIF-1 α mRNA. This would inhibit the translocation and the hetero-dimerization of HIF-1 α with HIF-1 β and thus prevent the binding to the HRE domain.

An additional useful genetic approach involves the use of two HIF-1 α variant inhibitory cDNAs. The first variant is called HIF-1 α Z, in relation to its induction by zinc. This is derived from a differently-sliced mRNA lacking exon 12, which generates a termination codon between exons 11 and 13 producing a shortened HIF-1 α protein that lacks C-terminal ODDD, TAD and NLS motifs. This protein loses the oxygen-dependent regulation and lacks the transactivation activity necessary for its function and, therefore, inhibits the hypoxic-induced activation of functional HIF-1 α via competing with HIF-1 α for dimerization with ARNT. The other HIF-1-inhibitory cDNA is called *HIF-1 α* ⁵¹⁶. This protein variant derives from mRNA lacking exons 11 and 12 resulting in the joining of exons 10 and 13, which produces a termination codon. This 516-amino acid polypeptide conserves its bHLH and PAS domains but, like *HIF-1 α Z*, lacks C-terminal ODDD and all TADs. In a similar manner to HIF-1 α Z, this variable protein inhibits HIF-1 α activity in hypoxia cells and down-regulates the expression of HIF target genes.⁹²

The inhibitory PAS domain protein (IPAS) is translated from an alternatively spliced variant of mouse HIF-3 α mRNA which inhibits HIF-1 heterodimerization. The protein structure of IPAS is similar to the human HIF-1 α variants, *HIF-1 α Z* and *HIF-1 α* ⁵¹⁶ and it also acts by inhibiting HIF-1 α target genes expression resulting in delayed tumour growth and reduced vasculature *in vivo*.

Even though these genetic approaches were all successful in achieving HIF-1 α inhibition in cell cultures, they could not achieve high therapeutic effects in patients, mostly because of problems associated with gene transfer.⁹²

2.3.3.2 Pharmacological approaches

An ever-increasing number of HIF-1 inhibitors are constantly being identified. These were mainly based on empirical approaches or cell-based screens. In this section, a number of known pharmacological inhibitors that have shown successful inhibition of HIF-1 α will be described (Figure 2.9).

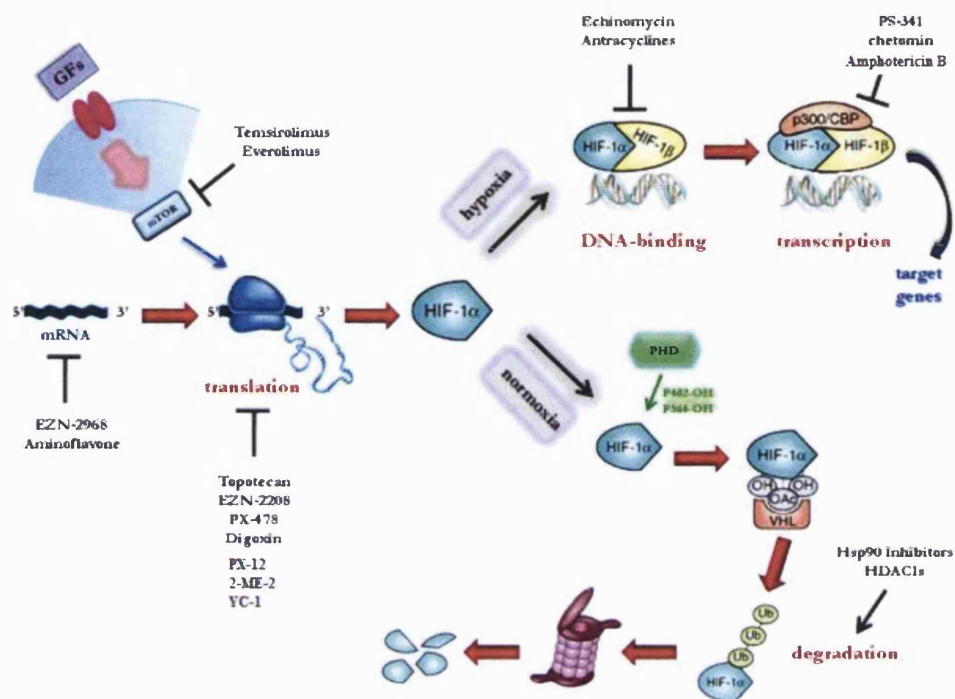


Figure 2.9 | HIF-1 α inhibitors and their proposed mechanism of action - Adapted from Onnis, B.; Rapisarda, A.; Melillo, G., 2009.⁹⁴

- Inhibitors of HIF-1 α m-RNA expression

It has been suggested that, under a hypoxic state, levels of HIF-1 α mRNA expression could control the rate of protein translation, which would eventually affect the rate of HIF-1 accumulation. As a result, HIF-1 α mRNA expression is a viable target for inhibition by small molecules.⁹⁵

EZN-2968 is an oligonucleotide that has been shown to bind to HIF-1 α mRNA and consequently inhibit it causing a significant reduction in HIF-1 α protein levels.⁹⁶ In tumour cell-based assays, this molecule inhibits tumour cell growth and exhibits the same effect when injected to mice with xenograft models of human prostate cancer. This oligonucleotide is undergoing phase I clinical trials in patients with advanced solid tumours. Furthermore, preliminary studies have shown that EZN-2968 can be beneficial in patients with metastatic renal cell carcinoma.

Similarly, HIF-1 α mRNA expression is affected by aminoflavone (GL-331, *Figure 2.10*) which is a ligand of the arylhydrocarbon receptor (AhR) and is currently in phase I clinical trials in metastatic cancer patients.⁹⁴ Melillo's group is currently exploring AF's role in downgrading HIF-1 α levels. The studies, which have just been submitted for publication by this group,⁹⁴ have shown that AF inhibits HIF-1 α accumulation by modulation of HIF-1 α mRNA expression. The exact mechanism is yet to be fully elucidated.

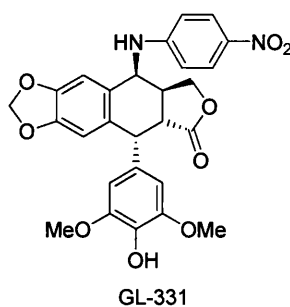


Figure 2.10 | GL-331, an aminoflavone inhibitor of HIF-1 α mRNA expression.

- Inhibitors of HIF-1 α protein translation

Inhibiting HIF-1 α protein translation is still not fully elucidated. However, there is a significant number of agents that affect this process, such as topoisomerase I and II inhibitors, receptor tyrosine kinase, cyclin-dependent kinase, oncogenic pathways, thioredoxin reductase, and p53 activators, as well as microtubule disruptors.

One of the earliest agents shown to inhibit HIF-1 α protein translation is topotecan. It is a small molecule inhibitor of HIF-1 α acting as a topoisomerase I inhibitor that induces DNA damage and cytotoxicity. This molecule was shown to be a potent inhibitor of HIF-1 α activity in a different mechanism to its cytotoxicity. Topotecan is also an FDA approved chemotherapeutic agent, clinically used to treat small cell lung cancer and ovarian cancer, and is in clinical trials for its role in HIF-1 inhibition.⁹⁷

Thioredoxin inhibitors were also shown to disrupt HIF-1 α protein accumulation. Thioredoxin-1 (Trx-1) is a redox protein, generally over-expressed in human cancers, and is associated with high levels of HIF-1 α proteins. However, while certain inhibitors of Trx-1 (e.g. PX-12, *Figure 2.11*) can reduce HIF-1 α protein levels, others (e.g. AJM 290) were proved to increase HIF-1 α in cancer cells.⁹⁸

Another method to inhibit HIF-1 α protein translation and its concurrent nuclear translocation is through microtubule disruption, which inhibits polymerization and stops

the mitosis. This can be achieved through the use of a natural oestrogen metabolite, 2-methoxyestradiol (2ME2, *Figure 2.11*), which suppresses the angiogenic effect of HIF-1 α . 2ME2 (Panzem™) is currently in phase I/II clinical trials.⁹⁹

Another example is YC-1 (*Figure 2.11*), an agent that also prevents the accumulation of HIF-1 α proteins, thereby down-regulating the expression of HIF-1 target genes, which reduces the angiogenesis and suppresses the tumour. Even though YC-1 was originally suggested as an activator of soluble guanylate cyclase (sGC), thus increasing the intracellular GMP levels, the relevance of this mechanism to HIF-1 α destabilization is still unknown.⁹⁹

PX-478 (*Figure 2.11*), currently in phase I clinical trials in patients with advanced metastatic cancer, is another recent molecule that was shown to destabilize HIF-1 α protein, inhibit its expression and reduce the plasma VEGF levels in a pVHL and p53 independent fashion. More recently, it was shown that PX-478 could exhibit its inhibition affecting the HIF-1 α levels at various stages.¹⁰⁰

Other inhibitors, including non-steroidal anti-inflammatory (NSAIDs) drugs, both selective (COX-2 inhibitors) and non-selective (e.g. ibuprofen, *Figure 2.11*), have been shown to inhibit angiogenesis in a number of tumours. In addition, flavopiridol (*Figure 2.11*)— a cyclin-dependent kinase inhibitor – inhibited VEGF mRNA expression in glioma cells.¹⁰¹

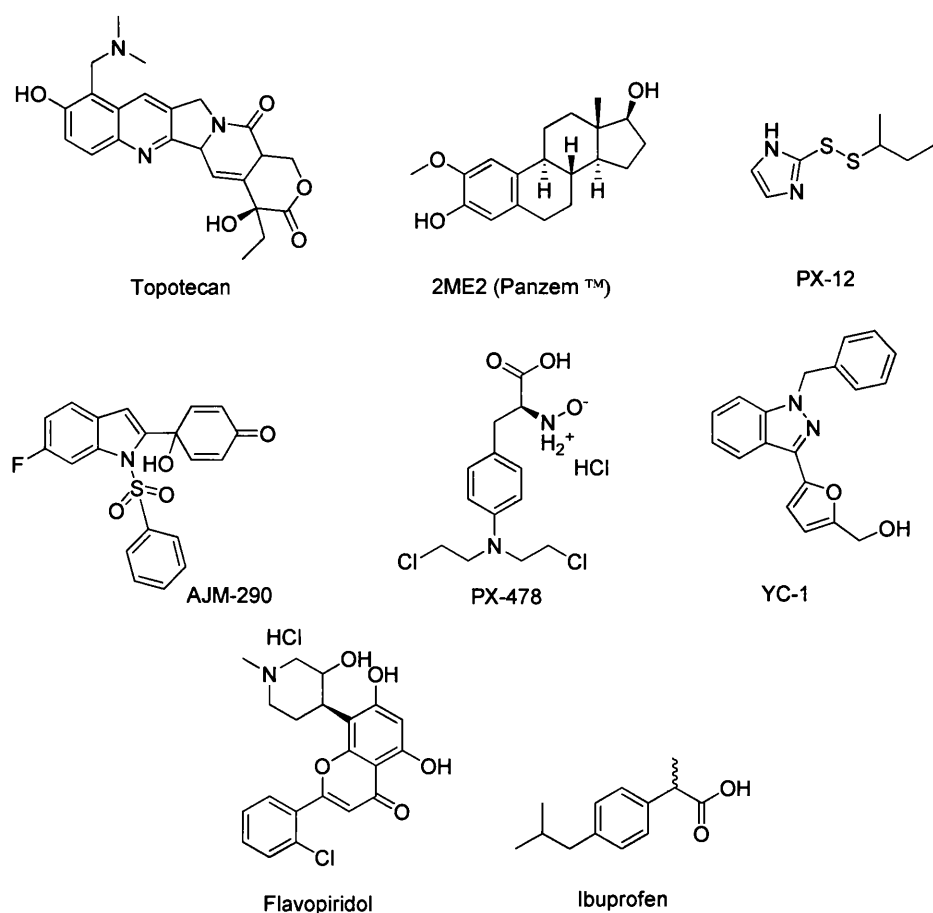


Figure 2.11 | Inhibitors of HIF-1 α protein translation.

- Inhibitors that affect HIF-1 α degradation pathway

Hsp90 is a molecular chaperone responsible for the proper folding of a number of protein kinases and transcription factors, including HIF-1 α . Molecules such as Geldanamycin (GA) and KF58333, which inhibit this chaperone *via* competing with its ATP binding site, also destabilize HIF-1 α through inducing its degradation in a VHL-independent manner. Analogues of GA (*Figure 2.12*), 17-AAG and 17-DMAG are in phase II clinical trials targeting a number of tumours.¹⁰²⁻¹⁰³

Another class of molecules inhibits the accumulation of HIF-1 α protein through the inhibition of histone deacetylase (HDAC). These inhibitors, also referred to as HDACI (*Figure 2.12*), were recently shown to induce HIF-1 α degradation *via* a VHL- and ubiquitin-independent, proteasome-dependent pathway.¹⁰⁴ HDACI are currently in phase I/II clinical trial testing on solid tumours and lymphomas.

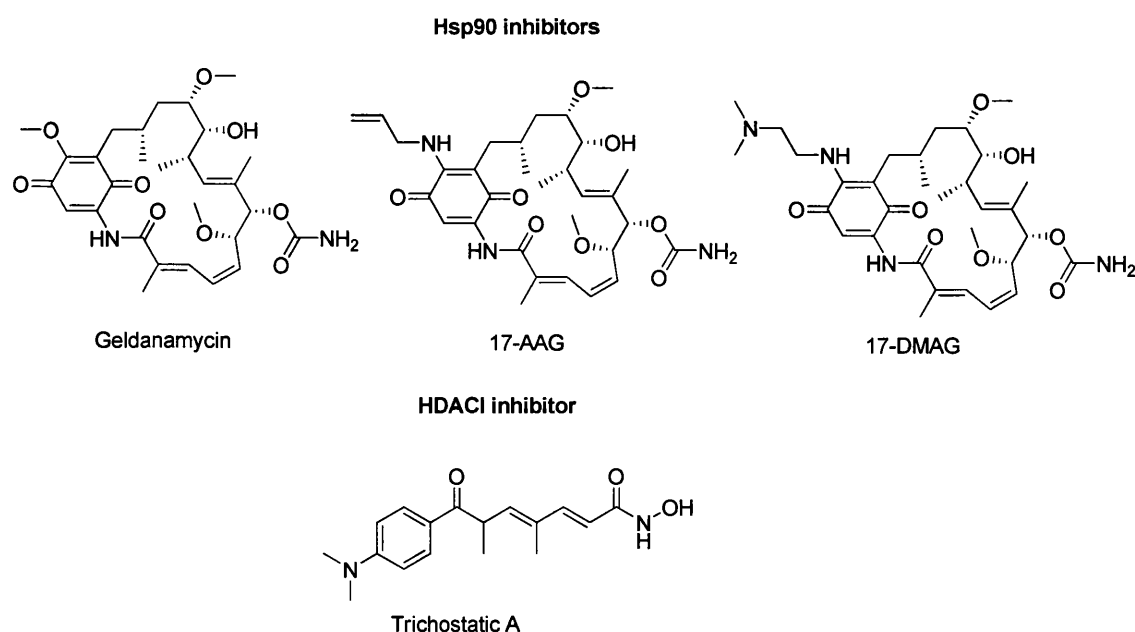


Figure 2.12 | Inhibitors that affect HIF-1 α degradation pathway (In blue are shown the structural differences between geldanamycin and its analogues).

- Inhibitors of HIF-1 α binding to DNA

Another family consists of inhibitors that block the binding of HIF-1 with its HRE domain on the DNA. The inhibition is specific to the bHLH region of the HIF-1 α :HIF-1 β dimer responsible for binding to the HRE. Polyamides, which consist of *N*-methylpyrrole and *N*-methylimidazole amino acids have been used to alter gene expression specifically. For example, polyamide-type molecules that could inhibit VEGF expression through binding to the HRE on its promoter region have been able to stop the HIF-induced expression of its mRNA.

Another inhibitor of the heterodimeric binding to HRE is a cyclic quinoxaline peptide, known as echinomycin (*Figure 2.13*). This molecule has shown potent inhibition of the HIF-1 binding to the VEGF HRE, thereby reducing VEGF mRNA expression in human cancer. The clinical testing of echinomycin for its anticancer properties has given negative results and was abandoned.¹⁰²

More recently, anthracyclines were shown to inhibit HIF-1 activity.¹⁰⁵ Molecules such as doxorubicin (*Figure 2.13*), and daunorubicin have been shown to block HIF-1 α binding to DNA.

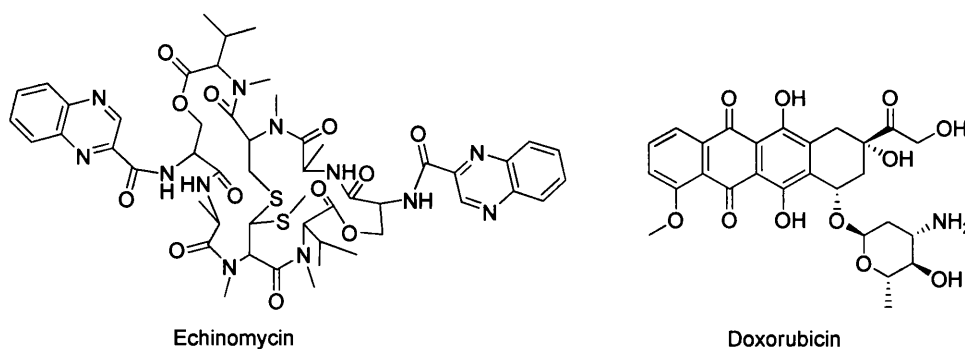


Figure 2.13 | Inhibitors of HIF-1 α binding to DNA.

- Inhibitors of HIF-1 α transcriptional activity

HIF-1 α inhibitors could work by blocking the transcriptional function of HIF-1. Therefore, they suppress the hypoxic induction of gene expression concurrently leading to tumour growth inhibition when tested in animal models. Chetomin (*Figure 2.14*), a dithiodiketopiperazine, was shown to bind to and alter the tertiary structure of the CH1 domain of p300. As a result, p300 is prevented from binding to HIF-1 α which leads to a reduction in HIF-1 transcriptional activity. This molecule was active in xenograft models of solid tumours.¹⁰⁶

Amphotericin B (*Figure 2.14*) is an antifungal agent which has recently been associated with inhibiting HIF-1 transcriptional activity without affecting its protein levels (e.g. by inducing FIH-1-mediated hydroxylation of Asn 803 thereby preventing p300 binding to the HIF-1 α subunit).¹⁰⁷

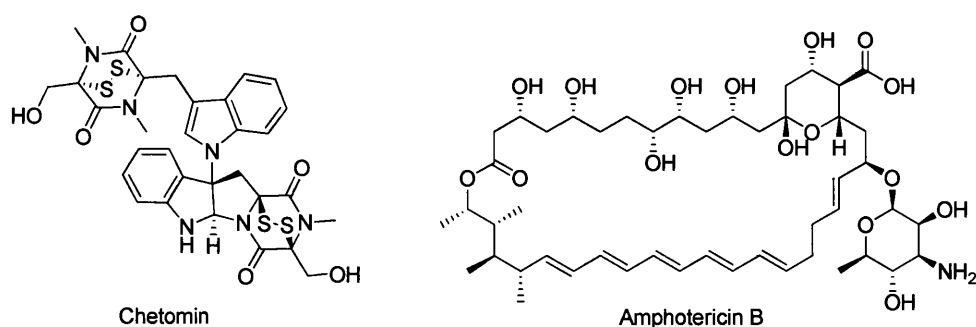


Figure 2.14 | Inhibitors of HIF-1 α transcriptional activity.

- Inhibitors of HIF-1 α heterodimerization process

The formation of the active HIF-1 heterodimer is achieved through the PPI between the PAS-A and PAS-B domains of the HIF-1 α and β subunits (*Figure 2.15*). The evidence that supports the critical role of the PAS domains for heterodimerization was brought up

based on the molecular structure of HIF-2 α ¹⁰⁸ as well as HIF-1 β -PAS-B domain.⁷⁸ Disrupting HIF-2 α -PAS domains also suppressed HIF function.

Prof. Melillo and co-workers recently demonstrated that over-expression of the HIF-1 α PAS-A domain in cells is sufficient to block hypoxic induction of HIF-1-dependent luciferase expression, and that inhibition of HIF-1 α -PAS-A domain was able to suppress HIF-1 transactivation.⁸⁸ This led to identification of the PAS-A domains of HIF-1 α and β as viable drug targets. Protein domains that mediate dimerisation of transcription factors are challenging targets for small-molecule inhibitors, especially when detailed structural information regarding regions of protein contact (*i.e.* “hot spots”) is unavailable. However, the Melillo group has developed an ELISA assay as a screening tool to identify inhibitors of the HIF-1 heterodimerisation process. Two chemical libraries were screened using the PAS-A based ELISA: the NCI diversity set, which includes 1992 compounds that represent chemical diversity, and the HIF-1 library. The latter was obtained from the HRE-luciferase screening of 140,000 compounds. The two screens first came up with 4 hits, which did not, however, pass validation assays. The NCI diversity set identified NSC50325 (rolitetracycline) (*Figure 2.16*) as a selective, dose-dependent inhibitor of the HIF-1 α :HIF-1 β PAS-A-mediated interaction with an IC₅₀ = 1.4 μ M. Unfortunately, due to cell-permeability issues, rolitetracycline was inactive in cell-based assays, both in intact cells and in nuclear proteins from hypoxic cells. Because of this, rolitetracycline per se cannot inhibit protein-protein interactions in cells.

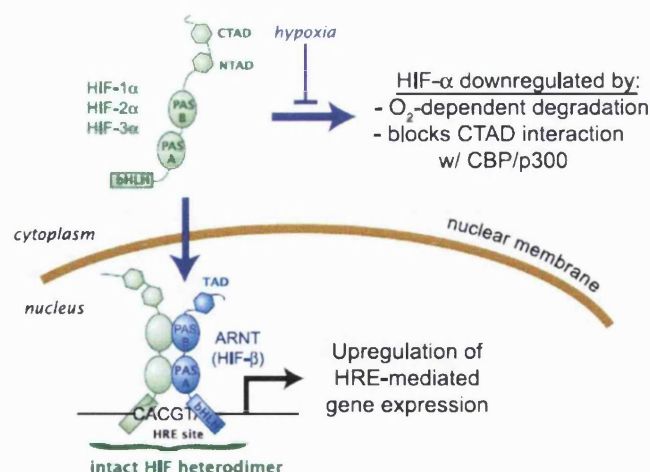


Figure 2.15 | Schematic representation of the structure of HIF protein, which shows the heterodimerisation process between HIF-1 α and HIF-1 β under hypoxia – reproduced from Erbel, P.J.A., et al, 2003.¹⁰⁸

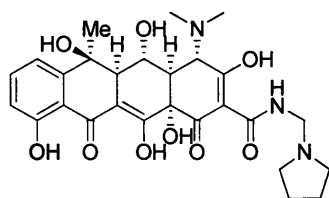


Figure 2.16 | NSC50325: rolitetraacycline. The red colour shows the core of the molecule giving it a rigid 3D geometry.

- Inhibitors which suppress oncogenic signalling pathways involved in HIF-1 α activation

The first examples are the inhibitors of mammalian targets of the rapamycin (mTOR) pathway. This pathway has been involved in growth factor-dependent upregulation of HIF-1 α translation in normoxia. In neoplastic mouse models, mTOR inhibition triggers apoptosis of the neoplastic epithelial cancer cell and reversal of the neoplasia. There are a number of mTOR inhibitors in clinical trials, including temsirolimus (*Figure 2.17*), a successful inhibitor in many cancer cell lines, as well as everolimus.¹⁰⁹ Both molecules are implicated in the inhibition of HIF-1 α and its downstream targets.

Other inhibitors that target HIF-1 α activation are the suppressors of the epidermal growth factor receptor (EGFR). This receptor pathway is responsible for inducing HIF-1 α translation. Indeed, it was shown that inhibitors of EGFR expression, such as gefitinib (*Figure 2.17*) and erlotinib, also down regulate HIF-1 α expression and have been clinically approved for treatment of lung cancer.¹¹⁰

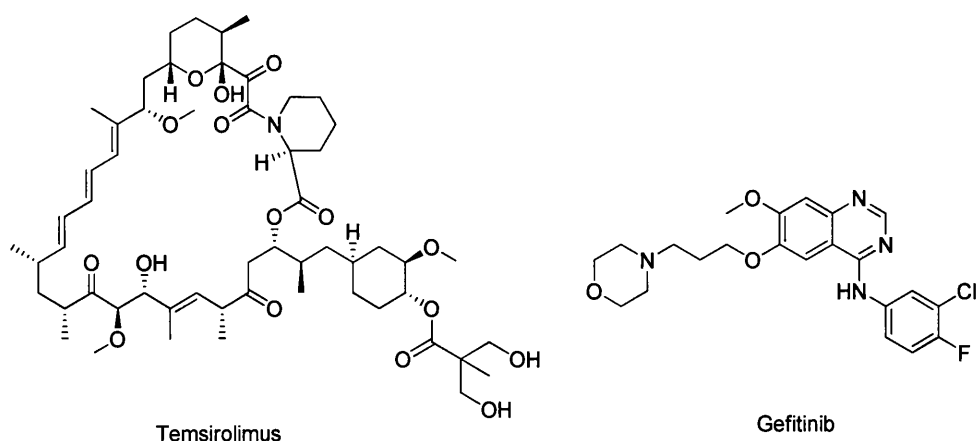


Figure 2.17 | Indirect inhibitors of HIF-1 α .

2.4 Conclusion

Hypoxia is a major hindrance to effective solid tumour therapy. The hypoxic portion of tumours is resistant to traditional therapies such as radiotherapy and chemotherapy.

HIF, a heterodimer comprising one of two HIF- α subunits (HIF-1 α or HIF-2 α) and HIF-1 β , is the master regulator of the hypoxia response by tumours. It regulates a large number of genes required for the adaptation to hypoxia. HIF-1 α has been highly ranked on the list of targets for cancer therapy because of its key role in regulating tumour survival and growth under hypoxic stress. Increased understanding of the molecular processes underlying HIF signalling pathway has enriched the development of strategies to target these for anticancer therapy.

The discovery of new approaches for targeting previous poorly characterized pathways triggered by hypoxia in the tumour microenvironment is hindered by the lack of specific and effective small molecules for HIF-1 inhibition. Nonetheless, validation of available small molecules in preclinical models or in early clinical trials could provide a key opportunity to inhibit hypoxia-induced pathways of clinical significance. Efforts to identify novel small molecule inhibitors should be considered along with well-designed, pharmacodynamic-based early clinical trials of promising HIF-1 inhibitors in order to validate their activity and discover agents that can be used in combination strategies.

CHAPTER 3

Diels-Alder reaction

Contents

3.1	The Diels Alder reaction	47
3.1.1	Background	47
3.1.2	Dienes and dienophiles	47
3.1.3	Pericyclic, ionic and radical Diels-Alder reactions	48
3.1.4	Regiochemistry	49
3.1.5	Stereoselectivity	52
3.1.6	Multiple Diels-Alder reaction	53
3.1.7	Lewis-acid catalysed Diels-Alder reactions	56
3.1.8	Applications of DA to the total synthesis of natural products	60
3.2	The cross-conjugated trienes	64
3.2.1	3-Methylene-1,4-pentadiene	64
3.2.2	Substituted cross-conjugated trienes	67
3.2.3	Conclusion	69

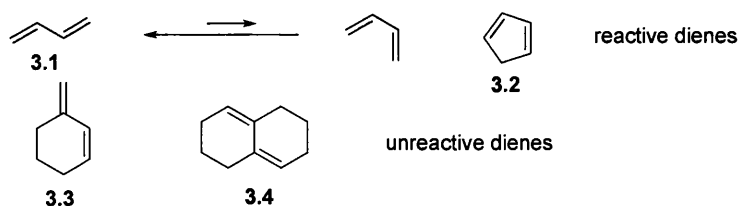
3.1 The Diels Alder reaction

3.1.1 Background

The $[4\pi + 2\pi]$ cyclization of a diene and an alkene (dienophile) to form a cyclohexene is known as Diels-Alder (DA) cycloaddition. This type of cycloaddition was discovered in the early 20th century. In 1928, Otto Diels and Kurt Alder, established the correct structure of the product from the reaction between *p*-quinone and cyclopentadiene.¹¹¹⁻¹¹² The DA cycloaddition is considered one of the most powerful and widely used pericyclic reactions in organic synthesis, and has been recognised as a major breakthrough that has enabled and shaped the total synthesis of a wide number of natural products.¹¹¹ A number of key features contribute to the synthetic value of this reaction. First, the DA reaction can generate multiple rings and up to four stereocentres in a single step. It is also highly diastereospecific and can be enantioselective with the use of a chiral Lewis acid as a catalyst. The DA reaction can also be regioselective when unsymmetrical dienes and dienophiles are used. Furthermore, the *cis* (*Z*) or *trans* (*E*) conformation of the dienophiles is preserved in the product.

3.1.2 Dienes and dienophiles

The DA cycloaddition requires that conjugated dienes assume a *cisoid* geometry in order to react. The *transoid* dienes would provide sterically unfavoured 6-membered ring transition states presenting a *trans* double bond. This is why cyclic dienes react more readily than open-chain ones (*Scheme 3.1*)



Scheme 3.1 | Reactive and unreactive dienes

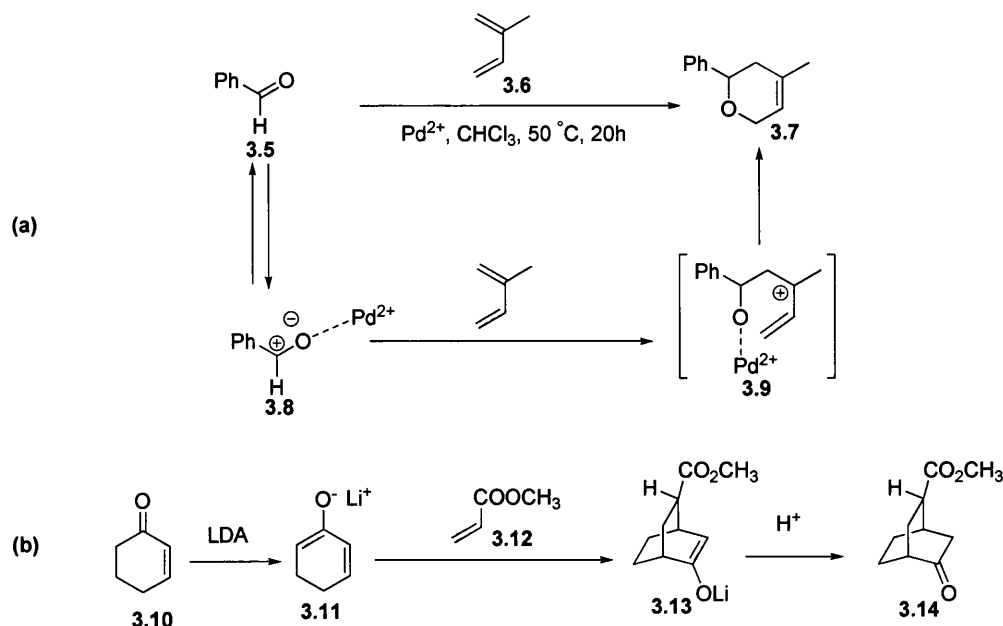
The reactivity of the dienes is also affected by their substituents. A diene substituted with electron-donating groups reacts faster with a dienophile bearing electron withdrawing groups. This is known as a ‘normal electron-demand Diels-Alder’.¹¹³ An ‘inverse electron-demand Diels-Alder’ is when the diene and the dienophile bear electron-withdrawing and electron-donating substituents, respectively.¹¹⁴

Dienophiles can either possess a double or a triple bond as reactive functionality, and be cyclic or non-cyclic. Very often, dienophiles are conjugated with a carbonyl group that enhances their reactivity. Examples include maleic anhydrides, maleimides, benzoquinones, naphthoquinones, and acroelins.

3.1.3 Pericyclic, ionic and radical Diels-Alder reactions

Thermal DA reactions and those involving apolar dienes and dienophiles, occur in a concerted fashion. They are hence described as pericyclic cycloadditions and involve concerted synchronous six-membered transition states.¹¹⁵ For instance, reactions between 1,3-butadiene and ethene have been heavily investigated and shown to occur in a concerted synchronous way.¹¹⁶

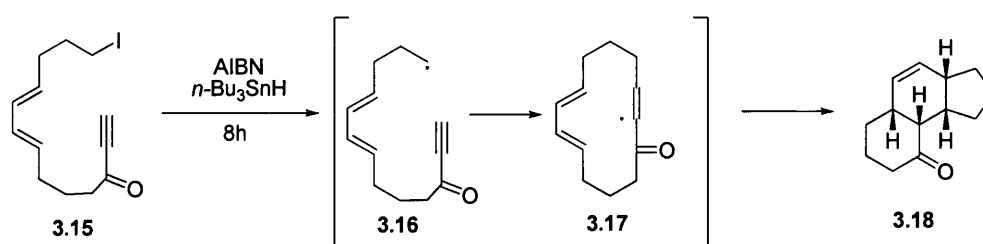
However, DA cycloadditions are not always pericyclic. When conjugated anions, cations and radicals are involved, the formation of the two σ bonds proceeds stepwise and not in a concerted fashion. Cationic dienophiles, such as allyl cations, could be considered as 2π -electron components in a normal electron-demand DA reaction. It was reported that the cationic palladium(II) complex $[\text{Pd}(\text{dppp})(\text{PhCN}_2)](\text{BF}_4)_2$ coordinates the carbonyl oxygen of the benzaldehyde enabling the carbon of the carbonyl to attack the isoprene, forming an allyl cation. This latter undergoes a cationic stepwise DA reaction giving the 4-methyl-6-phenyl-5,6-dihydro-2H-pyran - *Scheme 3.2 (a)*.¹¹⁷



Scheme 3.2 | Examples of a (a) cationic Diels Alder and (b) anionic Diels Alder reactions.

Anionic Diels-Alder reactions are less studied compared with their previous counterpart. These are sometimes regarded as double Michael additions, although a stepwise Diels-Alder mechanism is usually preferred. Examples include the cycloaddition of enolates of α,β -unsaturated ketones with olefins - *Scheme 3.2 (b)*.¹¹⁸

Radical Diels-Alder reactions are generally a powerful tool to form polycyclic molecules in one step. One example to note is the formation of a tricyclic enone¹¹⁹ (*Scheme 3.3*). The reaction proceeds after treatment of iodoenynone with *n*-tributyltin hydride/2,2'-azobisisobutyronitrile (AIBN) forming a vinyl radical intermediate that cyclises fairly rapidly.

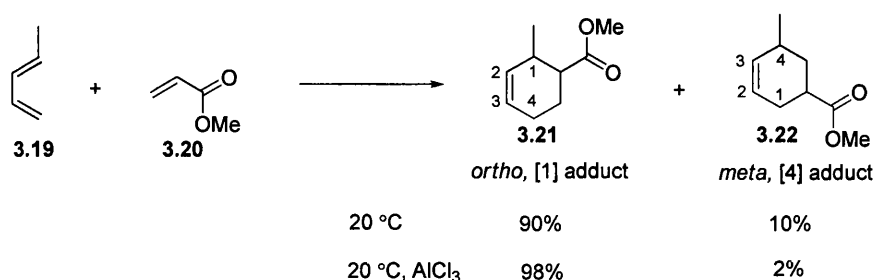


Scheme 3.3 | Example of a radical Diels-Alder reaction

3.1.4 Regiochemistry

The synthetic value of the DA reaction is owed greatly to its high regio- and stereo-selectivity. When an unsymmetrical diene is reacted with an unsymmetrical dienophile, two products would normally be expected. However, it is more often the case to see one predominant regioisomeric adduct.¹²⁰

The numbering of the various regioisomer adducts follows a nomenclature proposed by Fruiguelli and Wenkert.¹²⁰ The numbering starts from the original diene atoms, the lowest number being the atom closest to the electron withdrawing substituent in the product. The regioisomer adducts are named as *ortho*, *meta* and *para* followed by the number set in brackets then the word *adduct* – *Scheme 3.4*.

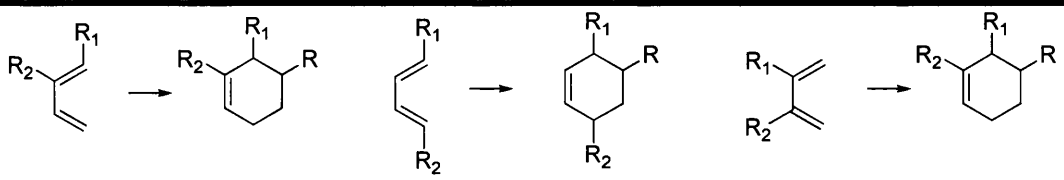


Scheme 3.4 | Nomenclature rules for different regioisomers.

The DA reaction is a cycloaddition with an aromatic transition state that is mainly *ortho* and *para* directing. However, the regioselectivity of this reaction depends on the number, nature and position of substituents on the dienes and dienophiles. In addition, the conditions of the reaction (i.e., presence and nature of the catalyst, pressure, temperature and solvent) can also affect the regiochemistry.

The *ortho* and *para* adducts are obtained when considering the reactions of 1- and 2-monosubstituted butadienes, respectively, with a monosubstituted dienophile. In the case of a disubstituted butadiene, one group on the diene will act as a regiodirector, as shown in *Table 3.1*.¹²¹ Exceptions to this rule have been observed which makes the prediction of the regioselectivity more difficult.

Table 3.1 | Diene substituent effect on regiochemical outcome in Diels-Alder reaction when reacted with monosubstituted ethene ($RCH=CH_2$).¹²²

					
R_1	R_2	R_1	R_2	R_1	R_2
Me	Ph	Me	SiEt ₃	Ph	Me
Me	OEt	Ph	Me	SPh	Me
Me	OAc	NHCO ₂ Et	Me	SPh	OMe
Me	Cl	NHCO ₂ Bu	SPh	SPh	OAc
Bn	NHCOCH ₃	OAc	Et	Cl	Me
SPh	OMe	SPh	OAc		

The *ortho* and *para* rule can be better explained by the frontier molecular orbital theory (FMO) by considering the atomic orbital coefficients to form the σ bond.¹²³

The DA reaction is controlled by the suprafacial *in phase* interaction of the highest occupied molecular orbital (HOMO) of either the diene or dienophile and the corresponding lowest unoccupied molecular orbital (LUMO). The highest reactivity is when the energy difference between the HOMO and the LUMO is minimal. This energy difference is affected by substituents present on both components. An electron-donating group (x-) raises the energy of the HOMO and LUMO of both the diene and the

dienophile, whereas an electron-withdrawing substituent (z-) lowers both energies. An extra conjugation (c-) raises the energy of the HOMO, but reduces the energy of the LUMO. By having a (x-) group on the diene and a (z-) group on the dienophile, the HOMO of the diene and the LUMO of the dienophile is reduced, which increases the rate of the reaction. This is known as a normal electron-demand Diels Alder. The opposite case, where the LUMO of the diene reacts with the HOMO of the dienophile, and is known as the inverse-electron demand Diels Alder. These concepts are displayed in *Figure 3.1*.

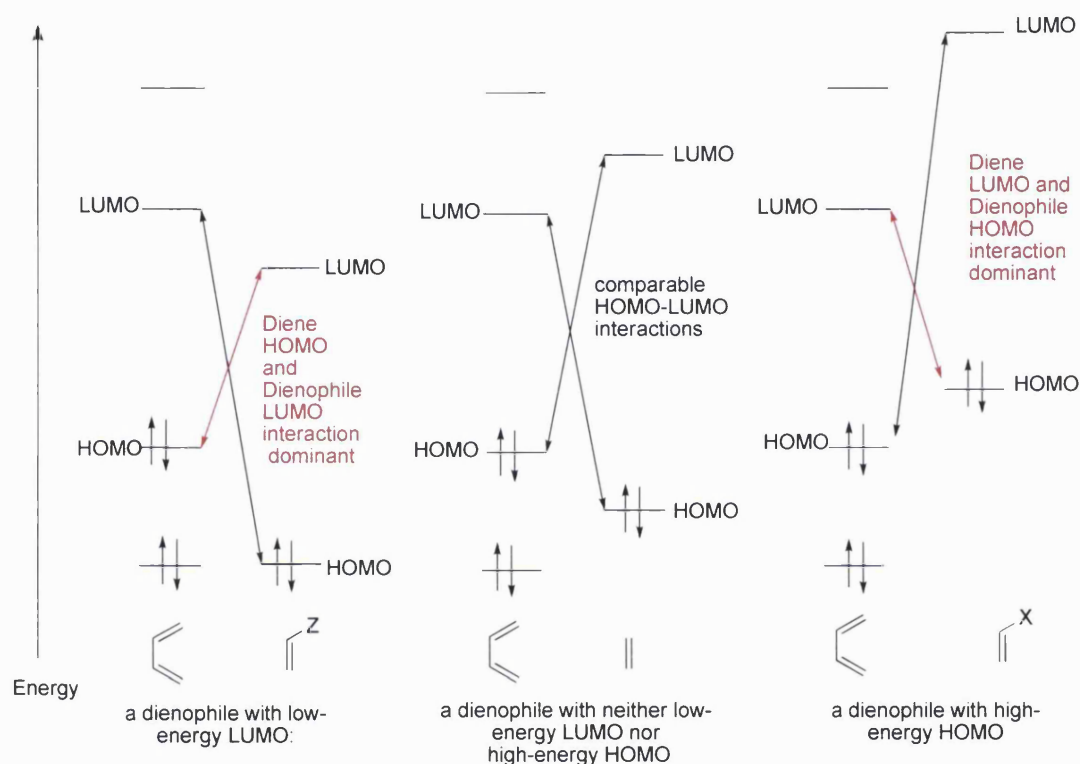
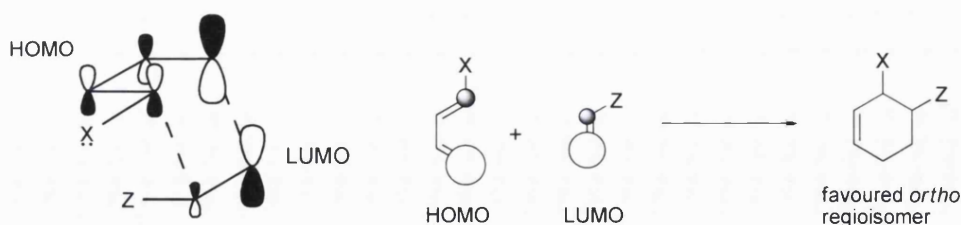


Figure 3.1 | Frontier orbital interactions for the DA reactions.¹²³

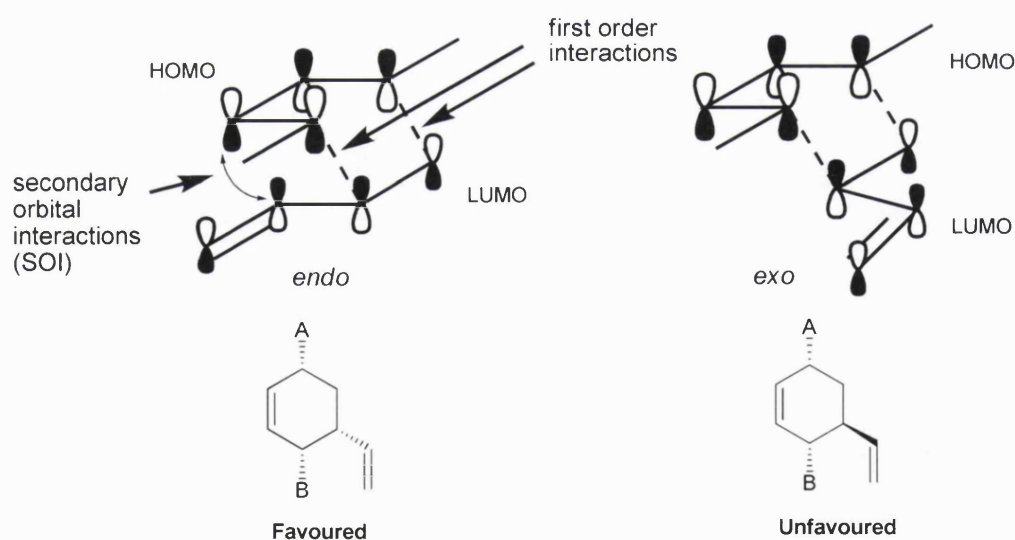
The regiochemistry is determined by the overlap of the orbitals with larger coefficients at each end of dienes and dienophiles. Within the one component, the greater the difference between orbital coefficients at both ends, the more regioselective the cycloaddition is. This concept is demonstrated in *Scheme 3.5*.¹²³ The circles in this figure represent the lobes of the *p* orbital, and the shaded and unshaded ones are of opposite signs. Lobes with large size and hence coefficient interact better leaving the ones with small size interacting together. The more different the coefficient values at each end, the more regioselective the Diels-Alder is.



Scheme 3.5 | Regioselectivity in Diels-Alder explained using FMO theory.

3.1.5 Stereoselectivity

DA reaction is suprafacial, which allows maintaining the relative stereochemistry of the substituents forming the new stereogenic centres in the cycloadduct *via* two suprafacial arrangements named as *endo* and *exo*. This is a very crucial feature that has led to widespread use of the reaction in the synthesis of complex natural products. The favoured arrangement of the DA reaction is the *endo* transition state, which can be explained by secondary orbital interactions (SOI) theory (*Scheme 3.6*), even though other factors such as solvent effects, steric interactions, hydrogen bonds and electrostatic forces can affect this diastereoselectivity¹²⁴.

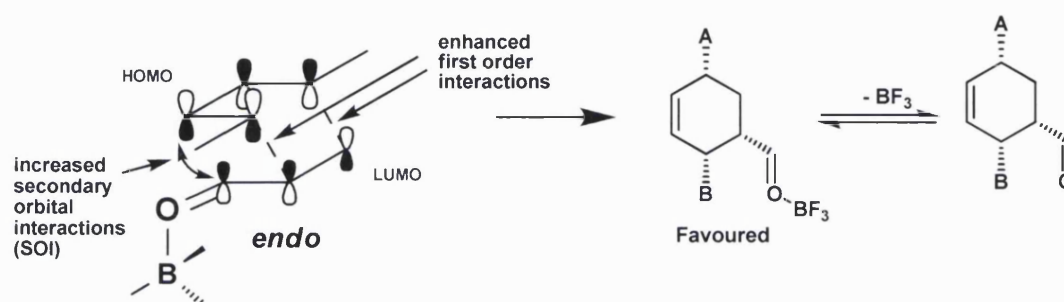


Scheme 3.6 | *Endo* Vs *exo* selectivity in Diels-Alder cycloaddition.

The Alder *endo* rule is displayed by the parallel arrangement of the diene and dienophile and the most stable transition state is ensured through maximum orbital overlap. In other terms, secondary orbital interactions involve the alkene bulky substituent orbitals and the diene HOMO, thereby ensuring a tighter transition state and a kinetically favored *endo* product. As a general rule, the *endo* product of Diels-Alder reaction can be

easily recognized as the one where there is a *cis* relationship between the electron withdrawing group on the dienophile and the substituent that is *trans* in the diene.

In the presence of a Lewis acid (e.g. $\text{BF}_3 \cdot \text{Et}_2\text{O}$ or SnCl_4), the *endo* diastereoselectivity is enhanced (Scheme 3.7) due to the complex formed between Lewis acid and the dienophile that reduces the energy gap between the LUMO of the dienophile and the HOMO of the diene, thus decreasing the activation energy for the cycloaddition to occur.¹¹¹ As a result, the *endo* transition state is enhanced due to the more significant SOI, increased by the presence of Lewis acid.



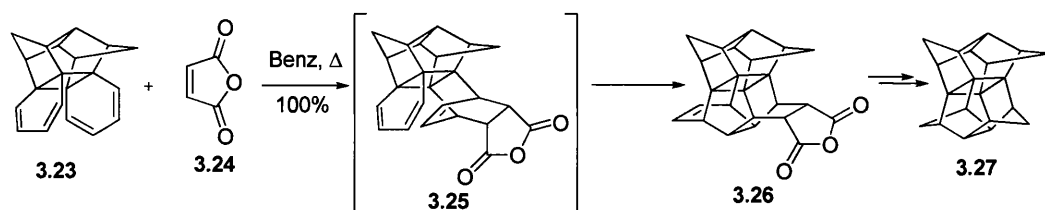
Scheme 3.7 | Enhancement of *endo* diastereoselectivity when using Lewis acid.

3.1.6 Multiple Diels-Alder reaction

It has always been one of the long-standing aims of synthetic chemists to create complex molecules in few steps. To this end, there has been a growing effort to develop and optimise successive chemical reactions occurring in one-pot. Such reactions may reduce the cost by cutting down on energy and materials use, which consequently reduces the chemical waste. In pericyclic chemistry, and more specifically the DA reaction, a number of one-pot multistep processes have been developed involving: domino, cascade, tandem, timed, consecutive, transmissive events, etc.¹²²

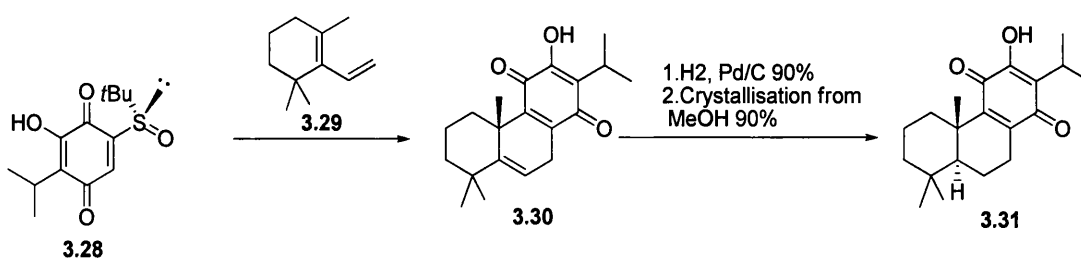
Domino processes are time-resolved transformations, named after the domino stones where one stone tips over the next, in a way that they all fall in turn.¹²⁵ Pericyclic domino reactions involve one pot, multistep pericyclic transformations, such as cycloadditions, sigmatropic rearrangements, electrocyclic reactions and ene reactions with each other, and also with non-pericyclic transformations. These reactions are very often carried out under the same reaction conditions without adding another reagent or catalyst such that the next reaction is the consequence of the functionality obtained from the one that precedes it. Most of the published pericyclic domino reactions involve two successive cycloadditions, mostly as $[4+2]/[4+2]$ combinations, but there are also

several cases of [2+2], [2+5], [4+3] (Nazarov), [5+2], and [6+2] cycloadditions. Diels and Alder described in the literature the combination of two successive [4+2] for the reaction of dimethyl acetylenedicarboxylate with an excess of furan.¹²⁶ There have been several applications since then, for instance, the synthesis of pagodane **3.27** by Prinzbach,¹²⁷ in which an intermolecular Diels–Alder reaction of **3.23** and **3.24** gave **3.25**, followed by another intramolecular Diels–Alder to furnish **3.26**, which was subjected to further reactions to furnish pagodane **3.27** (Scheme 3.8).



Scheme 3.8 | Domino Diels–Alder/Diels–Alder reaction applied to the synthesis of pagodane.¹²⁷

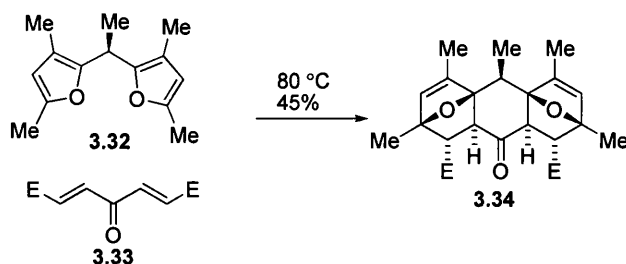
An example of a domino Diels–Alder reaction and 2,3-sigmatropic rearrangement can be found in Carreno, Ruano and coworkers enantioselective synthesis of the natural product (+)-royleanone.¹²⁸ The enantiopure sulfoxide 1,4-benzoquinone was reacted with the diene in CH_2Cl_2 under high pressure furnishing the tricyclic compound with 97% ee and 60% yield as a result of a sigmatropic rearrangement of the chiral sulfoxide. (+)-Royleanone was obtained after hydrogenation of the enantiopure intermediate (Scheme 3.9)



Scheme 3.9 | Domino Diels–Alder/2,3-sigmatropic rearrangement applied to the synthesis of (+)-royleanone.¹²⁸

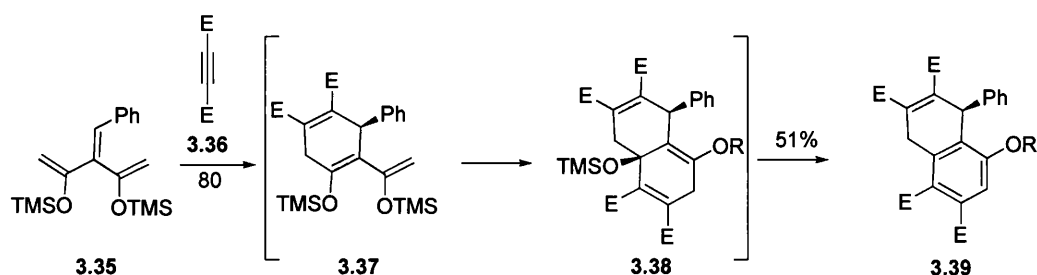
Tandem reactions are a different type of multiple reactions occurring in one pot. Tse-Lok Ho has described tandem reactions as ‘combinations of two or more reactions whose occurrence is in a specific order, and if they involve sequential addition of reagents the secondary reagents must be integrated into the products’.¹²⁹ Tandem Diels–Alder reaction could therefore be in combination with a non-pericyclic (e.g. elimination,

or pericyclic) reaction, for example another Diels-Alder or a retro-Diels-Alder, and would offer a powerful tool for synthesis. Tandem Diels-Alder/ Diels-Alder reaction was described by Fringuelli as a process that involves two separate Diels-Alder reactions occurring at the same time.¹²² Vogel and Marchionni have applied this strategy to synthesize polypropionate fragments (*Scheme 3.10*).¹³⁰⁻¹³¹ The tandem thermal Diels-Alder reaction of **3.32** and **3.33** gives **3.34** in 45% yield after simultaneously occurring double Diels-Alder to afford a stereochemically rich polycyclic ring system, which underscores the utility of this strategy.



Scheme 3.10 | Tandem double Diels-Alder applied to the synthesis of polypropionates.¹³¹

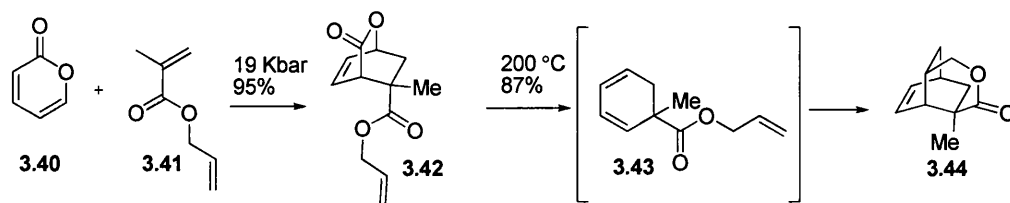
In addition, Winkler highlighted that tandem Diels-Alder cycloaddition could also occur sequentially.¹³¹ A useful example is the cycloaddition of bis-dienes **3.35** - also known as cross-conjugated trienes, with dimethylacetylenedicarboxylate **3.36** leading to the formation of **3.37**. This intermediate then reacts with another equivalent of the dienophile **3.36** to give **3.39** in 51% overall yield (*Scheme 3.11*).¹³² This sequential reaction could not be mistaken with a simultaneous tandem as the diene in the second reaction is the product of the first Diels-Alder reaction. These reactions have also been termed diene-transmissive.¹³¹



Scheme 3.11 | Tandem sequential Diels-Alder reaction.

A different scenario is when an initial Diels-Alder does not promote the second unless the experimental conditions are changed. One could refer to this multistep approach as consecutive or timed, as described by Marko and co-workers in their studies of *R*-

pyrone cycloaddition.¹³³ At high pressure, *R*-pyrone **3.40** reacts with the substituted acrylate **3.41** leading to the formation of the CO₂ Diels-Alder cycloadduct **3.42** in 95% yield. After subjecting this stable intermediate to high temperature (above 200 °C), CO₂ was extruded leading to the formation of the second diene **3.43**, which reacts intramolecularly generating the another Diels-Alder cycloadduct **3.44**, as shown in *Scheme 3.12*.



Scheme 3.12 | Example of a consecutive/ timed Diels-Alder reaction.¹³³

It can sometimes be difficult to distinguish between the different types of multiple Diels-Alder or other reactions. However, this methodology leads to unique approaches to the synthesis of polycyclic ring systems. From complex cage systems to anthracyclines, fused aromatics and molecular belts; cascade, sequential, tandem and domino Diels-Alder still impresses by showing that it can generate one of the most complex chemical structures with multiple stereocentres, all happening, most often, in one-pot and in a single step.¹²⁹

3.1.7 Lewis-acid catalysed Diels-Alder reactions

DA reactions are not influenced by polar changes. More often, a change in the reaction solvent has little impact on the reaction velocity and yield. However, Lewis-acid catalysis can have dramatic effects on their reactivity. Lewis-acid catalysed DA reactions are not only faster and more reactive, but even more regioselective and stereoselective than the uncatalysed ones. For this reason, increasing attention has been focusing on exploiting this family of catalysts. Yates and Eaton¹³⁴ were the first to report the effect of aluminium chloride on accelerating the reaction of anthracene with maleic anhydride. Several Lewis acid catalysts have been widely studied in DA processes, including conventional strong Lewis acids such as AlCl₃, TiCl₄, SnCl₄, ZnCl₂ and ZnBr₂ as well as lanthanide complexes such as Sc(OTf)₃ and Y(OTf)₃.

The activity that Lewis acids display on Diels-Alder reaction could be explained by the effect these have on the LUMO of the dienophile,^{123, 135} as discussed in section 3.1.5. With unsymmetrical dienophiles, a Lewis acid bound to the electron-withdrawing group of the dienophile catalyses the reaction lowering the LUMO of the dienophile further. In

addition, the Lewis acid increases the difference between the coefficients in the LUMO thus increasing the regio- and stereo- selectivity.

3.1.7.1 Classification of Lewis acids

Kobayashi and co-workers classified metal chlorides, being the most common type of Lewis acids, as follows: A, active; B, weak and C, inactive for the activation of aldehydes and aldimines (*Figure 3.2*).¹³⁶ Group A was further divided into A-1, A-2 and A-3. The first two subgroups are aldehyde and aldimine selective, respectively, whereas the third was classified as being neutral. Group B was divided in the same fashion into B-1, B-2 and B-3, whereas group C includes metal chlorides that do not display any Lewis acidity. These findings show that metal chlorides of the following atoms Ti, Zr, Hf, Nb, B, Al, Ga, Sn and Sb have the best Lewis-acidity with respect to aldehydes. On the other hand, metal chlorides of Sc, Fe, In and Bi are the strongest Lewis acids with respect to aldimines. This chart represents an important reference for Lewis acid selection when looking at the chelation of both O- and N- containing dienophiles.

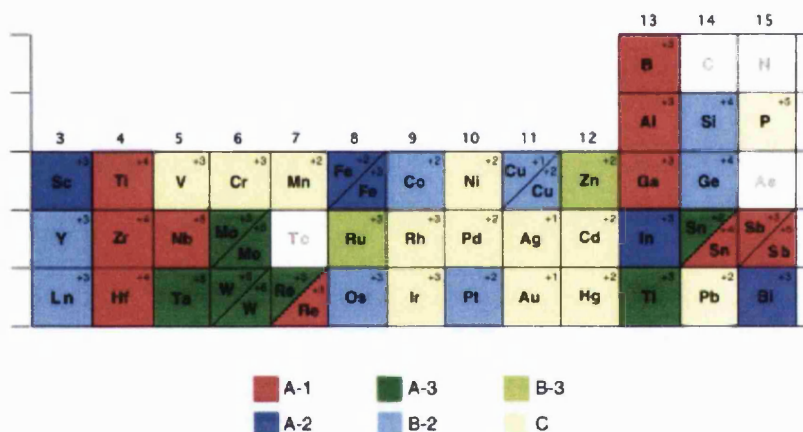


Figure 3.2 | Classification of Lewis acids.¹³⁶

3.1.7.2 Rare earth metals and derivatives

Lanthanide triflates have had an ever increasing role in organic synthesis. This has been recognized by a number of review articles covering various aspects of lanthanide-mediated synthetic organic chemistry.¹³⁷⁻¹³⁸ Scandium is in group 3 of the periodical table, and its radius is considerably smaller than that of any other rare-earth element. Its chemical behaviour is somewhere between aluminium and other lanthanides.¹³⁸ Scandium and other lanthanide triflates are strong Lewis acid catalysts in cycloaddition reactions, as well as other carbon-carbon bond forming reactions.¹³⁷ These compounds chelate strongly the carbonyl group of the dienophile due to their strong character and

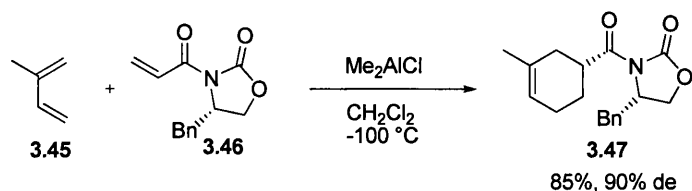
the electron-withdrawing trifluoromethanesulphonyl groups attached to them. A number of lanthanide triflates has already been used in DA including $\text{Sc}(\text{OTf})_3$, $\text{Y}(\text{OTf})_3$, and $\text{Yb}(\text{OTf})_3$, and clearly $\text{Sc}(\text{OTf})_3$ is more effective as catalyst in DA synthesis.¹³⁹ While more than stoichiometric amounts of Lewis acids such as AlCl_3 and $\text{BF}_3 \cdot \text{Et}_2\text{O}$ are needed as the Lewis-acid is consumed due to the coordination with the products, a catalytic amount of $\text{Sc}(\text{OTf})_3$ is enough for the reaction to be completed. In addition, Kobayashi and co-workers reported that in the presence of 10 mol.% $\text{Y}(\text{OTf})_3$ or $\text{Yb}(\text{OTf})_3$, only a negligible amount of the DA product was obtained for the reaction between methyl vinyl ketone with isoprene in comparison with 91% yield in the presence of the same catalytic amount of $\text{Sc}(\text{OTf})_3$.¹⁴⁰ Lanthanide triflate-catalysed reactions can be carried out in either water or a mixture of water and organic solvents (such as THF). Furthermore, the catalyst could be easily recovered from the aqueous layer after extraction and reused with insignificant decrease of the yield of the DA.¹⁴⁰ From a viewpoint of green chemistry, it is preferable to use water instead of organic solvents as a reaction solvent, since water is a safe, harmless, and environmentally benign solvent.

3.1.7.3 Boron derivatives

The boron atom possesses an empty *p*-orbital, allowing boron-based compounds to function as Lewis acids in organic syntheses. Boron tri-halide Lewis acids exist as boron trifluoride (BF_3), boron trichloride (BCl_3), boron tribromide (BBr_3), and boron triiodide (BI_3), in this order of increasing Lewis acidity. Whereas BX_3 ($x = \text{Cl}, \text{Br}, \text{I}$) are mainly used for the cleavage of the (C-O) bond in ethers, the milder BF_3 has had more successful applications in Diels-Alder reactions. Furthermore, a number of boron – based chiral catalysts have been developed over the years and successfully used in Diels-Alder chemistry.¹³⁹

3.1.7.4 Aluminium derivatives

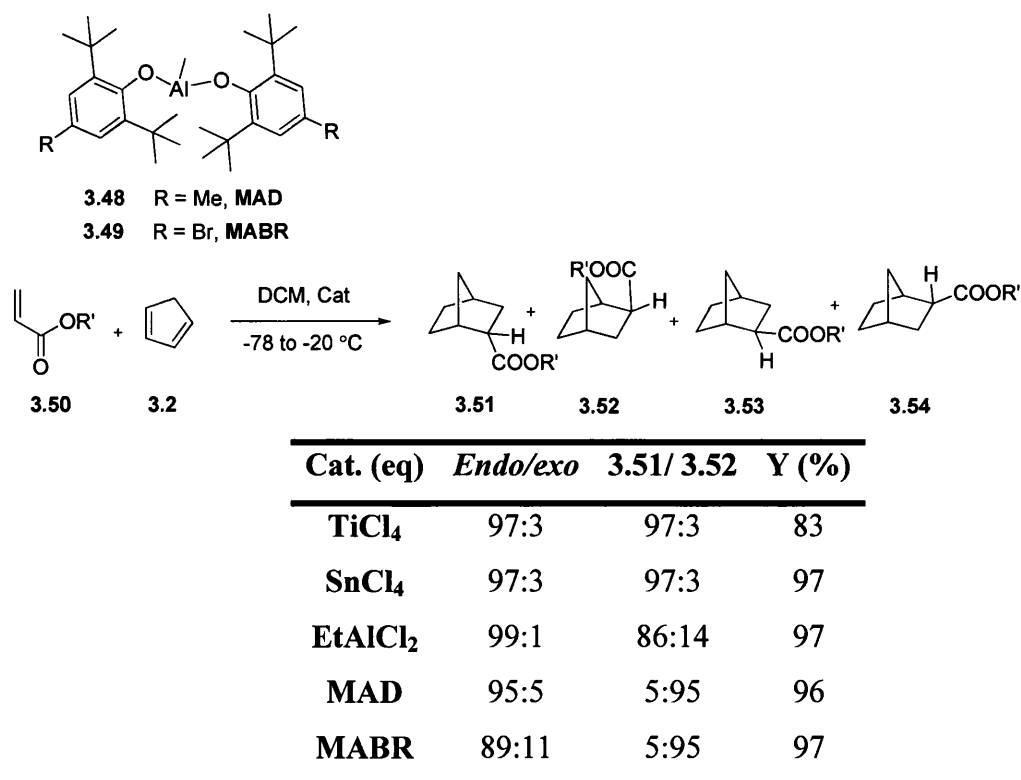
Aluminium (III) complexes are widely used as Lewis acids in DA chemistry. In particular, aluminium halide complexes (e.g., AlCl_3 , AlBr_3) that are commercially available have been widely explored. Organoaluminium compounds have a stronger Lewis acidity and could react with oxygen in the air. Dimethylaluminium chloride (Me_2AlCl) has been significantly used to catalyse various Diels-Alder reactions and works under very low temperatures, as shown in *Scheme 3.13*.¹³⁹



Scheme 3.13 | Organo-aluminium catalysts in Diels-Alder reaction.

3.1.7.5 Bulky Lewis acids

It is often the case that the regio- or stereochemical outcome using a chelating metal-based Lewis-acid does not furnish the desired product. In those circumstances, non-chelating Lewis acids could be explored. These are usually bulky metal-based Lewis acids such as methylaluminium-bis-(4-methyl-2,6-di-*tert*-butylphenoxide) (MAD) **3.48** and methyl-aluminium-bis-(4-bromo-2,6-di-*tert*-butylphenoxide) (MABR) **3.49** (Scheme 3.14). Due to the steric hindrance these catalysts exhibit towards one or more sites of the dienophile, electronic factors could govern the regio- or stereochemical control in the product. The comparative example of MAD and MABR catalytic control of a Diels-Alder reaction between acrylate **3.50** with cyclopentadiene **3.2** (Scheme 3.14) demonstrates this concept.¹⁴¹



Scheme 3.14 | Stereo- and regiochemical control of DA reaction using bulky Lewis acids.

3.1.7.6 Transition-metal-based catalysts

Transition-metal-based Lewis acid catalysts include molybdenum and tungsten nitrosyl complexes. Ruthenium(ii) complex, *trans*-[Ru(salen)(NO)(H₂O)] SbF₆ **3.55** (Figure 3.2) is stable when exposed to air and tolerant towards non-dry solvents.¹⁴² The catalyst works better with dienophiles having an aldehyde or a ketone and less with an ester. Other catalysts include cyclopentadienyl triflate complexes of zirconium **3.56** and titanium **3.57** (Figure 3.3). These catalysts increase the rate of the reaction between 10³ and >10⁵ over the corresponding thermal conditions, even at very low loading and are tolerant towards a variety of solvents, without the need to dry them.¹⁴³

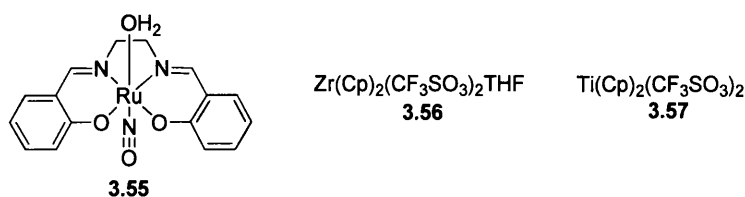
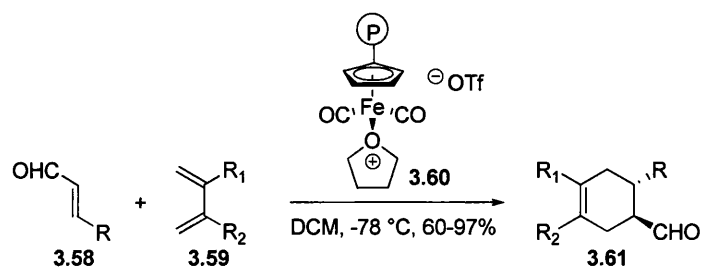


Figure 3.3 | Homogenous/ transition metal-based catalysts.

3.1.7.7 Polymer-supported catalysts

Polymer-supported Lewis acid catalysts, also known as heterogeneous Lewis acid catalysts, offer several advantages including operational simplicity, filterability and reusability. Conventionally used supports could be classified into high surface area (>1m²/g) such as silica, alumina, magnesia, activated-carbon, and carbon black. Low surface (<1m²/g) supports include kieselguhur, pumice, and silicon carbide.¹⁴⁴ A polymer-bound iron Lewis-acid catalyst¹⁴⁵ **3.60** was shown to be active in the cycloaddition of α,β -unsaturated aldehydes with a number of dienes (Scheme 3.15). Several silica-bound Lewis acids can now be readily purchased from suppliers such as Sigma Aldrich, including silica-bound AlCl₃ and BF₃.

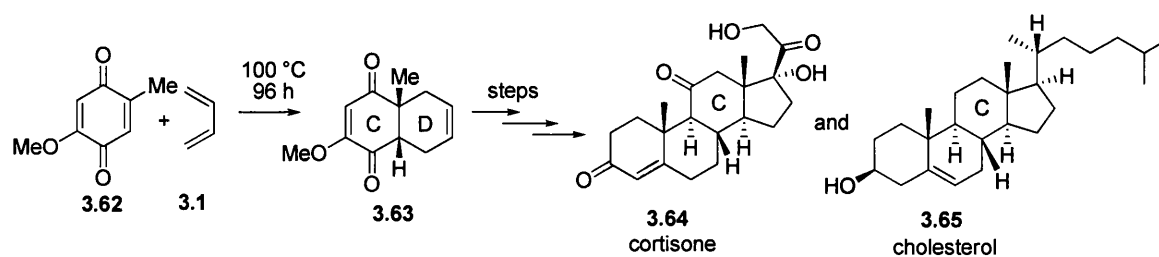


Scheme 3.15 | Polymer-bound Lewis-acid catalysis in Diels-Alder.

3.1.8 Applications of DA to the total synthesis of natural products

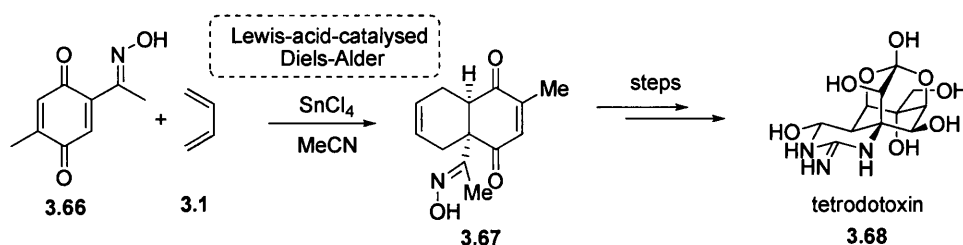
Otto Diels and Kurt Alder published in their landmark 1928 paper the first account of the reaction that would later bear their name.¹⁴⁶ In the same paper they anticipated the

importance of their discovery, when they wrote “Thus it appears to us that the possibility of synthesis of complex compounds related to or identical with natural products such as terpenes, sesquiterpenes, perhaps even alkaloids, has been moved to the near prospect.” However, the inventors reserved the application of their discovery to themselves and it was only in 1951 that Stork et al published their total synthesis of cantharidin employing this pericyclic reaction. Later, in the same year, Gates and Tschudi reported the use of the Diels-Alder in the synthesis of morphine.¹¹¹ However, perhaps the most significant application of Diels-Alder in its early years came from Woodward, who reported the total synthesis of cholesterol **3.65** and cortisone **3.64** in 1952 (*Scheme 3.16*),¹⁴⁷ and of reserpine in 1956.¹⁴⁸ This was the beginning for a new ‘school of thought’,¹¹¹ which involved the use of rational synthetic strategies in the total synthesis of complex natural products, placing Diels-Alder as a key reaction to solve challenging synthetic questions.



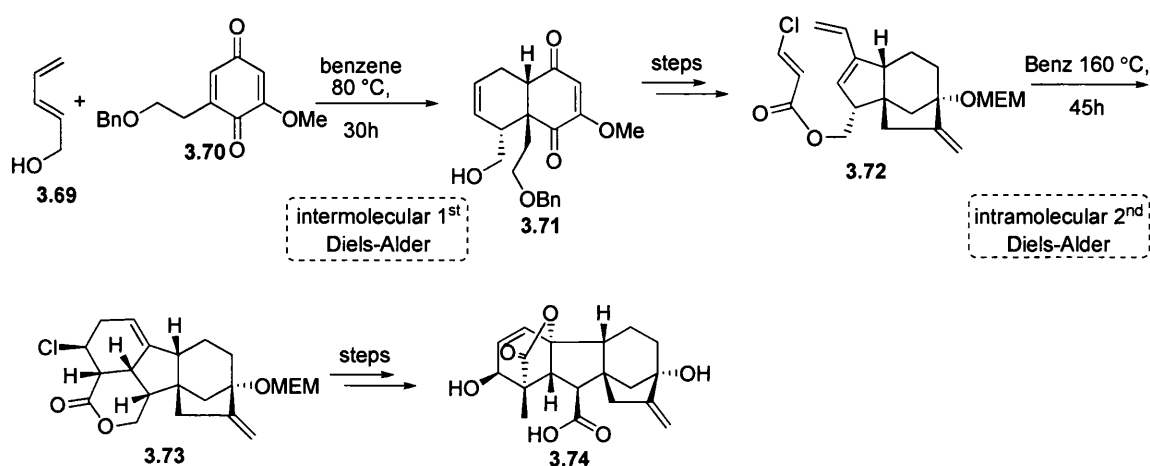
Scheme 3.16 | Woodward’s application of quinone-based DA in the synthesis of cortisone and cholesterol.¹⁴⁷

The use of Lewis acids allowed further progress for the application of the DA reaction for the total synthesis of tetrodotoxin by Kishi et al.¹⁴⁹ The use of SnCl_4 enabled the exclusive reaction of the olefinic bond of the quinone adjacent to the oxime (*Scheme 3.17*).



Scheme 3.17 | Kishi’s application of Lewis-acid-catalysed quinone Diels Alder reaction in the synthesis of tetrodotoxin.

Danishefsky designed a new diene system to achieve full regioselectivity and introduce useful functional groups. The 1-methoxy-3-trimethylsilyloxybutadiene has become a powerful component of the DA allowing a highly regioselective and *endo*-specific adduct. The synergistic effects of the two incorporated oxygens towards reinforcing the electronic effects of the diene has proved substantially useful where Lewis-acid catalysis is not applicable. Danishefsky's diene was used for the successful synthesis of natural products such as disodium prephenate¹⁵⁰ and myrocin-C¹⁴⁸; and the gibberellic acid **3.74**.¹⁵¹ Two DA reactions were used in this synthesis: an initial one between quinone **3.70** and dienol **3.69**, which affords regio- and chemospecifically the adduct **3.71** offering the backbone for the second DA occurring intra-molecularly (scheme 3.18).



Scheme 3.18 | Corey's use of both inter- and intramolecular DA reactions in the synthesis of gibberellic acid.¹⁵¹

The extent to which the cycloaddition developed by Otto Diels and Kurt Alder impacted the total synthesis of natural products has been immense. Since Woodward's synthesis of reserpine and Danishefsky's incorporation of his dienes, the reaction has been extensively explored and continues to be. Looking at some of the most impressive natural products syntheses, the DA reaction has shown to be a major presence as an assembly process for tailor-made compounds. From estrone and cytochalasin B to aloperine, ambruticin, aloperine and taxol (*Figure 3.4*), Diels and Alder would have been enormously satisfied to know of the many elegant and important applications of their reaction in the art of total synthesis.

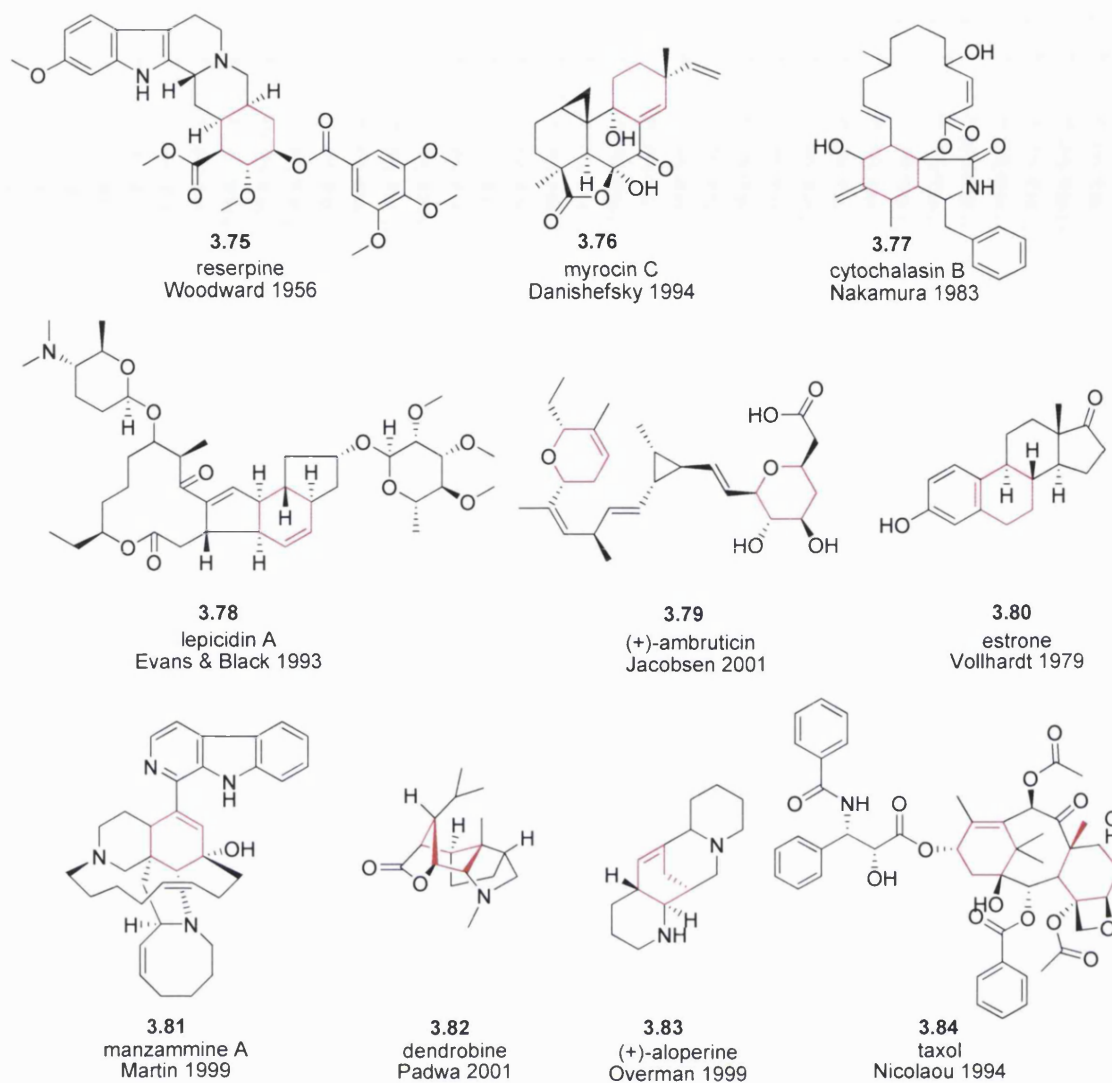


Figure 3.4 | Selected examples of natural products where DA reaction was applied to their total synthesis (rings shown in red were formed through the DA reaction.)

3.2 The cross-conjugated trienes

In DA reactions involving conjugated systems six types of unsaturated hydrocarbons could be produced which would differ from one another chemically, physically and also in terms of their synthetic applicability. Those classes are: linear polyenes **3.85**; annulenes **3.86-3.87**; radialenes **3.88-3.89**; fulvenes **3.90-3.91**; dendralenes **3.92-3.93**; and cumulenes **3.94-3.96** (Figure 3.5).¹⁵²⁻¹⁵⁴

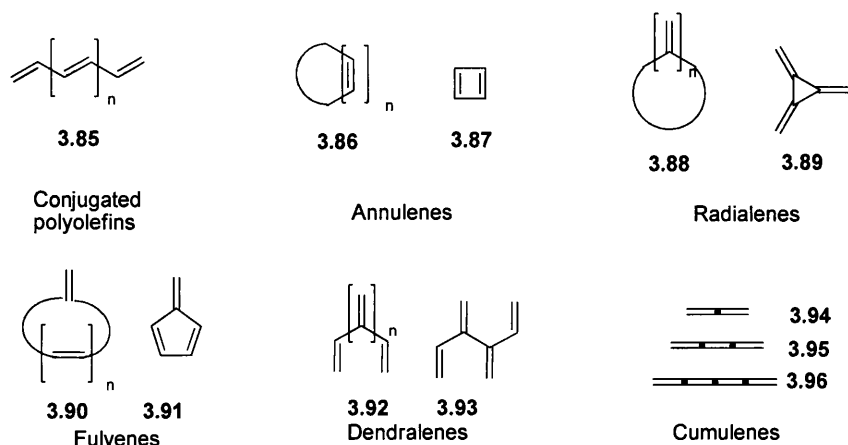


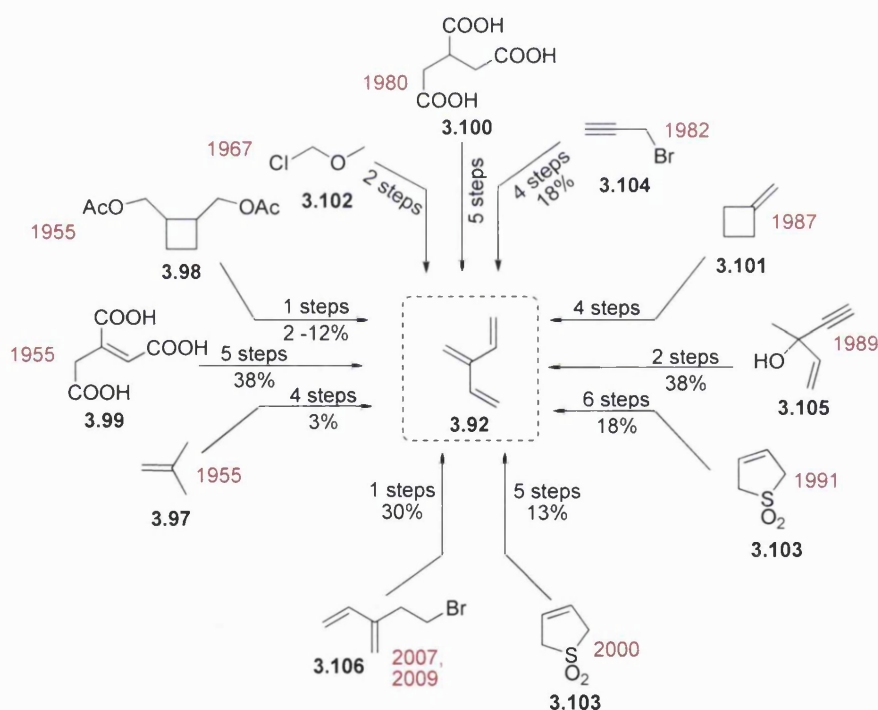
Figure 3.5 | The six different classes of double unsaturated hydrocarbons.^{152-153, 155}

Dendralenes, which have until recent years been one of the least studied polyene hydrocarbons, are acyclic and cyclic cross-conjugated polyenes derived from 3-methylene-1,4-pentadienes as the most basic component. Cross-conjugated trienes are a fraction of dendralenes (**3.92**, $n=1$) which serve as precursors to polycyclic natural product-like structures, by undergoing domino or tandem pericyclic reactions. In this section an overview is presented of the synthesis, stability and chemical and physical properties of cross-conjugated trienes, starting from the smallest member (**3.92**) to more complex aromatic-substituted cross-conjugated trienes.

3.2.1 3-Methylene-1,4-pentadiene

For over 50 years, the synthesis of 3-methylene-1,4-pentadiene (**3.92**) has involved pyrolytic elimination as a major route to prepare these unstable conjugated systems (scheme 3.19).¹⁵⁶ In 1955, Blomquist and Verdol reported the pyrolysis of 3-methylene-1,5-pentadienol diacetate, the product of the thermal condensation of isobutylene (**3.97**), at 485 °C, but the yield was only 3% after 4 steps.¹⁵⁷ In the same year, two papers were published on the pyrolysis of 1,2-di(acetoxymethyl)cyclobutane **3.98**, which furnished better yields and in fewer steps.¹⁵⁸⁻¹⁵⁹ Bailey and Economy also reported a different method starting from asconic acid (**3.99**) in which pyrolysis at 540 °C afforded the

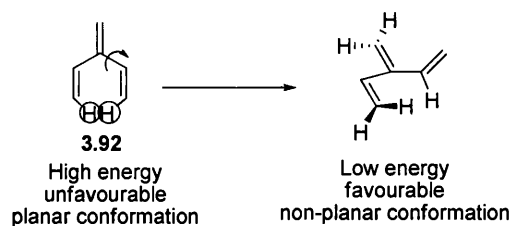
cross-conjugated triene in 38% yield over 5 steps.¹⁶⁰ Another group reported the preparation of **3.92** through Hoffman elimination of propane-1,2,3-tricarboxylic acid (**3.100**) at 180 °C/12 Torr yielding 40-55%.¹⁶¹ Vinylcyclobutene (**3.101**) has also been used as a precursor in a flash thermolysis reactor to afford 3-methylene-1,4-pentadiene by complete conversion at 335 °C.¹⁶² Other routes include the acid-catalysed elimination of a chloroether precursor (**3.102**) at 140-160 °C, and the pyrolysis of 3-vinyl-3-sulfolene (**3.103**) at 550 °C over 6 steps,¹⁶³ and 450 °C over 5 steps.¹⁶⁴ Hopf and Priebe in 1982 proposed a different synthesis of triene (**3.92**) starting from propargyl bromide (**3.104**), which was dimerized and subsequently isomerised at 500 °C.¹⁶⁵ A few years later, Hopf's group devised an alternative synthesis through the pyrolytic dehydration of a vinyl propargyl alcohol (**3.105**) over molecular sieves at 300 °C.¹⁶⁶ More recently, Sherburn's group developed a simpler and quicker method to the triene **3.92**.^{156, 167} Starting from 5-bromo-3-methylene-pent-1-ene (**3.106**), which is eliminated by slow addition of DBU in DMSO, the triene is obtained in gram-scale as a pure oil.



Scheme 3.19 | Existing synthetic routes to the simplest acyclic branched triene.¹⁵⁶

[3] Dendroles are non-planar structures. Hopf performed a comparison between the UV spectra of 3-methylene-1,4-pentadiene (**3.92**) ($\lambda_{\text{max}} = 224 \text{ nm}$, $\log \epsilon = 4.41$) and that of 1,3-butadiene (217 nm, 4.32).¹⁵⁴ The difference in the UV spectra would have been more significant if the triene (**3.92**) was planar. As indicated in *Scheme 3.20*, planar structures for **3.92** would be high in energy and thus unfavourable due to the steric

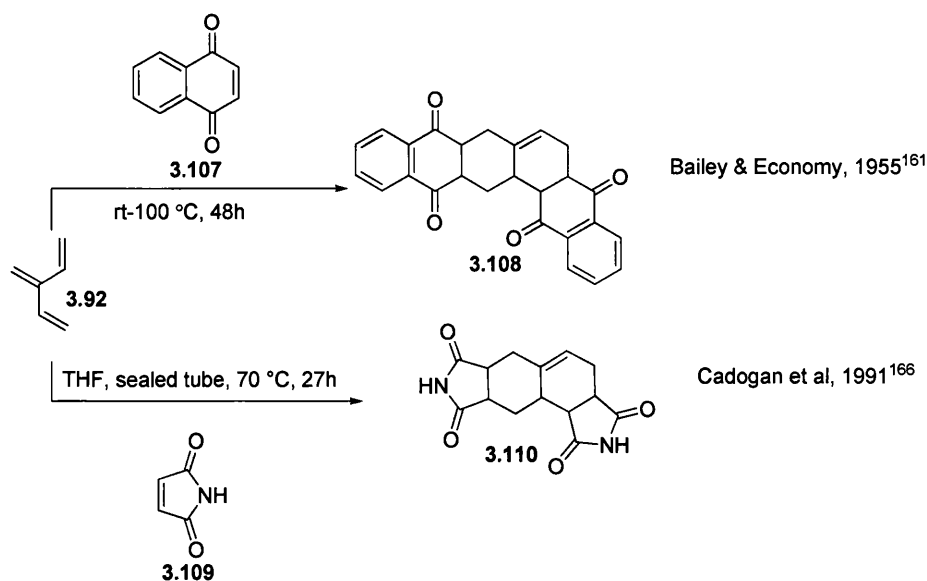
hindrance between the *–endo* hydrogen atoms. A twisted conformation is thus responsible for the non-planarity which prevents the parallel alignment of the *p*-orbitals shifting the absorption maxima to lower wavelengths.



Scheme 3.20 | Conformations of [3] dendralene.

As previously noted, [3]dendralenes are not very stable hydrocarbons and degradation is prone to occur if not well stored. Sherburn's group noted that only slight (<10%) degradation is observed when stored for one month at -20 °C. A dimer of the triene was the most observed form of degradation/ polymerization when stored for either 36h at -5 °C or at room temperature for 3 days.¹⁵⁶

[3]Dendralenes have a unique feature when it comes to their application to the DA reaction. These hydrocarbons are able to undergo double, also known as diene-transmissive, cycloadditions with maleic anhydrides,^{158, 160} various quinines,^{160, 163} *N*-phenyl-1,2,4-triazoline-3,5-dione,¹⁶³ dimethylacetylenedicarboxylate¹⁶³ and maleimides¹⁶³ (Scheme 3.21).



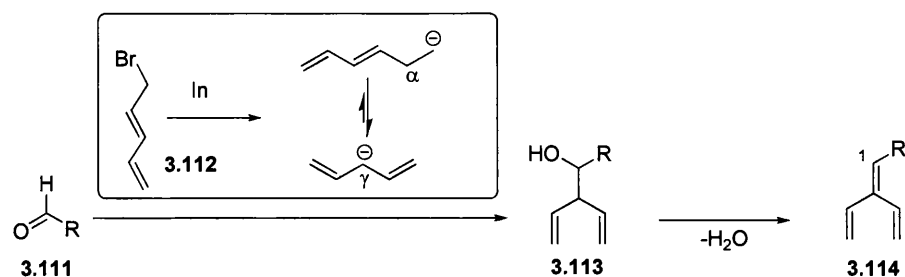
Scheme 3.21 | Diene-transmissive DA of [3]dendralene.^{158, 163}

The reactivity of these cross-conjugated trienes could be controlled to undergo a single cycloaddition reaction. This could be achieved by running reactions at low temperatures and using a Lewis acid, as will be shown in the next sections. Tsuge et al reported that the reaction of a substituted cross-conjugated triene with maleimides and maleic anhydrides could lead to the selective formation of mono- and bis- adducts by varying the amounts of dienophiles used.¹⁶⁸

This section has presented an insight into the most significant syntheses of the simplest cross-conjugated triene, 3-vinyl-1,4-pentadiene, also known as [3]dendralene. These highly volatile, low-molecular weight molecules react with almost any dienophile affording, sometimes in a single step, natural product-like polycyclic systems. As a result, there has been interest in making substituted cross-conjugated trienes to generate a more varied library of polycycles, as presented in the next section.

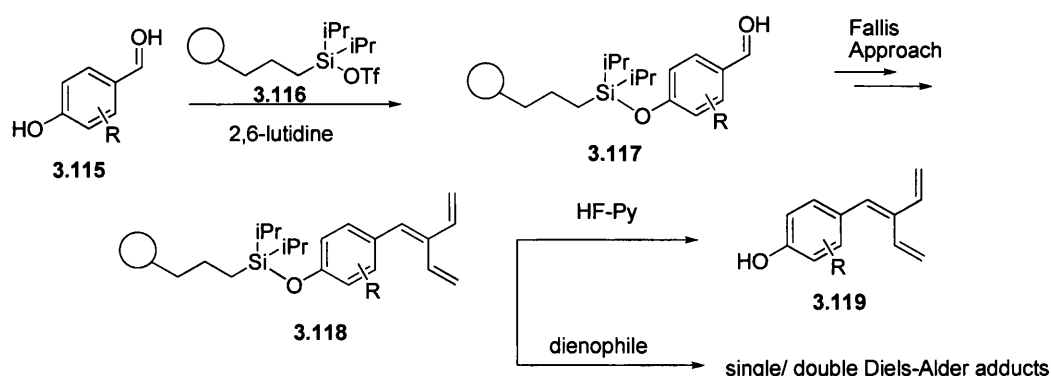
3.2.2 Substituted cross-conjugated trienes

There have been limited attempts to making substituted [3]dendralenes. The synthesis of mono-substituted, especially 1-substituted, trienes has been achieved by a number of groups including Fallis, Sherburn and Schreiber. This group reported the synthesis of 1-substituted-cross-conjugated trienes **3.114** using allylindium reagents which were added to carbonyl groups under various conditions – *Scheme 3.22*.¹⁶⁹ The choice of indium metal for the allylation was demonstrated by Chan and colleagues, who conducted the γ -allylation of carbonyl compounds **3.111** with labile dimethyl acetals in water, where zinc and tin reagents failed.¹⁷⁰ When the reaction was carried out in DMF, as opposed to water, the γ -adduct **3.113** was obtained exclusively. Dehydration of the 1,4-dienes **3.113** was achieved under Mitsunobu-type conditions (PPh₃, DEAD, benzene, 80 C°), or through mesylation and consecutive β -elimination with DBU (1,8-Diazabicyclo[5.4.0]undec-7-en). The Fallis protocol is still considered the best way to make 1-substituted trienes allowing the preparation of diverse gram-scale trienes. The cost of the reagents, namely indium, could be considered as the major downside. This reaction will be discussed in further detail in the upcoming chapters.



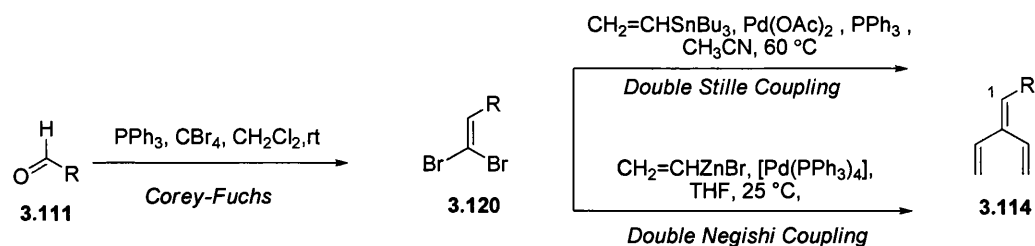
Scheme 3.22 | Fallis synthesis of 1-substituted cross-conjugated trienes.¹⁷¹

This synthetic protocol was also performed on solid-supported macrobeads. Schreiber's group used phenolic aldehyde-loaded macrobeads **3.117** to generate Fallis-type trienes. The group loaded 64 hydroxyaldehydes (e.g. **3.115**) onto macrobeads **3.116** through silylation of their hydroxyl groups, then separately reacted the protected aldehydes **3.117** with indium dust and 5-bromo-1,3-pentadiene **3.112** in DMF. After dehydration, the supported trienes were reacted with a set of dienophiles to afford single/ double cycloaddition adducts. The macrobeads were cleaved with HF-py furnishing a varied library of trienes **3.119** (Scheme 3.23).¹⁷²



Scheme 3.23 | Schreiber's solid phase synthesis of cross-conjugated trienes.¹⁷²

More recently, Sherburn proposed an alternative route to make these trienes. The aldehydes were reacted *via* Corey–Fuchs dibromomethylenation to afford a dibromoadduct **3.120**. This latter underwent two-fold Stille or Negishi coupling to furnish triene in good yields (Scheme 3.24).¹⁷³ Although this method could be cheaper and more amenable to scaling up, the purification could prove to be a challenge.



Scheme 3.24 | Sherburn protocol to synthesise 1-substituted trienes.¹⁷²

3.2.3 Conclusion

[3]Dendralenes or cross-conjugated trienes are truly powerful building blocks that have inspired several natural product synthetic chemists in the synthesis of fused cyclic systems. Their unique ability to act as a ‘double hook’ gives the chance to tailor a step-wise or tandem diene-transmissive cycloaddition reaction simply by varying the temperature and the amount of dienophile. However, there is still a need to explore them to have a more thorough assessment of their regiocontrol as well as reactivity. The upcoming chapters will be presenting our efforts to that end.



CHAPTER 4

AIMS AND OBJECTIVES

4.1 Aims and objectives

The aim of this research project was to identify small molecule inhibitors of the HIF-1 α :HIF-1 β interactions as potential cancer chemotherapy.

The project is based on earlier studies by Melillo who established an ELISA assay to identify inhibitors of the HIF-1 α :HIF-1 β PAS-A domain interaction.⁸⁸ The screening of NCI libraries allowed identification of the synthetically-modified natural product rolitetracycline as a potential protein-protein interaction (PPI) inhibitor (*Figure 4.1-a*). Although Semenza and co-workers have reported the use of a cell-based split-*Rluc* assay to identify acriflavine, a mixture of 3,6-diamino-10-methylacridinium chloride (trypaflavin) and 3,6-diaminoacridine (proflavine) (*Figure 4.1-a*), that inhibit HIF-1 heterodimerisation by binding to PAS-B subdomain of HIF-1 α and HIF-2 α , it is not selective.¹⁷⁴ Therefore, rolitetracycline remains the most promising hit, in terms of PPI target specificity, and the most amenable scaffold to library generation, although one major drawback is its poor cellular penetration properties.

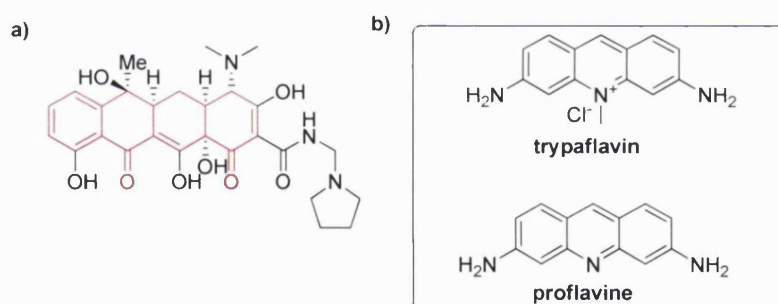


Figure 4.1 | **a)** Rolitetracycline structure showing the rigid tetracyclic scaffold (in red). **b)** Acriflavine.

As the structural basis of the PAS-domain interaction of HIF-1 α and HIF-1 β has not been elucidated, it is not fully understood how their macromolecular surfaces interact. Therefore, the main objective of this project was to synthesize libraries of rolitetracycline-based compounds to establish SAR, improve cellular penetration properties and to obtain lead molecules. A secondary objective was to make them available as chemical tools for probing the PAS-A domain interactions.

The 3D structure of rolitetracycline is defined by a rigid core (shown in red in *Figure 4.1*). The first generation of novel analogues planned was based on the fused four-ring scaffold of the parent compound.

In addition, further molecules were planned based on chemically-modified natural and synthetic commercially available tetracyclines, and by employing the efficient synthetic approach developed by Myers.¹⁷⁵

The focus will be on five points of chemical variations as shown in *Figure 4.2*.

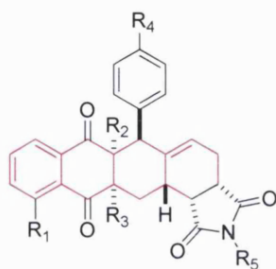


Figure 4.2 | Structure of proposed tetracycline mimetics with the rigid tetracyclic scaffold shown in red and the main points of chemical variation labelled as R₁ to R₅.

The biological objective was to screen all novel compounds for their PPI inhibitory effect using the ELISA assay established by Melillo.⁸⁸

Any hit molecules resulting from this screen would then be further investigated in a screening cascade in the Melillo laboratory to establish the effect on downstream target proteins of the HIF signalling pathway. Molecules with structure potency and selectivity would then be considered for progression into suitable pre-clinical models.

CHAPTER 5

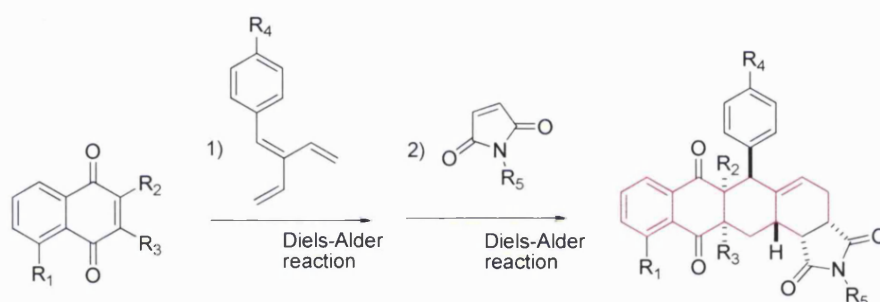
Design, Synthesis and Biological Evaluation of Novel Molecules Inhibitors of HIF-1 α : HIF-1 β PPI Interactions: Results and Discussion

Contents:

5.1	Tetracycline mimetics	74
5.2	Retrosynthetic analysis of tetracycline mimetics	74
5.3	Synthesis of tetracycline mimetics	75
5.3.1	Synthesis of the cross-conjugated triene building blocks	75
5.3.2	Synthesis of the naphthoquinones	82
5.3.3	Synthesis of the maleimides	83
5.3.4	Synthesis of anthraquinones via DA cycloaddition	83
5.3.5	Synthesis of the pentacyclic compounds via DA reaction	90
5.3.6	Conclusion	97
5.4	Biological evaluation of the tetracyclic mimetics	97
5.4.1	Screening protocol	97
5.4.2	The first-generation library (5.79-5.89 and 5.98-5.109)	100
5.4.3	The second-generation library (5.90-5.97, 5.115-5.118 and 5.124-5.127)	110
5.5	Conclusions	118

5.1 Tetracycline mimetics

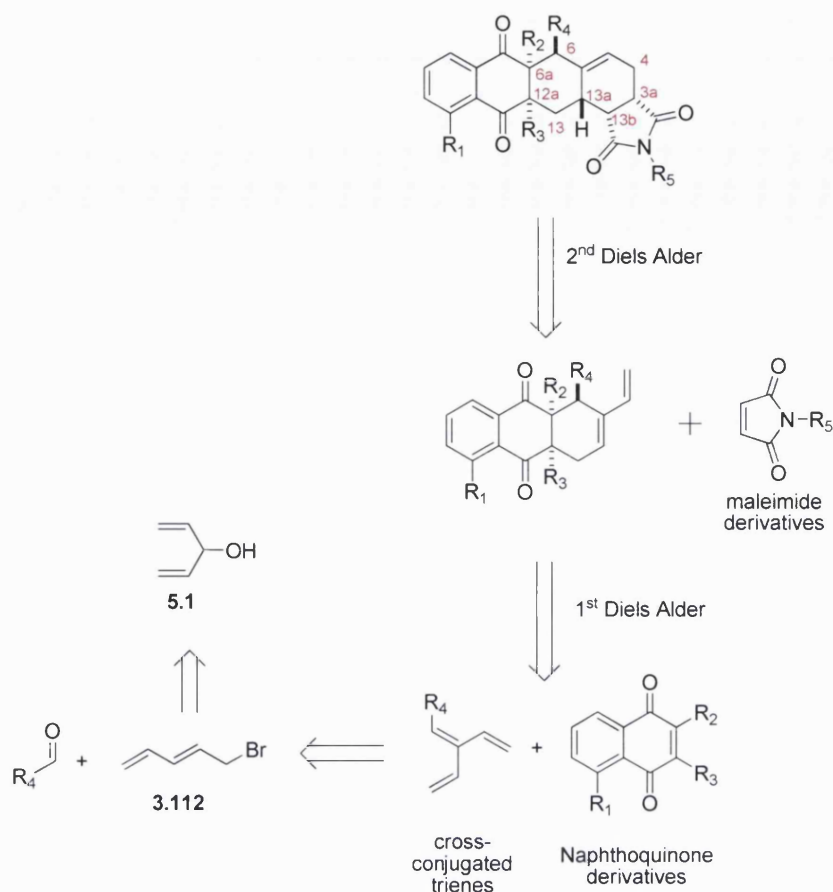
The potential inhibitors of the HIF-1 α :HIF-1 β interaction studied in this project were based on tetracycline mimetics. The specific molecules chosen preserve the original four-ring carbocyclic structure of tetracycline as the core skeleton. The synthetic route to these molecules required fewer steps and allowed more scope for variation in comparison to other routes to rolitetracycline and its analogues. Molecules of this type have been proposed by Kormann and coworkers to be inducers of the tetracycline-inducible repressor protein (TetR) and synthesized using solution phase parallel synthesis.¹⁷⁶ Their synthetic approach involved cross-conjugated trienes as central building blocks to facilitate two consecutive stereoselective DA reactions with different dienophiles (*Scheme 5.1*). This approach is particularly useful, as it allows the synthesis of diverse tetracycline mimetics.



Scheme 5.1 | Consecutive DA reactions for the preparation of tetracycline mimetics.

5.2 Retrosynthetic analysis of tetracycline mimetics

The synthetic route for the preparation of the pentacyclic compounds is based on results published by Kormann, and co-workers¹⁷⁶ (*Scheme 5.2*), which employed DA cycloaddition as a key reaction. Disconnection of bonds 4-3a and 13a-13b result in generation of tricyclic and maleimide intermediates (*Scheme 5.2*). The tricyclic intermediates can be prepared from DA reaction of cross-conjugated trienes with naphthoquinone derivatives. The trienes can, in turn, be generated by addition of 5-bromo-1,3-pentadiene onto the carbonyl function of aldehyde starting materials. Bromination of the penta-1,4-dien-3-ol alcohol produces the desired 5-bromo-1,3-pentadiene. The naphthoquinones can be readily prepared from the corresponding naphthalene derivatives *via* oxidation.



Scheme 5.2 | Retrosynthetic analysis of tetracycline mimetics.

5.3 Synthesis of tetracycline mimetics

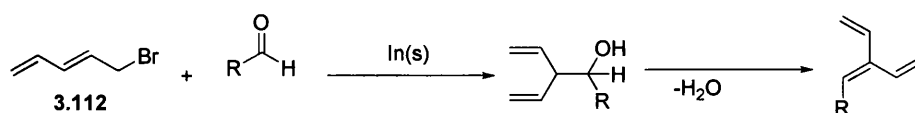
In this section, the synthesis of each building block that constitutes the backbone of the tetracyclic frameworks is explored. These are the cross-conjugated trienes, the naphthoquinone and the maleimide derivatives. In addition, the two DA syntheses are discussed.

5.3.1 Synthesis of the cross-conjugated triene building blocks

The construction of these building blocks was based essentially on the Fallis approach.¹⁶⁹ A different approach by Sherburn is also discussed.¹⁷³

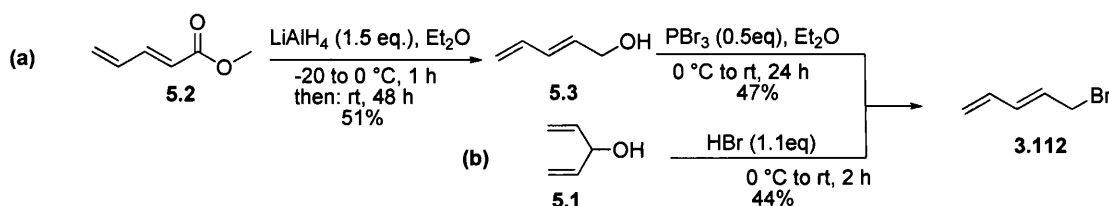
5.3.1.1 Fallis approach

A key building block for the DA reaction is the cross-conjugated triene which reacts consecutively with two dienophiles to furnish the final compounds. The triene synthesis involves γ -pentadienylation of commercially available benzaldehydes in the presence of indium metal to form a secondary alcohol (Section 3.2.2) (Scheme 5.3).¹⁶⁹ The following step is the dehydration of the secondary alcohol.



Scheme 5.3 | Fallis approach for the synthesis of the cross-conjugated trienes.

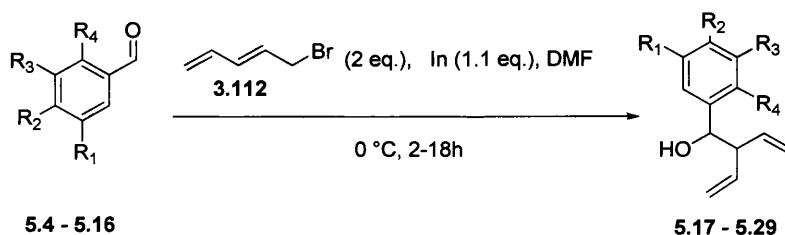
Synthesis of 5-bromo-1,3-pentadiene **3.112** can be achieved *via* two methods.¹⁷⁷⁻¹⁷⁸ The first one proceeds through reduction of the methyl ester **5.2** using LiAlH_4 over 48 hours with 51% yield. The resulting primary alcohol **5.3** reacts with phosphorous tribromide (PBr_3) over 24 hours to form 5-bromo-1,3-pentadiene **3.112** in 47% yield (*Scheme 5.4a*). This method was initially used, but was abandoned since it was time-consuming and uses a starting material (**5.2**), which is unstable to heat and light (*Scheme 5.4a*). Furthermore, the optimum yield for this two-step synthesis was 23% (30% in literature¹⁷⁷). Alternatively, synthesis of the 5-bromo-1,3-pentadiene **3.112** using another method developed by Prevost¹⁷⁹ (*Scheme 5.4b*) was considerably more efficient (single step, 2 hour reaction). This proceeds through the reaction of 1,4-pentadien-3-ol (**5.1**) with 1.1 eq. hydrobromic acid (HBr) at room temperature. The yield of this reaction synthesis was 44%.



Scheme 5.4 | Two approaches for the synthesis of 5-bromo-1,3-pentadiene.

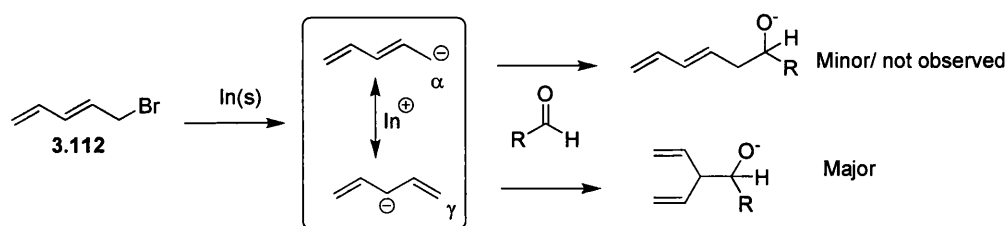
Synthesis of the unconjugated secondary alcohols (**5.17-5.29**) was achieved *via* condensation of benzaldehyde derivatives (**5.4-5.16**) using 2 eq. of 5-bromo-1,3-pentadiene **3.112** and 1.1 eq. of indium metal catalyst. The reaction proceeded in *N,N*-dimethylformamide (DMF) at 0°C for 2-18 hours with yields ranging from 41 to 95%. The products were purified using column chromatography in *n*-hexane: ethyl acetate 11:1 (*Table 5.1*).

Table 5.1 | Preparation of unconjugated secondary alcohols using indium-mediated condensation.



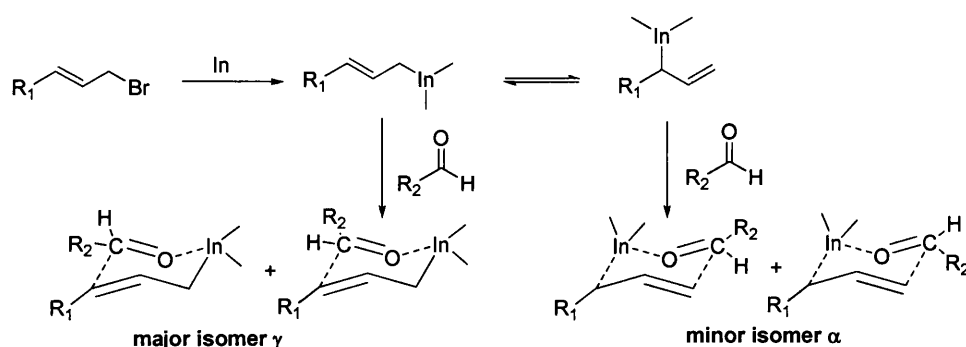
Entry	Benzaldehyde	R ₁	R ₂	R ₃	R ₄	Product	Yd%	Reaction Time
1	5.4	H	CF ₃	H	H	5.17	74	5h
2	5.5	H	CF ₃	H	CF ₃	5.18 [†]	85	5h
3	5.6	CF ₃	H	CF ₃	H	5.19 [†]	86	5h
4	5.7	H	H	H	CF ₃	5.20 [†]	95	5h
5	5.8	H	OCH ₃	H	H	5.21 [†]	93	5h
6	5.9	H	H	H	H	5.22	75	5h
7	5.10	H	Br	H	H	5.23	85	5h
8	5.11	H	F	H	H	5.24 [†]	74	5h
9	5.12	H	Cl	H	H	5.25 [†]	93	2h
10	5.13	H	H	H	Br	5.26 [†]	92	2h
11	5.14	H	Br	H	F	5.27 [†]	94	5h
12	5.15	Br	H	Br	H	5.28 [†]	41	18h
13	5.16	Br	H	H	H	5.29 [†]	66	5h

Fallis and co-workers demonstrated that the penta-2,4-dienyl-indium reagent obtained from 5-bromo-1,3-pentadiene **3.112** and indium metal in (DMF) condenses with aldehydes in a regioselective manner to produce non-conjugated compounds bearing a secondary alcohol at the γ -position (*Scheme 5.5*).¹⁶⁹ The mechanism for this regioselective allylation has not been fully determined, but a number of plausible mechanisms have been proposed.¹⁸⁰⁻¹⁸¹



Scheme 5.5 | Pentadienyl anion condensation.

Chan and co-workers suggested that indium-mediated coupling of allylic bromides with aldehydes in aqueous media proceeds through formation of an allyl indium, which exists in equilibrium with its regioisomer. During coupling with an aldehyde, the reaction proceeds through a number of possible cyclic transition states with the carbonyl oxygen coordinating with the tetravalent indium (*Scheme 5.6*).¹⁸¹ In view of the close structural similarity between pentadienyl and allyl indium species, Chan's transition-state model can also be used to explain the regioselective γ -pentadienylation of benzaldehydes. The γ - is favoured over the α -product when the size of the γ -substituent (R_1) is relatively small and vice versa.

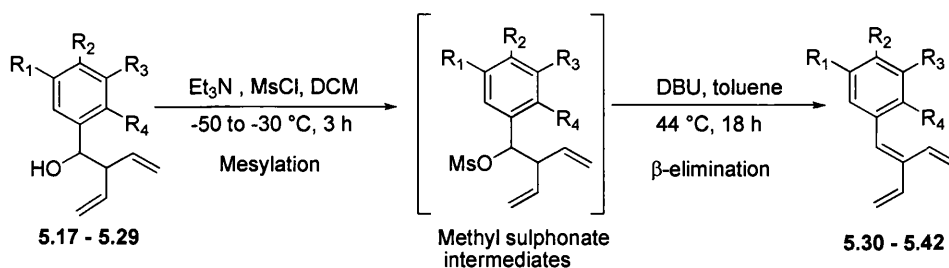


Scheme 5.6 | Transition state models for allylation of benzaldehyde proposed by Chan *et al.*¹⁸¹

The next step, to prepare the cross-conjugated trienes, involves the dehydration of the unconjugated secondary alcohols **5.17-5.29**. Several methods have been tried to optimize this reaction. The mesylation of the secondary alcohol followed by β -elimination with 1,8-diazabicyclo(5.4.0)undec-7-ene (DBU) resulted in the best yields for the preparation of the desired trienes. The mesylation was completed in 3 hours using 2 eq. of mesyl chloride and 2.2 eq. of triethylamine. The reaction was started at -50 °C and allowed to reach -30 °C by completion. The crude methyl sulphonate was then reacted with DBU in toluene at 44 °C leading to the desired cross-conjugated

trienes **5.30-5.42** (Table 5.2), which were purified using flash column chromatography in *n*-hexane to give yields varying between 44-92%.

Table 5.2 | Dehydration of secondary alcohols *via* mesylation and β -elimination to form cross-conjugated trienes.



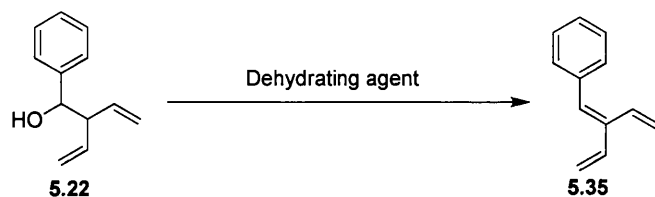
Entry	Dienes	R ₁	R ₂	R ₃	R ₄	Triene	%Yd-2 steps	Reaction Time
1	5.17	H	CF ₃	H	H	5.30	88	18h
2	5.18	H	CF ₃	H	CF ₃	5.31	65 [†]	18h
3	5.19	CF ₃	H	CF ₃	H	5.32	85 [†]	18h
4	5.20	H	H	H	CF ₃	5.33	72 [†]	18h
5	5.21	H	OCH ₃	H	H	5.34	44 [†]	24h
6	5.22	H	H	H	H	5.35	88	18h
7	5.23	H	Br	H	H	5.36	92	18h
8	5.24	H	F	H	H	5.37	77 [†]	18h
9	5.25	H	Cl	H	H	5.38	53 [†]	24h
10	5.26	H	H	H	Br	5.39	75 [†]	24h
11	5.27	H	Br	H	F	5.40	85 [†]	18h
12	5.28	Br	H	Br	H	5.41	83 [†]	18h
13	5.29	Br	H	H	H	5.42	60 [†]	18h

Preparation of the desired cross-conjugated trienes following the procedure described above was achieved in two steps. To obtain the target cross-conjugated trienes in one-step, alternative dehydration procedures based on the divinyl secondary alcohol have been explored.

The use of Martin's sulphurane¹⁸² **5.43** was investigated as a dehydrating agent.¹⁸³ The unconjugated alcohol **5.22** was added to 4 eq. of MS at 44 °C (Table 5.3). This led to formation of the dehydration product **5.35** in a single step, but in very low yield (10%).

Due to the high cost of this reagent, no further attempts were made to explore different conditions.

Tal [†]These compounds have been prepared by Kazi Sharmin Nahar and Dr Dyeison Antonow. The experimental details have not been included in this thesis.



Entry	Reagent(s)	Solvent	Temp. °C	T (h)	Y. %	Ref.
1	Martin's sulphurane 5.43	Toluene	44	4	<10	183
2	Burgess reagent 5.44	THF	0 – 25	24	<10	184
3	Triflic anhydride 5.45	CH ₂ Cl ₂	0 – 25	18	<10	185
4	PPh ₃ , DIAD	CH ₂ Cl ₂	25	96	<10	186
5	Copper triflate 5.46	Hexane	50	18	<10	187
6	Mesyl chloride then DBU	CH ₂ Cl ₂ / Toluene	-30 then 50	24	90	186

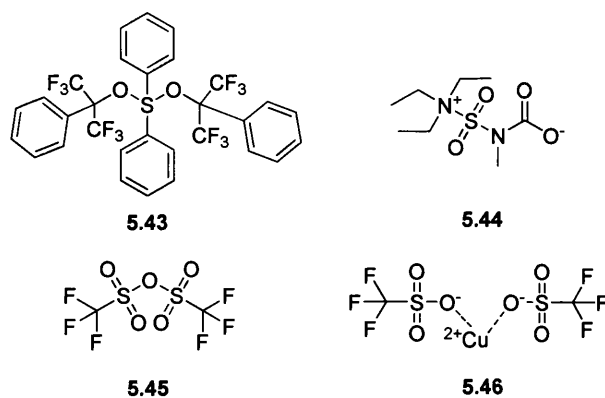


Figure 5.1 | Sulphur-containing dehydrating agents.

Burgess reagent **5.44** was used following standard reaction conditions (THF, 25 °C).¹⁸⁴ However, its use did not prove to be more successful than Martin's sulphurane **5.43**, as the product was isolated in low yield (*Table 5.3, entry 2*) after 24h reaction.

The addition of triflic anhydride **5.45** (Tf₂O) and pyridine (5 eq.) to the secondary alcohol **5.22** has also been attempted to dehydrate the secondary alcohol. The reaction

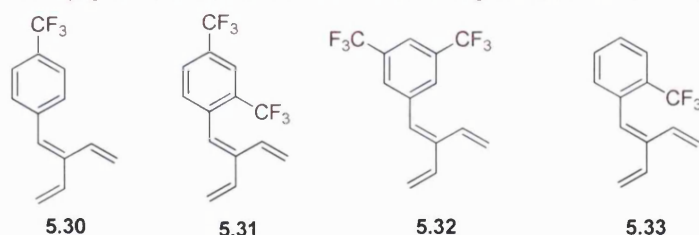
was conducted in CH_2Cl_2 at room temperature.¹⁸⁵ However, this was unsuccessful, as only 6% of the product was isolated (*Table 5.3, entry 3*).

Performing the reaction under standard Mitsunobu conditions: diisopropyl azodicarboxylate (DIAD) and triphenylphosphine (PPh_3) at room temperature over a period of four days furnished only 8% of the product due to problems with isolating the triphenylphosphine oxide byproduct (*Table 5.3, entry 4*).

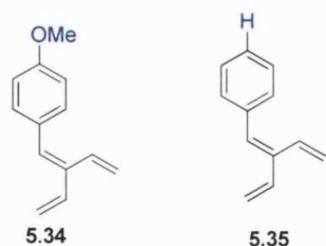
Copper triflate catalysed dehydration¹⁸⁷ using a catalytic amount of reagent **5.46** (0.1 eq.) has also been investigated. A mixture including the secondary alcohol **5.22** was left to stir in CH_2Cl_2 at room temperature providing a yield of <10% (*Table 5.3, entry 5*).

Another approach involved mesylation followed by β -elimination in DBU (*Table 5.3, entry 6*), 13 cross-conjugated trienes were obtained from different divinyl alcohol starting materials (*Figure 5.2*). The benzaldehydes were selected to provide more electronically and sterically versatile final compounds. These will be further discussed at a later stage in this chapter.

Cross conjugated trienes with electron-withdrawing substituents on the phenyl



Cross conjugated trienes with electron-donating substituents/ no substituents on the phenyl



Cross conjugated trienes with halogen-substituted phenyls

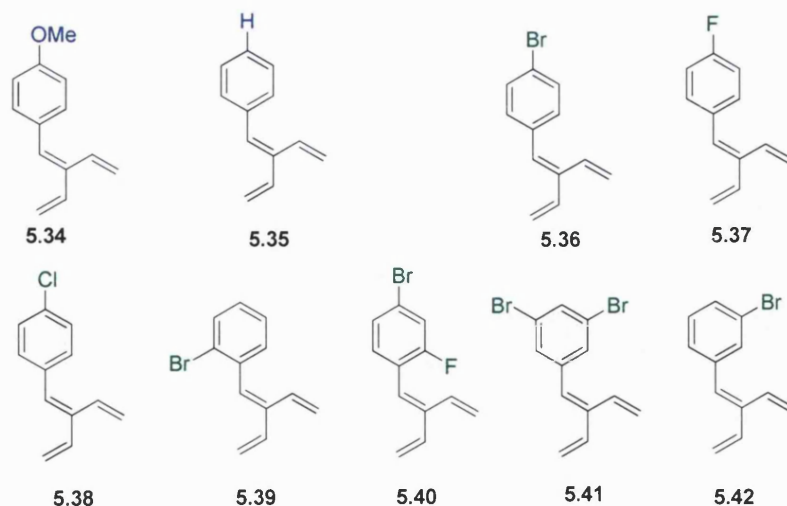
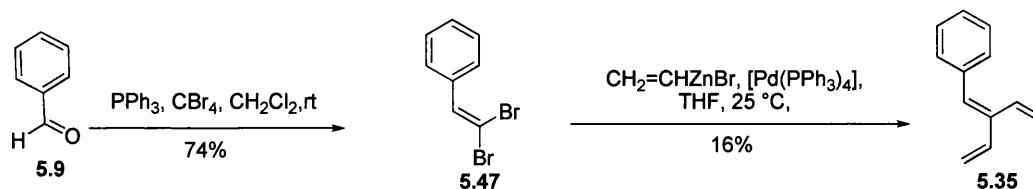


Figure 5.2 | Electronic classification of phenylic cross-conjugated trienes.

5.3.1.2 Sherburn approach

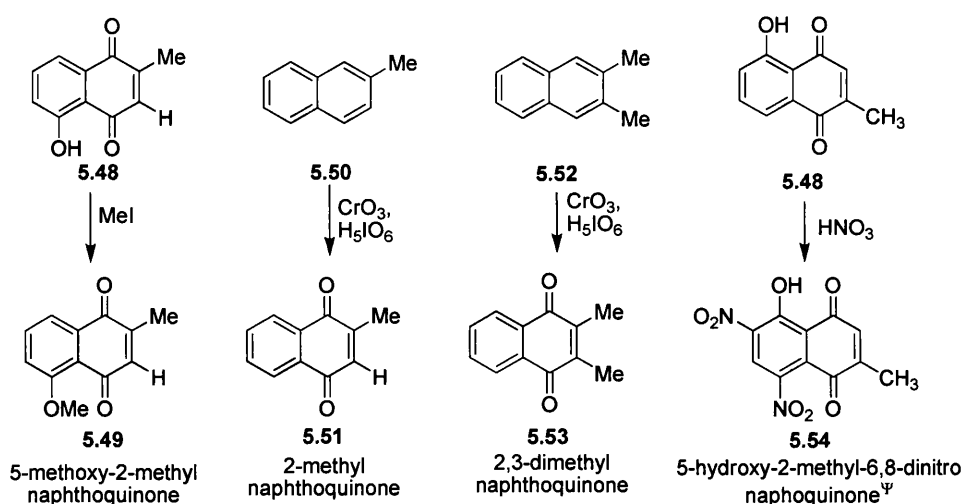
Sherburn's route was also investigated as a route to make the cross-conjugated trienes (also known as [3]dendralenes) (section 3.2.2).¹⁷³ An initial Corey-Fuchs reaction of benzaldehyde **5.9** furnished the vinyl dibromide in 76% yield. The next step was a Negishi double cross-coupling reaction, which was monitored until completion (*Scheme 5.7*). Separation of the resulting mixture, however, resulted in poor yields (20%). This route was abandoned in favour of the Fallis approach.



Scheme 5.7 | Using Sherburn's approach for the synthesis of cross-conjugated triene **5.35**.

5.3.2 Synthesis of the naphthoquinones

Naphthoquinone building blocks were prepared either in a single step (*Scheme 5.8*) or otherwise obtained commercially (*Figure 5.3*).



Scheme 5.8 | Preparation of naphthoquinone building blocks.

One of the methods investigated to prepare 2-methyl- and 2,3-dimethyl-naphthoquinones was *via* oxidation of the corresponding naphthalene. Naphthalenes **5.50** and **5.52** were treated with a catalytic amount of CrO_3 and excess of periodic acid (H_5IO_6) to afford naphthoquinones **5.51** and **5.53** in yields up to 60%.¹⁸⁸ Naphthoquinone **5.49** was prepared by methylation of commercially available (**5.48**) in iodomethane (MeI). The same naphthoquinone **5.48** was also doubly nitrated in nitric

acid (HNO₃) to afford another naphthoquinone **5.54**. Naphthoquinones which were obtained commercially included **3.107** and the unsubstituted naphthoquinone **5.48** (Figure 5.3).

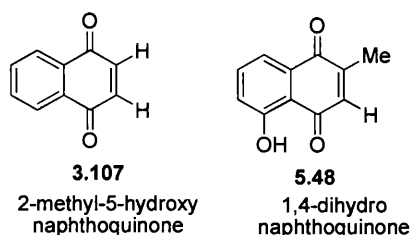


Figure 5.3 | Commercially available naphthoquinones.

5.3.3 Synthesis of the maleimides

The other dienophiles used in the Diels-Alder reaction for the synthesis of tetracycline mimetics are maleimides. Maleimides are widely used as dienophiles for their stability, high reactivity and a commercial availability (sigma Aldrich supplies over 140 types including bioreagents). In the synthesis of tetracycline mimetics, four different types of maleimides were employed (Figure 5.4). Whereas the propanoic acid-substituted maleimide **5.55** was prepared in one step, all the remaining maleimides were commercially obtained.

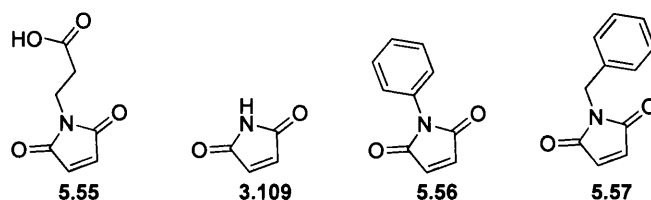
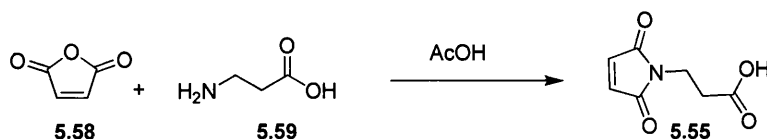


Figure 5.4 | Maleimides used in the synthesis of tetracycline mimetics.

Maleic anhydride **5.58** was reacted with β -alanine **5.59** in acetic acid under reflux (115 °C) and the reaction was left overnight until it turned orange.¹⁸⁹⁻¹⁹⁰ After purification, the product **5.55** was isolated in 70% yield and stored at -20 °C (Scheme 5.9).



Scheme 5.9 | Synthesis of propanoic-acid maleimide **5.84**.

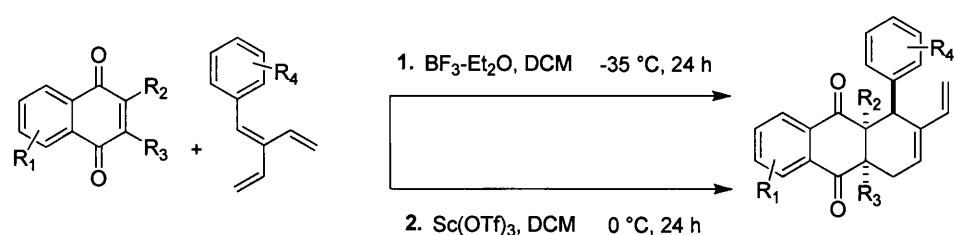
5.3.4 Synthesis of anthraquinones *via* DA cycloaddition

a) Synthetic library

The DA reaction of naphthoquinones has been widely studied, not only because quinones are good dienophiles but also because the cycloadducts of their reaction with a diene provides the fundamental skeleton of many important biologically active compounds such as the anthracyclines.¹⁹¹⁻¹⁹²

The DA reactions between the naphthoquinones presented above and the different types of cross-conjugated trienes were performed in CH₂Cl₂ at low temperatures (-35 to -45 °C) using BF₃.Et₂O as a catalyst. In reactions where BF₃ was not efficient, Sc(OTf)₃ catalysis was carried out (*Table 5.4*).

Table 5.4 | The Lewis acid-catalysed DA reaction to prepare tricyclic compounds.



Entry	Quinone	Triene	Cat.	Temp. °C	%Y	Product
1	5.48	5.30	BF ₃ .Et ₂ O	-35	65	5.60
2	3.107	5.30	BF ₃ .Et ₂ O	-35	56	5.61
3	5.48	5.36	BF ₃ .Et ₂ O	-35	92	5.62
4	5.48	5.35	BF ₃ .Et ₂ O	-35	62	5.63
5	5.51	5.30	BF ₃ .Et ₂ O	-35	86	5.64
6	5.51	5.36	BF ₃ .Et ₂ O	-35	83	5.65
7	5.51	5.35	BF ₃ .Et ₂ O	-35	78	5.66
8	5.49	5.30	BF ₃ .Et ₂ O	-35	76	5.67
9	5.49	5.36	BF ₃ .Et ₂ O	-35	81	5.68
10	5.53	5.36	Sc(OTf) ₃	0	80	5.69
11	5.53	5.30	Sc(OTf) ₃	0	77	5.70
12	5.51	5.37	BF ₃ .Et ₂ O	-35	66	5.71 [†]
13	5.51	5.40	BF ₃ .Et ₂ O	-35	73	5.72 [†]
14	5.51	5.32	BF ₃ .Et ₂ O	-35	79	5.73 [†]
15	5.51	5.41	BF ₃ .Et ₂ O	-35	57	5.74 [†]
16	5.51	5.34	BF ₃ .Et ₂ O	-35	22	5.75 [†]
17	5.51	5.38	BF ₃ .Et ₂ O	-35	47	5.76 [†]
18	5.51	5.39	BF ₃ .Et ₂ O	-35	29	5.77 [†]

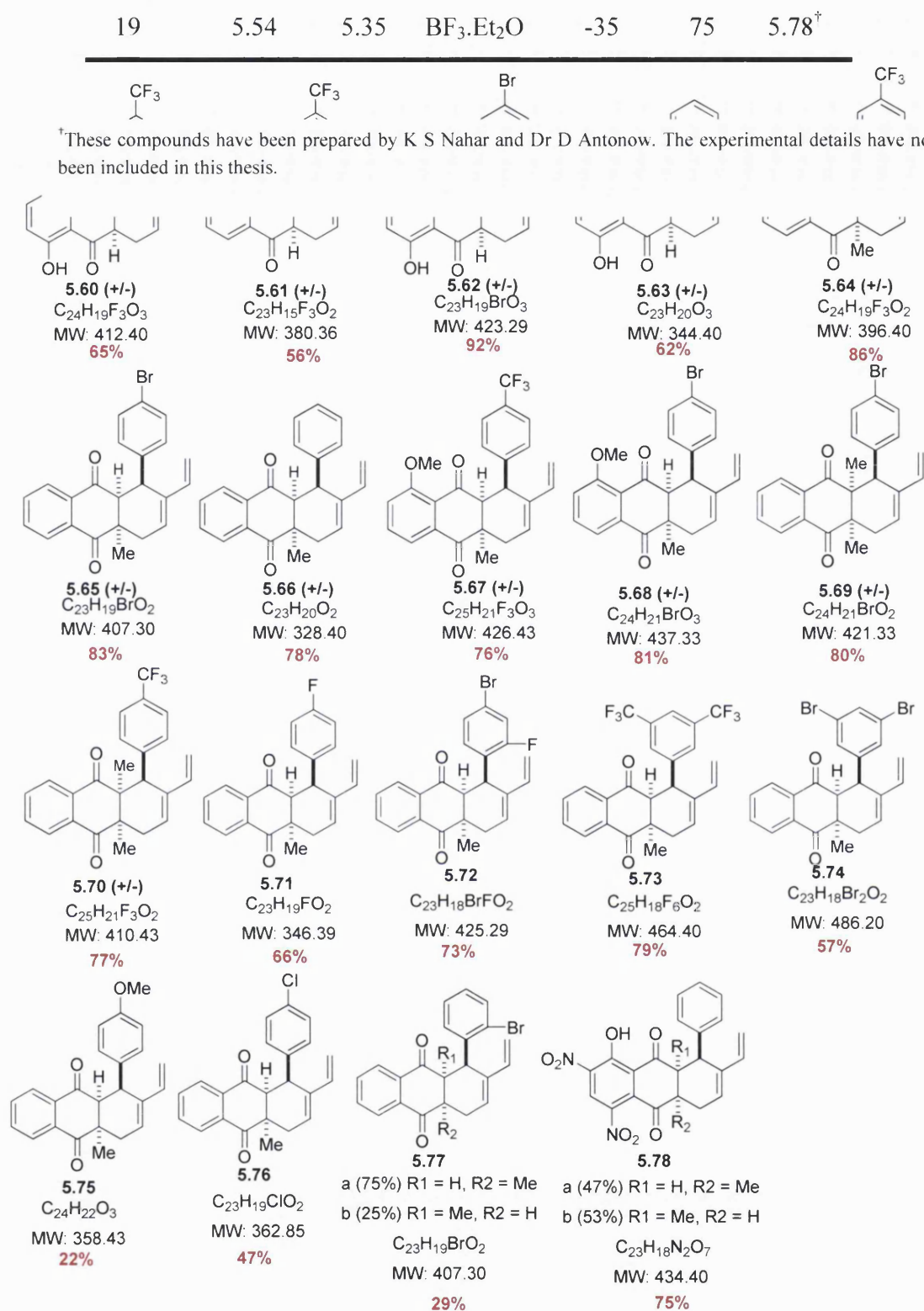


Figure 5.5 | Tricyclic compounds synthesised *via* DA reaction.

The workup associated for both catalysts involved water extraction from *n*-hexane. This was followed by freezing the water layer at -60 °C and pipetting out the organic component. Chromatography using silica gel was then used to remove non-polar

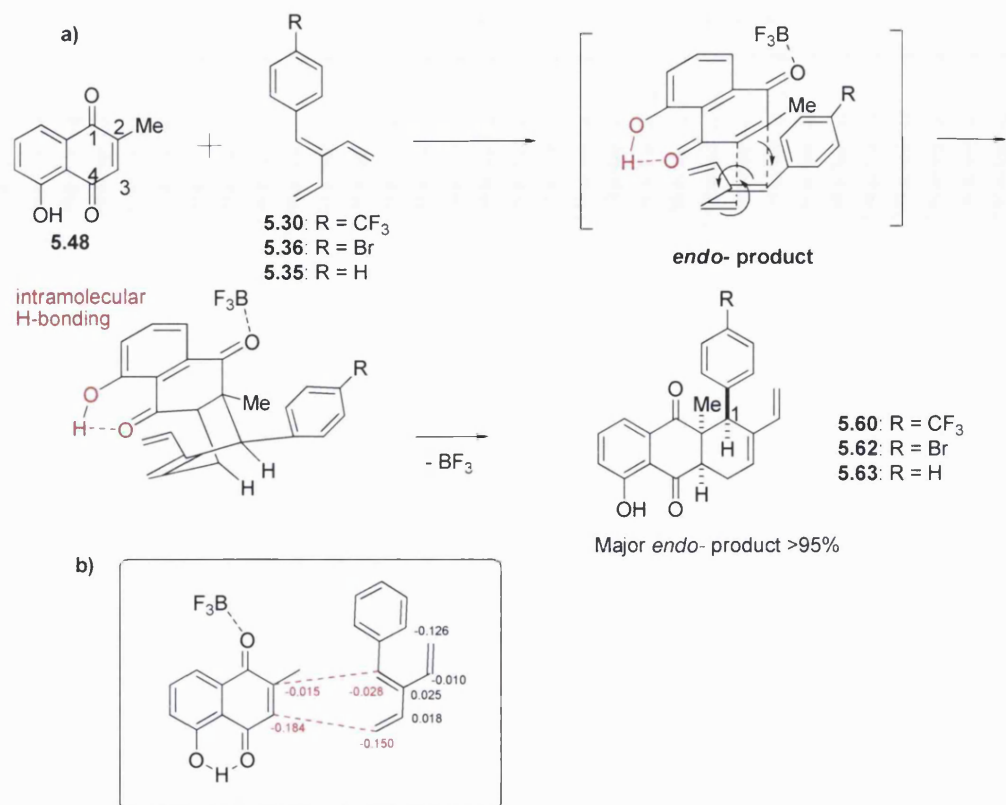
impurities. The tricyclic compounds (**5.60** – **5.78**) were obtained in yields varying from 22-92%.

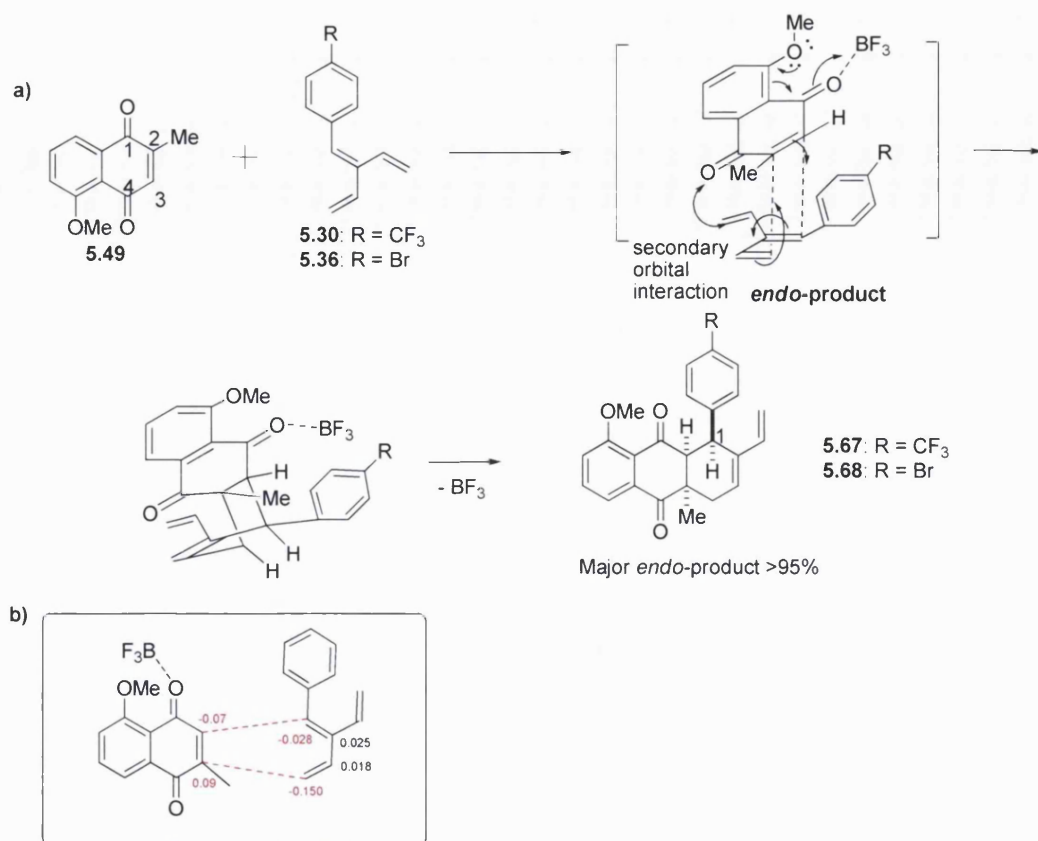
b) Regio/stereochemical considerations

In order to study the mechanism of the DA reactions including the regio- and stereochemistry of the observed tricyclic substrates, we considered the dienophiles (naphthoquinones) as the major driving force for the observed adducts.

The reaction involving naphthoquinone **5.48** and trienes **5.30**, **5.35**, **5.36** gave products **5.60**, **5.63** and **5.62**, respectively. These reactions were highly regioselective providing about 95% of the *ortho* regioisomer, i.e. the phenyl on the triene was *ortho*- to the methyl of the naphthoquinone.

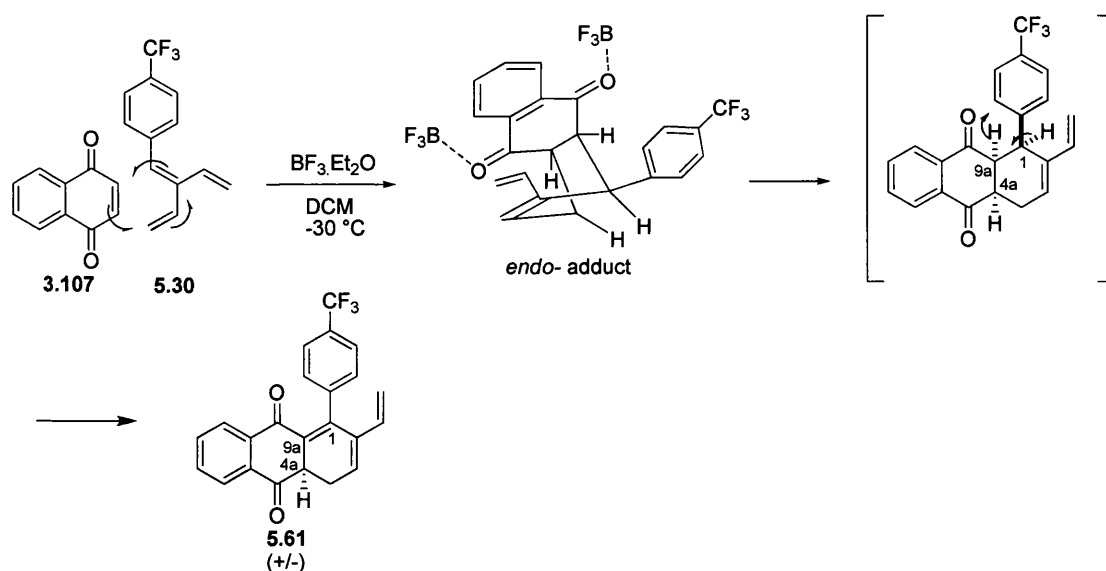
This regioselectivity was enhanced by the presence of the Lewis acid, $\text{BF}_3 \cdot \text{Et}_2\text{O}$, which is known to complex with carbonyl substituents. The strong hydrogen bond present in naphthoquinone **5.48** acts as an internal strong Lewis acid.¹⁹³ The $\text{BF}_3 \cdot \text{Et}_2\text{O}$ Lewis acid presumably coordinates with the free carbonyl group and, as a result, the electron withdrawing effect of the internally-coordinated carbonyl **C-4** is enhanced thus creating an electron deficient **C-3** position of the dienophile (HOMO) that reacts with the electron rich unsubstituted portion of the diene (LUMO). This directs the product towards the major conformation shown in *Scheme 5.9*. The regioselectivity was confirmed by ^1H NMR of compounds **5.60**, **5.62** and **5.63**, in which **H-1** appeared as a singlet. The COSY NMR also showed good correlation between the proton adjacent to the carbonyl and the two protons vicinal to it. The presence of 5% of the other regioisomer (*para*) was confirmed by ^1H NMR of compounds **5.62** and **5.63**. The ^1H NMR spectrum of compound **5.60** did not show any traces of the other regioisomer. This reaction was highly diastereoselective and provided only the *endo* adducts. Two-dimensional experiments such as NOESY and COSY also confirmed these findings.





Scheme 5.10 | a) Outcome of DA reactions involving 5-methoxy-2-methylnaphthoquinone (**5.49**). b) Computed charge distribution based on Huckel predictions for naphthoquinone **5.49** and the cross-conjugated triene **5.35**.

When the unsubstituted naphthoquinone **3.107** was used, reaction was complete within two hours. However, reaction was accompanied by a loss of two protons (**H-1** and **H-9a**) and formation of the conjugated triene. This is known as tandem cycloaddition/aromatisation, and has been previously reported when unsubstituted quinones are used.¹⁹⁵⁻¹⁹⁶ However, aromatisation was only partial, and it was assumed that the least acidic proton, **H-4a**, in the new ring remained intact. This partial aromatisation may have contributed to the increased rate of the reaction, which was complete within 2 hours. As a result, a new scaffold was obtained, which contained only one stereocentre **H-4a** (Scheme 5.11).

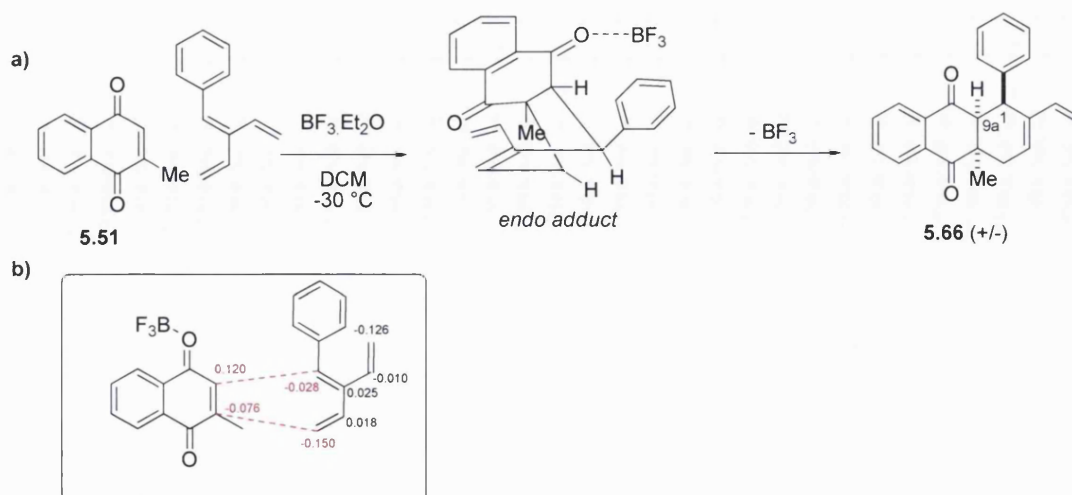


Scheme 5.11 | Tandem cycloaddition/partial aromatisation.

The DA reaction involving the naphthoquinone **5.51** and cross-conjugated trienes **5.30-5.39** and **5.41-5.42** generated the tricyclic compounds shown in *Figure 5.5*. In these, the 2-methyl on the newly formed ring is *meta*- to the phenyl substituent, as shown in *Scheme 5.12*.

Regarding the different rates of reactivity for the naphthoquinones, it has been noted that BF_3 displays unusual regioselective features in Diels-Alder reactions of benzo- and naphthoquinones, often the opposite to that of other Lewis acids explored for these types of substrates.^{193, 197-200} For example, with naphthoquinone **5.51**, the BF_3 preferentially chelates the oxygen atom of the C4-carbonyl where steric factors (*i.e.*, the C2-methyl) take precedence over electronic ones. Thus, in this case, the chelation properties of BF_3 promote formation of the thermodynamically favoured product **6.38** (for similar example, see total synthesis of Colombiasin A by Nicolaou²⁰¹).

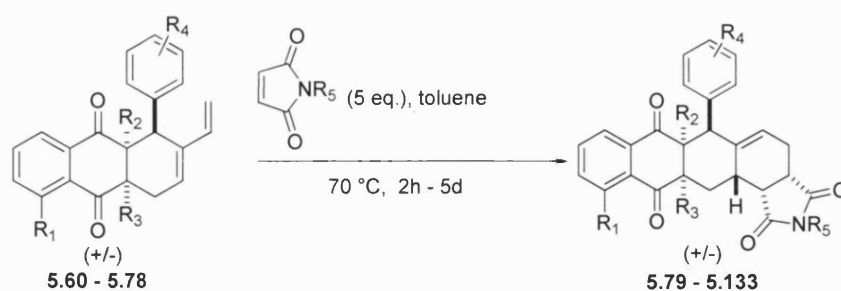
This observation was confirmed by NMR experiments with a strong correlation between H1 and H9a on COSY, as well as with an appearance of a doublet for both H1 and H9a in the ^1H NMR).



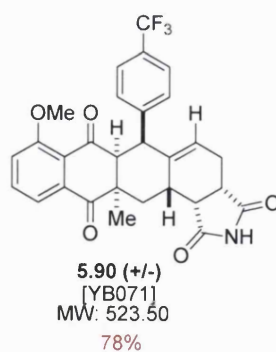
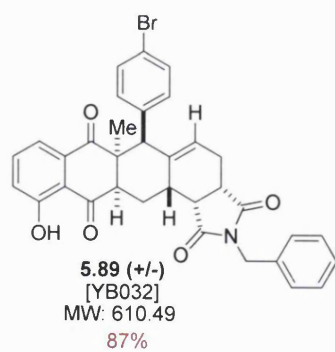
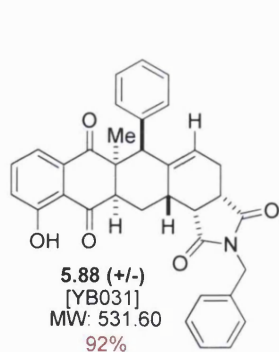
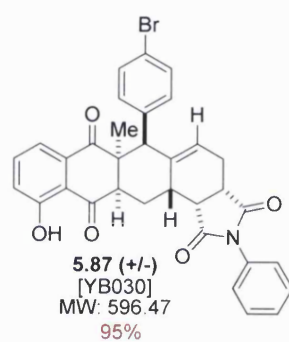
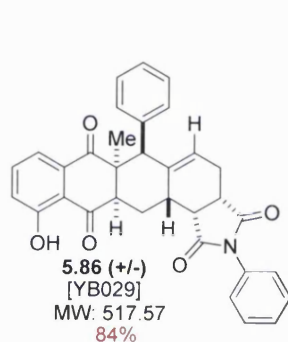
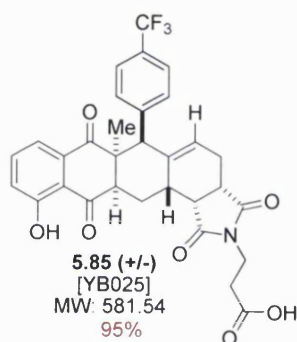
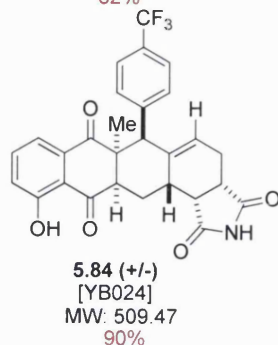
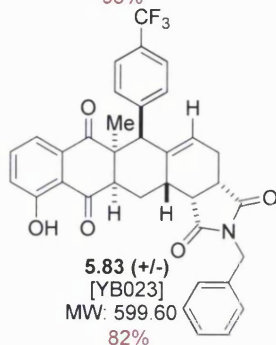
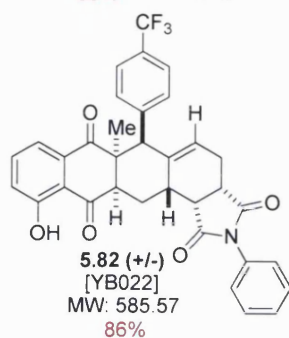
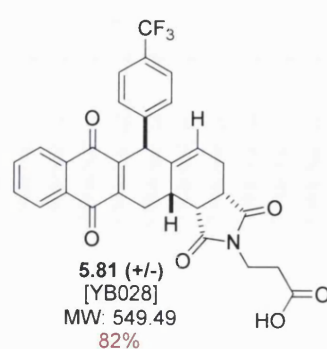
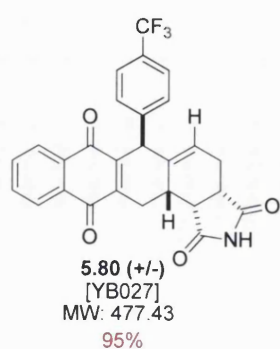
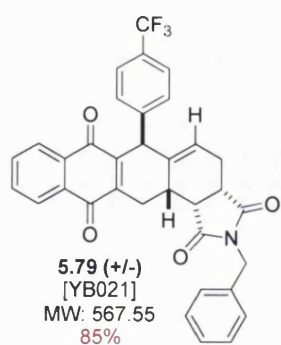
Scheme 5.12 | a) Lewis acid-catalysed DA reaction between the 2-methylnaphthoquinone **5.51** and the cross-conjugated triene **5.35**. b) Computed charge distribution based on Hückel predictions for naphthoquinone **5.51** and cross-conjugated triene **5.35**.

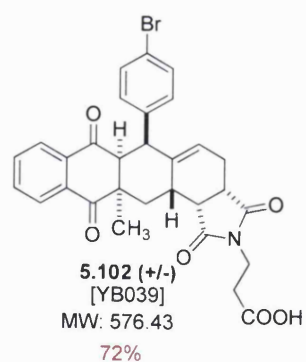
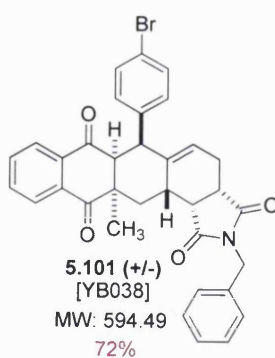
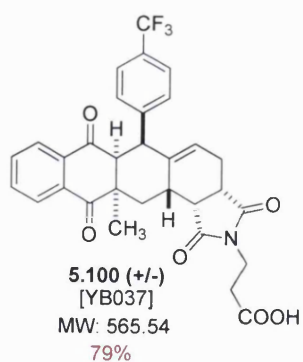
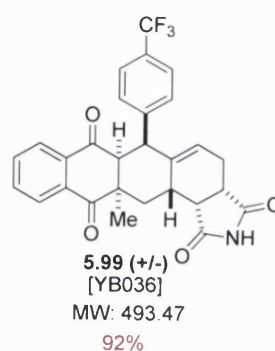
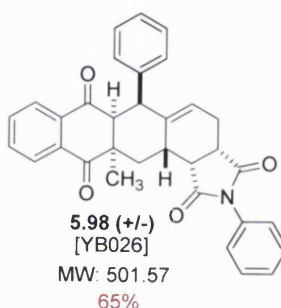
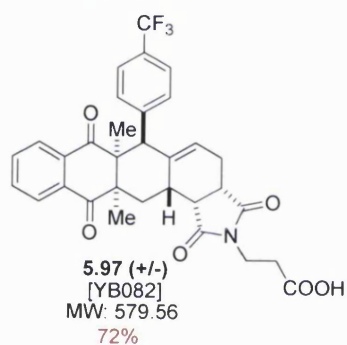
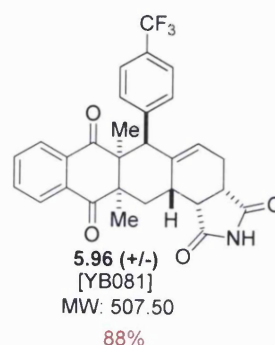
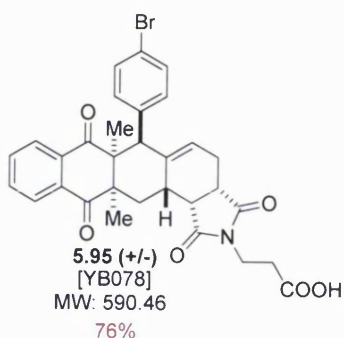
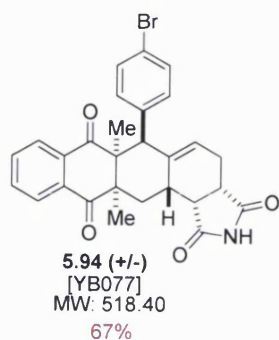
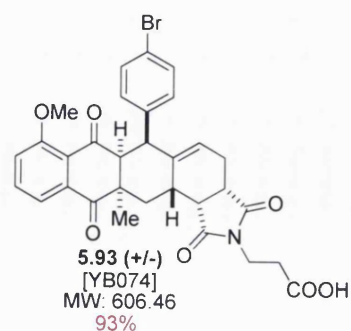
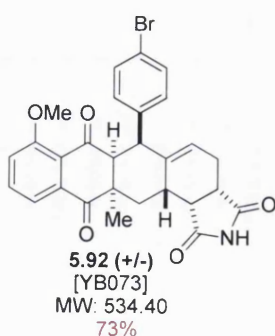
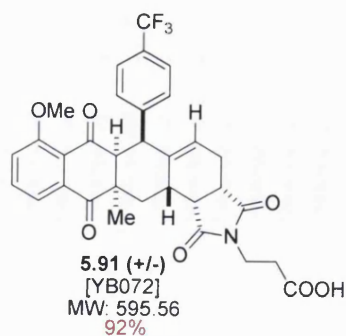
5.3.5 Synthesis of the pentacyclic compounds via DA reaction

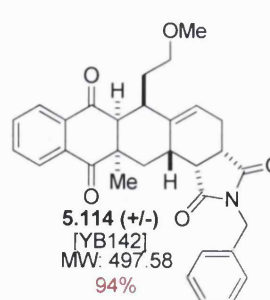
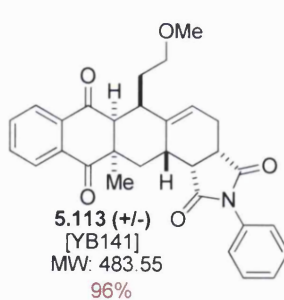
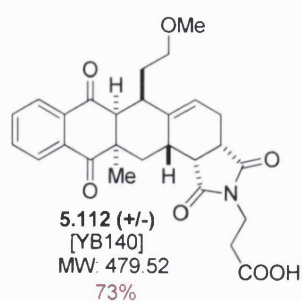
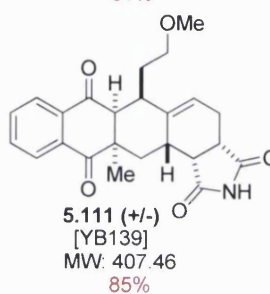
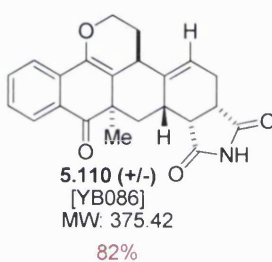
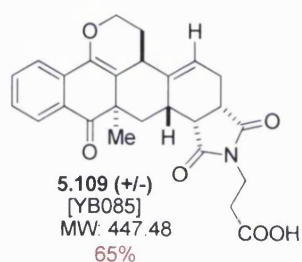
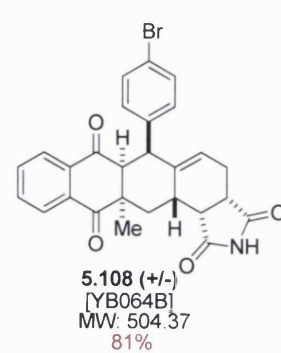
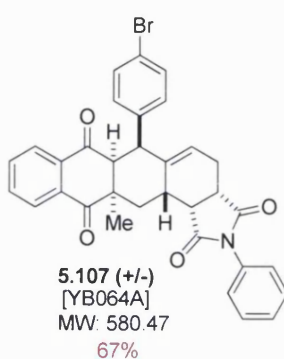
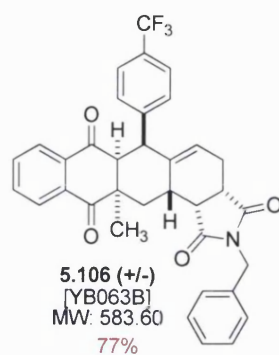
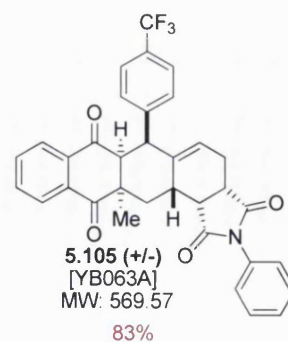
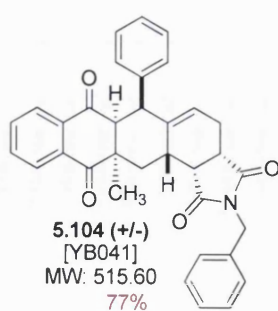
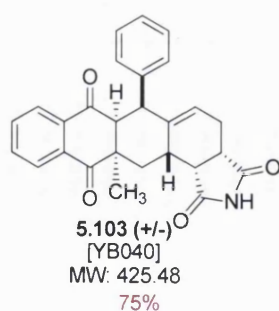
In order to build the pentacyclic final molecules, anthraquinone intermediates **5.60** – **5.78** from the initial DA were reacted with a number of commercially available *N*-maleimides **5.55**, **5.56**, **5.57** and **3.109** (Figure 5.4). These reactions were carried out in dry toluene at 70 °C for a period of time ranging from 2 hours to 5 days. The final compounds (**5.89-5.133**) were separated using either gravity column chromatography or semi-preparative HPLC to give yields varying from 19-96% (Scheme 5.13 and Figure 5.8).

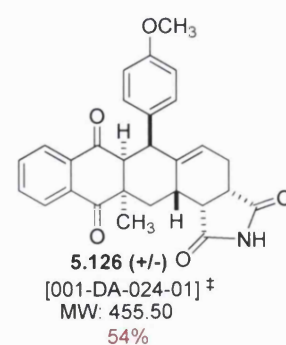
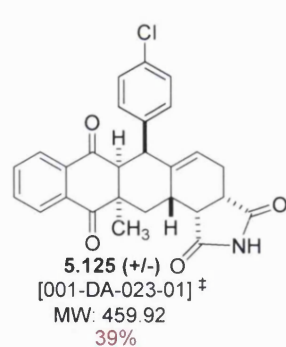
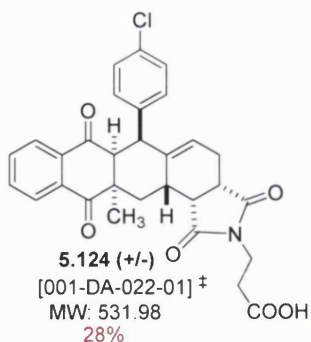
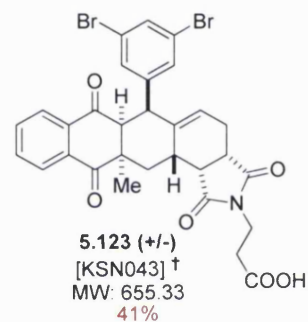
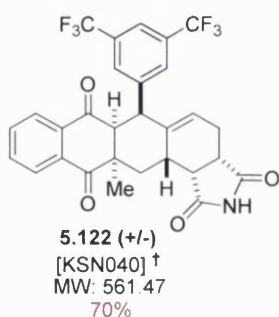
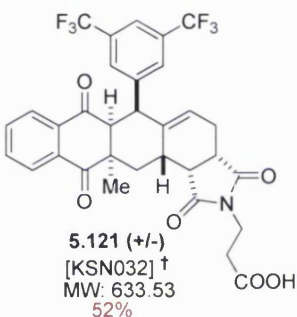
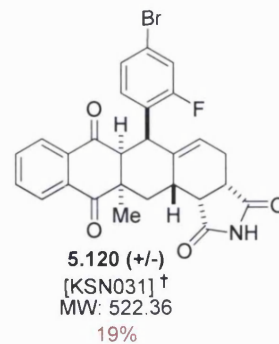
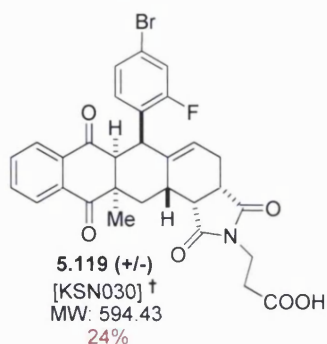
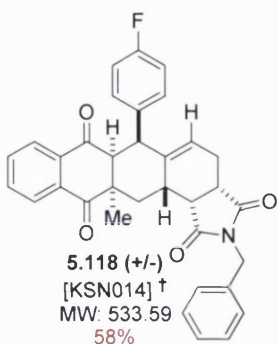
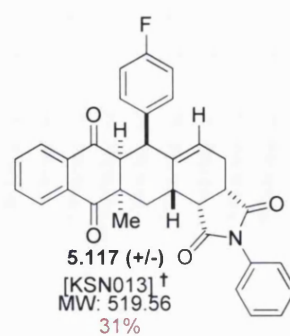
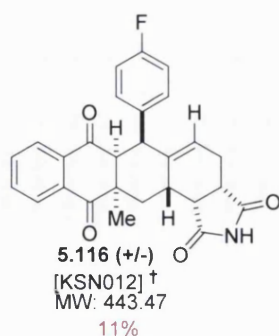
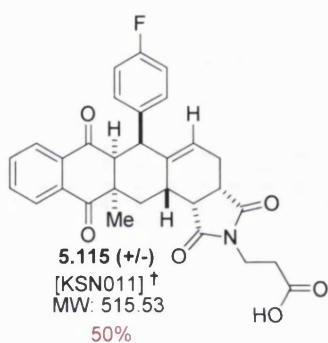


Scheme 5.13 | Procedure for DA synthesis of the tetracyclic compounds.









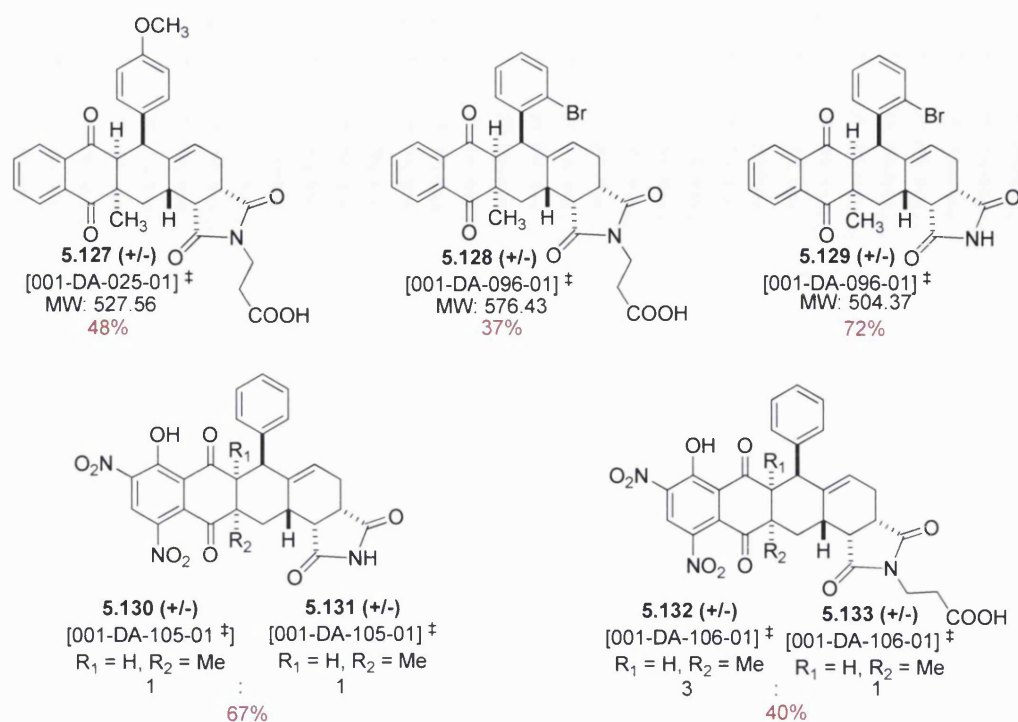
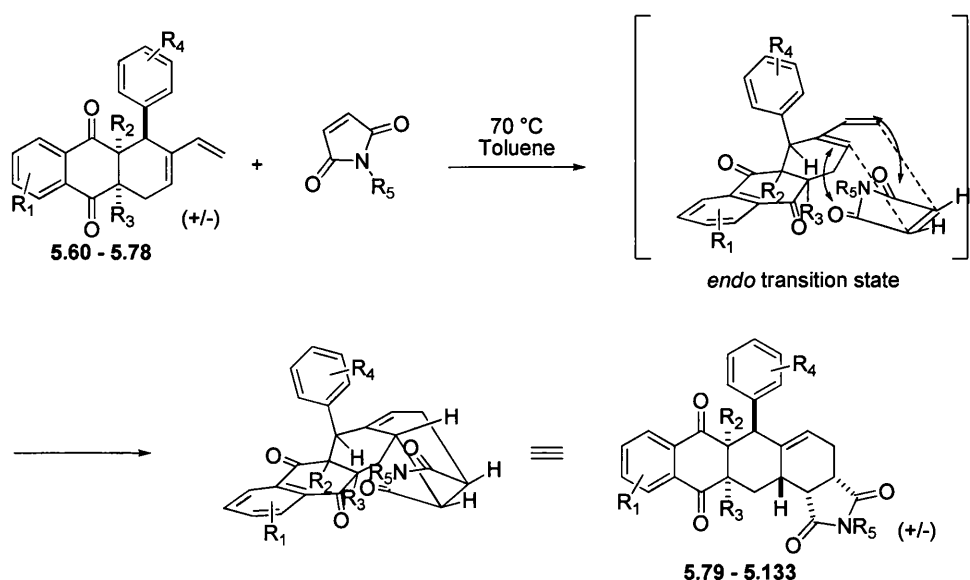


Figure 5.6 | Structures of the 54 tetracyclic compounds synthesised as potential HIF-1 α : HIF-1 β inhibitors.¹

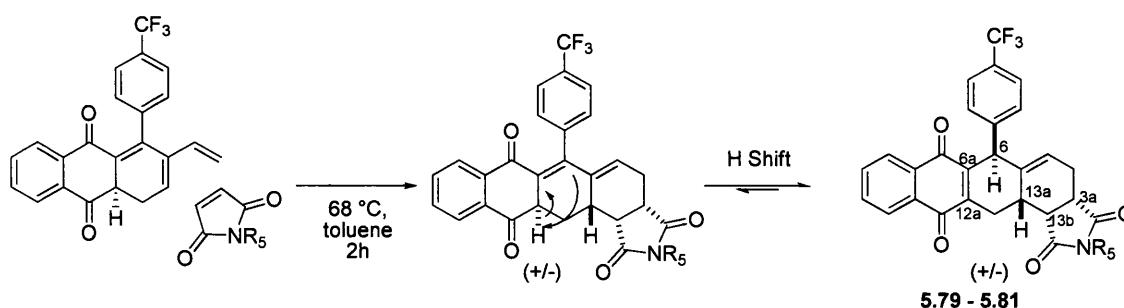
This time, there were no issues relating to regioselectivity in the second DA step, as all the maleimides used were symmetrical. Furthermore, the final compounds were pure diastereoisomers furnished from the *endo* transition state. This observation was supported by the fact that NOESY spectra which were consistent with a *cis*-selective *endo* approach of the dienophile (maleimide) opposite to the phenyl substituent of the diene (anthraquinone), an optimum orientation to avoid steric clash between these two substituents (*Scheme 5.14*). Therefore, the phenyl substituent always points in the opposite direction with respect to the maleimide. The final compounds were racemic mixtures but constitute a single diastereoisomer. The racemic nature was confirmed for a number of these compounds by a chiral separation using a normal phase chiral columns (CHIRAL-ODH and CHIRAL-IC). The enantioselective synthesis and isolation of these compounds is discussed in further detail in chapter 7.

¹ The original compound code is provided as a reference for the results shown in the biological results section. The yields for the final DA step are shown in red under each compound. The structures are grouped based on the original naphthoquinone used in their synthesis. The synthesis of compounds **5.109-5.114** will be presented in Chapter 6.



Scheme 5.14 | Suggested mechanism of action of the second and final DA cycloaddition reaction between anthraquinones **5.60–5.178** and the maleimides. The 3D model shown is a suggested schematic representation that provides a rationale for the diastereospecificity of this step.

As shown before, the first DA reaction of the unsubstituted naphthoquinone (1,4-dihydronaphthoquinone) (**3.107**) with a cross-conjugated triene generated a different type of anthraquinone derivative missing the H1 and H9a protons, and with a relatively planar shape and only one stereocentre. This intermediate was then reacted with a number of maleimides to generate a product as a single regioisomer. However, the observed products were different from that initially predicted (*Scheme 5.15*). A double bond had shifted from between C-6 and C-6a to between C-6a and C-12a, most likely driven by the re-aromatisation of the naphthoquinone. This was accompanied by a proton transfer to the C-6 position to creating a new stereocentre. The C-6-phenyl substituent was on the same surface as H-13a, but the opposite surface to that of the newly formed pyrrolidine, as shown in *Scheme 5.15*. These results were confirmed by NOESY experiments in which no correlation between H6 and H3a and H13b could be observed (refer to appendix). Furthermore, a good correlation was observed between H-13a and the protons on the phenyl substituent of C-6.



Scheme 5.15 | A possible tandem DA/ aromatisation.

5.3.6 Conclusion

In summary, the combinatorial synthesis of 54 rolitetracycline mimetics was achieved with good yields and high purities (90-99%). Each compound was prepared in 6 steps starting from 5-bromopentadiene. These molecules were progressed to biological evaluation in both cellular and cell-free assays as described below.

5.4 Biological evaluation of the tetracyclic mimetics

The interest in the synthesis and screening of tetracycline mimetics was first reported following the discovery of NSC-50352 (rolitetracycline) in the NCI diversity set as an inhibitor of HIF-1 α -PAS-A/HIF-1 β -PAS-A interaction in a cell-free assay. NSC-50352 inhibited this interaction in a concentration-dependent manner with an IC₅₀ of 1.4 μ M. However, it did not affect HIF-1-dependent luciferase expression in a cell-based assay or have any effect, which was explained by a lack of ability to permeate cells due to its polarity. The goal of this research project was to produce analogues of rolitetracycline with cell permeation properties and greater HIF-1 α /HIF-1 β interaction inhibition properties. Therefore, the biological assays described below were designed to evaluate the compounds for these properties.

5.4.1 Screening protocol

HIF-1 targeted cell-based high-throughput screens (HTS) utilise the ability of HIF-1 to bind to the hypoxia responsive element (HRE), a recognition sequence in the DNA, in order to trigger transcription.²⁰² Generally, almost all mammalian cell-lines that have been deprived of oxygen, either under a natural or induced conditions, respond by inducing HIF-1 transcriptional activity.²⁰³ Cell-based screens are performed by growing cells under hypoxic conditions (0.1-1% O₂) or by treating them with HIF-1 inducers, such as CoCl and DFO (desferoxamine). It is important to note that hypoxia mimetic

agents do not mimic the hypoxic state overall but simply work as HIF-1 α activators, and an understanding of this is crucial for interpreting the results.

Luciferase is the most commonly used reporter gene in screening assays. It offers easy measurement by non-invasive imaging of bioluminescence. One way it can be introduced is by stable transfection of HRE-luciferase reporter plasmids in cancer cell lines. In his review, Melillo has observed that this technique cannot be compared with transient transfection experiments, but is still robust enough to be used in HTS.²⁰⁴ The technique was validated initially by comparing the induction of luciferase expression when U251-HRE cells generated in Melillo's lab were subjected to hypoxia. An 8- to 12- fold induction was noted compared with untreated normoxic cells.

The detailed cell-based HTS protocol has been reported in Melillo's review. U251 human glioma cells co-transfected with pGL2-TK-HRE containing the inducible nitric oxide synthase (iNOS). The cells are maintained under normoxic conditions and hypoxia is induced by flushing the incubating flask with 1% O₂, 5%CO₂, and 94% N₂. Plasmids with mutated HRE (p-GL3-HRE) containing luciferase were used to transfect U251 cells which were employed as a secondary screen to evaluate the specificity for HIF-1 inhibition. A bright luciferase reagent is added, and, after 3 min, luminescence is measured. The toxicity of the compounds is also assayed in parallel using a fluorescent dye exclusion technique.²⁰⁴ When multiple doses of the compounds are used, the ratio of the EC₅₀ observed in control versus HRE cells (e.g., U251-pGL3/U251-HRE) should provide a fairly reliable indicator of specificity, as well as a measure of toxicity of the compounds.

Cell-based HIF-1-targeted HTS also allows for the identification of small molecules that inhibit unidentified components of the hypoxic cell signaling pathway. As a result, a number of validation assays are required to fully elucidate the mechanism of action of potential inhibitors identified in the HTS. This is shown schematically in *Figure 5.7*.

Hits from the HTS are first evaluated for their effect on inducing messenger RNA (mRNA) expression of endogenous HIF-1 target genes in hypoxic cells.²⁰⁵ A number of genes that are generally expressed in a HIF-1-dependent fashion in the majority of mammalian cells, such as vascular endothelial growth factor (VEGF), glucose transporter 1 (Glut-1) and glycolytic enzymes are assessed.

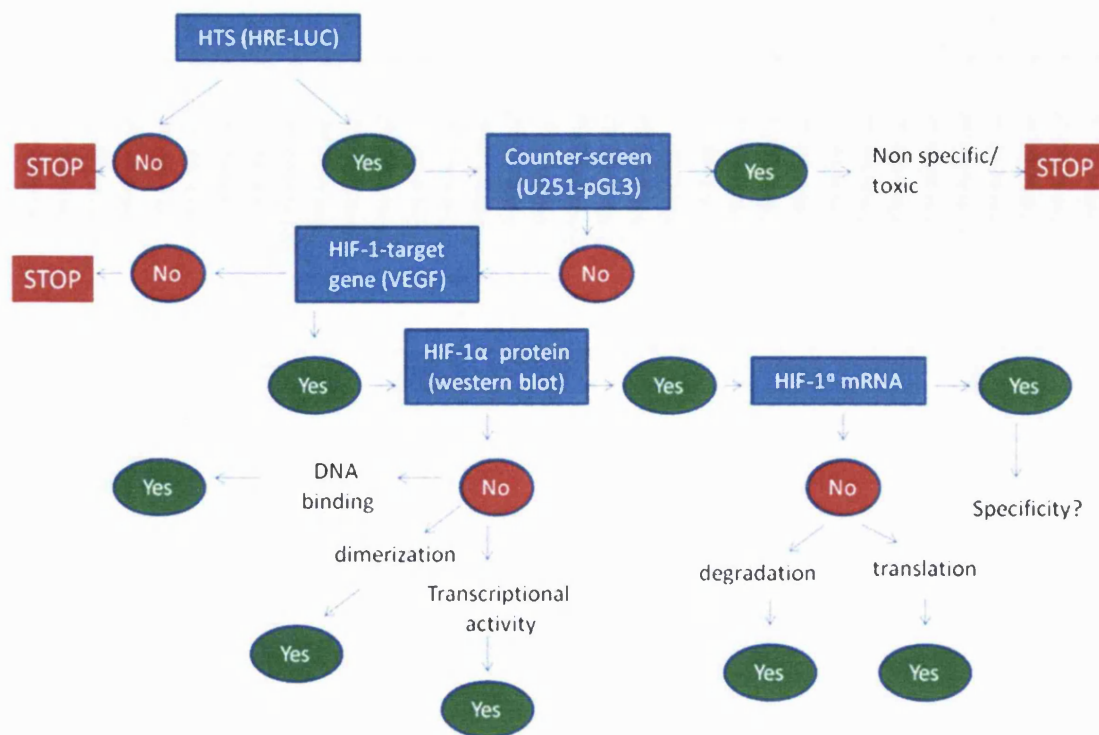


Figure 5.7 | Melillo's algorithm for validation of 'hits' identified in the HIF-1 HTS.²⁰⁴

The next stage is to perform Western blot analysis to measure the effect of inhibitors on the levels of HIF-1 α protein in cells subjected to a hypoxic state. Decreased levels of HIF-1 α protein may reflect either a decrease in protein translation or an increase in degradation. To investigate this further, the effect of inhibiting VHL-dependent proteasomal degradation with proteasome inhibitors such as PS-341 or MG-132 can be studied. However, these inhibitors can render the HIF-1 protein transcriptionally inactive.²⁰⁶ Thus, a more thorough investigation could require more sophisticated experiments using 'pulse-chase' techniques and an assessment of *de novo* HIF-1 α protein synthesis. In order to rule out an effect on mRNA expression, levels of HIF-1 α mRNA also need to be assessed.

If hypoxic induction of HIF-1 α protein accumulation is negative, this suggests that the inhibitor is affecting DNA binding, dimerization, and/or transcriptional activity. Inhibition of HIF-1 DNA binding can then be evaluated using enzyme-linked immunosorbent assay (ELISA), DNA binding, electromobility gel shift assay (EMSA) and chromatin immunoprecipitation (ChIP) assays.

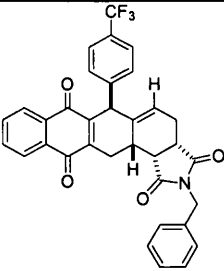
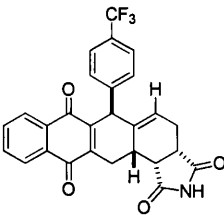
Protein-protein interaction inhibition can also be evaluated in cell-free systems using expressed proteins or in immunoprecipitation experiments on nuclear proteins from hypoxia-treated cells.⁸⁸

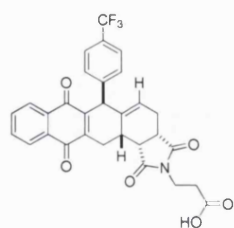
5.4.2 The first-generation library (5.79-5.89 and 5.98-5.109)

• HIF-1 α inhibition in UR51-HRE cell-based assay

The first generation library (18 members) has been screened in U251-HRE cells expressing the luciferase reporter gene in a HIF-1-dependent fashion, and in U251-pGL3 control cells (*Table 5.5* and *Figure 5.6*). Of the 18 compounds evaluated, an early SAR was obtained, and three novel compounds **5.84** (YB024), **5.99** (YB36) and **5.102** (YB39) inhibited HIF-1-dependent luciferase expression with EC₅₀ values of 6.7 μ M, 2.3 μ M and 1.4 μ M, respectively, without significantly affecting constitutive luciferase expression (as shown by the EC₅₀ (PG3/HRE) ratio in *Table 5.4*).

Table 5.5 | Results from the U251-HRE cell-based screening of the first generation library consisting of 18 tetracyclic mimetics. Topotecan (NSC-2609699) was used as a control.

Structure	Code	MW	Formula	EC ₅₀ HRE (μ M)	EC ₅₀ pGL3 (μ M)	pGL3/HRE
	5.79 [YB021]	567.55	C ₃₄ H ₂₄ F ₃ NO ₄	>20	>20	<1
	5.80 [yb027]	477.43	C ₂₇ H ₁₈ F ₃ NO ₄	>20	>20	<1



5.81
[yb028]

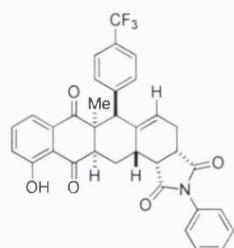
549.49

$C_{30}H_{22}F_3NO_6$

>20

>20

<1



5.82
[YB022]

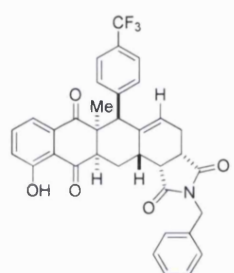
585.57

$C_{34}H_{26}F_3NO_5$

>20

>20

<1



5.83
[YB023]

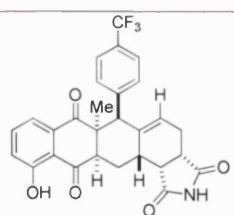
599.60

$C_{35}H_{28}F_3NO_5$

>20

>20

<1



5.84
[YB024]

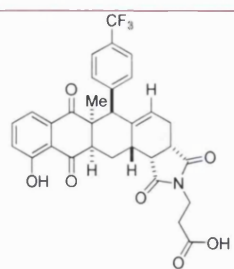
509.47

$C_{28}H_{22}F_3NO_5$

6.7

>20

>3



5.85
[YB025]

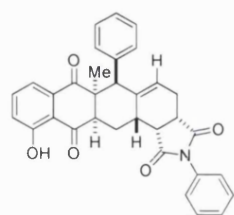
581.54

$C_{31}H_{26}F_3NO_7$

>20

>20

<1



5.86
[YB029]

517.57

$C_{33}H_{28}NO_5$

>20

>20

<1



5.87
[YB030]

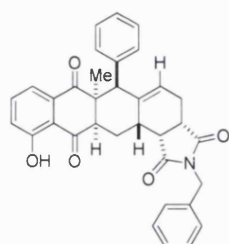
596.47

$C_{33}H_{26}BrNO_5$

>20

>20

<1



5.88
[YB031]

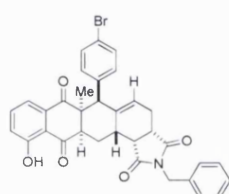
531.60

$C_{34}H_{29}NO_5$

>20

>20

<1



5.89
[YB032]

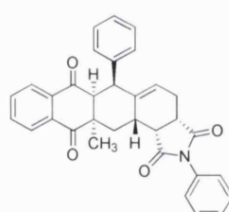
610.49

$C_{34}H_{28}BrNO_5$

>20

>20

<1



5.98
[YB026]

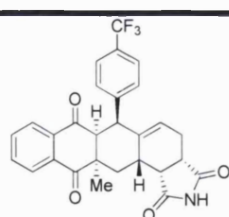
501.57

$C_{33}H_{27}NO_4$

>20

>20

<1



5.99
[YB036]

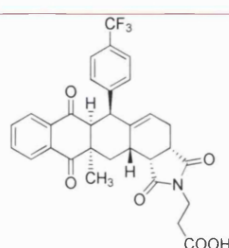
493.47

$C_{28}H_{22}F_3NO_4$

2.3

>20

>8.6



5.100
[YB037]

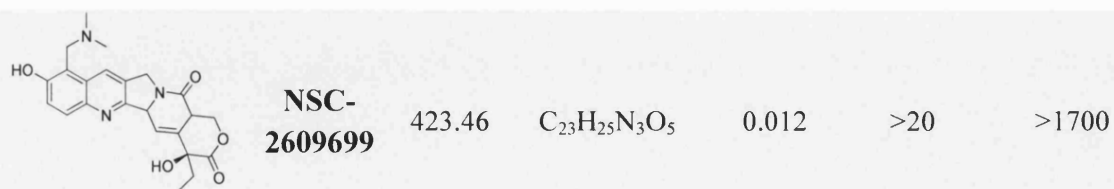
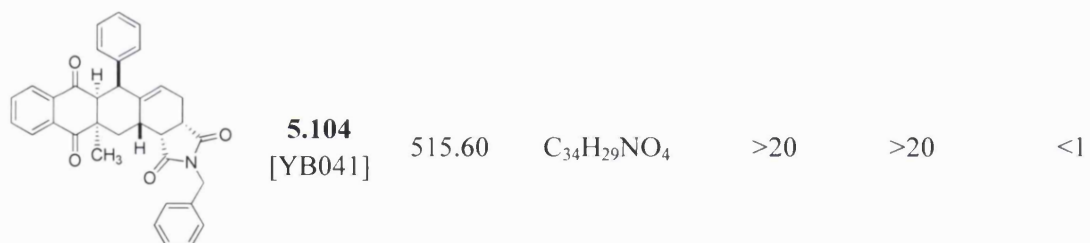
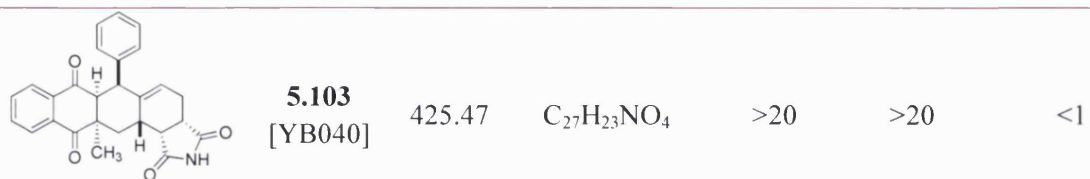
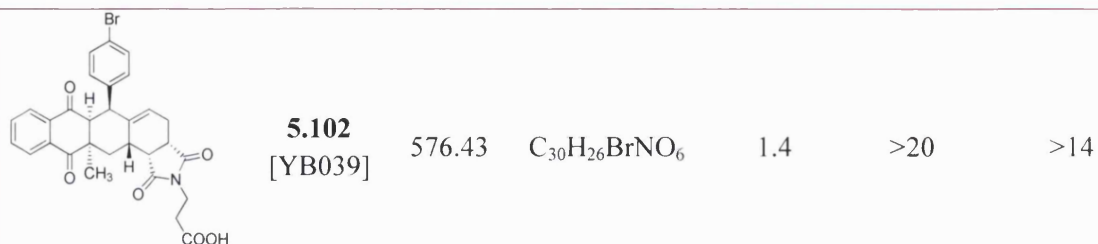
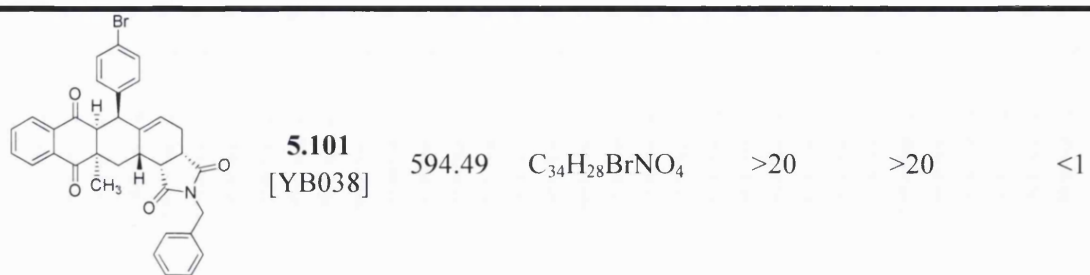
565.53

$C_{31}H_{26}F_3NO_6$

>20

>20

<1



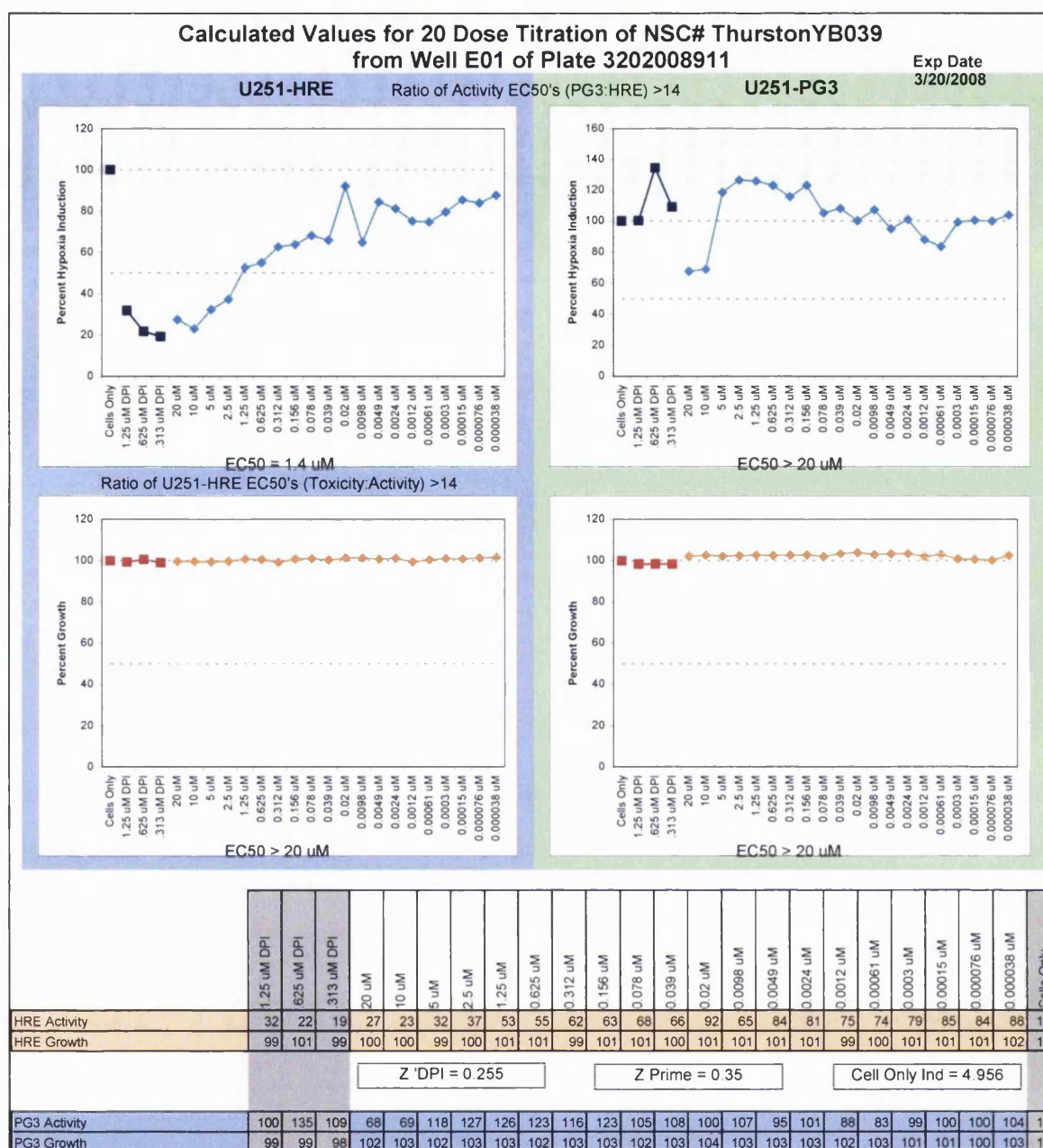


Figure 5.8 | Screening results for **5.102** (YB039) in U251-HRE cell lines (graph on the top left). The counter-screen in U251-pGL3 control cells is shown on the top right. The graphs in the lower half show no toxic/non-specific inhibition of glioma and control cell lines by this molecule. The two tables in the lower portion show the data points used in the plots.

Even though minimal structural differences exist between compounds in the initial screening batch, the structures of the top three active compounds allowed an early insight into structural features that might be responsible for the selective effect on the U251-HRE cells, as shown in *Figure 5.9*.

The presence of a double bond between the **B** and **C** rings in compounds **5.79**, **5.80** and **5.81** appeared to have no significant effect on the biological activity. The presence of this double bond in compound **5.80** ($EC_{50} > 20$) is the only significant difference compared to **5.99** ($EC_{50} = 2.3$). This suggested that cellular activity may not be associated with pentacycles possessing a double bond between rings **B** and **C**. Compounds possessing this double bond tend to have a flat architecture compared with the more concave/convex shapes formed by molecules with saturation at this position as has been demonstrated by the crystal structure.¹⁷⁶

Substitution of the *N*-pyrrolidinone (**E**-ring) appears to be crucial for the biological activity in U251-HRE cells. However, in this library, compounds possessing *N*-phenyl (**5.82**, **5.86**, **5.87** and **5.98**) and *N*-benzyl (**5.83**, **5.88**, **5.89**, **5.101** and **5.104**) substituents were not shown to inhibit luciferase expression to a significant degree $EC_{50} > 20$.

The *para*-substituent of the phenyl group attached to the **C**-ring also appeared to be important for biological activity. The absence of substituents at this position in compounds **5.86**, **5.88**, **5.98**, **5.103** and **5.104** is correlated with the absence of overall biological activity.

Another interesting observation with regard to SAR at this early stage was the association between the *para*-CF₃- group of the phenyl substituent of the **C**-ring and the NH- pyrrolidinone as reflected in the two active compounds **5.84** and **5.99**. Conversely, absence of activity is noted in **5.85** and **5.97**, which have pentanoic acid fragment present in the *N*-pyrrolidinone **E**-ring and a *para*-CF₃- on the phenyl substituent of the **C**-ring. Furthermore, the presence of *para*-Br at the phenyl of the **C**-ring seems to be only of importance when the substituent at the **E**-ring is propanoic acid (**5.102**). This association could be confirmed through the synthesis and biological evaluation of a compound bearing a *para*-Br-phenyl on the **C**-ring and no substituent in the **E**-ring.

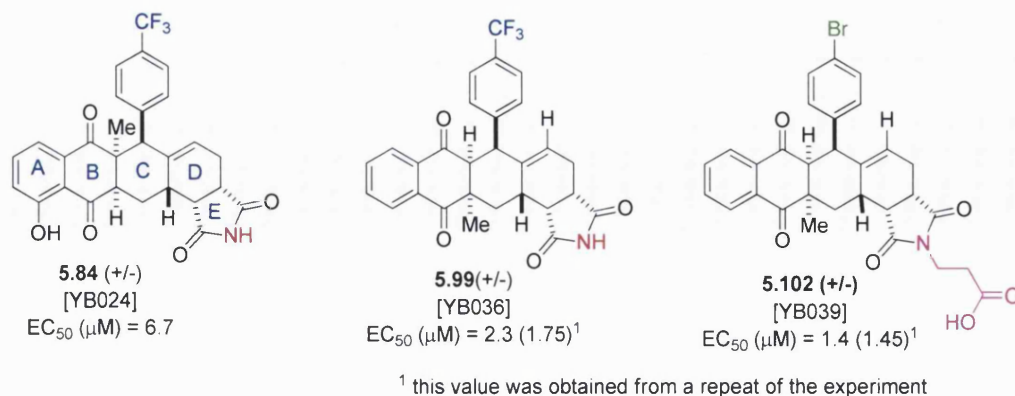
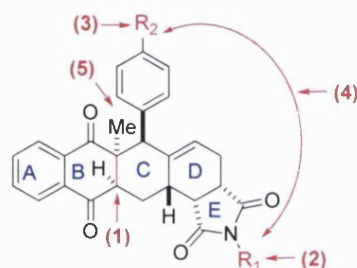


Figure 5.9 | The top three hits identified from screening the first generation library in cell-based assay.

Summary of the initial SAR for significant biological activity



- 1) The pentacyclic scaffold should not have a double bond between rings **C** and **B**.
- 2) No activity was observed with phenyl- and benzyl-substituted *N*-pyrrolidinone portion.
- 3) *Para*-Br and *para*-CF₃ substituents on the phenyl substituent attached to ring **C** show the most significant activity compared to those with unsubstituted phenyl rings.
- 4) There could be an association between *para*-CF₃-phenyl and NH-pyrrolidinone and between *para*-Br-phenyl and propanoic acid-*N*-pyrrolidinone.
- 5) The orientation of the methyl substituent (i.e. *ortho*- or *para*-) to the phenyl substituent on ring **C** has a small but not substantial effect on the activity of the overall molecule with the *para*- positioning giving the smallest EC_{50} .

• Effects on mRNA expression of a downstream target (VEGF)

Validation of the two leading HIF-1 inhibitors **5.99** (YB036) and **5.102** (YB039) was initially carried out by studying their effect on the hypoxic induction of VEGF mRNA expression. Under hypoxic conditions, compounds YB036 and YB039 inhibited the induction of VEGF mRNA expression. Inhibition was measured after 16 hours using

two concentrations. At 1 μ M, YB036 and YB039 inhibited VEGF mRNA expression by 35% and 45% respectively, whereas at 10 μ M the inhibition reached 59% and 69%, respectively (*Figure 5.10*).

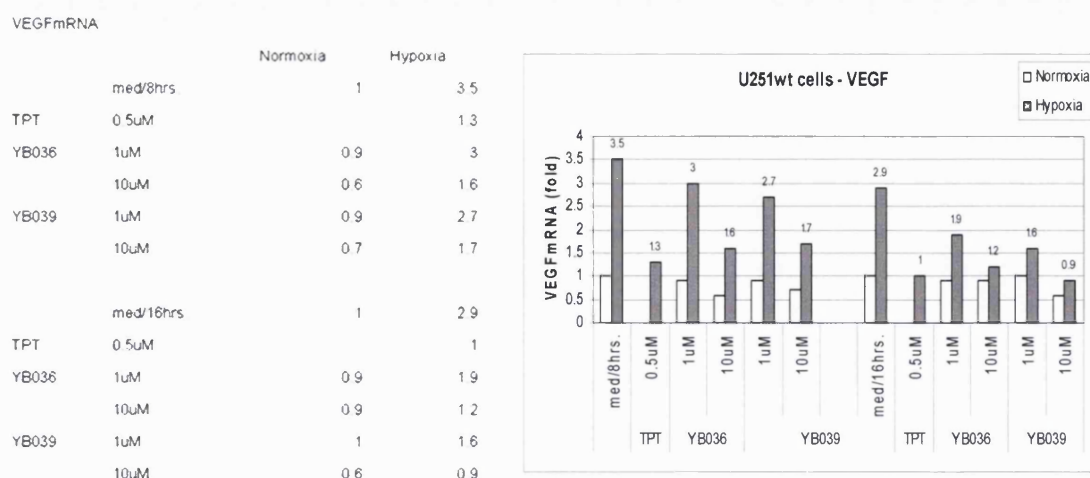


Figure 5.10 | Inhibition of induction of VEGF mRNA expression.

- Effects on HIF-1 α mRNA expression**

Levels of HIF-1 α mRNA were also measured to investigate the direct effect of YB036 and YB039 on protein expression. Inhibition of HIF-1 α mRNA expression in U251 wt cells cultured under hypoxic conditions, evaluated after 8 hours of adding YB036 and YB039, showed a decrease of 29% and 43%, respectively (*Figure 5.11*). After 16 hours, the inhibition increased to 43% and 78% respectively.

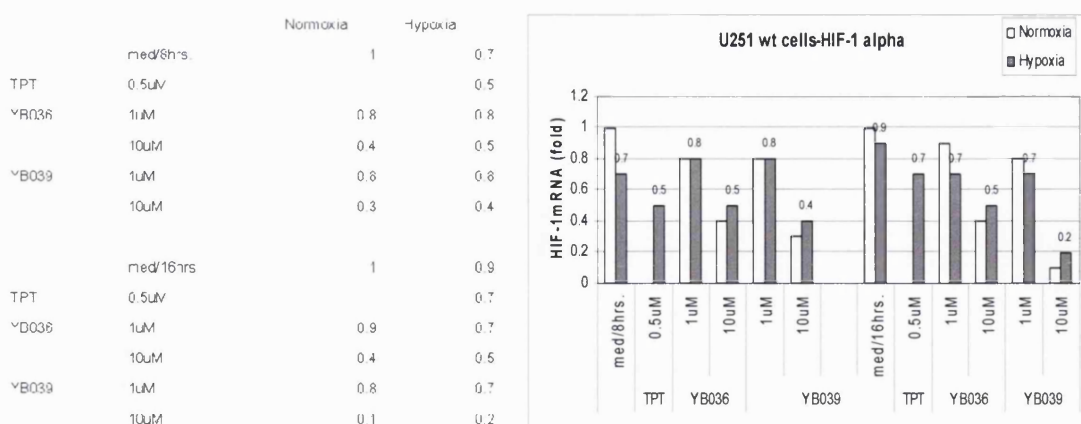


Figure 5.11 | Inhibition of the induction of HIF-1 α mRNA expression.

- **Evaluation of the inhibition of HIF-1 α protein accumulation**

Further studies to elucidate the mechanism of action of compounds **5.99** (YB036) and **5.102** (YB039) involved Western blot analysis to measure the accumulation of HIF-1 α protein in cells cultured under hypoxia compared those growing under normoxia.

In summary, both molecules inhibited hypoxic induction of HIF-1 α protein accumulation in U251 wt cells in a dose-dependent fashion. A full inhibition at 5 μ M was observed for YB039, whereas YB036 gave a complete inhibition at 10 μ M. A similar level of inhibition was also observed under normoxic conditions after 16h. Neither of the molecules had any effect on HIF-1 β (*Figure 5.12*).

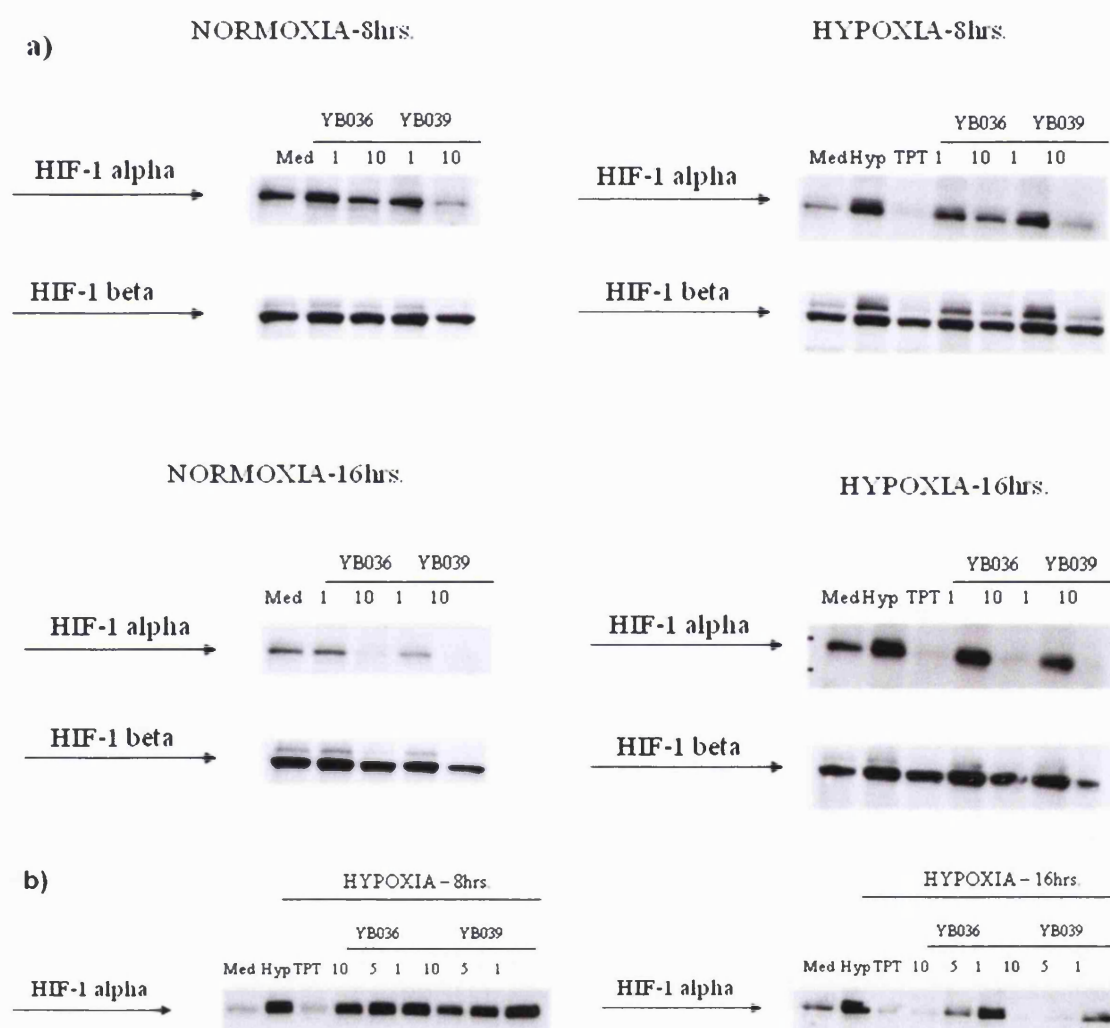
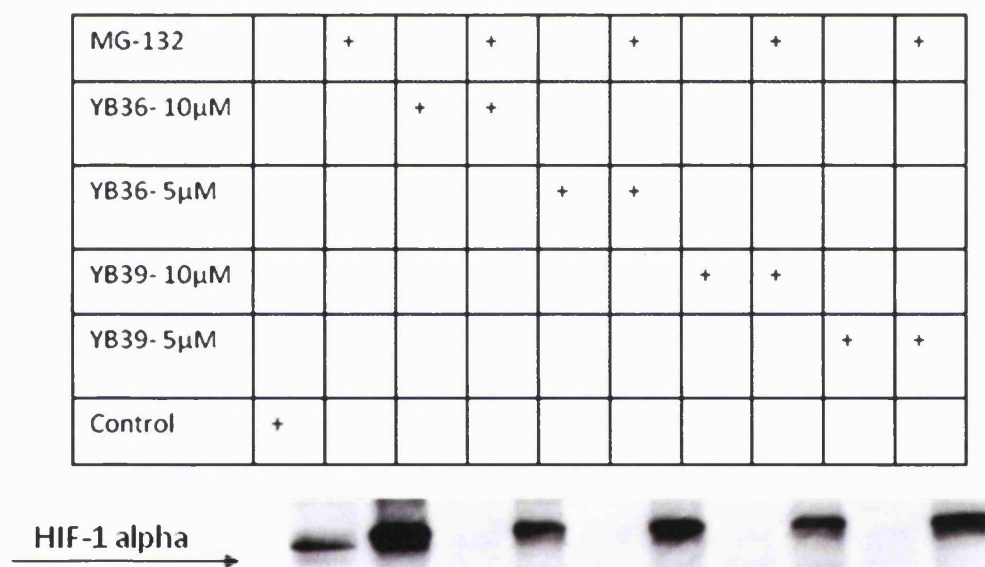


Figure 5.12 | a) The effect of **5.99** (YB036) and **5.102** (YB039) on HIF-1 α and HIF-1 β expression in U251 wt cells compared with topotecan (TPT). **b)** Exploring a wider range of concentrations.

- **Studies on Interference with proteasomal degradation of HIF-1 α**

To evaluate the involvement of VHL-dependent proteasomal degradation, a similar Western blot analysis was conducted in the presence of the proteasomal inhibitor, MG-132, in an experiment in which HIF-1 α was constitutively expressed under normal oxygen levels. The second column from the left in *Figure 5.13* shows the accumulation of HIF-1 α under normoxia as a result of the presence of MG-132. YB036 or YB039, without MG-132 gave complete inhibition of HIF-1 α protein expression (*Figure 5.13*). A mixture of MG-132 and either YB036 and YB039 allowed the accumulation of HIF-1 α protein to a level similar to that found in the control, suggesting that YB036 and YB039 can overcome the effect of proteasomal inhibition. One possibility is that YB036 and YB039 induce proteasomal degradation of the HIF-1 α protein although potential mechanism would require further studies.¹⁰²



Cells were seeded in a 100 mm dish. The following day, they were pre-treated with MG-132 (20 μ M) for 30 minutes, then compounds YB036 and YB039 were added at 5 and 10 μ M for 16hrs under normoxia. Lysed cells, run 80 μ g protein in 4-20% Tris-Glycine gel for 1.5 hours, then transferred for 3hrs.

Figure 5.13 | Evaluation of the effect on the modulation of proteasomal inhibition of HIF-1 α expression in U251 wt cells by **5.99** (YB036) and **5.102** (YB039).

Summary after the first generation screening:

- The first library screening in U251-HRE cells enabled the identification of three hit molecules: **5.84** (YB024, EC₅₀ = 6.7 μ M), **5.99** (YB036, EC₅₀ = 2.3 μ M) and **5.102** (YB039, EC₅₀ = 1.4 μ M) with development of an early SAR.

- The specificity of these hits was confirmed by measuring the ratio of the EC₅₀ observed in control *versus* HRE cells. The high values obtained were indicative of specificity.
- The two top hits, **5.99** and **5.102**, were further evaluated for their mode of action, and initially shown to inhibit the hypoxic induction of messenger RNA expression of an endogenous HIF-1 target gene (VEGF). This suggested that they were working by disrupting the HIF-1 signalling pathway.
- Next, Western Blot evaluation of the HIF-1 α protein showed an inhibitory effect for **5.102** (YB039) at 5 μ M, and for **5.99** (YB036) at 10 μ M after 16 hours of incubation under hypoxia. This observation suggested that these molecules impair HIF-1 α protein translation or enhance its degradation. The results of further experiments in the presence of proteasome inhibitors suggested that the top two hits may induce VHL-dependent proteasomal degradation of HIF-1 α .
- **5.99** (YB036) and **5.102** (YB039) inhibited HIF-1 α messenger RNA expression by 43% and 78%, respectively after 16 hours. This suggests a different mode of action for these molecules than that intended or possibly a “feedback loop” mechanism that could account for reduced expression of HIF-1 α .⁹⁷

5.4.3 The second-generation library (5.90-5.97, 5.115-5.118 and 5.124-5.127)

These encouraging results and the SAR information obtained (*Figure 5.14*) led to the synthesis of a second library (22 members) **5.90-5.97**, **5.115-5.118** and **5.124-5.127**, in order to improve potency and to further evaluate SAR. This library was screened in U251-HRE cells expressing the luciferase reporter gene in a HIF-1-dependent fashion, and in U251-pGL3 control cells (*Table 5.5*).

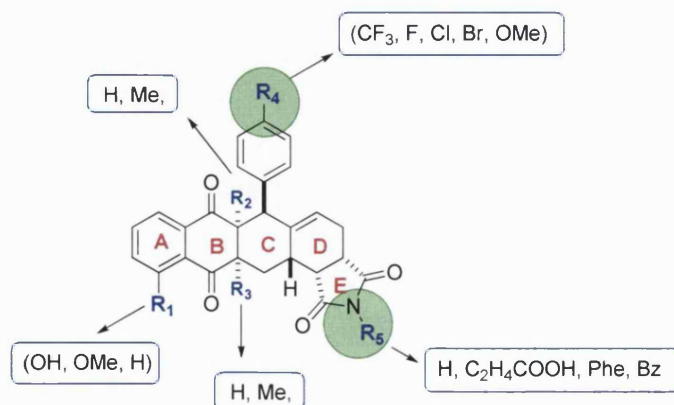

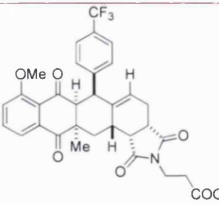
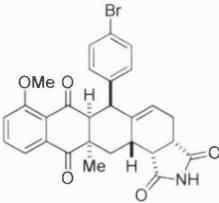

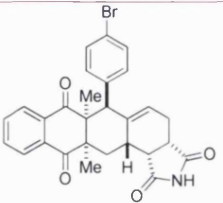
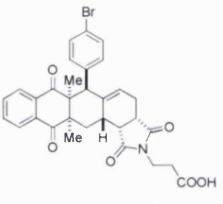
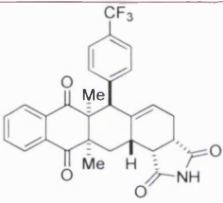
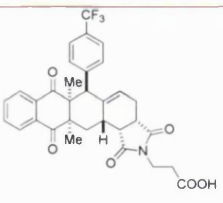
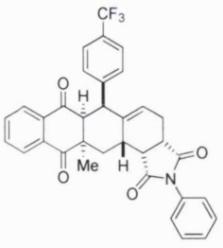
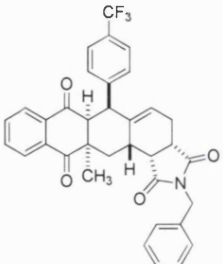


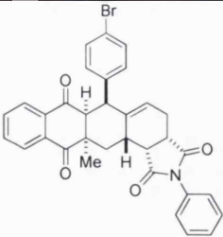
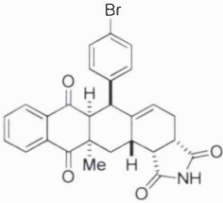
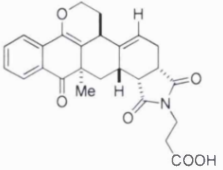
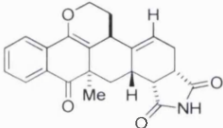
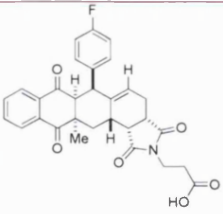
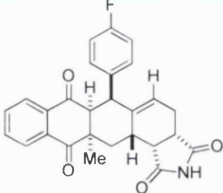
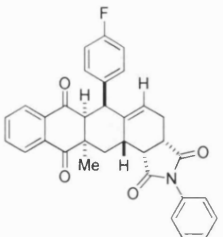
Figure 5.14 | Essential points of variation as derived from the initial screening. The circled substituents were shown to significantly alter the biological activity.

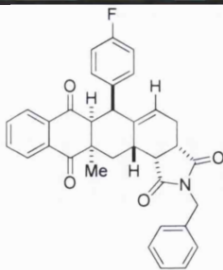
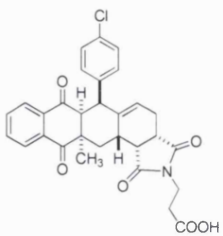
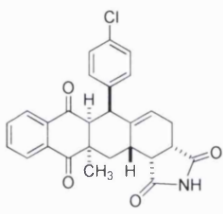
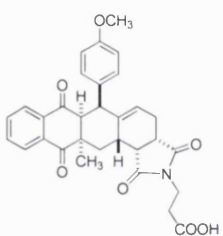
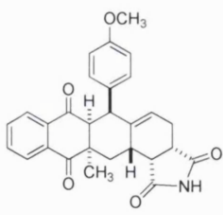
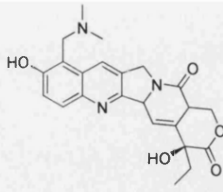
Of the 22 compounds, three novel compounds **5.93** (YB074), **5.96** (YB081) and **5.115** (KSN011) inhibited HIF-1-dependent luciferase expression with EC₅₀ values of 15.5 μM, 7.8 μM and 4.1 μM, respectively (Table 5.6). Although the potency of those compounds was comparable to the hits from the previous library, **5.93** (YB074) and **5.96** (YB081) did not affect luciferase expression in the pGL3 cell line, thus potentially allowing a therapeutic index.

Table 5.6 | Results of the U251-HRE cell-based screening of the second library consisting of 22 tetracyclic mimetics **5.90-5.97**, **5.115-5.118** and **5.124-5.127**, and compared with topotecan (NSC-2609699).

Structure	Code	MW	Formula	EC ₅₀ HRE (μM)	EC ₅₀ pGL3 (μM)	pGL3/HRE
	5.90 [YB071]	523.50	C ₂₉ H ₂₄ F ₃ NO ₅	6.7	>20	>3
	5.91 [YB072]	595.56	C ₃₂ H ₂₈ F ₃ NO ₇	>20	>20	<1
	5.92 [YB073]	534.40	C ₂₈ H ₂₄ BrNO ₅	>20	>20	<1

	5.93 [YB074]	606.46	$C_{31}H_{28}BrNO_7$	15.5	>20	>1.4
	5.94 [YB077]	518.40	$C_{28}H_{24}BrNO_4$	>20	>20	<1
	5.95 [YB078]	590.46	$C_{31}H_{26}BrNO_6$	>20	>20	<1
	5.96 [YB081]	507.17	$C_{29}H_{24}F_3NO_4$	7.8	>20	>2.7
	5.97 [YB082]	579.56	$C_{32}H_{28}F_3NO_6$	>20	>20	<1
	5.105 [YB063a]	569.57	$C_{34}H_{26}F_3NO_4$	>20	>20	<1
	5.106 [YB063b]	583.60	$C_{34}H_{26}F_3NO_4$	>20	>20	<1

	5.107 [YB064a]	580.47	$C_{35}H_{26}BrNO_4$	>20	>20	<1
	5.108 [YB064b]	504.37	$C_{27}H_{22}BrNO_4$	>20	>20	<1
	5.109 [YB085]	465.50	$C_{26}H_{27}NO_7$	>20	>20	<1
	5.110 [YB086]	393.43	$C_{23}H_{23}NO_5$	>20	>20	<1
	5.115 [KSN011]	515.53	$C_{30}H_{26}FNO_6$	4.1	8.7	2.15
	5.116 [KSN012]	443.47	$C_{27}H_{22}FNO_4$	>20	>20	<1
	5.117 [KSN013]	519.56	$C_{33}H_{26}FNO_4$	>20	>20	<1

	5.118 [KSN014]	533.59	$C_{34}H_{26}FNO_4$	>20	>20	<1
	5.124 [001-DA-022-01]	531.98	$C_{30}H_{26}ClNO_6$	>20	>20	<1
	5.125 [001-DA-023-01]	459.92	$C_{27}H_{22}ClNO_4$	>20	>20	<1
	5.126 [001-DA-025-01]	527.56	$C_{31}H_{29}NO_7$	>20	>20	<1
	5.127 [001-DA-024-01]	455.50	$C_{28}H_{25}NO_5$	>20	>20	<1
	NSC 2609699	423.46	$C_{23}H_{25}N_3O_5$	0.047	>20	>4200

These results confirmed the earlier SAR but did not provide any significantly new information (*Figure 5.15*). Therefore, the synthesis of a third small library was proposed

(Figure 5.16) to investigate changes to 5.111, 5.112, 5.113, 5.114, 5.119, 5.120, 5.121, 5.122, 5.123, 5.128, 5.129, 5.130, and 5.132.

None of these compounds showed any significant activity (i.e. $<20 \mu\text{M}$) in either the U251-HRE or U251-pGL3 cell lines. However, at the time of testing, the NCI reported having growth problems with their cell lines and the third library will be re-tested in the future (results not available at this time).

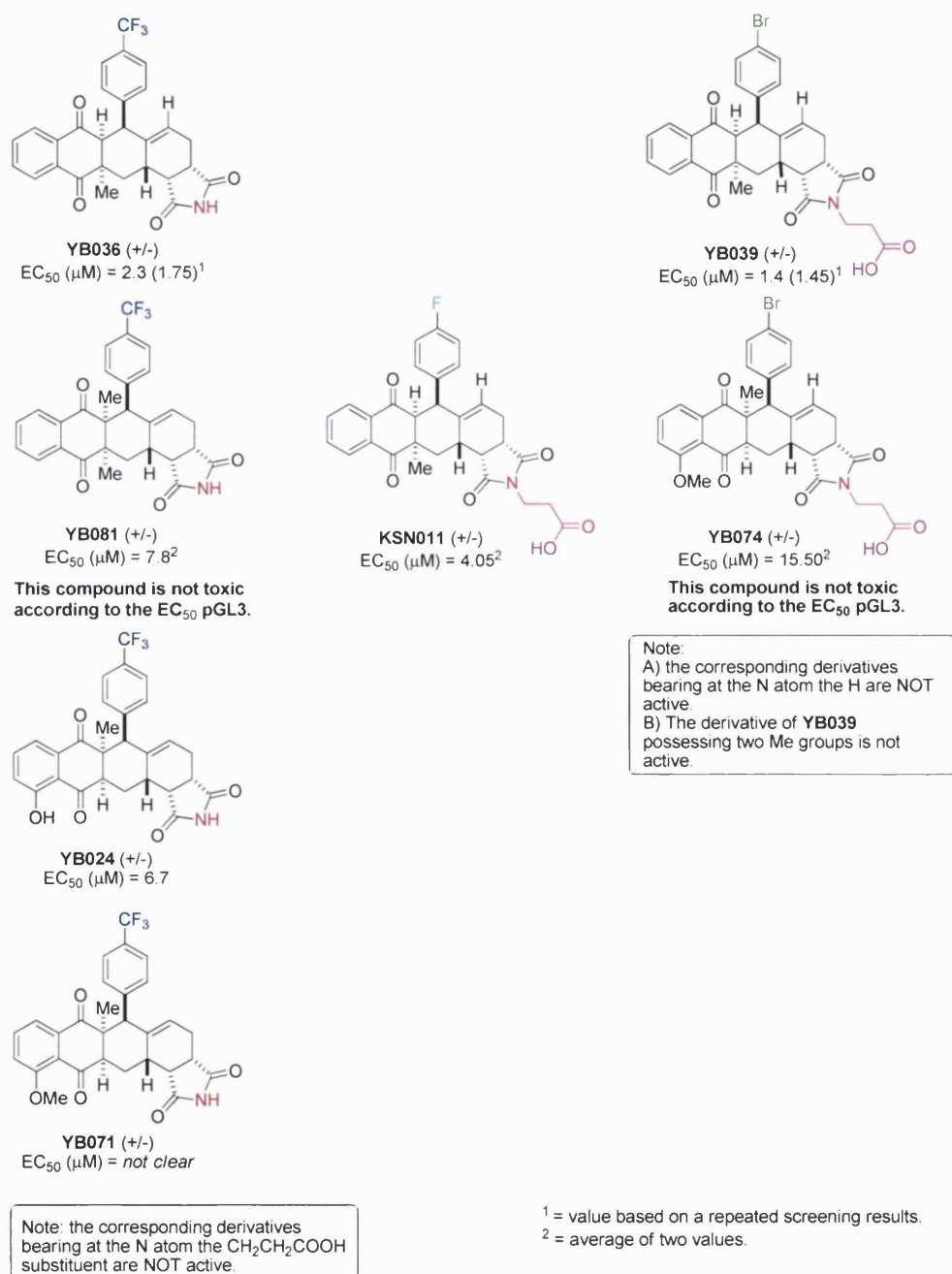


Figure 5.15 | The most active compounds derived from two generation library screenings and their activity and structural features.

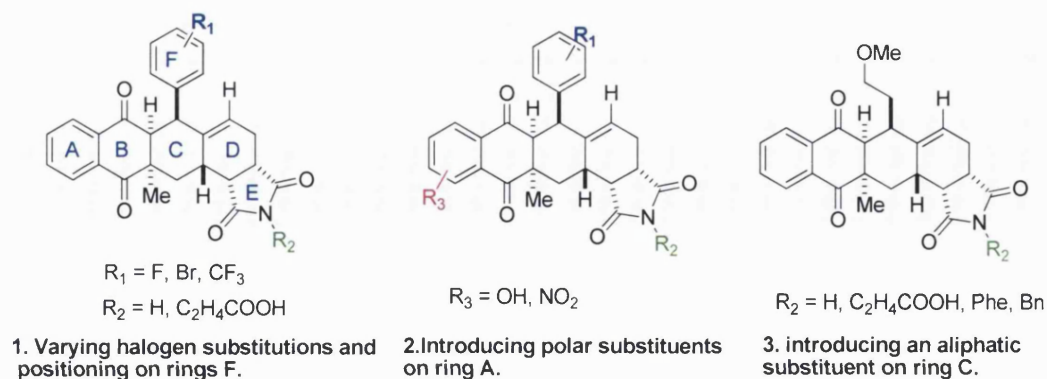


Figure 5.16 | Proposed structural modifications for the preparation of a third library.

Finally, due to the structural similarities of library with naturally-occurring tetracyclines, it was decided to screen a number of the synthesised molecules for antibacterial activity in gram-negative and gram-positive bacteria (*Table 5.7*). Only one molecule (**5.115**, KSN011) showed some activity in streptococcus pneumonia with MIC of 8 $\mu\text{g/ml}$. This activity was 32 fold lower than for tetracycline itself.

Table 5.7 | Minimum inhibitory concentrations for tetracycline (TET) and tetracycline mimetics against Gram-negative and Gram-positive bacteria

Organism	Minimum inhibitory concentration (µg/ml)													
	TET	YB024	YB030	YB036	YB038	YB039	YB040	YB071	YB074	YB081	YB085	YB086	KSN011	
Gram-negative														
<i>Escherichia coli</i>	0.5	>64	>64	>64	>64	>64	>64	>64	>64	>64	>64	>64	>64	
<i>Escherichia coli</i> G69	>64	>64	>64	>64	>64	>64	>64	>64	>64	>64	>64	>64	>64	
<i>Klebsiella pneumoniae</i> 344	2	>64	>64	>64	>64	>64	>64	>64	>64	>64	>64	>64	>64	
<i>Proteus mirabilis</i> 10830	>64	>64	>64	>64	>64	>64	>64	>64	>64	>64	>64	>64	>64	
<i>Pseudomonas aeruginosa</i>	32	>64	>64	>64	>64	>64	>64	>64	>64	>64	>64	>64	>64	
<i>Acinetobacter baumannii</i> 19606	4	>64	>64	>64	>64	>64	>64	>64	>64	>64	>64	>64	>64	
<i>Stenotrophomonas maltophilia</i>	2	>64	>64	>64	>64	>64	>64	>64	>64	>64	>64	>64	>64	
Gram-positive														
<i>Enterococcus faecalis</i> 13379	2	64	>64	>64	64	>64	>64	>64	>64	>64	>64	>64	>64	
<i>Enterococcus faecalis</i> 12697	16	32	64	>64	32	>64	>64	>64	>64	>64	>64	>64	>64	
<i>Staphylococcus aureus</i> 12981	0.25	>64	>64	>64	>64	>64	>64	>64	>64	>64	>64	>64	>64	
<i>Staphylococcus aureus</i> 13373	0.25	32	>64	>64	>64	>64	>64	>64	>64	>64	>64	>64	>64	
<i>Streptococcus pneumoniae</i>	0.25	64	>64	>64	>64	>64	>64	>8	>64	>8	>8	>64	8	

Notes:

1. MIC values were determined following Clinical Laboratory Standards Institute guidelines.
2. The tetracycline MIC values for reference isolates are within acceptable quality control ranges.

5.5 Conclusions

The aim of this project was to develop molecules that share essential structural features with rolitetracycline,⁸⁸ a naturally-occurring compound shown to inhibit the HIF-1 α :HIF-1 β protein protein interaction in cell-free (ELISA) assays, but with cell permeability characteristics, and a greater potency and selectivity.

A series of rolitetracycline mimetics were designed that possessed a similar tetracyclic scaffold to rolitetracycline and that could be prepared in 6 steps. The route was also sufficiently versatile to allow a broad range of structural modifications and subsequent patterns to examine SARs. The synthesis started with by the construction of a cross-conjugated triene (4 steps) which could then be reacted with naphthoquinone and maleimide fragments in two consecutive stereoselective DA cycloadditions to afford the final pentacyclic structures.

A first generation library (18 tetracycline mimetics) was screened at the NCI in a cell-based assay using U251-HRE cells expressing a HIF-1 dependent luciferase reporter gene. Specificity was monitored using a control assay in U251-pGL3 cells lacking the HIF-1 promotor. Of the 18 compounds, a discernable SAR was obtained, and three compounds **5.84** (YB024), **5.99** (YB036) and **5.102** (YB039) were identified as inhibitors of HIF-1-dependent luciferase expression with EC₅₀ values of 6.7 μ M, 1.75 μ M and 1.45 μ M, respectively. Interestingly, **5.99** (YB036) and **5.102** (YB039) also inhibited hypoxic induction of HIF-1 α protein accumulation in U251 wt cells in a dose-dependent fashion, but had no effect on constitutively expressed HIF-1 β . These molecules also inhibited induction of VEGF mRNA expression by 59% and 69%, respectively, in U251 wt cells cultured under hypoxic conditions, confirming that some element of the HIF-1 signalling pathway was being down-regulated.

A second generation library (22 compounds) identified three novel compounds **5.93** (YB074), **5.96** (YB081) and **5.115** (KSN011), which inhibited HIF-1-dependent luciferase expression with EC₅₀ values of 15.5 μ M, 7.8 μ M and 4.1 μ M, respectively. A third generation library of 13 compounds failed to show any activity, although this was thought to be due to a malfunction of the NCI assay and these compounds will be re-tested in the future.

Finally, all library members were evaluated for antimicrobial activity against tetracycline as a control, however none was significantly active.

In conclusion, through the synthesis of 54 rolitetracycline mimetics, this work has produced some lead molecules of low micromolar potency that clearly down-regulate the HIF-1 signalling pathway. Most significantly, the goal was achieved of producing some analogues of rolitetracycline with the ability to penetrate cell membranes. Furthermore, some of the molecules have a selective ability to down-regulate HIF-1 α in comparison to HIF-1 β . It is possible that, based on the SAR information obtained in this study, future generations of molecules could be designed with sub-micromolar potency that might be progressed to *in vivo* evaluation.

CHAPTER 6

One-pot synthesis of fused-tetracyclic scaffolds employing a
Lewis acid-catalyzed domino reaction of naphthoquinones

Contents:

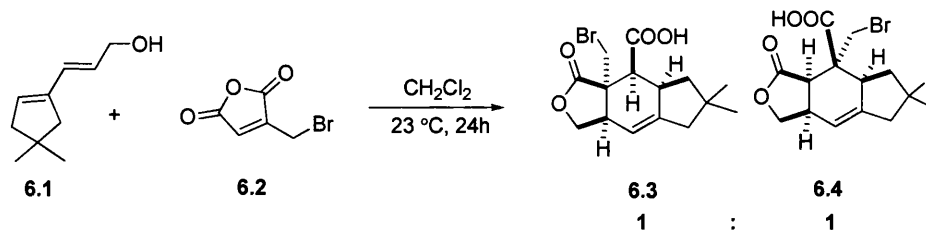
6.1	Introduction	121
6.2	Results and discussion	123
6.3	Conclusions	131

6.1 Introduction

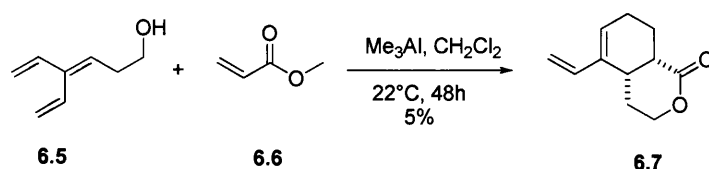
The scaffolds of many potent and selective protein-protein interaction (PPI) inhibitors²⁰⁷ are naturally occurring molecular frameworks possessing tetra- or pentacyclic fused rings containing at least one phenyl system. This confers a rigid 3-D geometry crucial for target selectivity. Endocyclic nitrogen and/or oxygen atoms are also often present in these frameworks.¹ In the course of searching for novel PPI inhibitors,²⁰⁸ our synthetic efforts have focused on tetracyclic templates utilizing the Diels-Alder cycloaddition for efficient and stereospecific construction of fused-carbocyclic rings. In particular, use of a 1,4-naphthoquinone as a dienophile allows direct introduction of a phenyl moiety, and 1-hydroxyl- or 1-amino-functionalized dienes can afford fused heterocyclic systems *via* hemiacetal or imine formation in a domino process with an intermolecular Diels-Alder cycloaddition.

There are only four previous examples that describe a similar domino process. However, the use of *monodentate* Lewis acids has never been investigated,²⁰⁹⁻²¹² The Woodward-Greenlee synthesis of marasmic acid²⁰⁹ (*Scheme 6.1 - a*) and the synthetic studies of Fallis and co-workers²¹⁰ (*Scheme 6.1 - b*) involved simple dienophiles such as methyl acrylate **6.6** or maleic anhydride **6.2**, with only oxygen-based dienes such as the 1-hydroxyl cross-conjugate triene **6.5** and 3-(4,4-dimethylcyclopent-1-enyl)-prop-2-en-1-ol **6.1**. Furthermore, the Woodward-Greenlee synthetic approach involved a thermal Diels-Alder cycloaddition and no Lewis acid catalyst was used, whereas Fallis and co-workers investigated a domino process with the use of *bidentate* Lewis acids (AlMe₃). In both these reaction sequences, the Diels-Alder cycloadditions were shown to be intermolecular followed by formation of the lactone. The other two examples involved the use of quinones as dienophiles.

a) Woodward-Greenlee synthesis of marasmic acid



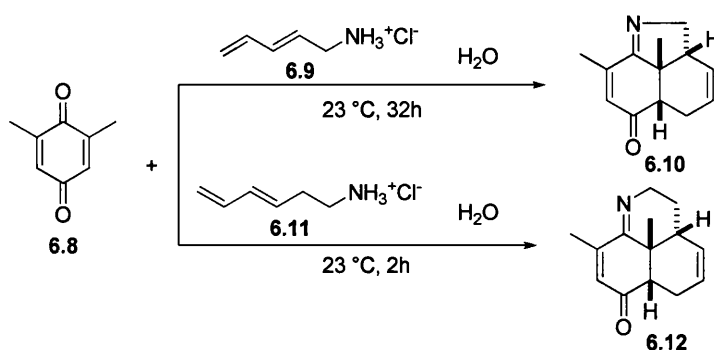
b) Fallis trienol Diels-Alder



Scheme 6.1 | *a)* Woodward-Greenlee's uncatalysed domino Diels-Alder cycloaddition and lactam ring formation during marasmic acid synthesis. *b)* Fallis' bidentate Lewis acid-catalysed domino Diels-Alder reaction and cyclisation.

Grieco and co-workers²¹² reported a more similar domino process to the one we describe here for nitrogen-based dienes. This involved Diels-Alder cycloaddition of symmetrically substituted (*i.e.*, 2,6- or 2,5-substitued) benzoquinones with dienyl ammonium chlorides (**6.9** and **6.11**) in which the formation of cyclic imines (**6.10** and **6.12**) was observed (*Scheme 6.2*). This domino process, however, was conducted in a protic solvent (*i.e.*, water) using a Brønsted acid (*i.e.*, HCl), and Lewis-acid catalysis was not investigated. Furthermore, the sequence of reactions in such a domino process was not discussed (*i.e.*, Diels-Alder reaction or imine formation first).

Grieco Brønsted acid-catalysed Diels-Alder

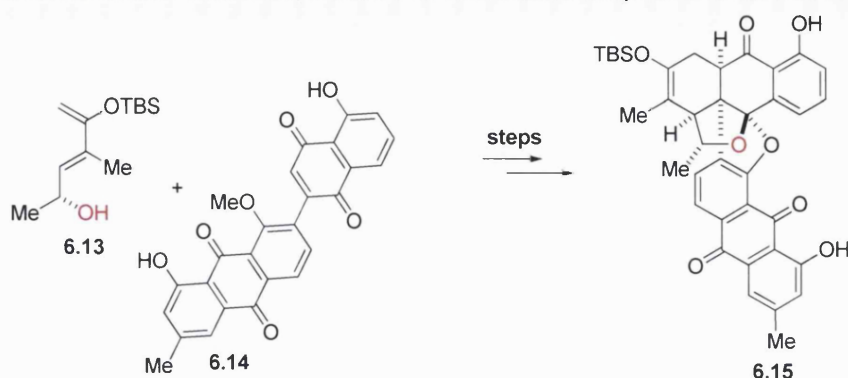


Scheme 6.2 | Grieco protocol to synthesise cyclic imines.

Finally, Nicolaou and co-workers have described a reaction sequence with a substituted naphthoquinone **6.14** and a dienol **6.13** involving hemiacetal formation

for the synthesis of the natural product BE-43472B.²¹¹ This domino process, however, was carried out only in thermal conditions, and the use of a Lewis acid was not investigated (*Scheme 6.3*).

Nicolaou cascade Diels-Alder, hemiketal formation and nucleophilic aromatic substitution

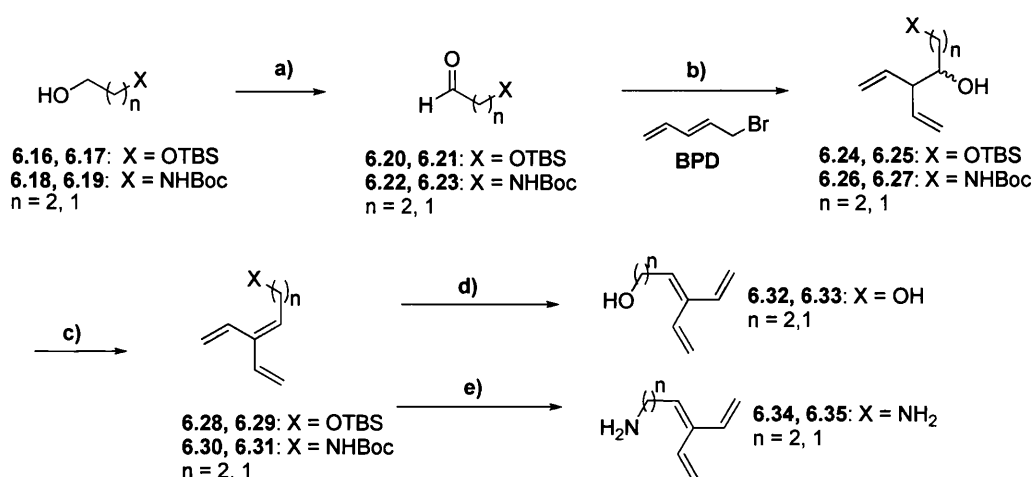


Scheme 6.3 | Nicolaou's key Diels-Alder followed by hemiketal formation step in the synthesis of BE-43472B.

We report here the use of asymmetrically substituted naphthoquinones, and oxygen and nitrogen-based derivatives of cross-conjugated trienes and dienes in domino reactions using *monodentate* Lewis acids. The studies also provide further insight into the mechanism of domino reactions of this type. Furthermore, the chemistry described here offers facile one-pot access to novel polycyclic scaffolds for the preparation of potential PPI inhibitors, and other useful intermediates not previously available.

6.2 Results and discussion

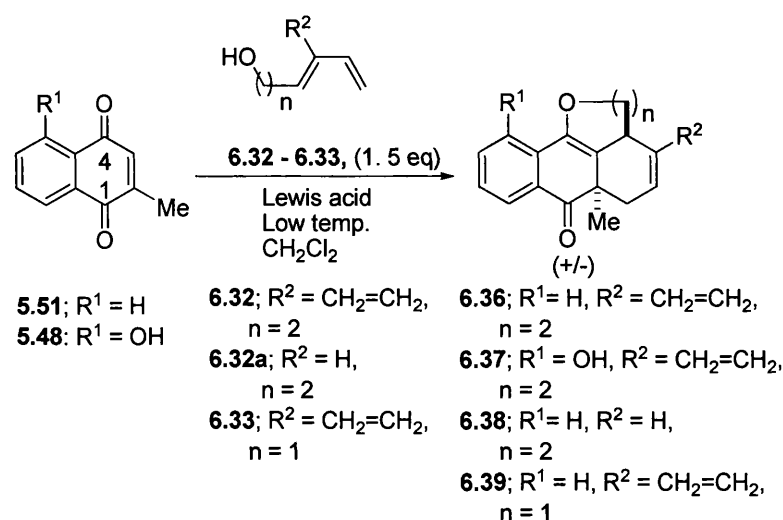
The cross-conjugated trienes **6.32** – **6.35** were prepared by the linear synthesis illustrated in *Scheme 6.4*.¹⁶⁹



a) Dess-Martin Periodinane, CH₂Cl₂, 0 °C, 30 min, 60-70%; b) In, DMF, 10 °C, 3 h, 75-90 %; c) i. MsCl, Et₃N, CH₂Cl₂, 0 °C, 1 h; ii. DBU, Toluene, 60 °C, 5-18 h, 80-92% over two steps; d) TBAF, THF, rt, 18 h, 80-96%; e) TFA, CH₂Cl₂, 50 °C, 18 h, 80-90%.

Scheme 6.4 | Synthesis of cross-conjugated trienes.

This commenced with the formation of aldehydes **6.20** – **6.21**, followed by Br-pentadienyl indium (**BPD**) addition and sulfonylation of the resulting secondary alcohols, followed by β -elimination and removal of the protecting groups. Formation of the novel scaffolds started with the 2-methyl and 5-hydroxy-2-methyl-1,4-naphthoquinone derivatives **5.51** and **5.48** (Table 6.1). An excess of the triene **6.32** was reacted at low temperature in dichloromethane with **5.51** using boron trifluoride diethyletherate or scandium trifluoro-methanesulfonate. In both cases the tetrahydro-2*H*-anthra[9,1-*bc*]pyran-7-one **6.36** was the only product isolated, and complete consumption of **5.51** was observed.²¹³ The reaction using BF₃ progressed to completion at –45 °C, and in these optimized conditions **6.36** was isolated in 80% yield.²¹⁴ The use of Sc(OTf)₃ also afforded **6.36** as a single compound, but in lower yield (65%). The reaction was also investigated using the Brønsted acid HCl (5M) in THF:water (1:1) at 50 °C, and the same product was isolated in 50% yield. Employing plumbagin **5.48**, the analogous product **6.37** was isolated in 75% yield as a single diastereoisomer, requiring 0 °C for the reaction to start. The use of the diene **6.32a** was also investigated and, as expected, based on stabilizing secondary orbital interactions, this diene was less reactive. For the reaction of **5.51** with triene **6.33**, Sc(OTf)₃ allowed formation of the dihydro-2*H*-anthra[9,1-*bc*]furan-7-one skeleton **6.39**⁶ in good yield at 0 °C (formation of this product or the sole Diels-Alder adduct were not observed with BF₃).

Table 6.1 | Synthesis of anthra[9,1-*bc*]pyranone and furanone scaffolds.⁹

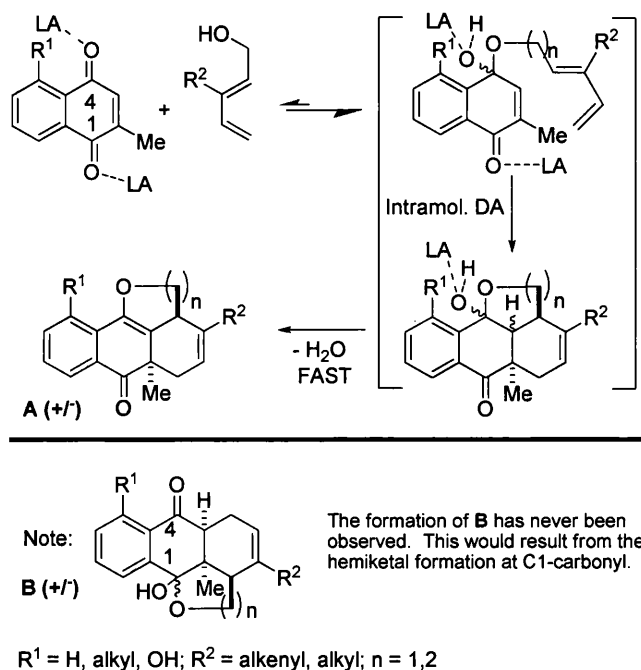
Naphthoquinone	Triene	Lewis acid	Temp (°C)	Time (h)	Yield (%)	Product
5.51	6.32	$\text{BF}_3\text{-Et}_2\text{O}^a$	-45	5	80	6.36
5.51	6.32	$\text{Sc}(\text{OTf})_3^b$	0	2	65	6.36
5.48	6.32	$\text{BF}_3\text{-Et}_2\text{O}^a$	0	2.5	75	6.37
5.51	6.32a	$\text{Sc}(\text{OTf})_3^b$	0	24	50	6.38
5.51	6.33	$\text{Sc}(\text{OTf})_3^b$	0	4.5	65	6.39

^a2 eq; ^b0.5 eq.

The sequence of the domino process is assumed to commence with formation of the hemiketal at C4 (Scheme 2), followed by intramolecular Diels-Alder cycloaddition to give the fused-cyclic hemiketal. This then undergoes elimination to afford the conjugated enol ether system. The driving force of the reaction, and regio-control of hemiketal formation, is presumably based on formation of the thermodynamically-favoured skeleton containing the conjugated enol ether system. The process is catalyzed at low temperature by the Lewis acid that promotes both formation of the hemiketal intermediate and the intramolecular [4+2]-cycloaddition with full stereospecific control (*endo* transition state). Hemiketal formation as the initial intermediate also ensures formation of the mono-Diels-Alder adduct, as in the tethered intramolecular Diels-Alder reactions investigated by Fallis and co-workers.⁷ Indeed, the double adduct resulting from the reaction of **A** with another molecule of naphthoquinone is not observed. As anticipated by this reaction sequence, formation

of the opposite regioisomer, the fused-cyclic hemiketal derivative **B**, or the sole Diels-Alder product are not observed.

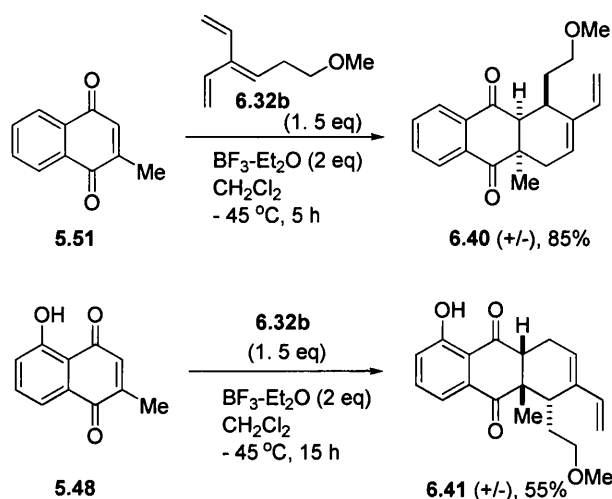
Regarding the different rates of reactivity for the naphthoquinones, it has been noted that BF_3 displays unusual regioselective features in Diels-Alder reactions of benzo- and naphthoquinones, often opposite to other Lewis acids explored for these types of substrates.^{193, 197-200} For example, with naphthoquinone **5.51**, the BF_3 preferentially chelates the oxygen atom of the C4-carbonyl where steric factors (*i.e.*, the C2-methyl) take precedence over electronic ones. Thus, in this case, the chelation properties of BF_3 promote formation of the thermodynamically favoured product **6.36**.



Scheme 6.5 | Proposed mechanism of the domino process and cascade sequence.

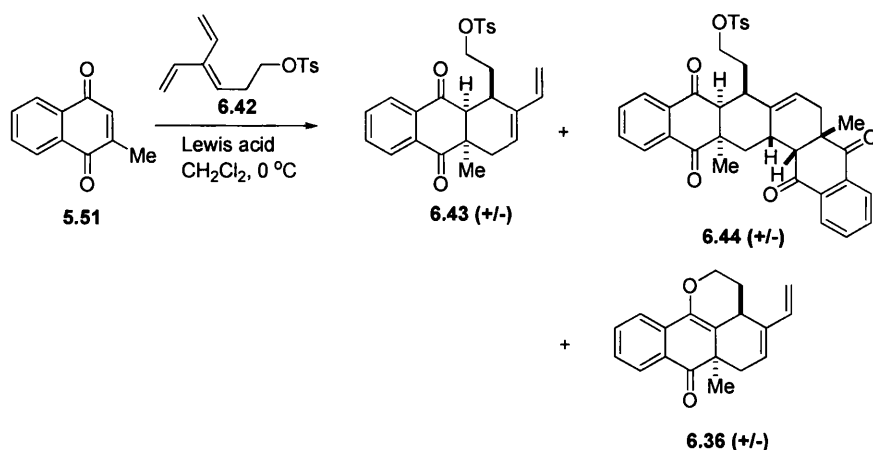
However, for naphthoquinone **5.48**, hemiketal formation is promoted at both the C1-carbonyl (*i.e.*, BF_3 chelation according to the literature¹⁰⁻¹⁴) and C4-carbonyl (*i.e.*, intramolecular hydrogen bonding) positions. Thus, an equilibrium between the regiomer hemiketals at C1 and C4 may be possible, although the formation of the thermodynamically favoured product presumably shifts the equilibrium towards hemiketal formation at C4 to afford **6.37**. This could explain why a higher temperature and longer reaction time are required compared with the same reaction for naphthoquinone **5.51**.

To help confirm the proposed mechanistic sequence, **5.51** and **5.48** were reacted with the methyl ether derivative **6.32b** (*Scheme 6.6*), in which only the formation of the cycloaddition adduct is possible. These reactions were conducted under conditions optimized for formation of the tetracyclic skeleton **6.36** using BF_3 . The tricyclic compounds **6.40** and **6.41** were obtained as single regioisomers. In both cases, the regiochemical outcome of the cycloaddition was in accordance with the chelation features of BF_3 in Diels-Alder reactions with naphthoquinones.¹⁰⁻¹⁴ Thus, the regioselective outcome for **5.48**, which is reversed compared with its reaction with the 1-hydroxyl triene **6.32** (*Table 6.1*), supports the proposed reaction sequence in *Scheme 6.6*.



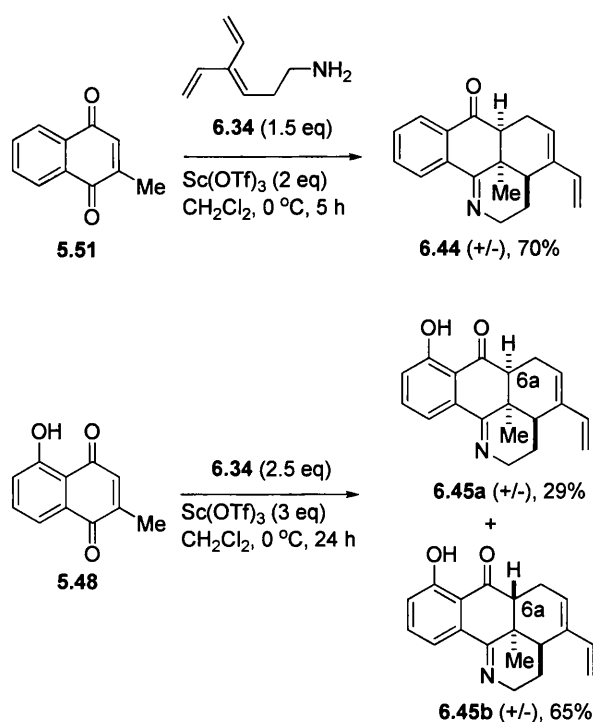
Scheme 6.6 | Synthesis of tricyclic skeletons **6.40** and **6.41**⁹.

Tosyl-protected triene **6.42** has also explored to investigate the mechanism. This was reacted with **5.51**, using BF_3 (1.5 eq.). The reaction furnished the double-DA adduct **6.44** as major product. Only 4% of the mono-DA adduct **6.43** was isolated, whereas 21% of the hemiketal **6.36** was formed. When we used 1eq. of BF_3 , the amount of the mono-DA **6.43** formed was 18% whereas the other two compounds were formed in the same proportion as before. The double-DA adduct is favored when a tosyl substituent is introduced.

Table 6.2 | Synthesis of the tricyclic skeleton **6.43**.⁹

Triene	Eq. triene	Lewis acid	Eq. Lewis acid	Time (h)	Yield (%)		
					6.43	6.44	6.36
6.42	1.5	$\text{BF}_3\text{-Et}_2\text{O}$	1.5	18	4	69	21
6.42	1.5	$\text{BF}_3\text{-Et}_2\text{O}$	1	18	18	69	21

The domino process was then investigated for application to hetero-tetracyclic skeletons containing an endocyclic nitrogen atom. Reaction of the naphthoquinones **5.51** and **5.48** was carried out with the 1-amino-functionalised trienes **6.34** (Scheme 6.7). In both cases no reaction was observed employing BF_3 as the Lewis acid. However, using $\text{Sc}(\text{OTf})_3$, the anthra[9,1-*bc*]pyridine tetracyclic skeletons **6.44** and **6.45a,b** were obtained. Two equivalents of the Lewis acid were required for full consumption of **5.51** and isolation of **6.44** in good yield. The reaction was also carried out in aqueous medium using HCl (5 M) as catalyst at 50°C . Identical regio- and diastereoselectivity was observed, but **6.44** was isolated in lower yield (60%). In the reaction with **5.48**, triene **6.34** proved to be much less reactive, and harsher conditions were required for complete consumption of **5.48** to form the tetracyclic compound in a good yield. However, due to the prolonged reaction time, racemization at C6a of **6.45a** was observed (monitored by LC-MS), with formation of *cis* (**6.45a**) and *trans* (**6.45b**) diastereoisomers in an approximate ratio of 1:2 (Scheme 6.7).



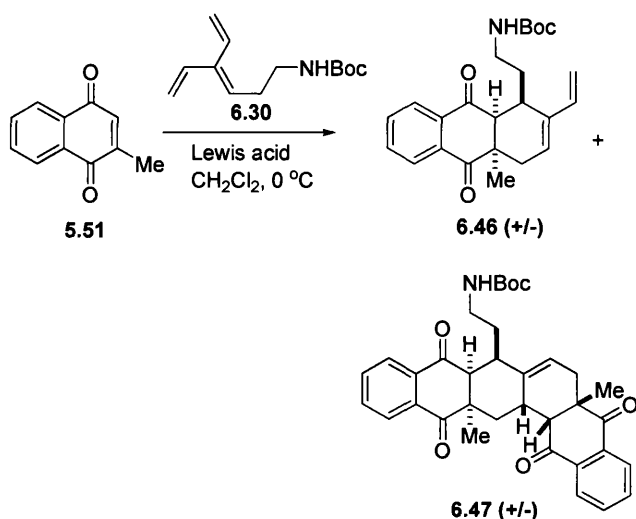
Scheme 6.7 | Synthesis of anthra[9,1-*bc*]pyridine scaffolds⁹.

The proposed sequence of reactions involving initial formation of the imine followed by intramolecular DA cycloaddition was supported by the results shown in Table 2. Reaction of **5.51** with the *N*-Boc triene derivative **6.30** was investigated employing either Sc(OTf)₃ or BF₃ as Lewis acid, respectively. In both cases the *meta* regiochemistry was observed, opposite to the *ortho* regiocontrol of the domino process afforded for both products, as shown in *Scheme 6.7*.

The reversal of regiochemistry, as occurred with the *O*-derivatives **6.37** and **6.41**, was a key result to validate the cascade sequence. The reaction using the scandium-based catalyst afforded **6.46** in good yield, with only traces of the double-DA adduct **6.47**. With BF₃ the same regiochemistry was observed, but the reaction proceeded poorly. In this case, the larger amount of Lewis acid and longer reaction time promoted the second DA cycloaddition with formation of a 1.3:1 ratio of **6.46**:**6.47**. Formation of the anthra[9,1-*bc*]pyrrole scaffold **6.48** required harsher reaction conditions (*i.e.*, 3 eq of Sc(OTf)₃, 2 eq of triene, rt and 18 h) for its isolation in moderate yield (*Scheme 6.8*). Full regio- and diastereoselectivity were achieved, but interestingly the regio-outcome was the opposite to **6.44**. In this case, the regioselectivity appeared to be controlled by steric factors for the formation of the heterocyclic five-membered ring during the intramolecular Diels-Alder reaction, as, after imine formation, the product **6.48** is favoured. It is interesting to note that in Grieco's study⁸ the reaction of 2,6-dimethyl 1,4-benzoquinone with 2,4-pentadienyl

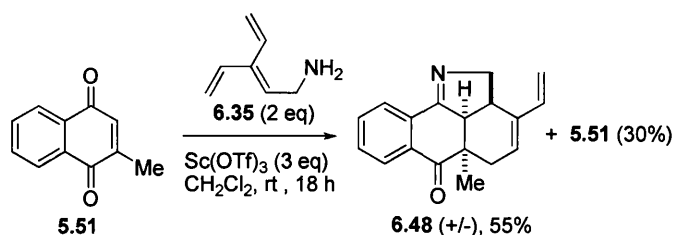
ammonium chloride in water at room temperature, gave the *ortho* regiochemistry, as anticipated if the Diels-Alder reaction occurs first, based on FMO theory. In our case, use of a Lewis acid with a naphthoquinone afforded the *meta* regiochemistry consistent with the proposed cascade sequence. Direct comparison between Lewis acid-catalyzed and water/HCl reaction conditions for the preparation of **6.48** was not possible as no products were observed in the case of **5.51** and **6.35** in water and HCl at room temperature.

Table 6.3 | Synthesis of the tricyclic skeleton **6.44**.⁹



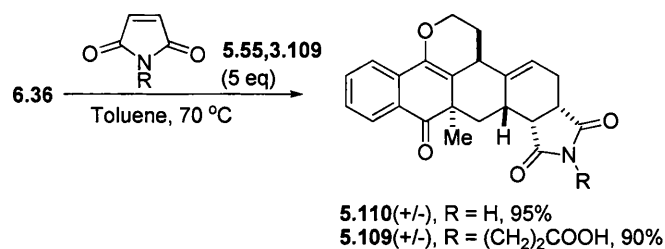
Triene	Eq. triene	Lewis acid	Eq. Lewis acid	Time (h)	Yield (%)	
					6.46	6.47
6.30	1.5	Sc(OTf) ₃	1.5	2.5	70	3
630	2.5	BF ₃ ·Et ₂ O	5	36	25 ^a	19 ^a

^a 25% of **5.51** was recovered.



Scheme 6.8 | Synthesis of anthra[9,1-*bc*]pyrrole scaffold⁹.

With these novel scaffolds in hand, we have started to investigate formation of more-complex structures. For example, the scaffold **6.36** was reacted with the symmetric dienophiles **5.55** and **3.109** in toluene in a thermal Diels-Alder cycloaddition to form the novel fused-polycyclic compounds **5.110** and **5.109**, containing endocyclic oxygen and nitrogen atoms. These were both isolated as single diastereoisomers in good yields (*Scheme 6.9*).



Scheme 6.9 | Synthesis of fused polycyclic skeletons⁹.

6.3 Conclusions

In summary, these studies have provided access to novel hetero-tetracyclic-fused skeletons in a one-pot synthesis and in a regio- and diastereo-specific manner. They have also provided further insight into the domino process that allows efficient inclusion of oxygen and nitrogen heterocycles into these ring systems. These complex skeletons should find use in the preparation of compound libraries for drug discovery, in particular in the protein-protein interaction area where the size and complexity of molecular frameworks are known to be important.¹

CHAPTER 7

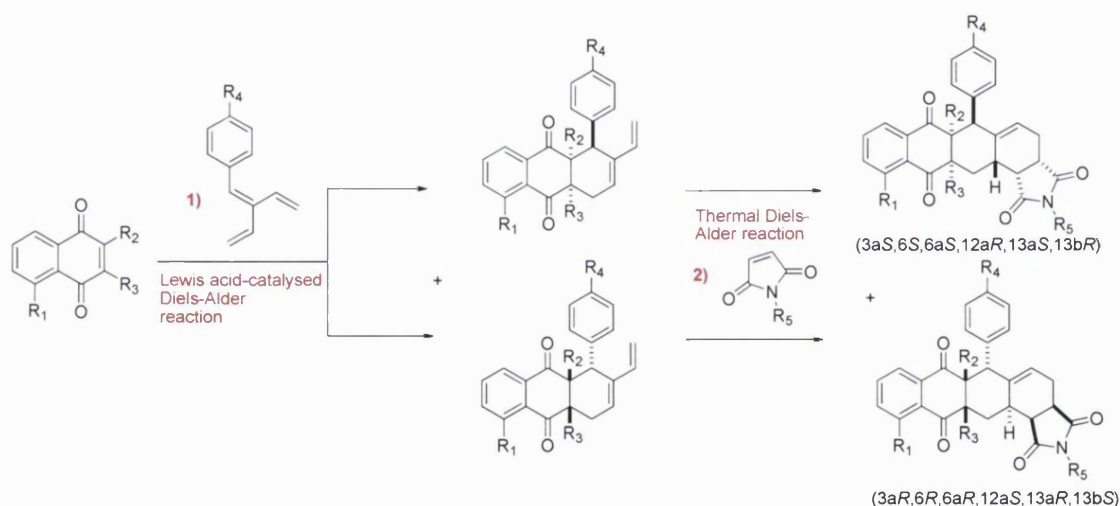
Development of chiral Bronsted/ Lewis acid-catalysed
enantioselective naphthoquinone Diels-Alder cycloaddition

Contents:

7.1	Introduction	133
7.2	Results and Discussion	137
7.3	Conclusions	144

7.1 Introduction

During attempts to identify novel HIF-1 α : HIF-1 β inhibitors, molecules possessing a pentacyclic framework were synthesised using essentially two consecutive Diels-Alder cycloadditions. The final compounds are present as racemic mixtures. It is essential at this stage of drug discovery to understand where the biological activity resides by exploring each enantiomer separately and comparing the activity with the racemic mixture.²¹⁵ The aim was to design a robust synthetic method to synthesise enantiopure pentacyclic HIF-1 α : HIF-1 β inhibitors. In order to achieve this, the focus was on the initial Lewis acid-catalysed Diels-Alder cycloaddition. As previously shown, the second thermal Diels-Alder furnishes a unique pentacyclic enantiomer for each component of the tricyclic racemic mixture (*Scheme 7.1*).



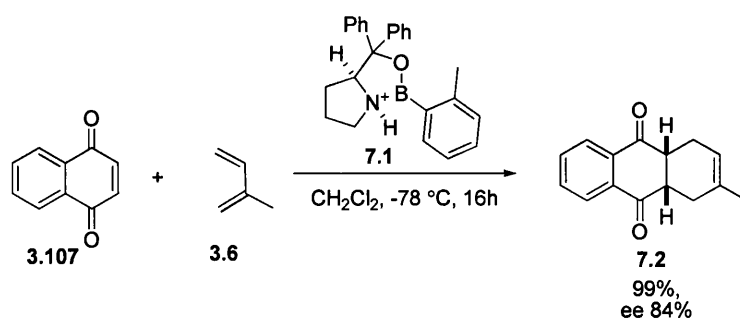
Scheme 7.1 | Consecutive Diels-Alder for the synthesis of HIF-1 inhibitors.

A significant number of syntheses of complex natural products employing the quinone Diels-Alder reaction have been reported over the last six decades. Examples include some of the biggest successes in the total synthesis of natural products, including: steroids,¹⁴⁸ reserpine,²¹⁶ ibogamine,²¹⁷ dendrobine,²¹⁸ gibberellic acid,²¹⁹ trichodermol,²²⁰ and euonyminol.²²¹ In those examples, the Diels-Alder reaction generated a racemic adduct setting a requirement to have a subsequent resolution step, accompanied by a significant loss of material (>50%). There is still a need to develop methodology for enantioselective Diels-Alder reaction with quinones as dienophiles due to the inefficiency of the standard Lewis acid catalysts employed in other subtypes of this cycloaddition.²²²

Naphthoquinones in particular have been extensively employed as dienophile systems in Diels-Alder reactions, but with very limited reports over their use in catalysed asymmetric cycloadditions.²²³⁻²²⁶ In addition, the few examples that have been published use a simple 1,4-naphthoquinone which does not present any challenge in terms of reactivity or regioselectivity. At present, methodology is not available for conducting complex naphthoquinone Diels-Alder reactions for synthesis employing complex triene systems. Nevertheless, examples with 1,4-naphthoquinones will be used as starting points in order to screen for and design the most efficient catalyst in the synthesis.

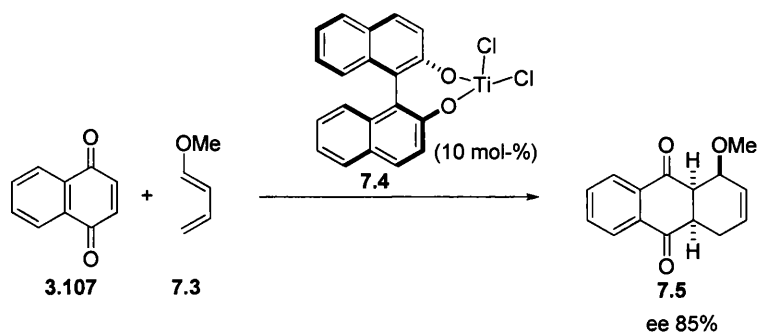
Corey and co-workers reported the use of chiral proline-derived oxazaborolidine, traditionally used in asymmetric reduction, as precatalysts for the asymmetric Diels-Alder reaction, and triflic acid,²²⁶ triflimide,²²⁷ or AlBr_3 ²²⁸ as activators to generate a potent cationic Lewis acid. A rationale behind the application of oxazaborolidinium to the enantioselective catalysis of Diels-Alder reactions of α,β -unsaturated aldehydes and ketones was proposed by Corey and co-workers.²²⁶ The coordination of the most Lewis basic α,β -enol portion of the quinone to the catalyst was suggested to lead to an organized C-H \cdots O hydrogen bonded complex (shown in *Scheme 7.8*). Exploring the formed complex, the electron-deficient α,β -enol subunit could attract the *cis* aromatic group on C₍₅₎ of the oxazaborolidine ring by a π - π -donor-acceptor interaction. This attractive interaction is sustained in the Diels-Alder transition state since the keto carbon has a strong positive charge during the reaction.²²⁹

These catalysts work at low temperatures, ranging from -20 to -90°C, depending on the substrates used.²²⁶ The catalysts are prepared in one step from the boroxines, and their activation is performed *in situ*. This enabled the synthesis of different variants of the catalysts by changing the substituents on the boron. In addition, there are two commercially available precatalysts.⁴³ In the example cited in *Scheme 7.2*, Corey and co-workers successfully synthesised highly enantiopure anthraquinone using 1,4-naphthoquinone and 2-methyl-1,3-diene.



Scheme 7.2 | Corey's enantioselective naphthoquinone Diels-Alder reaction catalysed by oxazaborolidines.²³⁰

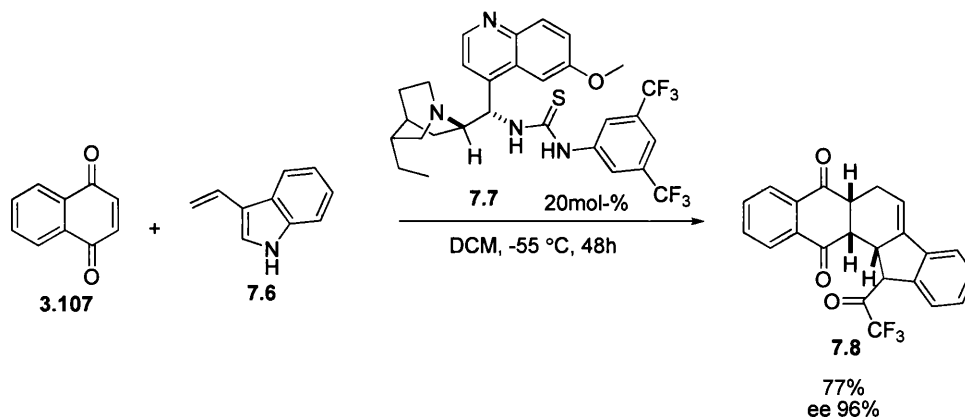
In 1991, Mikami and co-workers reported the use of a chiral bidentate titanium binaphthol complex that catalyses Diels-Alder reactions for the synthesis of anthraquinones.²³¹ These catalysts have been widely used in this cycloaddition since then. Although Mikami and co-workers originally reported that Diels-Alder reactions involving this catalyst, prepared *in situ*, were facilitated by 4Å molecular sieves (MS), certain substrates were shown to work better in the absence of MS.²²⁴ These catalysts were shown to work at temperatures below 0 °C, as well as at room temperature. The catalysts are also shown to be stable at higher temperatures. *Scheme 7.3* illustrates an example where Mikami's catalyst was used in the synthesis of an anthraquinone.



Scheme 7.3 | Mikami's enantioselective naphthoquinone Diels-Alder catalysed by Ti-BINOL-ate.^{224, 232}

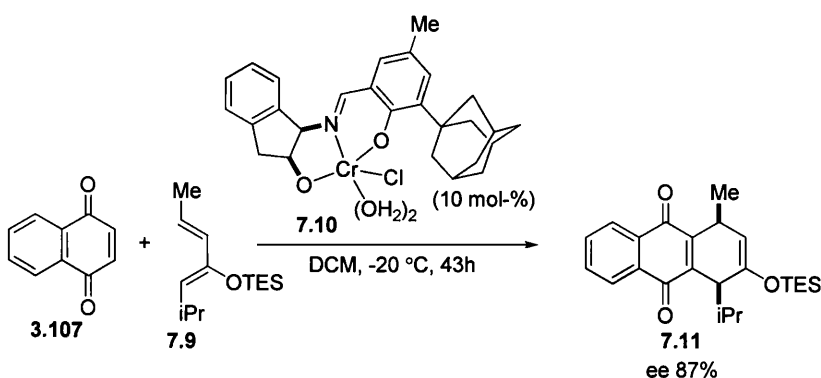
Bifunctional acid-base organic catalysts became widely popular in asymmetric catalytic reactions, including Diels-Alder cycloadditions.^{223, 233-235} In Diels-Alder, the catalysis was achieved through a hydrogen bonding coordination to both dienes and dienophiles. This resulted in a highly organised transition state and gave rise to a cycloadduct with good stereoselectivity. These catalysts commonly contain a mild acidic thiourea, which is responsible for the hydrogen-bonding and the ligand could contribute to it.²³³ Bifunctional thiourea catalysts were obtained from isothiocyanate, which was reacted

with another amine to which a chiral ligand is attached.²³⁶ Ricci and co-workers reported chiral naphthoquinone Diels-Alder cycloadditions with 3-vinylindoles catalysed by a number of bifunctional thioureas. The best result (ee = 96%) was achieved using 0.2 e.q. of hydroquinine-containing thiourea (*Scheme 7.4*).



Scheme 7.4 | Bifunctional thiourea-catalysed naphthoquinone Diels-Alder cycloaddition.²³³

Jacobsen and co-workers developed a new monomeric [(Schiff base)Cr^{III}] complex in quinone Diels-Alder cycloaddition.²³⁷⁻²³⁸ This Lewis acid catalyst, the mechanism of action of which has not been elucidated, is known to act through a one-point ligation by activating the most Lewis basic carbonyl. The Schiff base catalyst was prepared in three steps, the last of which is carried out inside a glove box. A 3N HCl workup condition was shown to be essential to avoid polymerisation. The delicate preparation method limits its use as a first choice, although it was shown to achieve highly enantioselective quinone Diels-Alder cycloadditions (*Scheme 7.5*).^{225, 239}

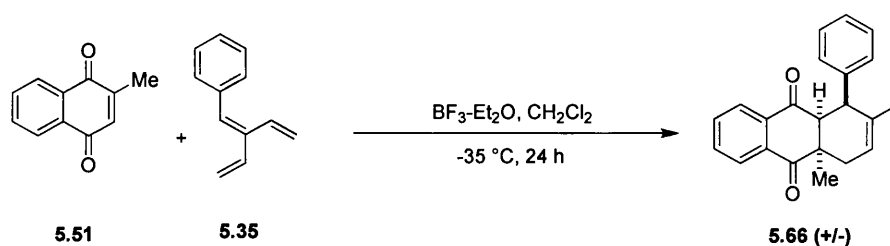


Scheme 7.5 | Schiff base-catalysed enantioselective naphthoquinone Diels-Alder cycloaddition.²²⁵

In summary, the search for catalysts that mediate the Diels-Alder reaction of naphthoquinones has yet to provide a widely applicable catalyst. There are numerous other successful catalysts used in asymmetric Diels-Alder reaction, including MacMillan imidazolidinones,²⁴⁰ Kobayashi lanthanide triflates,²⁴¹ Carreno tolyl sulfinyl auxiliaries,²⁴² and others.

7.2 Results and Discussion

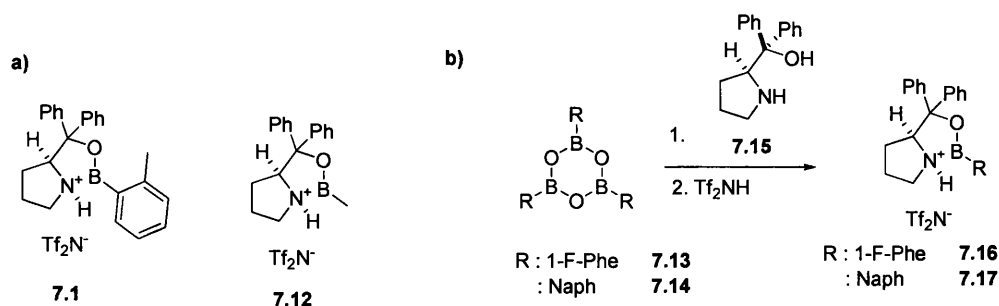
The enantioselectivity of a Diels-Alder reaction between 2-methyl-1,4-naphthoquinone **5.51** and (2-vinylbuta-1,3-dienyl)benzene **5.35** was evaluated (*Scheme 7.6*). The racemic reaction was previously reported in chapter five using $\text{BF}_3 \cdot \text{Et}_2\text{O}$ as a catalyst.



Scheme 7.6 | The achiral Lewis acid-catalysed Diels-Alder synthesis of an anthraquinone derivative.

- *CBS-Oxazaborolidine-Catalysed Naphthoquinone Diels-Alder*

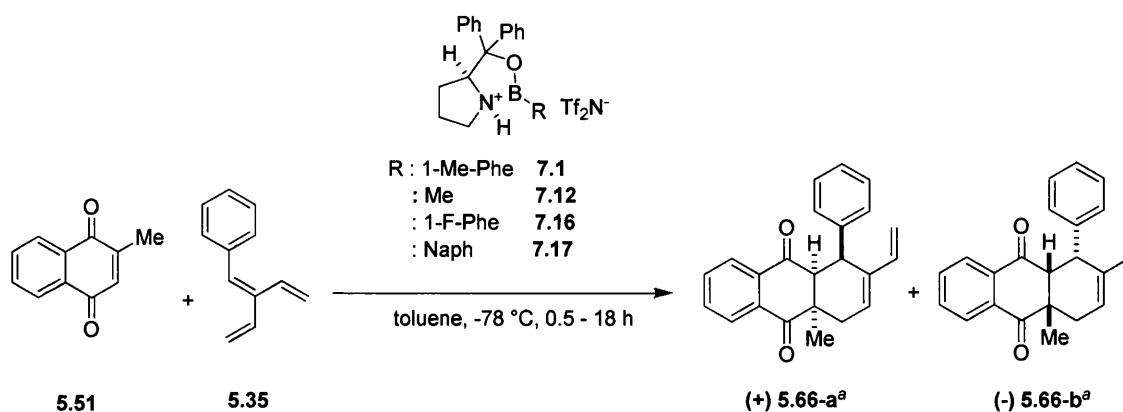
Chiral catalysis using oxazaborolidines was explored. Some of these catalysts were purchased and activated *in situ* using 1,1,1-trifluoro-*N*-(trifluoromethylsulfonyl) methanesulphonamide, also known as triflimide (*Scheme 7.7 – a*). The strong acid protonated the nitrogen on the pyrrolidine ring affording the active species. Other oxazaborolidine catalysts were prepared in one step from the corresponding boroxine, as shown in *Scheme 7.7 - b*. This enabled to explore different substituents on the boron in order to identify the most suitable chiral catalyst for the reaction.



Scheme 7.7 | a) Commercially available activated (*S*)-oxazaborolidinium catalysts. b) Synthesis of (*S*)-oxazaborolidinium catalysts.

After determination of the most favourable parameters for Diels-Alder reactions catalyzed by the cationic Lewis acids, the scope of this process for **7.1**, **7.12**, **7.16** and **7.17** was studied with the results shown in *Table 7.1*.

Table 7.1 | Investigation of the asymmetric Diels-Alder reaction using oxazaborolidines.



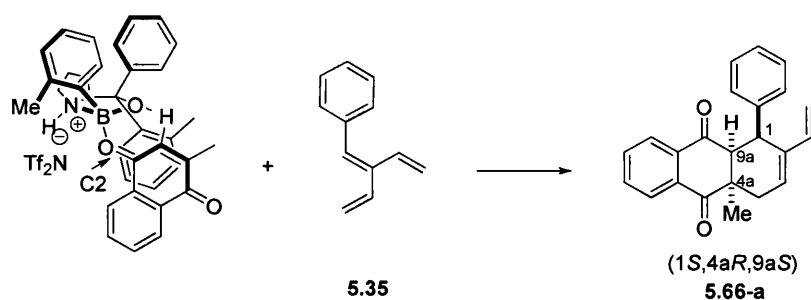
Entry	Catalyst	Temp.	Time (h)	Yield (%)	% ee ^b	(a : b) ratio	d.r. ^c . (exo:endo)
1	7.16	-78	0.5	90	10	55:45	50:1
2	7.17	-78	2	90	10	55:45	50:1
3	7.1 (<i>S</i>)	-78	7	92	8	54:46	50:1
4	7.1 (<i>R</i>) ^d	-78	3	85	10	45:55	50:1
5	7.12	-78	18	82	12	56:44	50:1

^aAbsolute configuration has been assigned by measurement of the optical rotation and based on mechanistic prediction (*Scheme 7.8*). ^bEnantioselectivities determined by chiral HPLC.

^cexo:endo ratio determined by ¹H NMR and confirmed by chiral HPLC. ^dThe catalyst structure has been shown in the experimental section.

Excellent yields (82 -92 %), but poor enantioselectivities (8-12 %), were obtained with the oxazaborolidine catalysts tested.

The absolute stereochemical outcome of the Diels-Alder reaction may be suggested based on the catalyst-naphthoquinone complex and the pre-transition assembly shown in *Scheme 7.8*. In *S*-oxazaborolidine, the chelated carbonyl carbon is situated above C(2) of the nearby phenyl group, which effectively prevents the rear face of the complexed *S-trans*- α,β -ketone from attack by the triene component. Addition of the cross-conjugated triene to the *re* (front) face of the α,β -double bond leads to the enantiomers shown.²³⁰



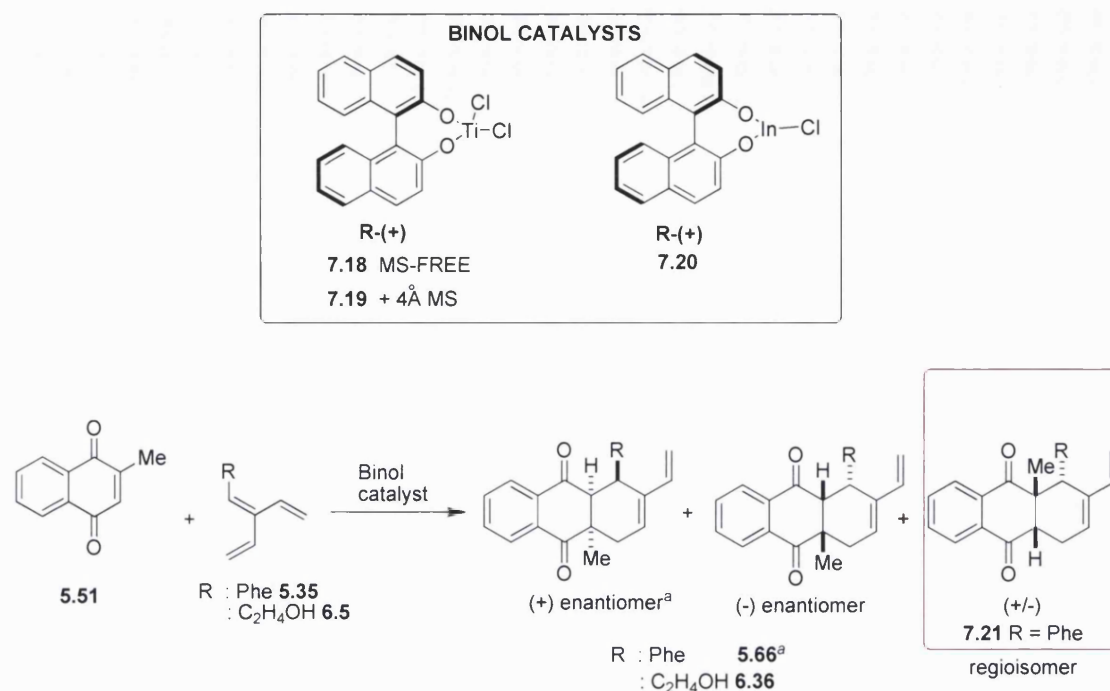
Scheme 7.8 | Pre-transition assembly of the *S*-oxazaborolidine and 2-Me-naphthoquinone.

Oxazaborolidines are powerful catalysts in the enantioselective Diels-Alder synthesis but may not be suitable for the asymmetric synthesis of the substrates that were explored. Perhaps more fundamental structural changes need to be assessed. Such modifications include altering the substituents on the carbon adjacent to the oxygen of the oxazaborolidine ring, or the use of different Lewis acids, such as AlBr_3 , to obtain the ammonium.

- *BINOL derivatives-catalysed naphthoquinone Diels-Alder*

Chiral binaphthol-derived titanium complex (BINOL-Ti), known as Mikami catalyst,²²⁴ was explored in the asymmetric Diels-Alder reaction between 2-methylnaphthoquinone **5.51** and cross-conjugated triene **5.35**. The catalyst was prepared *in situ* from commercially available (*S*)-BINOL and $\text{TiCl}_2(i\text{Pr})_2$, freshly prepared.²²⁴ The reactions were performed in the presence of 4 Å molecular sieves (MS), although an inertly prepared MS-free catalyst was also used. In addition, the use of a chiral (*S*)-BINOL-In(III) as precatalyst and allyltributylstannane as activator was investigated to generate another potent Lewis acid in the presence of $[\text{hmim}][\text{PF}_6^-]$ ionic liquid.²⁴³ The results are shown in *Table 7.2*.

Table 7.2 | Investigation of the asymmetric Diels-Alder reaction using BINOL catalysts.



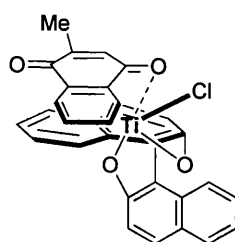
Entry	Triene	Catalyst	Temp.	Time (h)	Yield %	% ee ^b	a:b (+):(-) ratio	d.r. ^c (exo:endo)	% Regioisomer 7.21^d
1	6.5	7.18	23 - 50 °C	74	25	2	55:45	50:1	0
2	5.35	7.18	23 - 50 °C	88	35	40	30:70	50:1	95
3	5.35	7.20	-40 - 50 °C	48	75	90	95:5	50:1	29
4	6.5	7.19	23 - 50 °C	72	0	-	-	-	-
5	5.35	7.19	23 - 50 °C	72	0	-	-	-	-

^aAbsolute configuration was assigned by measurement of the optical rotation and based on mechanistic prediction (Scheme 7.8). ^bEnantioselectivities were determined by chiral HPLC. ^cexo:endo ratio determined by ¹H NMR and confirmed by chiral HPLC. ^dThe regioisomeric ratio was determined by ¹H NMR and confirmed by HPLC analysis.

Reactions carried in the presence of BINOL-Ti catalyst **7.19**, i.e. with 4Å MS, did not show any progress (table 7.2, entries **4** and **5**). When BINOL-Ti catalyst **7.18** (from which MS were centrifuged off) was used, the reactions proceeded with both trienes **5.35** and **6.5** with 35% and 25% yields, respectively (entries **1** and **2**). The reaction of BINOL-Ti catalyst and triene **5.35** (entry **2**) progressed almost exclusively towards the regioisomer **7.21**, opposite to the one expected, as confirmed by ¹H NMR and chiral HPLC. The *ee* for the other regioisomer could not be assessed using the HPLC gradient

method used. The elevated temperature required for these reactions to proceed (50 °C) may be an important factor to account for the elevated proportion of the opposite regioisomer (entries **2** and **3**). Perhaps the best result to note was from table entry **3**, where the use of BINOL-In(III) catalyst in ionic liquid furnished the desired regioisomer **5.66** in 71% of the mixture and with an enantiomeric excess ($ee = 90\%$) (95:5 ratio of enantiomers + / -). However, the other regioisomer was still obtained in 29% of the product mixture and the reaction did not advance without heating. This is certainly a promising result, but further work was required to optimise the reaction.

In order to rationalise the observed enantioselectivity, a possible pre-transition assembly is shown in *Scheme 7.9*. This model demonstrates the π - π -interactions between (*S*)-BINOL-Ti catalyst and 2-methyl-naphthoquinone **5.51** allowing the exposure of only one face of 2-methyl-naphthoquinone to the cross-conjugated triene **5.35**. This model was based on similar ones proposed by White,²³² and Ward and co-workers.²⁴⁴

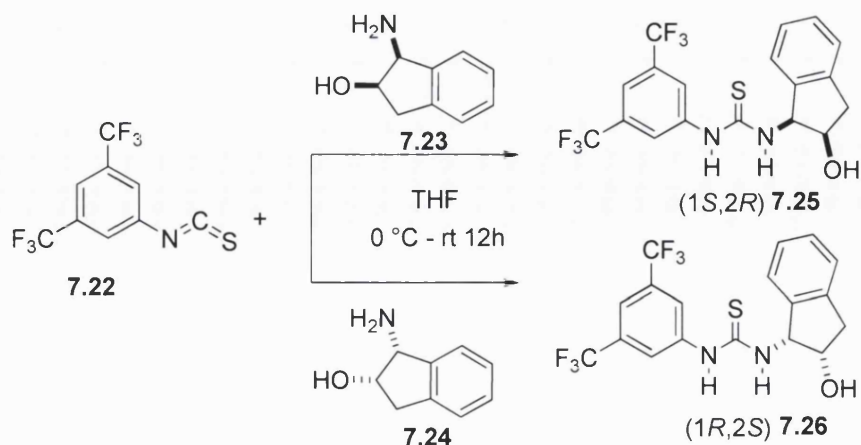


Scheme 7.9 | Model to rationalise the observed pre-transition assembly of the (*S*)-BINOL-Ti complex and 2-methyl-naphthoquinone **5.51**.²³¹

In summary, the use of BINOL-Ti and BINOL-In(III) catalysts achieved a much more improved enantiomeric control compared with the oxazaborolidines. An enantioselective excess (ee) of 90% was obtained with the use of BINOL-In(III). This positive could be optimised to develop highly asymmetric DA reaction for these substrates. However, so far, controlling the regioselectivity still needs to be done. These reactions warrant further in order to achieve a better regio- and enantiocontrol.

- *Thiourea derivatives-Catalysed Naphthoquinone Diels-Alder*

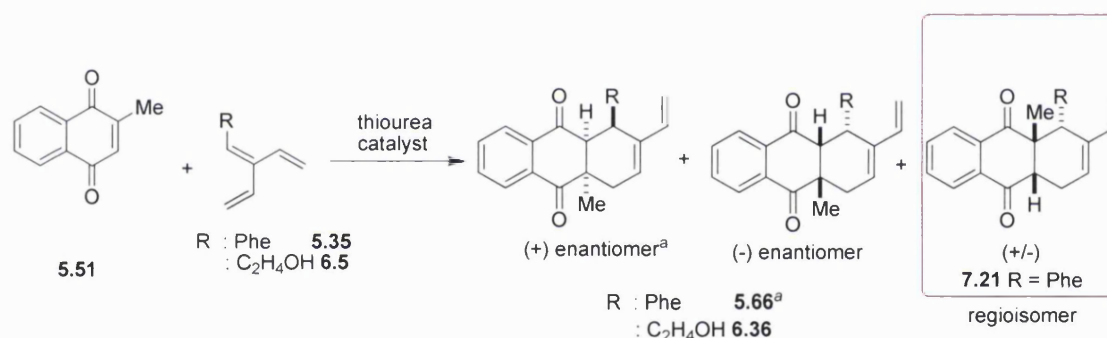
Organocatalytic Diels-Alder cycloaddition between 2-methyl-naphthoquinone **5.51** and two cross-conjugated trienes (**5.35** and **6.5**) was tried using thiourea derivatives. The chiral organic hydrogen bond donor used was prepared in a single step from a reaction of di(trifluoromethyl)phenyl-isothiocyanate and an amine to which was attached a chiral auxiliary (*Scheme 7.10*).²³⁶



Scheme 7.10 | The synthesis of thiourea organocatalysts used in Diels-Alder synthesis.

These results of the chiral Diels-Alder synthesis catalysed by **7.25** and **7.26** are shown in *Table 7.3*.

Table 7.3 | Investigation of the asymmetric Diels-Alder reaction using thiourea catalysts.



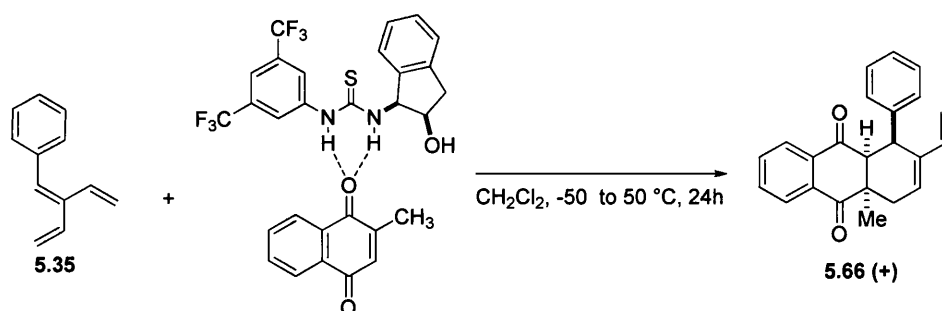
Entry	Triene	Catalyst	Temp. °C	Time (h)	Prod.	Y %	% ee ^b	a:b (+):(-) ratio	d.r. ^c (<i>exo:endo</i>)
1	5.35	7.25	-50 – 50	24	(6.36:7.21)(1:4) ^d	80	94	97:3	50:1
2	5.35	7.26	-50 – 50	24	7.21	60	0	50:50	-
3	6.5	7.25	-50 – 50	24	5.66	60	4	52:48	50:1

^aAbsolute configuration was assigned by measurement of the optical rotation and based on mechanistic prediction (*Scheme 7.10*). ^bEnantioselectivities were determined by chiral HPLC. ^c*exo:endo* ratio determined by ¹H NMR and confirmed by chiral HPLC. ^dThe regioisomeric ratio was determined by ¹H NMR and confirmed by HPLC analysis.

The DA reaction of 2-methyl-naphthoquinone **5.51** and triene **5.35** using 1-(3,5-bis(trifluoromethyl)phenyl)-3-((1*S*,2*R*)-2-hydroxy-2,3-dihydro-1*H*-inden-1-yl)thiourea

7.25 gave a (1:4) mixture of regioisomers (**5.66**:**7.21**) (table 7.3, entry **1**). Further HPLC studies showed that **7.21** was obtained as a racemic mixture. The minor regioisomer **5.66** had a higher enantioselectivity (+)-**5.66-a**/ (-)-**5.66-b** (97:3). The DA reaction exclusively furnished regioisomer **7.21** when catalyst **7.26** was used (entry **2**). No enantioselectivity was observed when catalyst **7.26** was tried on a different cross-conjugated triene **6.5** (table entry **3**).

To understand the chiral catalysis by the organocatalysts employed, we looked at the pre-transition state between the thiourea and the naphthoquinone. The most Lewis-basic carbonyl group of the dienophile was activated by the thiourea with the chiral auxiliary shielding one face of the naphthoquinone from the triene attack (*Scheme 7.11*). It was also been shown that the chiral auxiliary could chelate the substituents on the diene/dienophile through hydrogen-bonding, which would allow tweaking of the catalyst towards this end. This chelation may not be possible in the case of the cross-conjugated triene **5.66** which lacks any hydrogen bond donors/ acceptors. The non-regioselectivity may be due to the non-selective chelation of the catalyst to either carbonyl on the naphthoquinone. Increasing the temperature could again be the most significant factor responsible for the lack of regioisomeric control.



Scheme 7.11 | Model to rationalise the observed pre-transition assembly of the (1*S*,2*R*)-thiourea complex and 2-methyl-naphthoquinone **5.51**.²⁴⁵

Even though the synthesis of the desired compound **5.66** was achieved in 94% ee using an organocatalyst thiourea, about 80% of the undesired regioisomeric compound was obtained as well. To overcome this, the reactions could be further optimised. Such steps could include using different auxiliaries on the catalyst, such as quinine and quinidine derivatives,²³³ or varying reaction conditions.

- *Schiff base-Catalysed Naphthoquinone Diels-Alder*

Schiff base catalyst **7.7** was prepared in three steps, starting from 2-adamantyl-*p*-cresol, following Jacobsen's method.²²⁵ The Diels-Alder reaction of 2-methylnaphthoquinone **5.51** and naphthoquinone **5.35** has not shown any progress, even after heating. As a result, no further experiments were tried using this catalyst.

7.3 Conclusions

In conclusion, the results presented here could help to develop enantioselective synthesis of anthraquinone derivatives through catalysis of the Diels-Alder cycloaddition between 2-methylnaphthoquinone **5.51** and cross-conjugated triene **5.35**. Perhaps the most noteworthy enantiomeric ratio was achieved using BINOL-In(III) catalyst (table 2, entry 3), although a third of the product mixture consisted of the other undesired regioisomer **7.21**. Organocatalyst **7.25** has also achieved high enantioselectivity (table 3, entry 1) but the high ratio of the undesired regioisomer is a significant limitation under the current reaction conditions. It is not understood at this stage why the regioisomer **7.21** is obtained in high amounts, or exclusively, with certain catalysts.

A chiral resolution of compound **5.99** (YB036) has been attempted but epimerisation was a problem. These results are shown in the appendix.



CHAPTER 8

Conclusions and Future Work

Contents:

8.1	Concluding remarks	146
8.2	Future work	149

8.1 Concluding remarks

- *Design, synthesis and biological evaluation of novel HIF-1 α :HIF-1 β PPI inhibitors*

A series of rolitetracycline mimetics have been designed that possess a similar tetracyclic scaffold to rolitetracycline and that could be prepared in 6 steps. The route was sufficiently versatile to allow a broad range of structural modifications and substitution patterns to examine SARs. The synthesis started with by construction of a cross-conjugated triene (4 steps) which was then reacted with naphthoquinone and maleimide fragments in two consecutive stereoselective DA cycloadditions to afford the final pentacyclic structures.

A first generation library (18 tetracycline mimetics) was screened at the NCI in a cell-based assay using U251-HRE cells expressing a HIF-1 dependent luciferase reporter gene. Specificity was monitored using a control assay in U251-pGL3 cells lacking the HIF-1 promotor. Of the 18 compounds tested, a discernable SAR was obtained, and three compounds **5.84** (YB024), **5.99** (YB036) and **5.102** (YB039) were identified as inhibitors of HIF-1-dependent luciferase expression with EC₅₀ values of 6.7 μ M, 1.75 μ M and 1.45 μ M, respectively. Interestingly, **5.99** (YB036) and **5.102** (YB039) also inhibited hypoxic induction of HIF-1 α protein accumulation in U251 wt cells in a dose-dependent fashion, but had no effect on constitutively expressed HIF-1 β . These molecules also inhibited induction of VEGF mRNA expression by 59% and 69%, respectively, in U251 wt cells growing under hypoxic conditions, confirming that a component of the HIF-1 signalling pathway was being selectively down-regulated (*Table 8.1*).

A second generation library (22 compounds) afforded three novel compounds, **5.93** (YB074), **5.96** (YB081) and **5.115** (KSN011), that inhibited HIF-1-dependent luciferase expression with EC₅₀ values of 15.5 μ M, 7.8 μ M and 4.1 μ M, respectively. A third generation library of 13 compounds failed to show any activity, although this was thought to be due to a malfunction of the NCI assay, and these compounds will be re-tested in the future.

In conclusion, through the synthesis and evaluation of 54 rolitetracycline analogues, this work has produced some lead molecules of low micromolar potency that clearly down-regulate the HIF-1 signalling pathway (*Table 8.1*). Most significantly, the goal was

achieved of producing some analogues of rolitetracycline with the ability to penetrate cell membranes. Furthermore, some of the molecules have a selective ability to down-regulate HIF-1 α in comparison to HIF-1 β . It is possible that, based on the SAR information obtained in this study, future generations of molecules might be designed with sub-micromolar potency that might be progressed to *in vivo* evaluation.

Table 8.1 | Summary of biological activity for the two hits.



YB036	Biological investigation	YB039
2.3	EC ₅₀ (μ M)	1.4
-	General cytotoxicity ¹	-
+	Inhibition of HIF-1 target gene ²	+
+	Inhibition of HIF-1 α mRNA expression ³	+
+	Inhibition of HIF-1 α protein accumulation ⁴	+
+	Induction of proteasomal degradation	+
N/A	Inhibitor of HIF-1 α :HIF-1 β PPI	N/A

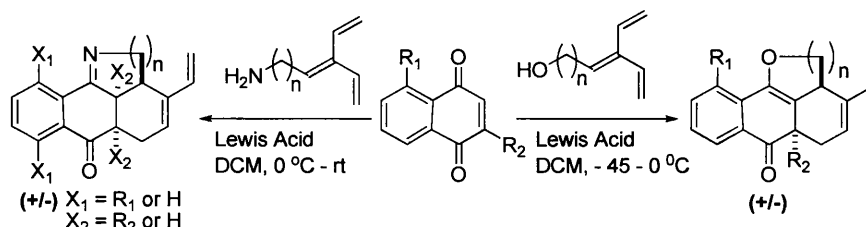
¹This was performed in pGL3 control cells, non-toxic values EC₅₀ pGL3 >20.

²Inhibition of VEGF mRNA expression at 10 μ M was 59% and 69% for YB036 and YB039, respectively. ³After 16 hours post inoculation, the inhibition attained 43% and 78% respectively. ⁴A full inhibition was attained at 5 μ M for YB039 and 10 μ M for YB036.

- *One-pot synthesis of fused-tetracyclic scaffolds employing a Lewis acid-catalyzed domino reaction of naphthoquinones*

Studies of the domino Diels-Alder cycloaddition have provided access to novel heterotetracyclic-fused skeletons in a one-pot synthesis and in a regio- and diastereo-specific manner (*Scheme 8.1*). They have also provided further insight into the domino process that allows efficient inclusion of oxygen and nitrogen heterocycles into these ring

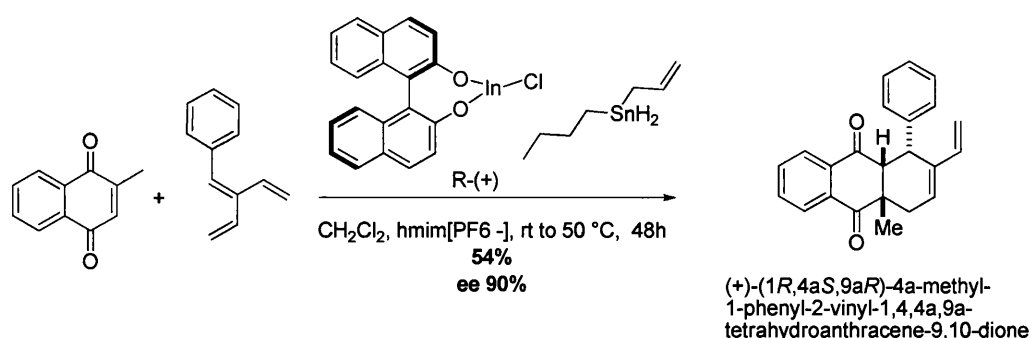
systems. These complex skeletons should find use in the preparation of compound libraries for drug discovery, in particular in the protein-protein interaction area where the size and complexity of molecular frameworks are known to be important.¹



Scheme 8.1 | Synthesis of oxygen and nitrogen containing heterocycles *via* domino Diels-Alder cycloaddition.

- *Development of chiral Bronsted/Lewis acid-catalysed enantioselective naphthoquinone Diels-Alder cycloaddition*

The synthetic studies reported herein provide results that could help in the development of an asymmetric synthesis of anthraquinone derivatives through catalysis of the Diels-Alder cycloaddition between 2-methylnaphthoquinone **5.78** and the cross-conjugated triene **5.63**. After screening a range of Lewis and Bronsted acid catalysts, the optimal enantiomeric ratio was achieved using the BINOL-In(III) catalyst (*Scheme 8.2*), although some of the regioisomer **7.21** was also isolated. A high enantiomeric ratio was also attained using a thiourea-based organocatalyst **7.25**, but the amount of the other regioisomer produced was found to be a significant limitation.



Scheme 8.2 | Asymmetric synthesis of anthraquinone derivatives using the BINOL-In(III) catalyst.

8.2 Future work

- *The design, synthesis and biological evaluation of novel HIF-1 α :HIF-1 β PPI inhibitors*

An SAR has been established following the screening of two libraries (40 molecules). We are currently awaiting the results of screening of a third generation library of 13 compounds. The third screening is aimed at providing further SAR insights towards the preparation of HIF-1 inhibitors with greater potency and selectivity than those produced in this study.

In addition, a FRET assay is currently being developed to screen the active lead compounds for their PPI inhibitory effect.

- *One-pot synthesis of fused-tetracyclic scaffolds employing a Lewis acid-catalyzed domino reaction of naphthoquinones*

Future studies could build on the novel domino process that has been used to prepare tetracyclic frameworks with 5- and 6-membered heterocyclic rings containing either nitrogen or oxygen. In addition to exploring the potential PPI inhibitory effect of these molecules on HIF-1 α :HIF-1 β interactions, further synthetic studies could be carried out. For example, the O-containing molecules are closely related to a number of natural compounds such as morindafurone from *Morinda citrifolia* Linn. (Figure 8.1) which is known to possess antimicrobial, antioxidant, pesticidal, anti-HIV, anti-leishmaniasis, and hypotensive activity.²⁴⁶ The N-containing molecules are closely related to the aporphinoid alkaloids (Figure 8.1) from *Menispermum dauricum*, which have been reported to have cytotoxicity in certain cancer cells.²⁴⁷⁻²⁵⁰

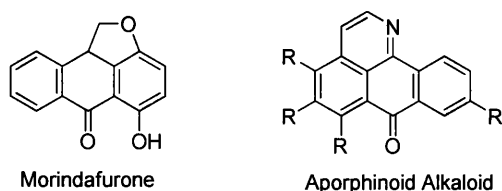
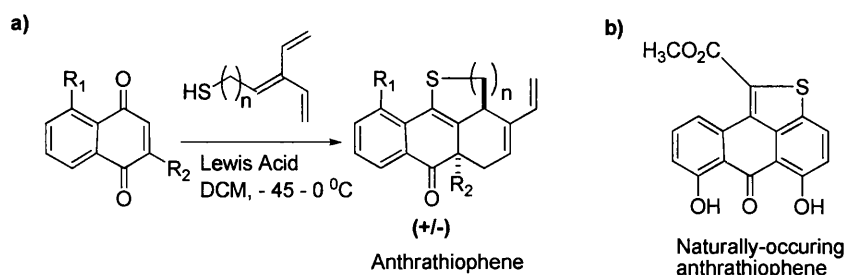


Figure 8.1 | Natural products containing O- and N- heterocycles.

Also, it should be possible to explore the domino Diels-Alder synthesis on a wider range of unsymmetrical naphthoquinones and heterocycles containing cross-conjugated trienes. For example, in this laboratory, the use of sulphur-containing trienes is being explored to prepare anthrathiophene derivatives (*Scheme 8.3-a*) which resemble some naturally-occurring pigments (*Scheme 8.3-b*).²⁵¹



Scheme 8.3 | a) Prospective synthesis of anthrathiophene derivatives. b) A naturally-occurring anthrathiophene.

- *Further development of chiral Bronsted/Lewis acid-catalysed enantioselective naphthoquinone Diels-Alder cycloaddition*

The attempts in these studies to establish an asymmetric naphthoquinone Diels-Alder synthesis have demonstrated that high enantiomeric ratios using BINOL-In(III) and thioureas organocatalyst derivatives but yields are low, mainly due to the formation of the undesired regioisomer. Therefore, future studies could focus on optimising the asymmetric potential of these catalysts and in improving regioselectivity. These future studies could explore different reaction conditions (solvents and temperature), ligands (for thiourea and oxazaborolidine catalysts), metals (for BINOL catalysts), and Lewis acid complexes (e.g. AlBr_3 for oxazaborolidines) (*Figure 8.2*). Other cross-conjugated triene building blocks (e.g., *p*- CF_3 -triene and *p*-Br-triene) could also be studied.

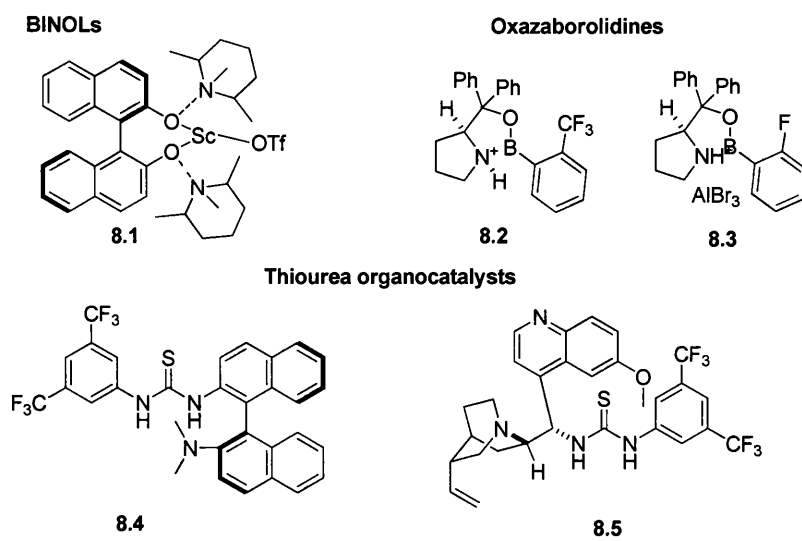


Figure 8.2 | Some of the catalysts that could be investigated in the future.

CHAPTER 9

Experimental Section

Contents:

9.1	Synthesis of HIF-1α:HIF-1β PPI inhibitors	153
9.1.1	General Procedure for the Synthesis of the cross-conjugated Trienes	154
9.1.2	General Procedure for the Synthesis 2-methyl- and 2,3-dimethyl-naphthoquinone	160
9.1.3	General Procedure for the Synthesis of the tricyclic compounds: 1 st Diels-Alders reaction	162
9.1.4	General Procedure for the synthesis of the pentacyclic compounds: 2 nd Diels-Alders reaction	170
9.2	One-pot synthesis of fused-tetracyclic scaffolds employing a Lewis acid-catalyzed domino reaction of naphthoquinones	207
9.2.1	Synthesis of dienes and cross-conjugated trienes	207
9.2.2	Synthesis of the tricyclic scaffolds	219
9.2.3	Synthesis of the tetracyclic scaffolds	226
9.2.4	Synthesis of polycyclic derivatives	234
9.3	Development of chiral Bronsted/ Lewis acid-catalysed enantioselective naphthoquinone Diels-Alder cycloaddition	237
9.3.1	Asymmetric Diels-Alder using Oxazaborolidine derivatives	238
9.3.2	Asymmetric Diels-Alder using Binaphthol derivatives	243
9.3.3	Asymmetric Diels-Alder using thiourea derivatives	245

9.1 Design, synthesis and biological evaluation of novel HIF-1 α :HIF-1 β PPI inhibitors

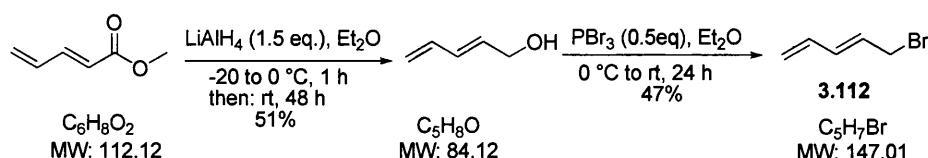
General experimental details

All reagents and solvents used were supplied from commercial sources unless otherwise indicated. Reactions requiring anhydrous conditions were conducted in glassware, which had been oven-dried overnight and used the following day. All reactions were carried under dry N₂ conditions unless otherwise stated. All reactions were monitored by analytical thin-layer chromatography (TLC) performed using indicated solvent on silica gel 60 (0.25 mm). TLC plates were visualized using UV light (254 or 360nm) and/or staining with a cerium sulfate-ammonium molybdate solution or basic potassium permanganate KMnO₄ followed by heating. LC-MS, liquid chromatography coupled with mass spectrophotometer, was also used to monitor the progress of the reactions. Solvents were removed by rotary evaporator at or below 40 °C and the compounds further dried using low-pressure vacuum pumps. Compounds with low boiling points such as bromo-pentadiene, pendienol and the trienes were dried at 100 mmHg at 30 °C. An immersion cooler was used to perform overnight reactions at very low temperatures e.g. -45 °C. The purification of the compounds was achieved by column chromatography using silica gel (230 – 400mesh). ¹H and ¹³C NMR were recorded at 400MHz or 500MHz for ¹H NMR and 100MHz or 125MHz for ¹³C NMR. Chemical shifts (δ H) are quoted in ppm (parts per million) and referenced to CDCl₃ residual chloroform signal ¹H δ = 7.26, ¹³C δ = 77.2 or *d6*-DMSO residual dimethyl-sulphoxide signal ¹H δ = 2.54, ¹³C δ = 40.45. Multiplicities in ¹H NMR spectra are quoted as: s = singlet, d = doublet, q = quartet, m = multiplet, dd = double doublet, ddd = double double doublet, dt = double triplet, td = triple doublet, ddt = double double triplet. High resolution mass spectra (HRMS) were obtained on a mass spectrometer coupled with to LC using electrospray (ES) ionization and time-of-flight (TOF) mass spectrometry. Infrared spectra were recorded 1000 using neat conditions. All the reactions were carried out under N₂ flow, and in anhydrous conditions and dry solvents, unless water was used as solvent or co-solvent.

9.1.1 General Procedure for the Synthesis of the cross-conjugated Trienes

Procedure for the synthesis of 5-Br-1,3-pentadiene (3.112)

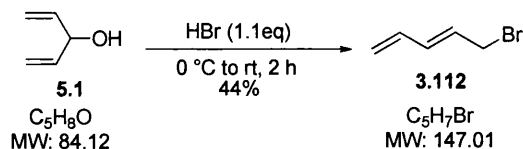
Method A¹⁷⁷



$LiAlH_4$ solution (40.12 mmol, 1.0 M in Et_2O , 1.5 eq.) was added dropwise to a vigorously stirred solution of methyl-2,4-pentadienoate (**1**) (26.75 mmol, 1.0 eq.) in anhydrous Et_2O (about 300 ml for every 100 mmol of (**1**)) at -20 °C and under N_2 . The solution was left to stir for 24h at room temperature, protected from light at all time (using aluminium foil). Powdered sodium sulfate decahydrate (13.38 g) was then added portionwise at 0 °C to quench the reaction and the resultant slurry was left to stir for 2h at room temperature. Filtration through a pad of magnesium sulfate followed by washing with Et_2O gave a dilute solution that was washed with aq. $NaHCO_3$ and H_2O , dried over $MgSO_4$ and filtered. After the solvent was removed at 250 mmHg/ 15 °C, the residue was distilled to give 2,4-pentadienol (**2**) (51%) as a clear yellow oil. b.p. 25 °C/2 mmHg; 1H NMR and ^{13}C NMR data in accordance with those reported.¹⁷⁷ R_f 0.71 (Silica gel, $EtOAc/n$ -hexane 7:3). Yellow oil.

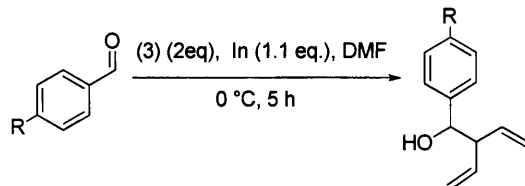
PBr_3 (4.82 g, 17.83 mmol, 0.5 eq.) was added to a stirred solution of 2,4-pentadienol **5.1** (3 g, 35.66 mmol, 1.0 eq.) in dry Et_2O (15 ml) at -10 °C under dry N_2 atmosphere. The mixture was stirred for 24h at room temperature, and then poured into ice water and extracted with Et_2O . The Et_2O solution was washed with sat. aq. $NaHCO_3$ and H_2O , dried over $MgSO_4$ and filtered. After the solvent was removed at 250 mmHg/ 15 °C, the residue was distilled to give 47% yield of **3.112** as clear yellow oil. b.p. 43 °C/ 19 mmHg; 1H NMR and ^{13}C NMR data were identical to those reported in literature. R_f 0.36 (Silica gel, $EtOAc/n$ -hexane 1:10). Clear yellow oil.

*Method B*¹⁷⁸



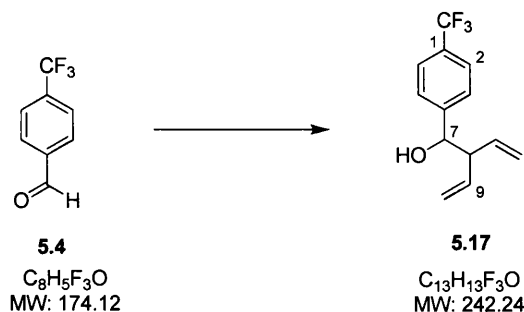
A solution of 48% hydrobromic acid (HBr) (11.33 mmol, 1.1 eq.) was added dropwise to a vigorously stirred 1,4-pentadien-3-ol **5.1** oil (10.3 mmol, 1.0 eq.) at 0 °C. The addition of HBr makes the mixture become cloudy which is left to stir for 2h at room temperature. The mixture was then diluted in 15ml Et₂O and washed 3 times with an equivalent amount of crushed ice. The organic phase was then dried over MgSO₄, filtered, and concentrated at 250mmHg/15 °C. The crude (about 80% pure) was used as such without further purification. The yield of this reaction was 44%. *R_f* 0.36 (Silica gel, EtOAc/*n*-hexane 1:10). Clear yellow oil.

Procedure for the indium-mediated γ -pentadienylation of benzaldehydes¹⁷⁶



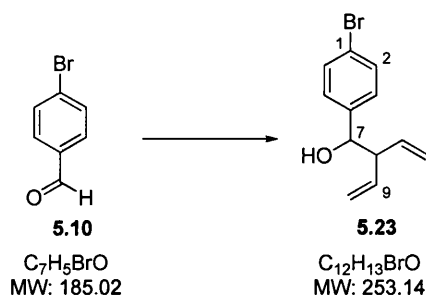
Indium powder (100mesh, 13.07 mmol, 1.1 eq.) was added in portions to a solution of 5-bromo-1,3-pentadiene **3.112** (23.78 mmol, 2.0 eq.) and aromatic benzaldehyde (11.89 mmol, 1.0 eq.) in DMF (12 ml). After stirring for 5h at 0 °C, temperature was allowed to rise to 10 °C. The mixture was diluted with CH₂Cl₂ (60 ml) and poured into Et₂O (950 ml). The resulting turbid mixture was filtered through a pad of silica gel and washed with an additional amount of Et₂O. Evaporation of the solvent at 11mmHg/40 °C and purification of the intermediate by gravity chromatography on silica gel, using *n*-hexane/EtOAc 20:1 increased gradually to 8:2 EtOAc, resulted in the secondary alcohol (8.79 mmol, 74%).

7-(1-(trifluoromethyl)phenyl)-8-vinylbut-9-en-7-ol (5.17)



Compound **5.17** was isolated as a clear yellow oil; **Y** = 74%; **R_f** 0.16 (Silica gel, *n*-hexane/EtOAc 10:1); 1H NMR (400MHz, $CDCl_3$): δ 7.59 (2H, d, J = 8.2Hz, $H^{2,6}$), 7.43 (2H, d, J = 8.2Hz, $H^{3,5}$), 5.82 (1H, ddd, J = 17.2, 10.3, 8.2 Hz, H^9), 5.70 (1H, ddd, J = 17.2, 10.2, 7.2 Hz, H^9), 5.25 (1H, dd, J = 10.2, 1.0Hz, H^{11}), 5.17 (1H, dt, J = 17.2, 1.1Hz, H^{11}), 5.09 (1H, dt, J = 10.4, 1.2Hz, H^{11}), 5.02 (1H, dt, J = 17.2, 1.2Hz, H^{11}), 4.66 (1H, dd, J = 6.8, 2.9Hz, H^8), 3.08 (1H, q, J = 7.2Hz, H^7), 2.32 (1H, d, J = 3.2Hz, OH); ^{13}C NMR (100MHz, $CDCl_3$): δ 144.7 (C^4), 135.1 (C^9), 134.9 (C^9), 128.6 (C^1 , q, J = 32Hz), 126.1 (C^3 & C^5), 123.95 (C^2 & C^6), 123.2 (CF_3 , q, J = 270Hz), 117.8 (C^{10}), 116.7(C^{10}), 74.5 (C^8), 55.2 (C^7); **HRMS**: Found 281.0547 $[M+K]^+$, $C_{13}H_{13}F_3KO$ theoretical mass = 281.0556; **Elemental analysis**, calculated for $C_{13}H_{13}F_3O$: C 64.46%, H 5.41%; found: C 64.48%, H 5.21%

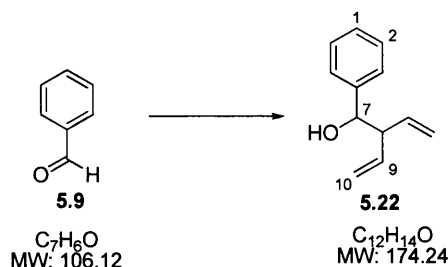
7-(1-bromophenyl)-8-vinylbut-9-en-7-ol (5.23)



Compound **5.23** was isolated as clear yellow oil; **Y** = 85%; **R_f** 0.13 (Silica gel, *n*-hexane/EtOAc 10:1); 1H NMR (400MHz, $CDCl_3$): δ 7.46 (2H, d, J = 8.4Hz, $H^{2,6}$), 7.19 (2H, d, J = 8.4Hz, $H^{3,5}$), 5.80 (1H, ddd, J = 17.2, 10.3, 8.2 Hz, H^9), 5.64 (1H, ddd, J = 17.2, 10.2, 7.2 Hz, H^9), 5.25 (1H, dd, J = 10.2, 1.0Hz, H^{10}), 5.17 (1H, dt, J = 17.2, 1.1Hz, H^{10}),

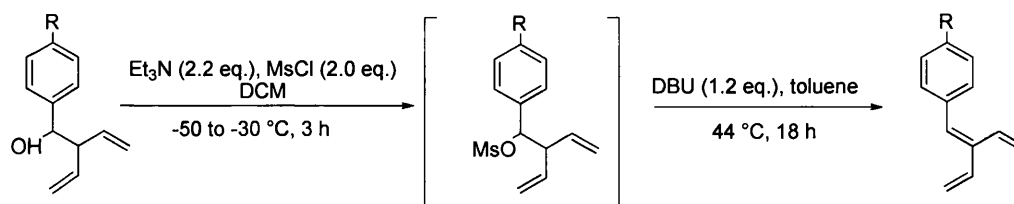
5.07 (1H, dt, $J = 10.4, 1.2\text{Hz}$, H^{10}), 5.01 (1H, dt, $J = 17.2, 1.2\text{Hz}$, H^{10}), 4.56 (1H, dd, $J = 6.8, 2.9\text{Hz}$, H^8), 3.04 (1H, q, $J = 7.2\text{Hz}$, H^7), 2.18 (1H, d, $J = 3.2\text{Hz}$, OH); MS (ESI): $m/z = 251.19$ [$\text{M}-\text{H}^+$, 100%], calculated for same isomer = 253.022 [$\text{M}+\text{H}$] $^+$.

7-phenyl-8-vinylbut-9-en-7-ol (5.22)



Compound **5.22** was isolated as clear yellow oil; R_f 0.18 (Silica gel, *n*-hexane/ EtOAc 10:1). Spectroscopic data in accordance with those reported in literature¹⁷⁶.

Procedure for the synthesis of cross conjugated trienes

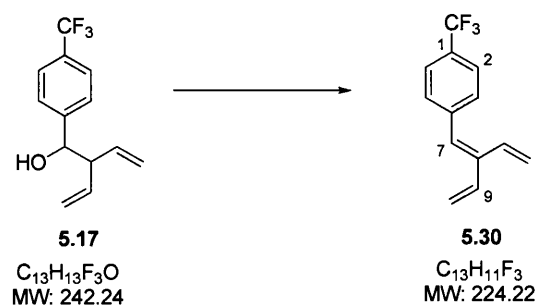


Mesyl chloride (1.27 mmol, 1.3 eq.) was added dropwise to a solution of the secondary alcohol (0.95 mmol, 1.0 eq.) and triethylamine (1.42 mmol, 1.5 eq.) in CH_2Cl_2 (10 ml) at $-50\text{ }^\circ\text{C}$ under constant N_2 flow. After 45min, another amount of mesyl chloride (0.63 mmol, 0.7 eq.) was added dropwise followed by triethylamine (0.67 mmol, 0.7 eq.) at $-50\text{ }^\circ\text{C}$. The mixture was allowed to warm to $-30\text{ }^\circ\text{C}$ over 2h and 15min and poured into half saturated aqueous solution of NaHCO_3 (10 ml). This mixture was subsequently extracted with Et_2O (3 x 10 ml), dried onto Na_2SO_4 pad, filtered and the solvent was concentrated under high vacuum pump to form unstable methyl sulfonate salt [99%, R_f 0.24 (Silica gel, *n*-hexane/EtOAc 10:1)].

The intermediate was dissolved in dry toluene (10ml), treated with 1,8-diazabicyclo[5.4.0]undec-7-ene (1.14 mmol, 1.2 eq.) and gently heated at $44\text{ }^\circ\text{C}$ for 18h. The crude mixture was dissolved in a mixture of methanol/*n*-hexane 5:5 then preloaded onto dry silica powder and purified using flash column chromatography in *n*-hexane to

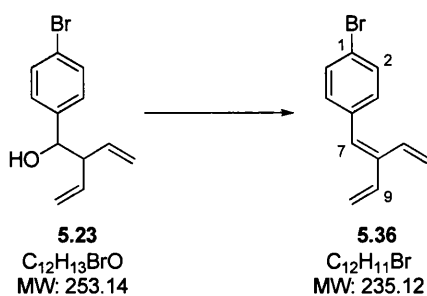
furnish the triene (85%). The solvent evaporation following the column was performed at 70 mmHg/40 °C for 2h due to the volatile nature of this compound. The general yield over 2 steps (i.e. condensation, mesylation and elimination) was 20 – 62%.

1-(trifluoromethyl)-4-(8-vinylbuta-7,9-dienyl)benzol (5.30)



Compound **5.30** was isolated as clear oil; **Y** = 88%; **R_f** 0.11 (Silica gel, *n*-hexane/EtOAc 10:1); ¹H NMR (400MHz, CDCl₃): δ 7.59 (2H, d, *J* = 8.2Hz, H^{2,6}), 7.43 (2H, d, *J* = 8.2Hz, H^{3,5}), 6.71-6.63 (1H, dd, *J* = 17.1, 11.2 Hz, H^{9/9'}), 6.65 (1H, s, H⁷), 6.63-6.55 (1H, ddd, *J* = 17.2, 10.7, 0.7Hz, H^{9/9'}), 5.61 (1H, dd, *J* = 17.2, 1.3Hz, H^{10/10'}), 5.52 (1H, dd, *J* = 17.6, 1.2Hz, H^{10/10'}), 5.44 (1H, dt, *J* = 11.2, 1.2Hz, H^{10/10'}), 5.30 (1H, dd, *J* = 10.7, 1.3Hz, H^{10/10'}); ¹³C NMR (100MHz, CDCl₃): δ 140.67 (C⁴), 139.9 (C⁸), 137.7 (C⁹), 132.8 (C⁹), 129.7 (C³ & C⁵), 129.2 (C¹, q, *J* = 32Hz), 127.8 (C⁷), 125.0 (C² & C⁶), 124.2 (CF₃, q, *J* = 270Hz), 119.6 (C¹⁰), 117.4 (C¹⁰).

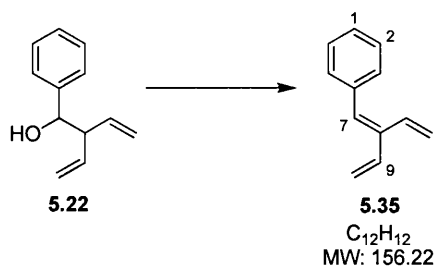
1-bromo-4-(2-vinylbuta-1,3-dienyl)benzene (5.36)



Compound **5.36** was isolated as clear colourless oil; **Y** = 92%; **R_f** 0.06 (Silica gel, *n*-hexane/EtOAc 10:1); ¹H NMR (400MHz, CDCl₃): δ 7.46 (2H, d, *J* = 8.5Hz, H^{2,6}), 7.23 (2H, d, *J* = 8.5Hz, H^{3,5}), 6.62 (1H, dd, *J* = 17.6, 11.0 Hz, H^{9/9'}), 6.54 (1H, s, H⁷), 6.53 (1H, ddd, *J* = 17.3, 10.7, 0.9Hz, H^{9/9'}), 5.55 (1H, dd, *J* = 17.3, 1.3Hz, H^{10/10'}), 5.48 (1H, dd, *J* = 17.6, 1.2Hz, H^{10/10'}), 5.38 (1H, dt, *J* = 11.2, 1.2Hz, H^{10/10'}), 5.23 (1H, dd, *J* = 10.7, 1.3Hz,

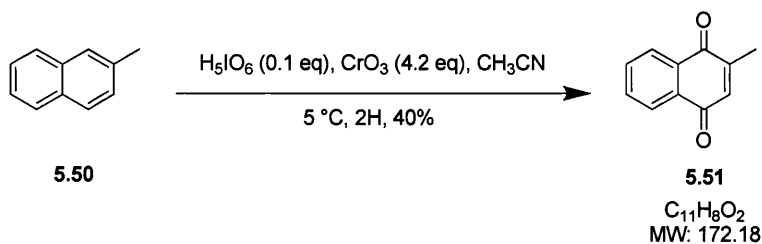
$H^{10/10'}$); ^{13}C NMR (100MHz, $CDCl_3$): δ 138.6 (C^4), 137.7 (C^7), 133.1 (C^9), 132.8 (C^9), 131.3 (C^3 , C^5), 131.2 (C^2 , C^6), 128.2 (C^9), 121.0 ($C1$), 119.1 (C^{10}), 116.5 (C^{10}); **MS (EI)**: m/z = 233.60 [$M-H^+$, 100%], calculated = 235.0122 [$M+H$] $^+$.

(8-vinylbuta-7,9-dienyl)benzene (5.35)



Compound **5.35** was isolated as clear oil. $Y = 88\%$; R_f 0.12 (Silica gel, *n*-hexane/EtOAc 10:1). Spectroscopic data in accordance with those reported in literature¹⁷⁶.

9.1.2 General Procedure for the Synthesis 2-methyl- and 2,3-dimethyl-naphthoquinone¹⁸⁸

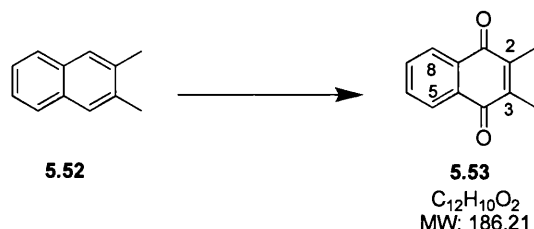


H_5IO_6 (3.52 mmol, 1.0 eq.) was dissolved in acetonitrile (65 ml) with vigorous stirring, and CrO_3 (0.352 mmol, 0.1 eq.) was dissolved to the solution. The resulted solution was cooled at 5 °C. 2-Methylnaphthalene **5.50** (3.52 mmol, 1.0 eq.) dissolved in mlacetonitrile (5 ml) was added to the previous solution with stirring. A white precipitate formed immediately with exothermic reaction. After 2h stirring at 5 °C, the supernatant liquid of the reaction mixture was decanted to a flask, and the solvent was removed by evaporation. The residues after decantation and evaporation were dissolved in H_2O and CH_2Cl_2 , combined and then extracted with CH_2Cl_2 (10 ml \times 2). The collected organic extracts were washed with aq. NaOH. The aqueous phase was acidified with 1 M aq. HCl and extracted with CH_2Cl_2 . 2-Naphthoic acid (55 mg, 9%) was obtained from acidified aqueous solution by CH_2Cl_2 extraction. The organic layer was washed with brine, and dried over MgSO_4 . The solvent was concentrated under reduced pressure. The raw product obtained was recrystallized from ethanol to afford 2-methyl-1,4-naphthoquinone **5.51** (40%) as yellow crystals.¹⁸⁸

2-methyl-naphthoquinone (5.51)

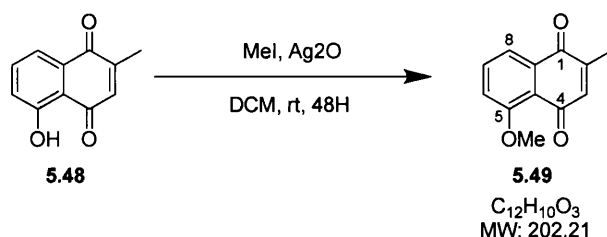
$\text{Y} = 40\%$; R_f 0.24 ($\text{CH}_2\text{Cl}_2/n\text{-hexane}$ 50:50); $^1\text{H NMR}$ (400 MHz, CDCl_3): δ 8.06 – 8.13 (2H, m, H^6 & H^7), 7.75 (2H, dd, H^7 & H^6), 6.87 (1H, s, H^3), 2.22 (3H, s, CH_3); $^{13}\text{C NMR}$ (100 MHz, CDCl_3): δ 195.0 (C^1 & C^4), 156.0 (C^2 & C^3), 138.0 (C^{4a} & C^{8a}), 135.7 (C^7), 133.7 (C^6), 126.5 (C^5), 126.1 (C^8), 18.0 (CH_3).

2,3-dimethyl-1,4-naphthoquinone (5.53)



5.53 was isolated as a yellow solid. **Y** = 45%; **R_f** 0.25 (Silica gel, CH₂Cl₂); **IR**: 2924, 1656, 1620, 1592, 1458, 1371, 1334, 1293, 790, 695 cm⁻¹. **¹H NMR** (400 MHz, CDCl₃): δ 8.06 – 8.13 (2H, m, H^{6,7}), 7.75 (2H, dd, H^{7,6}), 6.87 (1H, s, H³), 2.22 (3H, s, CH₃); **¹³C NMR** (100 MHz, CDCl₃): δ 184.7 (C^{1,4}), 143.3 (C^{2,3}), 133.2 (C^{5,6}), 132.0 (C^{7,8}), 126.1 (C^{4a, 8a}), 12.8 (2 × CH₃); **HRMS**: found MH⁺ 181.0756, C₁₂H₁₁O₂ requires 181.0759. Spectroscopic data in accordance with those reported in literature²⁵²

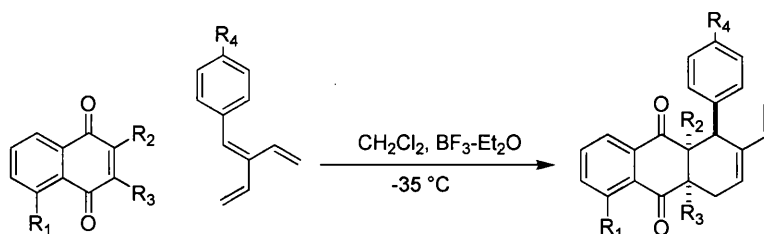
5-methoxy-2-methylnaphthoquinone (5.49)



5.49 was isolated as yellow compound; **Y** = 99%; **R_f** 0.27 (Silica gel, CH₂Cl₂); **IR**: 2950, 1663, 1583, 1282, 1256 cm⁻¹; **Mp.** 93-95 °C; **¹H NMR** (400 MHz, CDCl₃): δ 7.74 (d, 1H, *J* = 6.9 Hz, H⁸), 7.65 (t, 1H, *J* = 7.8 Hz, H⁷), 7.29 (d, 1H, *J* = 8.1 Hz, H⁷), 6.73 (d, 1H, *J* = 1.5 Hz, H³), 4.00 (s, 3H, CH₃O), 2.13 (s, 3H, CH₃); **¹³C NMR** (100 MHz, CDCl₃): δ 185.7 (C^{1/4}), 184.4 (C^{1/4}), 159.3 (C⁵), 145.3 (C²), 137.8 (C³), 134.5 (C⁷), 134.3 (C^{8a}), 119.8 (C^{4a}), 119.3 (C⁸), 117.6 (C⁶), 56.4 (CH₃O), 15.7 (CH₃); **Elemental analysis**, Calcd for C₁₂H₁₀O₃: C 71.28%, H 4.98%; found C 71.01%, H 5.05%.

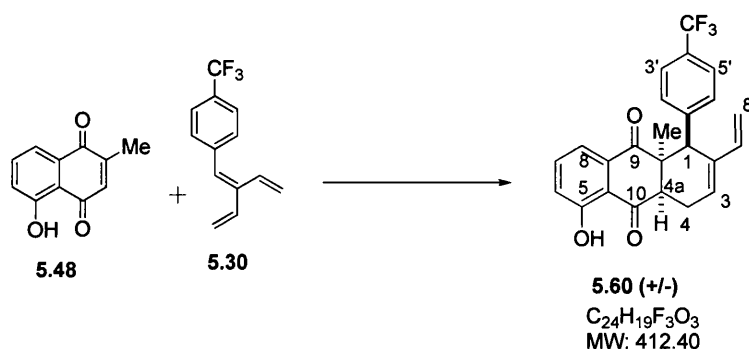
Spectroscopic data in accordance with those reported in literature²⁵³

9.1.3 General Procedure for the Synthesis of the tricyclic compounds: 1st Diels-Alders reaction



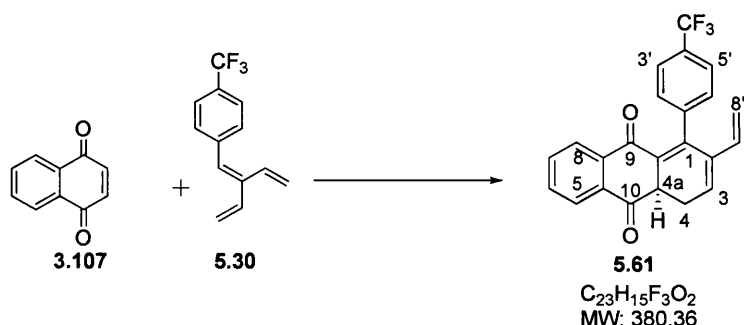
A solution of quinone (0.14 mmol, 1.0 eq.) and cross-conjugated triene (0.21 mmol, 1.5 eq.) in CH_2Cl_2 (5 ml) was cooled to $-35\text{ }^\circ\text{C}$ (acetonitrile in immersion cooler) under inert atmosphere. Boron trifluoride Et_2O ate (0.37 mmol, 2.5 eq.) was added dropwise within 5 min. After stirring for 1 h, the reaction mixture was treated with an additional amount of **cross-conjugated triene** (0.068 mmol, 0.5 eq.). The solution was allowed to stir overnight at $-35\text{ }^\circ\text{C}$. After addition of H_2O (5 ml) the reaction mixture was allowed to warm to $0\text{ }^\circ\text{C}$ under vigorous stirring. Treatment with *n*-hexane (5 ml) followed by cooling to $-60\text{ }^\circ\text{C}$ (acetone/MeOH 1:1 and dry ice) resulted in freezing of the aqueous layer. The supernatant organic phase was removed by pipetting and evaporated under reduced pressure. Purification of the resulting residue was performed by adsorption to silica gel; the unreacted triene and nonpolar side-products were removed by washing with *n*-hexane (500 ml). Elution using CH_2Cl_2 (500 ml) and subsequent evaporation of the solvent afforded the tricyclic compound.¹⁷⁶

(1SR,4aRS,9aSR)-5-hydroxy-9a-methyl-1-(4-(trifluoromethyl)phenyl)-2-vinyl-1,4,4a,9a-tetrahydroanthracene-9,10-dione (5.60)



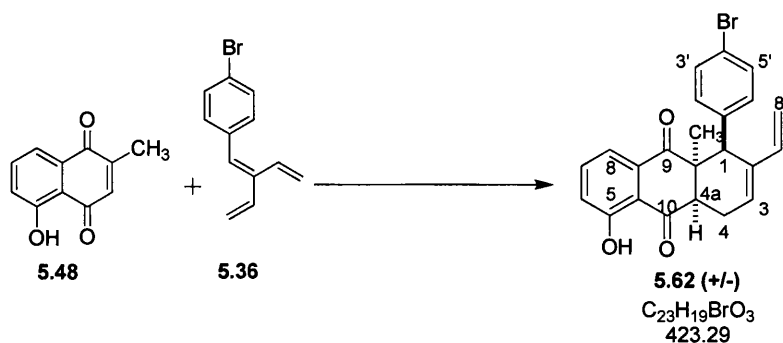
Compound **5.60** is a yellow solid; **Y** = 65%; **R_f** 0.51 (Silica gel, CH₂Cl₂), **Mp** = 114-118 °C; **IR** 2917, 2873, 1690, 1642, 1453, 1418, 1320, 1264, 1162, 1063, 902, 816, 725 cm⁻¹; **¹H NMR** (400MHz, CDCl₃): δ 11.59 (1H, s, OH), 7.34 (2H, dd, *J* = 7.6, 1.6 Hz, H^{6/8}), 7.30 (1H, t, *J* = 7.6Hz, H⁷), 7.06 (2H, d, *J* = 8.2Hz, H^{5',3'}), 6.94 (2H, d, *J* = 8.3Hz, H^{6',2'}), 6.89 (1H, dd, *J* = 7.8, 1.6Hz, H⁸), 6.27 (1H, dd, *J* = 17.6, 10.9Hz, H^{7'}), 6.16 (1H, t, *J* = 3.9Hz, H³), 4.81 (1H, d, *J* = 10.9Hz, H^{8'cis}), 4.65 (1H, d, *J* = 17.6Hz, H^{8'trans}), 4.21 (1H, d, *J* = 6.1Hz, H⁴), 3.78 (1H, s, H¹), 3.14 (1H, d, *J* = 7.9Hz, H^{4a}), 2.43 (1H, dd, *J* = 20.16, 7.9Hz, H⁴), 1.65 (3H, s, CH₃); **¹³C NMR** (100MHz, CDCl₃): δ 202.1 (C^{9/10}), 199.5 (C^{9/10}), 159.8 (0), 142.3 (0), 137.5 (C⁶), 135.8 (C⁸), 134.2 (0), 134.1 (0), 129.5 (C^{6',2'}), 128.2 (C³), 124.5 (q, *J* = 4Hz, C^{5'/3'}), 123.8 (q, *J* = 270Hz, CF₃), 123.1 (C⁷), 118.2 (C^{7'}), 117.5 (0), 113.3 (C^{8'}), 52.1 (0), 49.5 (C¹), 48.1 (C^{4a}), 23.9 (CH₃), 20.3 (C⁴); **MS** (EI): *m/z* 411.53 (M-H⁺) (100); **HRMS**: Found MH⁺ 413.1356, C₂₄H₁₉F₃O₃ requires *MH*, 413.1364.

(RS)-4-(4-(trifluoromethyl)phenyl)-3-vinyl-1,9a-dihydroanthracene-9,10-dione (5.61)



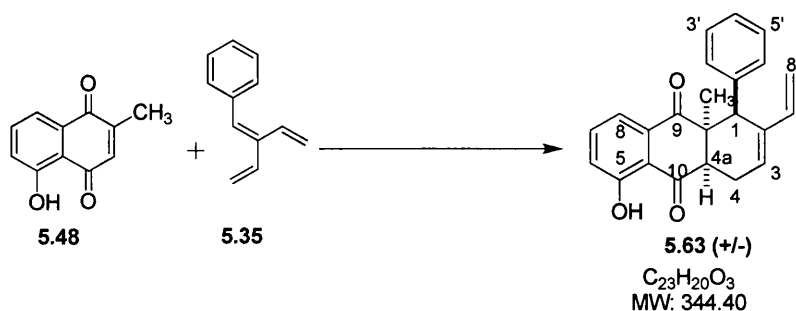
5.61 is a yellow solid; **Y** = 56%; **R_f** 0.52 (Silica gel, CH₂Cl₂); **Mp** = 127-130 °C; **IR** 2359, 2330, 1661, 1594, 1416, 1290, 1163, 1121, 1017, 840 cm⁻¹; **¹H NMR** (400MHz, CDCl₃): δ 8.07 (1H, m, H^{5/8}), 8.03 (1H, m, H^{5/8}), 7.69 (2H, m, H^{7,6}), 7.50 (4H, dd, *J* = 11.96, 8.8Hz, H^{6',2',5',3'}), 6.34 (1H, dd, *J* = 17.6, 10.9Hz, H^{7'}), 6.21 (1H, t, *J* = 2.5Hz, H³), 5.30 (1H, t, H^{4a}), 5.26 (1H, d, *J* = 17.6Hz, H⁸), 5.04 (1H, d, *J* = 10.9Hz, H^{8'}), 3.7 (1H, dt, *J* = 24.8, 4.6Hz, H⁴), 3.46 (1H, ddd, *J* = 22.8, 4.6, 2.5, H⁴); **MS** (EI): *m/z* 381.25 (M+H⁺) (100); **HRMS**: Found MNa⁺ 403.0928, C₂₃H₁₅F₃O₂ requires *MNa*, 403.0922; **Purity** 95 %. Spectroscopic data in accordance with those reported in literature.¹⁷⁶

(1S,4aR,9aS)-1-(4-bromophenyl)-5-hydroxy-9a-methyl-2-vinyl-1,4,4a,9a-tetrahydroanthracene-9,10-dione (5.62)



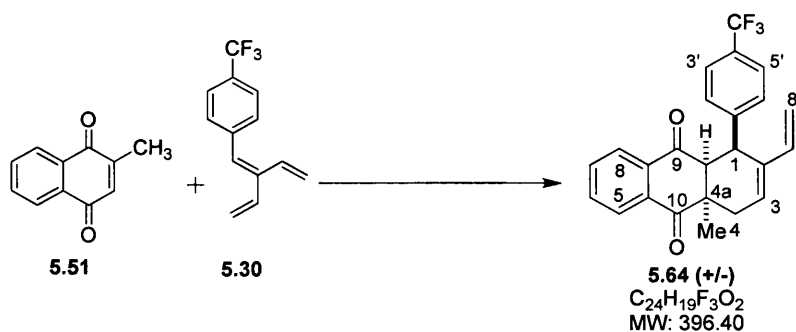
5.62 is a dark yellow solid; **Y** = 92%; **R_f** 0.26 (Silica gel, CH₂Cl₂/*n*-hexane 5:5); **IR** 2975, 2923, 1688, 1639, 1452, 750 cm⁻¹; **¹H NMR** (400MHz, CDCl₃): δ 11.60 (1H, s, OH), 7.60 (2H, m, H^{3',5'}), 7.36 (1H, m, H⁸), 7.26 (2H, d, *J* = 4.3Hz, H^{2',6'}), 6.94 (1H, m, H⁷), 6.68 (1H, m, H⁶), 6.24 (1H, m, H^{7'}), 6.12 (1H, d, *J* = 3.3 Hz, H³), 4.80 (1H, dd, *J* = 10.9, 3.3 Hz, H⁸), 4.67 (1H, dd, *J* = 17.5, 3.2 Hz, H⁸), 3.70 (1H, s, H¹), 3.58 (1H, dd, *J* = 16.1, 4.1 Hz, H⁴), 3.02 (1H, dd, *J* = 7.7, 3.7 Hz, H^{4a}), 2.41 (dd, 1H, *J* = 18.3, 2.5 Hz, H⁴), 1.62 (3H, s, CH₃); **MS** (EI): *m/z* 424.38 (M-H⁺) (100); **Purity** 95 %. Spectroscopic data in accordance with those reported in literature.¹⁷⁶

(1S,4aR,9aS)-5-hydroxy-9a-methyl-1-phenyl-2-vinyl-1,4,4a,9a-tetrahydroanthracene-9,10-dione (5.63)



5.63 is a yellow solid; **Y** = 62%; **R_f** 0.27 (Silica gel, CH₂Cl₂/*n*-hexane 5:5); **IR**: 2971, 2926, 2868, 1690, 1641, 1452, 753 cm⁻¹; **¹H NMR** (400MHz, CDCl₃): δ 11.67 (1H, s, OH), 7.37 (1H, dd, *J* = 8.2, 1.1 Hz, H⁷), 7.30 (1H, t, *J* = 8.0Hz, H⁸), 6.88 (1H, dd, *J* = 8.2, 1.1Hz, H⁶), 6.81 (5H, m, H^{2'-6'}), 6.26 (1H, dd, *J* = 17.6, 10.9Hz, H^{7'}), 6.12 (1H, t, *J* = 3.9Hz, H³), 4.73 (1H, d, *J* = 17.6 Hz, H^{8'}), 3.76 (1H, s, H¹), 3.61 (1H, dd, 20.1, 4.6, H⁴), 3.01 (1H, d, *J* = 8.0Hz, H^{4a}), 2.43 (dd, 1H, *J* = 20.3, 7.8Hz, H⁴); 1.64 (3H, s, CH₃); **MS** (EI): *m/z* 343.64 (M-H⁺) (100); **Purity** 95 %. Spectroscopic data in accordance with those reported in literature.¹⁷⁶

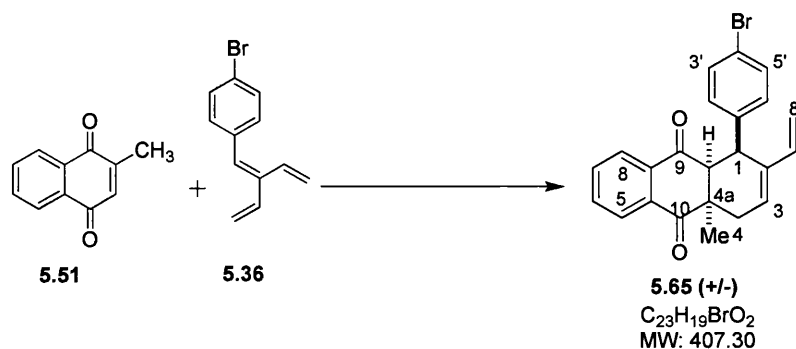
(1SR,4aRS,9aSR)-4a-methyl-1-(4-(trifluoromethyl)phenyl)-2-vinyl-1,4,4a,9a-tetrahydroanthracene-9,10-dione (5.64)



5.64 was obtained as yellow solid; **Y** = 86%; **R_f** 0.36 (Silica gel, chloroform); **Mp** = 79.2 – 78.3 °C; **IR** 3385, 2919, 2358, 1688, 1616, 1592, 1420, 1252, 1163, 1122, 1068, 979, 720 cm⁻¹; **¹H NMR** (400MHz, CDCl₃): δ 7.69 (1H, m, H^{7/6}), 7.54 (1H, m, H^{7/6}), 7.37 (2H, m, H^{5,8}), 6.97 (2H, d, *J* = 8.2Hz, H^{3'}, H^{5'}), 6.87 (2H, d, *J* = 8.2Hz, H^{2',6'}), 6.21 (1H, dd, *J* = 17.6, 10.9Hz, H^{7'}), 6.12 (1H, t, *J* = 4Hz, H³), 4.77 (1H, d, *J* = 10.9Hz, H^{8'cis}), 4.63 (1H, d, *J* = 17.6Hz, H^{8'trans}), 4.23 (1H, d, *J* = 6.4Hz, H^{9a}), 3.67 (1H, dd, *J* = 20.1, 4.6Hz, H⁴), 3.42 (1H, d, *J* = 6.5Hz, H¹), 2.08 (d, 1H, *J* = 20.1Hz, H⁴), 1.26 (3H, s, CH₃); **¹³C NMR** (100MHz, CDCl₃): δ 199.4 (C^{9/10}), 199.3 (C^{9/10}), 142.2, 137.2 (C^{7'}),

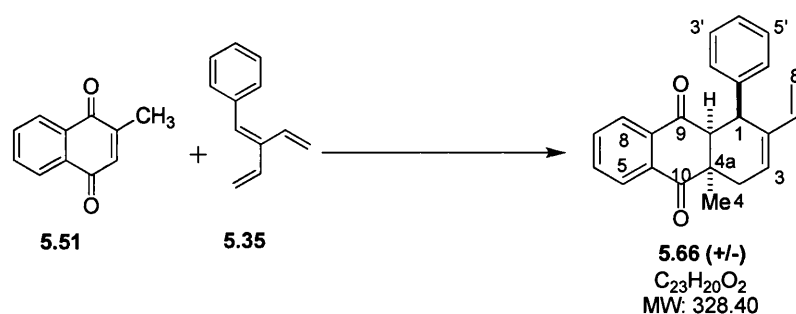
134.9, 134.6, 134.1 ($C^{5/8}$), 133.6, 133.5 ($C^{5/8}$), 130.3 (C^2), 129.9 ($C^{2',6'}$), 126.8 ($C^{7/6}$), 126.1 ($C^{7/6}$), 125.1 ($C^{3',5'}$), 123.9 (CF_3 , q, $J = 270\text{Hz}$), 113.6 ($C^{8'}$), 59.5 (C^1), 45.8 (C^{4a}), 43.9 (C^{9a}), 32.1 (C^4), 30.5 (CH_3); **MS** (EI): m/z 397.47 ($M+H^+$) (100). **HRMS**: Found MNa^+ 419.1254, $C_{24}H_{19}F_3O_2$ requires MNa , 419.1235; **Purity** 95 %.

(1SR,4aRS,9aSR)-1-(4-bromophenyl)-4a-methyl-2-vinyl-1,4,4a,9a-tetrahydroanthracene-9,10-dione (5.65)



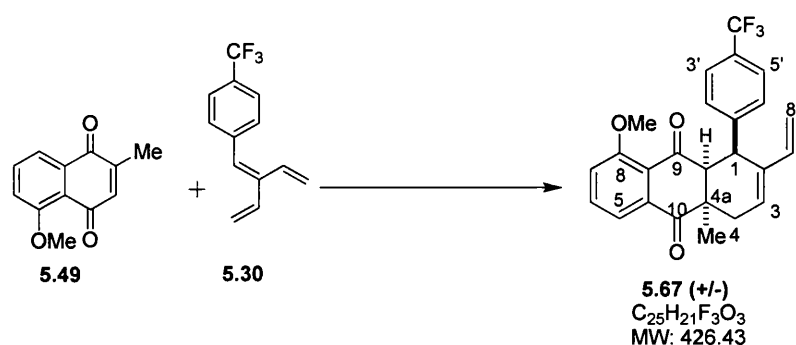
5.65 was obtained as yellow solid; **Y** = 83%; **R_f** 0.33 (Silica gel, chloroform); **Mp** = 85.2 – 86.4 °C; **IR**: 2964, 2359, 2335, 1591, 1485, 1407, 1281, 1249, 1072, 1009, 800, 736 cm^{-1} ; **¹H NMR** (400MHz, $CDCl_3$): δ 7.72 (1H, m, $H^{7/6}$), 7.58 (1H, m, $H^{7/6}$), 7.45 (2H, m, $H^{5,8}$), 6.84 (2H, d, $J = 8.4\text{Hz}$, $H^{3',5'}$), 6.61 (2H, d, $J = 8.4\text{Hz}$, $H^{2',6'}$), 6.19 (1H, dd, $J = 17.6, 10.9\text{Hz}$, H^7), 6.08 (1H, t, $J = 4\text{Hz}$, H^3), 4.76 (1H, d, $J = 10.9\text{Hz}$, $H^{8'cis}$), 4.65 (1H, d, $J = 17.6\text{Hz}$, $H^{8'trans}$), 4.14 (1H, d, $J = 6.2\text{Hz}$, H^{9a}), 3.64 (1H, dd, $J = 20.1, 4.4\text{Hz}$, H^4), 3.38 (1H, d, $J = 6.4\text{Hz}$, H^1), 2.05 (1H, d, $J = 20.0\text{Hz}$, H^4), 1.25 (3H, s, CH_3); **¹³C NMR** (100MHz, $CDCl_3$): δ 199.4 ($C^{9/10}$), 199.1 ($C^{9/10}$), 137.3 (C^3), 137.1, 135.0, 134.9, 133.9 ($C^{5/8}$), 133.7, 133.6 ($C^{5/8}$), 131.2 ($C^{2'/6'/3'/5'}$), 131.1 ($C^{2'/6'/3'/5'}$), 130.0 (C^7), 126.9 ($C^{7/6}$), 126.1 ($C^{7/6}$), 121.2 (0), 113.5 ($C^{8'}$), 59.6 (C^1), 45.6 (C^{4a}), 43.4 (C^{9a}), 31.9 (C^4), 30.4 (CH_3); **MS** (EI): m/z 407.33 ($M+H^+$) (100); **HRMS**: Found MNa^+ 429.0456, $C_{23}H_{19}BrO_2$ requires MNa , 429.0466; **Purity** 95 %.

(1SR,4aRS,9aSR)-4a-methyl-1-phenyl-2-vinyl-1,4,4a,9a-tetrahydroanthracene-9,10-dione (5.66)



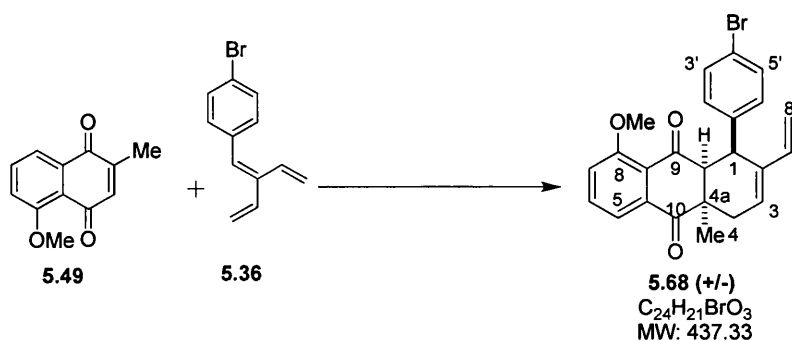
5.66 was obtained as yellow solid; **Y** = 78%; **R_f** 0.36 (Silica gel, chloroform); **Mp** = 77.4 °C; **IR** 2926, 2359, 1592, 1492, 1453, 1282, 1251, 979, 701 cm⁻¹; **¹H NMR** (400MHz, CDCl₃): δ 7.69 (1H, m, H^{7/6}), 7.54 (1H, m, H^{7/6}), 7.35 (2H, m, H^{5,8}), 6.64 - 6.79 (5H, m, H^{2'-6'}), 6.20 (1H, dd, *J* = 17.6, 10.9Hz, H^{7'}), 6.06 (1H, t, *J* = 3.8Hz, H³), 4.75 (1H, d, *J* = 10.9Hz, H^{8'cis}), 4.68 (1H, d, *J* = 17.6Hz, H^{8'trans}), 4.18 (1H, d, *J* = 6.3Hz, H^{9a}), 3.57 (1H, dd, *J* = 20.1, 4.4Hz, H⁴), 3.39 (1H, d, *J* = 6.4Hz, H¹), 2.05 (1H, d, *J* = 20.0Hz, H⁴), 1.24 (3H, s, CH₃); **¹³C NMR** (100MHz, CDCl₃): δ 199.8 (C^{9/10}), 199.4 (C^{9/10}), 137.8 (C³), 137.4 (0), 135.4 (0), 134.9 (0), 133.7 (C^{5/8}), 133.6 (0), 133.2 (C^{5/8}), 129.5 (C^{2'-6'}), 129.4 (C^{2'-6'}), 128.1 (C^{7'}), 127.2 (C^{7/6}), 126.6 (C^{7/6}), 125.9 (0), 113.3 (C^{8'}), 59.8 (C¹), 45.8 (C^{4a}), 44.2 (C^{9a}), 32.1 (C⁴), 30.7 (CH₃); **MS** (EI): *m/z* 329.39 (M+H⁺) (100); **HRMS**: Found MNa⁺, 351.1362, C₂₃H₂₀O₂ requires *MNa*, 351.1361; **Purity** 95 %.

(1SR,4aRS,9aSR)-8-methoxy-4a-methyl-1-(4-(trifluoromethyl)phenyl)-2-vinyl-1,4,4a,9a-tetrahydroanthracene-9,10-dione (5.67)



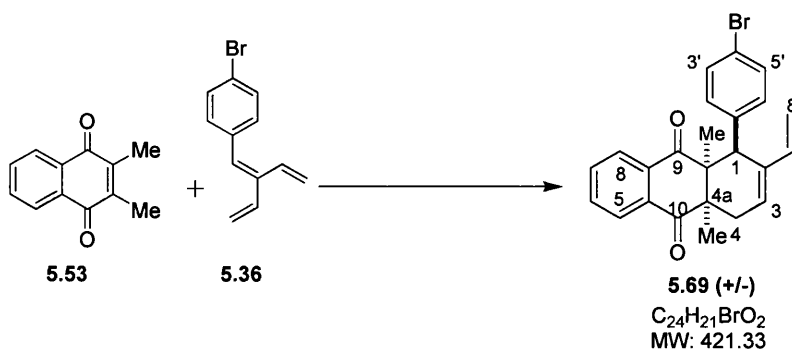
5.67 was obtained as yellow solid; **Y** = 76%; **R_f** 0.28 (Silica gel, chloroform); **Mp** = 107.9 - 110.3 °C; **IR**: 3374, 2931, 2358, 1684, 1585, 1468, 1277, 1231, 1163, 1120, 1068, 993 cm⁻¹; **¹H NMR** (500MHz, CDCl₃): δ 7.32 (1H, t, *J* = 8.0Hz, H⁶), 7.24 (1H, m, H^{7/5}), 7.02 (2H, d, *J* = 8.2Hz, H^{3',5'}), 6.94 (2H, d, *J* = 8.3Hz, H^{2',6'}), 6.92 (1H, dd, *J* = 8.4, 1.0Hz, H^{5/7}), 6.22 (1H, dd, *J* = 17.6, 11.0Hz, H^{7'}), 6.13 (1H, t, *J* = 4.0Hz, H³), 4.78 (1H, d, *J* = 10.9Hz, H^{8'cis}), 4.62 (1H, d, *J* = 17.6Hz, H^{8'trans}), 4.26 (1H, d, *J* = 6.9Hz, H^{9a}), 3.89 (s, 3H, CH₃), 3.58 (1H, dd, *J* = 19.8, 4.9Hz, H⁴), 3.37 (1H, d, *J* = 6.5Hz, H¹), 2.08 (1H, d, *J* = 19.8Hz, H⁴), 1.31 (3H, s, CH₃); **¹³C NMR** (125MHz, CDCl₃): δ 199.0 (C^{9/10}), 198.9 (C^{9/10}), 158.1 (C⁸), 142.8 (C^{1'}), 137.2 (C^{7'}), 135.3 (C^{5a}), 134.5 (C⁶), 134.1 (C^{8a}), 130.1 (C³), 129.8 (C²), 129.4 (C^{5',6'}), 124.6 (C^{2'/3'}), 124.6 (C^{2'/3'}), 124.0 (CF₃, q, *J* = 270Hz), 118.8 (C^{5/7}), 116.8 (C^{5/7}), 113.4 (C^{8'}), 61.0 (C¹), 56.3 (CH₃), 45.6 (C^{4a}), 43.1 (C^{9a}), 31.9 (C⁴), 29.3 (CH₃); **MS** (EI): *m/z* 427.33 (M+H⁺) (100); **HRMS**: Found MNa⁺, 449.1351, C₂₅H₂₁F₃O₃ requires *MNa*, 449.1341; **Purity** 95 %.

(1SR,4aRS,9aSR)-1-(4-bromophenyl)-8-methoxy-4a-methyl-2-vinyl-1,4,4a,9a-tetrahydroanthracene-9,10-dione (5.68)



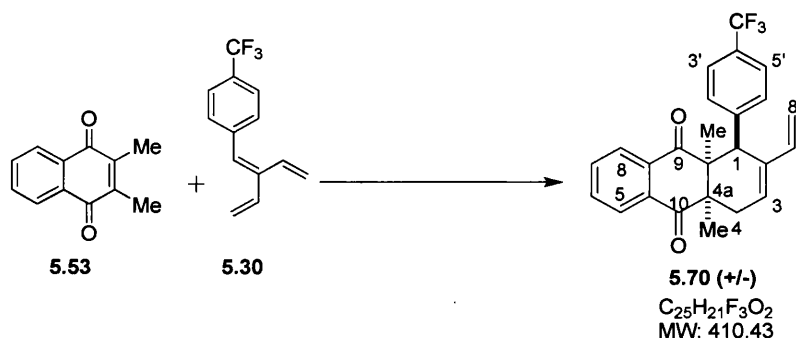
5.68 was obtained as yellow solid; **Y** = 81%; **R_f** 0.29 (Silica gel, chloroform); **Mp** = 115.2 – 116.9 °C; **IR**: 3400, 2964, 2359, 1680, 1584, 1485, 1467, 1275, 1229, 1069, 992 cm⁻¹; **¹H NMR** (500MHz, CDCl₃): δ 7.32 (1H, t, *J* = 8.0Hz, H⁶), 7.24 (1H, m, H^{7/5}), 7.02 (2H, d, *J* = 8.2Hz, H^{3',5'}), 6.94 (2H, d, *J* = 8.3Hz, H^{2',6'}), 6.92 (1H, dd, *J* = 8.4, 1.0Hz, H^{5/7}), 6.22 (1H, dd, *J* = 17.6, 11.0Hz, H^{7'}), 6.08 (1H, t, *J* = 4.0Hz, H³), 4.77 (1H, d, *J* = 10.9Hz, H^{8'cis}), 4.64 (1H, d, *J* = 17.6Hz, H^{8'trans}), 4.16 (1H, d, *J* = 6.7Hz, H^{9a}), 3.91 (s, 3H, CH₃), 3.56 (1H, dd, *J* = 19.8, 4.8Hz, H⁴), 3.33 (1H, d, *J* = 6.9Hz, H¹), 2.04 (1H, dd, *J* = 19.8, 2.0Hz, H⁴), 1.29 (3H, s, CH₃); **¹³C NMR** (125MHz, CDCl₃): δ 199.2 (C^{9/10}), 198.2 (C^{9/10}), 158.2 (C⁸), 137.6 (C^{1'}), 137.1 (C^{7'}), 135.4 (C^{5a}), 134.4 (C^{8a}), 134.3 (C⁶), 130.8 (C^{2',6'}), 130.7 (C^{3',5'}), 129.8 (C³), 123.4 (C²), 120.8 (C^{4'}), 118.9 (C^{5/7}), 116.8 (C^{5/7}), 113.3 (C^{8'}), 61.2 (C¹), 56.4 (CH₃), 45.5 (C^{4a}), 42.8 (C^{9a}), 31.9 (C⁴), 29.3 (CH₃); **MS** (EI): *m/z* 437.22 (M+H⁺) (100); **HRMS**: Found MH⁺, 437.0737, C₂₄H₂₁BrO₃ requires *M*, 437.0752; **Purity** 95 %.

(1SR,4aRS,9aSR)-1-(4-bromophenyl)-4a,9a-dimethyl-2-vinyl-1,4,4a,9a-tetrahydroanthracene-9,10-dione (5.69)



5.69 was obtained as yellow solid; **Y** = 80%; **R_f** 0.39 (Silica gel, chloroform); **Mp** = 103.8 - 105.4 °C; **IR** 3441, 2969, 2359, 2330, 1741, 1680, 1592, 1370, 1262, 1010, 980 cm⁻¹; **¹H NMR** (400MHz, CDCl₃): δ 7.75 (1H, m, H^{5/8}), 7.57 (1H, m, H^{8/5}), 7.44 (2H, m, H^{7,6}), 6.84 (2H, d, *J* = 8.3Hz, H^{3',5'}), 6.63 (2H, dd, *J* = 8.7, 1.0Hz, H^{2',6'}), 6.22 (1H, dd, *J* = 17.6, 10.9Hz, H^{7'}), 6.12 (1H, t, *J* = 4.0Hz, H³), 4.76 (1H, d, *J* = 10.9Hz, H^{8'cis}), 4.57 (1H, d, *J* = 17.7Hz, H^{8'trans}), 3.74 (1H, s, H¹), 3.55 (1H, dd, *J* = 19.8, 4.4Hz, H⁴), 2.06 (1H, ddt, *J* = 19.7, 2.0, 1.0Hz, H⁴), 1.57 (3H, s, CH₃), 1.14 (3H, s, CH₃); **¹³C NMR** (100MHz, CDCl₃): δ 201.5 (C^{9/10}), 199.8 (C^{9/10}), 137.6 (C^{7'}), 137.2 (C²), 134.6 (C^{1'/4'}), 134.0 (C^{8a}), 133.9 (C^{9a}), 133.3 (C^{6/7}), 133.1 (C^{6/7}), 131.5 (C^{2',6'}), 130.8 (C^{3',5'}), 129.4 (C³), 126.1 (C^{5,8}), 121.0 (C^{1'/4'}), 113.1 (C^{8'}), 55.8 (C^{4a/9a}), 52.1 (C¹), 49.3 (C^{4a/9a}), 30.8 (C⁴), 26.7 (CH₃), 19.8 (CH₃); **MS** (EI): *m/z* 443.07 (M+Na⁺) (100); **HRMS**: Found MNa⁺ 443.0604, C₂₄H₂₁BrO₂ requires *MNa*, 443.0623; **Purity** 95%.

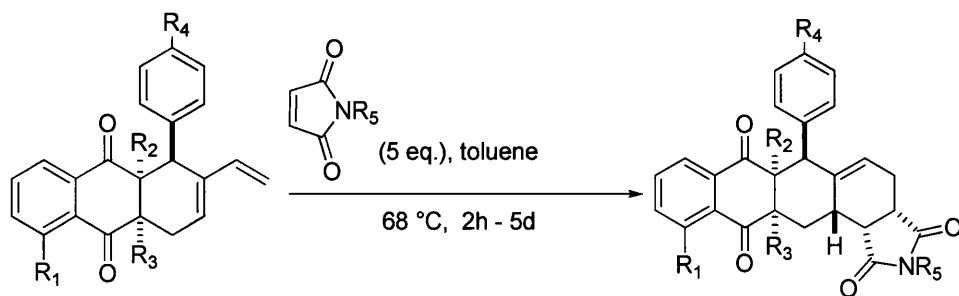
(1S,4aR,9aS)-4a,9a-dimethyl-1-(4-(trifluoromethyl)phenyl)-2-vinyl-1,4,4a,9a-tetrahydroanthracene-9,10-dione (5.70)



5.70 was obtained as yellow solid; **Y** = 77%; **R_f** 0.37 (Silica gel, chloroform); **Mp** = 122.7 – 124.3 °C; **IR** 2985, 2873, 2358, 1681, 1615, 1594, 1419, 1262, 1111, 980 cm⁻¹; **¹H NMR** (400MHz, CDCl₃): δ 7.71 (1H, m, H^{8/5}), 7.50 (1H, m, H^{8/5}), 7.34 (2H, m, H^{7,6}), 6.94 (2H, d, *J* = 8.1Hz, H^{3',5'}), 6.87 (2H, dd, *J* = 8.2Hz, H^{2',6'}), 6.21 (1H, dd, *J* = 17.6, 11.0Hz, H^{7'}), 6.14 (1H, t, *J* = 3.9Hz, H³), 4.72 (1H, d, *J* = 11.0Hz, H^{8'cis}), 4.53 (1H, d, *J* = 17.6Hz, H^{8'trans}), 3.81 (1H, s, H¹), 3.55 (1H, dd, *J* = 19.8, 4.9Hz, H⁴), 2.05 (1H, dt, *J* = 19.8, 0.9Hz, H⁴), 1.57 (3H, s, CH₃), 1.11 (3H, s, CH₃); **¹³C NMR** (100MHz, CDCl₃): δ 201.2 (C^{9/10}), 199.6 (C^{9/10}), 142.4 (C²), 137.6 (C^{7'}), 134.6 (C^{1',4'}), 133.8 (C^{8a}), 133.7 (C^{9a}), 133.5 (C^{6/7}), 133.2 (C^{6/7}), 130.2 (C^{3',5'}), 129.7 (C^{2',6'}), 129.4 (C³), 126.1 (C^{5,8}), 124.6 (C⁸), 124.0 (q, *J* = 270Hz, CF₃), 113.3 (C^{8'}), 55.8 (C^{4a/9a}), 52.4 (C¹), 49.3 (C^{4a/9a}), 30.8 (C⁴), 26.7 (CH₃), 19.9 (CH₃); **MS** (EI): *m/z* 410.52 (M+H⁺) (100); **HRMS**: Found MH⁺, 411.1552, C₂₅H₂₁F₃O₂ requires *M*, 411.1572; **Purity** 95%.

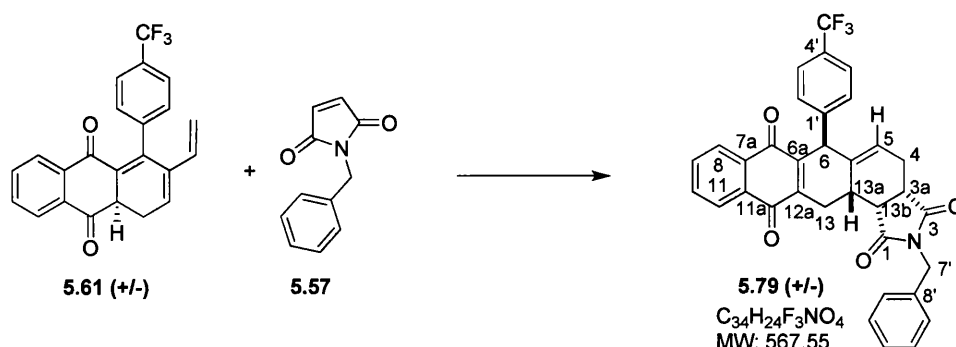
9.1.4 General Procedure for the synthesis of the pentacyclic compounds: 2nd

Diels-Alders reaction



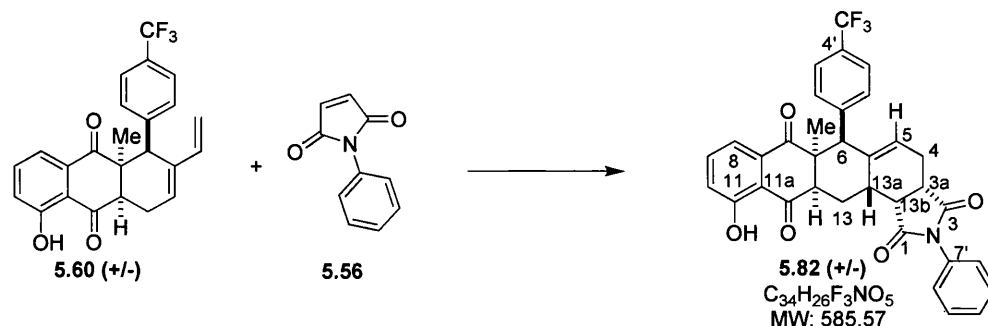
Each tricyclic intermediate was placed in a sealed glass tube under dry, inert conditions. Different maleimides (up to 5 equiv) were added to the glass tube in addition to toluene (1-10 mL). The solution was stirred for 2h – 3 days at 70 °C. Removal of the solvent under reduced pressure followed by flash column chromatography afforded the pentacyclic compounds in various yields¹⁷⁶.

(3aSR,6SR,13aSR,13bRS)-2-benzyl-6-(4-(trifluoromethyl)phenyl)-3a,4,13,13a-tetrahydro-1H-anthra[2,3-e]isoindole-1,3,7,12(2H,6H,13bH)-tetraone (5.79)



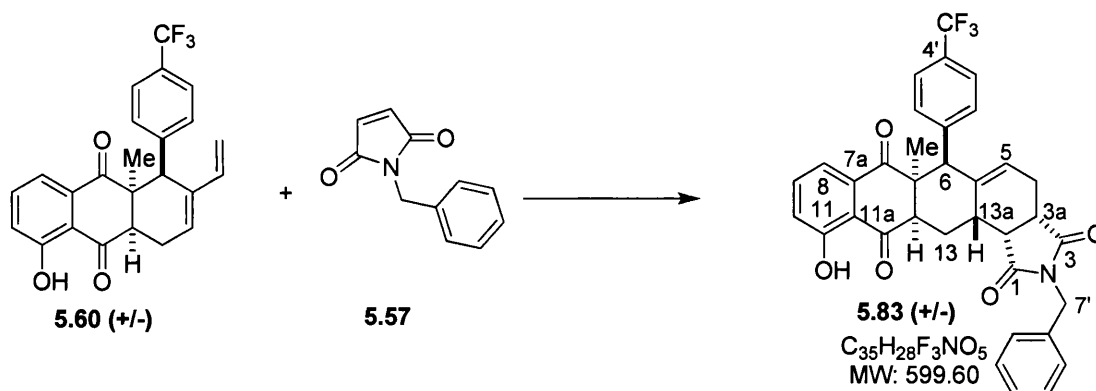
5.79 was obtained as a clear yellow solid; **Y** = 85%; **R_f** 0.09 (Silica gel, CH₂Cl₂); **Mp** = 145-150 °C; **IR**: 2363, 2339, 1707, 1325, 1165, 668 cm⁻¹; **¹H NMR** (400MHz, CDCl₃): δ 8.20 (m, 1H, H^{8/11}), 8.08 (m, 1H, H^{8/11}), 7.73 (m, 2H, H^{9,10}), 7.47 (d, 2H, *J* = 8.3Hz, H^{5',3'}), 7.22 (d, 2H, *J* = 8.4Hz, H^{2',6'}), 7.14 (t, 1H, *J* = 7.4Hz, H^{11'}), 7.04 (t, 2H, *J* = 7.3Hz, H^{10',12'}), 6.89 (d, 2H, *J* = 7.2Hz, H^{9',13'}), 6.00 (m, 1H, H⁵), 5.08 (s, 1H, H⁶), 4.41 (d, 1H, *J* = 14.2Hz, H^{7'}), 4.30 (d, 1H, *J* = 14.2Hz, H^{7'}), 3.71 (d, 1H, *J* = 17.4Hz, H¹³), 3.20 (m, 1H, H^{13b}), 3.17 (dt, 1H, *J* = 8.7, 1.1Hz, H^{3a}), 3.01 (m, 1H, H^{13a}), 2.91 (ddd, 1H, *J* = 14.9, 7.2, 1.4Hz, H⁴), 2.44 (dd, 1H, *J* = 17.4, 9.3Hz, H¹³), 2.30 (ddd, 1H, *J* 15.4, 6.6, 2.9 Hz, H⁴); **¹³C NMR** (100MHz, CDCl₃): δ 183.3 (C¹²), 182.9 (C⁷), 178.8 (C³), 177.2 (C¹), 146.4 (0), 144.2 (0), 141.7 (0), 139.2 (0), 135.5 (0), 133.7 (C^{9/10}), 133.4 (C^{9/10}), 132.1 (C^{6a/12a}), 131.8 (C^{6a/12a}), 128.4 (C^{10',12'}), 127.7 (C^{11'}), 127.6 (C^{9',3'}), 127.4 (C^{2',6'}), 126.7 (C^{8/11}), 126.5 (C^{8/11}), 125.5 (C^{5',3'}), 124.1 (C⁵), 124.0 (q, CF₃, *J* = 270Hz), 44.1 (C^{13b}), 43.1 (C⁶), 42.2 (C^{7'}), 39.2 (C^{3a}), 32.8 (C^{13a}), 24.9 (C⁴), 23.6 (C¹³); **MS** (EI): *m/z* 568.41 (M+H⁺) (100); **HRMS** (ESI): Found 568.1752 [M+H]⁺, calculated for C₃₄H₂₅F₃NO₄ 568.1736; **Elemental analysis** calculated for C₃₄H₂₄F₃NO₄: C, 71.95; H, 4.26; N, 2.47. Found: C, 72.02; H, 4.20; N, 2.56.

(3aSR,6SR,6aSR,13aSR,13bRS)-11-hydroxy-6a-methyl-2-phenyl-6-(4-(trifluoromethyl)phenyl)-3a,4,6,6a,13,13a-hexahydro-1H-anthra[2,3-e]isoindole-1,3,7,12 (2H,12aH,13bH)-tetraone (5.82)



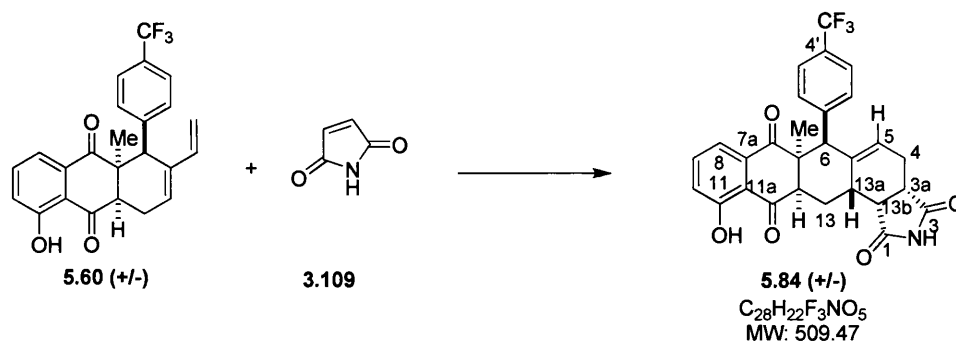
5.82 was obtained as a yellow solid; **Y** = 86%; **R_f** 0.08 (Silica gel, CH₂Cl₂); **Mp** = 125-127 °C; **IR**: 2909, 1976, 1707, 1325, 1165 cm⁻¹; **¹H NMR** (400MHz, CDCl₃): δ 11.91 (s, 1H, OH), 7.53 (t, 1H, *J* = 7.9Hz, H⁹), 7.5 (dd, 2H, *J* = 5.6, 1.4Hz, H^{8',12'}), 7.45 (m, 3H, H^{9',10',11'}), 7.41 (d, 2H, *J* = 8.4, H^{5',H3'}), 7.32 (dd, 1H, *J* = 7.5, 0.8Hz, H¹⁰), 7.25 (d, 2H, *J* = 8.0 Hz, H^{2',6'}), 7.13 (d, 1H, *J* = 5.3Hz, H⁸), 5.41 (dt, 1H, *J* = 5.9, 2.7Hz, H⁵), 3.51 (s, 1H, H⁶), 3.35 (dd, 1H, *J* = 11.6, 5.8Hz, H^{12a}), 3.33 (dd, 1H, *J* = 9.4, 5.8Hz, H^{13b}), 3.28 (dd, 1H, *J* = 8.3, 1.7Hz, H^{3a}), 3.03 (ddd, 1H, *J* = 14.5, 8.6, 6.3 Hz, H¹³), 2.86 (m, 1H, H^{13a}), 2.72 (ddd, 1H, *J* = 15.7, 7.0, 1.3Hz, H⁴), 2.60 (ddd, 1H, *J* = 14.9, 8.4, 6.8 Hz, H¹³), 2.21 (m, 1H, H⁴), 1.36 (s, 3H, CH₃); **¹³C NMR** (100MHz, CDCl₃): δ 204.3 (C¹²), 199.3 (C⁷), 178.3 (C³), 177.5 (C¹), 161.1 (C¹¹), 142.8 (C^{1'/7a}), 140.5 (C^{5a}), 136.9 (C⁹), 135.6 (C^{7'}), 131.7 (C^{4'}), 131.3 (C^{2',6'}), 129.2 (C^{9',C11'}), 128.8 (C^{10'}), 126.4 (C^{8',12'}), 124.9 (C^{5',3'}), 124.0 (q, CF₃, *J* = 270Hz), 123.9 (C⁵), 123.4 (C⁸), 118.6 (C¹⁰), 116.6 (C^{11a}), 56.2 (C⁶), 53.9 (C^{12a}), 52.7 (C^{6a}), 44.7 (C^{13b}), 40.2 (C^{3a}), 32.8 (C^{13a}), 25.6 (C⁴), 25.1 (CH₃), 24.2 (C¹³); **MS** (EI): *m/z* = 584.74 (M-H⁺) (100); **HRMS**: Found 586.1816 [M+H]⁺, calculated for C₃₄H₂₇F₃NO₅ 586.1841; **Elemental analysis** calculated for C₃₄H₂₆F₃NO₅: C, 69.74; H, 4.48; N, 2.39. Found: C, 69.75; H, 4.23; N, 2.36.

(3aSR,6SR,6aSR,13aSR,13bRS)-2-benzyl-11-hydroxy-6a-methyl-6-(4-(trifluoromethyl)phenyl)-3a,4,6,6a,13,13a-hexahydro-1H-anthra[2,3-e]isoindole-1,3,7,12 (2H,12aH,13bH)-tetraone (5.83)



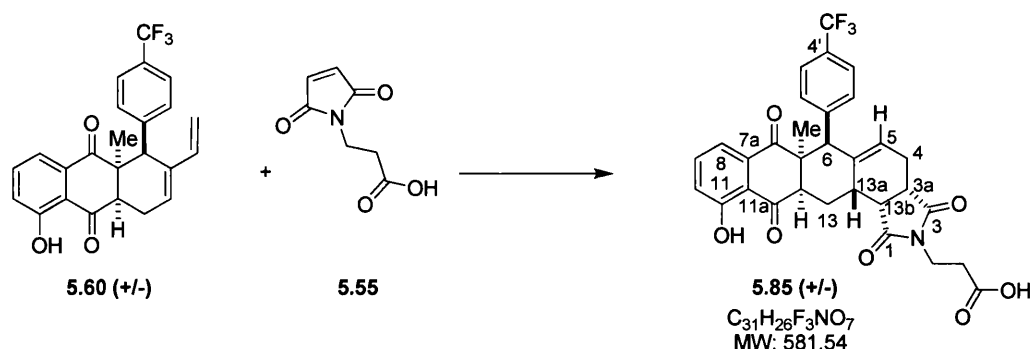
5.83 was obtained as a clear yellow solid; **Y** = 82%; **R_f** 0.09 (Silica gel, CH₂Cl₂); **Mp** = 120-122 °C; **IR**: 2032, 1695, 1396, 1163, 1111, 1068, 699 cm⁻¹; **¹H NMR** (400MHz, CDCl₃): δ 11.87 (s, 1H, OH), 7.49 (t, 1H, *J* = 8.0Hz, H⁹), 7.33 (d, 2H, *J* = 8.2Hz, H^{3',5'}), 7.28 (d, 1H, *J* = 8.7Hz, H¹⁰), 7.25 (m, 5H, H^{8'-13'}), 7.12 (d, 1H, *J* = 8.3Hz, H⁸), 7.03 (d, 2H, *J* = 8.2Hz, H^{2',H6'}), 5.21 (dt, 1H, *J* = 5.8, 2.7Hz, H⁵), 4.61 (d, 1H, *J* = 14.1Hz, H^{7'}), 4.54 (d, 1H, *J* = 14.1Hz, H^{7'}), 3.25 (t, 1H, *J* = 6.5Hz, H^{12a}), 3.18 (s, 1H, H⁶), 3.14 (m, 2H, H^{3a,13b}), 2.95 (ddd, 1H, *J* = 14.6, 8.2, 6.4Hz, H¹³), 2.74 (m, 1H, H^{13a}), 2.63 (dd, 1H, *J* = 15.4, 7.6, H⁴), 2.50 (ddd, 1H, *J* = 15.0, 8.5, 7.0Hz, H¹³), 2.12 (tdd, 1H, *J* = 17.65, 6.31, 3.27 Hz, H⁴), 1.22 (s, 3H, CH₃); **¹³C NMR** (100MHz, CDCl₃): δ 204.4 (C¹²), 199.3 (C⁷), 178.9 (C³), 178.0 (C¹), 161.1 (C¹¹), 142.8 (C^{1',4'}), 140.3 (C^{5a}), 136.9 (C⁹), 135.8 (C⁸), 135.6 (C^{7a}), 131.6 (C^{2',6'}), 128.7 (C C^{9'/10'/12'/13'}), 128.4 (C^{9'/10'/12'/13'}), 127.8 (C^{11'}), 124.7 (C^{5',3'}), 124.0 (q, CF₃, *J* = 270Hz), 123.9 (C⁵), 123.3 (C⁸), 118.6 (C¹⁰), 116.5 (C^{11a}), 56.8 (C⁶), 54.1 (C^{12a}), 52.6 (C^{6a}), 44.6 (C^{13b}), 42.4 (C^{7'}), 40.1 (C^{3a}), 32.6 (C^{13a}), 25.2 (C⁴), 25.1 (CH₃), 24.2 (C¹³); **MS** (EI): *m/z* 600.64 (M+H⁺) (100); **HRMS** (EI): Found 600.2014 [M+H]⁺, calculated for C₃₅H₂₉F₃NO₅ 600.1998 [M+H]⁺; **Elemental analysis** calculated for C₃₅H₂₈F₃NO₅: C, 70.11; H, 4.71; N, 2.34. Found: C, 70.09; H, 4.51; N, 2.29.

(3aSR,6SR,6aSR,13aSR,13bRS)-11-hydroxy-6a-methyl-6-(4-(trifluoromethyl)phenyl)-3a,4,6,6a,13,13a-hexahydro-1H-anthra[2,3-e]isoindole-1,3,7,12(2H,12aH,13bH)-tetraone (5.84)



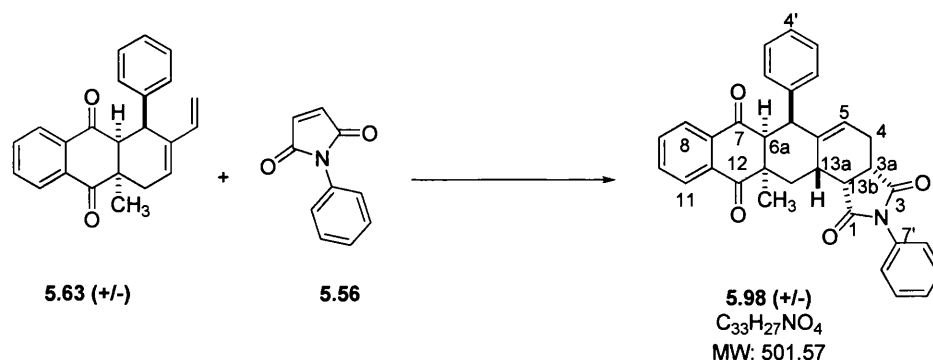
5.84 was obtained as a dark yellow solid; **Y** = 90%; **R_f** 0.08 (Silica gel, CH₂Cl₂); **Mp** = 273-280 °C; **IR**: 3356, 2364, 2355, 2174, 2049, 1641 cm⁻¹; **¹H NMR** (400MHz, CDCl₃): δ 11.85 (s, 1H, OH), 8.8 (br s, 1H, NH), 7.49 (t, 1H, *J* = 7.9Hz, H⁹), 7.34 (d, 2H, *J* = 8.3Hz, H^{3',5'}), 7.28 (dd, 1H, *J* = 7.55, 0.97Hz, H¹⁰), 7.22 (d, 2H, *J* = 8.2Hz, H^{2',6'}), 7.11 (dd, 1H, *J* = 8.3, 0.95Hz, H⁸), 5.37 (m, 1H, H⁵), 3.54 (s, 1H, H⁶), 3.28 (t, 1H, *J* = 6.22Hz, H^{12a}), 3.22 (dd, 1H, *J* = 8.7, 5.5Hz, H^{13b}), 3.15 (td, 1H, *J* = 8.3, 1.4Hz, H^{3a}), 2.97 (ddd, 1H, *J* = 15.5, 9.2, 6.5Hz, H¹³), 2.78 (m, 1H, H^{13a}), 2.57 (m, 1H, H⁴), 2.50 (m, 1H, H¹³), 2.13 (m, 1H, H⁴), 1.25 (s, 3H, CH₃); **¹³C NMR** (100MHz, CDCl₃): δ 204.5 (C¹²), 199.3 (C⁷), 179.8 (C³), 178.9 (C¹), 160.7 (C¹¹), 143.3 (C^{1',4'}), 140.1 (C^{5a}), 136.9 (C⁹), 135.8 (C^{7a}), 131.4 (C^{2',6'}), 124.7 (C^{5',3'}), 124.2 (C⁵), 124.0 (q, CF₃, *J* = 270Hz), 123.3 (C⁸), 118.6 (C¹⁰), 116.9 (C^{11a}), 55.8 (C⁶), 53.4 (C^{12a}), 52.8 (C^{6a}), 44.5 (C^{13b}), 41.1 (C^{3a}), 32.3 (C^{13a}), 25.1 (CH₃), 24.9 (C⁴), 23.6 (C¹³); **MS (EI)**: *m/z* 510.41 (M+H⁺) (100); **HRMS**: Found 532.1348 [M+Na]⁺, C₂₈H₂₂F₃NNaO₅, calculated 532.1348 [M+Na]⁺; **Elemental analysis** calculated for C₂₈H₂₂F₃NO₅: C, 66.01; H, 4.35; N, 2.75. Found: C, 66.67; H, 4.27; N, 2.66.

3-((3aSR,6SR,6aSR,13aSR,13bRS)-11-hydroxy-6a-methyl-1,3,7,12-tetraoxo-6-(4-(trifluoromethyl)phenyl)-3a,4,6a,7,12,12a,13,13a-octahydro-1H-anthra[2,3-e]isoindol-2(3H,6H,13bH)-yl)propanoic acid (5.85)



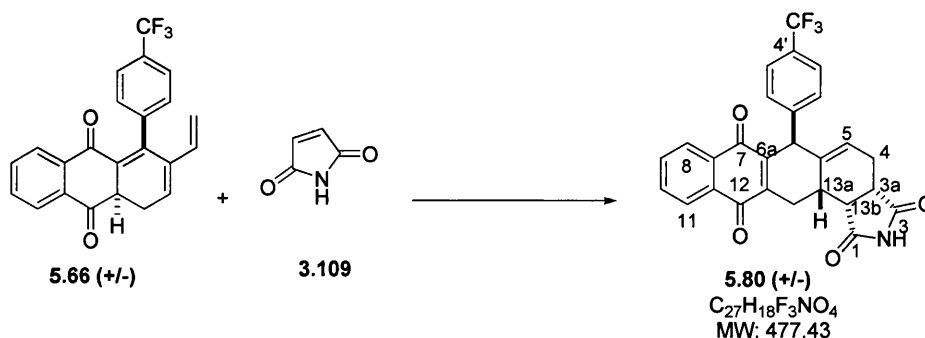
5.85 was obtained as an orange solid; **Y** = 95%; **R_f** 0.14 (Silica gel, EtOAc); **Mp** = 129-132 °C; **IR**: 2919, 2360, 2335, 2167, 2140, 1990, 1699 cm⁻¹. **¹H NMR** (400MHz, CDCl₃): δ 11.82 (s, 1H, OH), 10.43 (br s, 1H, COOH), 7.46 (t, 1H, *J* = 7.9Hz, H⁹), 7.32 (d, 2H, *J* = 8.3Hz, H^{3',5'}), 7.23 (dd, 1H, *J* = 7.4, 0.8Hz, H¹⁰), 7.22 (d, 2H, *J* = 8.2Hz, H^{2',6'}), 7.07 (dd, 1H, *J* = 8.4, 0.9Hz, H⁸), 5.25 (m, 1H, H⁵), 3.78 (t, 2H, *J* = 7.1Hz, H^{7'}), 3.45 (s, 1H, H⁶), 3.27 (t, 1H, *J* = 6.3Hz, H^{12a}), 3.16 (t, 1H, *J* = 9.5Hz, C^{13b}), 3.13 (m, 1H, H^{3a}), 2.94 (m, 1H, H¹³), 2.74 (m, 1H, H^{13a}), 2.64 (t, 2H, *J* = 7.1Hz, H^{8'}), 2.56 (m, 1H, H⁴), 2.51 (dt, 1H, *J* = 16.0, 9.0 Hz, H¹³), 2.10 (m, 1H, H⁴), 1.31 (s, 3H, CH₃); **¹³C NMR** (100MHz, CDCl₃): δ 204.5 (C¹²), 199.3 (C⁷), 179.3 (C³), 178.7 (C¹), 176.0 (C^{9'}), 160.7 (C¹¹), 143.3 (C^{1',4'}), 140.1 (C^{5a}), 136.9 (C⁹), 135.5 (C^{7a}), 131.4 (C^{2',C6'}), 124.7 (C^{5',3'}), 124.0 (C⁵), 124.0 (q, CF₃, *J* = 270Hz), 123.3 (C⁸), 118.6 (C¹⁰), 116.6 (C^{11a}), 55.7 (C⁶), 53.5 (C^{12a}), 52.8 (C^{6a}), 44.3 (C^{3a}), 39.8 (C^{13b}), 33.3 (C^{7'}), 32.4 (C^{13a}), 32.5 (C^{8'}), 25.1 (C⁴), 25.0 (CH₃), 23.6 (C¹³). **MS (EI)**: *m/z* 604.49 (M+Na⁺) (100); **HRMS**: Found 604.0683 [M+Na]⁺, calculated for C₃₁H₂₆F₃NNaO₇ 604.1559 [M+Na]⁺; **Elemental analysis**, calculated for C₃₁H₂₆F₃NO₇: C, 64.03; H, 4.51; N, 2.41. Found: C, 64.03; H, 4.24; N, 2.61.

(3aSR,6aSR,6aSR,12aRS,13aSR,13bRS)-12a-methyl-2,6-diphenyl-3a,4,6,6a,13,13a - hexahydro-1H-anthra[2,3-e]isoindole-1,3,7,12(2H,12aH,13bH)-tetraone



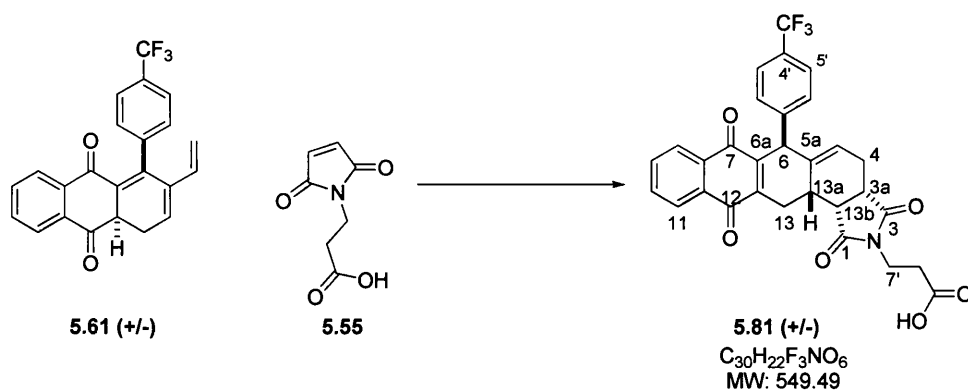
5.98 was obtained as a white solid; **Y** = 82%; **R_f** 0.07 (Silica gel, CH₂Cl₂); **Mp** = 127-130 °C; **IR**: 2922, 2359, 2165, 2011, 1958, 1683, 694 cm⁻¹. **¹H NMR** (400MHz, CDCl₃): δ 7.93 (d, 1H, *J* = 7.6Hz, H^{8/11}), 7.58 (m, 3H, H^{8/11,9,10}), 7.35–7.48 (m, 3H, H^{3'-5'}), 7.14 (m, 2H, H^{2',6'}), 6.97 (dd, 3H, *J* = 5.1, 1.8Hz, H^{9'-11'}), 6.68 (dd, 2H, *J* = 7.9, 2.4Hz, H^{8',12'}), 5.48 (dt, 1H, *J* = 5.8, 2.5 Hz, H⁵), 4.15 (d, 1H, *J* = 8.9Hz, H⁶), 3.45 (d, 1H, *J* = 10.3Hz, H^{6a}), 3.38 (dd, 1H, *J* = 8.5, 5.1Hz, H^{13b}), 3.28 (td, *J* = 8.3, 1.9Hz, 1H, H^{3a}), 3.06 (dtd, 1H, *J* = 8.1, 6.0, 2.3 Hz, H^{13a}), 2.78 (dd, 1H, *J* = 13.8, 6.4, H¹³), 2.67 (ddd, 1H, *J* = 15.7, 6.7, 1.6Hz, H⁴), 2.50 (dd, 1H, *J* = 13.5, 0.9Hz, H¹³), 2.0 (dddd, 1H, *J* = 15.4, 7.5, 5.7, 3.6 Hz, 1H, H⁴), 1.35 (s, 3H, CH₃); **¹³C NMR** (100MHz, CDCl₃): δ 200.3 (C¹²), 198.4 (C⁷), 178.5 (C³), 177.4 (C¹), 140.3 (C^{5a}), 139.0 (C^{7'}), 135.9 (C^{7a/11a}), 134.0 (C¹⁰), 133.8 (C⁹), 133.6 (C^{7a/11a}), 132.1 (C^{1'}), 129.9 (C^{8',12'}), 129.2 (C^{3',5'}), 128.7 (C^{4'}), 127.9 (C^{9',11'}), 127.0 (C^{2',6'}), 126.5 (C^{10'}), 126.5 (C^{8,11}), 124.2 (C⁵), 61.1 (C^{6a}), 48.5 (C^{12a}), 47.8 (C⁶), 43.6 (C^{13b}), 40.2 (C^{3a}), 34.3 (C^{13a}), 33.1 (C¹³), 29.7 (CH₃), 25.4 (C⁴). **MS (EI)**: *m/z* 500.58 (M-H⁺) (100); **HRMS**: Found 502.2031 [M+H]⁺, calculated for C₃₃H₂₈NO₄ 502.2018 [M+H]⁺; **Elemental analysis** calculated for C₃₃H₂₇NO₄: C, 79.02; H, 5.43; N, 2.79. Found: C, 79.03; H, 5.24; N, 2.79.

(3aSR,6SR,13aSR,13bRS)-6-(4-(trifluoromethyl)phenyl)-3a,4,13,13a-tetrahydro-1H-anthra[2,3-e]isoindole-1,3,7,12(2H,6H,13bH)-tetraone (5.80)



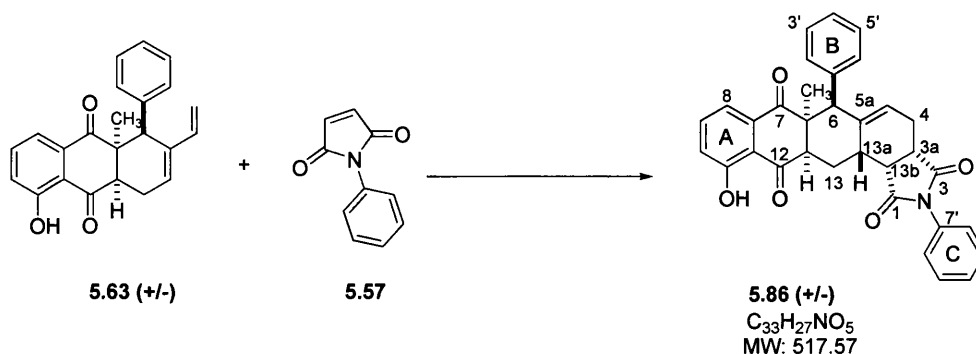
5.80 was obtained as a dark yellow solid; **Y** = 95%; **R_f** 0.29 (Silica gel, Et₂O); **Mp** = 310-315 °C; **IR** : 2914, 2171, 2098, 2152, 2009, 1986 cm⁻¹, **¹H NMR** (400MHz, DMSO): δ 10.10 (s, 1H, NH), 8.20 (m, 1H, H^{8/11}), 8.12 (m, 1H, H^{8/11}), 7.74 (m, 1H, H^{9,10}), 7.51 (d, 2H, *J* = 8.3Hz, H^{5',3'}), 7.27 (d, 2H, *J* = 8.3Hz, H^{2',6'}), 6.15 (dd, 1H, *J* = 6.5, 3.0Hz, H⁵), 5.29 (s, 1H, H⁶), 3.61 (dd, 1H, *J* = 17.5, 1.6Hz, H¹³), 3.25 (dt, 2H, *J* = 13.5, 10.5Hz, H^{3a,13b}), 3.00 (m, 1H, H^{13a}), 2.88 (dd, 1H, *J* = 7.0, 5.0Hz, H⁴), 2.52 (dd, 1H, *J* = 17.5, 9.1Hz, H¹³), 2.34 (m, 1H, H⁴); **¹³C NMR** (100MHz, CD₂Cl₂): δ 204.9 (C¹²), 199.6 (C⁷), 179.2 (C³), 178.5 (C¹), 161.3 (C^{6a/11a}), 161.1 (C^{6a/11a}), 143.9 (C^{7a,5a}), 140.4 (C^{11a}), 136.8 (C^{9/10}), 136.1 (C^{9/10}), 133.1 (C^{4'}), 131.9 (C^{2',6'}), 129.4 (C^{3',5'}), 129.1 (C^{1'}), 125.6 (C^{8/11}), 124.5 (CF₃), 123.4 (C^{8/11}), 117.2 (C⁵), 51.4 (C⁶), 44.7 (C^{13b}), 40.3 (C^{3a}), 34.5 (C^{13a}), 32.9 (C¹³), 24.1 (C⁴); **MS (EI)**: *m/z* 478.39 (M+H⁺) (100). **HRMS**: Found 478.1277 [M+H]⁺, calculated for C₂₇H₁₉F₃NO₄ 478.1266. **Elemental analysis**, calculated for C₂₇H₁₈F₃NO₄: C, 67.92; H, 3.80; N, 2.93. Found: C, 67.12; H, 3.98; N, 2.49.

3-((3a*S*,6*S*,13a*S*,13b*R*)-1,3,7,12-tetraoxo-6-(4-(trifluoromethyl)phenyl)-3a,4,13,13a-tetrahydro-1*H*-anthra[2,3-*c*]isoindol-2(3*H*,6*H*,7*H*,12*H*,13b*H*)-yl)propanoic acid (5.81)



5.81 was obtained as an orange solid; **Y** = 82%; **R_f** 0.37 (Silica gel, CH₂Cl₂/methanol 85:15); **Mp** = 160-162 °C; **IR**: 2355, 2181, 2157, 2030, 1697, 1323, 1112, 1066, 646 cm⁻¹; **¹H NMR** (400MHz, DMSO): δ 9.88 (s, 1H, COOH), 8.07-8.28 (m, 2H, H^{9,10}), 7.88-8.00 (m, 2H, H^{3',5'}), 7.78-7.88 (m, 2H, H^{8,11}), 7.56-7.65 (m, 2H, H^{2',6'}), 7.27 (d, 2H, *J* = 8.3Hz, H^{2',6'}), 6.14 (m, 1H, H⁵), 5.45 (s, 1H, H⁶), 3.59 (m, 2H, H^{7'}), 3.31 (m, 1H, H¹³), 2.51(m, 2H, H⁸), 2.19 (m, 2H, H^{3a,13b}), 2.13 (m, 1H, H^{13a}), 2.02 (m, 1H, H⁴), 1.93 (m, 1H, H¹³), 1.74 (m, 1H, H⁴); **¹³C NMR** (100MHz, CD₂Cl₂) δ 204.9 (C¹²), 199.6 (C⁷), 179.3 (C³), 178.4 (C¹), 161.2 (C^{6a/11a}), 160.1 (C^{6a/11a}), 144.2 (C^{7a,5a}), 140.3 (C^{11a}), 136.5 (C^{9/10}), 136.2 (C^{9/10}), 133.1 (C^{4'}), 131.2 (C^{2',6'}), 129.5 (C^{3',5'}), 129.0 (C^{1'}), 125.2 (C^{8/11}), 124.0 (CF₃), 123.5 (C^{8/11}), 117.2 (C⁵), 51.3 (C⁶), 44.8 (C^{13b}), 40.2 (C^{3a}), 35.1 (C^{13a}), 34.2 (C^{7'}), 31.9 (C¹³), 31.5 (C^{8'}), 24.1 (C⁴); **MS (EI)**: *m/z* 548.42 (M-H⁺) (100); **HRMS (EI)**: Found 550.1501 [M+H]⁺, calculated for C₃₀H₂₃F₃NO₆ 550.1477 [M+H]⁺; **Elemental analysis**, calculated for C₃₀H₂₂F₃NO₆: C, 65.57; H, 4.04; N, 2.55. Found: C, 65.63; H, 4.06; N, 2.50.

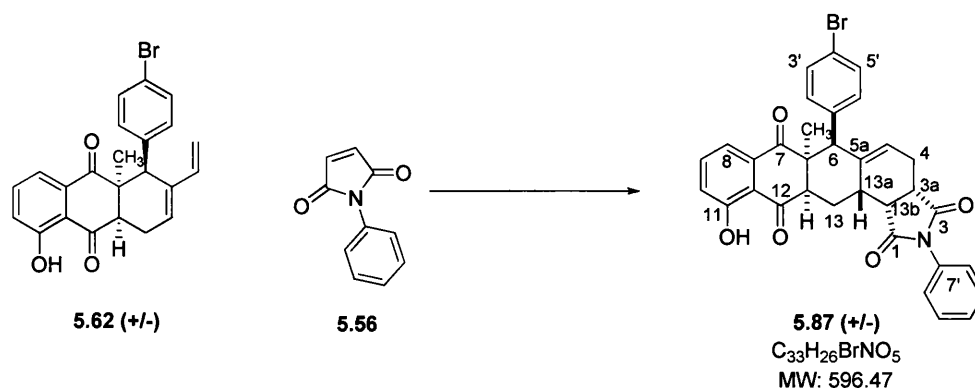
(3aSR,6SR,6aSR,13aSR,13bRS)-11-hydroxy-6a-methyl-2,6-diphenyl-3a,4,6,6a,13,13a-hexahydro-1H-anthra[2,3-e]isoindole-1,3,7,12(2H,12aH,13bH)-tetraone (5.86)



5.86 was obtained as a dark yellow solid; **Y** = 84%; **R_f** 0.67 (Silica gel, EtOAc); **Mp** = 150-152 °C; **IR**: 2914, 2363, 2192, 2164, 1708, 615 cm^{-1} ; **¹H NMR** (400MHz, CDCl_3): δ 1.25 (s, 3H, CH_3), 1.80 (dd, 1H, J = 24.6, 13.0, H^4), 2.53 (td, 1H, J = 19.0Hz, H^{13}), 2.59 (m, 2H, $\text{H}^{4,13}$), 2.95 (d, 1H, J = 19.0Hz, H^{13a}), 3.21 (t, 1H, J = 8.4Hz, H^{3a}), 3.27 (m, 1H, H^{13b}), 3.97 (dd, 1H, J = 11.3, 3.8 Hz, H^{12a}), 4.13 (s, 1H, H^6), 5.91 (t, 1H, J = 3.30 Hz, H^5), 7.13 (d, 2H, J = 7.5 Hz, Ar^C), 7.17 (t, 1H, J = 7.2 Hz, Ar^C), 7.24 (dd, 2H, J = 6.3, 1.3 Hz, Ar^C), 7.28 (dd, 1H, J = 9.1, 4.2 Hz, C^{10}), 7.38-7.34 (m, 2H, Ar^B), 7.46-7.41 (m, 1H, Ar^B), 7.53 (t, J = 7.66 Hz, 2H, Ar^B), 7.68-7.64 (m, 2H, $\text{C}^{8,9}$), 11.68 (s, 1H, OH).; **¹³C NMR** (100MHz, CDCl_3): δ 204.5 (C^{12}), 199.4 (C^7), 178.5 (C^3), 177.6 (C^1), 160.8 (C^{11}), 140.6 (C^{5a}), 138.8 (C^{7a}), 136.0 ($\text{C}^{7'}$), 130.7 ($\text{C}^{1'}$), 129.3 (Ar^B), 128.8 (Ar^B), 128.7 (Ar^C), 128.4 (Ar^C), 126.5 (Ar^B), 125.5 (Ar^C), 124.5 (C^{10}), 122.4 (C^5), 119.6 ($\text{C}^{8,9}$), 117.1 (C^{11a}), 56.5 (C^6), 53.5 (C^{12a}), 52.9 (C^{6a}), 44.4 (C^{13b}), 40.3 (C^{3a}), 33.1 (C^{13a}), 25.5 (C^4), 25.2 (CH_3), 23.5 (C^{13}); **MS (EI)**: m/z 519.49 ($\text{M}+\text{H}^+$) (100); **HRMS (EI)**: Found 518.1976 $[\text{M}+\text{H}]^+$, calculated for $\text{C}_{33}\text{H}_{27}\text{NO}_5$ 518.1967 $[\text{M}+\text{H}]^+$; **Elemental Analysis** calculated for $\text{C}_{33}\text{H}_{27}\text{NO}_5$: C, 76.58; H, 5.26; N, 2.71. Found: C, 76.25; H, 5.32; N, 2.71.

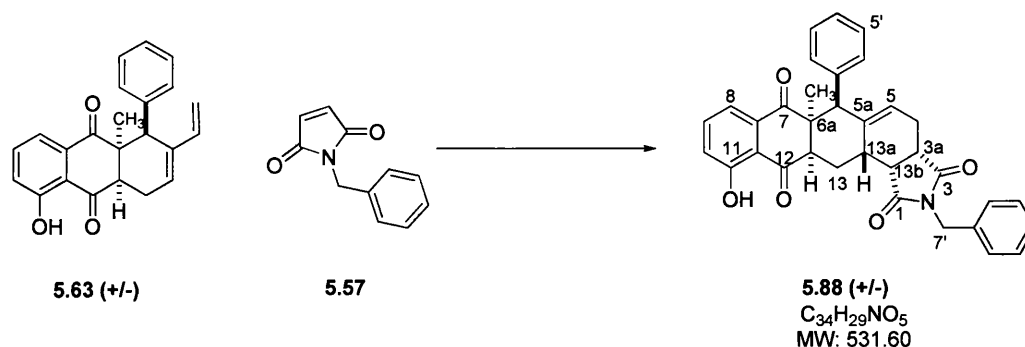
Spectroscopic data in accordance with those reported in literature.¹⁷⁶

(3aSR,6SR,6aSR,13aSR,13bRS)-6-(4-bromophenyl)-11-hydroxy-6a-methyl-2-phenyl-3a,4,6,6a,13,13a-hexahydro-1H-anthra[2,3-c]isoindole-1,3,7,12(2H,12aH,13bH)-tetraone (5.87)



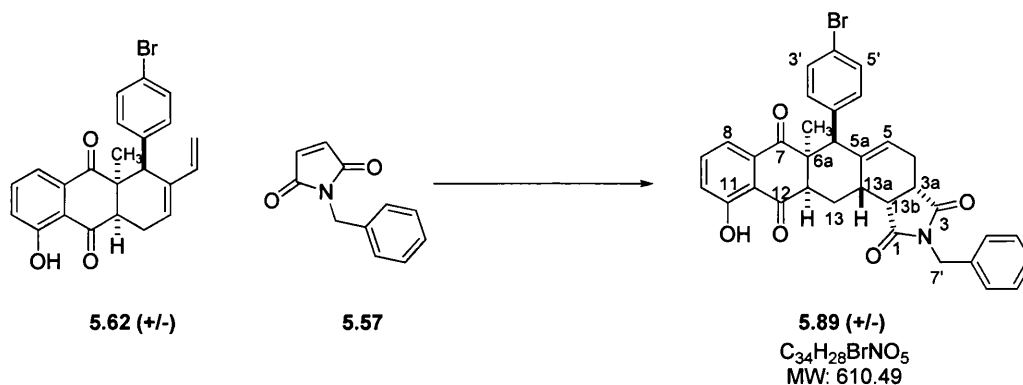
5.87 was obtained as a yellow solid; **Y** = 95%; **R_f** 0.67 (Silica gel, EtOAc); **Mp** = 167 - 169 °C; **IR**: 3738, 2361, 2173, 2033, 1987, 1958, 1541 cm^{-1} ; **¹H NMR** (400MHz, $CDCl_3$): δ 11.90 (s, 1H, OH), 7.55 (t, 1H, J = 8.0Hz, H^9), 7.39-7.49 (3H, m, $H^{9'-11'}$), 7.33 (dd, 1H, J = 7.6, 1.2Hz, H^8), 7.29 (d, 2H, J = 8.45Hz, $H^{3',5'}$), 7.17 (dd, 1H, J = 8.4, 1.0Hz, H^{10}), 7.12 (dd, 2H, J = 7.1, 1.5Hz, $H^{8',12'}$), 6.99 (dd, 2H, J = 6.8, 1.8Hz, $H^{2',6'}$), 5.42 (m, 1H, H^5), 3.9 (s, 1H, H^6), 3.33 (dd, 1H, J = 8.6, 5.3, H^{12a}), 3.28 (m, 2H, $H^{3a,13b}$), 2.82 (m, 1H, H^{13a}), 2.82 (ddd, 1H, J = 14.7, 9.1, 6.1Hz, H^{13}), 2.71 (ddd, 1H, J = 16.6, 7.1, 1.4Hz, H^4), 2.59 (ddd, 1H, J = 14.7, 8.3, 6.6Hz, H^{13}), 2.21 (m, 1H, H^4), 1.35 (s, 3H, CH_3); **¹³C NMR** (100MHz, $CDCl_3$): δ 204.5 (C^{12}), 199.4 (C^7), 178.3 (C^3), 177.5 (C^1), 161.0 (C^{11}), 140.7 ($C^{1'}$), 137.5 (C^{5a}), 136.9 (C^9), 135.7 ($C^{7'}$), 132.7 ($C^{2'/6'}$), 131.7 (C^4), 131.2 ($C^{3',5'}$), 129.2 ($C^{9'}$), 128.8 ($C^{11'}$), 126.4 ($C^{8',12'}$), 123.6 (C^{10}), 123.2 (C^5), 121.3 (C^{7a}), 118.6 (C^8), 116.7 (C^{11a}), 55.9 (C^6), 53.9 (C^{12a}), 52.7 (C^{6a}), 44.7 (C^{13b}), 40.2 (C^{3a}), 33.0 (C^{13a}), 25.6 (C^4), 25.1 (CH_3), 24.3 (C^{13}); **MS (EI)**: m/z 595.50 ($M-H^+$) (100); **HRMS**: Found 596.1064 $[M+H]^+$, calculated for $C_{33}H_{27}BrNO_5$ 596.1073 $[M+H]^+$; **Elemental analysis**, calculated for $C_{33}H_{26}BrNO_5$: C, 66.45; H, 4.39; N, 2.35. Found: C, 66.65; H, 4.18; N, 2.15.

(3aSR,6aSR,13aSR,13bRS)-2-benzyl-11-hydroxy-6a-methyl-6-phenyl-3a,4,6,6a,13,13a-hexahydro-1H-anthra[2,3-e]isoindole-1,3,7,12(2H,12aH,13bH)-tetraone (5.88)



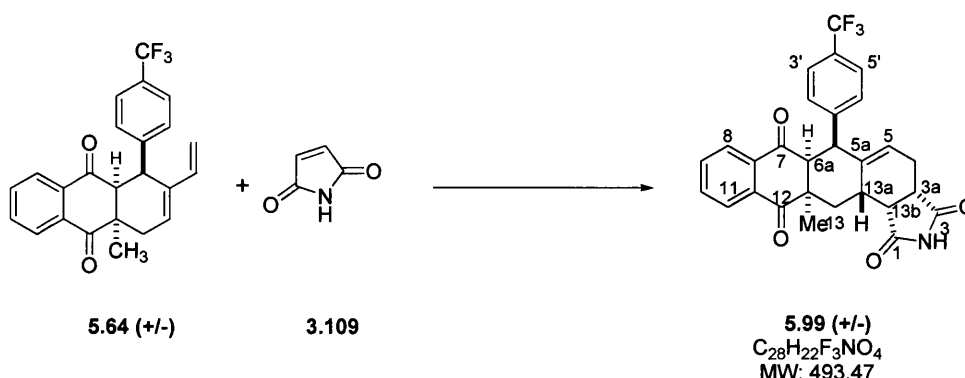
5.88 was obtained as a yellow solid, **Y** = 92%; **R_f** 0.67 (Silica gel, EtOAc); **Mp** = 187 - 188 °C; **IR**: 3338, 2924, 2364, 2330, 2150, 2032, 1959 cm^{-1} . **¹H NMR** (400MHz, $CDCl_3$): δ 11.84 (s, 1H, OH), 7.48 (t, 1H, J = 7.9Hz, H^9), 7.26-7.28 (2H, m, H^8), 7.22-7.27 (m, 5H, $H^{2'-6'}$), 7.09 (dd, 1H, J = 8.3, 1.0Hz, H^{10}), 7.06 (m, 3H, $H^{10'-12'}$), 6.88 (m, 2H, $H^{9',13'}$), 5.32 (m, 1H, H^5), 4.60 (d, 2H, J = 12.2Hz, $H^{7'}$), 3.25 (s, 1H, H^6), 3.20 (t, 1H, J = 5.9Hz, H^{12a}), 3.16 (dd, 1H, J = 8.4, 3.14Hz, H^{13b}), 3.12 (td, 1H, J = 8.6, 1.4Hz, H^{3a}), 2.94 (ddd, 1H, J = 15.3, 9.4, 6.0Hz, H^{13}), 2.79 (m, 1H, H^{13a}), 2.61 (ddd, 1H, J = 16.7, 7.2, 1.34Hz, H^4), 2.55 (ddd, 1H, J = 14.1, 8.0, 5.8Hz, H^{13}), 2.11 (m, 1H, H^4), 1.28 (s, 3H, CH_3); **¹³C NMR** (100MHz, $CDCl_3$): δ 204.5 (C^{12}), 199.5 (C^7), 179.1 (C^3), 178.0 (C^1), 160.7 (C^{11}), 140.5 (C^{5a}), 138.9 ($C^{1'}$), 136.7 (C^9), 135.9 (C^{7a}), 135.7 ($C^{8'}$), 130.8 ($C^{9',13'}$), 128.7 ($C^{2'-6'}$), 128.3 ($C^{2'-6'}$), 127.8 ($C^{2'-6'}$), 127.0 ($C^{2'-6'}$), 123.9 (C^5), 122.8 (C^{10}), 118.5 (C^8), 117.0 (C^{11a}), 56.0 (C^6), 53.5 (C^{12a}), 52.7 (C^{6a}), 44.3 (C^{13b}), 42.4 ($C^{7'}$), 40.1 (C^{3a}), 32.7 (C^{13a}), 25.2 (CH_3), 25.1 (C^4), 23.4 (C^{13}); **MS (EI)**: m/z 530.55 ($M-H^+$) (100); **HRMS**: Found 532.2097 [$M+H$] $^+$, calculated for $C_{34}H_{30}NO_5$ 532.2119 [$M+H$] $^+$; **Elemental analysis**, calculated for $C_{34}H_{29}NO_5$: C, 76.82; H, 5.50; N, 2.63. Found: C, 76.39; H, 5.55; N, 2.54.

(3aSR,6SR,6aSR,13aSR,13bRS)-2-benzyl-6-(4-bromophenyl)-11-hydroxy-6a-methyl-3a,4,6,6a,13,13a-hexahydro-1H-anthra[2,3-e]isoindole-1,3,7,12(2H,12aH,13bH)-tetraone (5.89)



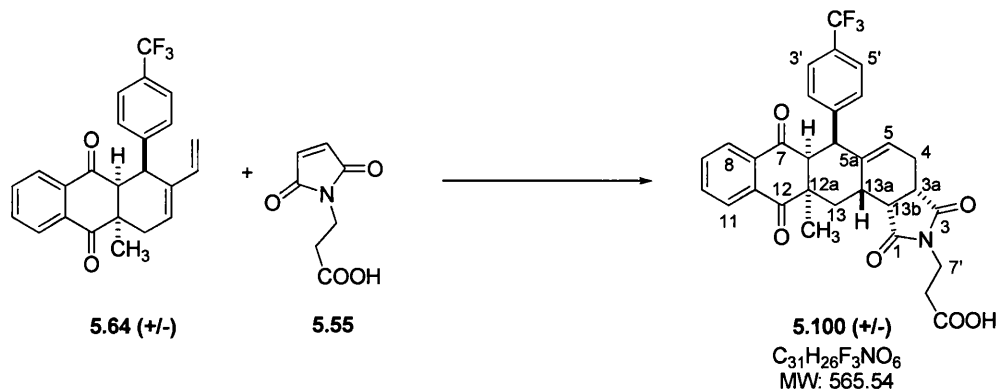
5.89 was obtained as a yellow solid; **Y** = 87%; **R_f** 0.67 (Silica gel, EtOAc); **Mp** = 210-211 °C; **IR**: 2361, 2196, 2047, 2015, 1960, 1940 cm^{-1} ; **¹H NMR** (400MHz, $CDCl_3$): δ 11.84 (s, 1H, OH), 7.53 (t, 1H, J = 8.0Hz, H^9), 7.25 (d, 1H, H^8), 7.22-7.30 (5H, m, $H^{9'}$, $^{13'}$), 7.22 (d, 2H, J = 6.7Hz, $H^{3',5'}$), 7.15 (dd, 1H, J = 8.4, 0.9Hz, H^{10}), 6.80 (d, 2H, J = 8.5Hz, $H^{2',6'}$), 5.24 (m, 1H, H^5), 4.58 (d, 2H, J = 9.2Hz, H^7), 3.22 (t, 1H, J = 6.0, H^{12a}), 3.11 (m, 2H, $H^{3a,13b}$), 3.07 (br s, 1H, H^6), 2.94 (ddd, 1H, J = 14.6, 8.3, 6.3Hz, H^{13}), 2.70 (m, 1H, H^{13a}), 2.62 (dd, 1H, J = 15.0, 7.3Hz, H^4), 2.48 (ddd, 1H, J = 15.0, 8.4, 7.0Hz, H^{13}), 2.09 (m, 1H, H^4), 1.22 (s, 3H, CH_3); **¹³C NMR** (100MHz, $CDCl_3$): δ 204.5 (C^{12}), 199.5 (C^7), 178.9 (C^3), 178.0 (C^1), 161.0 (C^{11}), 140.5 (C^{5a}), 137.5 ($C^{1'}$), 136.9 (C^9), 135.8 (C^{7a}), 135.7 (C^8), 132.9 ($C^{3'/5'}$), 128.7 ($C^{9',13'}$), 128.3 ($C^{10',12'}$), 127.8 ($C^{11'}$), 123.7 (C^{10}), 123.2 (C^5), 121.1 ($C^{4'}$), 118.5 (C^8), 116.5 (C^{11a}), 55.6 (C^6), 54.1 (C^{12a}), 52.6 (C^{6a}), 44.6 (C^{13b}), 42.4 ($C^{7'}$), 40.1 (C^{3a}), 32.7 (C^{13a}), 25.2 (C^4), 25.1 (CH_3), 23.4 (C^{13}); **MS (EI)**: m/z 608.55 ($M-H^+$) (100) **HRMS (EI)**: Found 610.1218 [$M+H$] $^+$, calculated for $C_{34}H_{29}BrNO_5$ 610.1229 [$M+H$] $^+$; **Elemental analysis**, calculated for $C_{34}H_{28}BrNO_5$: C, 66.89; H, 4.62; N, 2.29. Found: C, 66.85; H, 4.52; N, 2.12.

(3aSR,6SR,6aSR,12aRS,13aSR,13bRS)-12a-methyl-6-(4'-(trifluoromethyl) phenyl)-3a,4,6,6a,13,13a-hexahydro-1H-anthra[2,3-e]isoindole-1,3,7,12(2H,12aH, 13bH)-tetraone (5.99)



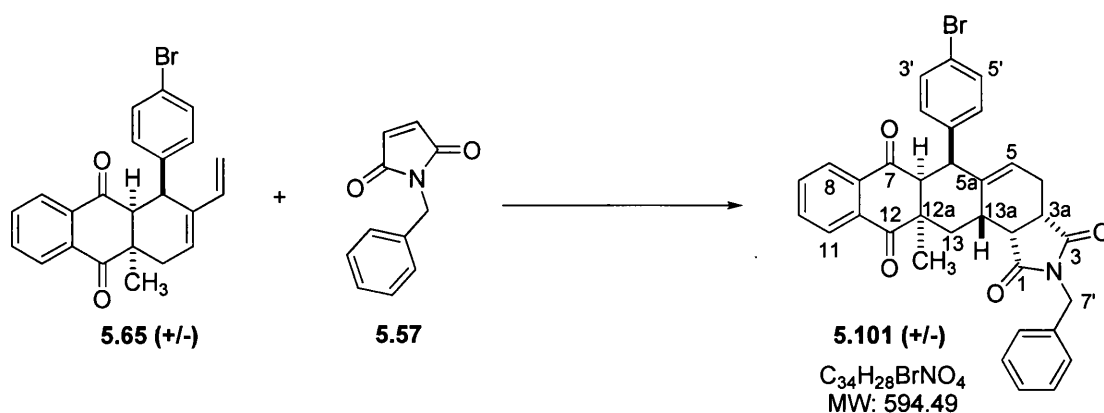
5.99 was obtained as a white solid; **Y** = 92%; **R_f** 0.39 (Silica gel, Et₂O); **Mp** = 204 - 207 °C; **IR**: 2362, 2335, 1705, 1325 cm⁻¹. **¹H NMR** (400MHz, CDCl₃): δ 7.90 (br s, 1H, -NH), 7.89 (d, 1H, *J* = 7.7Hz, H⁹), 7.59 (m, 1H, H¹¹), 7.51 (m, 2H, H^{8,10}), 7.15 (d, 2H, *J* = 8.1Hz, H^{3',5'}), 6.78 (d, 2H, *J* = 8.1Hz H^{2',6'}), 5.48 (dd, 1H, *J* = 6.1, 3.0Hz, H⁵), 4.25 (d, 1H, *J* = 8.0Hz, H⁶), 3.47 (d, 1H, *J* = 10.2Hz, H^{6a}), 3.28 (dd, 1H, *J* = 8.6, 5.7Hz, H^{13b}), 3.18 (td, 1H, *J* = 8.5, 1.8Hz, H^{3a}), 3.01 (m, 1H, H^{13a}), 2.73 (dd, 1H, *J* = 13.9, 6.6Hz, H¹³), 2.58 (ddd, 1H, *J* = 15.9, 6.8, 1.6Hz, H⁴), 2.45 (dd, 1H, *J* = 13.7, 12.5Hz, H¹³), 2.15 (m, 1H, H⁴), 1.35 (s, 3H, CH₃); **¹³C NMR** (100MHz, CDCl₃): δ 200.0 (C¹²), 198.1 (C⁷), 178.9 (C³), 178.1 (C¹), 144.0 (C^{4'}), 139.6 (C^{5a}), 135.6 (C^{7a}), 134.1 (C^{10/11}), 134.0 (C^{10/11}), 133.6 (C^{11a}), 130.3 (C^{2',6'}), 128.9 (C^{1'}), 126.5 (C^{8/9}), 126.4 (C^{8/9}), 125.1 (C⁵), 124.6 (C^{3'/5'}), , 124.0 (q, CF₃, *J* = 270Hz), 60.5 (C^{6a}), 48.2 (C^{12a}), 46.9 (C⁶), 44.7 (C^{13b}), 41.2 (C^{3a}), 33.6 (C^{13a}), 32.7 (C¹³), 29.7 (CH₃), 24.9 (C⁴); **HRMS**: Found 494.1593 [M+H]⁺, calculated for C₂₈H₂₃F₃NO₄ 494.1574 [M+H]⁺. **Elemental analysis**, calculated for C₂₈H₂₂F₃NO₄: C, 68.15; H, 4.49; N, 2.84. Found: C, 67.98; H, 4.25; N, 2.72.

3-((3a*S*,6*S*,6a*S*,12a*R*,13a*S*,13b*R*)-12a-methyl-1,3,7,12-tetraoxo-6-(4'-(trifluoromethyl)phenyl)-3a,4,6a,7,12,12a,13,13a-octahydro-1*H*-anthra[2,3-*e*]isoindol-2(3*H*,6*H*,13b*H*)-yl)propanoic acid (5.100)



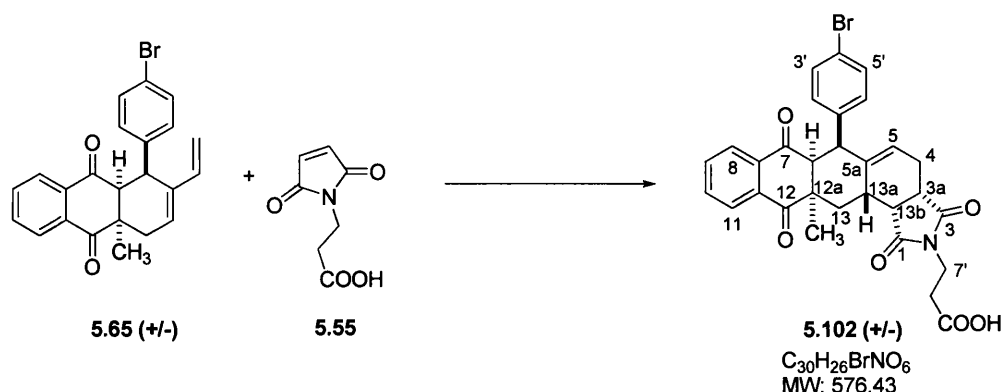
5.100 was obtained as a white solid; **Y** = 79%; **R_f** 0.43 (Silica gel, AcOH/EtOAc 1:99); **Mp** = 140.8 – 142.1 °C; **IR**: 2890, 2366, 1692, 1325, 1163 cm⁻¹; **¹H NMR** (400MHz, CDCl₃): δ 7.87 (d, 1H, *J* = 7.7Hz, H⁹), 7.58 (m, 1H, H¹¹), 7.51 (m, 2H, H^{8,10}), 7.15 (d, 2H, *J* = 8.1Hz, H^{3',5'}), 6.75 (d, 2H, *J* = 8.1Hz H^{2',6'}), 5.38 (dd, 1H, *J* = 6.1, 2.9Hz, H⁵), 4.22 (d, 1H, *J* = 8.8Hz, H⁶), 3.76 (m, 2H, *J* = 6.8Hz, H^{7'}), 3.46 (d, 1H, *J* = 10.0Hz, H^{6a}), 3.22 (dd, 1H, *J* = 8.5, 5.7Hz, H^{13b}), 3.14 (td, 1H, *J* = 8.6, 1.4Hz, H^{3a}), 3.02 (m, 1H, H^{13a}), 2.78 (dd, 1H, *J* = 14.0, 6.9Hz, H¹³), 2.60 (t, 2H, *J* = 6.8, H^{8'}), 2.58 (m, 1H, H⁴), 2.48 (dd, 1H, *J* = 13.9, 12.0Hz, H¹³), 2.12 (m, 1H, H⁴), 1.37 (s, 3H, CH₃); **¹³C NMR** (100MHz, CDCl₃): δ 200.0 (C¹²), 198.7 (C⁷), 179.0 (C³), 177.1 (C¹), 174.9 (COOH), 144.4 (C^{4'}), 139.6 (C^{5a}), 135.5 (C^{7a}), 134.1 (C^{10,11}), 133.6 (C^{11a}), 130.3 (C^{2',6'}), 128.9 (C^{1'}), 126.5 (C^{8/9}), 126.4 (C^{8/9}), 125.2 (C⁵), 124.6 (C^{3',5'}), 124.0 (q, CF₃, *J* = 270Hz), 60.2 (C^{6a}), 48.1 (C^{12a}), 46.7 (C⁶), 43.7 (C^{13b}), 39.9 (C^{3a}), 34.3 (C^{7'}), 33.7 (C^{13a}), 32.4 (C¹³), 31.8 (C^{8'}), 29.7 (CH₃), 25.1 (C⁴); **HRMS**: Found 566.1805 [M+H]⁺, calculated for C₃₁H₂₇F₃NO₆ 566.1785 [M+H]⁺; **Elemental analysis**, calculated for C₃₁H₂₆F₃NO₆: C, 68.84; H, 4.63; N, 2.48. Found: C, 65.73; H, 4.58; N, 2.54.

(3aSR,6SR,6aSR,12aRS,13aSR,13bRS)-2-benzyl-6-(4-bromophenyl)-12a-methyl-3a,4,6,6a,13,13a-hexahydro-1H-anthra[2,3-e]isoindole-1,3,7,12(2H,12aH,13bH)-tetraone (5.101)



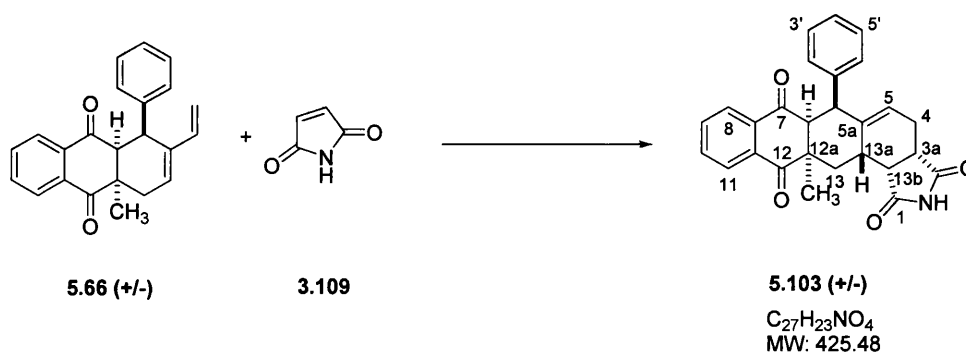
5.101 was obtained as a white solid; **Y** = 72%; **R_f** 0.67 (Silica gel, EtOAc); **Mp** = 177.5 – 179.1 °C; **IR**: 2935, 2354, 1693, 1397, 701 cm⁻¹; **¹H NMR** (400MHz, CDCl₃): δ 7.93 (dd, 1H, *J* = 7.6, 1.2 Hz, H⁸), 7.64 (dt, 1H, *J* = 7.5, 1.4Hz, H¹⁰), 7.58 (dt, 1H, *J* = 7.3, 1.0Hz, H⁹), 7.52 (dd, 1H, *J* = 7.7, 1.4Hz, H¹¹), 7.25 (m, 5H, H^{9'-13'}), 7.04 (d, 2H, *J* = 8.4Hz, H^{3',5'}), 6.35 (d, 2H, *J* = 8.4Hz, H^{2',6'}), 5.25 (dd, 1H, *J* = 6.6, 3.2Hz, H⁵), 4.58 (d, 2H, *J* = 8.2Hz, C^{7'}), 3.80 (dt, 1H, *J* = 10.6, 1.5Hz, H⁶), 3.34 (d, 1H, *J* = 10.7Hz, H^{6a}), 3.18 (dd, 1H, *J* = 8.5, 5.5Hz, H^{13b}), 3.14 (td, 1H, *J* = 8.6, 1.3Hz, H^{3a}), 2.90 (m, 1H, H^{13a}), 2.65 (dd, 1H, *J* = 13.8, 6.5Hz, H¹³), 2.56 (ddd, *J* = 15.7, 7.2, 1.3Hz, 1H, H⁴), 2.41 (dd, 1H, *J* = 13.5, 12.6Hz, H¹³), 2.08 (m, 1H, H⁴), 1.32 (s, 3H, CH₃); **¹³C NMR** (100 MHz, CDCl₃): δ 200.0 (C¹²), 198.2 (C⁷), 179.0 (C³), 178.0 (C¹), 139.9 (C^{5a}), 138.0 (C^{4'}), 135.8 (C^{7a}), 134.2 (C⁹), 134.0 (C¹⁰), 133.5 (C^{11a}), 131.7 (C^{2',6'}), 130.8 (C^{3',5'}), 128.7 (C^{10',11'}), 128.2 (C^{9',13'}), 127.8 (C^{11'}), 126.6 (C^{8/11}), 126.5 (C^{8/11}), 124.6 (C⁵), 120.8 (C^{8',1'}), 60.7 (C^{6a}), 48.3 (C^{12a}), 46.3 (C⁶), 43.7 (C^{13b}), 42.3 (C^{7'}), 40.2 (C^{3a}), 34.2 (C^{13a}), 32.6 (C¹³), 29.7 (CH₃), 25.2 (C⁴); **HRMS**: Found 594.1251 [M+H]⁺, calculated for C₃₄H₂₉BrNO₄ 594.1280 [M+H]⁺; **Elemental analysis**, calculated for C₃₄H₂₈BrNO₄: C, 68.69; H, 4.75; N, 2.36. Found: C, 68.68; H, 4.63; N, 2.45.

3-((3aSR,6SR,6aSR,12aRS,13aSR,13bRS)-6-(4-bromophenyl)-12a-methyl-1,3,7,12-tetraoxo-3a,4,6a,7,12,12a,13,13a-octahydro-1H-anthra[2,3-e]isoindol-2(3H,6H,13bH)-yl)propanoic acid (5.102)



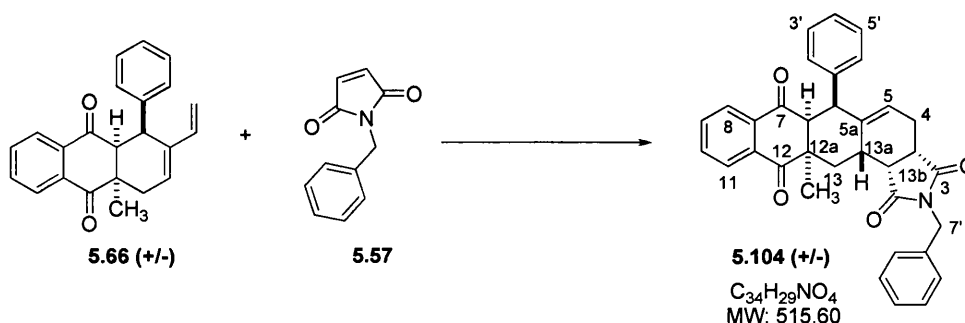
5.102 was obtained as a white solid; **Y** = 72%; **R_f** 0.43 (Silica gel, AcOH/EtOAc 1:99); **Mp** = 160.7 – 161.2 °C; **IR**: 2940, 2356, 2160, 1688 cm^{-1} ; **¹H NMR** (400MHz, CDCl_3): δ 7.89 (d, 1H, J = 7.3Hz, H^8), 7.63 (td, 1H, H^{10}), 7.56 (m, 2H, $\text{H}^{11,9}$), 7.20 (d, 2H, J = 8.4Hz, $\text{H}^{3',5'}$), 6.5 (d, 2H, J = 8.5Hz $\text{H}^{2',6'}$), 5.35 (dd, 1H, J = 6.3, 2.9Hz, H^5), 4.09 (d, 1H, J = 9.5Hz, H^6), 3.75 (m, 2H, $\text{H}^{7'}$), 3.43 (d, 1H, J = 10.1Hz, H^{6a}), 3.20 (dd, 1H, J = 8.6, 5.7Hz, H^{13b}), 3.12 (td, 1H, J = 8.6, 1.3Hz, H^{3a}), 2.95 (m, 1H, H^{13a}), 2.74 (dd, 1H, J = 13.9, 6.7Hz, H^{13}), 2.59 (t, 2H, J = 7.0, $\text{H}^{8'}$), 2.57 (m, 1H, H^4), 2.46 (dd, 1H, J = 13.9, 12.1Hz, H^{13}), 2.10 (m, 1H, H^4), 1.36 (s, 3H, CH_3); **¹³C NMR** (100MHz, CDCl_3): δ 200.1 (C^{12}), 198.8 (C^7), 179.0 (C^3), 177.0 (C^1), 174.8 (COOH), 139.8 (C^{5a}), 138.7 ($\text{C}^{4'}$), 135.7 (C^{7a}), 134.1 ($\text{C}^{10,9}$), 134.0 ($\text{C}^{10,9}$), 133.6 (C^{11a}), 131.6 ($\text{C}^{2',6'}$), 130.8 ($\text{C}^{3',5'}$), 126.6 ($\text{C}^{8/11}$), 126.5 ($\text{C}^{8/11}$), 124.8 (C^5), 120.9 ($\text{C}^{1'}$), 60.4 (C^{6a}), 48.1 (C^{12a}), 46.5 (C^6), 43.7 (C^{13b}), 40.0 (C^{3a}), 34.2 ($\text{C}^{7'}$), 33.9 (C^{13a}), 32.5 (C^{13}), 31.8 ($\text{C}^{8'}$), 29.7 (CH_3), 25.1 (C^4); **HRMS**: Found 576.1041 $[\text{M}+\text{H}]^+$, calculated for $\text{C}_{30}\text{H}_{27}\text{BrNO}_6$ 576.1016 $[\text{M}+\text{H}]^+$; **Elemental Analysis**, calculated for $\text{C}_{30}\text{H}_{26}\text{BrNO}_6$: C, 62.51; H, 4.55; N, 2.43. Found: C, 62.60; H, 4.56; N, 2.43.

(3aSR,6SR,6aSR,12aRS,13aSR,13bRS)-12a-methyl-6-phenyl-3a,4,6a,13,13a-hexahydro-1H-anthra[2,3-e]isoindole-1,3,7,12(2H,12aH,13bH)-tetraone (5.103)



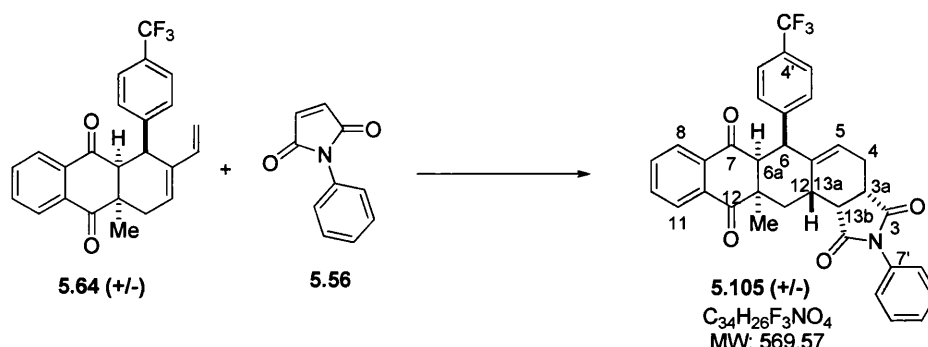
5.103 was obtained as a white solid; **Y** = 75%; **R_f** 0.35 (Silica gel, Et₂O); **Mp** = 223.4 – 225.1 °C; **IR**: 3230, 2356, 1706, 1682, 701 cm⁻¹; **¹H NMR** (400MHz, CDCl₃): 7.90 (ddd, 1H, *J* = 7.5, 1.1, 0.7Hz, H¹¹), 7.58 (ddd, 1H, *J* = 7.7, 6.1, 2.6Hz, H⁹), 7.53 (m, 2H, H^{8,10}), 6.93 (m, 1H, H^{4'}), 6.93 (dd, 2H, *J* = 4.9, 2.1Hz, H^{3',5'}), 6.66 (dd, 2H, *J* = 7.2, 2.1Hz H^{2',6'}), 5.46 (dt, 1H, *J* = 6.0, 2.7Hz, H⁵), 4.17 (dd, 1H, *J* = 10.2, 3.1Hz, H⁶), 3.47 (t, 1H, *J* = 10.2Hz, H^{6a}), 3.28 (dd, 1H, *J* = 8.6, 5.8Hz, H^{13b}), 3.15 (td, 1H, *J* = 8.4, 2.0Hz, H^{3a}), 2.99 (m, 1H, H^{13a}), 2.72 (dd, 1H, *J* = 13.7, 6.4Hz, H¹³), 2.56 (ddd, 1H, *J* = 15.9, 6.8, 1.9Hz, H⁴), 2.42 (dd, 1H, *J* = 13.7, 12.4Hz, H¹³), 2.13 (m, 1H, H⁴), 1.35 (s, 3H, CH₃); **¹³C NMR** (100MHz, CDCl₃): δ 200.3 (C¹²), 198.5 (C⁷), 179.1 (C³), 178.1 (C¹), 140.1 (C^{5a}), 139.4 (C^{7a}), 135.9 (C^{11a}), 133.9 (C^{9/10}), 133.7 (C^{9/10}), 133.6 (C^{1'}), 129.9 (C^{2',6'}), 127.8 (C^{3',5'}), 126.5 (C^{8/11}), 126.9 (C^{4'}), 126.4 (C^{8/11}), 124.2 (C⁵), 60.9 (C^{6a}), 48.4 (C^{12a}), 46.5 (C⁶), 44.7 (C^{13b}), 41.2 (C^{3a}), 33.8 (C^{13a}), 33.0 (C¹³), 29.7 (CH₃), 24.9 (C⁴); **HRMS**: Found 426.1722 [M+H]⁺, calculated for C₂₇H₂₄NO₄ 426.1700 [M+H]⁺; **Elemental analysis**, calculated for C₂₇H₂₃NO₄: C, 76.22; H, 5.45; N, 3.29. Found: C, 75.98; H, 5.28; N, 3.38.

(3aS,6S,6aS,12aR,13aS,13bR)-2-benzyl-12a-methyl-6-phenyl-3a,4,6,6a,13,13a-hexahydro-1H-anthra[2,3-e]isoindole-1,3,7,12(2H,12aH,13bH)-tetraone (5.104)



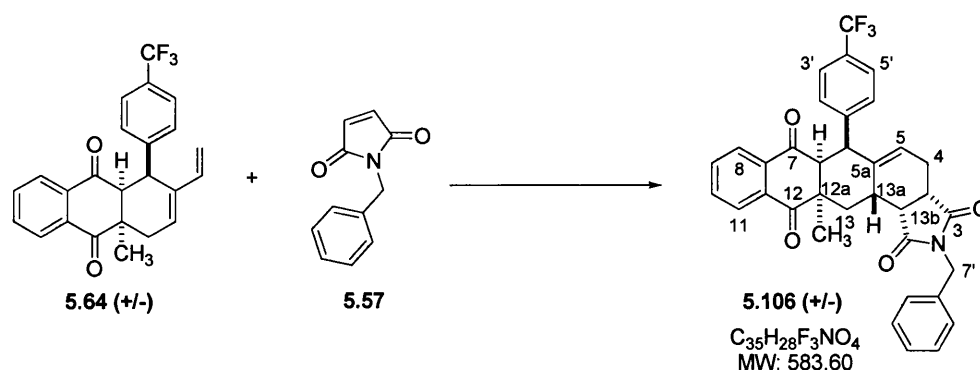
5.104 was obtained as a white solid; **Y** = 77%; **R_f** 0.67 (Silica gel, EtOAc); **Mp** = 190.5 - 193.1 °C; **IR**: 2914, 2362, 1694, 1398 cm⁻¹; **¹H NMR** (400MHz, CDCl₃): δ 7.92 (dt, 1H, *J* = 7.2, H⁸); 7.60 (ddd, 1H, *J* = 7.7, 6.6, 2.1Hz, H¹⁰), 7.52 (m, 2H, H^{11,9}), 7.25 (m, 5H, H^{9'-13'}), 6.93 (m, 3H, H^{3',4',5'}), 6.52 (dd, 2H, *J* = 7.9, 1.4Hz H^{2',6'}), 5.32 (dt, 1H, *J* = 6.1, 2.8Hz, H⁵), 4.58 (s, 2H, C^{7'}), 3.89 (dd, 1H, *J* = 10.5, 3.4Hz, H⁶), 3.36 (d, 1H, *J* = 10.6Hz, H^{6a}), 3.20 (dd, 1H, *J* = 8.5, 5.6Hz, H^{13b}), 3.12 (td, 1H, *J* = 8.4, 1.6Hz, H^{3a}), 2.93 (m, 1H, H^{13a}), 2.65 (dd, 1H, *J* = 13.8, 6.5Hz, H¹³), 2.57 (ddd, 1H, *J* = 15.6, 7.0, 1.6Hz, H⁴), 2.40 (dd, 1H, *J* = 13.6, 12.5Hz, H¹³), 2.10 (m, 1H, H⁴), 1.31 (s, 3H, CH₃); **¹³C NMR** (100MHz, CDCl₃): δ 200.3 (C¹²), 198.4 (C⁷), 179.1 (C³), 178.0 (C¹), 140.1 (C^{5a}), 138.9 (C^{1'}), 136.1 (C^{7a}), 135.8 (C⁸), 134.0 (C⁹), 133.7 (C¹⁰), 133.6 (C^{11a}), 130.1 (C^{2',6'}), 128.7 (C^{10',11'}), 128.1 (C^{9',13'}), 127.8 (C^{11'}), 127.7 (C^{3',5'}), 126.9 (C^{4'}), 126.6 (C^{8/11}), 126.5 (C^{8/11}), 124.3 (C⁵), 60.9 (C^{6a}), 48.4 (C^{12a}), 47.2 (C⁶), 43.6 (C^{13b}), 42.3 (C^{7'}), 40.2 (C^{3a}), 34.1 (C^{13a}), 33.0 (C¹³), 29.6 (CH₃), 25.1 (C⁴); **HRMS**: Found 596.2159 [M+H]⁺, calculated for C₃₄H₃₀NO₄ 596.2175 [M+H]⁺; **Elemental Analysis**: calculated for C₃₄H₂₉NO₄: C, 79.20; H, 5.67; N, 2.72. Found: C, 78.99; H, 5.72; N, 2.85.

(3aSR,6SR,6aSR,12aRS,13aSR,13bRS)-12a-methyl-2-phenyl-6-(4(trifluoromethyl)phenyl)-3a,4,6,6a,13,13a-hexahydro-1H-anthra[2,3-e]isoindole-1,3,7,12(2H,12aH,13bH)-tetraone (5.105)



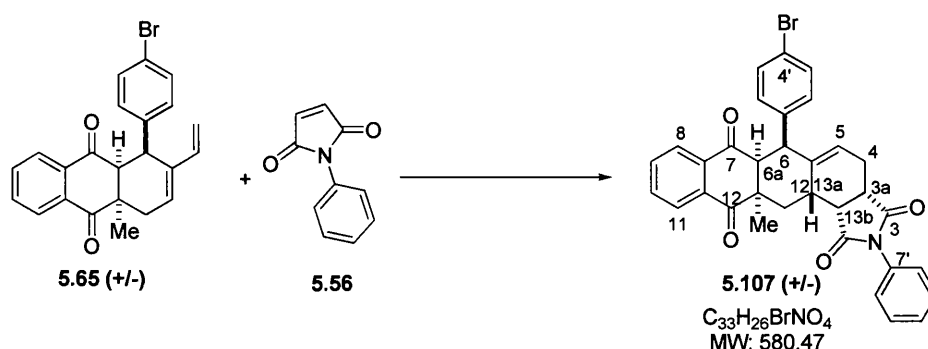
5.105 was obtained as a white solid; **Y** = 83%; **R_f** 0.69 (Silica gel, EtOAc); **Mp** = 250.1 °C; **IR**: 3749, 2197, 1749, 1594, 1498, 1383, 1111, 981, 743 cm^{-1} ; **¹H NMR** (500MHz, $CDCl_3$): δ 7.92 (d, 1H, J = 7.7Hz, H^9), 7.62 (m, 1H, H^{11}), 7.55 (m, 2H, $H^{8,10}$), 7.46 (t, 2H, J = 7.3Hz, $H^{8',12'}$), 7.39 (t, 1H, J = 7.5Hz, $H^{10'}$), 7.19 (d, 2H, J = 8.2Hz, $H^{3',5'}$), 7.15 (d, 2H, J = 7.3Hz, $H^{9',11'}$), 6.79 (d, 2H, J = 8.1Hz, $H^{2',6'}$), 5.47 (dd, 1H, J = 6.2, 3.1Hz, H^5), 4.23 (dd, 1H, J = 10.2, 2.6Hz, H^6), 3.47 (d, 1H, J = 10.7Hz, H^{6a}), 3.41 (dd, 1H, J = 8.6, 5.6Hz, H^{13b}), 3.31 (td, 1H, J = 8.4, 1.8Hz, H^{3a}), 3.01 (m, 1H, H^{13a}), 2.79 (dd, 1H, J = 13.9, 6.6Hz, H^{13}), 2.69 (ddd, 1H, J = 15.9, 6.9, 1.8Hz, H^4), 2.54 (dd, 1H, J = 13.8, 12.3Hz, H^{13}), 2.25 (m, 1H, H^4), 1.36 (s, 3H, CH_3); **¹³C NMR** (125MHz, $CDCl_3$): δ 200.0 (C^{12}), 198.1 (C^7), 178.3 (C^3), 177.4 (C^1), 143.7 (C^{5a}), 139.9 ($C^{7'}$), 135.7 ($C^{7a/11a}$), 134.2 (C^{11}), 134.1 ($C^{8/10}$), 133.6 ($C^{7a/11a}$), 132.1 ($C^{1'}$), 130.3 ($C^{2',6'}$), 129.2 ($C^{8',12'}$), 128.8 ($C^{10'}$), 126.6 ($C^{9',11'}$), 126.5 (C^9), 126.4 ($C^{8/10}$), 125.0 (C^5), 124.7 ($C^{3',5'}$), 124.0 (q, CF_3 , J 270Hz), 122.7 ($C^{4'}$), 60.6 (C^{6a}), 48.3 (C^{12a}), 47.2 (C^6), 43.6 (C^{13b}), 40.2 (C^{3a}), 34.1 (C^{13a}), 32.8 (C^{13}), 29.7 (CH_3), 25.5 (C^4); **HRMS**: Found 570.1867 $[M+H]^+$, calculated for $C_{34}H_{27}F_3NO_4$ 570.1892 $[M+H]^+$; **Elemental analysis**, calculated for $C_{34}H_{26}F_3NO_4$: C, 71.70; H, 4.60; N, 2.46. Found: C, 71.58; H, 5.61; N, 2.41.

(3aSR,6SR,6aSR,12aRS,13aSR,13bRS)-2-benzyl-12a-methyl-6-(4-(trifluoromethyl)phenyl)-3a,4,6,6a,13,13a-hexahydro-1H-anthra[2,3-e]isoindole-1,3,7,12(2H,12aH,13bH)-tetraone (5.106)



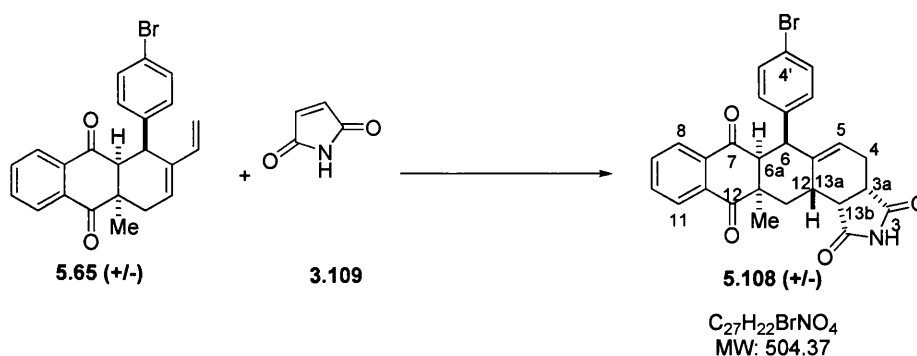
5.106 was obtained as a white solid; **Y** = 77%; **R_f** 0.64 (Silica gel, EtOAc); **Mp** = 109.1–111.6 °C; **IR**: 3749, 2489, 1690, 1594, 1397, 1321, 1163, 1121, 1067, 707 cm^{-1} ; **¹H NMR** (500MHz, $CDCl_3$): δ 7.91 (dd, 1H, J = 7.7, 0.6Hz, H^9), 7.61 (td, 1H, J = 7.7, 1.4Hz, H^{11}), 7.53 (td, 1H, J = 7.3, 1.2Hz, H^{10}), 7.47 (dd, 1H, J = 7.4, 0.9Hz, H^8), 7.27 (m, 3H, J = 7.3Hz, $H^{10'-12'}$), 7.24 (m, 2H, $H^{9',13''}$), 7.14 (d, 2H, J = 8.1Hz, $H^{3',5'}$), 6.60 (d, 2H, J = 8.1Hz, $H^{2',6'}$), 5.61 (d, 1H, J = 14.0Hz, $H^{7'}$), 5.25 (dd, 1H, J = 6.5, 3.1Hz, H^5), 4.55 (d, 1H, J = 14.0Hz, $H^{7'}$), 3.91 (dd, 1H, J = 10.5, 2.9Hz, H^6), 3.36 (d, 1H, J = 10.6Hz, H^{6a}), 3.21 (dd, 1H, J = 8.5, 5.6Hz, H^{13b}), 3.15 (td, 1H, J = 8.0, 1.4Hz, H^{3a}), 2.94 (m, 1H, H^{13a}), 2.67 (dd, 1H, J = 13.8, 6.6Hz, H^{13}), 2.59 (ddd, 1H, J = 15.6, 7.1, 1.4Hz, H^4), 2.43 (dd, 1H, J = 13.7, 12.4Hz, H^{13}), 2.11 (m, 1H, H^4), 1.32 (s, 3H, CH_3); **¹³C NMR** (100MHz, $CDCl_3$): δ 200.0 (C^{12}), 198.1 (C^7), 178.9 (C^3), 178.0 (C^1), 143.4 (C^{5a}), 139.6 (C^{5a}), 135.9 ($C^{4'}$), 135.7 (C^{7a}), 134.2 (C^{11}), 134.1 (C^{10}), 133.5 (C^{11a}), 130.5 ($C^{2',6'}$), 128.7 ($C^{9'-11'}$), 128.4 ($C^{8',12'}$), 127.9 (C^8), 126.6 (C^8), 126.4 (C^9), 125.0 (C^5), 124.5 ($C^{3',5'}$), 124.0 (q, CF_3 , J = 270Hz), 60.5 (C^{6a}), 48.3 (C^{12a}), 46.6 (C^6), 43.5 (C^{13b}), 42.4 ($C^{7'}$), 40.2 (C^{3a}), 34.1 (C^{13a}), 32.7 (C^{13}), 29.6 (CH_3), 25.2 (C^4); **HRMS**: Found 584.2014 $[M+H]^+$, calculated for $C_{35}H_{29}F_3NO_4$ 584.2049 $[M+H]^+$; **Elemental analysis**, calculated for $C_{35}H_{28}F_3NO_4$: C, 72.03; H, 4.84; N, 2.40. Found: C, 72.09; H, 4.88; N, 2.42.

(3aSR,6SR,6aSR,12aRS,13aSR,13bRS)-6-(4-bromophenyl)-12a-methyl-2-phenyl-3a,4,6,6a,13,13a-hexahydro-1H-anthra[2,3-e]isoindole-1,3,7,12(2H,12aH,13bH)-tetraone (5.107)



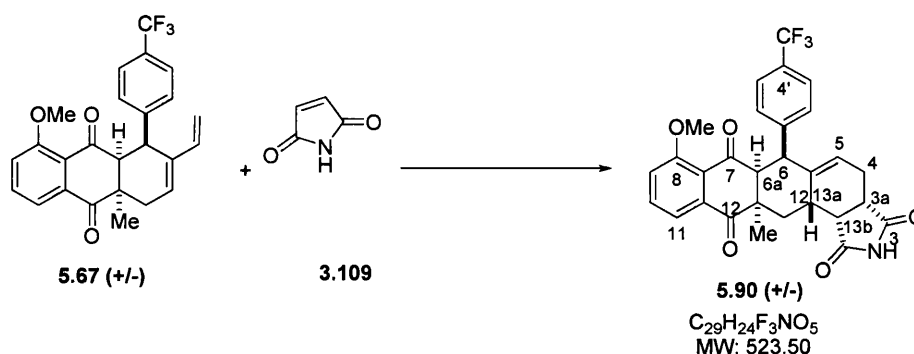
5.107 was obtained as a white solid; **Y** = 67%; **R_f** 0.72 (Silica gel, EtOAc); **Mp** = 141.7 - 145.4 °C; **IR**: 2197, 1700, 1593, 1488, 1383, 1293, 1199, 1150, 981, 693 cm⁻¹; **¹H NMR** (500MHz, CDCl₃): δ 7.94 (d, 1H, *J* = 7.6Hz, H⁹); , 7.66 (m, 1H, H¹¹), 7.60 (m, 2H, H^{8,10}), 7.46 (t, 2H, *J* = 6.9Hz, H^{9',11'}), 7.39 (t, 1H, *J* = 7.4Hz, H^{10'}), 7.12 (d, 2H, *J* = 7.2Hz, H^{8',12'}), 7.09 (d, 2H, *J* = 8.5Hz, H^{3',5'}), 6.53 (d, 2H, *J* = 8.5Hz H^{2',6'}), 5.45 (dd, 1H, *J* = 6.3, 3.2Hz, H⁵), 4.12 (dd, 1H, *J* = 7.9, 2.4Hz, H⁶), 3.44 (d, 1H, *J* = 10.4Hz, H^{6a}), 3.39 (dd, 1H, *J* = 8.6, 5.6Hz, H^{13b}), 3.29 (td, 1H, *J* = 8.4, 1.8Hz, H^{3a}), 3.03 (m, 1H, H^{13a}), 2.76 (dd, 1H, *J* = 13.8, 6.5Hz, H¹³), 2.68 (ddd, 1H, *J* = 15.7, 6.9, 1.7Hz, H⁴), 2.52 (dd, 1H, *J* = 13.7, 12.4Hz, H¹³), 2.20 (m, 1H, H⁴), 1.36 (s, 3H, CH₃); **¹³C NMR** (100MHz, CDCl₃): δ 200.1 (C¹²), 198.2 (C⁷), 178.4 (C³), 177.4 (C¹), 140.1 (C^{5a}), 138.2 (C^{7'}), 135.8 (C^{7a/11a}), 134.2 (C¹¹), 134.1 (C^{8/10}), 133.6 (C^{7a/11a}), 131.7 (C^{1'}), 131.6 (C^{2',6'}), 131.0 (C^{3',5'}), 129.2 (C^{9',11'}), 128.8 (C^{10'}), 126.6 (C⁹), 126.5 (C^{8/10}), 126.4 (C^{8',12'}), 124.6 (C⁵), 121.1 (C^{4'}), 60.8 (C^{6a}), 48.4 (C^{12a}), 46.9 (C⁶), 43.6 (C^{13b}), 40.3 (C^{3a}), 34.3 (C^{13a}), 32.9 (C¹³), 29.7 (CH₃), 25.5 (C⁴); **HRMS**: Found 580.1088 [M+H]⁺, calculated for C₃₃H₂₇BrNO₄ 580.1123 [M+H]⁺; **Elemental analysis**, calculated for C₃₃H₂₆BrNO₄: C, 68.28; H, 4.51; N, 2.41. Found: C, 67.89, H, 4.41, N, 2.33.

(3aSR,6SR,6aSR,12aRS,13aSR,13bRS)-6-(4-bromophenyl)-12a-methyl-3a,4,6,6a,13,13a-hexahydro-1H-anthra[2,3-e]isoindole-1,3,7,12(2H,12aH,13bH)-tetraone (5.108)



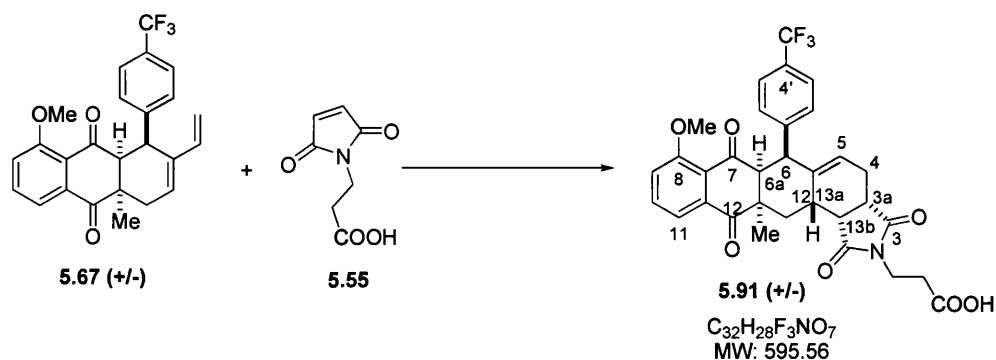
5.108 was obtained as a white solid; **Y** = 81%; **R_f** 0.33 (Silica gel, Et₂O); **Mp** = 254.9 °C; **IR**: 1681, 1592, 1487, 1360, 1253, 1009, 981, 712 cm⁻¹; **¹H NMR** (500MHz, CDCl₃): δ 8.09 (br s, 1H, -NH); 7.91 (d, 1H, *J* = 7.7Hz, H⁹), 7.64 (t, 1H, *J* = 7.3Hz, H¹¹), 7.56 (m, 2H, H^{8,10}), 7.04 (d, 2H, *J* = 8.2Hz, H^{3',5'}), 6.52 (d, 2H, *J* = 8.3Hz H^{2',6'}), 5.41 (dd, 1H, *J* = 6.0, 3.0Hz, H⁵), 4.12 (d, 1H, *J* = 7.9Hz, H⁶), 3.45 (d, 1H, *J* = 10.3Hz, H^{6a}), 3.26 (dd, 1H, *J* = 8.6, 5.8Hz, H^{13b}), 3.16 (td, 1H, *J* = 8.4, 7.3Hz, H^{3a}), 2.95 (m, 1H, H^{13a}), 2.70 (dd, 1H, *J* = 13.8, 6.5Hz, H¹³), 2.57 (dd, 1H, *J* = 15.3, 6.5Hz, H⁴), 2.44 (dd, 1H, *J* = 13.2, 12.9Hz, H¹³), 2.12 (m, 1H, H⁴), 1.36 (s, 3H, CH₃); **¹³C NMR** (100MHz, CDCl₃): δ 200.2 (C¹²), 198.4 (C⁷), 179.2 (C³), 178.3 (C¹), 139.9 (C^{4'}), 138.6 (C^{5a}), 135.7 (C^{7a}), 134.2 (C^{8/11}), 134.0 (C^{8/11}), 133.6 (C^{11a}), 131.6 (C^{2',6'}), 130.9 (C^{3',5'}), 126.6 (C^{10/9}), 126.5 (C^{10/9}), 124.7 (C⁵), 120.9 (C^{1'}), 60.7 (C^{6a}), 48.3 (C^{12a}), 46.6 (C⁶), 44.7 (C^{13b}), 41.3 (C^{3a}), 33.8 (C^{13a}), 32.8 (C¹³), 29.7 (CH₃), 24.9 (C⁴); **HRMS**: Found 504.0807 [M+H]⁺, calculated for C₂₇H₂₃BrNO₄ 504.0810 [M+H]⁺; **Elemental analysis**, calculated for C₂₇H₂₂BrNO₄: C, 64.30; H, 4.40; N, 2.78. Found: C, 64.08; H, 4.38; N, 2.81.

(3aSR,6SR,6aSR,12aRS,13aSR,13bRS)-8-methoxy-12a-methyl-6-(4-(trifluoromethyl)phenyl)-3a,4,6,6a,13,13a-hexahydro-1H-anthra[2,3-e]isoindole-1,3,7,12(2H,12aH,13bH)-tetraone (5.90)



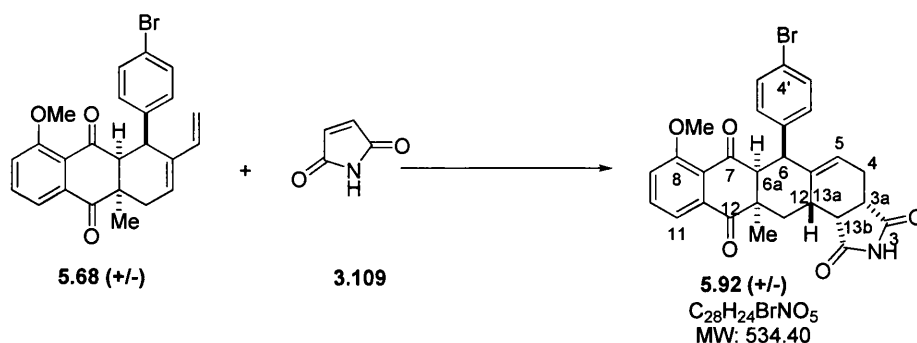
5.90 was obtained as a white solid; **Y** = 78%; **R_f** 0.42 (Silica gel, Et₂O); **Mp** = 90.6 °C; **IR**: 3244, 2328, 1674, 1586, 1467, 1278, 1156, 1104, 1065, 998, 730 cm⁻¹; **¹H NMR** (400MHz, CDCl₃): δ 8.35 (br s, 1H, -NH), 7.51 (m, 2H, H^{11,9}), 7.20 (d, 2H, *J* = 8.1Hz, H^{3',5'}), 7.02 (d, 1H, *J* = 8.2Hz, H¹⁰), 6.85 (d, 2H, *J* = 8.1Hz, H^{2',6'}), 5.42 (dd, 1H, *J* = 6.6, 3.5Hz, H⁵), 4.22 (m, 1H, H⁶), 3.72 (s, 1H, -OCH₃), 3.38 (d, 1H, *J* = 10.4Hz, H^{6a}), 3.21 (dd, 1H, *J* = 8.8, 5.6Hz, H^{13b}), 3.14 (td, 1H, *J* = 8.6, 1.6Hz, H^{3a}), 2.82 (m, 1H, H¹³), 2.60 (dd, 1H, *J* = 13.7, 6.4Hz, H^{13a}), 2.55 (dd, 1H, *J* = 8.6, 1.4Hz, H⁴), 2.50 (d, 1H, *J* = 12.2Hz, H¹³), 2.07 (m, 1H, H⁴), 1.37 (s, 3H, CH₃); **¹³C NMR** (100MHz, CDCl₃): δ 200.2 (C¹²), 196.7 (C⁷), 179.4 (C³), 178.4 (C¹), 157.9 (C⁸), 143.7 (C^{1',4'}), 139.6 (C^{5a}), 135.7 (C^{7a}), 134.5 (C^{11/9}), 130.4 (C^{2',6'}), 125.1 (C^{11a}), 124.6 (C^{5',3'}), 124.6 (C⁵), 124.0 (q, CF₃, *J* = 270Hz), 118.5 (C^{11/9}), 117.2 (C¹⁰), 62.4 (C^{6a}), 55.9 (C^{OMe}), 48.4 (C^{12a}), 45.8 (C⁶), 44.8 (C^{13b}), 41.4 (C^{3a}), 34.0 (C^{13a}), 33.2 (C¹³), 28.6 (CH₃), 25.0 (C⁴); **HRMS** (EI): Found 524.1683 [M+H]⁺, C₂₉H₂₅F₃NO₅, calculated 524.1685 [M+H]⁺; **Elemental Analysis**, calculated for C₂₉H₂₄F₃NO₅: C, 66.53; H, 4.62; N, 2.68. Found: C, 66.43; H, 4.77, N, 2.62.

3-((3aSR,6SR,6aSR,12aRS,13aSR,13bRS)-8-methoxy-12a-methyl-1,3,7,12-tetraoxo-6-(4-(trifluoromethyl)phenyl)-3a,4,6a,7,12,12a,13,13a-octahydro-1H-anthra[2,3-c]isoindol-2(3H,6H,13bH)-yl)propanoic acid (5.91)



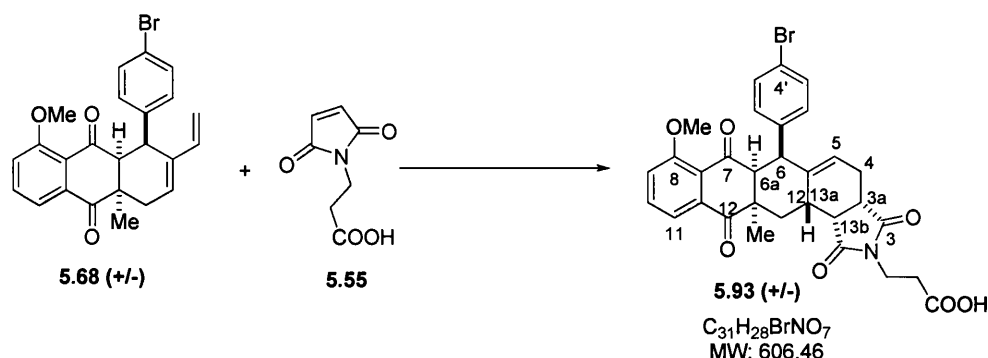
5.91 was obtained as a white solid; **Y** = 92%; **R_f** 0.45 (Silica gel, AcOH/EtOAc 1:99); **Mp** = 144.1 – 147.5 °C; **IR**: 3749, 2359, 1993, 1740, 1671, 1398, 1316, 1216, 1156, 1105, 990, 853 cm⁻¹; **¹H NMR** (500MHz, CDCl₃): δ 7.52 (m, 2H, H^{11,9}), 7.18 (d, 1H, *J* = 8.2Hz, H^{3',5'}), 7.02 (dd, 1H, *J* = 6.3, 3.0Hz, H¹⁰), 6.83 (d, 2H, *J* = 8.1, H^{2',6'}), 5.37 (dd, 1H, *J* = 6.6, 3.0Hz, H⁵), 4.19 (d, 1H, *J* = 7.7Hz, H₆), 3.74 (s, 3H, -OCH₃), 3.72 (m, 2H, H^{7'}), 3.38 (d, 1H, *J* = 10.2Hz, H^{6a}), 3.17 (dd, 1H, *J* = 8.6, 5.6Hz, C^{13b}), 3.11 (t, 1H, *J* = 7.7Hz, H^{3a}), 2.85 (m, 1H, H¹³), 2.66 (dd, 1H, *J* = 14.0, 6.7Hz, H^{13a}), 2.58 (dd, 1H, *J* = 16.1, 6.8Hz, H⁴), 2.57 (t, 2H, *J* = 7.0Hz, H^{8'}), 2.50 (dd, 1H, *J* = 13.6, 12.6 Hz, H¹³), 2.07 (m, 1H, H⁴), 1.39 (s, 3H, CH₃); **¹³C NMR** (125MHz, CDCl₃): δ 200.2 (C¹²), 197.2 (C⁷), 179.0 (C³), 177.8 (C¹), 174.5 (C^{9'}), 157.9 (C⁸), 144.0 (C^{1',4'}), 139.5 (C^{5a}), 135.7 (C^{7a}), 134.6 (C^{11/9}), 130.3 (C^{2',6'}), 128.9 (C^{11a}), 125.0 (C⁵), 124.5 (C^{3',5'}), 124.0 (q, CF₃, *J* = 270Hz), 118.5 (C^{11/9}), 117.2 (C¹⁰), 62.2 (C^{6a}), 55.9 (OCH₃), 48.2 (C^{12a}), 45.7 (C⁶), 43.7 (C^{3a}), 40.1 (C^{13b}), 34.3 (C^{7'}), 34.1 (C^{13a}), 32.9 (C¹³), 31.7 (C^{8'}), 28.7 (CH₃), 25.2 (C⁴); **HRMS** (EI): Found: 596.1920 [M+H]⁺, C₃₂H₂₉F₃NO₇, calculated 596.1896 [M+H]⁺; **Elemental Analysis**, calculated for C₃₂H₂₈F₃NO₇: C, 64.53; H, 4.72; N, 2.35. Found: C, 64.48; H, 4.69, N, 2.08.

(3aSR,6SR,6aSR,12aRS,13aSR,13bRS)-6-(4-bromophenyl)-8-methoxy-12a-methyl-3a,4,6,6a,13,13a-hexahydro-1H-anthra[2,3-e]isoindole-1,3,7,12(2H,12aH, 13bH)-tetraone (5.92)



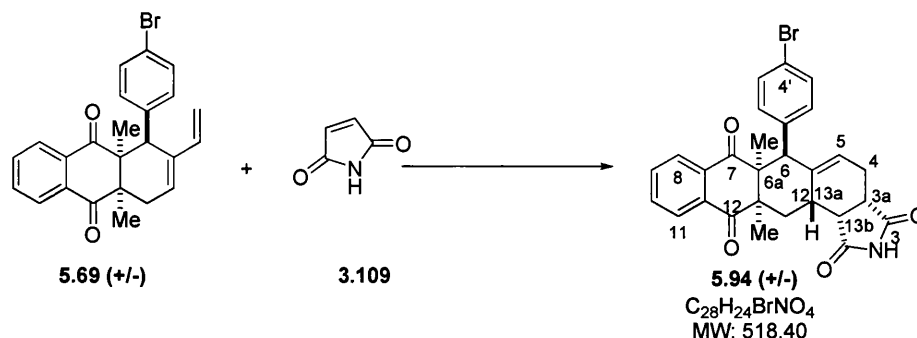
5.92 was obtained as a white solid; **Y** = 73%; **R_f** 0.35 (Silica gel, Et₂O); **Mp** = 170.0 – 173.1 °C; **IR**: 2927, 1692, 1583, 1434, 1362, 1273, 1231, 1183, 1148, 1076 cm⁻¹; **¹H NMR** (400MHz, CDCl₃): δ 7.77 (br s, 1H, -NH), 7.55 (m, 2H, H^{11,9}), 7.10 (d, 2H, *J* = 8.4Hz, H^{3',5'}), 7.02 (m, 1H, H¹⁰), 6.62 (d, 2H, *J* = 8.4Hz, H^{2',6'}), 5.43 (dd, 1H, *J* = 6.7, 3.2Hz, H⁵), 4.11 (m, 1H, H⁶), 3.80 (s, 1H, -OCH₃), 3.35 (d, 1H, *J* = 10.4Hz, H^{6a}), 3.20 (dd, 1H, *J* = 8.7, 5.4Hz, H^{13b}), 3.13 (td, 1H, *J* = 8.4, 1.5Hz, H^{3a}), 2.77 (m, 1H, H¹³), 2.58 (m, 1H, H^{13a}), 2.55 (dd, 1H, *J* = 7.2, 1.3Hz, H⁴), 2.50 (d, 1H, *J* = 12.8Hz, H¹³), 2.04 (m, 1H, H⁴), 1.38 (s, 3H, CH₃); **¹³C NMR** (100MHz, CDCl₃): δ 200.4 (C¹²), 196.9 (C⁷), 178.9 (C³), 178.0 (C¹), 157.9 (C⁸), 139.8 (C^{1'}), 138.2 (C^{5a}), 135.7 (C^{7a}), 134.4 (C^{11/9}), 131.7 (C^{2',6'}), 130.9 (C^{5',3'}), 125.4 (C^{11a}), 124.2 (C⁵), 120.7 (C^{4'}), 118.5 (C^{11/9}), 117.2 (C¹⁰), 62.6 (C^{6a}), 56.2 (C^{OMe}), 48.5 (C^{12a}), 45.5 (C⁶), 44.8 (C^{13b}), 41.4 (C^{3a}), 34.2 (C^{13a}), 33.3 (C¹³), 28.6 (CH₃), 25.1 (C⁴); **HRMS** (ESI): Found 534.0911 [M+H]⁺, C₂₈H₂₅BrNO₅, calculated 534.0916 [M+H]⁺; **Elemental analysis**, calculated for C₂₈H₂₄BrNO₅: C, 62.93; H, 4.52; N, 2.62. Found: C, 63.03; H, 4.36; N, 2.61.

3-((3aSR,6SR,6aSR,12aRS,13aSR,13bRS)-6-(4-bromophenyl)-8-methoxy-12a-methyl-1,3,7,12-tetraoxo-3a,4,6a,7,12,12a,13,13a-octahydro-1H-anthra[2,3-e]isoindol-2(3H,6H,13bH)-yl)propanoic acid (5.93)



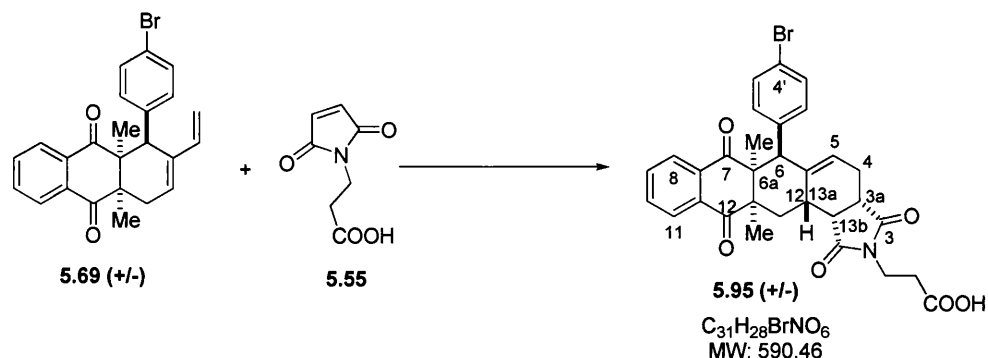
5.93 was obtained as a white solid; **Y** = 93%; **R_f** 0.49 (Silica gel, AcOH/EtOAc 1:99); **Mp** = 151.3 – 154.2 °C **IR**: 3853, 2173, 1740, 1666, 1561, 1293, 1029, 983, 710 cm⁻¹; **¹H NMR** (500MHz, CDCl₃): δ 7.53 (m, 2H, H^{11,9}), 7.08 (dd, 1H, *J* = 6.6, 2.8Hz, H¹⁰), 7.06 (d, 1H, *J* = 8.4Hz, H^{3',5'}), 6.58 (d, 2H, *J* = 8.4, H^{2',6'}), 5.37 (dd, 1H, *J* = 6.7, 3.1Hz, H⁵), 4.06 (dt, 1H, *J* = 8.6, 1.5Hz, H₆), 3.80 (s, 3H, -OCH₃), 3.72 (dd, 1H, *J* = 7.1, 6.6Hz, H^{7'}), 3.68 (dd, 1H, *J* = 7.0, 6.8Hz, H^{7'}), 3.34 (d, 1H, *J* = 10.3Hz, H^{6a}), 3.14 (dd, 1H, *J* = 8.6, 5.5Hz, C^{13b}), 3.09 (dt, 1H, *J* = 8.6, 1.1Hz, H^{3a}), 2.78 (m, 1H, H¹³), 2.61 (dd, 1H, *J* = 13.8, 6.5Hz, H^{13a}), 2.58 (dd, 1H, *J* = 7.4, 1.1Hz, H⁴), 2.54 (t, 2H, *J* = 7.0Hz, H^{8'}), 2.50 (dd, 1H, *J* = 13.6, 12.7 Hz, H¹³), 2.07 (m, 1H, H⁴), 1.38 (s, 3H, CH₃); **¹³C NMR** (125MHz, CDCl₃): δ 200.4 (C¹²), 197.4 (C⁷), 179.1 (C³), 177.9 (C¹), 174.7 (C^{9'}), 157.9 (C⁸), 139.7 (C^{1'}), 138.4 (C^{5a}), 135.7 (C^{4'}), 134.5 (C^{11/9}), 131.7 (C^{2',7'}), 130.3 (C^{3',5'}), 125.2 (C^{7a}), 124.4 (C⁵), 120.6 (C^{11a}), 118.5 (C^{11/9}), 117.2 (C¹⁰), 62.4 (C^{6a}), 56.2 (OCH₃), 48.3 (C^{12a}), 45.4 (C⁶), 43.6 (C^{3a}), 40.1 (C^{13b}), 34.3 (C^{13a}), 34.2 (C^{7'}), 33.1 (C¹³), 31.7 (C^{8'}), 28.7 (CH₃), 25.2 (C⁴); **HRMS** (EI): Found 606.1133 [M+H]⁺, C₃₁H₂₉BrNO₇, calculated 606.1127 [M+H]⁺; **Elemental analysis**, calculated for C₃₁H₂₈BrNO₇: C, 61.39; H, 4.65; N, 2.31. Found: C, 61.21; H, 4.48; N, 2.05.

(3aS,6S,6aS,12aR,13aS,13bR)-6-(4-bromophenyl)-6a,12a-dimethyl-3a,4,6,6a,13,13a-hexahydro-1H-anthra[2,3-e]isoindole-1,3,7,12(2H,12aH,13bH)-tetraone (5.94)



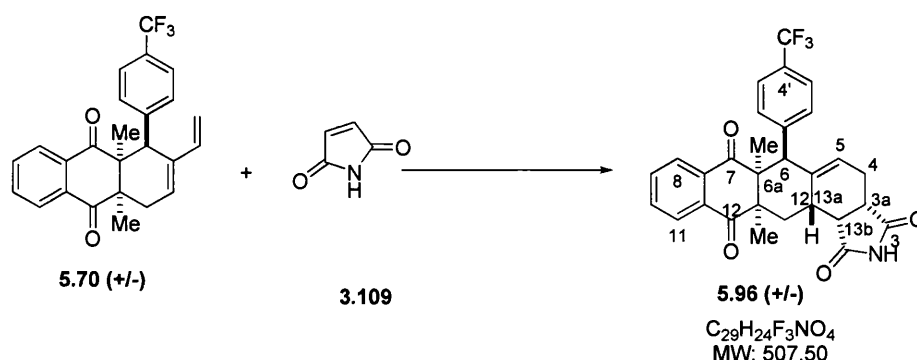
5.94 was obtained as a white solid; **Y** = 67%; **R_f** 0.37 (Silica gel, Et₂O); **Mp** = 90.8 – 95.2 °C; **IR**: 2981, 1702, 1682, 1594, 1486, 1361, 1262, 1198, 1076, 1009, 980, 788 cm⁻¹; **¹H NMR** (400MHz, CDCl₃): δ 8.23 (br s, 1H, -NH), 7.80 (d, 1H, *J* = 8.2Hz, H^{9/10}), 7.58 (dd, 1H, *J* = 7.2, 1.7Hz, H^{9/10}), 7.54 (dd, 1H, *J* = 7.3, 1.7Hz, H^{8/11}), 7.51 (td, 1H, *J* = 5.9, 1.5Hz, H^{8/11}), 6.92 (d, 2H, *J* = 8.5Hz, H^{3',5'}), 6.47 (d, 2H, *J* = 8.5Hz, H^{2',6'}), 5.41 (dd, 1H, *J* = 5.9, 2.8Hz, H⁵), 3.68 (s, 1H, H⁶), 3.28 (dd, 1H, *J* = 8.4, 5.6Hz, H^{13b}), 3.18 (td, 1H, *J* = 8.4, 2.0Hz, H^{3a}), 3.12 (m, 1H, H^{13a}), 2.76 (dd, 1H, *J* = 14.1, 12.0Hz, H¹³), 2.56 (ddd, 1H, *J* = 16.1, 6.7, 1.8Hz, H⁴), 2.53 (dd, 1H, *J* = 14.0, 7.5Hz, H¹³), 2.14 (m, 1H, H⁴), 1.55 (s, 1H, CH₃), 1.19 (s, 3H, CH₃); **¹³C NMR** (100MHz, CDCl₃): δ 201.0 (C¹²), 200.3 (C⁷), 179.4 (C³), 178.6 (C¹), 140.3 (C^{1'/4'}), 139.5 (C^{5a}), 135.6 (C^{7a/11a}), 133.8 (C^{8/11}), 133.7 (C^{7a/11a}), 133.6 (C^{9/10}), 131.7 (C^{2',6'}), 130.7 (C^{3',5'}), 126.8 (C^{8/11}), 126.0 (C⁵), 125.8 (C^{9/10}), 120.8 (C^{1'/4'}), 56.8 (C^{6a}), 56.4 (C⁶), 51.6 (C^{12a}), 44.4 (C^{13b}), 41.2 (C^{3a}), 33.7 (C^{13a}), 29.2 (C¹³), 26.7 (C^{6a}-CH₃), 25.1 (C⁴), 20.8 (C^{12a}-CH₃); **HRMS**: Found 518.0961 [M+H]⁺, calculated for C₂₈H₂₅BrNO₄ 518.0967 [M+H]⁺; **Elemental analysis**, calculated for C₂₈H₂₄BrNO₄: C, 64.87; H, 4.67; N, 2.70. Found: C, 65.03; H, 4.48; N, 2.61.

3-((3aSR,6SR,6aSR,12aRS,13aSR,13bRS)-6-(4-bromophenyl)-6a,12a-dimethyl-1,3,7,12-tetraoxo-3a,4,6a,7,12,12a,13,13a-octahydro-1H-anthra[2,3-e]isoindol-2(3H,6H,13bH)-yl)propanoic acid (5.95)



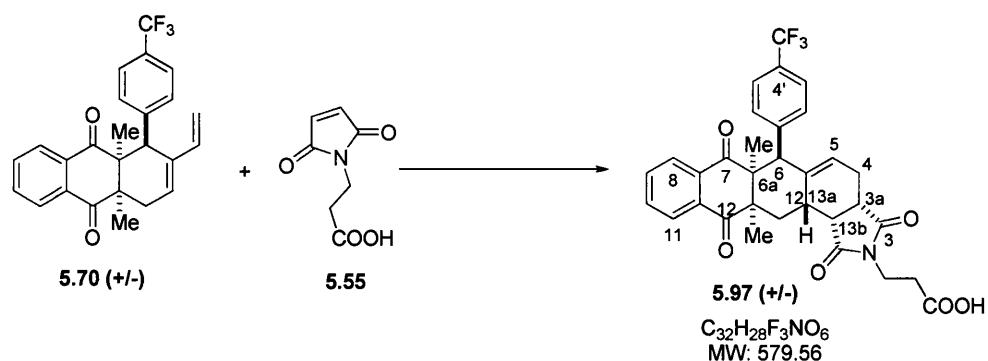
5.95 was obtained as a white solid; **Y** = 76%; **R_f** 0.40 (Silica gel, AcOH/EtOAc 1:99); **Mp** = 137.5 – 141.4°C; **IR**: 2981, 2356, 1738, 1692, 1594, 1486, 1364, 1262, 1219, 1009, 980, 631 cm^{-1} ; **¹H NMR** (500MHz, CDCl₃): δ 7.80 (dt, 1H, *J* = 7.6, 0.7Hz, H^{9/10}), 7.58 (m, 1H, H^{9/10}), 7.56 (dd, 1H, *J* = 7.4, 1.1Hz, H^{8/11}), 7.52 (td, 1H, *J* = 7.3, 0.9Hz, H^{8/11}), 6.95 (d, 2H, *J* = 8.3Hz, H^{3',5'}), 6.45 (d, 2H, *J* = 8.5Hz, H^{2',6'}), 5.32 (dd, 1H, *J* = 6.0, 2.8Hz, H⁵), 3.77 (dd, 1H, *J* = 13.7, 7.2Hz, H^{7'}), 3.72 (dd, 1H, *J* = 13.8, 6.8Hz, H^{7'}), 3.61 (s, 1H, H⁶), 3.20 (dd, 1H, *J* = 8.6, 5.6Hz, H^{13b}), 3.14 (td, 1H, *J* = 8.2, 1.4Hz, H^{3a}), 3.09 (m, 1H, H^{13a}), 2.82 (dd, 1H, *J* = 14.0, 12.0Hz, H¹³), 2.58 (m, 1H, H⁴), 2.54 (m, 2H, H⁸), 2.53 (dd, 1H, *J* = 8.9, 4.7Hz, H¹³), 2.12 (m, 1H, H⁴), 1.54 (s, 1H, CH₃), 1.21 (s, 3H, CH₃); **¹³C NMR** (100MHz, CDCl₃): δ 201.0 (C¹²), 200.3 (C⁷), 179.1 (C³), 178.2 (C¹), 175.2 (COOH), 140.1 (C^{1'/4'}), 139.5 (C^{5a}), 135.6 (C^{7a/11a}), 133.9 (C^{8/11}), 133.7 (C^{7a/11a}), 133.6 (C^{9/10}), 131.7 (C^{2',6'}), 130.7 (C^{3',5'}), 126.9 (C^{8/11}), 126.0 (C⁵), 125.7 (C^{9/10}), 120.8 (C^{1'/4'}), 56.8 (C^{6a}), 56.2 (C⁶), 51.6 (C^{12a}), 43.2 (C^{13b}), 40.0 (C^{3a}), 34.1 (C⁷), 34.0 (C^{13a}), 31.7 (C¹³), 29.2 (C⁸), 27.2 (C^{6a}-CH₃), 25.3 (C⁴), 20.8 (C^{12a}-CH₃); **HRMS**: Found 590.1172 [M+H]⁺, calculated for C₃₁H₂₉BrNO₆ 590.1178 [M+H]⁺; **Elemental analysis**, calculated for C₃₁H₂₈BrNO₆: C, 63.06; H, 4.78; N, 2.37. Found: C, 63.04; H, 4.75; N, 2.36.

(3aSR,6SR,6aSR,12aRS,13aSR,13bRS)-6a,12a-dimethyl-6-(4-(trifluoromethyl)phenyl)-3a,4,6,6a,13,13a-hexahydro-1H-anthra[2,3-e]isoindole-1,3,7,12(2H,12aH,13bH)-tetraone (5.96)



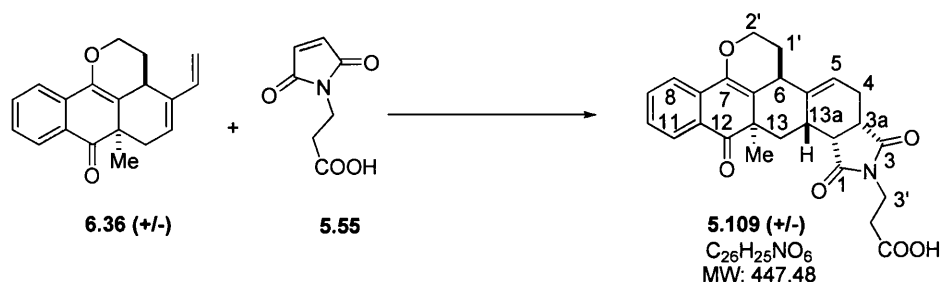
5.96 was obtained as a white solid; **Y** = 88%; **R_f** 0.45 (Silica gel, Et₂O); **Mp** = 137.5 – 142.1 °C; **IR**: 2909, 2165, 1596, 1558, 1416, 1361, 1323, 1263, 1122, 1067, 980, 828, 624 cm⁻¹; **¹H NMR** (400MHz, CDCl₃): δ 7.78 (dd, 1H, *J* = 7.5, 1.2Hz, H^{9/10}), 7.73 (br s, 1H, -NH), 7.55 (dd, 1H, *J* = 7.6, 1.3Hz, H^{9/10}), 7.50 (td, 1H, *J* = 7.3, 1.4Hz, H^{8/11}), 7.45 (td, 1H, *J* = 7.5, 1.4Hz, H^{8/11}), 7.05 (d, 2H, *J* = 8.2Hz, H^{3',5'}), 6.73 (d, 2H, *J* = 8.2Hz, H^{2',6'}), 5.44 (dd, 1H, *J* = 6.0, 3.1Hz, H⁵), 3.82 (s, 1H, H⁶), 3.32 (dd, 1H, *J* = 8.6, 5.9Hz, H^{13b}), 3.21 (td, 1H, *J* = 8.5, 2.0Hz, H^{3a}), 3.20 (m, 1H, H^{13a}), 2.78 (dd, 1H, *J* = 14.1, 11.9Hz, H¹³), 2.60 (d, 1H, *J* = 15.5Hz, H⁴), 2.56 (dd, 1H, *J* = 14.3, 7.6Hz, H¹³), 2.17 (m, 1H, H⁴), 1.59 (s, 1H, CH₃), 1.21 (s, 3H, CH₃); **¹³C NMR** (100MHz, CDCl₃): δ 201.0 (C¹²), 200.3 (C⁷), 179.4 (C³), 178.6 (C¹), 138.2 (C^{1'/4'}), 136.4 (C^{5a}), 135.4 (C^{7a/11a}), 133.8 (C^{8/11}), 133.7 (C^{7a/11a}), 133.6 (C^{9/10}), 130.4 (C^{2',6'}), 126.8 (C^{8/11}), 126.2 (C⁵), 125.9 (C^{9/10}), 124.5 (C^{1'/4'}), 124.4 (C^{3',5'}), 124.0 (q, CF₃, *J* = 270Hz), 56.7 (C^{6a}), 56.6 (C⁶), 51.5 (C^{12a}), 44.4 (C^{13b}), 41.2 (C^{3a}), 33.6 (C^{13a}), 29.1 (C¹³), 26.8 (C^{6a}-CH₃), 25.1 (C⁴), 20.7 (C^{12a}-CH₃); **HRMS**: Found 508.1731 [M+H]⁺, calculated for C₂₉H₂₅F₃NO₄ 508.1736 [M+H]⁺; **Elemental analysis**, calculated for C₂₉H₂₄F₃NO₄: C, 68.63; H, 4.77; N, 2.76. Found: C, 66.05; H, 4.63; N, 2.37.

(3aSR,6SR,6aSR,13aSR,13bRS)-2-benzyl-6-(4-bromophenyl)-11-hydroxy-6a-methyl-3a,4,6,6a,13,13a-hexahydro-1H-anthra[2,3-e]isoindole-1,3,7,12(2H,12aH,13bH)-tetraone (5.97)



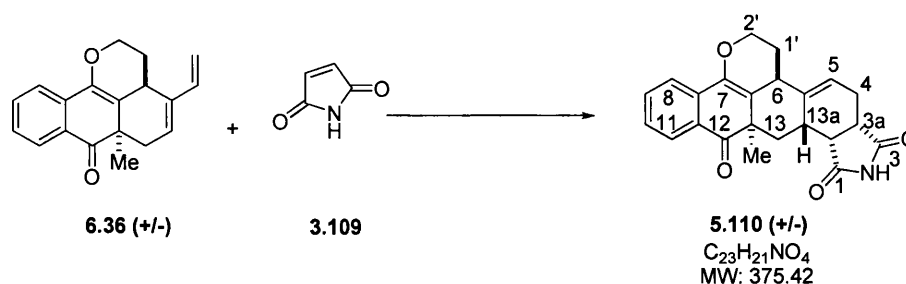
5.97 was obtained as a white solid; R_f 0.39 (Silica gel, AcOH/EtOAc 1:99); $\text{Mp} = 202.3$ – 207.8 °C; **IR**: 3731, 2987, 2335, 1741, 1681, 1556, 1396, 1310, 1262, 1157, 1067, 1019, 862 cm^{-1} ; **^1H NMR** (500MHz, CDCl_3): δ 7.80 (dd, 1H, $J = 7.7, 1.3\text{Hz}$, $\text{H}^{8/11}$), 7.54 (dd, 1H, $J = 7.6, 1.4\text{Hz}$, $\text{H}^{8/11}$), 7.50 (td, 1H, $J = 7.5, 1.4\text{Hz}$, $\text{H}^{9/10}$), 7.44 (td, 1H, $J = 7.5, 1.4\text{Hz}$, $\text{H}^{9/10}$), 7.04 (d, 2H, $J = 8.2\text{Hz}$, $\text{H}^{3',5'}$), 6.71 (d, 2H, $J = 8.2\text{Hz}$, $\text{H}^{2',6'}$), 5.35 (dq, 1H, $J = 6.0, 2.9\text{Hz}$, H^5), 3.78 (dd, 1H, $J = 13.9, 6.7\text{Hz}$, $\text{H}^{7'}$), 3.76 (s, 1H, H^6), 3.74 (dd, 1H, $J = 13.8, 6.8\text{Hz}$, $\text{H}^{7'}$), 3.23 (dd, 1H, $J = 8.6, 5.7\text{Hz}$, H^{13b}), 3.17 (td, 1H, $J = 8.4, 1.8\text{Hz}$, H^{3a}), 3.16 (m, 1H, H^{13a}), 2.85 (dd, 1H, $J = 14.2, 11.8\text{Hz}$, H^{13}), 2.60 (td, 1H, $J = 7.1, 1.1\text{Hz}$, H^4), 2.58 (d, 2H, $J = 7.3\text{Hz}$, $\text{H}^{8'}$), 2.55 (dd, 1H, $J = 7.3, 2.7\text{Hz}$, H^{13}), 2.15 (m, 1H, H^4), 1.57 (s, 1H, CH_3), 1.21 (s, 3H, CH_3); **^{13}C NMR** (125MHz, CDCl_3): δ 200.9 (C^{12}), 200.2 (C^7), 179.1 (C^3), 178.2 (C^1), 175.2 (COOH), 145.8 ($\text{C}^{1'/4'}$), 139.2 (C^{5a}), 135.5 ($\text{C}^{7a/11a}$), 133.9 ($\text{C}^{9/10}$), 133.7 ($\text{C}^{7a/11a}$), 133.6 ($\text{C}^{9/10}$), 130.4 ($\text{C}^{2',6'}$), 126.8 ($\text{C}^{8/11}$), 126.2 (C^5), 125.9 ($\text{C}^{9/10}$), 124.5 ($\text{C}^{3',5'}$), 124.4 ($\text{C}^{1'/4'}$), 124.0 (q, CF_3 , $J = 270\text{Hz}$), 56.8 (C^{6a}), 56.4 (C^6), 51.6 (C^{12a}), 43.2 (C^{13b}), 40.0 (C^{3a}), 34.2 ($\text{C}^{7'}$), 33.8 (C^{13a}), 31.7 (C^{13}), 29.1 ($\text{C}^{8'}$), 26.8 ($\text{C}^{6a}\text{-CH}_3$), 25.3 (C^4), 20.7 ($\text{C}^{12a}\text{-CH}_3$); **HRMS**: Found 580.1949 $[\text{M}+\text{H}]^+$, calculated for $\text{C}_{32}\text{H}_{29}\text{F}_3\text{NO}_6$ 580.1947 $[\text{M}+\text{H}]^+$; **Elemental analysis**, calculated for $\text{C}_{32}\text{H}_{28}\text{F}_3\text{NO}_6$: C, 66.32; H, 4.87; N, 2.42. Found: C, 66.52; H, 4.66; N, 2.40.

3'-((3aSR, 6SR, 12aRS, 13bRS,13aSR,)-12a-methyl-1,3,12-trioxo-1,3,3a,5a,6,12a,13,13a,13b, -decahydro-2H-naphtho[3',2',1':8,1]isochromeno[6,5-e]isoindol-2(5H)-yl)propanoic acid (5.109)



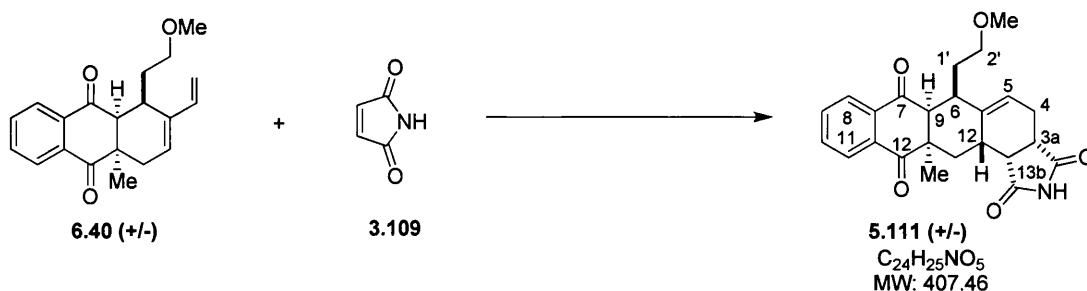
The reaction was carried out for 48h to afford compound **5.109** as white solid. **Y** = 65%; **R_f** 0.29 (Silica gel, AcOH/EtOAc 1:99); **Mp.** 207.6 – 210.1 °C; **IR:** 2928, 1738, 1694, 1399 cm^{-1} ; **¹H NMR** (400MHz, $CDCl_3$): δ 7.85 (dt, 1H, $J = 7.7, 0.6Hz$, $H^{11/8}$), 7.55 (td, 1H, $J = 7.3, 1.3Hz$, $H^{9,10}$), 7.52 (dd, 1H, $J = 7.8, 1.6Hz$, $H^{8/11}$), 7.33 (ddd, 1H, $J = 7.6, 6.9, 1.7Hz$, $H^{9/10}$), 5.49 (dd, 1H, $J = 7.0, 2.8Hz$, H^5), 4.10 (ddd, 1H, $J = 10.3, 6.4, 3.6Hz$, Hb^2), 4.03 (ddd, 1H, $J = 10.8, 8.2, 2.8Hz$, Ha^2), 3.76 (t, 2H, $J = 7.3Hz$, H^3), 3.16 (dd, 1H, $J = 8.8, 6.0Hz$, H^{13b}), 3.09 (td, 1H, $J = 8.1, 1.2Hz$, H^{3a}), 3.01 (m, 1H, H^{13a}), 2.99 (dd, 1H, $J = 14.1, 4.3Hz$, Hb^{13}), 2.71 (dd, 1H, $J = 15.0, 7.2Hz$, H^4), 2.61 (t, 2H, $J = 7.1Hz$, H^4), 2.29 (q, 1H, $J = 13.0Hz$, Ha^{13}), 2.16 (m, 1H, H^6), 2.20 (m, 1H, Hb^1), 2.02 (m, 1H, H^4), 2.11 (m, 1H, Ha^1), 1.37 (s, 3H, CH_3); **¹³C NMR** (100MHz, $CDCl_3$): δ 203.8 (C^{12}), 179.5 (C^3), 177.6 (C^1), 175.0 (COOH), 143.5 (C^7), 143.2 (C^{6a}), 135.0 ($C^{7a/11a}$), 133.8 ($C^{8/11}$), 129.0 ($C^{7a/11a}$), 127.9 ($C^{9/10}$), 126.7 ($C^{9/10}$), 121.6 ($C^{8/11}$), 117.8 (C^{5a}), 116.0 (C^5), 63.4 (C^2), 49.0 (C^{12a}), 43.3 (C^{13b}), 39.8 (C^{3a}), 34.7 (C^6), 34.3 (C^3), 31.8 (C^4), 31.7 (C^{13a}), 29.3 (C^{13}), 29.2 (CH_3), 25.0 (C^1), 24.5 (C^4); **MS** (EI): m/z 448.56 ($M+H^+$) (100); **HRMS:** Found M^+ 447.1584, $C_{26}H_{25}NO_6$ requires 447.1682; **Elemental analysis:** calculated for $C_{26}H_{25}NO_6$: C, 69.79; H, 5.63; N, 3.13; Found C, 69.90; H, 5.51; N, 3.02.

(3aSR,6SR,12aRS,13bRS,13aSR)-12a-methyl-1',3a,4,6,12a,13-hexahydro-2H-naphtho[3',2',1':8,1]isochromeno[6,5-e]isoindole-1,3,12(7H,8aH,8bH)-trione (5.110)



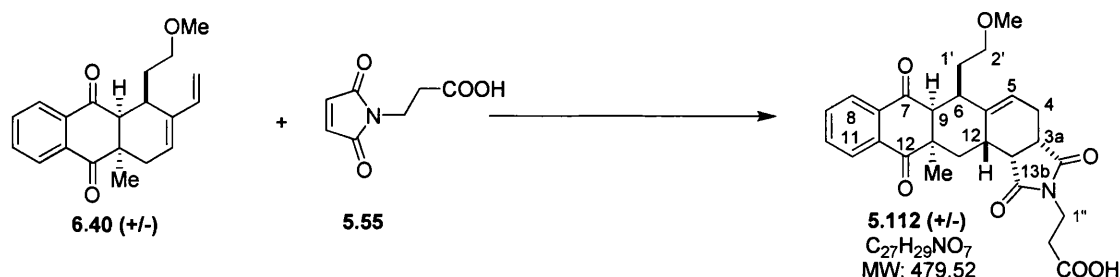
The reaction was carried out for 24h to afford compound **5.110** as white solid. **Y** = 82%; **R_f** 0.34 (Silica gel, Et₂O); **IR**: 1740, 1697, 1648, 1593, 1364 cm⁻¹; **Mp**. 246.5 – 247.1 °C; **¹H NMR** (400MHz, DMSO-d₆): δ 7.15 (ddd, 1H, *J* = 7.8, 1.4, 0.6Hz, H^{11/8}), 6.93 (ddd, 1H, *J* = 7.9, 7.2, 1.4Hz, H^{9/10}), 6.84 (dd, 1H, *J* = 7.7, 0.6Hz, H^{8/11}), 6.66 (td, 1H, *J* = 7.5, 1.1Hz H^{9/10}), 5.00 (dd, 1H, *J* = 5.5, 2.8Hz, H⁵), 3.49 (dt, 1H, *J* = 10.7, 3.5Hz, Hb^{2'}), 3.28 (td, 1H, *J* = 11.1, 1.9Hz, Ha^{2'}), 2.58 (s, 1H, H⁶), 2.31 (td, 1H, *J* = 9.1, 1.6Hz, H^{13b}), 2.29 (q, 1H, *J* = 6.1Hz, H^{3a}), 2.01 (m, 1H, H^{13a}), 1.67 (dd, 1H, *J* = 15.7, 6.3Hz, Hb⁴), 1.39 (m, 2H, Hb^{1'}, a⁴), 1.27 (t, 1H, *J* = 12.2Hz, Hb¹³), 1.21 (dd, 1H, *J* = 13.0, 7.2Hz, Ha¹³), 0.90 (tdt, 1H, *J* = 13.5, 10.7, 2.8Hz, Ha^{1'}), 0.45 (s, 3H, CH₃); **¹³C NMR** (100MHz, DMSO-d₆): δ 201.3 (C¹²), 180.9 (C³), 180.0 (C¹), 141.0 (C⁷), 138.7 (C^{6a}), 135.0 (C^{7a/11a}), 134.7 (C^{9/10}), 127.8 (C^{9/10}), 127.2 (C^{7a/11a}), 126.5 (C^{8/11}), 121.6 (C^{8/11}), 119.9 (C⁵), 117.4 (C^{5a}), 64.8 (C^{2'}), 46.2 (C^{12a}), 43.5 (C^{13b}), 40.0 (C^{3a}), 35.7 (C¹³), 33.5 (C⁶), 31.6 (C^{13a}), 28.9 (C^{1'}), 23.3 (C⁴), 21.5 (CH₃); **MS** (EI): *m/z* 376.52 (M+H⁺) (100); **HRMS**: Found 376.1536 [M+H]⁺, calculated for C₂₃H₂₂NO₄ 376.1549 [M+H]⁺; **Elemental analysis**, calculated for C₂₃H₂₁NO₄: C, 73.58; H, 5.64; N, 3.73; Found C, 73.55; H, 5.95; N, 3.63.

(3aSR,6RS,6aSR,12aRS,13aSR,13bRS)-6-(2-methoxyethyl)-12a-methyl-3a,4,6,6a,13,13a-hexahydro-1H-anthra[2,3-e]isoindole-1,3,7,12(2H,12aH,13bH)-tetraone (5.111)



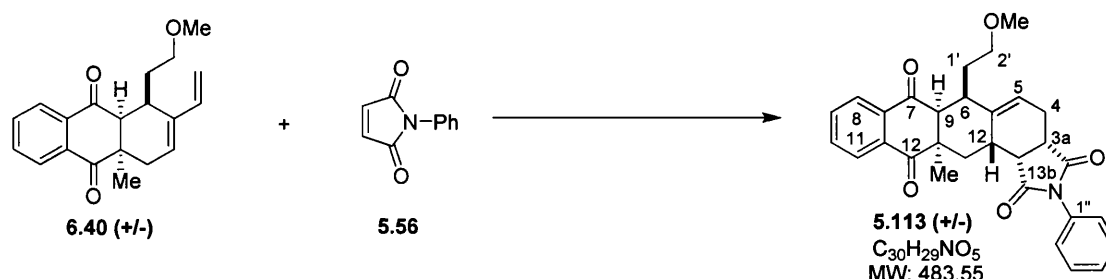
The reaction was carried out for 72h to afford compound **5.111** as white solid. **Y** = 85%; **R_f** 0.31 (Silica gel, CH₂Cl₂/Et₂O 50:50); **IR**: 3173, 3059, 2922, 2361, 1780, 1697, 1592, 1247, 1163, 728 cm⁻¹; **Mp.** 231.7 - 235.2 °C; **¹H NMR** (400MHz, CD₂Cl₂): δ 8.04 (m, 1H, H¹¹), 7.99 (m, 1H, H⁹), 7.75 (dd, 1H, *J* = 3.9, 2.4Hz, H^{10/8}), 7.73 (dd, 1H, *J* = 3.9, 2.3Hz, H^{10/8}), 5.61 (t, 1H, *J* = 3.9Hz, H⁵), 3.17 (t, 1H, *J* = 8.5Hz, H^{13b}), 3.07 (s, 3H, -CH₃O), 3.07 (m, 1H, H^{3a}), 3.00 (d, 1H, *J* = 5.7Hz, H^{6a}), 2.98 (t, 2H, *J* = 5.5Hz, H²), 2.87 (dt, 1H, *J* = 11.5, 5.6Hz, H⁶), 2.69 (dd, 1H, *J* = 13.1, 3.5Hz, H^{b13}), 2.68 (m, 1H, H^{13a}), 2.57 (dt, 1H, *J* = 18.5, 3.6Hz, H^{b4}), 2.30 (dddd, 1H, *J* = 18.5, 9.8, 3.9, 1.6Hz, H^{a4}), 1.25 (m, 1H, H^{b1}), 1.16 (s, 3H, CH₃), 1.07 (t, 1H, *J* = 13.5Hz, H^{a13}), 1.01 (m, 1H, H^{a1}); **¹³C NMR** (100MHz, CD₂Cl₂): δ 200.5 (C¹²), 198.1 (C⁷), 179.7 (C³), 178.1 (C¹), 138.6 (C^{5a}), 135.5 (C^{7a}), 134.9 (C^{11a}), 134.9 (C^{8/10}), 134.6 (C^{8/10}), 127.4 (C¹¹), 126.4 (C⁹), 119.6 (C⁵), 70.5 (C²), 62.3 (C^{6a}), 58.5 (CH₃O), 49.1 (C^{12a}), 45.3 (C⁶), 42.6 (C^{13b}), 38.5 (C^{3a}), 37.9 (C¹³), 29.4 (C^{13a}), 28.8 (C¹), 28.6 (CH₃), 21.1 (C⁴); **MS** (EI): *m/z* 408.37 (M+H⁺) (100); **HRMS**: Found 408.1825 [M+H]⁺, calculated for C₂₄H₂₆NO₅ 408.1811 [M+H]⁺; **Elemental analysis**, calculated for C₂₄H₂₅NO₅: C, 70.74; H, 6.18; N, 3.44; Found C, 70.44; H, 6.23; N, 3.41.

3-((3aSR,6RS,6aSR,12aRS,13aSR,13bRS)-6-(2-methoxyethyl)-12a-methyl-1,3,7,12-tetraoxo-3a,4,6a,7,12,12a,13,13a-octahydro-1H-anthra[2,3-e]isoindol-2(3H,6H,13bH)-yl)propanoic acid (5.112)



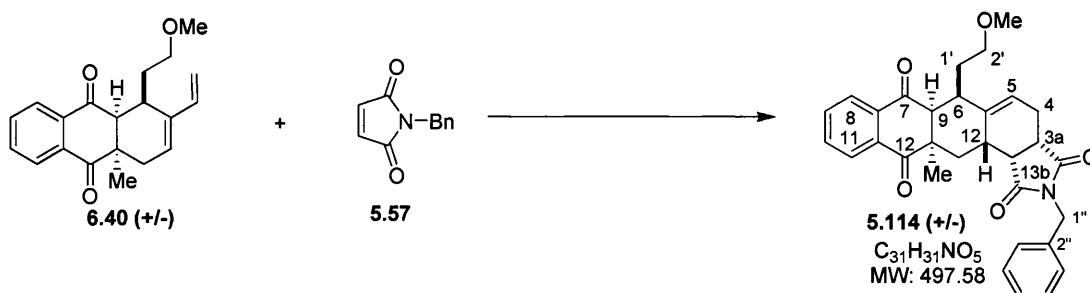
The reaction was carried out for 5 days to afford compound **5.112** as a white solid. **Y** = 73%; **R_f** 0.27 (Silica gel, AcOH/EtOAc 1:99); **IR**: 2930, 2363, 1695, 1591, 1392, 1248, 668 cm^{-1} ; **Mp.** 147.3 - 148.2 °C; **¹H NMR** (400MHz, CD₃OD): δ 8.08 (m, 1H, H¹¹), 8.02 (m, 1H, H⁹), 7.87 (m, 1H, H^{8/10}), 7.83 (m, 1H, H^{8/10}), 5.65 (t, 1H, *J* = 4.1Hz, H⁵), 3.79 (t, 2H, *J* = 7.2Hz, H^{1''}), 3.24 (t, 1H, *J* = 8.3Hz, H^{13b}), 3.18 (s, 3H, -CH₃O), 3.17 (dd, 2H, *J* = 6.7, 5.9Hz, H^{2'}), 3.13 (td, 1H, *J* = 8.9, 3.4Hz, H^{3a}), 3.03 (d, 1H, *J* = 6.0Hz, H^{6a}), 2.90 (dt, 1H, *J* = 11.0, 5.4Hz, H⁶), 2.67 (m, 1H, H^{13a}), 2.64 (m, 1H, H¹³), 2.63 (t, 2H, *J* = 7.1Hz, H^{2''}), 2.59 (dt, 1H, *J* = 17.7, 3.9Hz, H⁴), 2.29 (ddd, 1H, *J* = 18.1, 9.3, 4.0Hz, H⁴), 1.39 (ddt, 1H, *J* = 13.7, 11.2, 5.6Hz, H^{1'}), 1.27-1.21 (m, 1H, H¹³), 1.24 (s, 3H, CH₃), 1.17 (dtd, 1H, *J* = 13.7, 6.8, 4.8Hz, H^{1'}); **¹³C NMR** (100MHz, CD₃OD): δ 206.2 (COOH), 201.9 (C¹²), 199.6 (C⁷), 181.3 (C³), 179.7 (C¹), 140.1 (C^{5a}), 136.8 (C^{7a}), 136.2 (C^{11a}), 135.9 (C^{8/10}), 135.6 (C^{8/10}), 128.0 (C¹¹), 127.1 (C⁹), 120.6 (C⁵), 71.3 (C^{2'}), 62.5 (C^{6a}), 58.7 (CH₃O), 48.5 (C^{12a}), 45.2 (C⁶), 42.4 (C^{13b}), 38.7 (C¹³), 38.4 (C^{3a}), 35.6 (C^{1''}), 32.5 (C^{2''}), 30.5 (C^{13a}), 29.6 (CH₃), 29.4 (C¹), 22.5 (C⁴); **MS** (EI): *m/z* 480.22 (M+H⁺) (100); **HRMS**: Found 478.1890 [M+H]⁺, calculated for C₂₇H₃₀NO₇ 478.1866 [M+H]⁺; **Elemental analysis**, calculated for C₂₇H₂₉NO₇: C, 67.63; H, 6.10; N, 2.92; Found C, 67.48; H, 6.10; N, 2.72.

(3aS,6R,6aS,12aR,13aS,13bR)-6-(2-methoxyethyl)-12a-methyl-2-phenyl-3a,4,6,6a,13,13a-hexahydro-1H-anthra[2,3-e]isoindole-1,3,7,12(2H,12aH,13bH)-tetraone (5.113)



The reaction was carried out for 3 days to afford compound **5.113** as a white solid. **Y** = 96%; **R_f** 0.26 (Silica gel, Et₂O); **IR**: 2915, 2847, 1697, 1679, 1591, 1494, 1380, 1250, 1162, 1085, 699 cm⁻¹; **Mp**. 225.7 - 228.8 °C; **¹H NMR** (400MHz, CDCl₃): δ 8.07 (m, 1H, H¹¹), 8.03 (m, 1H, H⁹), 7.74 (m, 2H, H^{8,10}), 7.47 (m, 2H, H^{3'',5''}), 7.38 (m, 1H, H^{4''}), 7.30 (m, 2H, H^{2'',6''}), 5.68 (t, 1H, *J* = 3.9Hz, H⁵), 3.34 (t, *J* = 8.4Hz, H^{13b}), 3.21 (td, 1H, *J* = 9.1, 3.2Hz, H^{3a}), 3.13 (s, 3H, -CH₃O), 3.06 (dd, 2H, *J* = 7.0, 5.8Hz, H¹³), 3.03 (t, 1H, *J* = 6.2Hz, H^{13a}), 2.96 (td, 1H, *J* = 10.5, 5.6Hz, H^{6a}), 2.83 (dd, 2H, *J* = 12.7, 2.9Hz, H^{2'}), 2.78 (m, 1H, H⁴), 2.41 (dddd, 1H, *J* = 18.5, 9.6, 3.6, 1.1Hz, H⁴), 1.34 (m, 1H, H^{1'}), 1.27 (m, 1H, H⁶), 1.21 (s, 3H, CH₃), 1.14 (m, 1H, H^{1'}); **¹³C NMR** (100MHz, CDCl₃): δ 199.9 (C¹²), 197.9 (C⁷), 178.5 (C³), 176.8 (C¹), 138.5 (C^{5a}), 135.2 (C^{7a}), 134.6 (C^{8/10}), 134.5 (C^{11a}), 134.2 (C^{8/10}), 131.9 (C^{1''}), 129.2 (C^{3'',5''}), 128.5 (C^{4''}), 127.2 (C^{9/11}), 126.2 (C^{2'',6''}), 126.2 (C^{9/11}), 119.2 (C⁵), 70.4 (C^{2'}), 61.7 (C^{13a}), 58.5 (CH₃O), 48.7 (C^{12a}), 44.6 (C^{6a}), 41.4 (C^{13b}), 37.6 (C^{3a,6}), 37.5 (C¹³), 29.3 (CH₃), 28.4 (C^{1'}), 21.3 (C⁴); **MS** (EI): *m/z* 484.74 (M+H⁺) (100); **HRMS**: Found 484.2145 [M+H]⁺, calculated for C₃₀H₃₀NO₅ 484.2124 [M+H]⁺; **Elemental analysis**, calculated for C₃₀H₂₉NO₅: C, 74.52; H, 6.04; N, 2.90; Found C, 74.66; H, 6.10; N, 2.88.

(3aS,6R,6aS,12aR,13aS,13bR)-2-benzyl-6-(2-methoxyethyl)-12a-methyl-3a,4,6,6a,13,13a-hexahydro-1H-anthra[2,3-e]isoindole-1,3,7,12(2H,12aH,13bH)-tetraone (5.114)

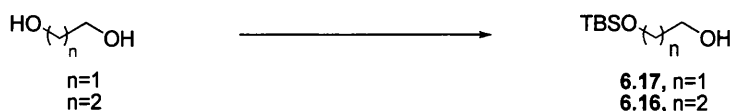


The reaction was carried out for 3 days to afford compound **5.114** as a white solid. **Y** = 94%; **R_f** 0.28 (Silica gel, Et₂O); **IR**: 3069, 2924, 2362, 1744, 1698, 15923, 1394, 1245, 1116, 978, 699 cm⁻¹; **Mp**. 157.1 - 158.3 °C; **¹H NMR** (400MHz, CDCl₃): δ 8.02 (m, 1H, H¹¹), 7.99 (m, 1H, H⁹), 7.73 (td, 1H, *J* = 6.0, 2.0Hz, H¹⁰), 7.70 (td, 1H, *J* = 5.9, 1.9Hz, H⁸), 7.43 (m, 2H, H^{3'',7''}), 7.28 (m, 2H, H^{4'',6''}), 7.21 (m, 1H, H^{5''}), 5.57 (t, 1H, *J* = 3.8Hz, H⁵), 4.67 (s, 2H, H^{1''}), 3.14 (t, 1H, *J* = 8.5Hz, H^{13b}), 3.11 (s, 3H, -CH₃O), 3.00 (dt, 2H, *J* = 14.9, 1.6Hz, H^{2'}), 2.98 (m, 1H, H^{3a}), 2.88 (d, 1H, *J* = 6.1Hz, H^{6a}), 2.83 (dt, 1H, *J* = 11.4, 5.5Hz, H⁶), 2.68 (m, 1H, H^{13a}), 2.66 (dt, 1H, *J* = 18.4, 3.5Hz, H^{b4}), 2.36 (dd, 1H, *J* = 12.8, 3.5Hz, H^{b13}), 2.30 (m, 1H, H^{a4}), 1.26 (m, 2H, H^{b1'}), 1.07 (m, 1H, H^{a1'}), 0.92 (s, 3H, CH₃), 0.71 (t, 1H, *J* = 13.1Hz, H^{a13}); **¹³C NMR** (100MHz, CDCl₃): δ 199.9 (C¹²), 198.0 (C⁷), 179.2 (C³), 177.5 (C¹), 138.4 (C^{5a}), 135.9 (C^{7a}), 135.1 (C^{2'',11a}), 134.5 (C^{8/10}), 134.2 (C^{8/10}), 129.3 (C^{3'',5''}), 128.6 (C^{4'',6''}), 127.9 (C^{5''}), 127.2 (C^{9/11}), 126.2 (C^{9/11}), 119.1 (C⁵), 70.4 (C^{2'}), 61.5 (C^{6a}), 58.5 (CH₃O), 48.5 (C^{12a}), 44.5 (C⁶), 42.3 (C^{1''}), 41.0 (C^{13b}), 37.2 (C¹³), 37.1 (C^{3a}), 29.0 (C^{13a}), 28.9 (CH₃), 28.3 (C^{1'}), 21.1 (C⁴); **MS** (EI): *m/z* 498.33 (M+H⁺) (100); **HRMS**: Found 498.2289 [M+H]⁺, calculated for C₃₁H₃₂NO₅ 498.2281 [M+H]⁺; **Elemental analysis**, calculated for C₃₁H₃₁NO₅: C, 74.83; H, 6.28; N, 2.81; Found C, 74.68; H, 6.22; N, 2.68.

9.2 One-pot synthesis of fused-tetracyclic scaffolds employing a Lewis acid-catalyzed domino reaction of naphthoquinones

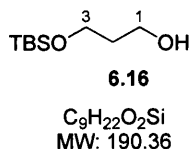
9.2.1 Synthesis of dienes and cross-conjugated trienes

General procedure for TBS monoprotection of diols



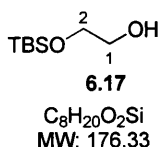
Propanediol or ethanediol was diluted in THF (0.5 M) at 0 °C and imidazole powder (2.4 eq.) was added to the solution under dry, inert condition. Upon stirring, TBDMSCl (0.95 eq.) powder was added to the mixture. The reaction was left to stir at room temperature for 18h. The crude was filtered on a pad of silica gel and washed with excess EtOAc. The crude was then concentrated at 100 mmHg, 40 °C, separated by column chromatography on silica gel using *n*-hexane and EtOAc (4:1). The desired products were isolated as colourless oils (98% purity assessed by NMR analysis and TLC).

3-(*tert*-butyldimethylsilyloxy)propan-1-ol (6.16):



Y = 60%; **R_f** 0.15 (silica gel, *n*-hexane/ EtOAc, 4:1); **IR**: 3453, 2922, 2356 cm^{-1} ; **¹H NMR** (400MHz, CDCl_3): δ 3.77 (4H, m, $\text{H}^{1,3}$), 2.76 (1H, s, OH), 1.74 (2H, q, J = 5.7 Hz, H^2), 0.90 (9H, s, $(\text{CH}_3)_3$), 0.04 (6H, s, $(\text{CH}_3)_2$); **¹³C NMR** (100MHz, CDCl_3): δ -5.8 (CH_3)₂, 25.6 ($\text{C}(\text{CH}_3)_3$), 25.8 ($(\text{CH}_3)_3$), 34.0 (C^2), 61.9 ($\text{C}^{1/3}$), 62.5 ($\text{C}^{1/3}$). Spectroscopic data are in accordance with those reported in literature.²¹⁰

3-(*tert*-butyldimethylsilyloxy)ethan-1-ol (6.17):



Y = 57%; **R_f** 0.17 (silica gel, *n*-hexane/ EtOAc, 4:1); **IR**: 2928, 2360, 1417, 1253 cm^{-1} ; **¹H NMR** (400MHz, CDCl_3): δ 3.71 (1H, dt, J = 6.4, 0.7 Hz, H^1), 3.70 (1H, d,

$J = 5.0$ Hz, H^1), 3.65 (2H, m, H^2), 0.91 (9H, s, $(CH_3)_3$), 0.08 (6H, s, $(CH_3)_2$); ^{13}C NMR (100MHz, $CDCl_3$): δ 64.1 ($C^{1/3}$), 63.7 ($C^{1/3}$), 25.9 ($(CH_3)_3$), 18.3 ($C(CH_3)_3$), -5.3 ($(CH_3)_2$). This compound is commercially available.

Synthesis of *N*-boc propanol (6.18)



The amino alcohol (0.50 g, 0.51 ml, 6.66 mmol) was diluted in THF (15 ml, 0.4 M) and transferred to a three necks flask. The solution was cooled to 0 °C and K_2CO_3 (0.92 g, 6.66 mmol, 1 eq.) and di-*tert*-butyldicarbonate (1.74 g, 7.99 mmol, 1.2 eq.) were added to the mixture. This was allowed to warm up to room temperature and left vigorously stirring for 18h. Then the reaction mixture was concentrated under reduced pressure and diluted in 35 ml EtOAc, washed with water (3 x) and brine. The aqueous phases were combined and extracted with EtOAc (3 x). The organic extracts were combined, dried over $MgSO_4$ and concentrated under vacuum. The crude mixture was purified by column chromatography on silica gel using *n*-hexane and EtOAc (1:1). Compound **3** was isolated as clear colourless oil (1.03 g, 88%) (98% purity assessed by NMR and LC-MS analysis). R_f 0.27 (silica gel, Et_2O); IR: 3349, 2934, 2330, 1682, 1164 cm^{-1} ; 1H NMR (400MHz, $CDCl_3$): δ 4.74 (1H, s, NH), 3.66 (2H, q, $J = 5.8$ Hz, H^1), 3.29 (2H, q, $J = 6.0$ Hz, H^1), 1.66 (2H, q, $J = 5.9$ Hz, H^2), 1.45 (9H, s, $(CH_3)_3$). ^{13}C NMR (100MHz, $CDCl_3$): δ 155.8 (COO), 79.7 ($C(CH_3)_3$), 59.2 (C^1), 36.8 (C^3), 32.9 (C^2), 28.4 ($(CH_3)_3$). Spectroscopic data are in accordance with those reported in literature.²⁵⁴

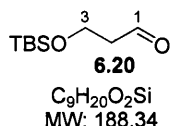
General procedure for the synthesis of aldehydes



At 0 °C, Dess-Martin periodinane (1.05 eq.) was added in one portion to a 0.4 M solution of alcohol in CH_2Cl_2 . The reaction mixture was left stirring for 30 min to 1.5 h, then quenched with a saturated solution of $NaHCO_3$ / Na_2SO_3 (1:1) and stirred at room temperature for 30 min. The aqueous layer was separated from the organic and extracted Et_2O (3 x). The combined organic phases were washed with water (3

x) and brine, dried over MgSO_4 , filtered and concentrated under reduced pressure. The crude mixture was purified by flash column chromatography on silica gel using *n*-hexane and EtOAc (20:1), to afford the desired compounds (98% purity assessed by NMR analysis and TLC).

3-(*tert*-butyldimethylsilyloxy)propanal (6.20):



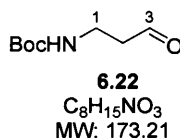
The reaction time was 1.5 h and compound **6.20** was isolated as colourless oil. **Y** = 75%; **R_f** 0.143 (silica gel, *n*-hexane/ EtOAc 20:1); **IR**: 2928, 2366, 1715, 1253, 1102 cm^{-1} ; **¹H NMR** (400MHz, CDCl₃): δ 9.80 (1H, s, H¹), 3.98 (2H, t, *J* = 6.0 Hz, H³), 2.59 (2H, td, *J* = 26.0, 2.1 Hz, H²), 0.88 (9H, s, (CH₃)₃), 0.07 (6H, s, (CH₃)₂); **¹³C NMR** (100MHz, CDCl₃): δ -5.5 (CH₃)₂, 18.2 (C(CH₃)₃), 25.8 ((CH₃)₃), 46.5 (C²), 57.4 (C³), 201.9 (C¹); **HRMS**: Found [M+H]⁺ 189.1316, C₉H₂₀O₂Si requires *MH*, 189.1311. Spectroscopic data are in accordance with those reported in literature.²¹⁰

3-(*tert*-butyldimethylsilyloxy)ethanal (6.21):



The reaction time was 1 h and compound **6.21** was isolated as colourless oil. **Y** = 65%; **R_f** 0.16 (silica gel, *n*-hexane/EtOAc 20:1); **IR**: 2917, 2849, 2365, 1739, 1263, 733 cm^{-1} ; **¹H NMR** (400MHz, CDCl₃): δ 9.70 (1H, s, H¹), 4.20 (2H, d, *J* = 0.8 Hz, H²), 0.93 (9H, s, (CH₃)₃), 0.11 (6H, s, (CH₃)₂). **¹³C NMR** (100MHz, CDCl₃): δ 202.3 (C¹), 69.6 (C²), 25.7 ((CH₃)₃), 18.3 (C(CH₃)₃), -5.4 (CH₃)₂; **HRMS**: Found [M+H]⁺ 175.1158, C₈H₁₈O₂Si requires *MH*, 175.1154. Spectroscopic data are in accordance with those reported in literature.²⁵⁵

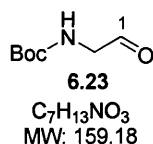
tert-butyl 3-oxopropylcarbamate (6.22):



The reaction time was 1 h and compound **6.22** was isolated as colourless oil. **Y** = 75%; **R_f** 0.4 (silica gel, Et₂O); **IR**: 2976, 2357, 1702, 1506, 1264 cm^{-1} ; **¹H NMR**

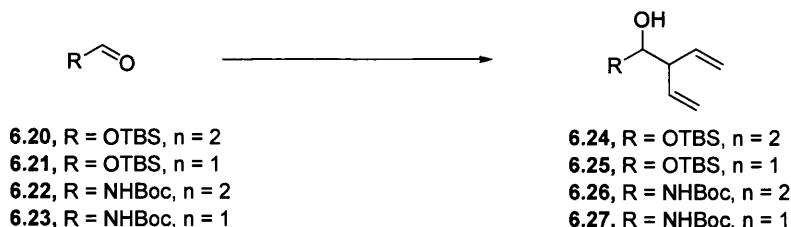
(400MHz, CDCl₃): δ 9.81 (1H, s, H³), 4.91 (1H, s, NH), 3.41 (2H, m, H¹), 2.71 (2H, m, H²), 1.42 (9H, s, (CH₃)₃); ¹³C NMR (100MHz, CDCl₃): δ 201.5 (C³), 155.8 (COO), 79.5 (C(CH₃)₃), 44.3 (C²), 34.0 (C¹), 28.4 ((CH₃)₃). Spectroscopic data are in accordance with those reported in literature.²⁵⁶

tert-butyl 2-oxoethylcarbamate (6.23):



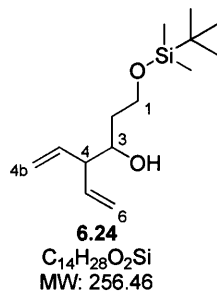
The reaction time was 30 min and compound **6.23** was isolated as colourless oil. **Y** = 99%; **R_f** 0.65 (silica gel, Et₂O); **IR**: 2977, 2356, 1686, 1630 cm⁻¹; ¹H NMR (400 MHz, CDCl₃): δ 9.63 (1H, s, H²), 5.23 (1H, s, NH), 4.05 (2H, d, *J* = 4.6 Hz, H¹), 1.44 (9H, s, (CH₃)₃); ¹³C NMR (100 MHz, CDCl₃): δ 197.46 (C²), 156.01 (COO), 51.73 (C¹), 31.90 (C(CH₃)₃), 28.62 ((CH₃)₃). **MS** (EI): 158.27 (M⁺ - 1) (20), 171.34 (M⁺ + 12); **HRMS**: Found [M+H]⁺ 160.0978, C₇H₁₃NO₃ requires *MH*, 160.0974; **Elemental analysis**: Calculated for C₇H₁₃NO₃ C, 52.82; H, 8.23; N, 8.80; Found C 52.62; H, 8.06; N, 8.69. Spectroscopic data are in accordance with those reported in literature.²⁵⁷

General procedure for allylation of aldehydes



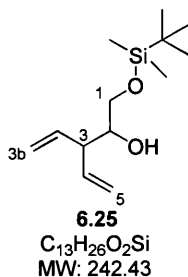
The 5-bromo-1,3-pentadiene (1.5 eq.), prepared according the procedure described by Prevost¹⁷⁸, was added to a solution of aldehyde in DMF (0.2 M). The reaction mixture was then cooled to 0 °C and indium powder 100 mesh (2 eq.) was added portion-wise under vigorous stirring. After 3 h the reaction was allowed to warm to 10 °C, diluted in CH₂Cl₂ (0.2 M) and poured into Et₂O (0.02 M) forming a cloudy mixture. This was filtered on a pad of silica gel and washed with excess of Et₂O (3 x). The solution was evaporated under reduced pressure and the crude product was purified by flash column chromatography on silica gel using *n*-hexane and Et₂O (4:1). Compounds **6.24** – **6.27** were obtained as colourless oils (98% purity assessed by NMR and LC-MS analysis).

1-(*tert*-butyldimethylsilyloxy)-4-vinylhex-5-en-3-ol (6.24):



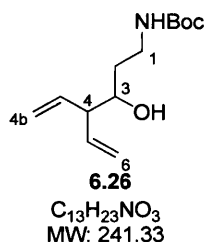
Y = 90%; **R_f** 0.48 (silica gel, *n*-hexane/ Et₂O 4:1); **IR**: 3462, 2956, 2364, 1253, 1086 cm⁻¹; **¹H NMR** (400MHz, CDCl₃): δ 5.90 (1H, ddd, *J* = 17.5, 10.6 Hz, H^{4a/5}), 5.83 (1H, ddd, *J* = 17.3, 10.9, 7.5 Hz, H^{4a/5}), 5.13 (4H, m, H^{4b,6}), 3.89 (1H, dt, *J* = 10.1, 5.0 Hz, H³), 3.81 (2H, m, H¹), 2.81 (1H, q, *J* = 7.0 Hz, H⁴), 1.77 (2H, m, H²), 0.90 (9H, s, (CH₃)₃), 0.07 (6H, s, (CH₃)₂). **¹³C NMR** (100 MHz, CDCl₃): δ 137.8 (C^{5/4a}), 137.3 (C^{5/4a}), 116.7 (C^{4b/6}), 116.4 (C^{4b/6}), 73.6 (C³), 62.6 (C¹), 54.7 (C⁴), 35.8 (C²), 25.8 ((CH₃)₃), 18.1 (C(CH₃)₃), -5.6 (CH₃)₂. **MS** (EI): *m/z* 238.88 (M⁺ - 18) (100), 256.89 (M⁺) (20); **HRMS**: Found [M+H]⁺ 257.1928, C₁₄H₂₈O₂Si requires *MH*, 257.1937. Spectroscopic data are in accordance with those reported in literature.²¹⁰

1-(*tert*-butyldimethylsilyloxy)-3-vinylpent-4-en-2-ol (6.25):



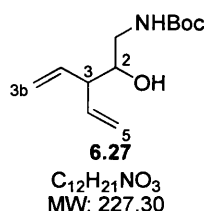
Y = 75%; **R_f** 0.50 (silica gel, *n*-hexane/ Et₂O 4:1); **IR**: 2927, 2360, 1636, 1471, 1107 cm⁻¹; **¹H NMR** (400MHz, CDCl₃): δ 5.92 (1H, dt, *J* = 17.4, 8.8 Hz, H^{3a/4}), 5.80 (1H, dt, *J* = 17.8, 8.8 Hz, H^{3a/4}), 5.12 (4H, m, H^{3b,5}), 3.63 (2H, m, H¹), 3.51 (1H, m, H²), 2.90 (1H, q, *J* = 7.4 Hz, H³), 2.41 (1H, d, *J* = 3.9 Hz, OH), 0.90 (9H, s, (CH₃)₃), 0.07 (6H, s, (CH₃)₂); **¹³C NMR** (100 MHz, CDCl₃): 137.2 (C^{3a/4}), 116.6 (C^{3b/5}), 73.4 (C²), 65.2 (C¹), 53.4 (C³), 25.9 ((CH₃)₃), 18.2 (C(CH₃)₃), -5.4 ((CH₂)₂); **MS** (EI): *m/z* 242.86 (M⁺) (10), 224.92 (M⁺ - 18) (100); **HRMS**: Found [M+Na]⁺ 265.1611, C₁₃H₂₆O₂Si requires *MNa*, 265.1600.

tert-butyl 3-hydroxy-4-vinylhex-5-enylcarbamate (6.26):



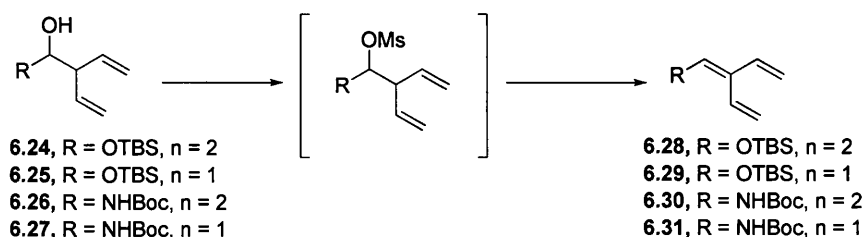
Y = 65%; **R_f** 0.15 (silica gel, EtOAc/ *n*-hexane 1:1); **IR**: 3351, 2977, 2353, 1682, 1508, 1166 cm^{-1} ; **¹H NMR** (400MHz, $CDCl_3$): δ 5.84 (2H, m, $H^{4a,5}$), 5.17 (4H, m, $H^{4b,6}$), 4.92 (1H, br s, NH), 3.63 (1H, td, $J = 6.2, 2.7$ Hz, H^3), 3.46 (1H, m, H^1), 3.17 (1H, dd, $J = 13.7, 5.4$ Hz, H^1), 2.81 (1H, q, $J = 7.4$ Hz, H^4), 2.73 (1H, br s, OH), 1.65 (1H, m, H^2), 1.52 (1H, m, H^2), 1.46 (9H, s, $(CH_3)_3$); **¹³C NMR** (100MHz, $CDCl_3$): δ 157.0 (COO), 137.7 ($C^{5, 4a}$), 136.5 ($C^{5, 4a}$), 117.7 ($C^{6, 4b}$), 116.5 ($C^{6, 4b}$), 79.5 ($-C(CH_3)_3$), 71.2 (C^3), 54.5 (C^4), 37.3 (C^1), 35.2 (C^2), 20.2 ($(CH_3)_3$). **MS** (EI): m/z 79.09 ($M^+ - 162$), 241.57 (M^+) (10), 264.55 (MNa^+) (5); **HRMS**: Found $[M+Na]^+$ 264.1578, $C_{13}H_{23}NO_3$ requires MNa , 264.1576.

1-(N-Boc)-3-vinylpent-4-en-2-ol (6.27):



Y = 72%; **R_f** 0.6 (*n*-hexane/ Et_2O 1:9); **IR**: 3361, 2977, 2360, 1682, 1512, 1392, 1366, 1246 cm^{-1} ; **¹H NMR** (400MHz, $CDCl_3$): δ 5.82 (2H, m, $H^{3a,4}$), 5.22-5.11 (4H, m, $H^{3b,5}$), 4.93 (1H, s, NH), 3.63 (1H, td, $J = 7.4$ Hz, H^2), 3.40 (1H, ddd, $J = 14.0, 6.7, 2.5$ Hz, H^1), 3.03 (1H, ddd, $J = 14.1, 8.1, 5.1$ Hz, H^1), 2.85-2.79 (m, 1H, H^3), 2.47 (1H, s, OH), 1.44 (9H, s, $(CH_3)_3$); **¹³C NMR** (100MHz, $CDCl_3$): δ 157.00 (COO), 136.94 ($C^{3b,5}$), 117.74 ($C^{3a,4}$), 66.19 (C^2), 53.36 (C^3), 44.80 (C^1), 31.92 ($C(CH_3)_3$), 28.72 ($(CH_3)_3$). **MS** (EI): m/z : 228.46 ($M^+ + 1$) (10), 250.42 ($M^+ + 23$); **HRMS**: Found $[M+Na]^+$ 250.1427, $C_{12}H_{21}NO_2$ requires MNa , 250.1419; **Elemental analysis**: Calculated for $C_{12}H_{21}NO_2$ C, 63.41; H, 9.31; N, 6.16; Found C, 63.54; H, 9.21; N, 6.26.

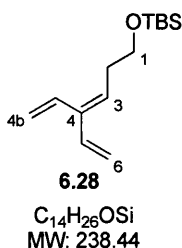
General procedure for the synthesis of cross-conjugated trienes



Triethylamine (2.0 eq.) was added at room temperature to a solution of the secondary alcohol in CH_2Cl_2 (0.25 M). Mesityl chloride (1.5 eq.) was then added dropwise at $-50\text{ }^\circ\text{C}$. The reaction was allowed to reach $0\text{ }^\circ\text{C}$ and stirred for 1 h. The reaction mixture was then poured into half saturated aqueous solution of NaHCO_3 . The separated aqueous layer was extracted with Et_2O (3 x), dried over MgSO_4 , and concentrated under reduced pressure to form the methyl sulfonate salt that was used in the next step without further purification.

The sulphonate salt was dissolved in benzene (0.25 M) and then 1,8-diazabicycloundec-7-ene (DBU) (1.05 eq.) was added. The mixture was heated at $80\text{ }^\circ\text{C}$ for 5-18 h. The solvent was evaporated under reduced pressure and the crude mixture was purified by column chromatography on silica gel using *n*-hexane, concentrated under reduced pressure (50 mmHg, $40\text{ }^\circ\text{C}$) to afford cross-conjugated trienes **6.28** – **6.31** as a clear colourless oils. (98% purity assessed by NMR analysis and TLC).

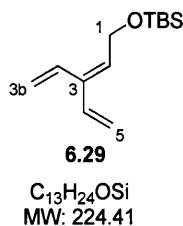
tert-butyldimethyl(4-vinylhexa-3,5-dienyloxy)silane (**6.28**):



Y = 92%; **R_f** 0.8 (silica gel, CH_2Cl_2); **IR**: 2954, 2362, 1471, 1253, 1096 cm^{-1} ; **¹H NMR** (400MHz, CDCl_3): δ 6.49 (1H, dd, $J = 18.2, 10.6\text{ Hz}$, $\text{H}^{4a/5}$), 6.40 (1H, dd, $J = 17.4, 10.7\text{ Hz}$, $\text{H}^{4a/5}$), 5.64 (1H, t, $J = 7.6\text{ Hz}$, H^3), 5.30 (1H, dd, $J = 1.9, 1.3\text{ Hz}$, $\text{H}^{4b/6}$), 5.26 (2H, m, $\text{H}^{4b/6}$), 5.03 (1H, dd, $J = 10.6, 1.5\text{ Hz}$, $\text{H}^{4b/6}$), 3.66 (2H, t, $J = 6.8\text{ Hz}$, H^1), 2.45 (2H, q, $J = 7.1\text{ Hz}$, H^2), 0.89 (9H, s, $(\text{CH}_3)_3$), 0.05 (6H, s, $(\text{CH}_3)_2$); **¹³C NMR** (100MHz, CDCl_3): δ 138.5 (C^4), 137.8 (C^3), 132.1 ($\text{C}^{5/4a}$), 128.5 ($\text{C}^{5/4a}$), 117.4 ($\text{C}^{4b/6}$), 114.0 ($\text{C}^{4b/6}$), 62.7 (C^1), 32.1 (C^2), 25.9 ($(\text{CH}_3)_3$), 18.4 ($\text{C}(\text{CH}_3)_3$), -5.3 ($(\text{CH}_3)_2$); **MS** (EI): m/z 239.17 (MH^+) (15), 123.29 ($\text{M} - 116$) (15); **HRMS**: Found

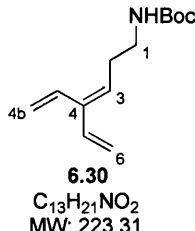
$[M+H]^+$ 239.1822, $C_{14}H_{26}OSi$ requires MH , 239.1831.

***tert*-butyldimethyl(3-vinylpenta-2,4-dienyloxy)silane (6.29):**



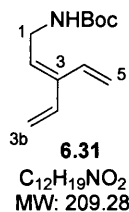
$Y = 80\%$; R_f 0.8 (silica gel, CH_2Cl_2); **IR**: 2928, 2363, 1471, 1253, 1096 cm^{-1} ; **1H NMR** (400MHz, $CDCl_3$): δ 6.43 (2H, dd, $J = 17.8, 10.9$ Hz, $H^{3a,4}$), 5.76 (1H, t, $J = 6.8$ Hz, H^2), 5.35 (2H, m, $H^{3b,5}$), 5.26 (1H, dd, $J = 17.6, 1.8$ Hz, $H^{3b/5}$), 5.13 (1H, dd, $J = 10.7, 1.0$ Hz, $H^{3b/5}$), 4.39 (2H, d, J 6.8 Hz, H^1), 0.90 (9H, s, $(CH_3)_3$), 0.07 (6H, s, $(CH_3)_2$). **^{13}C NMR** (100MHz, $CDCl_3$): δ 142.8 (C^3), 138.2 (C^2), 134.6 ($C^{4/3a}$), 126.5 ($C^{4/3a}$), 118.4 ($C^{3b/5}$), 115.7 ($C^{3b/5}$), 69.4 (C^1), 25.9 ($(CH_3)_3$), 18.3 ($C(CH_3)_3$), -5.3 ($(CH_3)_2$); **MS** (EI): m/z 224.92 (M^+) (100); **HRMS**: Found ($M^+ - 3$) 221.1178, $C_{13}H_{24}OSi$ requires MH , 224.1596.

1-(*N*-Boc)-4-vinylhexa-3,5-diene (6.30):



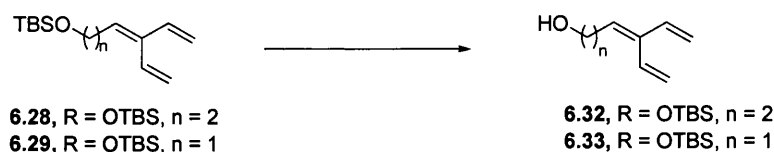
$Y = 65\%$; R_f 0.26 (silica gel, CH_2Cl_2); **IR**: 3350, 2976, 2357, 1682, 1506, 1163 cm^{-1} ; **1H NMR** (400MHz, $CDCl_3$): δ 6.46 (1H, dd, $J = 17.3, 11.0$ Hz, $H^{4a/5}$), 6.39 (1H, dd, $J = 16.9, 10.3$ Hz, $H^{4a/5}$), 5.56 (1H, t, $J = 7.7$ Hz, H^3), 5.31 (1H, d, $J = 11.1$ Hz, $H^{4b/6 \text{ cis}}$), 5.28 (2H, d, $J = 17.5$ Hz, $H^{4b,6 \text{ trans}}$), 5.06 (1H, d, $J = 10.7$ Hz, $H^{4b/6 \text{ cis}}$), 4.53 (1H, br s, NH), 3.20 (2H, q, $J = 6.1$ Hz, H^1), 2.41 (2H, q, $J = 7.1$ Hz, H^2), 1.44 (9H, s, $(CH_3)_3$); **^{13}C NMR** (100MHz, $CDCl_3$): δ 155.8 (COO), 139.3 (C^4), 137.6 ($C^{5/4a}$), 131.7 ($C^{5/4a}$), 128.3 (C^3), 117.9 ($C^{6/4b}$), 114.5 ($C^{6/4b}$), 79.5 ($-C(CH_3)_3$), 40.0 (C^1), 28.7 (C^2), 28.4 ($(CH_3)_3$); **MS** (EI): m/z 168.22 ($M^+ - 55$) (75), 224.30 (MH^+) (15); **HRMS**: Found $[M+Na]^+$ 246.1480, $C_{13}H_{21}NO_2$ requires MNa , 246.1470; **Elemental analysis**: Calculated for $C_{13}H_{21}NO_2$ C, 69.92; H, 9.48; N, 6.27; Found C, 69.91; H, 9.54; N, 5.99.

1-(*N*-Boc)-3-vinylpenta-2,4-diene (6.31):



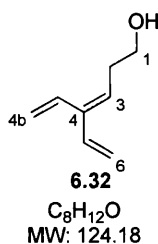
Y = 65%; **R_f** 0.3 (silica gel, CH₂Cl₂); **IR**: 2976, 1689, 1505, 1391, 1365, 1247, 1180 cm⁻¹; **¹H NMR** (400MHz, CDCl₃): δ 6.40 (2H, m, *J* = 17.6, 11.1 Hz, H^{3b/5}), 5.58 (1H, t, *J* = 7.0 Hz, H²), 5.38-5.09 (4H, m, H^{3b/5}), 4.55 (1H, s, NH), 3.92 (2H, t, H¹), 1.44 (9H, s, (CH₃)₃); **¹³C NMR** (100 MHz, CDCl₃): δ 156.11 (COO), 137.71 (C³), 131.59 (C^{3a/4}), 128.06 (C²), 119.53 (C^{3b/5}), 115.80 (C^{3b/5}), 38.98 (C¹), 31.25 (C(CH₃)₃), 28.77 ((CH₃)₃). **MS** (EI): *m/z* 232.50 (M⁺ + 23) (10); **HRMS**: Found [M+Na]⁺ 232.1320, C₁₂H₁₉NO₂ requires *MNa* 232.1313; **Elemental analysis**: Calculated for C₁₂H₁₉NO₂ C, 68.87; H, 9.15; N, 6.69; Found C, 68.8; H, 9.37; N, 6.91.

General procedure for the removal of the TBDMS protecting group



Tetra-*n*-butylammonium fluoride (TBAF) (1 M in THF, 2 eq.) was added at 0 °C to a solution of TBSO protected triene in THF (0.2 M). The mixture was left to stir at room temperature for 18 h. THF was evaporated under reduced pressure and the crude re-dissolved in CH₂Cl₂ (0.2 M), washed with saturated aq. NaHCO₃ solution (3 x), water (3 x) and brine, dried over MgSO₄ and concentrated under reduced pressure. The crude mixture was purified by column chromatography on silica gel using *n*-hexane and CH₂Cl₂ (4:1). Alcohols **6.32** and **6.33** were obtained as colourless oils (98% purity assessed by NMR analysis and TLC).

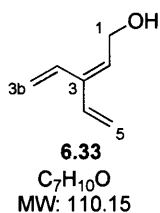
4-vinylhexa-3,5-dien-1-ol (6.32):



Y = 96%; **R_f** 0.18 (silica gel, CH₂Cl₂); **IR**: 3318, 2879, 2367, 1629, 1417 cm⁻¹; **¹H**

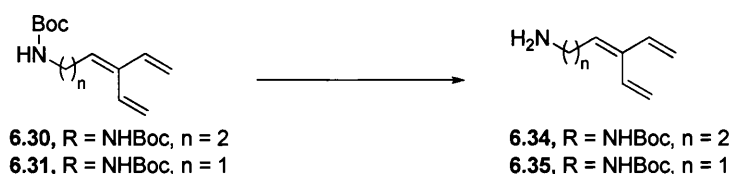
NMR (400MHz, CDCl₃): δ 6.50 (1H, dd, J = 17.2, 11.7 Hz, H^{4a/5}), 6.41 (1H, dd, J = 17.4, 10.7 Hz, H^{4a/5}), 5.64 (1H, t, J = 7.6 Hz, H³), 5.30 (3H, m, H^{4b/6}), 5.07 (1H, dd, J = 10.7, 1.3 Hz, H^{4b/6}), 3.71 (2H, dd, J = 11.7, 6.2 Hz, H¹), 2.51 (2H, dd, J = 13.9, 6.7 Hz, H²), 1.40 (1H, br s, OH); **¹³C NMR** (100MHz, CDCl₃): 139.6 (C⁴), 137.6 (C^{5/4a}), 131.8 (C^{5/4a}), 127.6 (C³), 118.0 (C^{4b/6}), 114.5 (C^{4b/6}), 62.4 (C¹), 31.8 (C²); **MS** (EI): m/z 124.34 (M⁺) (5), 104.90 (M⁺ - 19) (20); **HRMS**: Found [M+H]⁺ N/A, C₈H₁₂O requires MH , 125.0966.

4-vinylpenta-2,4-dien-1-ol (6.33):



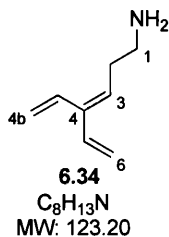
Y = 96%; **R_f** 0.20 (silica gel, CH₂Cl₂); **IR**: 3318, 2361, 1601, 1417, 986 cm⁻¹; **¹H NMR** (400MHz, CDCl₃): δ 6.42 (2H, dd, J = 17.8, 10.9 Hz, H^{3a,4}), 5.77 (1H, t, J = 6.8 Hz, H²), 5.35 (2H, m, H^{3b,5}), 5.26 (1H, dd, J = 17.6, 1.8 Hz, H^{3b/5}), 5.13 (1H, dd, J = 10.7, 1.0 Hz, H^{3b/5}), 4.35 (2H, d, J 6.8 Hz, H¹), 1.47 (1H, br s, OH); **¹³C NMR** (100MHz, CDCl₃): 139.2 (C³), 137.5 (C^{3/3a}), 131.3 (C^{4/3a}), 129.9 (C²), 119.2 (C^{3b/5}), 115.7 (C^{3b/5}), 59.5 (C¹); **MS** (EI): m/z 110.86 (M⁺) (85), 96.4 (M⁺ - 17) (55); **HRMS**: Found [M+H]⁺ 111.0813, C₇H₁₀O requires MH , 111.0810.

General procedure for the removal of the Boc protecting group



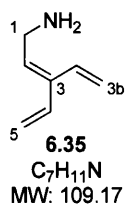
Trifluoroacetic acid (TFA) (4.0 eq.) was added at 0 °C to a solution of *N*-Boc protected triene in CH₂Cl₂ (0.2 M). The mixture was left to stir at 50 °C for 18 h. The solution was then left to cool at room temperature and activated amberlyst A-21 (8.0 eq.) was added. The heterogeneous mixture was stirred at room temperature for 1 h. Amberlyst was filtered off and the filtrate was concentrated at 40 mmHg, 40 °C. The crude mixture was purified by flash column chromatography on silica gel using EtOAc and triethylamine (9.5:0.5). Amines **6.34** and **6.35** were obtained as clear yellow oils (98% purity assessed by NMR and LC-MS analysis).

4-vinylhexa-3,5-dien-1-amine (6.34):



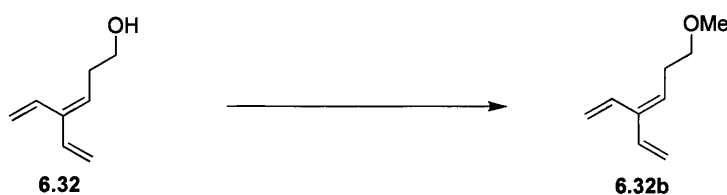
Y = 55%; **R_f** 0.26 (silica gel, EtOAc/diethyl amine 9.5:0.5); **IR**: 2935, 2365, 1684, 1166 cm^{-1} ; **¹H NMR** (400MHz, $CDCl_3$): δ 6.43 (1H, dt, J = 17.2, 11.4 Hz, $H^{4a/5}$), 6.34 (1H, ddd, J = 17.4, 10.6, 6.8 Hz, $H^{4a/5}$), 5.55 (1H, q, J = 6.5 Hz, H^{3s}), 5.22 (3H, m, $H^{4b/6}$), 4.98 (1H, dd, J = 10.7, 6.1 Hz, $H^{4b/6\ cis}$), 2.73 (2H, t, J = 6.8 Hz, H^1), 2.31 (2H, q, J = 7.1 Hz, H^2), 1.38 (1H, br s, NH); **¹³C NMR** (100MHz, $CDCl_3$): δ 138.8 (C^4), 137.4 ($C^{5/4a}$), 131.7 ($C^{5/4a}$), 129.2 (C^3), 117.5 ($C^{4b/6}$), 113.9 ($C^{4b/6}$), 41.7 (C^1), 29.4 (C^2); **MS** (EI): m/z 124.17 (MH^+) (25), 107.14 ($M^+ - 17$) (35); **HRMS**: Found $[M+H]^+$ 124.1120, $C_8H_{13}N$ requires MH , 124.1126.

3-vinylpenta-2,4-dien-1-amine (6.35):



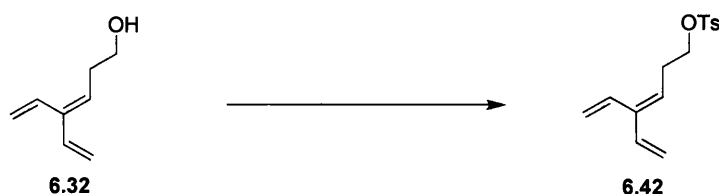
Y = 45%; **R_f** 0.20 (silica gel, EtOAc/diethyl amine 9.5:0.5); **IR**: 3260, 2922, 2357, 1661, 988 cm^{-1} ; **¹H NMR** (400 MHz; $CDCl_3$): δ 6.45 (1H, dd, J = 15.7, 9.2 Hz, $H^{3a/4}$), 6.38 (1H, dd, J = 15.7, 8.8 Hz, $H^{3a/4}$), 5.67 (1H, t, J = 7.0 Hz, H^2), 5.32 (1H, ddd, J = 11.1, 1.8, 1.0 Hz, $H^{3b/5}$), 5.30 (1H, dd, J = 17.4, 1.6Hz, $H^{3b/5}$), 5.25 (1H, dd, J = 17.6, 1.8 Hz, $H^{3b/5}$), 5.08 (1H, ddd, J = 10.7, 1.5, 0.4 Hz, $H^{3b/5}$), 3.48 (2H, d, J = 7.0 Hz, H^1), 1.36 (2H, s, NH_2); **¹³C NMR** (100MHz, $CDCl_3$): δ 137.7 ($C^{3a/4}$), 137.3 (C^3), 133.0(C^2), 131.6 ($C^{3a/4}$), 118.3 ($C^{3b/5}$), 114.8 ($C^{3b/5}$), 39.8 (C^1); **MS** (EI): m/z 106.08 ($M^+ - 3$) (100); **HRMS**: Found $[M+H]^+$ 110.0966, $C_7H_{11}N$ requires MH , 110.0970.

Synthesis of the cross-conjugated triene 6.32b



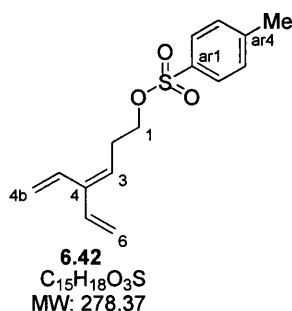
Silver (II) oxide (260.0 mg, 1.12 mmol, 2.0 eq.) and methyl iodide (4 eq, 1.12 ml, 2M in THF, 2.25 mmol, 4.0 eq.) were added to a vigorously stirred solution of the compound **6.32** (70.0 mg, 0.56 mmol, 1.0 eq.) in CH₂Cl₂ (0.2 M, 3 ml) into a sealed tube. The reaction mixture was left to stir at room temperature for 48 h. This was then filtered on a thin pad of celite and washed with CH₂Cl₂ (3 x 10 ml). The crude mixture was then concentrated under reduce pressure and purified by column chromatography on silica gel using *n*-hexane and CH₂Cl₂ (1:1). Compound **6.32b** was obtained in 70% yield as colourless oil (98% purity assessed by NMR analysis and TLC). *R_f* 0.28 (silica gel, *n*-hexane/CH₂Cl₂ 50:50); IR: 3297, 2926, 2358, 1641, 1015 cm⁻¹; ¹H NMR (400MHz, CDCl₃): δ 6.47 (1H, dd, *J* = 17.5, 11.4 Hz, H^{4a/5}), 6.39 (1H, dd, *J* = 17.4, 10.7 Hz, H^{4a/5}), 5.63 (1H, t, *J* = 7.5 Hz, H³), 5.29 (2H, m, H^{4b/6}), 5.25 (1H, m, H^{4b/6}), 5.03 (1H, dd, *J* = 10.7, 1.6 Hz, H^{4b/6}), 3.42 (2H, q, *J* = 6.8 Hz, H¹), 3.34 (3H, s, -OCH₃), 2.49 (2H, q, *J* 7.0 Hz, H²); ¹³C NMR (100 MHz, CDCl₃): δ 138.6 (C⁴), 137.8 (C^{5/4a}), 131.8 (C^{5/4a}), 128.2 (C³), 117.7 (C^{4b/6}), 114.2 (C^{4b/6}), 72.2 (CH₃), 58.6 (C¹), 30.9 (C²); MS (EI): *m/z* 139.18 (MH⁺) (50), 133.10 (M⁺ - 5) (25); HRMS: Found [M - H]⁺ 137.0656, C₉H₁₄O requires *M* - *H*, 137.0966.

Synthesis of the cross-conjugated triene **6.42**



Pyridine (328 mg, 4.84 mmol, 4.0 eq.), tosyl chloride (1.38 g, 7.24 mmol, 6.0 eq.) and 4-dimethylaminopyridine DMAP (74.0 mg, 0.60 mmol, 0.5 eq.) were successively added to a solution of compound **6.32** (150 mg, 1.21 mmol, 1.0 eq.) in chloroform (0.1 M) at 0 °C. The mixture was left to stir at room temperature for 12h. The reaction was quenched with water and the separated aqueous phase was extracted with Et₂O (3x). The combined organic phases were dried over MgSO₄, filtered, concentrated under reduced pressure and the residue was purified by flash column chromatography on silica gel with *n*-hexane and CH₂Cl₂ (1:1) as solvent system. Compound **6.42** was isolated as clear colourless oil in 85% yield (98% purity assessed by NMR and LCMS analysis).

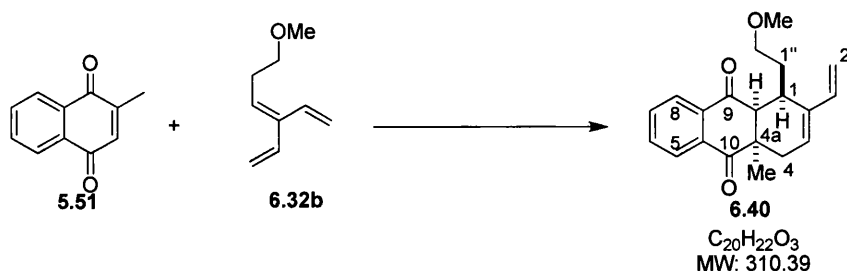
1-Tosyloxy-4-vinylhexa-3,5-diene (6.42)



R_f 0.30 (silica gel, *n*-hexane/dichloromethane 50:50); IR: 2923, 1597, 1188 cm^{-1} ; 1H NMR (400MHz, $CDCl_3$): δ 7.78 (2H, d, $J = 8.3Hz$, H^{ar}), 7.33 (2H, d, $J = 7.9Hz$, H^{ar}), 6.34 (1H, dd, $J = 17.6, 11.2Hz$, $H^{4a/5}$), 6.31 (1H, dd, $J = 17.3, 10.7Hz$, $H^{4a/5}$), 5.42 (1H, t, $J = 7.5Hz$, H^3), 5.29 (2H, dt, $J = 11.2, 1.4Hz$, $H^{4b/6}$), 5.23 (1H, dt, $J = 17.7, 2.1Hz$, $H^{4b/6}$), 5.06 (1H, dd, $J = 10.7, 1.5Hz$, $H^{4b/6}$), 4.06 (2H, t, $J = 6.8Hz$, H^1), 2.57 (2H, q, $J = 7.0Hz$, H^2), 2.45 (3H, s, CH_3); ^{13}C NMR (100 MHz, $CDCl_3$): δ 144.7 ($C^{ar1/4}$), 140.2 ($C^{ar1/4}$), 137.4 ($C^{4a/5}$), 133.2 (C^4), 131.4 ($C^{5/4a}$), 129.8 ($C^{ar2,ar3}$), 127.9 ($C^{ar5,ar6}$), 124.8 (C^3), 118.6 ($C^{4b/6}$), 115.1 ($C^{4b/6}$), 69.5 (C^1), 28.1 (C^2), 21.6 (CH^3); MS (EI): m/z : 278.96 (M^+) (30), 189.88 ($M^+ - 89$) (55); HRMS: Found MNa^+ 301.0874, $C_{15}H_{18}O_3S$ requires MNa , 301.0872.

9.2.2 Synthesis of the tricyclic scaffolds.

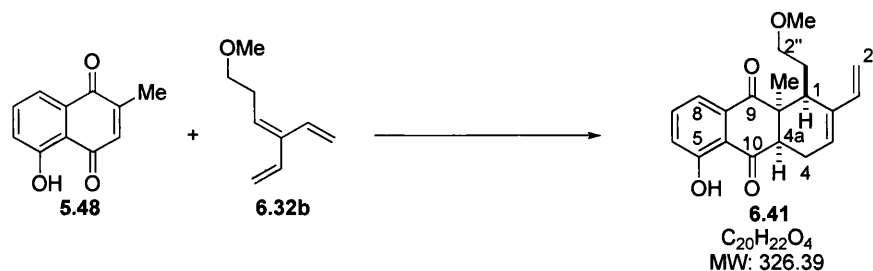
(1*RS*,4*aRS*,9*aSR*)-1-(2'-methoxyethyl)-4*a*-methyl-2-vinyl-1,4,4*a*,9*a*-tetrahydroanthracene-9,10-dione (6.40)



2-methyl naphthoquinone **5.51** (30 mg, 0.17 mmol) and methoxy triene **6.32b** (36 mg, 0.26 mmol, 1.5 eq.) in CH_2Cl_2 (1.5 ml) were added to a sealed glass tube. The mixture was cooled at $-45^\circ C$, and then borontrifluoride diethyletherate (49.5 mg, 0.043 ml, 0.35 mmol, 2 eq.) was added very slowly. The reaction mixture was left to stir at this temperature for 7h, and then quenched with ice water (5 ml). After phase separation, the aqueous phase was extracted with CH_2Cl_2 (3 x 5 ml). The

combined organic phases were washed with water and brine, dried over MgSO_4 and concentrated under reduced pressure. The crude mixture was purified by flash column chromatography on silica gel using *n*-hexane and Et_2O (80:20) to afford the compound **6.40** (46.0 mg, 85%) as yellow oil (98% purity assessed by NMR and LC-MS analysis). R_f 0.42 (silica gel, *n*-hexane/ Et_2O 1:1); IR: 2915, 2359, 1685, 1247, 628 cm^{-1} ; ^1H NMR (500MHz, CDCl_3): δ 8.09 (2H, m, $\text{H}^{6,7}$), 7.75 (2H, m, $\text{H}^{5,8}$), 6.31 (1H, dd, $J = 17.5, 10.9$ Hz, $\text{H}^{1'}$), 5.75 (1H, dd, $J 5.0, 3.6$ Hz, H^3), 5.22 (1H, d, $J 17.6$ Hz, $\text{H}^{2'}$), 4.97 (1H, d, $J 10.9$ Hz, $\text{H}^{2'}$), 3.56 (1H, dd, $J = 19.9, 2.5$ Hz, H^1), 3.10 (1H, m, H^{9a}), 3.04 (1H, d, $J = 4.5$ Hz, H^4), 3.03 (3H, s, OCH_3), 2.98 (2H, t, $J = 6.5$ Hz, $\text{H}^{2''}$), 2.05 (1H, dd, $J = 19.9, 5.4$ Hz, H^4), 1.32 (2H, m, $\text{H}^{1''}$), 1.31 (3H, s, CH_3); ^{13}C NMR (125 MHz, CDCl_3): δ 200.8 (C^9), 198.9 (C^{10}), 139.9 ($\text{C}^{4b/8a}$), 138.1 ($\text{C}^{1'}$), 134.8 ($\text{C}^{4b/8a}$), 134.6 ($\text{C}^{5/6/7/8}$), 134.1 ($\text{C}^{5/6/7/8}$), 133.9 (C^2), 127.5 ($\text{C}^{5/6/7/8}$), 126.7 ($\text{C}^{5/6/7/8}$), 126.4 (C^3), 111.5 ($\text{C}^{2'}$), 70.6 ($\text{C}^{2''}$), 58.9 (C^{9a}), 58.1 (OCH_3), 46.2 (C^{4a}), 34.6 (C^1), 31.6 (C^4), 31.5 ($\text{C}^{1''}$), 30.9 (CH_3); MS (EI): m/z 311.20 (MH^+) (70), 279.35 ($\text{M}^+ - 32$) (100); HRMS: Found $[\text{M}+\text{H}]^+$ 311.1649, $\text{C}_{20}\text{H}_{22}\text{O}_3$ requires MH , 311.1647; Elemental analysis: Calculated for $\text{C}_{20}\text{H}_{22}\text{O}_3$ C, 77.39; H, 7.14; Found C, 77.43; H, 7.22.

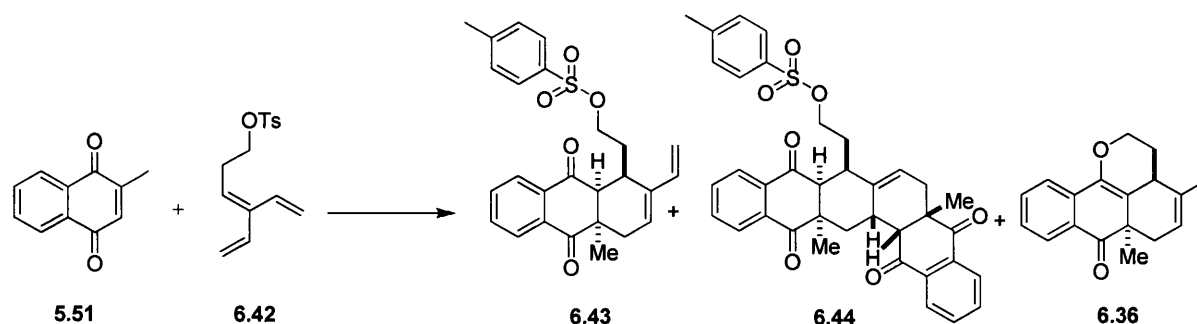
(1*SR*,4*aRS*,9*aSR*)-5-hydroxy-1-(2''-methoxyethyl)-9*a*-methyl-2-vinyl-1,4,4*a*,9*a*-tetrahydroanthracene-9,10-dione (6.41**)**



2-methyl-5-hydroxynaphthoquinone **5.48** (20 mg, 0.11 mmol) and methoxy triene **6.32b** (22 mg, 0.16 mmol, 1.5 eq.) in CH_2Cl_2 (1 ml) were added to a sealed glass tube. The mixture was cooled at -45°C , and then borontrifluoride diethyletherate (49.5 mg, 0.026 ml, 0.21 mmol, 2 eq.) was added slowly. The reaction mixture was left to stir at this temperature for 7 h, and then quenched with ice water (5 ml), and the organic and aqueous phases separated. The latter was extracted with CH_2Cl_2 (3 x 5 ml). The combined organic phases were washed with water and brine, dried over MgSO_4 and concentrated under reduced pressure. The crude mixture was purified by flash column chromatography on silica gel using *n*-hexane and Et_2O (80:20) to afford the compound **6.41** (19.2 mg, 55%) as yellow oil (98% purity assessed by

NMR and LC-MS analysis). R_f 0.55 (Silica gel, Et₂O/*n*-hexane 2:1); **IR**: 2926, 1690, 1641, 1577, 1452, 1370, 1333, 1266 cm⁻¹; **¹H NMR** (500MHz; CDCl₃): δ 11.89 (1H, s, OH), 7.68 (1H, dd, J = 7.6, 1.4 Hz, H⁸), 7.64 (1H, t, J = 7.8 Hz, H⁷), 7.24 (1H, dd, J = 8.1, 1.4 Hz, H⁶), 6.37 (1H, dd, J = 17.5, 10.9 Hz, H^{1'}), 5.75 (1H, t, J = 3.8 Hz, H³), 5.30 (1H, d, J = 17.6 Hz, H^{2'}), 5.02 (1H, d, J = 10.9, H²), 3.65 (1H, dd, J = 9.8, 7.1 Hz, H^{4a}), 3.44 (1H, ddd, J = 9.4, 8.0, 6.0 Hz, H^{2''}), 3.37 (1H, ddd, J = 9.4, 6.6, 5.6 Hz, H^{2''}), 3.15 (1H, dd, J = 4.7, 2.5 Hz, H¹), 3.13 (3H, s, -OCH₃), 2.71 (1H, ddd, J = 20.4, 7.1, 4.2 Hz, H^{b4}), 2.65 (1H, ddd, J = 20.5, 9.9, 3.8 Hz, H^{a4}), 1.90 (1H, dddd, J = 14.1, 7.8, 6.5, 5.0 Hz, H^{1''}), 1.64 (1H, ddt, J = 13.7, 7.5, 6.0 Hz, H^{1''}), 1.11 (3H, s, CH₃); **¹³C NMR** (125MHz, CDCl₃): δ 205.3 (C¹⁰), 198.7 (C⁹), 160.7 (C⁵), 139.3 (C²), 139.2 (C¹), 136.6 (C⁷), 133.5 (C^{8a}), 125.4 (C³), 123.5 (C⁶), 119.0 (C⁸), 117.1 (C^{4b}), 111.5 (C^{2'}), 71.0 (C^{2''}), 58.9 (-OCH₃), 50.8 (C^{9a}), 44.8 (C^{4a}), 37.2 (C¹), 34.5 (C^{1''}), 23.1 (C^{4'}), 21.4 (CH₃); **MS** (EI): m/z 327.69 (MH⁺) (25), 295.63 (M⁺ - 32) (100); **HRMS**: Found MH⁺ 327.1610, C₂₀H₂₂O₄ requires M⁺, 327.1596.

Synthesis of the tricyclic compound 6.43



Procedure 1:

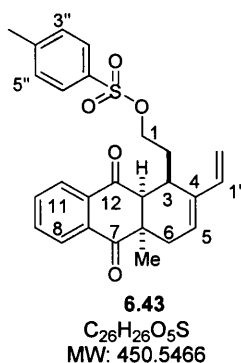
2-methylnaphthoquinone **5.51** (50 mg, 0.29 mmol) and a solution of triene **6.42** (121 mg, 0.44 mmol) in CH₂Cl₂ (3 mL, 0.2 M) were added to a sealed tube. The solution mixture was cooled to 0 °C and boron trifluoride diethyletherate (136 mg, 0.071 mL, 0.58 mmol) was added very slowly. The reaction mixture was left to stir at this temperature for 18h and quenched with ice water (15 mL). After phase separation, the aqueous phase was extracted with CH₂Cl₂ (3x 10 mL). The combined organic phases were washed with water and brine, dried over MgSO₄, filtered and concentrated under reduced pressure. The crude mixture was purified by flash column chromatography on silica gel with *n*-hexane and Et₂O (1:1) as solvent system to afford compounds **6.43** (5.5

mg, 4%), **6.44** (62 mg, 69%) and **6.36** (17 mg, 21%) as yellow oils (98% purity assessed by NMR and LCMS analysis).

Procedure 2:

2-methylnaphthoquinone **5.51** (50 mg, 0.29 mmol) and a solution of triene **6.42** (121 mg, 0.44 mmol) in CH₂Cl₂ (3 mL, 0.2 M) were added to a sealed tube. The solution mixture was cooled to 0 °C and boron trifluoride diethyletherate (68 mg, 0.035 mL, 0.29 mmol) was added very slowly. The reaction mixture was left to stir at this temperature for 18h and quenched with ice water (15 mL). After phase separation, the aqueous phase extracted with CH₂Cl₂ (3 x 10 mL). The combined organic phases were washed with water and brine, dried over MgSO₄, filtered and concentrated under reduced pressure. The crude mixture was purified by flash column chromatography on silica gel with *n*-hexane and Et₂O (1:1) as solvent system to afford compounds **6.43** (25 mg, 18%), **6.44** (52 mg, 69%) and **6.36** (23 mg, 21%) as yellow oils.

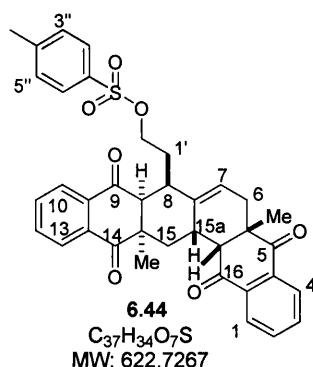
(2-((3*RS*,6*aRS*,12*aSR*)-6*a*-methyl-7,12-dioxo-4-vinyl-3,6,6*a*,7,12,12*a*-hexahydroanthracen-3-yl)ethyl 4''-methylbenzenesulfonate (6.43**)**



R_f 0.26 (*n*-hexane/Et₂O 1:1); **IR**: 3338, 2924, 1685, 1593, 1100 cm⁻¹; **¹H-NMR** (400 MHz; CDCl₃): δ 8.06 (1H, m, H^{9/10}), 8.02 (1H, m, H^{9/10}), 7.77 (2H, m, H^{8,11}), 7.62 (2H, d, *J* = 8.2Hz, H^{3'', 5''}), 7.27 (2H, dd, *J* = 6.7, 0.7Hz, H^{2'', 4''}), 6.24 (1H, dd, *J* = 17.6, 11.0Hz, H^{1'}), 5.74 (1H, dd, *J* = 5.2, 3.3Hz, H⁵), 5.07 (1H, d, *J* = 17.5Hz, H^{2'trans}), 4.91 (1H, d, *J* = 11.0Hz, H^{2'cis}), 3.72 (2H, t, *J* = 6.7Hz, H¹), 3.38 (1H, dd, *J* = 20.3, 3.0Hz, Hb⁶), 2.97 (2H, m, *J* = 2.2Hz, H^{3, 12a}), 2.42 (3H, s, CH₃), 2.01 (1H, dd, *J* = 19.9, 5.1Hz, Ha⁶), 1.49 (2H, q, *J* = 6.9Hz, H²), 1.30 (3H, s, CH₃); **¹³C NMR** (100MHz, CDCl₃): δ 200.3 (C^{7/12}), 198.3 (C^{7/12}), 144.7 (C^{1''}), 139.0 (C^{7a/11a}), 138.4 (C^{1'}), 134.8 (C^{8/10}), 134.5 (C^{7a/11a}), 134.3 (C^{8/10}), 133.6 (C^{4''}), 132.9 (C⁴), 129.7 (C^{3'', 5''}), 127.8 (C^{1'', 6''}), 127.6

(C^{9/11}), 126.7 (C^{9/11}), 126.4 (C⁵), 112.2 (C^{2'}), 68.5 (C¹), 57.7 (C^{12a}), 46.4 (C^{6a}), 33.8 (C³), 31.7 (C⁶), 30.1 (C²), 29.6 (CH₃), 20.9 (H₃C-Phe); **MS (EI)**: *m/z*: 451.01 (MH⁺) (60), 432.89 (M⁺ - 19) (5); **HRMS**: Found MH⁺ 451.1514, C₂₆H₂₆O₅S requires *MH*, 451.1579.

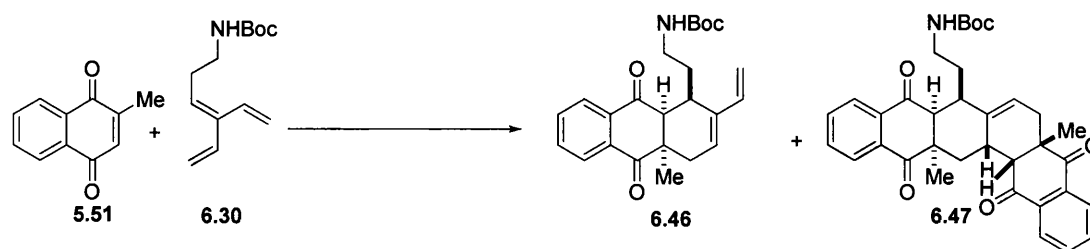
(5a*RS*,8*RS*,8a*SR*,14a*RS*,15a*SR*,15b*SR*)-8-(2'-tolylloxy)-5a,14a-dimethyl-5a,6,8,8a,15,15a-hexahydrohexaphene-5,9,14,16(14aH,15bH)-tetraone (6.44)



R_f 0.1 (*n*-hexane/Et₂O 1:1); **IR**: 2935, 2357, 1692, 1175 cm⁻¹; **¹H-NMR** (400MHz; CDCl₃): δ 8.18 (1H, m, H^{1/10}), 8.01 (1H, m, H^{1/10}), 7.98 (1H, t, *J* = 4.5Hz, H^{3/12}), 7.94 (1H, t, *J* = 4.5Hz, H^{3/12}), 7.75 (2H, t, *J* = 4.1Hz, H^{11,13}), 7.70 (2H, m, H^{2,4}), 7.67 (2H, d, *J* = 8.2Hz, H^{2'',6''}), 7.34 (2H, d, *J* = 8.0Hz, H^{3'',5''}), 5.51 (1H, d, *J* = 4.4Hz, H⁷), 3.72 (1H, dt, *J* = 9.9, 5.1Hz, H^{2'}), 3.64 (1H, td, *J* = 9.2, 5.2Hz, H^{2'}), 3.13 (1H, d, *J* = 7.1Hz, H^{15b}), 3.06 (1H, dd, *J* = 18.1, 5.3Hz, Hb⁶), 2.91 (1H, d, *J* = 6.0Hz, H^{8a}), 2.78 (1H, ddd, *J* = 12.7, 5.9, 3.9Hz, H⁸), 2.65 (1H, m, H^{15a}), 2.47 (3H, s, CH₃), 1.84 (1H, dd, *J* = 12.6, 3.2Hz, Hb¹⁵), 1.71 (1H, d, *J* = 18.2Hz, Ha⁶), 1.27 (3H, s, CH₃), 1.13 (1H, m, H^{1'}), 0.99 (1H, m, H^{1'}), 0.82 (3H, s, CH₃), 0.50 (1H, t, *J* = 13.0Hz, Ha¹⁵); **¹³C NMR** (100MHz; CDCl₃): δ 200.0 (C=O), 199.4 (C=O), 198.5 (C=O), 197.3 (C=O), 144.9 (C^{1''}), 135.4 (C^{7a}), 135.1 (C^{4''}), 134.7 (C^{4a,13a}), 134.7 (C²), 134.5 (C⁴), 134.3 (C¹¹), 134.2 (C¹³), 134.1 (C^{9a}), 132.8 (C^{16a}), 129.9 (C^{3'',5''}), 127.8 (C^{2'',6''}), 127.1 (C^{3/12}), 127.0 (C^{3/12}), 126.35 (C^{1/10}), 126.30 (C^{1/10}), 122.1 (C⁷), 67.7 (C^{2'}), 61.1 (C^{8a}), 57.0 (C^{15b}), 48.2 (C^{5a/14a}), 46.2 (C^{5a/14a}), 44.5 (C⁸), 38.5 (C¹⁵), 32.0 (C^{15a}), 31.0 (C⁶), 29.4 (CH₃), 28.9 (CH₃), 27.9 (C²), 21.7 (CH₃-Ar); **MS (EI)**: *m/z*: 623.09 (MH⁺) (75), 451.01 (M⁺ - 172) (55); **HRMS**: Found MH⁺ 623.2114, C₃₇H₃₄O₇S requires *MH*, 623.2103.

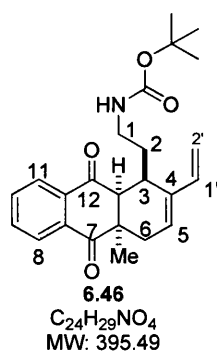
Full characterization for compound **6.36** is shown separately in the following experimental procedure.

***tert*-butyl-2-((3*RS*,6*aRS*,12*aSR*)-6*a*-methyl-7,12-dioxo-4-vinyl-3,6,6*a*,7,12,12*a*-hexahydroanthracen-3-yl)ethylcarbamate (**6.46**)**



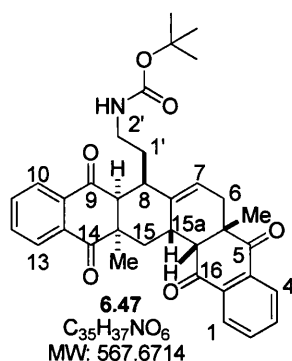
Procedure 1: 2-methylnaphthoquinone **5.51** (39 mg, 0.23 mmol) and a solution of triene **6.30** (75 mg, 0.34 mmol) in CH₂Cl₂ (1 ml, 0.2 M) were added to a sealed glass tube. The solution mixture was then cooled to 0 °C and scandium triflate (165 mg, 0.34 mmol) was added all at once. The reaction mixture was left to stir at this temperature for 2.5h, then quenched with ice water (5 ml), and the organic and aqueous phases separated. The latter was extracted with CH₂Cl₂ (3 x 5 ml). The combined organic phases were washed with water and brine, dried over MgSO₄ and concentrated under reduced pressure. The crude mixture was purified by flash column chromatography on silica gel using *n*-hexane and Et₂O (8:2) to afford **6.46** (63 mg, 70 %) and **6.47** (2 mg, 3%) as yellow oils (98% purity assessed by NMR and LC-MS analysis).

Procedure 2: 2-methylnaphthoquinone **5.51** (100 mg, 0.58 mmol) and a solution of triene **6.30** (323 mg, 1.45 mmol) in CH₂Cl₂ (3 ml, 0.2 M) were added to a sealed glass tube. The solution mixture was then cooled to 0 °C and boron trifluoride diethyletherate (681 mg, 0.36 ml, 2.9 mmol) was added very slowly. The reaction mixture was left to stir at this temperature for 36 h, then quenched with ice water (15 ml), and the organic and aqueous phases separated. The latter was extracted with CH₂Cl₂ (3 x 10 ml). The combined organic phases were washed with water and brine, dried over MgSO₄ and concentrated under reduced pressure. The crude mixture was purified by flash column chromatography on silica gel using *n*-hexane and Et₂O (8:2) to afford **6.46** (57 mg , 25%) and **6.47** (31 mg, 19%) and SM **5.51** (25%) as yellow oils (98% purity assessed by NMR and LC-MS analysis).



6.46: R_f 0.24 (Silica gel, Et₂O/*n*-hexane 1:1); **IR:** 3379, 2971, 1684, 1509, 1247 cm⁻¹; **¹H NMR** (400MHz; CDCl₃): δ 8.10 (2H, dtd, J = 6.1, 3.4, 2.5 Hz, H^{9,11}), 7.74-7.81 (2H, m, H^{8,10}), 6.33 (1H, dd, J = 17.6, 11.0 Hz, H^{1'}), 5.78 (1H, dd, J = 5.1, 3.5 Hz, H⁵), 5.15 (1H, d, J = 17.5 Hz, H^{2'} trans), 5.00 (1H, d, J = 10.9 Hz, H^{2'} cis), 4.15 (1H, s, NH), 3.54 (1H, d, J = 20.2 Hz, Hb⁶), 3.06 (1H, d, J = 4.4 Hz, H^{12a}), 2.98 (1H, dd, J = 12.8, 5.4 Hz, H³), 2.79 (2H, q, J = 6.8 Hz, H¹), 2.06 (1H, dd, J = 19.8, 5.5 Hz, Ha⁶), 1.33 (9H, s, (CH₃)₃), 1.32 (3H, s, CH₃), 1.25 (2H, m, H²); **¹³C NMR** (100MHz, CDCl₃): δ 200.3 (C^{7/12}), 198.9 (C^{7/12}), 155.4 (COO), 139.4 (C^{7a/11a}), 137.9 (C^{1'}), 134.7 (C^{8/10}), 134.6 (C^{8/10}), 133.8 (C^{7a/11a}), 132.3 (C⁴), 127.7 (C^{9/11}), 127.6 (C^{9/11}), 126.4 (C⁵), 111.6 (C^{2'}), 79.5 (-C(CH₃)₃), 58.6 (C^{12a}), 46.2 (C^{6a}), 39.4 (C¹), 35.5 (C³), 31.7 (C⁶), 28.4 (C²), 28.3 (CH₃), 28.2 ((CH₃)₃); **MS** (EI): m/z 396.27 (MH⁺) (45), 340.20 (M⁺ - 56) (45), 296.33 (M⁺ - 99) (100); **HRMS:** Found [M+H]⁺ 396.2174, C₂₄H₂₉NO₄ requires MH , 396.2175.

(5aR,8R,8aS,14aR,15aS,15bS)-8-(2'-N-*tert*-Butyloxycarbonyl)-5a,14a-dimethyl-5a,6,8,8a,15,15a-hexahydrohexaphene-5,9,14,16(14aH,15bH)-tetraone (6.47):

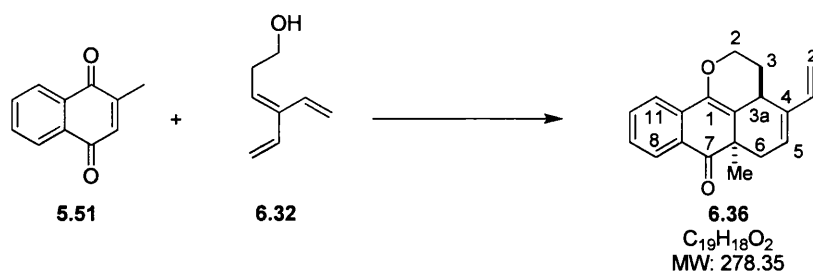


R_f 0.05 (Silica gel, Et₂O/*n*-hexane 1:1); **IR:** 3364, 2922, 2362, 1690, 1592, 1246 cm⁻¹; **¹H NMR** (400MHz; CDCl₃): δ 8.21 (1H, m, H^{2/11}), 8.03 (2H, m, H^{4,13}), 7.99 (1H, m, H^{2/11}), 7.76 (2H, m, H^{12,10}), 7.71 (2H, m, H^{1,3}), 5.68 (1H, d, J = 4.7 Hz, H⁷), 3.25 (1H, d, J = 7.1 Hz, H^{5b}), 3.16 (1H, dd, J = 18.2, 5.5 Hz, Hb⁶), 2.95 (1H, d, J =

6.0 Hz, H^{8a}), 2.82 (2H, m, H^{2'}), 2.80 (1H, m, H^{15a}), 2.76 (1H, m, H⁸), 1.90 (1H, dd, $J = 12.4, 3.4$ Hz, Ha⁶), 1.88 (1H, dt, $J = 18.1, 1.8$ Hz, Hb¹⁵), 1.39 (9H, s, (CH₃)₃), 1.31 (3H, s, CH₃), 1.26 (3H, s, CH₃), 0.85 (2H, m, H^{2'}), 0.54 (1H, t, $J = 12.9$ Hz, Ha¹⁵); ¹³C NMR (100 MHz; CDCl₃): δ 201.2 (C=O), 200.6 (C=O), 199.6 (C=O), 199.1 (C=O), 155.3 (COO), 135.5 (C^{7a}), 134.7 (C^{4a,13a}), 134.6 (C²), 134.5 (C⁴), 134.2 (C¹¹), 134.1 (C¹³), 134.1 (C^{9a}), 133.1 (C^{16a}), 127.3 (C^{3/12}), 127.2 (C^{3/12}), 126.4 (C^{1/10}), 126.30 (C^{1/10}), 121.5 (C⁷), 80.0 (-C(CH₃)₃), 61.6 (C^{8a}), 57.2 (C^{15b}), 48.2 (C^{5a/14a}), 46.3 (C^{5a/14a}), 46.1 (C^{2'}), 44.5 (C⁸), 38.7 (C¹⁵), 34.2 (C^{15a}), 32.2 (C^{1'}), 31.0 (C⁶), 29.0 (CH₃), 28.9 (CH₃), 28.4 ((CH₃)₃); MS (EI): m/z 468.37 (M⁺ - Boc) (70), 296.25 (M⁺ - 172) (25); HRMS: Found [M+Na]⁺ 590.2510, C₃₅H₃₇NO₆ requires *MNa*, 590.2518.

9.2.3 Synthesis of the tetracyclic scaffolds

(3a*SR*,6a*RS*)-6a-methyl-4-vinyl-3,3a,6,6a-tetrahydro-2*H*-anthra[9,1-*bc*]pyran-7-one (23)



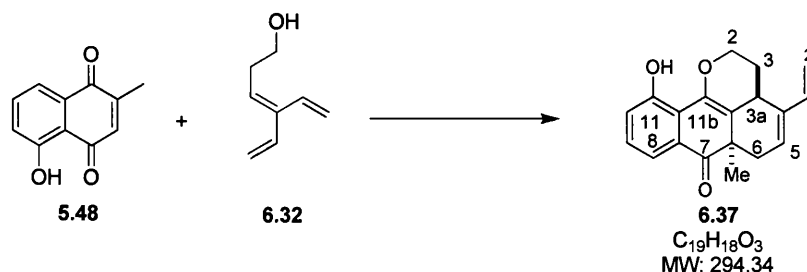
Procedure 1: 2-methyl-naphthoquinone **5.51** (25 mg, 0.15 mmol) and triene **6.32** (27 mg, 0.22 mmol, 1.5 eq.) in CH₂Cl₂ (0.5 ml) were added to a sealed glass tube. The mixture was cooled at -45 °C and then boron trifluoride diethyletherate (68.2 mg, 0.035 ml, 0.29 mmol, 2 eq.) was added very slowly. The reaction mixture was left to stir at this temperature for 5 h, and then quenched with ice water (5 ml), and the organic and aqueous phases separated. The latter was extracted with CH₂Cl₂ (3 x 5 ml). The combined organic phases were washed with water and brine, dried over MgSO₄, filtered and concentrated under reduced pressure. The crude mixture was purified by flash column chromatography on silica gel using *n*-hexane and Et₂O (95:5) to afford **6.36** (32.3 mg, 80%) as yellow solid (98% purity assessed by NMR and LC-MS analysis).

Procedure 2: 2-methylnaphthoquinone **5.51** (18 mg, 0.11 mmol) was diluted with HCl aq. (5 M, 0.07 ml) and the solution was added at 0 °C to a solution of triene **6.32** (39 mg, 0.31 mmol, 3 eq.) in THF: water (0.2 ml). The reaction mixture was

vigorously stirred at 50 °C for 18 h, then diluted with 15 ml CH₂Cl₂ and washed with 15 ml of a saturated solution of NaHCO₃. After shaking, the two phases were separated and the aqueous extracted with CH₂Cl₂ (5 x 5 ml). The combined organic extracts were washed with water and brine, dried over MgSO₄ and concentrated under reduced pressure. The crude mixture was purified by flash column chromatography on silica gel using *n*-hexane and Et₂O (1:1) to afford **6.36** (15 mg, 50%) as yellow solid.

R_f 0.54 (silica gel, CH₂Cl₂); **IR**: 2914, 2323, 1648, 1300 cm⁻¹; **Mp**. 118.9 °C; **¹H NMR** (500MHz, CDCl₃): δ 8.09 (1H, dd, *J* = 7.8, 1.3 Hz, H^{8/11}), 7.75 (1H, dd, *J* = 7.9, 0.9 Hz, H^{8/11}), 7.63 (1H, td, *J* = 7.6, 1.4 Hz, H^{9/10}), 7.38 (1H, td, *J* = 7.5, 1.1 Hz, H^{9/10}), 6.30 (1H, dd, *J* = 17.7, 11.0 Hz, H^{1'}), 5.84 (1H, d, *J* = 6.2 Hz, H⁵), 5.18 (1H, d, *J* = 17.7 Hz, H^{2'trans}), 5.08 (1H, d, *J* = 11.1 Hz, H^{2'cis}), 4.46 (1H, ddd, *J* = 10.8, 3.7, 2.5 Hz, Hb²), 4.17 (1H, ddd, *J* = 12.7, 10.8, 1.9 Hz, Ha²), 3.38 (1H, m, H^{3a}), 2.53 (1H, ddt, *J* = 13.7, 5.6, 2.2 Hz, Hb³), 2.46 (1H, dd, *J* = 17.9, 6.2 Hz, Hb⁶), 2.20 (1H, d, *J* = 18.0 Hz, Ha⁶), 1.64 (1H, dddd, *J* = 13.6, 12.7, 11.5, 3.7 Hz, Ha³), 1.33 (3H, s, CH₃); **¹³C NMR** (125MHz, CDCl₃): δ 200.4 (C⁷), 140.1 (C^{11a}), 137.8 (C⁴), 137.1 (C^{1'}), 135.9 (C^{7a/11a}), 134.5 (C^{8/11}), 127.9 (C^{7a/11a}), 127.6 (C^{9/10}), 127.0 (C^{8/11}), 125.1 (C⁵), 122.1 (C^{9/10}), 115.8 (C^{11b}), 112.5 (C^{2'}), 65.7 (C²), 44.7 (C^{6a}), 37.1 (C⁶), 31.8 (C^{3a}), 28.5 (C³), 32.6 (CH₃); **MS** (EI): *m/z* 278.91 (M⁺) (100), 250.81 (M⁺ - 28) (10), 301.00 (MNa⁺) (10); **HRMS**: Found [M+H]⁺ 279.1391, C₁₉H₁₈O₂ requires *MH*, 279.1385; **Elemental analysis**: Calculated for C₁₉H₁₈O₂ C, 81.99; H, 6.52; Found C, 81.89; H, 6.41.

(3a*SR*,6a*RS*)-11-hydroxy-6a-methyl-4-vinyl-3,3a,6,6a-tetrahydro-2*H*-anthra[9,1-*bc*]pyran-7-one (6.37)

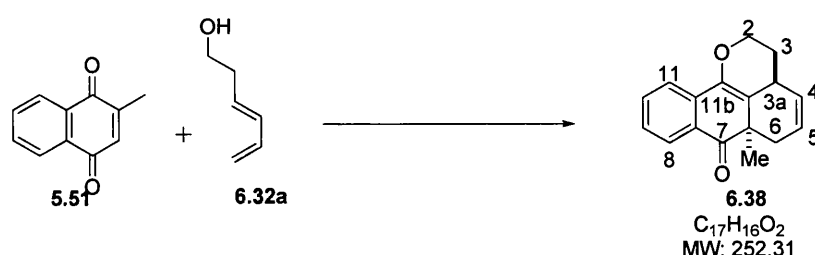


2-methyl-5-hydroxynaphthoquinone **5.48** (25 mg, 0.13 mmol) and triene **6.32** (24 mg, 0.20 mmol, 1.5 eq.) in CH₂Cl₂ (0.5 ml) were added to a sealed glass tube. The mixture was cooled at -45 °C and then borontrifluoride diethyletherate (61.1 mg, 0.031 ml, 0.26 mmol) was added very slowly. The reaction mixture was left to stir at this temperature for 5h, then quenched with ice water (5 ml). After phase separation,

the aqueous layer was extracted with CH₂Cl₂ (3 x 5 ml). The combined organic phases were washed with water and brine, dried over MgSO₄ and concentrated under reduced pressure. The crude mixture was purified by flash column chromatography on silica gel using *n*-hexane and Et₂O (95:5) to afford **6.37** (29 mg, 75%). as yellow solid (98% purity assessed by NMR and LC-MS analysis). *R_f* 0.5 (Silica gel, CH₂Cl₂) **IR**: 3390, 2924, 2847, 2361, 1690, 1646, 1455, 1263, 1033 cm⁻¹; **Mp**. 112.5 °C; **¹H NMR** (400MHz, CDCl₃): δ 9.25 (1H, s, OH), 7.68 (1H, dt, *J* = 7.7, 1.1 Hz, H⁸), 7.28 (1H, t, *J* = 7.9 Hz, H⁹), 7.13 (1H, dt, *J* = 8.1, 1.1 Hz, H¹⁰), 6.29 (1H, dd, *J* = 17.8, 11.1 Hz, H¹), 5.85 (1H, d, *J* = 6.2 Hz, H⁵), 5.17 (1H, d, *J* = 17.7 Hz, H^{2'-trans}), 5.10 (1 H, d, *J* = 11.1 Hz, H^{2'-cis}), 4.53 (1H, ddd, *J* = 10.6, 3.7, 2.6 Hz, Hb²), 4.25 (1H, ddd, *J* = 12.6, 10.6, 2.0 Hz, Ha²), 3.37 (1H, m, H^{3a}), 2.56 (1H, ddt, *J* = 13.9, 5.5, 2.4 Hz, Hb³), 2.45 (1H, dd, *J* = 18.0, 6.2 Hz, Hb⁶), 2.21 (1H, d, *J* = 17.0 Hz, Ha⁶), 1.71 (1H, m, Ha³), 1.32 (3H, s, CH₃); **¹³C NMR** (100MHz, CDCl₃): δ 201.6 (C⁷), 154.3 (C¹¹), 141.7 (C^{11a}), 137.4 (C⁴), 136.8 (C^{1'}), 129.4 (C^{7a}), 129.3 (C⁹), 125.2 (C⁵), 123.6 (C¹⁰), 119.4 (C⁸), 119.2 (C^{11b}), 115.3 (C^{11c}), 112.7 (C^{2'}), 66.4 (C²), 44.4 (C^{6a}), 37.0 (C⁶), 31.4 (C^{3a}), 27.9 (C³), 22.6 (CH₃); **MS** (EI): *m/z* 294.81 (M⁺) (35), 213.74 (M⁺ - 80) (100); **HRMS**: Found [M+H]⁺ 295.1325, C₁₉H₁₈O₃ requires *MH*, 295.1334, and [M+Na]⁺ 317. 1156 requires *MNa*, 317.1154; **Elemental analysis**: Calculated for C₁₉H₁₈O₃ C, 77.53; H, 6.56; Found C, 77.46; H, 6.66.

(3a*SR*,6a*RS*)-6a-methyl-3,3a,6,6a-tetrahydro-2*H*-anthra[9,1-*bc*]pyran-7-one

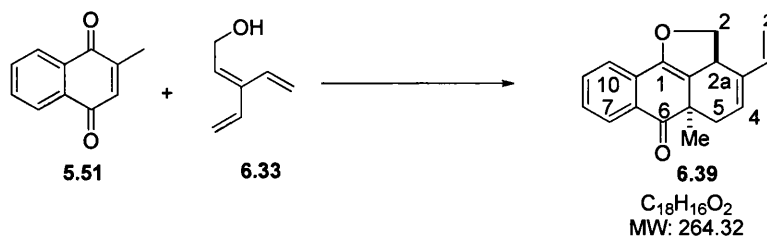
(25)



2-methyl naphthoquinone **5.51** (50 mg, 0.29 mmol) and diene **6.32a** (142 mg, 1.45 mmol) (which was prepared according to the procedure by DeBoef²⁵⁸) in CH₂Cl₂ (0.5 ml) were added to a sealed tube. The mixture was cooled at -45 °C and then borontrifluoride diethyletherate (411.3 mg, 0.21 ml, 1.74 mmol) was added very slowly. The reaction mixture was left to stir at 0 °C for 5h, and then quenched with ice water (1 ml), and the organic and aqueous phases separated. The latter was extracted with CH₂Cl₂ (3 x 5 ml). The combined organic phases were washed with water and brine, dried over MgSO₄ and concentrated under reduced pressure. The

crude mixture was purified by flash column chromatography on silica gel using *n*-hexane and Et₂O (95:5) to afford **25** (37.5 mg, 50%) as yellow solid (98% purity assessed by NMR and LC-MS analysis). *R_f* 0.35 (silica gel, CHCl₃); **IR**: 2971, 2927, 2863, 1675, 1648, 1595, 1288, 1098 cm⁻¹; **Mp.** 82.4 °C; ¹H NMR (400MHz, CDCl₃): δ 8.09 (1H, dd, *J* = 7.8, 1.4 Hz, H⁸), 7.72 (1H, dt, *J* = 7.9, 0.6 Hz, H¹¹), 7.62 (1H, tdd, *J* = 7.6, 1.4, 0.4, H⁹), 7.37 (1H, td, *J* = 7.5, 1.2 Hz, H¹⁰), 5.72 (1H, ddt, *J* = 9.6, 4.7, 2.3 Hz, H⁴), 5.67 (1H, dt, *J* = 10.0, 2.2 Hz, H⁵), 4.43 (1H, ddd, *J* = 10.7, 3.6, 2.7 Hz, H^{b2}), 4.09 (1H, ddd, *J* = 12.4, 10.6, 1.9, H^{a2}), 3.14 (1H, ddtt, *J* = 9.0, 6.4, 2.3, 2.0 Hz, H^{3a}), 2.39 (1H, ddd, *J* = 17.6, 4.8, 1.4 Hz, H^{b6}), 2.17 (1H, dq, *J* = 6.2, 2.2 Hz, H^{a6}), 2.13 (1H, m, H^{b3}), 1.73 (1H, dtd, *J* = 13.2, 12.0, 3.6 Hz, H^{a3}), 1.41 (3H, s, CH₃); ¹³C NMR (100MHz; CDCl₃): δ 202.74 (C⁷), 139.69 (C^{11b}), 135.77 (C^{7a}), 134.44 (C⁹), 128.55 (C⁵), 127.93 (C^{11a}), 127.54 (C¹⁰), 127.05 (C⁸), 124.11 (C⁴), 121.97 (C¹¹), 116.21 (C^{11c}), 65.36 (C²), 44.98 (C^{6a}), 36.86 (C⁶), 31.21 (C^{3a}), 29.40 (C³), 23.57 (CH₃); **MS** (EI): *m/z* 253.29 (MH⁺) (100), 235.55 (M⁺ - 18) (55); **HRMS**: Found MH⁺ 253.1223, C₁₇H₁₈O₂ requires *MH*, 253.1384; **Elemental analysis**: Calculated for C₁₇H₁₈O₂ C, 80.28; H, 7.13; Found C, 80.21; H, 7.11.

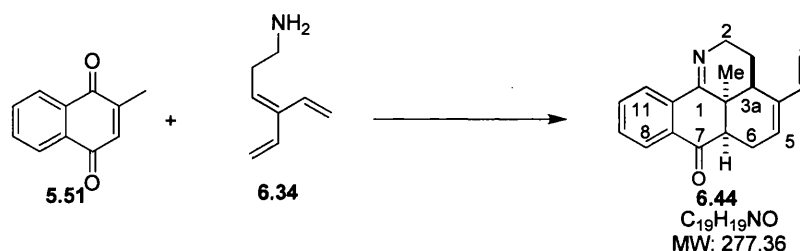
(2a*SR*,5a*RS*)-5a-methyl-3-vinyl-5,5a-dihydro-2*H*-anthra[9,1-*bc*]furan-6(2a*H*)-one (6.39)



2-methylnaphthoquinone **5.51** (30 mg, 0.17 mmol) and triene **18** (29 mg, 0.26 mmol, 1.5 eq.) in CH₂Cl₂ (0.5 ml) were added to a sealed glass tube. The mixture was cooled at -20 °C and then scandium trifluoromethanesulfonate (43 mg, 0.087 mmol, 0.5 eq.) was added portion-wise to the mixture, which was then warmed up to 0 °C. The reaction mixture was left to stir at this temperature for 5h, quenched with ice water (5 ml), and the organic and aqueous phases separated. The latter was extracted with CH₂Cl₂ (3 x 5 ml). The combined organic phases were washed with water and brine, dried over MgSO₄ and concentrated under reduced pressure. The crude mixture was purified by flash column chromatography on silica gel using *n*-hexane/Et₂O (95:5) to afford **6.39** (30.3 mg, 65%) as yellow solid (98% purity assessed by NMR and LC-MS analysis). *R_f* 0.53 (silica gel, CH₂Cl₂); **IR**: 2361,

1683, 1596, 1265, 769 cm^{-1} ; **Mp.** 130.9 °C; ^1H NMR (500MHz, CDCl_3): δ 7.61 (1H, td, $J = 7.5, 1.3$ Hz, $\text{H}^{7/10}$), 7.41 (1H, dt, $J = 7.7, 0.6$ Hz, $\text{H}^{7/10}$), 7.37 (2H, td, $J = 7.6, 1.2$ Hz, $\text{H}^{8,9}$), 6.33 (1H, dd, $J = 17.7, 10.8$ Hz, H^1), 5.74 (1H, m, $J = 6.2$ Hz, H^4), 5.09 (1H, dd, $J = 9.8, 8.6$ Hz, Hb^2), 5.07 (1H, d, $J = 10.3$ Hz, $\text{H}^{2'cis}$), 4.94 (1H, d, $J = 17.6$ Hz, $\text{H}^{2'trans}$), 4.15 (1H, dd, $J = 10.1, 8.6$ Hz, Ha^2), 4.04 (1H, t, $J = 11.0$ Hz, H^{2a}), 2.51 (1H, dd, $J = 18.2, 5.4$ Hz, Hb^5), 2.34 (1H, d, $J = 21.3$ Hz, Ha^5), 1.35 (3H, s, CH_3); ^{13}C NMR (125MHz, CDCl_3): δ 202.7 (C^6), 144.3 ($\text{C}^{10a/6a}$), 139.0 (C^3), 137.6 ($\text{C}^{1'}$), 134.4 ($\text{C}^{7/10}$), 131.8 ($\text{C}^{6a/10a}$), 129.4 (C^1), 128.3 ($\text{C}^{7/10}$), 127.8 (C^4), 127.6 ($\text{C}^{8/9}$), 121.4 ($\text{C}^{8/9}$), 117.8 (C^{10b}), 112.6 ($\text{C}^{2'}$), 76.7 (C^2), 43.8 (C^{5a}), 39.9 (C^{2a}), 38.1 (C^4), 20.9 (CH_3); **MS** (EI): m/z 264.92 (M^+) (15), 281.89 ($\text{M}^+ + 17$) (100); **HRMS**: Found $[\text{M}+\text{H}]^+$ 265.1231, $\text{C}_{18}\text{H}_{16}\text{O}_2$ requires MH , 265.1229; **Elemental analysis**: Calculated for $\text{C}_{18}\text{H}_{16}\text{O}_2$ C, 81.71; H, 6.10; Found C, 81.97; H, 6.15.

(3aSR,11cSR,6aRS)-11c-methyl-4-vinyl-2,3,3a,6,6a,11c-hexahydro-anthra[9,1-bc]pyridine-7-one (6.44)



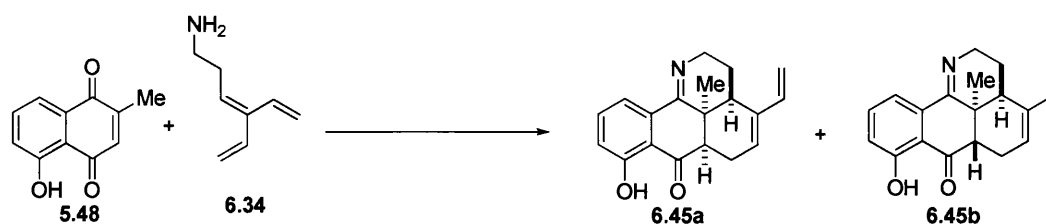
Procedure 1: 2-methyl naphthoquinone **5.51** (20.0 mg, 0.12 mmol) and triene **6.34** (22 mg, 0.18 mmol, 1.5 eq.) in CH_2Cl_2 (1 ml) were added to a sealed glass tube. The mixture was cooled at -5 °C and then scandium trifluoromethanesulfonate (118 mg, 0.24 mmol, 2 eq.) was added. The reaction mixture was left to stir at 0 °C for 15h, then quenched with ice water (1 ml) and the organic and aqueous phases separated. The latter was extracted with CH_2Cl_2 (3 x 5 ml). The combined organic phases were washed with water and brine, filtered and dried over MgSO_4 and concentrated under reduced pressure. The crude mixture was purified by flash column chromatography on silica gel with *n*-hexane and Et_2O (1:1) to afford **6.44** (23.3 mg, 70%) as yellow oil (98% purity assessed by NMR and LC-MS analysis).

Procedure 2: 2-methylnaphthoquinone **5.51** (24 mg, 0.14 mmol) was diluted with HCl aq. (5 M, 0.07 ml) and the solution was added at 0 °C to a solution of triene **6.34** (51 mg, 0.42 mmol, 3 eq.) in water (0.12 ml). The reaction mixture was vigorously stirred at 50 °C for 2.5h, then diluted with 15 ml CH_2Cl_2 and washed with 15 ml of a saturated solution of NaHCO_3 . After shaking, the two phases were

separated and the aqueous extracted with CH₂Cl₂ (5 x 5 ml). The combined organic extracts were washed with water and brine, dried over MgSO₄, filtered and concentrated under reduced pressure. The crude mixture was purified by flash column chromatography on silica gel with *n*-hexane and Et₂O (1:1) to afford **6.44** (22 mg, 57%) as yellow oil.

R_f 0.18 (silica gel, *n*-hexane/Et₂O 50:50); **IR**: 2950, 2918, 2852, 2361, 1633, 1455, 1279 cm⁻¹; **¹H NMR** (500MHz, CDCl₃): 8.01 (1H, ddd, *J* = 7.8, 1.4, 0.5 Hz, H^{8/11}), 7.89 (1H, dd, *J* = 7.8, 1.0 Hz, H^{8/11}), 7.64 (1H, td, *J* = 7.5, 1.4 Hz, H^{9/10}), 7.50 (1H, td, *J* = 7.6, 1.3 Hz, H^{9/10}), 6.30 (1H, dd, *J* = 17.7, 11.0 Hz, H¹), 5.86 (1H, d, *J* = 5.2, 2.6 Hz, H⁵), 5.14 (1H, d, *J* = 17.7 Hz, H^{2'trans}), 5.03 (1H, d, *J* = 10.9 Hz, H^{2'cis}), 4.18 (1H, ddd, *J* = 17.2, 3.8, 1.7 Hz, Hb²), 3.66 (1H, ddd, *J* = 10.8, 3.7, 2.5 Hz, Ha²), 3.01 (1H, ddd, *J* = 12.7, 10.8, 1.9 Hz, H^{6a}), 2.74 (1H, dt, *J* = 19.8, 5.7 Hz, Hb⁶), 2.47 (1H, dd, *J* = 12.7, 1.8 Hz, H^{3a}), 2.20 (1H, m, Hb³), 2.40 (1H, m, Ha⁶), 1.05 (3H, s, CH₃), 1.43 (1H, m, Ha³); **¹³C NMR** (100MHz, CDCl₃): 198.3 (C⁷), 170.4 (C^{11b}), 139.9 (C⁴), 138.4 (C^{1'}), 136.1 (C^{7a/11a}), 134.3 (C^{9/10}), 132.2 (C^{7a/11a}), 130.0 (C^{9/10}), 126.3 (C^{8/11}), 126.0 (C⁵), 125.9 (C^{8/11}), 111.2 (C^{2'}), 50.8 (C²), 47.7 (C^{6a}), 41.6 (C^{3a1}), 41.3 (C^{3a}), 26.9 (C³), 22.9 (C⁶), 20.7 (CH₃); **MS** (EI): *m/z* 277.97 (M⁺) (100), 296.60 (M⁺ + 18) (15); **HRMS**: Found MH⁺ 278.1539, C₁₉H₁₉NO requires *MH*, 278.1545; **Elemental analysis**: Calculated for C₁₉H₁₉NO C, 82.28; H, 6.90, N, 5.05; Found C, 82.28; H, 6.61; N, 4.98.

(3aSR,11cSR,6aRS)-8-hydroxy-11c-methyl-4-vinyl-2,3,3a,6,6a,11c-hexahydro-anthra[9,1-*bc*]pyridine-7-one (6.45a)

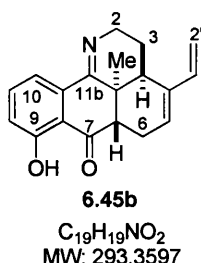


2-methyl-5-hydroxynaphthoquinone **5.48** (30 mg, 0.16 mmol) and triene **6.34** (52 mg, 0.4 mmol, 2.5 eq.) in CH₂Cl₂ (1 ml) were added to a sealed glass tube. The mixture was cooled to -20 °C and then scandium trifluoromethanesulfonate (325 mg, 0.48 mmol, 3 eq.) was added. The reaction mixture was left to stir at 0 °C for 24h, then quenched with ice water (1 ml) and the organic and aqueous phases separated. The latter was extracted with CH₂Cl₂ (3 x 5 ml). The combined organic phases were washed with water and brine, dried over MgSO₄ and concentrated under reduced pressure. The crude mixture was purified by flash column chromatography on silica

gel with *n*-hexane and Et₂O (1:1) to afford **6.45a** (14 mg, 29%) and **6.45b** (31 mg, 65%) as colourless oils (98% purity assessed by NMR and LC-MS analysis).

R_f 0.38 (silica gel, Et₂O/*n*-hexane 2:1); **IR**: 2972, 2918, 2847, 2361, 1641, 1452, 1249, 820 cm⁻¹; **¹H NMR** (400MHz, CDCl₃): δ 12.01 (1H, s, OH), 7.52 (1H, t, *J* = 7.9 Hz, H¹⁰), 7.47 (1H, dd, *J* = 7.7, 1.4 Hz, H¹¹), 7.04 (1H, dd, *J* = 8.1, 1.4 Hz, H⁹), 6.24 (1H, dd, *J* = 17.7, 11.1 Hz, H¹), 5.98 (1H, m, H⁵), 5.19 (1H, d, *J* = 17.7 Hz, H²), 5.08 (1H, d, *J* = 11.1 Hz, H^{2'}), 3.84 (1H, ddt, *J* = 18.7, 4.4, 1.3 Hz, Hb²), 3.52 (1H, ddd, *J* = 18.6, 12.5, 4.2 Hz, Ha²), 2.65 (1H, m, H^{3a}), 2.63 (1H, dd, *J* = 11.9, 4.9 Hz, H^{6a}), 2.32 (1H, m, Hb⁶), 2.19 (1H, m, Ha⁶), 2.13 (1H, dddt, *J* = 12.4, 5.8, 3.0, 1.5 Hz, Hb³), 1.90 (1H, ddt, *J* = 13.6, 12.7, 4.3 Hz, Ha³), 1.39 (3H, s, CH₃); **¹³C NMR** (100MHz; CDCl₃): δ 206.7 (C⁷), 165.5 (C^{11b}), 161.9 (C⁸), 138.8 (C^{11a}), 137.1 (C¹), 137.0 (C⁴), 136.8 (C¹⁰), 127.2 (C⁵), 119.6 (C⁹), 117.4 (C¹¹), 113.8 (C^{7a}), 113.2 (C^{2'}), 53.7 (C^{6a}), 46.5 (C²), 41.0 (C^{11c}), 38.4 (C^{3a}), 28.2 (C⁶), 26.4 (CH₃), 21.2 (C³); **MS** (EI): *m/z* 294.50 (MH⁺) (100), 295.50 (M⁺ + 2) (50); **HRMS**: Found [M+H]⁺ 294.1505, C₁₉H₁₉NO₂ requires *MH*, 294.1494; **Elemental analysis**: Calculated for C₁₉H₁₉NO₂ C,77.79; H,6.53; N,4.77; Found C,77.75; H,6.55; N,4.80.

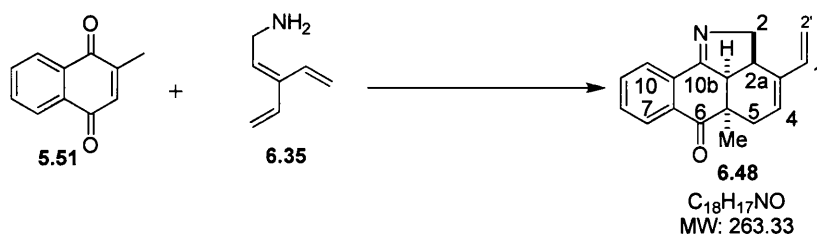
(3aSR,11cSR,6aSR)-8-hydroxy-11c-methyl-4-vinyl-2,3,3a,6,6a,11c-hexahydro-anthra[9,1-*bc*]pyridine-7-one (6.45b):



R_f 0.27 (silica gel, Et₂O/*n*-hexane 2:1); **IR**: 2951, 2919, 2853, 2362, 1633, 1455, 1279, 820 cm⁻¹; **¹H NMR** (400MHz, CDCl₃): δ 12.13 (1H, s, OH), 7.53 (1H, dd, *J* = 8.3, 7.6 Hz, H¹⁰), 7.34 (1H, dd, *J* = 7.6, 1.1 Hz, H¹¹), 7.01 (1H, dd, *J* = 8.4, 1.1 Hz, H⁹), 6.30 (1H, dd, *J* = 17.7, 11.0 Hz, H¹), 5.85 (1H, dd, *J* = 5.3, 2.5 Hz, H⁵), 5.15 (1H, d, *J* = 17.8 Hz, H²), 5.05 (1H, d, *J* = 11.0 Hz, H^{2'}), 4.16 (1H, ddd, *J* = 17.2, 3.8, 1.7 Hz, Hb²), 3.63 (1H, ddd, *J* = 17.2, 12.1, 3.6 Hz, Ha²), 3.07 (1H, dd, *J* = 10.9, 6.1 Hz, H^{6a}), 2.76 (1H, dt, *J* = 19.7, 5.7 Hz, Hb⁶), 2.47 (1H, d, *J* = 12.6 Hz, Hb³), 2.37 (1H, dd, *J* = 19.4, 10.6 Hz, Ha⁶), 2.20 (1H, dtd, *J* = 13.9, 3.3, 1.7 Hz, H^{3a}), 1.40 (1H, ddd, *J* = 12.5, 3.9, 1.3 Hz, Ha³), 1.08 (3H, s, CH₃); **¹³C NMR** (100MHz, CDCl₃): δ 204.9 (C⁷), 169.8 (C^{11b}), 161.4 (C⁸), 140.5 (C^{11a}), 138.2 (C¹), 137.0 (C¹⁰), 136.3 (C⁴), 125.8 (C⁵), 119.1 (C⁹), 117.0 (C¹¹), 116.2 (C^{7a}), 111.5 (C^{2'}), 50.8 (C^{6a}), 47.6

(C²), 41.3 (C^{11c}), 41.1 (C^{3a}), 26.9 (C⁶), 22.5 (C³), 20.4 (CH₃); **MS** (EI): *m/z* 294.52 (MH⁺) (100), 295.55 (M⁺+2) (45); **HRMS**: Found [M+H]⁺ 294.1505, C₁₉H₁₉NO₂ requires *MH*, 294.1494; **Elemental analysis**: Calculated for C₁₉H₁₉NO₂ C,77.79; H,6.53; N,4.77; Found C,77.88; H,6.39; N,4.75.

(2a*RS*,10b*SR*,5a*RS*)-5a-methyl-3-vinyl-2,2a,5,5a-tetrahydro-2*H*-anthra[9,1-*bc*]pyrrole-6-one (6.48)



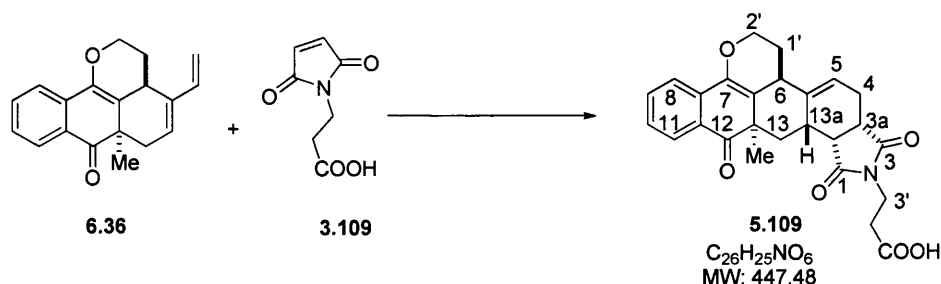
2-methylnaphthoquinone **5.51** (20 mg, 0.12 mmol) and triene **6.35** (19 mg, 0.17 mmol, 1.5 eq.) in CH₂Cl₂ (0.5 ml) were added to a sealed glass tube. The mixture was cooled at -5 °C and then scandium trifluoromethanesulfonate (285 mg, 0.60 mmol, 5 eq.) was added portion-wise to the mixture which was left stirring at room temperature for 18h. The reaction mixture was then quenched with ice water (1 ml), and the organic and aqueous phases separated. The latter was extracted with CH₂Cl₂ (3 x 5 ml). The combined organic phases were washed with water and brine, dried over MgSO₄ and concentrated under reduced pressure. The crude mixture was purified by flash column chromatography on silica gel using CH₂Cl₂ and Et₂O (1:1) to afford **6.48** (18.0 mg, 55%) as yellow oil (purity assessed by NMR and LC-MS analysis). *R_f* 0.23 (silica gel, *n*-hexane/Et₂O 1:1); **IR**: 2924, 2852, 2359, 2330, 1684, 159, 1260, 730 cm⁻¹; **¹H NMR** (400MHz, CDCl₃): 8.04 (1H, t, *J* = 8.1 Hz, H^{7/10}), 7.72 (1H, t, *J* = 8.6 Hz, H^{7/10}), 7.65 (2H, t, *J* = 7.5 Hz, H^{8,9}), 6.29 (1H, dd, *J* = 17.7, 11.1 Hz, H^{1'}), 5.75 (1H, dt, *J* = 7.2, 0.9 Hz, H⁴), 5.11 (1H, d, *J* = 17.8 Hz, H^{2'}), 5.08 (1H, d, *J* = 10.8 Hz, H^{2'}), 4.24 (2H, t, *J* = 2.8 Hz, H²), 3.44 (1 H, m, H^{2a}), 3.33 (1H, td, *J* = 7.1, 3.3 Hz, H^{10c}), 2.28 (2H, d, *J* = 18.5 Hz, Hb⁵), 1.92 (1H, dd, *J* = 18.2, 6.5 Hz, Ha⁵), 1.34 (3H, s, CH₃); **¹³C NMR** (100MHz, CDCl₃): 196.5 (C⁶), 168.9 (C^{10b}), 137.8 (C³), 136.5 (C^{1'}), 133.2 (C^{8/9}), 133.1 (C^{6a/10a}), 132.8 (C^{6a/10a}), 130.6 (C^{8/9}), 128.1 (C^{7/10}), 126.2 (C⁴), 125.3 (C^{7/10}), 110.7 (C^{2'}), 66.8 (C²), 54.2 (C^{10c}), 45.4 (C^{5a}), 34.1 (C^{2a}), 29.7 (C⁵), 20.4 (CH₃); **MS** (EI): *m/z* 264.54 (MH⁺) (100), 214.50 (M⁺ - 50) (25); **HRMS**: Found [M+H]⁺ 264.1384, C₁₈H₁₇NO requires *MH*, 264.1388; **Elemental analysis**: calculated for C₁₈H₁₇NO C,82.10; H,6.51; N,5.32; Found C,82.13; H,6.48; N,5.32.

9.2.4 Synthesis of polycyclic derivatives

General procedure for the synthesis of the polycyclic scaffolds

Anthraquinolic diene in toluene (0.5 M) and maleimide (5.0 eq.) were added to a sealed glass tube. The reaction mixture was stirred at 70 °C for 28 to 48h. Removal of the solvent under reduced pressure followed by flash column chromatography on silica gel using a mixture of *n*-hexane and Et₂O afforded the polycyclic compound (98% purity assessed by NMR and LC-MS analysis).

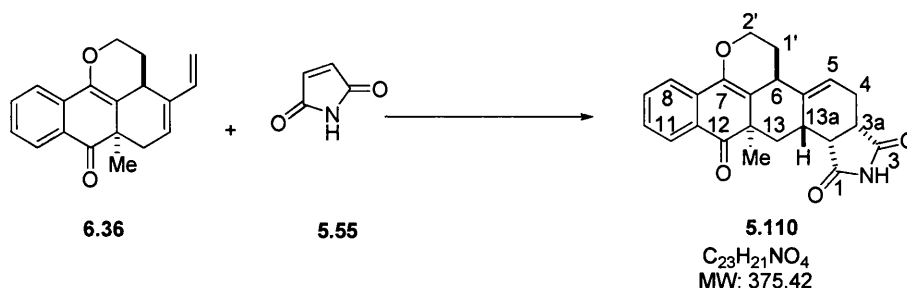
(3a*SR*,6*SR*,12a*RS*,13b*RS*,13a*SR*)-12a-methyl-1',3a,4,6,12a,13-hexahydro-2*H* naphtho[3',2',1':8,1]isochromeno[6,5-*e*]isoindole-1,3,12(7*H*,8a*H*,8b*H*)-trione (5.109):



The reaction time was 24h to afford **5.109** as white solid. **Y** = 95%; **R_f** 0.34 (silica gel, Et₂O); **IR**: 1740, 1697, 1648, 1593, 1364 cm⁻¹; **Mp**. 246.5 °C; **¹H NMR** (400MHz, DMSO-*d*₆): δ 7.15 (ddd, 1H, *J* = 7.8, 1.4, 0.6 Hz, H^{11/8}), 6.93 (ddd, 1H, *J* = 7.9, 7.2, 1.4 Hz, H^{9/10}), 6.84 (dd, 1H, *J* 7.7, 0.6 Hz, H^{8/11}), 6.66 (td, 1H, *J* 7.5, 1.1 Hz H^{9/10}), 5.00 (dd, 1H, *J* 5.5, 2.8 Hz, H⁵), 3.49 (dt, 1H, *J* 10.7, 3.5 Hz, Hb^{2'}), 3.28 (td, 1H, *J* 11.1, 1.9 Hz, Ha^{2'}), 2.58 (s, 1H, H⁶), 2.31 (td, 1H, *J* 9.1, 1.6 Hz, H^{13b}), 2.29 (q, 1H, *J* = 6.1 Hz, H^{3a}), 2.01 (m, 1H, H^{13a}), 1.67 (dd, 1H, *J* 15.7, 6.3 Hz, Hb⁴), 1.39 (m, 2H, Hb^{1'}, a⁴), 1.27 (t, 1H, *J* = 12.2 Hz, Hb¹³), 1.21 (dd, 1H, *J* = 13.0, 7.2 Hz, Ha¹³), 0.90 (tdt, 1H, *J* = 13.5, 10.7, 2.8 Hz, Ha^{1'}), 0.45 (s, 3H, CH₃); **¹³C NMR** (100MHz, DMSO-*d*₆): δ 201.3 (C¹²), 180.9 (C³), 180.0 (C¹), 141.0 (C⁷), 138.7 (C^{6a}), 135.0 (C^{7a/11a}), 134.7 (C^{9/10}), 127.8 (C^{9/10}), 127.2 (C^{7a/11a}), 126.5 (C^{8/11}), 121.6 (C^{8/11}), 119.9 (C⁵), 117.4 (C^{5a}), 64.8 (C^{2'}), 46.2 (C^{12a}), 43.5 (C^{13b}), 40.0 (C^{3a}), 35.7 (C¹³), 33.5 (C⁶), 31.6 (C^{13a}), 28.9 (C^{1'}), 23.3 (C⁴), 21.5 (CH₃); **MS (EI)**: *m/z* 376.52

(MH^+) (100); **HRMS**: Found $[M+H]^+$ 376.1536, $C_{26}H_{26}NO_6$ requires MH , 376.1549; **Elemental analysis**: Calculated for $C_{26}H_{25}NO_6$ C, 73.58; H, 5.64; N, 3.73; Found C, 73.55; H, 5.66; N, 3.70 .

3'-((3aSR, 6SR, 12aRS, 13bRS, 13aSR)-12a-methyl-1,3,12-trioxo-1,3,3a,5a, 6,12a,13,13a,13b, -decahydro-2H-naphtho[3',2',1':8,1]isochromeno[6,5-e] isoindol-2(5H)-yl)propanoic acid (5.110):



The reaction time was 48h to afford **5.110** as white solid. **Y** = 90%; **R_f** 0.29 (silica gel, EtOAc/AcOH 99:1); **Mp.** 207.6 °C; **IR**: 2928, 1738, 1694, 1399 cm^{-1} ; **¹H NMR** (400MHz, $CDCl_3$): δ 7.85 (dt, 1H, J = 7.7, 0.6 Hz, $H^{11/8}$); 7.55 (td, 1H, J = 7.3, 1.3 Hz, $H^{9,10}$), 7.52 (dd, 1H, J = 7.8, 1.6 Hz, $H^{8/11}$), 7.33 (ddd, 1H, J = 7.6, 6.9, 1.7 Hz $H^{9/10}$), 5.49 (dd, 1H, J = 7.0, 2.8 Hz, H^5), 4.10 (ddd, 1H, J = 10.3, 6.4, 3.6 Hz, $Hb^{2'}$), 4.03 (ddd, 1H, J = 10.8, 8.2, 2.8 Hz, $Ha^{2'}$), 3.76 (t, 2H, J = 7.3 Hz, $H^{3'}$), 3.16 (dd, 1H, J = 8.8, 6.0 Hz, H^{13b}), 3.09 (td, 1H, J = 8.1, 1.2 Hz, H^{3a}), 3.01 (m, 1H, H^{13a}), 2.99 (dd, 1H, J = 14.1, 4.3 Hz, Hb^{13}), 2.71 (dd, 1H, J = 15.0, 7.2 Hz, H^4), 2.61 (t, 2H, J = 7.1, $H^{4'}$), 2.29 (q, 1H, J = 13.0 Hz, Ha^{13}), 2.16 (m, 1H, H^6), 2.20 (m, 1H, $Hb^{1'}$), 2.02 (m, 1H, H^4), 2.11 (m, 1H $Ha^{1'}$), 1.37 (s, 3H, CH_3); **¹³C NMR** (100MHz, $CDCl_3$): δ 203.8 (C^{12}), 179.5 (C^3), 177.6 (C^1), 175.0 (COOH), 143.5 (C^7), 143.2 (C^{6a}), 135.0 ($C^{7a/11a}$), 133.8 ($C^{8/11}$), 129.0 ($C^{7a/11a}$), 127.9 ($C^{9/10}$), 126.7 ($C^{9/10}$), 121.6 ($C^{8/11}$), 117.8 (C^{5a}), 116.0 (C^5), 63.4 ($C^{2'}$), 49.0 (C^{12a}), 43.3 (C^{13b}), 39.8 (C^{3a}), 34.7 (C^6), 34.3 ($C^{3'}$), 31.8 ($C^{4'}$), 31.7 (C^{13a}), 29.3 (C^{13}), 29.2 (CH_3), 25.0 ($C^{1'}$), 24.5 (C^4); **MS** (EI): m/z 448.56 (MH^+) (100); **HRMS**: Found $[M+H]^+$ 447.1584, $C_{23}H_{22}NO_4$ requires MH , 447.1682; **Elemental analysis**: Calculated for $C_{23}H_{21}NO_4$ C, 69.79; H, 5.63; N, 3.13; Found C, 69.77; H, 5.60; N, 3.11.

9.3 Development of chiral Bronsted/ Lewis acid-catalysed enantioselective naphthoquinone Diels-Alder cycloaddition

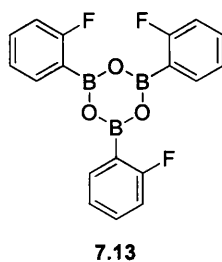
General Method:

All reagents and solvents used were supplied from commercial sources unless otherwise indicated. Reactions requiring anhydrous conditions were conducted in glassware, which had been oven-dried overnight and used the following day. All reactions were carried under dry N₂ conditions unless otherwise stated. All reactions were monitored by analytical thin-layer chromatography (TLC) performed using indicated solvent on silica gel 60 (0.25 mm). TLC plates were visualized using UV light (254 or 360nm) and/or staining with a cerium sulfate-ammonium molybdate solution or basic potassium permanganate KMnO₄ followed by heating. LC-MS, liquid chromatography coupled with mass spectrophotometer, was also used to monitor the progress of the reactions. Solvents were removed by rotary evaporator at or below 40 °C and the compounds further dried using low-pressure vacuum pumps. An immersion cooler was used to perform overnight reactions at very low temperatures e.g. -45 °C. The purification of the compounds was achieved by column chromatography using silica gel (230 – 400mesh). Optical rotations were measured on a Perkin-Elmer 241 polarimeter. The enantiomeric excess (*ee*) of the products was determined by chiral stationary phase HPLC (Daicel Chiralpak-IC), using a UV detector operating at 254 nm. Analytical grade solvents and commercially available reagents were used as received, unless otherwise stated.

The cross-conjugated trienes were prepared following a method cited previously. Reagents used to prepare CBS-oxazaborolidine were purchased from Sigma-Aldrich. These catalysts were prepared then activated *in situ* using Corey's method²⁵⁹ unless otherwise stated. Binaphthols were obtained from Sigma-Aldrich and the catalysts prepared following the method specified in the experiment^{224, 260}. Thioureas were prepared following Schreiner's method.²³⁶

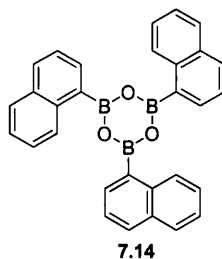
9.3.1 Asymmetric Diels-Alder using Oxazaborolidine derivatives

Tri-*o*-fluorophenylboroxine (7.13).



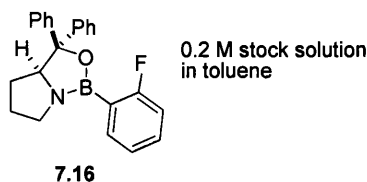
Following Corey's protocol,²⁵⁹ a round-bottomed flask to which was added a short-path distillator was charged with *o*-fluorophenylboronic acid (278.0 mg, 2 mmol). The boronic acid was dehydrated by azeotropic distillation with 3 x 10 mL benzene to afford the corresponding boroxine (242.0 mg, 100%). Further recrystallization from benzene-hexanes afforded the boroxine as a white solid which was used without further purification to prepare the corresponding catalyst.

2,4,6-tri(naphthalen-1-yl)-boroxine (7.14).



The procedure cited above was applied with naphthalen-1-ylboronic acid (344.0 mg, 2 mmol) to afford the corresponding boroxine (340.0 mg, 100%) as a white solid, which was used without further purification to prepare the corresponding catalyst.

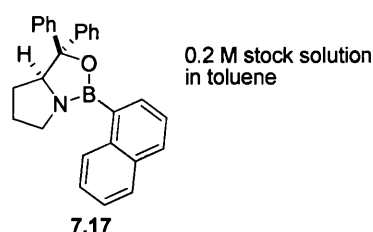
(3*aS*,7*S*)-1-(2-fluorophenyl)-3,3-diphenylhexahydro-1*H*-pyrrolo[1,2-*c*][1,3,2]oxazaborol-7-ium (7.16)



Following Corey's protocol,²⁵⁹ a round-bottomed flask was fitted with a pressure-equalizing addition funnel (containing a cotton plug and 4Å molecular sieves, and functioning as a Soxhlet extractor) fitted on top with a reflux condenser and a nitrogen inlet adaptor. (*S*)-(-)- α,α -diphenyl-2-pyrrolidinemethanol (200 mg, 0.789 mmol, 3 eq.),

tri-*o*-fluorophenylboroxine (96.5 mg, 0.263 mmol, 1 eq.) and 35 mL of toluene were added to the flask. The resulting solution was heated to reflux (155 °C) for 4 hours then the reaction mixture was cooled to 60 °C and a short-path distillation head was placed instead of the addition funnel. The mixture was concentrated by distillation. The distillation was repeated three times by re-charging with 3 x 5 mL of toluene. The solution was then allowed to cool to room temperature, the distillation head was quickly replaced with a vacuum adaptor and the solution was concentrated *in vacuo* (ca. 1 mmHg, 1 h). Toluene (3.9 mL) was then added and a rubber septum containing a nitrogen inlet line was placed. The resulting 0.2 M stock solution of oxazaborolidine catalyst precursor was used immediately in the asymmetric synthesis.

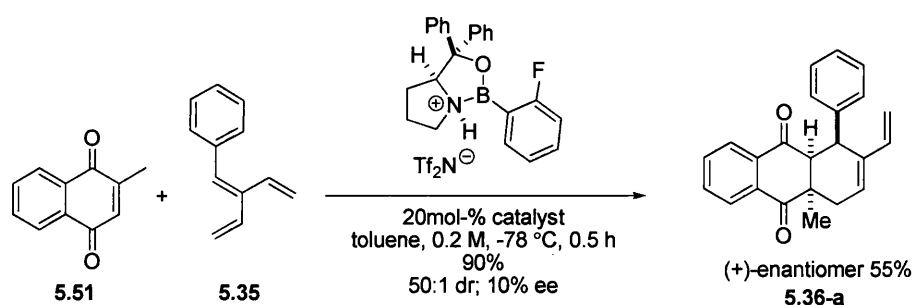
(S)-1-(naphthalen-1-yl)-3,3-diphenylhexahydropyrrolo[1,2-c][1,3,2]oxazaborole



Following the procedure cited above, (*S*)-(-)- α,α -diphenyl-2-pyrrolidinemethanol (200.2 mg, 0.789 mmol, 3eq.), 2,4,6-tri(naphthalen-1-yl)-boroxine (122.1 mg, 0.263 mmol, 1 eq.) and 35 mL of toluene were added. At the end of the reaction, 0.2 M stock solution of the oxazaborolidine catalyst precursor was used immediately in the asymmetric synthesis.

General procedure for oxazaborolidine-catalysed asymmetric Diels-Alder reaction

Fluorophenyl-(S)-CBS-oxazaborolidinium-catalysed Diels-Alder (Table 7.1, entry 1)

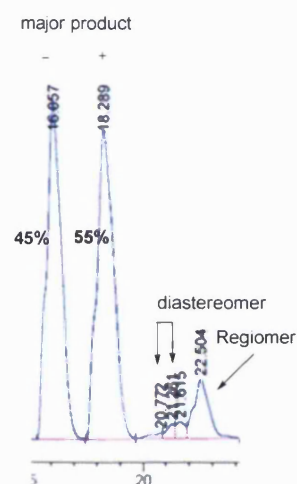


(1*S*,4*aR*,9*aS*)-9*a*-methyl-1-phenyl-2-vinyl-1,4,4*a*,9*a*-tetrahydroanthracene-9,10-dione (5.36-a)

To a 0.2 M of fluorophenyl-CBS-oxazaborolidine precursor in toluene (0.087 mmol, 90 μ L, 0.5 eq.) was added trifluoromethanesulfonimide (0.20 M solution in toluene, freshly

prepared by adding 21mg in 0.4mL toluene) dropwise at $-25\text{ }^{\circ}\text{C}$. After 10 min at $-25\text{ }^{\circ}\text{C}$, a colourless homogeneous catalyst solution was ready for use in the Diels-Alder reactions.

To a catalyst solution in toluene were successively added a solution of 2-methyl,1,4-naphthoquinone (30.0 mg, 0.174 mmol, 1 eq.) in CH_2Cl_2 (0.3 mL) and (2-vinylbuta-1,3-dienyl)benzene (55 μL , 54.0 mg, 0.348 mmol, 2 eq.), at $-78\text{ }^{\circ}\text{C}$. The reaction mixture was stirred at this temperature and monitored by LCMS and TLC. After 30 min, the solvents were removed by rotary evaporation and water (3 mL) and CH_2Cl_2 (3 mL) were added. The aqueous layer was extracted with CH_2Cl_2 (4 x 3mL). The combined extracts were dried over anhydrous MgSO_4 , concentrated in vacuo and purified by column chromatography on silica gel (hexane: Et_2O 9:1) to afford the product as a clear yellow solid (52.0 mg, 90%).



Enantioselectivity and diastereoselectivity were determined by HPLC analysis using Chiral-IC (1% \rightarrow 5% \rightarrow 10% \rightarrow 15% CH_2Cl_2 in hexane), **5.36**, 50:1 dr; ee = 10% ($\text{rt}_{(-)\text{-enantiomer}}$ = 16.0 min; $\text{rt}_{(+)\text{-enantiomer}}$ = 18.3 min).

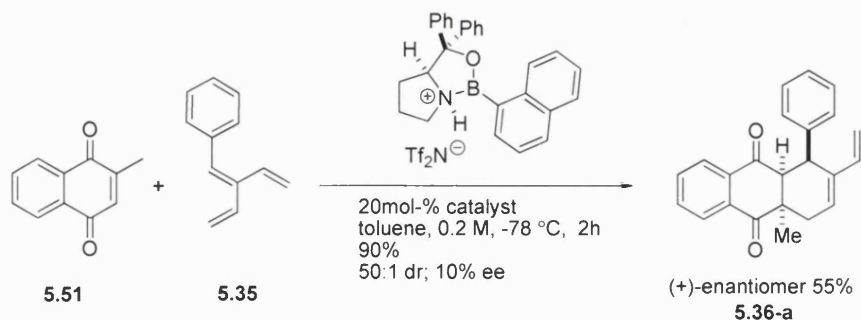
$[\alpha]_D^{25}$ (c = 2%, CHCl_3) = $+7^{\circ}$

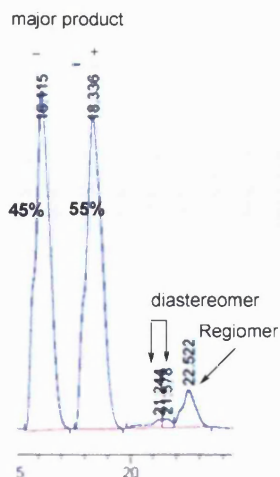
The absolute configuration was assigned by measurement of optical rotation and based on mechanistic prediction. (scheme 7.8).

A full characterisation of this compound has previously been reported.

The corresponding racemic product for the determination of enantioselectivity was prepared by using Boron trifluoride diethyletherate (1.5 eq.). ($\text{rt}_{\text{enantiomer 1}}$ = 16.4 min; $\text{rt}_{\text{enantiomer 2}}$ = 18.6 min).

Naphthalenyl-(S)-CBS-oxazaborolidinium-catalysed Diels-Alder (Table 7.1, entry 2)



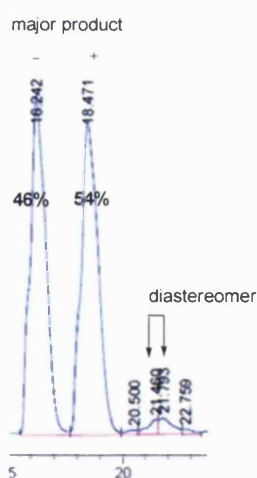
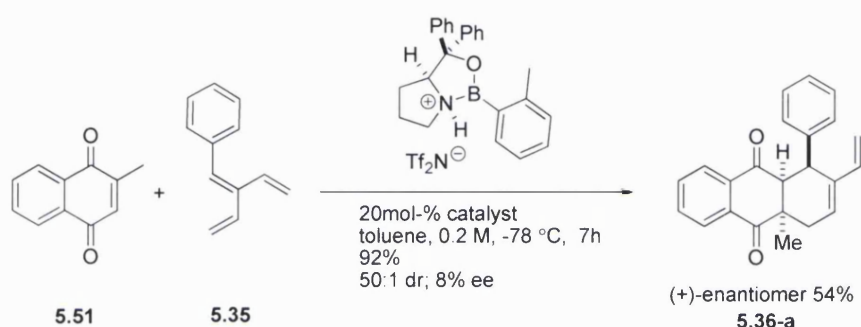


The product was obtained as a clear yellow solid (52.0 mg, 90%). Enantioselectivity and diastereoselectivity were determined by HPLC analysis using Chiral-IC (1% → 5% → 10% → 15% CH₂Cl₂ in Hexane), **5.36**, 50:1 dr; ee = 10% (rt_{minor enantiomer} = 16.1 min; rt_{major enantiomer} = 18.3 min).

$[\alpha]^{25}_D$ (c = 2%, CH₃Cl₃) = +3.2°

The absolute configuration was assigned by measurement of optical rotation and based on mechanistic prediction. (scheme 7.8).

Tolyl-(S)-CBS-oxazaborolidinium-catalysed^{H3} Diels-Alder (Table 7.1, entry 3)

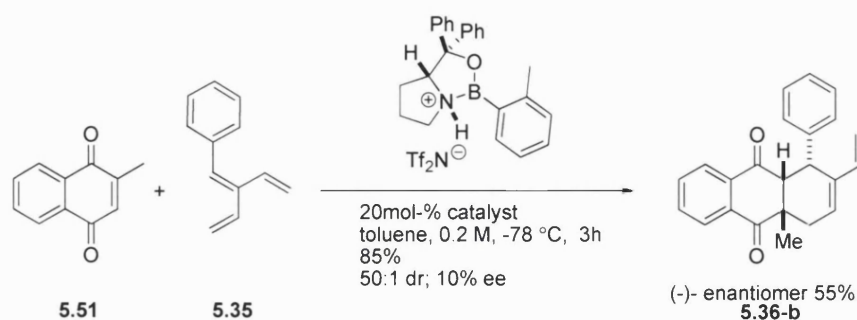


The product was obtained as a clear yellow solid (52mg, 92%). Enantioselectivity and diastereoselectivity were determined by HPLC analysis using Chiral-IC (1% → 5% → 10% → 15% CH₂Cl₂ in hexane), 50:1 dr; ee = 8% (rt_{minor enantiomer} = 16.2 min; rt_{major enantiomer} = 18.4 min).

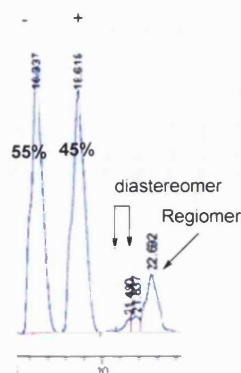
$[\alpha]^{25}_D$ (c = 2%, CHCl₃) = +10°

The absolute configuration was assigned by measurement of optical rotation and based on mechanistic prediction. (scheme 7.8).

Tolyl-(R)-CBS-oxazaborolidinium-catalysed^{H3} Diels-Alder (Table 7.1, entry 4)



major product

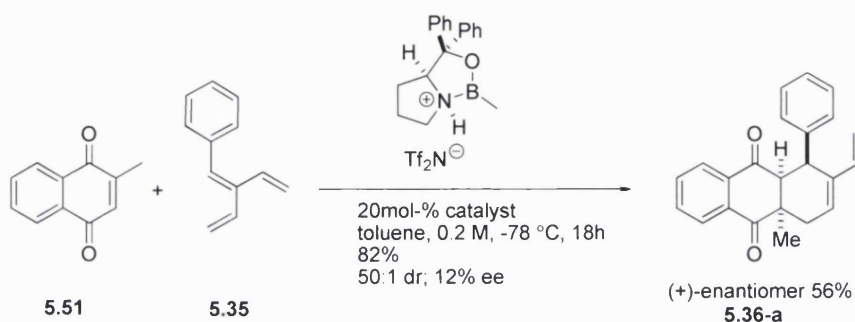


The product was obtained as a clear yellow solid (48mg, 85%). Enantioselectivity and diastereoselectivity were determined by HPLC analysis using Chiral-IC (1% → 5% → 10% → 15% CH₂Cl₂ in hexane), **5.36**, 50:1 dr; ee = 10% (rt_{minor enantiomer} = 16.3 min; rt_{major enantiomer} = 18.6 min).

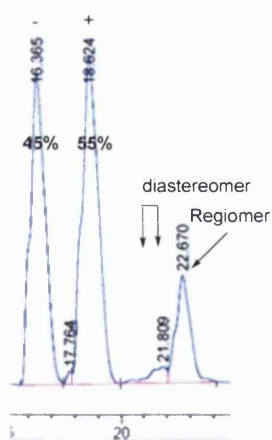
$[\alpha]^{25}_D$ (c = 2%, CHCl₃) = - 6°

The absolute configuration was assigned by measurement of optical rotation and based on mechanistic prediction. (Scheme 7.8).

Methyl-(S)-CBS-oxazaborolidinium-catalysed^{H3} Diels-Alder (Table 7.1, entry 5)



major product



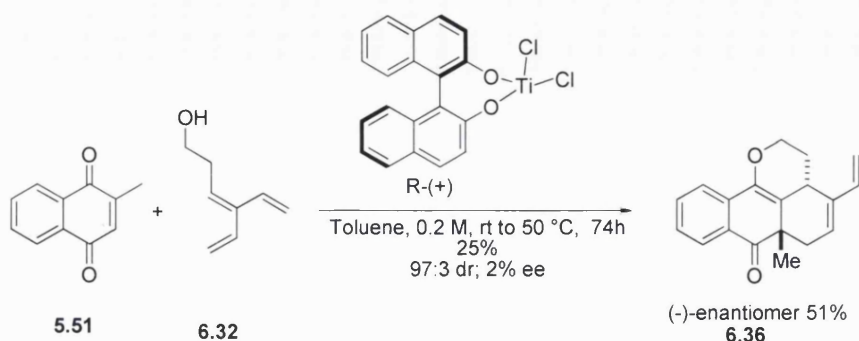
The product was obtained as a clear yellow solid (46.0 mg, 82%). Enantioselectivity and diastereoselectivity were determined by HPLC analysis using Chiral-IC (1% → 5% → 10% → 15% CH₂Cl₂ in hexane), **5.36**, 50:1 dr; ee = 12% (rt_{minor enantiomer} = 16.3 min; rt_{major enantiomer} = 18.6 min).

$[\alpha]^{25}_D$ (c = 2%, CHCl₃) = +10°

The absolute configuration was assigned by measurement of optical rotation and based on mechanistic prediction. (Scheme 7.8).

9.3.2 Asymmetric Diels-Alder using Binaphthol derivatives

chlorotitanium-(*R,R*)- 1,1'-binaphthoxide-catalysed Diels-Alder (Table 7.2, entry 1)

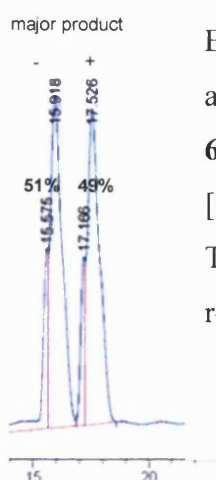


(3*aS*,6*aS*)-6*a*-methyl-4-vinyl-3,3*a*,3*a*1,6,6*a*,11*b*-hexahydrodibenzo[*de,h*]chromen-7(2*H*)-one (6.38)

Molecular sieves-free chlorotitanium-(*R,R*)- 1,1'-binaphthoxide (70 mg, 0.17 mmol) prepared following Mikami's protocol²²⁴ was dissolved in toluene (0.5 mL). 2-methyl-1,4-naphthoquinone (30.0 mg, 0.17 mmol) was added to the solution followed by 4-vinylhexa-3,5-dien-1-ol (55 μ L, 54 mg, 0.44 mmol) at 0 $^\circ$ C. The mixture was left to stir at room temperature for 2h then heated to 50 $^\circ$ C and stirred for a further 3 days. The reaction was stopped and cooled down to ambient temperature. The crude mixture was concentrated under vacuum and purified by column chromatography on silica gel (hexane: Et₂O 9:1), to afford the product as a clear yellow solid (13.0 mg, 25%).

A full characterisation of this compound has previously been reported.

The corresponding racemic product used for the determination of enantioselectivity was prepared by using Boron trifluoride diethyletherate (1.5 eq.). (*r*_t_{enantiomer 1} = 15.3 min; *r*_t_{enantiomer 2} = 16.9 min).

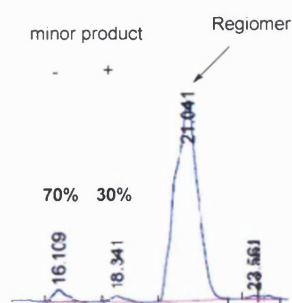
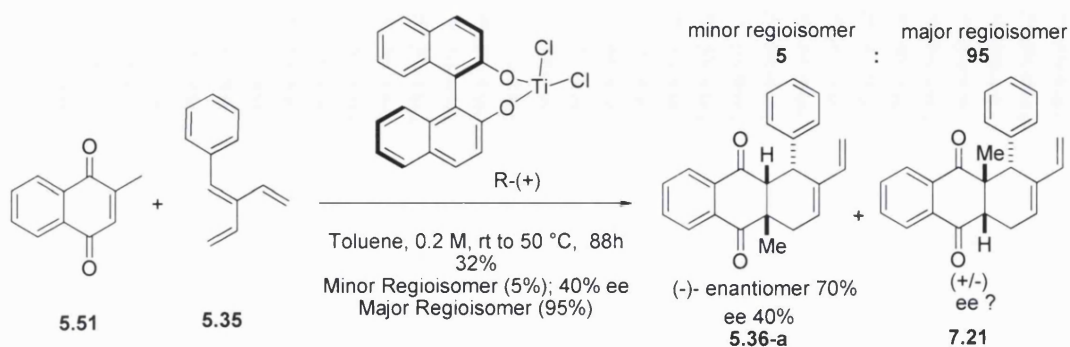


Enantioselectivity and diastereoselectivity were determined by HPLC analysis using Chiral-IC (1% \rightarrow 5% \rightarrow 10% \rightarrow 15% CH₂Cl₂ in hexane), **6.36**, ee = 2% (*r*_t_{minor enantiomer} = 15.9 min; *r*_t_{major enantiomer} = 17.5 min).

$[\alpha]_D^{25}$ (c = 2%, CHCl₃) = 0 $^\circ$

The absolute configuration was assigned by measurement of optical rotation and based on mechanistic prediction. (Scheme 7.9).

(1R,4aS,9aR)-4a-methyl-1-phenyl-2-vinyl-1,4,4a,9a-tetrahydroanthracene-9,10-dione (Table 7.2, entry 2)

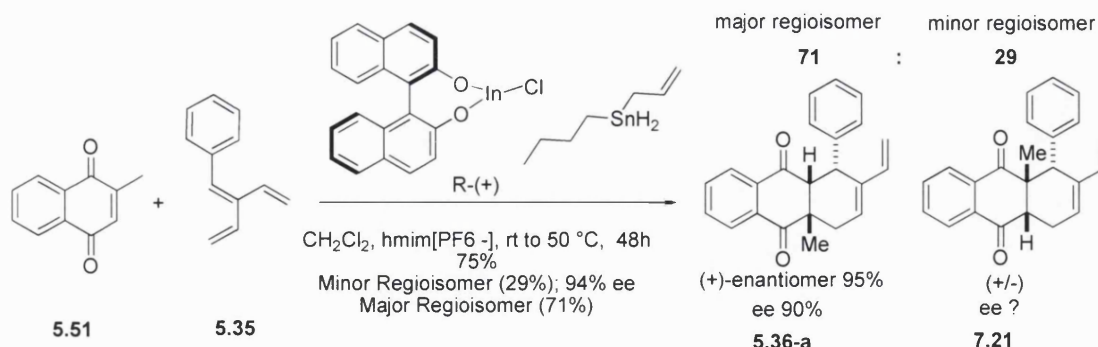


(2-vinylbuta-1,3-dienyl)benzene (71 μ L, 0.44 mmol, 2.5 eq.) was used following the previous method. Enantioselectivity and regioselectivity were determined by NMR and HPLC analysis using Chiral-IC (1% \rightarrow 5% \rightarrow 10% \rightarrow 15% CH_2Cl_2 in *n*-hexane); **minor regioisomer 5.36** (5%) ee = 40% ($\text{rt}_{\text{minor enantiomer}}$ = 18.3 min; $\text{rt}_{\text{major enantiomer}}$ = 16.1 min); **major regioisomer 7.21** (95%) (see below for characterisation).

$$[\alpha]^{25}_D (c = 2\%, \text{CHCl}_3) = +6^\circ$$

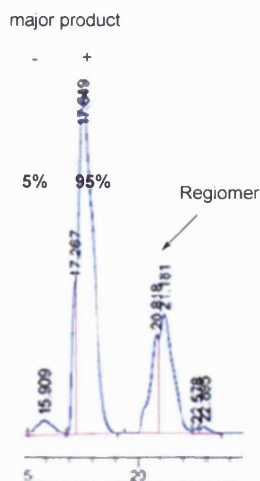
The absolute configuration was assigned by measurement of optical rotation and based on mechanistic prediction. (Scheme 7.9).

Indium(III) (*R*)-1,1'-binaphthyl-2,2'-bis(olate) chloride-catalysed Diels-Alder (Table 7.2, entry 3)



To a round-bottom flask equipped with a magnetic stirring bar was added InCl_3 (15.4 mg, 0.07 mmol, 0.2 eq.). The solid was azeotropically dried with anhydrous tetrahydrofuran twice (2 mL x 2) before the addition of 1 mL of CH_2Cl_2 . (*R*)-BINOL (22.0 mg, 0.07 mmol 0.2 eq.) and 4 Å molecular sieves (10.0 mg) were added, and the

mixture was stirred under nitrogen at room temperature for 2h. Allyltributylstannane (0.063 mL, 0.21 mmol, 0.6 eq.) was added to the resulting mixture and stirred for 10 min followed by addition of 0.7 mL of hmim[PF₆⁻] to the preformed catalyst. The organic solvent was removed *in vacuo*, and subsequent dropwise addition of (2-vinylbuta-1,3-dienyl)benzene (84 μ L, 0.52 mmol, 1.5 eq.) and 2-methyl-1,4-naphthoquinone (60.0 mg, 0.35 mmol, 1 eq.) was carried out. The reaction mixture was stirred at room temperature for 24 h then heated to 50 °C for another 24h. After the reaction was stopped, the mixture was extracted with ether (10 mL x 3). The combined organic extracts were washed with brine, dried over anhydrous MgSO₄, filtered and concentrated *in vacuo*. The residual crude product was purified by column chromatography on silica gel in (hexane: Et₂O 9:1) to afford the Diels-Alder adduct as a yellow solid (85 mg, 75% yield).



Enantioselectivity and regioselectivity were determined by NMR and HPLC analysis using Chiral-IC (1% \rightarrow 5% \rightarrow 10% \rightarrow 15% CH₂Cl₂ in *n*-hexane); **major regioisomer 5.36** (71%), ee = 90% (rt_{minor enantiomer} = 15.9 min; rt_{major enantiomer} = 17.6 min); **minor regioisomer 7.21** (29%) (See below for characterisation).

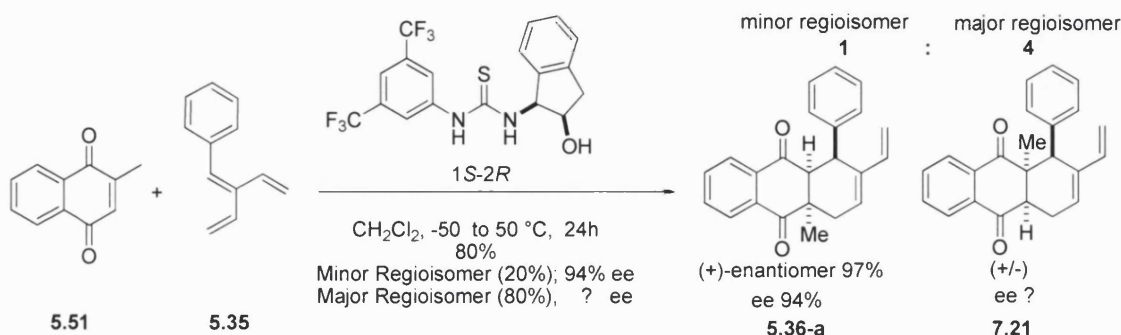
$[\alpha]_D^{25}$ (c = 0.5%, CHCl₃) = +12°

The absolute configuration was assigned by measurement of optical rotation and based on mechanistic prediction. (Scheme 7.9).

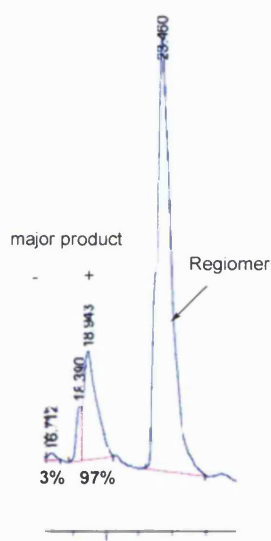
9.3.3 Asymmetric Diels-Alder using thiourea derivatives

Thiourea-catalysed Diels-Alder for the synthesis of (1R,4aS,9aR)-4a-methyl-1-phenyl-2-vinyl-1,4,4a,9a-tetrahydroanthraquinone.

- *1S,2R*-Thiourea (Table 7.3, entry 1)



To a round bottomed flask equipped with a magnetic stirring bar were sequentially added the 2-methyl-1,4-naphthoquinone (30.1 mg, 0.17 mmol), CH₂Cl₂ (1 mL) and catalyst 1-(3,5-bis(trifluoromethyl)phenyl)-3-((1*S*,2*R*)-2-hydroxy-2,3-dihydro-1*H*-inden-1-yl)thiourea (36.7 mg, 0.087 mmol), which was prepared following a method by Schreiner²³⁶. After cooling to -55 °C, a pre-cooled solution of (2-vinylbuta-1,3-dienyl)benzene (55 µL, 54 mg, 0.44 mmol) in CH₂Cl₂ (0.50 mL), was added dropwise. The mixture was stirred at the same temperature for 1h, and then allowed to warm up to room temperature and slowly heated up to 50 °C. After 24h, the mixture was allowed to cool down to room temperature then the mixture was concentrated *in vacuo*. The residual crude product was purified by column chromatography on silica gel in (hexane: Et₂O 9:1) to afford the Diels-Alder adduct as a yellow solid (85 mg, 80% yield).

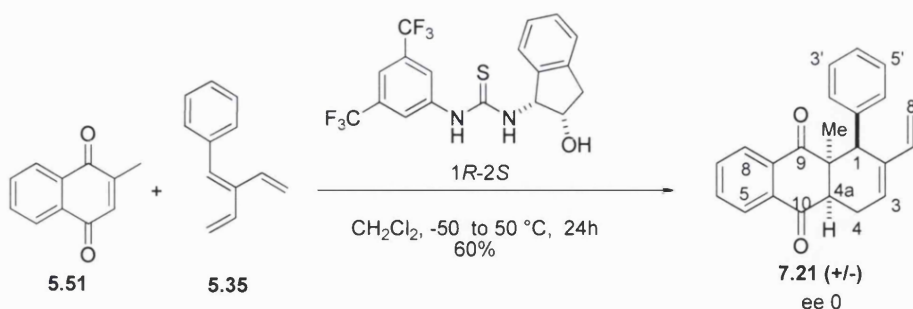


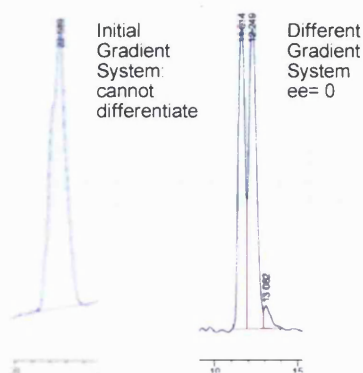
Enantioselectivity and regioselectivity were determined by NMR and HPLC analysis using Chiral-IC (1% → 5% → 10% → 15% CH₂Cl₂ in *n*-hexane); **major regioisomer 7.21** (71%); **minor regioisomer 5.36** (29%) ee = 94% (rt_{minor enantiomer} = 16.7 min; rt_{major enantiomer} = 18.9 min); (see below for characterisation)

$[\alpha]_D^{25}$ (c = 0.5%, CHCl₃) = +24°

The absolute configuration was assigned by measurement of optical rotation and based on mechanistic prediction. (*Scheme 7.10*).

- 1*R*,2*S*-Thiourea (*Table 7.3, entry 2*)

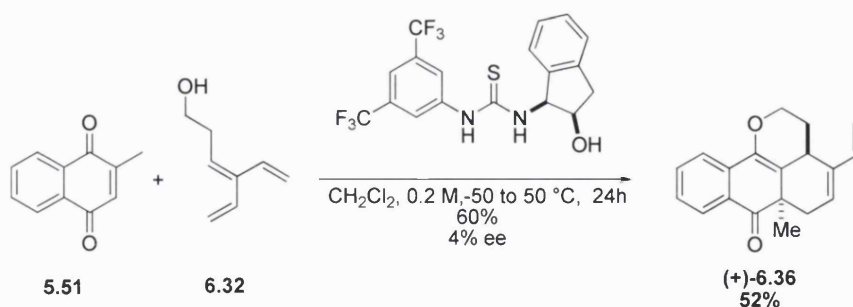


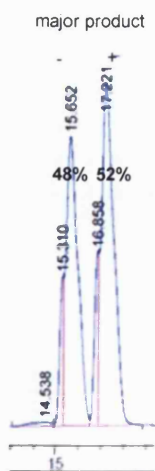


Enantioselectivity was determined by HPLC analysis using Chiral-IC (10% \rightarrow 11% \rightarrow 12% \rightarrow 13% CH_2Cl_2 in *n*-hexane); **7.21**, ee = 0 ($\text{rt}_{\text{enantiomer 1}}$ = 11.6 min; $\text{rt}_{\text{enantiomer 2}}$ = 12.5 min).
 $[\alpha]^{25}_D$ (c = 1.5%, CHCl_3) = 0°

7.21 was obtained as yellow solid; **Y** = 60%; **R_f** 0.35 (Silica gel, chloroform); **Mp** = 78.2 °C; **IR** 2924, 2361, 1591, 1492, 1455, 1281, 1250 cm^{-1} ; **¹H NMR** (400MHz, CDCl_3): δ 7.82 (1H, m, $\text{H}^{7/6}$), 7.60 (1H, m, $\text{H}^{7/6}$), 7.39 (2H, m, $\text{H}^{5,8}$), 6.82-6.67 (5H, m, $\text{H}^{2'-6'}$), 6.26 (1H, dd, J = 17.6, 10.9Hz, $\text{H}^{7'}$), 6.13 (1H, t, J = 4.0Hz, H^3), 4.77 (1H, d, J = 10.9Hz, $\text{H}^{8' \text{ cis}}$), 4.70 (1H, d, J = 17.6Hz, $\text{H}^{8' \text{ trans}}$), 3.77 (1H, s, H^1), 3.63 (1H, dd, J = 20.0, 4.4Hz, H^4), 2.97 (1H, d, J = 6.4Hz, H^{4a}), 2.43 (1H, dd, J = 19.8, 8.0Hz, H^4), 1.66 (3H, s, CH_3); **¹³C NMR** (100MHz, CDCl_3): δ 200.9 ($\text{C}^{9/10}$), 196.1 ($\text{C}^{9/10}$), 138.1 (C^3), 138.0 (0), 135.2 (0), 134.7 (0), 133.1 ($\text{C}^{5/8}$), 133.0 (0), 129.6 ($\text{C}^{2'-6'}$), 127.9 ($\text{C}^{2'-6'}$), 127.8 ($\text{C}^{7'}$), 126.9 ($\text{C}^{7/6}$), 126.6 ($\text{C}^{7/6}$), 125.4 (0), 112.8 ($\text{C}^{8'}$), 67.1 (C^1), 52.6, 50.1 (C^{4a}), 49.0 (C^{9a}), 24.5 (C^4), 21.1 (CH_3); **MS** (EI): m/z 329.38 ($\text{M}+\text{H}^+$) (100); **Purity** 95%.

Thiourea-catalysed Diels-Alder for the synthesis of (3aR,6aS)-6a-methyl-4-vinyl-3,3a,6,6a-tetrahydrodibenzo[de,h]chromen-7(2H)-one (Table 7.3, entry 3)





Enantioselectivity was determined by HPLC analysis using Chiral-IC (1% \rightarrow 5% \rightarrow 10% \rightarrow 15% CH_2Cl_2 in *n*-hexane); **6.36**, ee = 4% ($\text{rt}_{\text{minor enantiomer}} = 15.6 \text{ min}$; $\text{rt}_{\text{major enantiomer}} = 17.2 \text{ min}$);

$[\alpha]_D^{25}$ (c = 1%, CHCl_3) = +1°

The absolute configuration was assigned by measurement of optical rotation and based on mechanistic prediction. (*Scheme 7.10*).



CHAPTER 10

References

1. A. Loregian and G. Palu, *Journal of Cellular Physiology*, 2005, **204**, 750-762.
2. P. L. Toogood, *Journal of Medicinal Chemistry*, 2002, **45**, 1543-1558.
3. D. P. Ryan and J. M. Matthews, *Current Opinions in Structural Biology*, 2005, **15**, 441-446.
4. P. M. Fischer, *Drug Design Reviews - Online*, 2005, **2**, 179-207.
5. J. Gerrard, C. Hutton and M. Perugini, *Mini Reviews in Medicinal Chemistry*, 2007, **7**, 151-157.
6. G. Verdone and L. Walensky, *Clinical Cancer Research*, 2007, **13**, 7264.
7. D. Spring, *Chemical Society Reviews*, 2005, **34**, 472-482.
8. H. Arndt, *Angewandte Chemie International Edition*, 2006, **45**, 4552-4560.
9. T. A. Graham, C. Weaver, F. Mao, D. Kimelman and W. Xu, *Cell*, 2000, **103**, 885-896.
10. L. Tong, T. C. Warren, J. King, R. Betageri, J. Rose and S. Jakes, *Journal of Molecular Biology*, 1996, **256**, 601-610.
11. J. A. Wells and C. L. McClendon, *Nature*, 2007, **450**, 1001-1009.
12. O. Keskin, A. Gursoy, B. Ma and R. Nussinov, *Chemical Reviews*, 2008, **108**, 1225-1244.
13. S. W. Fesik, *Nature Reviews: Cancer*, 2005, **5**, 876-885.
14. S. Cory and J. M. Adams, *Nature Reviews: Cancer*, 2002, **2**, 647-656.
15. G. Lessene, P. E. Czabotar and P. M. Colman, *Nature Reviews: Drug Discovery*, 2008, **7**, 989-1000.
16. M. Vogler, D. Dinsdale, M. J. S. Dyer and G. M. Cohen, *Cell Death & Differentiation*, 2008, **16**, 360-367.
17. M. Bruncko, T. K. Oost, B. A. Belli, H. Ding, M. K. Joseph, A. Kunzer, D. Martineau, W. J. McClellan, M. Mitten, S.-C. Ng, P. M. Nimmer, T. Oltersdorf, C.-M. Park, A. M. Petros, A. R. Shoemaker, X. Song, X. Wang, M. D. Wendt, H. Zhang, S. W. Fesik, S. H. Rosenberg and S. W. Elmore, *Journal of Medicinal Chemistry*, 2007, **50**, 641-662.
18. A. Ventura, D. Kirsch, M. McLaughlin, D. Tuveson, J. Grimm, L. Lintault, J. Newman, E. Reczek, R. Weissleder and T. Jacks, *Nature*, 2007, **445**, 661-665.
19. C. Martins, L. Brown-Swigart and G. Evan, *Cell*, 2006, **127**, 1323-1334.

20. E. Rayburn, R. Zhang, J. He and H. Wang, *Current Cancer Drug Targets*, 2005, **5**, 27-41.
21. S. Shangary and S. Wang, *Annual Review of Pharmacology and Toxicology*, 2009, **49**, 223-241.
22. L. Vassilev, *Trends in Molecular Medicine*, 2007, **13**, 23-31.
23. C. Tovar, J. Rosinski, Z. Filipovic, B. Higgins, K. Kolinsky, H. Hilton, X. Zhao, B. Vu, W. Qing and K. Packman, *Science Signalling: Signal Transduction Knowledge Environment*, 2006, **103**, 1888.
24. S. Shangary, D. Qin, D. McEachern, M. Liu, R. Miller, S. Qiu, Z. Nikolovska-Coleska, K. Ding, G. Wang and J. Chen, *Proceedings of the National Academy of Sciences*, 2008, **105**, 3933.
25. L. T. Vassilev, B. T. Vu, B. Graves, D. Carvajal, F. Podlaski, Z. Filipovic, N. Kong, U. Kammlott, C. Lukacs, C. Klein, N. Fotouhi and E. A. Liu, *Science*, 2004, **303**, 844-848.
26. R. Mohammad, J. Wu, A. Azmi, A. Aboukameel, A. Sosin, S. Wu, D. Yang, S. Wang and A. Al-Katib, *Molecular Cancer*, 2009, **8**, 115.
27. D. C. Fry and L. T. Vassilev, *Journal of Molecular Medicine*, 2005, **83**, 955-963.
28. E. Sprinzak, Y. Altuvia and H. Margalit, *Proceedings of the National Academy of Sciences*, 2006, **103**, 14718.
29. K. Gunasekaran, C. Tsai, S. Kumar, D. Zanuy and R. Nussinov, *Trends in biochemical sciences*, 2003, **28**, 81-85.
30. O. Keskin and R. Nussinov, *Structure*, 2007, **15**, 341-354.
31. N. Burgoyne and R. Jackson, *Bioinformatics*, 2006, **22**, 1335.
32. C. Tsai, A. del Sol and R. Nussinov, *Journal of Molecular Biology*, 2008, **378**, 1-11.
33. N. Goodey and S. Benkovic, *Nature Chemical Biology*, 2008, **4**, 474-482.
34. T. Clackson and J. Wells, *Science*, 1995, **267**, 383-383.
35. I. Moreira, P. Fernandes and M. Ramos, *Proteins: Structure, Function, and Bioinformatics*, 2007, **68**, 803-812.
36. A. Shulman-Peleg, M. Shatsky, R. Nussinov and H. Wolfson, *BMC biology*, 2007, **5**, 43.
37. M. Landon, D. Lancia Jr, J. Yu, S. Thiel and S. Vajda, *Journal of Medicinal Chemistry*, 2007, **50**, 1231-1240.
38. G. Zinzalla and D. E. Thurston, *Future Medicinal Chemistry*, 2009, **1**, 65-93.

39. D. Gonzalez-Ruiz and H. Gohlke, *Current medicinal chemistry*, 2006, **13**, 2607-2625.
40. J. R. Proudfoot, R. Betageri, M. Cardozo, T. A. Gilmore, S. Glynn, E. R. Hickey, S. Jakes, A. Kabcenell, T. M. Kirrane, A. K. Tibolla, S. Lukas, U. R. Patel, R. Sharma, M. Yazdanian, N. Moss, P. L. Beaulieu, D. R. Cameron, J. M. Ferland, J. Gauthier, J. Gillard, V. Gorys, M. Poirier, J. Rancourt, D. Wernic and M. Llinas-Brunet, *Journal of Medicinal Chemistry*, 2001, **44**, 2421-2431.
41. A. M. Finch, A. K. Wong, N. J. Paczkowski, S. K. Wadi, D. J. Craik, D. P. Fairlie and S. M. Taylor, *Journal of Medicinal Chemistry*, 1999, **42**, 1965-1974.
42. D. Newman, *Journal of Medicinal Chemistry*, 2008, **51**, 2589-2599.
43. G. Rishton, *The American Journal of Cardiology*, 2008, **101**, 43-49.
44. A. Ganesan, *Current Opinions in Chemical Biology*, 2008, **12**, 306-317.
45. F. Koehn and G. Carter, *Nature Reviews Drug Discovery*, 2005, **4**, 206-220.
46. D. Morton, S. Leach, C. Cordier, S. Warriner and A. Nelson, *Angewandte Chemie*, 2009, **121**, 110-115.
47. A. Whitty and G. Kumaravel, *Nature Chemical Biology*, 2006, **2**, 112-118.
48. E. Park, D. Kong, R. Fisher, J. Cardellina, R. Shoemaker and G. Melillo, *Cell Cycle*, 2006, **5**, 1847-1853.
49. A. Kung, S. Zabudoff, D. France, S. Freedman, E. Tanner, A. Vieira, S. Cornell-Kennon, J. Lee, B. Wang and J. Wang, *Cancer Cell*, 2004, **6**, 33-43.
50. C. A. Lipinski, F. Lombardo, B. W. Dominy and P. J. Feeney, *Advanced Drug Delivery Reviews*, 1997, **23**, 3-25.
51. M.-Q. Zhang and B. Wilkinson, *Current Opinion in Biotechnology*, 2007, **18**, 478-488.
52. H. Yin and A. D. Hamilton, *Angewandte Chemie-International Edition*, 2005, **44**, 4130-4163.
53. A. R. Yeager, G. K. Min, J. A. Porco and S. E. Schaus, *Organic Letters*, 2006, **8**, 5065-5068.
54. T. M. Gierasch, Z. Shi and G. L. Verdine, *Organic Letters*, 2003, **5**, 621-624.
55. L. Soucek, M. Helmer-Citterich, A. Sacco, R. Jucker, G. Cesareni and S. Nasi, *Oncogene*, 1998, **17**, 2463.
56. X. Lu, P. Vogt, D. Boger and J. Lunec, *Oncology Reports*, 2008, **19**, 825.
57. A. Kiessling, B. Sperl, A. Hollis, D. Eick and T. Berg, *Chemical Biology*, 2006, **13**, 745-751.

58. M. Huang, Y. Cheng, C. Liu, S. Lin and H. Liu, *Experimental Hematology*, 2006, **34**, 1480-1489.
59. J. L. Wang, D. Liu, Z. J. Zhang, S. Shan, X. Han, S. M. Srinivasula, C. M. Croce, E. S. Alnemri and Z. Huang, *Proceedings of the National Academy of Sciences of the United States of America*, 2000, **97**, 7124-7129.
60. G. Lauri and P. A. Bartlett, *Journal of Computer-Aided Molecular Design*, 1994, **8**, 51-66.
61. L. Neckers, T. W. Schulte and E. Mimnaugh, *Investigational New Drugs*, 1999, **17**, 361-373.
62. B. J. Weigel, S. M. Blaney, J. M. Reid, S. L. Safgren, R. Bagatell, J. Kersey, J. P. Neglia, S. P. Ivy, A. M. Ingle, L. Whitesell, R. J. Gilbertson, M. Krailo, M. Ames and P. C. Adamson, *Clinical Cancer Research*, 2007, **13**, 1789-1793.
63. G. Chiosis, M. N. Timaul, B. Lucas, P. N. Munster, F. F. Zheng, L. Sepp-Lorenzino and N. Rosen, *Chemical Biology*, 2001, **8**, 289-299.
64. J. Chin, R. Grotzfeld, M. Fabian and A. Schepartz, *Bioorganic & Medicinal Chemistry Letters*, 2001, **11**, 1501-1505.
65. A. Gemperli, S. Rutledge, A. Maranda and A. Schepartz, *Journal of American Chemical Society*, 2005, **127**, 1596-1597.
66. J. Kritzer, R. Zutshi, M. Cheah, F. Ran, R. Webman, T. Wongjirad and A. Schepartz, *Chemical and Biological Chemistry*, 2006, **7**, 29-31.
67. H. Volkman, S. Rutledge and A. Schepartz, *Journal of the American Chemical Society*, 2005, **127**, 4649-4658.
68. C. E. Schafmeister, J. Po and G. L. Verdine, *Journal of the American Chemical Society*, 2000, **122**, 5891-5892.
69. F. Bernal, A. Tyler, S. Korsmeyer, L. Walensky and G. Verdine, *Journal of the American Chemical Society*, 2007, **129**, 2456-2457.
70. L. Walensky, K. Pitter, J. Morash, K. Oh, S. Barbuto, J. Fisher, E. Smith, G. Verdine and S. Korsmeyer, *Molecular cell*, 2006, **24**, 199-210.
71. J. Choi, J. Chen, S. Schreiber and J. Clardy, *Science*, 1996, **273**, 239-242.
72. T. Corson, N. Aberle and C. Crews, *ACS Chemical Biology*, 2008, **3**, 677-692.
73. J. M. Brown and W. R. Wilson, *Nature Reviews*, 2004, **4**, 437-447.
74. K. Lee, R. A. Roth and J. J. LaPres, *Pharmacology and Therapeutics*, 2007, **113**, 229-246.
75. J. I. Bardos and M. Ashcroft, *Bioessays*, 2004, **26**, 262-269.

76. R. J. Kewley, M. L. Whitelaw and A. Chapman-Smith, *The International Journal of Biochemistry & Cell Biology*, 2004, **36**, 189-204.
77. J. I. Bardos and M. Ashcroft, *Biochimica Et Biophysica Acta-Reviews on Cancer*, 2005, **1755**, 107-120.
78. P. B. Card, P. J. A. Erbel and K. H. Gardner, *Journal Molecular Biology*, 2005, **353**, 664-677.
79. J. S. Yang, L. Zhang, P. J. A. Erbel, K. H. Gardner, K. Ding, J. A. Garcia and R. K. Bruick, *Journal of Biological Chemistry*, 2005, **280**, 36047-36054.
80. R. K. Bruick and S. L. McKnight, *Science*, 2001, **294**, 1337-1340.
81. P. J. Ratcliffe, *The Journal of Clinical Investigation*, 2007, **117**, 862-865.
82. C. J. Hu, S. Iyer, A. Sataur, K. L. Covello, L. A. Chodosh and M. C. Simon, *Molecular and Cellular Biology*, 2006, **26**, 3514-3526.
83. C. J. Hu, L. Y. Wang, L. A. Chodosh, B. Keith and M. C. Simon, *Molecular and Cellular Biology*, 2003, **23**, 9361-9374.
84. C. P. Bracken, M. L. Whitelaw and D. J. Peet, *Cellular and Molecular Life Sciences*, 2003, **60**, 1376-1393.
85. J. W. Lee, S. H. Bae, J. W. Jeong, S. H. Kim and K. W. Kim, *Experimental & Molecular Medicine*, 2004, **36**, 1-12.
86. G. L. Semenza, *Nature Reviews*, 2003, **3**, 721-732.
87. K. S. Hewitson and C. J. Schofield, *Drug Discovery Today*, 2004, **9**, 704-711.
88. E. J. Park, D. Kong, R. Fisher, J. Cardellina, R. H. Shoemaker and G. Melillo, *Cell Cycle*, 2006, **5**, 1847-1853.
89. A. Giaccia, B. G. Siim and R. S. Johnson, *Nature Reviews Drug Discovery*, 2003, **2**, 803-811.
90. S. A. M. Paul, J. W. Simons and N. J. Mabweesh, *Journal of Cellular Physiology*, 2004, **200**, 20-30.
91. G. Melillo, *Molecular Cancer Research*, 2006, **4**, 601-605.
92. E. J. Yeo, Y. S. Chun and J. W. Park, *Biochemical Pharmacology*, 2004, **68**, 1061-1069.
93. X. Sun, J. R. Kanwar, E. Leung, K. Lehnert, D. Wang and G. W. Krissansen, *Gene therapy*, 2001, **8**, 638-645.
94. B. Onnis, A. Rapisarda and G. Melillo, *Journal of Cellular and Molecular Medicine*, 2009, **13**, 2780.
95. H. Chang, K. Shyu, C. Lee, S. Tsai, B. Wang, Y. Hsien Lee and S. Lin, *Biochemical and Biophysical Research Communications*, 2003, **302**, 95-100.

96. L. Greenberger, I. Horak, D. Filpula, P. Sapra, M. Westergaard, H. Frydenlund, C. Albæk, H. Schröder and H. Ørum, *Molecular Cancer Therapeutics*, 2008, **7**, 3598.
97. A. Rapisarda, J. Zalek, M. Hollingshead, T. Braunschweig, B. Uranchimeg, C. A. Bonomi, S. D. Borgel, J. P. Carter, S. M. Hewitt, R. H. Shoemaker and G. Melillo, *Cancer Research*, 2004, **64**, 6845-6848.
98. D. T. Jones and A. L. Harris, *Molecular Cancer Therapeutics*, 2006, **5**, 2193-2202.
99. H. Sun, Y. Liu, Y. Huang, S. Pan, D. Huang, J. Guh, F. Lee, S. Kuo and C. Teng, *Oncogene*, 2007, **26**, 3941-3951.
100. M. Koh, T. Spivak-Kroizman, S. Venturini, S. Welsh, R. Williams, D. Kirkpatrick and G. Powis, *Molecular Cancer Therapeutics*, 2008, **7**, 90.
101. E. W. Newcomb, M. A. Ali, T. Schnee, L. Lan, Y. Lukyanov, M. Fowkes, D. C. Miller and D. Zagzag, *Neuro-Oncology*, 2005, **7**, 225-235.
102. G. Melillo, *Cancer Metastasis Reviews*, 2007, **26**, 341-352.
103. L. Neckers, *Current Topics in Medicinal Chemistry*, 2006, **6**, 1163-1171.
104. X. Kong, Z. Lin, D. Liang, D. Fath, N. Sang and J. Caro, *Molecular and Cellular Biology*, 2006, **26**, 2019-2028.
105. K. Lee, D. Qian, S. Rey, H. Wei, J. Liu and G. Semenza, *Proceedings of the National Academy of Sciences*, 2009, **106**, 2353.
106. A. L. Kung, S. D. Zabudoff, D. S. France, S. J. Freedman, E. A. Tanner, A. Vieira, S. Cornell-Kennon, J. Lee, B. Wang, J. Wang, K. Memmert, H. U. Naegeli, F. Petersen, M. J. Eck, K. W. Bair, A. W. Wood and D. M. Livingston, *Cancer Cell*, 2004, **6**, 33-43.
107. E. J. Yeo, J. H. Ryu, Y. S. Cho, Y. S. Chun, L. E. Huang, M. S. Kim and J. W. Park, *Blood*, 2006, **107**, 916-923.
108. P. J. Erbel, P. B. Card, O. Karakuzu, R. K. Bruick and K. H. Gardner, *Proceedings of the National Academy of Sciences of the United States of America*, 2003, **100**, 15504-15509.
109. M. Calvani, A. Rapisarda, B. Uranchimeg, R. H. Shoemaker and G. Melillo, *Blood*, 2006, **107**, 2705-2712.
110. N. Pore, Z. Jiang, A. Gupta, G. Cerniglia, G. D. Kao and A. Maity, *Cancer Research*, 2006, **66**, 3197-3204.
111. K. C. Nicolaou, S. A. Snyder, T. Montagnon and G. Vassilikogiannakis, *Angewandte Chemie International Edition English*, 2002, **41**, 1668-1698.

112. L. Kürti and B. Czako, *Strategic Applications of Named Reactions in Organic Synthesis*, Elsevier Academic Press, 2005.
113. F. Fringuelli, L. Minuti, F. Pizzo and A. Taticchi, *Acta Chemica Scandinavica*, 1993, **47**, 255-255.
114. G. Bodwell and Z. Pi, *Tetrahedron Letters*, 1997, **38**, 309-312.
115. M. J. S. Dewar, S. Olivella and J. J. P. Stewart, *Journal of the American Chemical Society*, 1986, **108**.
116. K. N. Houk, Y. T. Lin and F. K. Brown, *Journal of the American Chemical Society*, 1986, **108**.
117. S. Oi, K. Kashiwagi, e. Terada, K. Ohuchi and Y. Inoue, *Tetrahedron Letters*, 1996, **37**.
118. A. Kraus and H. Sugimoto, *Tetrahedron Letters*, 1977.
119. P. Jones, W. S. Li, G. Pattenden and N. M. Thomson, *Tetrahedron Letters*, 1997, **52**.
120. E. C. Angell, F. Fringuelli, L. Minuti, F. Pizzo, A. Taticchi and E. Wenkert, *Journal of Organic Chemistry*, 1986, **51**.
121. S. D. Kahn, C. F. Pau, L. E. Overman and W. J. Hehre, *Journal of the American Chemical Society*, 1986, **108**.
122. F. Fringuelli and A. Taticchi, *The Diels-alder Reaction: Selected Practical Methods*, John Wiley & Sons, Ltd
2002.
123. I. Fleming, *Frontier orbitals and organic chemical reactions*, Wiley New York, 2006.
124. J. I. Garcia, J. A. Mayoral and L. Salvatella, *Accounts of chemical research*, 2000, **33**, 658-664.
125. L. F. Tietze, G. Brasche and K. M. Gericke, *Domino Reactions in Organic Synthesis*, Wiley-VCH, 2006.
126. O. Diels and K. Alder, *Justus Liebigs Annals of Chemistry*, 1931, **490**.
127. W. D. Fessner, C. Grund, R. Pinkos, J. P. Melder and P. H., *Tetrahedron Letters*, 1989, **30**, 3137-3140.
128. M. C. Carreno, J. L. Garcia Ruano and M. A. Tuledo, *Chemistry: A European Journal*, 2000, **6**, 288-291.
129. T. L. Ho, *Tandem Organic Reactions*, Wiley-Interscience, 1992.
130. C. Marchionni, P. Vogel and P. Roversi, *Tetrahedron Letters* 1996, **37**.
131. J. D. Winkler, *Chemical Reviews*, 1996, **96**, 167-176.

132. L. Tsuge, E. Wada and S. Kanemasa, *Chemical Letters*, 1983, **12**, 239-242.
133. T. M. Swarbrick, I. E. Marko and L. Kennard, *Tetrahedron Letters*, 1991, **32**, 2549-2552.
134. P. Yates and P. Eaton, *Journal of the American Chemical Society*, 1960, **82**, 4436-4437.
135. P. V. Alston and R. M. Ottenbrite, *Journal of Organic Chemistry*, 1975, **40**, 1111-1116.
136. S. Kobayashi, T. Busujima and S. Nagayama, *Chemistry -A European Journal*, 2000, **6**, 3491-3494.
137. G. P. Steel, *Journal of the Chemical Society: Perkin Transactions 1*, 2001, **1**, 2727-2751.
138. S. Kobayashi, *European Journal of Organic Chemistry*, 1999, 15-27.
139. J. A. McCleverty and T. J. Meyer, in *Comprehensive Coordination Chemistry II*, ed. M. D. Ward, Elsevier Pergamon, 2004, vol. 9.
140. S. Kobayashi, I. Hachiya, M. Araki and I. H., *Tetrahedron Letters*, 1993, **34**, 3755-3758.
141. K. Maruoka, M. Oishi and H. Yamamoto, *Synlett*, 1993, 683-683.
142. W. Ellis and W. Odenkirk, *Chemical Communications*, 1998, **1998**, 1311-1312.
143. T. Hollis, N. Robinson and B. Bosnich, *Organometallics*, 1992, **11**, 2745-2748.
144. G. Smith and F. Notheisz, *Heterogeneous Catalysis in Organic Chemistry*, Academic Press, 1999.
145. A. K. Saha and M. M. Hossain, *Tetrahedron Letters*, 1993, **34**, 3833-3836.
146. O. Diels and K. Alder, *Justus Liebig's Annalen der Chemie*, 1928, **460**, 98-122.
147. R. Woodward, F. Sondheimer, D. Taub, K. Heusler and W. McLamore, *Journal of the American Chemical Society*, 1952, **74**, 4223-4251.
148. R. Woodward, F. Sondheimer, D. Taub, K. Heusler and W. McLamore, *Journal of the American Chemical Society*, 1952, **74**, 4223-4251.
149. Y. Kishi, M. Aratani, T. Fukuyama, F. Nakatsubo and T. Goto, *Journal of the American Chemical Society*, 1972, **94**, 9217.
150. S. Danishefsky, M. Hirama, N. Fritsch and J. Clardy, *Journal of the American Chemical Society*, 1979, **101**, 7013-7018.
151. E. Corey, R. Danheiser, S. Chandrasekaran, P. Siret, G. Keck and J. Gras, *Journal of the American Chemical Society*, 1978, **100**, 8031-8034.
152. H. Hopf, *Angewandte Chemie-International Edition*, 2001, **40**, 705-706.
153. H. Hopf, *Nature*, 2009, **460**, 183-184.

154. H. Hopf, *Angewandte Chemie International Edition in English*, 1984, **23**, 948-960.
155. H. Hopf, *Angewandte Chemie-International Edition*, 2001, **40**, 705-706.
156. T. A. Bradford, A. D. Payne, A. C. Willis, M. N. Paddon-Row and M. S. Sherburn, *The Journal of Organic Chemistry*, 2010, **75**, 491-494.
157. A. T. Blomquist and J. A. Verdol, *Journal of the American Chemical Society*, 1955, **77**, 81-83.
158. W. J. Bailey, C. H. Cunov and L. Nicholas, *Journal of the American Chemical Society*, 1955, **77**, 2787-2790.
159. A. T. Blomquist and J. A. Verdol, *Journal of the American Chemical Society*, 1955, **77**, 1806-1809.
160. W. J. Bailey and J. Economy, *Journal of the American Chemical Society*, 1955, **77**, 1133-1136.
161. H. Martin, M. Eckert-Maksi and B. Mayer, *Angewandte Chemie International Edition in English*, 1980, **19**, 807-809.
162. V. M. Vdovin, E. S. Finkel'shtein, A. V. Shelkov and M. S. Yatsenko, *Russian Chemical Bulletin*, 1986, **35**, 2364-2366.
163. J. Cadogan, S. CRADOCK, S. GILLAM and I. GOSNEY, *Journal of the Chemical Society. Chemical communications*, 1991, 114-115.
164. S. Fielder, D. Rowan and M. Sherburn, *Angewandte Chemie-International Edition*, 2000, **39**, 4331-4332.
165. H. Priebe and H. Hopf, *Angewandte Chemie International Edition in English*, 1982, **21**, 286-287.
166. H. Bader, H. Hopf and H. Jäger, *Chemische Berichte*, 1989, **122**.
167. T. Bradford, A. Payne, A. Willis, M. Paddon-Row and M. Sherburn, *Org. Lett.*, 2007, **9**, 4861-4864.
168. O. Tsuge, S. Kanemasa, H. Sakoh and E. Wada, *Chemistry Letters*, 1984, **13**, 277-278.
169. S. Woo, N. Squires and A. G. Fallis, *Organic Letters*, 1999, **1**, 573-576.
170. T. Chan, C. Li, M. Lee and Z. Wei, *Canadian Journal of Chemistry*, 1994, **72**, 1181-1192.
171. A. G. Fallis, P. Forgione, S. Woo, S. Legoupy, S. Py, C. Harwig and T. Rietveld, *Polyhedron*, 2000, **19**, 533-535.
172. O. Kwon, S. Park and S. Schreiber, *Journal of American Chemical Society*, 2002, **124**, 13402-13404.

173. N. Miller, A. Willis, M. Paddon-Row and M. Sherburn, *Angewandte Chemie-International Edition*, 2007, **46**, 937-940.
174. K. Lee, H. Zhang, D. Qian, S. Rey, J. Liu and G. Semenza, *Proceedings of the National Academy of Sciences*, 2009, **106**, 17910.
175. M. G. Charest, D. R. Siegel and A. G. Myers, *Journal of Americal Chemical Society*, 2005, **127**, 8292-8293.
176. C. Kormann, F. W. Heinemann and P. Gmeiner, *Tetrahedron*, 2006, **62**, 6899-6908.
177. T. Mizawa, K. Takenaka and T. Shiomi, *Journal of Polymer Science: Part A: Polymer Chemistry*, 1999, **37**, 3464-3472.
178. C. Prévost, P. Miginiac and L. Miginiac-Groizeleau, *Bulletin de la Societe Chimique de France*, 1964, 2485-2492.
179. C. Prévost, P. Miginiac and L. Miginiac-Groizeleau, *Bulletin de la Societe Chimique de France*, 1964, 2485-2492.
180. L. A. Paquette, G. D. Bennett, A. Chhatrwalla and M. B. Isaac, *Journal of Organic Chemistry*, 1997, **62**, 3370-3374.
181. M. Isaac and T.-H. Chan, *Tetrahedron Letters*, 1995, **36**, 8957-8960.
182. R. Arhart and J. Martin, *Journal of the American Chemical Society*, 1972, **94**, 5003-5010.
183. A. G. Myers, P. C. Hogan, A. R. Hurd and S. D. Goldberg, *Angewandte Chemie (International edition)*, 2002, **41**, 1062-1067.
184. K. Nicolaou, D. Longbottom, S. Snyder, A. Nalbanadian and X. Huang, *Angewandte Chemie International Edition*, 2002, **41**, 3866-3870.
185. N. S. Mani, C. M. Mapes, J. Wu, X. Deng and T. K. Jones, *The Journal of Organic Chemistry*, 2006, **71**, 5039-5042.
186. P. Wuts and T. Greene, *Greene's protective groups in organic synthesis*, John Wiley and Sons, 2007.
187. L. Khosrow, R. J. Gerzina, C. M. Flajnik, C. M. Geric and A. M. Dombroski, *Helvetica Chimica Acta*, 1987, **70**, 607-611.
188. S. Yamazaki, *Tetrahedron Letters*, 2001, **42**, 3355-3357.
189. H. Y. Song, M. H. Ngai, Z. Y. Song, P. A. MacAry, J. Hobley and M. J. Lear, *Organic & Biomolecular Chemistry*, 2009, **7**, 3400-3406.
190. R. Bennes, M. S. Babiloni, W. Hayes and D. Philp, *Tetrahedron Letters*, 2001, **42**, 2377-2380.
191. M. Jung and J. Lowe, *The Journal of Organic Chemistry*, 1977, **42**, 2371-2373.

192. K. Kim, J. Reibenspies and G. Sulikowski, *The Journal of Organic Chemistry*, 1992, **57**, 5557-5559.
193. R. K. Boeckman, T. M. Dolak and K. O. Culos, *Journal of the American Chemical Society*, 1978, **100**, 7098-7100.
194. T. R. Kelly, J. W. Gillard, R. N. Goerner and J. M. Lyding, *Journal of the American Chemical Society*, 1977, **99**, 5513-5514.
195. J. T. Kuethe and D. L. Comins, *Tetrahedron Letters*, 2003, **44**, 4179-4182.
196. P. Nebois, R. Barret and H. Fillion, *Tetrahedron Letters*, 1990, **31**, 2569-2572.
197. Z. Stojanac, R. A. Dickinson, N. Stojanac, R. J. Woznow and Z. Valenta, *Canadian Journal of Chemistry*, 1975, **53**, 616-618.
198. T. R. Kelly, J. W. Gillard, R. N. Goerner and J. M. Lyding, *Journal of the American Chemical Society*, 1975, **99**, 5513-5514.
199. B. M. Trost, J. Ippen and W. C. Vladuchick, *Journal of the American Chemical Society*, 1977, **99**, 8116-8118.
200. J. Motoyoshiya, T. Kameda, M. Asari, M. Miyamoto, S. Narita, H. Aoyama and S. Hayashi, *Journal of the Chemical Society, Perkin Transactions 2: Physical Organic Chemistry*, 1997, **9**, 1845-1850.
201. K. C. Nicolaou and S. A. Snyder, *Classics in Total Synthesis II: More Targets, Strategies, Methods*, Wiley-VCH Verlag GmbH, 2003.
202. B. Jiang, E. Rue, G. Wang, R. Roe and G. Semenza, *Journal of Biological Chemistry*, 1996, **271**, 17771.
203. G. L. Wang and G. L. Semenza, *Proceedings of the National Academy of Science USA*, 1993, **90**, 4304-4308.
204. G. Melillo, *Methods in enzymology*, 2007, **435**, 385.
205. A. Rapisarda, B. Uranchimeg, D. A. Scudiero, M. Selby, E. A. Sausville, R. H. Shoemaker and G. Melillo, *Cancer research*, 2002, **62**, 4316-4324.
206. S. Kaluz, M. Kaluzova and E. Stanbridge, *Molecular and Cellular Biology*, 2006, **26**, 5895.
207. G. Zinzalla and D. E. Thurston, *Future Medicinal Chemistry*, 2009, **1**, 65-93.
208. Y. Bendiabdellah, G. Zinzalla, U. Badarch, K. S. Nahar, D. Antonow, K. M. Rahman, R. H. Shoemaker, G. Melillo and D. E. Thurston, *Proceeding of AACR 100th Meeting* 2009, 4646.
209. W. Greenlee and R. Woodward, *Journal of the American Chemical Society*, 1976, **98**, 6075-6076.

210. M. S. Souweha, A. Arab, M. A. Simon and A. G. Fallis, *Organic Letters*, 2007, **9**, 615-618.
211. K. C. Nicolaou, L. Yee Hwee and B. Jochen, *Angewandte Chemie International Edition*, 2009, **48**, 3444-3448.
212. P. A. Grieco, P. Galatsis and R. F. Spohn, *Tetrahedron*, 1986, **42**, 2847-2853.
213. The reactions were monitored by LC-MS and TLC on silica gel.
214. The structures and relative stereochemistries were unambiguously determined by 1D and 2D NMR experiments (including NOESY). Full characterisation of the novel skeletons with their NMR data and spectra are included in the Supporting Information.
215. A. J. Hutt, in *Introduction to the Principles of Drug Design and Action*, eds. H. J. Smith and H. Williams, CRC PRESS, 2006.
216. R. B. Woodward, F. E. Bader, H. Bickel, A. J. Frey and R. W. Kierstead, *Tetrahedron*, 1958, **2**, 1-57.
217. S. I. Sallay, *Journal of the American Chemical Society*, 1967, **89**, 6762-6763.
218. W. R. Roush, *Journal of the American Chemical Society*, 1978, **100**, 3599-3601.
219. E. J. Corey, R. L. Danheiser, S. Chandrasekaran, P. Siret, G. E. Keck and J. L. Gras, *Journal of the American Chemical Society*, 1978, **100**, 8031-8034.
220. W. C. Still and M.-Y. Tsai, *Journal of the American Chemical Society*, 1980, **102**, 3654-3655.
221. J. D. White, N. S. Cutshall, T.-S. Kim and H. Shin, *Journal of the American Chemical Society*, 1995, **117**, 9780-9781.
222. M. Breuning and E. J. Corey, *Organic Letters*, 2001, **3**, 1559-1562.
223. M. Gaunt, C. Johansson, A. McNally and N. Vo, *Drug Discovery Today*, 2007, **12**, 8-27.
224. K. Mikami, Y. Motoyama and M. Terada, *Journal of the American Chemical Society*, 1994, **116**, 2812-2820.
225. E. Jarvo, B. Lawrence and E. Jacobsen, *Angewandte Chemie International Edition*, 2005, **44**, 6043-6046.
226. E. Corey, T. Shibata and T. Lee, *Journal of the American Chemical Society*, 2002, **124**, 3808-3809.
227. E. Corey, *J. Am. Chem. Soc.*, 2003, **125**, 6388-6390.
228. D. Liu, E. Canales and E. Corey, *Journal of the American Chemical Society*, 2007, **129**, 1498-1499.

229. Y. Hayashi, J. J. Rohde and E. J. Corey, *Journal of the American Chemical Society*, 1996, **118**, 5502-5503.
230. G. Zhou and E. Corey, *Journal of the American Chemical Society*, 2004, **126**, 4800-4802.
231. K. Mikami, M. Terada, Y. Motoyama and T. Nakai, *Tetrahedron: Asymmetry*, 1991, **2**, 643-646.
232. J. White and Y. Choi, *Helvetica Chimica Acta*, 2002, **85**, 4306-4327.
233. C. Gioia, A. Hauville, L. Bernardi, F. Fini and A. Ricci, *Angewandte Chemie International Edition*, 2008, **47**, 9236-9239.
234. X. Yu and W. Wang, *Chemistry-An Asian Journal*, 2008, **3**, 516-532.
235. A. Doyle and E. Jacobsen, *Chemical Reviews*, 2007, **107**, 5713-5743.
236. M. Kotke and P. Schreiner, *Tetrahedron*, 2006, **62**, 434-439.
237. Alexander G. Dossetter, Timothy F. Jamison and Eric N. Jacobsen, *Angewandte Chemie*, 1999, **111**, 2549-2552.
238. K. Gademann, D. E. Chavez and E. N. Jacobsen, *Angewandte Chemie International Edition*, 2002, **41**, 3059-3061.
239. A. Boezio, E. Jarvo, B. Lawrence and E. Jacobsen, *Angewandte Chemie International Edition*, 2005, **44**, 6046-6050.
240. Q. Chu, W. Zhang and D. Curran, *Tetrahedron Letters*, 2006, **47**, 9287-9290.
241. S. Kobayashi, H. Ishitani, M. Araki and I. Hachiya, *Tetrahedron Letters*, 1994, **35**, 6325-6328.
242. M. Carreno, S. Garcia-Cerrada, A. Urbano and C. Di Vitta, *Journal of Organic Chemistry*, 2000, **65**, 4355-4363.
243. F. Fu, Y. Teo and T. Loh, *Organic Letters*, 2006, **8**, 5999-6001.
244. D. Ward and J. Shen, *Organic Letters*, 2007, **9**, 2843-2846.
245. M. Linder and T. Brinck, *Organic & Biomolecular Chemistry*, 2009, **7**, 1304-1311.
246. B. Siddiqui, F. Sattar, F. Ahmad and S. Begum, *Natural Product Research*, 2008, **22**, 1128-1136.
247. H. Guinaudeau, M. Lebouf and A. Cavé, *Journal of Natural Products*, 1994, **57**, 1033-1135.
248. B. Yu, L. Meng, J. Chen, T. Zhou, K. Cheng, J. Ding and G. Qin, *Journal of Natural Products*, 2001, **64**, 968-970.
249. L. Killmer, F. Vogt, A. Freyer, M. Menachery and C. Adelman, *Journal of Natural Products*, 2003, **66**, 115-118.

250. E. Sobarzo-Sánchez, B. Cassels and L. Castedo, *Magnetic Resonance in Chemistry*, 2003, **41**, 545-548.
251. T. R. Kelly, Y. Fu, J. T. Sieglén and H. De Silva, *Organic Letters*, 2000, **2**, 2351-2352.
252. C. Commandeur, C. Chalumeau, J. Dessolin and M. Laguerre, *European Journal of Organic Chemistry*, 2007, **2007**, 3045-3052.
253. L. S. Liebeskind, K. L. Granberg and J. Zhang, *The Journal of Organic Chemistry*, 2002, **57**, 4345-4352.
254. M. Ito, L. W. Koo, A. Himizu, C. Kobayashi, A. Sakaguchi and T. Ikariya, *Angew Chem Int Edit*, 2009, **48**, 1324-1327.
255. E. Abraham, S. G. Davies, N. L. Millican, R. L. Nicholson, P. M. Roberts and A. D. Smith, *Org Biomol Chem*, 2008, **6**, 1655-1664.
256. A. Negro, M. J. Garzon, J. F. Martin, A. Elmarini, M. L. Roumestant and R. Lazaro, *Synthetic Commun*, 1991, **21**, 359-369.
257. C. Dose and O. Seitz, *Bioorg Med Chem*, 2008, **16**, 65-77.
258. B. DeBoef, W. R. Counts and S. R. Gilbertson, *The Journal of Organic Chemistry*, 2007, **72**, 799-804.
259. T. Lee and E. Corey, *Journal of the American Chemical Society*, 2002, **124**, 9992-9993.
260. F. Fu, Y. Teo and T. Loh, *Organic Letters*, 2006, **8**, 5999-6001.
261. D. L. Comins, Y. M. Zhang and X. L. Zheng, *Chemical Communications*, 1998, 2509-2510.
262. U. Jacquemard, V. Beneteau, M. Lefoix, S. Routier, J. Y. Merour and G. Coudert, *Tetrahedron*, 2004, **60**, 10039-10047.
263. Q. Dong, C. E. Anderson and M. A. Ciufolini, *Tetrahedron Letters*, 1995, **36**, 5681-5682.
264. A. M. Felix, *Journal of Organic Chemistry*, 1974, **39**, 1427-1429.



CHAPTER 11

Appendix

Contents:

11.1	Enantiomeric Resolution of YB036	265
11.2	U251-HRE 3 rd generation screening assay	271
11.3	Materials and Methods describing the biological screening	272
11.4	Selected NMR spectra	279

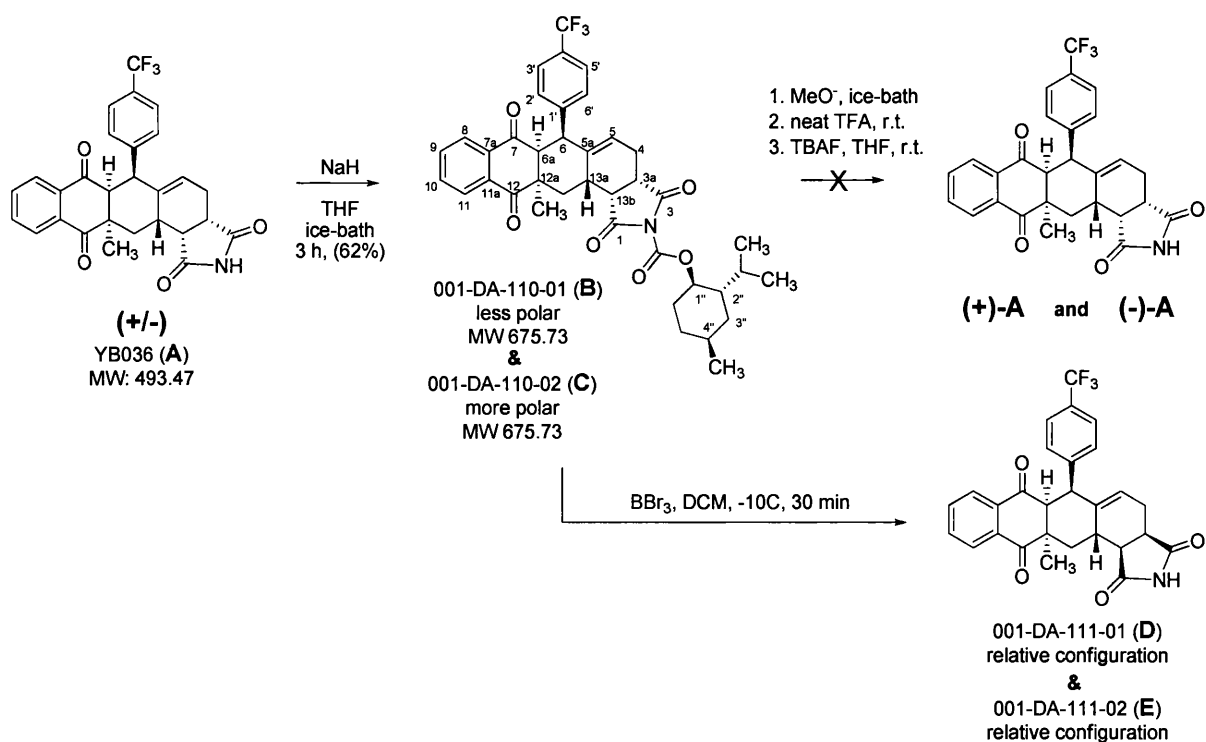
11.1 Enantiomeric resolution of YB036

Background

The aim of this project is to obtain enantiomerically pure YB-tetracycline compounds by means of chiral derivatization. These compounds have shown to down-regulate the expression of HIF-1 α in cells artificially subjected to hypoxic conditions, which is suggestive of their potential antitumor properties. However, YB-tetracycline compounds are currently being obtained as a mixture of enantiomers and it is crucial that these isomers are produced separately in order to progress to clinical use.

Results/Discussion

The synthetic strategy devised for this project involves the derivatization of YB036 (**A**), a hit compound selected by HTS assays. The chiral derivatizing agent chosen for this study was (1R)-(-)-menthyl chloroformate due to its inexpensiveness. This reagent was coupled to **A** in the presence of sodium hydride through its succinimidic nitrogen. This reaction proceeded smoothly in 62% yield to give the diastereoisomeric carbamate products **B** and **C**, which were then separated by column chromatography. These products (**B** and **C**) were scaled-up (40 mg of each diastereoisomer) in order to obtain sufficient amounts of material for spectroscopic analysis and final nitrogen deprotection. At this point extensive NOESY analysis was carried out to determine the absolute configuration of the tetracycline part of these molecules. However, no NOE was observed between the reference menthyl protons and the tetracycline protons in **B** and **C**. This lack of transmagnetization between these two sets of spin systems within the same molecule was not foreseen and may represent a problem to determine the absolute configuration of the final compounds.



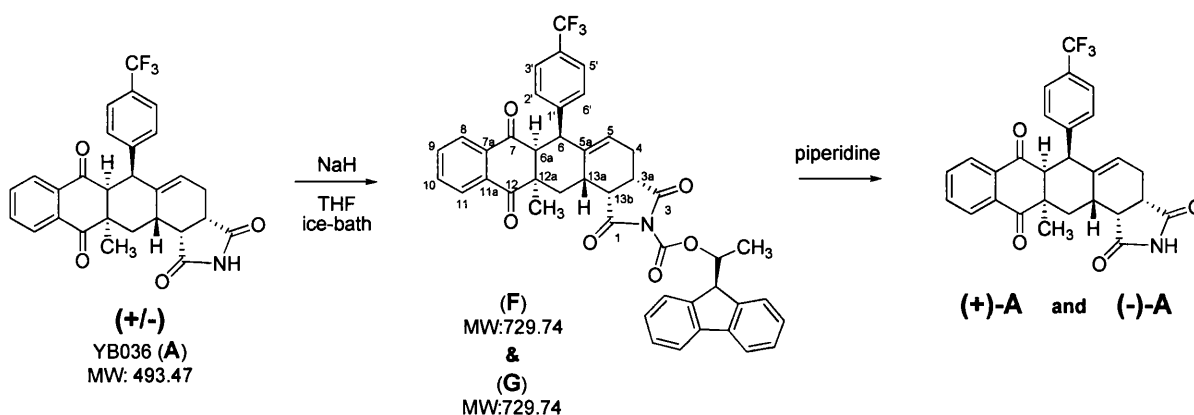
Although the absolute configuration of **B** and **C** was not possible the enantiomeric resolution of **A** was pursued via removal of the (R)-menthyl unit. The literature of protecting-groups provides a substantial amount of methodologies to cleave carbamate groups. However, there is only one example²⁶¹ in which the carbamate group had been removed from a succinimidic group. This method employed sodium methoxide and was unsuccessful for **B** and **C**. Several other reagents and conditions were then investigated to remove the (R)-menthyl moiety including neat TFA, TBAF,²⁶² 10% Cd/Pb couple²⁶³ and BBr₃.²⁶⁴ With the exception of 10% Cd/Pb couple and BBr₃, all other reagents failed to remove (R)-menthyl. Treatment with 10% Cd/Pb couple led to degradation. In the case of BBr₃, TLC clearly showed that this reagent induced structural changes elsewhere in the tetracycline ring systems of both **B** and **C** upon cleavage, as indicated by the presence of two products with *R_f* different of **A**. Extensive NMR investigation of one of this products (**D**) has indicated that epimerization has occurred in the succinimidic ring. It is very likely that this has occurred due to increased acidity of protons 3a and 13b upon complexation of their vicinal carbonyls with BBr₃ (enolization). The relative stereochemistry assigned for the succinimidic moiety of **D** is consistent with two products for this reaction.

Conclusions

The separation of the two diastereoisomers **B** and **C** was accomplished but their absolute configuration was not determined. Removal of the (R)-menthyl derivatizing moiety seems to be resistant to traditional cleavage methods described in literature. When deprotection was achieved using BBr_3 epimerization occurred.

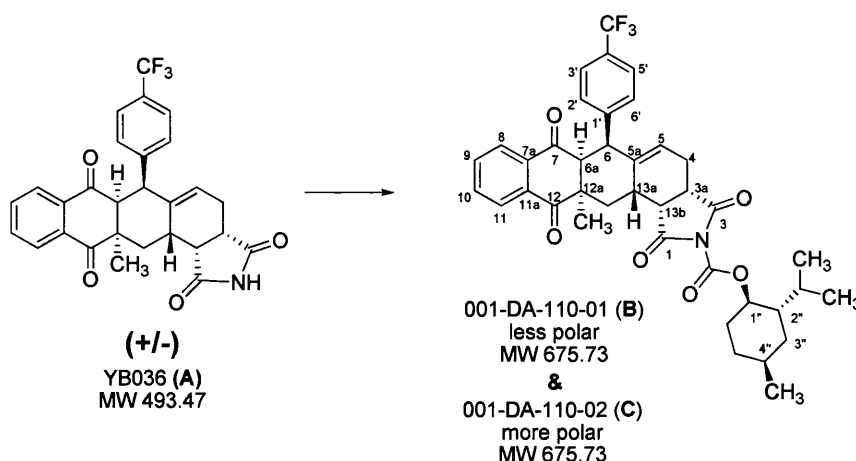
Future work

(-)-1-(9-Fluorenyl)ethyl chloroformate will be used as chiral derivatizing agent. This chiral moiety could then be coupled to YB036 (**A**) under the same conditions (NaH) and offers the possibility of mild deprotection conditions employing piperidine e/or pyrrolidine. However, the efficient diastereoisomeric separation encountered for **B** and **C** may not result the same for **F** and **G**. In addition, the stock batch of YB036 (**A**) is currently at ~50 mg and may need to be re-synthesised.



Experimental

Synthesis of (3a*S*,6*S*,6a*S*,12a*R*,13a*S*,13b*R*)-((1*R*,2*S*,4*S*)-2-isopropyl-4-methylcyclohexyl) 12a-methyl-1,3,7,12-tetraoxo-6-(4-(trifluoromethyl)phenyl)-3a,4,6,6a,7,12,12a,13,13a,13b-decahydro-1*H*-anthra[2,3-*e*]isoindole-2(3*H*)-carboxylate



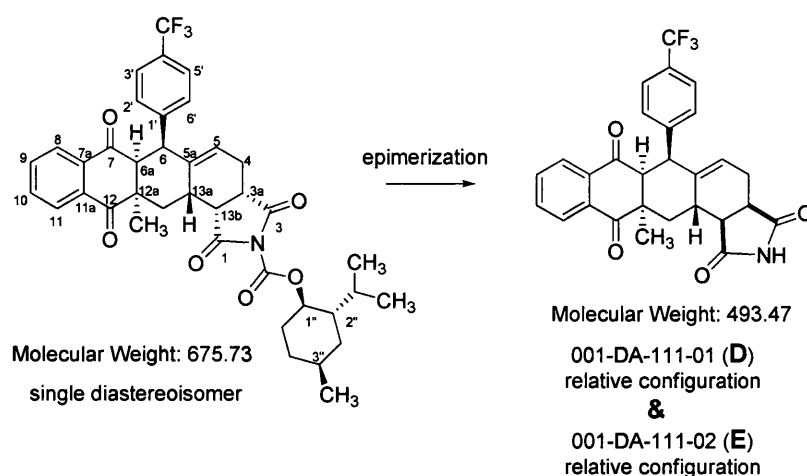
60% NaH in mineral oil (8.0 mg, 0.2 mmol, 3.4 Equiv.) was added to a solution of **001-DA-109-01** (40 mg, 0.06 mmol, 1.0 Equiv.) in anhydrous THF (1.0 mL) under argon atmosphere in a sealed tube in a ice-bath. After 20 min a solution of (1*R*)-(+)-Menthyl chloroformate (27 mg, 0.13 mmol, 2.1 Equiv.) in THF (1.0 mL) was slowly added to the reaction mixture (ice-bath) through a syringe. After 1h the ice-bath was removed and the mixture was allowed to stir for further 2h. The mixture was then diluted with diethyl ether (5 mL) and washed with sat. NaHCO₃ solution (2 x 5 mL), dried over MgSO₄, filtrated, and concentrated under vacuum. The remaining oil was redissolved in small amounts of DCM (< 1 mL) and subjected to flash chromatography purification (Hexane/EtOAc 1:0→1:1) to afford **001-DA-010-01** (higher *R_f*, 16 mg) and **001-DA-010-02** (lower *R_f*, 10 mg) as a colourless oils. (26 mg, 62%).

001-DA-010-01 (higher *R_f*): **HRMS**: Theoretical mass [*M* + *H*]⁺, 698.2706; Measured mass [*M* + *Na*]⁺, 698.2689 (δ 2 ppm). [*α*]_D^{25°C} = -4° (CHCl₃). **001-DA-010-02** (lower *R_f*): **IR** (ATR, λ_{max}/cm⁻¹): 2956, 2916, 2842, 1811, 1765, 1687, 1593, 1324, 1248, 1164, 1123, 1070, 1016, 979, 946, 909, 866, 730, 622. **¹H NMR** (CDCl₃, 400 MHz) δ 0.81 (d, 2 H, *J* = 6.9 Hz, 4''-CH₃), 0.93-0.96 (m, 6 H, 2''-CHCH₃), 1.08-1.30 (m, 4 H, H3'', H5'', H6'', and H13), 1.25 (s, 3 H, CH₃), 1.50-1.57 (m, 1 H, 6''H), 1.70-1.76 (m, 2 H, H3'' and H5''), 2.05-2.27 (m, 4 H, H2'', H4□, H4'', and 2''-CHCH₃), 2.55-2.65 (m, 1 H, H4□), 2.882.91 (m, 1 H, H13b), 3.04-3.10 (m, 2 H, H3a and H13), 3.31 (d, 1 H, *J* = 7.7 Hz, H6a), 3.42 (d, 1 H, *J* = 8.0 Hz, H13a), 4.22 (d, 1 H, *J* = 7.7 Hz, H6), 4.86 (td, 1 H, *J* = 4.4, 10.9 Hz, H1''), 5.75 (s, 1 H, H5), 6.93 (d, 2 H, *J* = 8.2 Hz, H2' and H6'),

7.03 (d, 2 H, $J = 8.2$ Hz, H3' and H5'), 7.40-7.48 (m, 2 H, H9 and H10), 7.63 (d, 1 H, $J = 8.0$ Hz, H11), 7.21 (d, 1 H, $J = 7.8$ Hz, H8). **MS** (ESI⁻) m/z (relative intensity): 675.34 ($[M + H]^-$, 90%). **HRMS**: Theoretical mass $[M + H]^+$, 698.2706; Measured mass $[M + Na]^+$, 698.2704 (Δ 1 ppm). $\alpha_D^{25^\circ C} = -13^\circ$ (CHCl₃).

Synthesis of (3aS,6S,6aS,12aR,13aS,13bR)-12a-methyl-6-(4-(trifluoromethyl)phenyl)-3a,4,6,6a,13,13a-hexahydro-1H-anthra[2,3-e]isoindole-1,3,7,12(2H,12aH,13bH)-tetraone*

* According to Felix, A. M. *J. Org. Chem.*, 39(10), 1427, 1974



A 1 M solution of BBr₃ in DCM (0.03 mL, 0.03 mmol, 2.0 Equiv.) was added to a solution of **001-DA-110-02** (10 mg, 0.015 mmol, 1.0 Equiv.) in anhydrous DCM (1.0 mL) under argon atmosphere in a ice-bath with acetone (-10°C). After 30 min, TLC analysis showed the formation of two products at lower R_f (possibly two diastereoisomers), the reaction was then quenched with water and the organic phase was dried over MgSO₄, filtrated, and concentrated under vacuum. The remaining oil was redissolved in small amounts of DCM (< 1 mL) and subjected to flash chromatography purification (Hexane/EtOAc 1:0→1:1) to afford **001-DA-111-01** and **001-DA-111-02** as a colourless oils. (4 mg, 54%).

001-DA-111-02 (more polar): ¹H NMR (CDCl₃, 400 MHz) δ 1.15 (m, 1 H, H13a), 1.19 (s, 3 H, CH₃), 2.18-2.23 (m, 1 H, H4a), 2.48-2.52 (m, 1 H, H4b), 2.75 (dd, 1 H, $J = 5.7, 8.5$ Hz, H13b), 3.00-3.04 (m, 1 H, H3a), 3.06-3.12 (m, 1 H, H13a), 3.14-3.20 (m, 1 H, H13a), 3.25 (d, 1 H, $J = 7.8$ Hz, H6a), 4.17 (d, 1 H, $J = 7.8$ Hz, H6), 5.68 (q, 1 H, $J = 2.8$ Hz, H5), 6.82 (d, 1 H, $J = 8.4$ Hz, H2' and H6'), 6.95 (d, 1 H, $J = 8.4$ Hz, H3' and

H5'), 7.32-7.41 (m, 1 H, H9 and H10), 7.55 (dd, 1 H, $J = 1.2, 7.5$ Hz, H11), 7.63 (m, 2 H, H8 and NH). **MS** (ESI⁺) m/z (relative intensity): 494.83 ($[M + H]^+$, 100 %).

11.2 U251-HRE 3rd generation screening assay.

Thurston Samples				25/08/2009
HIF-1 ASSAY				
New Samples Received 7/27/09				
NSC	20 concentration Titration (20-0.000038 uM)			
	EC50 HRE	EC50 pGLE	Ratio EC50's pGL3/HRE Hypoxia	
YB036 (3-20-08)	2.3	>20	>8.6	
YB036 (4-1-08)	1.2	>20	>16	
YB036 (8-5-09)	>20	>20	?	
YB036 (8-18-09)	1.2	>20	>17	
YB039 (3-20-08)	1.4	>20	>14	
YB039 (4-1-08)	1.5	>20	13.0	
YB039 (8-5-09)	>20	>20	?	
YB039 (8-13-09)	17	>20	>1.2	
YB039 (8-18-09)	1.7	>20	>12	
YB139	>20	>20	?	
YB140	20	>20	>1	
YB140 (8-13-09)	>20	>20	?	
YB140 (8-18-09)	>20	>20	?	
YB141	>20	>20	?	
YB142	>20	>20	?	
KSN017	>20	>20	?	
KSN030	>20	>20	?	
KSN030 (8-13-09)	>20	>20	?	
KSN031	>20	>20	?	
KSN032	>20	>20	?	
KSN040	>20	>20	?	
KSN043	>20	>20	?	
001DA09601	>20	>20	?	
001DA09601 (8-13-09)	>20	>20	?	
001DA09701	>20	>20	?	
001DA10501	>20	>20	?	
001DA10601	>20	>20	?	
001DA10901	>20	>20	?	
NSC 609699	0.00078	>20	>26000	Topotecan
NSC 609699	0.002	>20	>10000	Topotecan
NSC 609699	0.00042	>20	>47000	Topotecan
			>5.0	

11.3 Materials and methods describing the screening of tetracycline mimetics

The following experimental method has been reproduced from a journal article published by Melillo's group.²⁰⁵ It also describes the experimental method the group used to carry out the biological screening of molecules described in chapter 5.

Cell lines and reagents

We routinely maintained U251 human glioma cells in RPMI 1640 (Whittacker Bioproducts, Walkersville, MD) supplemented with 5% heat-inactivated fetal bovine serum (Whittacker Bioproducts), penicillin (50 IU/ml), streptomycin (50 µg/ml) and 2 mMglutamine (all purchased from Invitrogen-Life Technologies, Inc., Carlsbad, CA). Cells were maintained at 37°C in a humidified incubator containing 21% O₂, 5% CO₂ in air (referred to as normoxic conditions). Hypoxia treatment was performed by placing cells in a modular incubator chamber (Billupus-Rothemberg Inc., Del Mar, CA) and then flushing with a mixture of 1% O₂, 5% CO₂, and 94% nitrogen for 20 min. The chamber was then placed at 37°C. DFX was purchased from Sigma (St. Louis, MO), and ActD was purchased from Calbiochem (La Jolla, CA). Drugs from the NCI Training and Diversity Set (described elsewhere [5](#)) were initially dissolved in DMSO (Sigma) and diluted into complete medium for assay.

Plasmids

We generated pGL2-TK promoter plasmid by replacing the SV40 promoter of pGL2 promoter (Promega) with the herpes simplex virus TK promoter fragment (from -105 to +51).

The pGL2-TK-HRE plasmid was generated by subcloning three copies of the HRE (5'-GTGACTACGTGCTGCCTAG-3') from the inducible nitric oxide synthase promoter into the pGL2-TK promoter vector ([19](#)). Plasmids were sequenced at the Molecular Technology Laboratory, Science Applications International Corporation-Frederick, Inc.

pGL3-control (Promega) contains the firefly luciferase coding sequence under control of the SV40 promoter and enhancer sequences.

Plasmid p7, containing the VEGF 5'-flanking sequence (-1005 to +306) upstream of the luciferase reporter gene, and p11WT, encompassing the HIF-1-binding site of VEGF promoter at position -985 and -939, were generous gifts from Dr. Gregg Semenza.

Stable transfection and engineered cell lines

DNA plasmids were prepared using a commercially available kit (Endofree Maxi-Prep; Qiagen, Inc., Valencia, CA). Transfections were performed using Effectene Transfection Reagents (Qiagen, Inc.) according to the manufacturer's instructions. Stably transfected cells (U251-HRE, U251-TK, U251-pGL3, U251-p7, and U251-p11) were generated by cotransfection of the specific reporter plasmid (pGL2-TK-HRE, pGL2-TK promoter, pGL3-control, VEGF-p7, or VEGF-p11WT, respectively) with an expression vector carrying the neomycin resistance gene for selection in mammalian cells (ratio, 100:1). Twenty-four h after transfection, reagents were removed, and cells were allowed to recover for 24 h before the addition of selection medium containing the antibiotic G418 at 500 µg/ml (Invitrogen-Life Technologies, Inc.). Stably transfected cells were seeded at a concentration of 1×10^4 cells/well in 96-well optiplates the day before treatment and routinely treated for 16–24 h.

Luciferase reporter assays were performed in 96-well optiplates (Packard Instrument, Inc., Meriden, CT) using Bright Glo luciferase assay reagents (Promega, Inc., Madison, WI).

Nuclear extract preparation and immunoblotting (Western Blot)

Cells were collected and washed twice with ice-cold Dulbecco's PBS 1× (PBS) and pelleted by centrifugation at 1,200 rpm. The cell pellet was subsequently washed once in a hypotonic buffer [10 mM Tris-HCl (pH 7.5), 1.5 mM MgCl₂, 10 mM KCl, 2 mM DTT, 1 mM Pefabloc, 2 mM sodium vanadate, 4 µg/ml pepstatin, 4 µg/ml leupeptin, and 4 µg/ml aprotinin], resuspended in the same buffer, and incubated for 10 min on ice. The cell suspension was homogenized with 18–20 strokes in a glass Dounce homogenizer. The nuclear pellet was obtained after centrifugation at $1,000 \times g$ at 4°C for 10 min and resuspended in a hypertonic buffer [20 mM Tris-HCl (pH 7.5), 1.5 mM MgCl₂, 0.42 M KCl, 20% glycerol, 2 mM DTT, 1 mM Pefabloc, 2 mM sodium vanadate, 4 µg/ml pepstatin, 4 µg/ml leupeptin, and 4 µg/ml aprotinin] to obtain nuclear extracts. The nuclear suspension was rotated at 4°C for 30 min, and nuclear debris were pelleted by centrifugation at $15,000 \times g$ for 30 min at 4°C.

Typically, 50 µg of protein were separated on an 8% Tris-glycine gel (Invitrogen Corp., Carlsbad, CA) and electroblotted on an Immobilon-P membrane (Invitrogen Corp.). Membranes were blocked for 1 h at room temperature with blocking buffer A (1× PBS, 0.1% Tween 20, and 4% BSA) to detect HIF-1α and blocked with blocking buffer B (1× PBS, 0.1% Tween 20, and 5% nonfat dry milk) to detect HIF-1β before incubation with primary

antibodies (1 h at room temperature) in dilution buffer (1× PBS, 0.1% Tween 20, and 0.4% BSA). Monoclonal anti-HIF-1 α (clone H1 α 67) and monoclonal anti-HIF-1 β (clone H1B234) antibodies were purchased from Novus Biologicals (Littleton, CO). HIF-1 α was detected using a 1:1000 dilution of the specific antibody, whereas HIF-1 β antibody was diluted 1:1500. After washing three times in washing buffer (1× PBS and 0.1% Tween 20), membranes were incubated for 30 min at room temperature with a peroxidase-conjugated sheep antimouse antibody (diluted 1:20000 in dilution buffer) for both HIF-1 α and HIF-1 β (Amersham Pharmacia Biotech, Inc., Piscataway, NJ). Membranes were then washed three times in washing buffer, and chemiluminescence detection was performed using an enhanced chemiluminescence kit according to the manufacturer's protocol (Amersham Pharmacia Biotech, Inc.).

Electrophoretic mobility shift assay

Nuclear extracts, prepared as described previously, were dialyzed against one change of dialysis buffer [25 mM Tris-HCl (pH 7.5), 0.2 mM EDTA, 0.1 M KCl, 20% glycerol, 1 mM DTT, 0.2 mM Pefabloc, and 0.5 mM sodium vanadate]. The double-stranded oligonucleotide AB.2 (5'-GTGCTACGTGCTGCCTAG-3') encompassing the HIF-1 binding site was labeled with [32 P]dCTP using the Klenow enzyme (Invitrogen-Life Technologies, Inc.). To perform the binding reaction, 5 μ g of nuclear protein were incubated on ice in binding buffer [25 mM Tris-HCl (pH 7.5), 0.2 mM EDTA, 0.1 M KCl, 20% glycerol, and 0.4 μ g of denatured calf thymus DNA] in the presence or absence of antibodies for HIF-1 α for 30 min. Probe (1 \times 10⁴ cpm) was added, and the samples were incubated for an additional 20 min on ice. Samples were subjected to a 5% nondenaturing polyacrylamide gel, and electrophoresis was performed at 180 V in 0.3× Tris-borate EDTA at 4°C. Gel was allowed to dry using HydroTech gel drying system (Bio-Rad Laboratories, Hercules, CA) before being autoradiographed using Kodak XAR-5 film and intensifying screens at -80°C.

HTS Assay

U251-HRE cells were inoculated into 384 well white flat-bottomed plates (Costar catalogue number 3704) at 3000 cells/well with a Beckman Biomek 2000 Laboratory Automation Workstation in a volume of 25 μ l and incubated for 24 h at 37°C, 5% CO₂, and ambient O₂. Experimental agents at the appropriate concentrations were added in a volume of 25 μ l using the Biomek 2000, and after a 20-h incubation in a hypoxia chamber (Billups Rothenberg,

MIC 101) at 37°C, 5% CO₂, and 1% O₂, the plates were removed and incubated at room temperature, 5% CO₂, and ambient O₂ for 1.5 h. Forty µl of Bright Glo luciferase reagent (Promega catalogue number E26500) were added with the Biomek 2000, and after 3 min, luminescence was measured using a Tecan Ultra Multifunction Plate Reader in luminescence mode. Appropriate control cells were treated identically, except that they were treated at 37°C, 5% CO₂, and ambient O₂. Compound toxicity was assayed using the SRB assay as described previously in detail.

Real-time PCR

Total RNA from U251 cells was obtained using RNA Mini Kit (Qiagen, Inc.). One µg of total RNA was used to perform RT-PCR using RT-PCR kit (PE Biosystems, Foster City, CA). The conditions used for RT-PCR were as follows: 10 min at 25°C, 30 min at 48°C, and 5 min at 95°C. To measure human VEGF, COX-2, GLUT-3, and aldolase expression, real-time PCR was performed using an ABI-Prism 7700 Sequence Detector (Applied Biosystems, Foster City, CA). Typically 5 ng of reverse-transcribed cDNA per sample were used to perform real-time PCR in triplicate samples. Real-time PCR cycles started with 2 min at 50°C, 10 min at 95°C, and then 40 cycles of 15 s at 95°C and 1 min at 60°C. Primers and specific probes were obtained from Applied Biosystems. The following primers and probes were used: human VEGF forward, 5'-TACCTCCACCATGCCAAGTG-3'; human VEGF reverse, 5'-ATGATTCTGCCCTCCTCCTTC-3'; probe, 5'-FAM-TCCCAGGCTGCACCCATGGC-TAMRA-3'; human COX-2 forward, 5'-GAATCATTACACAGGCAAATTG-3'; human COX-2 reverse, 5'-TCTGTACTGCGGGTGGAACA-3'; probe, 5'-FAM-TGGCAGGGTTGCTGGTGGTAGGA-TAMRA-3'; human GLUT-3 forward, 5'-CGTGGCAGGACTTTTGAGGAT-3'; human GLUT-3 reverse, 5'-AGCAGGCTCGATGCTGTTCAT-3'; human aldolase forward, 5'-GCGCTGTGTGCTGAAAATCAG-3'; and human aldolase reverse, 5'-CCACAATAGGCACAATGCCATT-3'. Detection of 18S rRNA, used as internal control, was preformed using premixed reagents from Applied Biosystems. Detection of VEGF, COX-2, and 18S rRNA was performed using TaqMan Universal PCR Master Mix (Applied Biosystems), whereas GLUT-3 and aldolase detection was performed using Sybr Green PCR Master Mix (Applied Biosystems).

Relative quantitation values were expressed as follows: $2^{(\Delta C_{tr}-\Delta C_{tt})}$, where C is the value measured in each well, C_t is the mean of the replicate wells run for each sample, ΔC_t is the difference between the mean C_t values of the samples in the target wells and those of the endogenous control for the same wells (18S values), $\Delta C_{tr}-\Delta C_{tt}$ represents the difference between ΔC_t of the reference sample (medium) and ΔC_t of the tested samples (treatments). Values are expressed as fold increases relative to the reference sample (medium).

ELISA

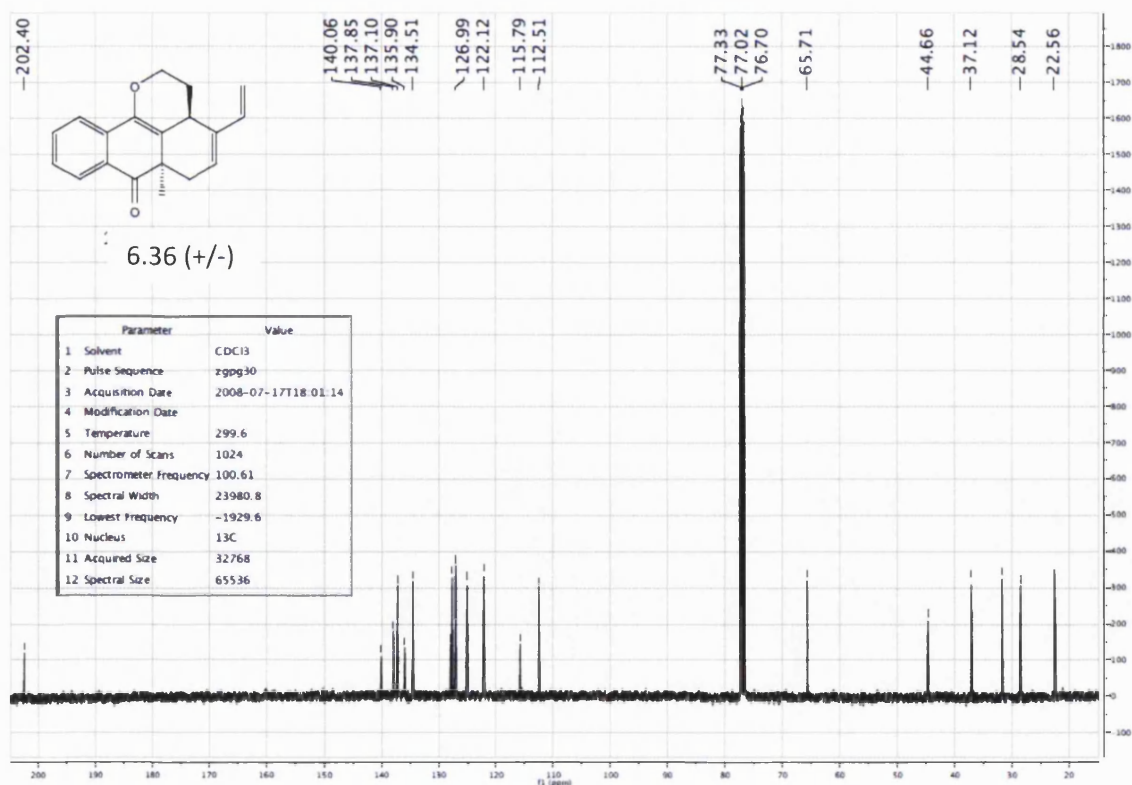
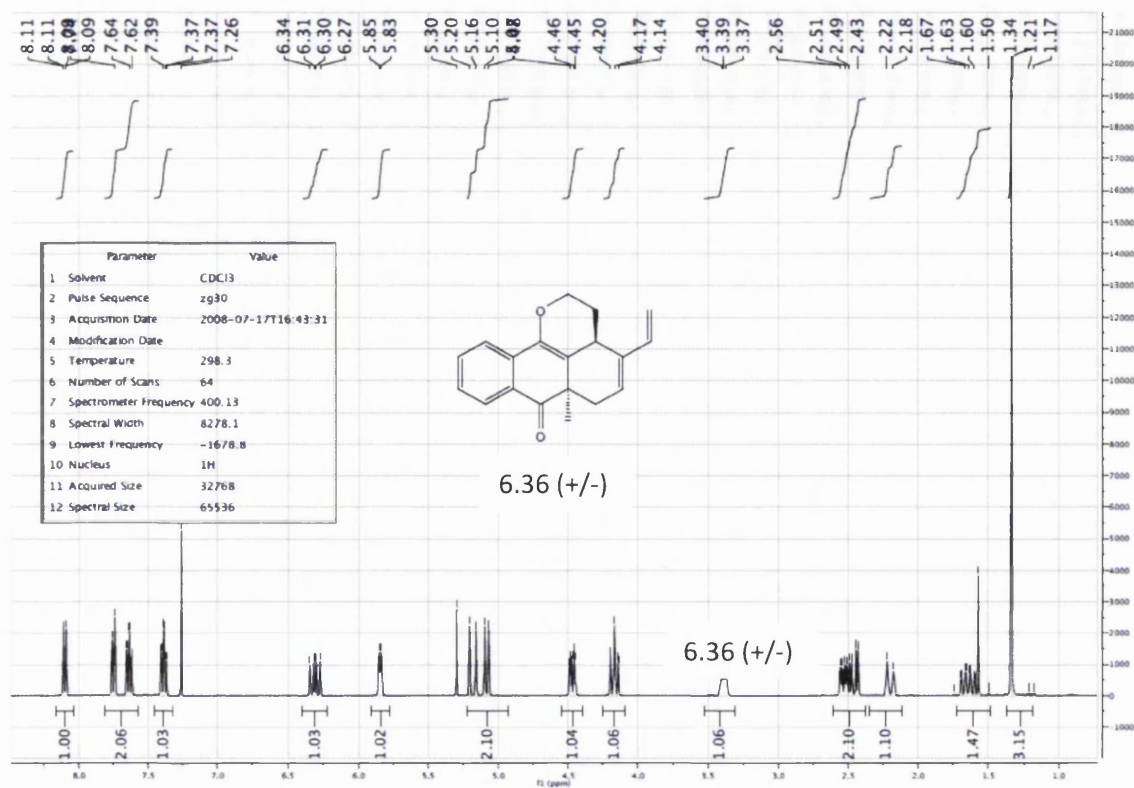
Supernatants were collected from U251 cells after 24 h of incubation under the indicated conditions. Total levels of VEGF protein were measured at the Lymphokine Testing Laboratory, Science Applications International Corporation-Frederick, Inc., NCI (Frederick, MD) using human VEGF DuoSet (R&D Systems, Minneapolis, MN).

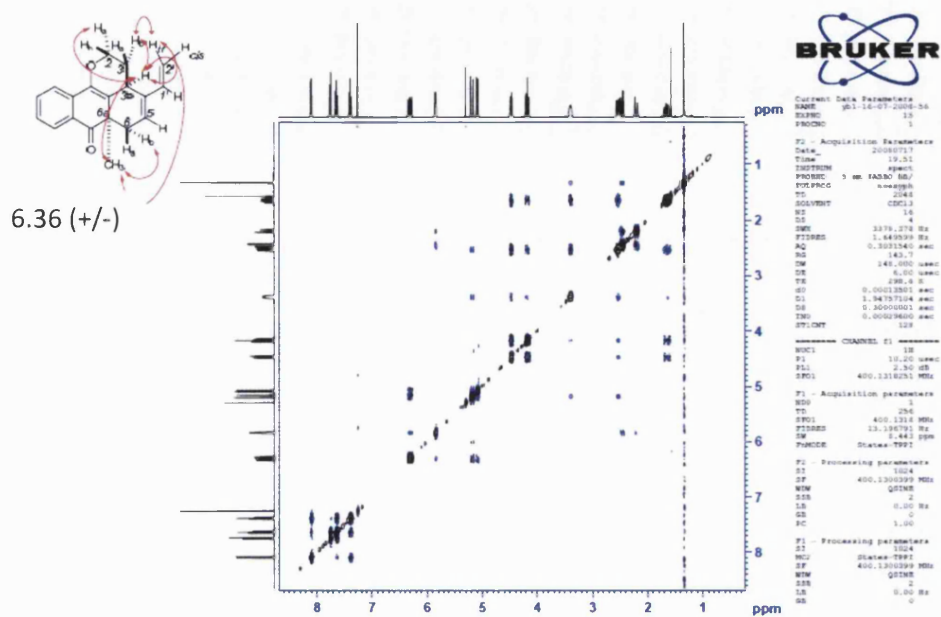
The following is the protocol used at the National Cancer Institute at Frederick for HIF-1 HTS using U251-HRE cells.

Generation of U251-HRE stable cell lines: U251 human glioma cells were co-transfected with pGL2-TK-HRE containing three copies of the inducible nitric oxide synthase (iNOS)-HRE in front of TK-luciferase and an expression vector carrying the neomycin resistance gene for selection in mammalian cells (ratio 1:100). Twenty-four hours following transfection, reagents were removed and cells were allowed to recover for 24 h before addition of selection medium containing the antibiotic G418 at 500 mM (Invitrogen-Life Technologies, Inc., Carlsbad, CA). U251-HRE are routinely maintained in RPMI 1640 medium (Whittaker Bioproducts, Walkersville, MD) supplemented with 5% heat-inactivated fetal bovine serum (Hyclone Laboratories, Logan, UT), penicillin (50 IU/ml), streptomycin (50 mg/ml), 2 mM glutamine (all from Invitrogen-Life Technologies, Inc., Carlsbad, CA), and 200 mg/ml G418. Cells are maintained at 37 °C in a humidified incubator containing 21% O₂, 5% CO₂ in air (referred to as normoxic conditions). Hypoxia treatment is performed by placing cells in a modular incubator chamber (Billups-Rotheberg Inc., Del Mar, CA), flushing them with a mixture of 1% O₂, 5% CO₂, and 94% nitrogen for 20 min, and then placing them at 37 °C. Plasmids with mutated HRE sequences can be used to confirm that the

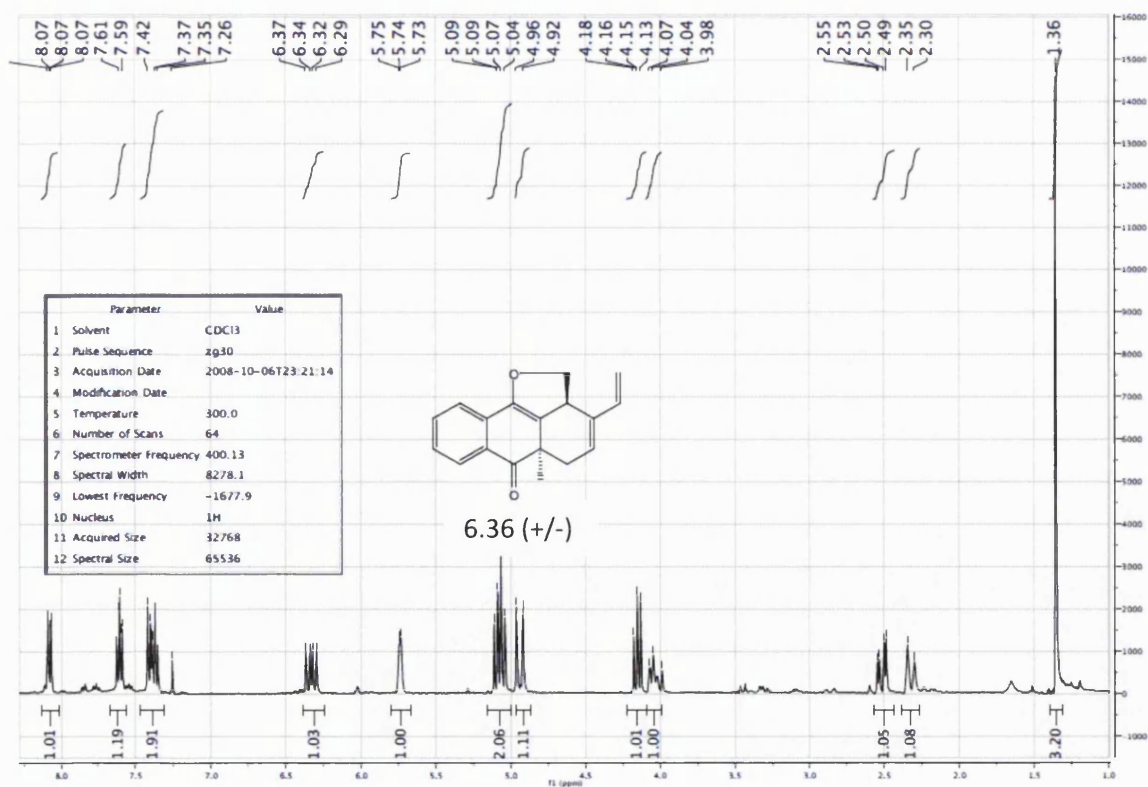
expression of luciferase is indeed HIF-1–dependent. U251-pGL3 control cell lines: U251 cells were transfected as previously stated with pGL3-control (Promega, Madison, WI), which contains the firefly luciferase coding sequence under control of the SV40 promoter and enhancer sequences. A secondary screen using control cell lines essential to validate the specificity of HIF-1 inhibitors can be run in parallel to a primary screen or to validate “hits” and generate a dose-response curve. U251-HRE cells are inoculated into 384-well white, flat-bottom plates (Costar, Catalog # 3704) at 3000 cells/well with a Beckman Biomek HIF-1 Inhibitors 389 2000 Laboratory Automation Workstation in a volume of 25 ml and incubated for 24 h at 37 °C , 5 % CO₂, and ambient O₂. Experimental agents at the appropriate concentrations are added in a volume of 25 ml using the Biomek 2000 and, after a 20-h incubation in a hypoxia chamber (Billups Rothenberg, MIC 101) at 37 °C, 5 % CO₂, and 1 % O₂, the plates are removed and incubated at room temperature, 5 % CO₂, and ambient O₂ for 1.5 h. 40 ml of Bright Glo luciferase reagent (Promega, Catalog # E26500) is added with the Biomek 2000, and, after 3 min, luminescence is measured using a Tecan Ultra Multifunction Plate Reader in luminescence mode. Appropriate control cells are treated identically except that they are incubated at 37 °C, 5 % CO₂, and ambient O₂. Compound toxicity is assayed in parallel utilizing the sulphorhodamine B or Alamar blue assays.

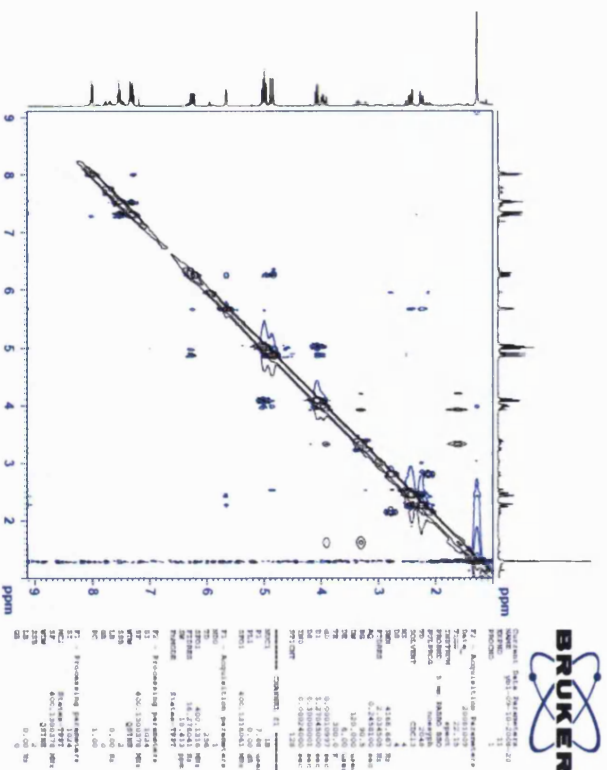
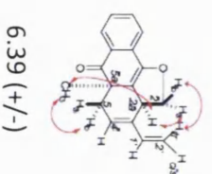
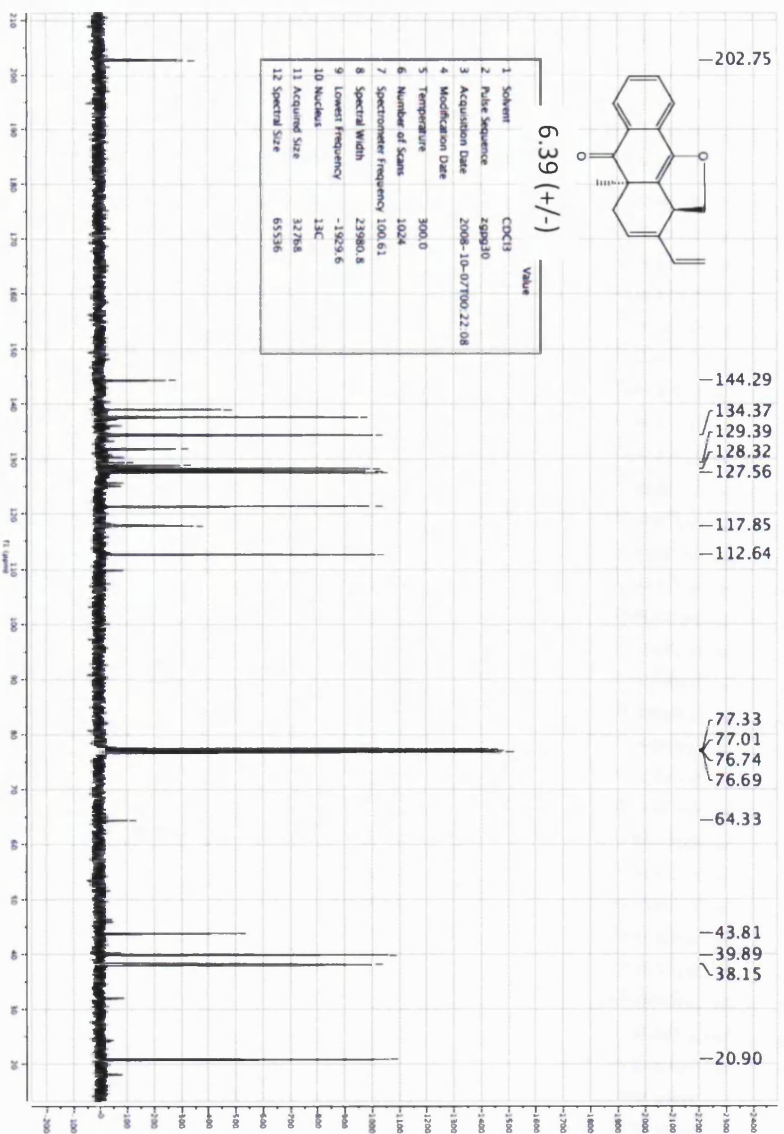
11.4 Selected NMR spectra

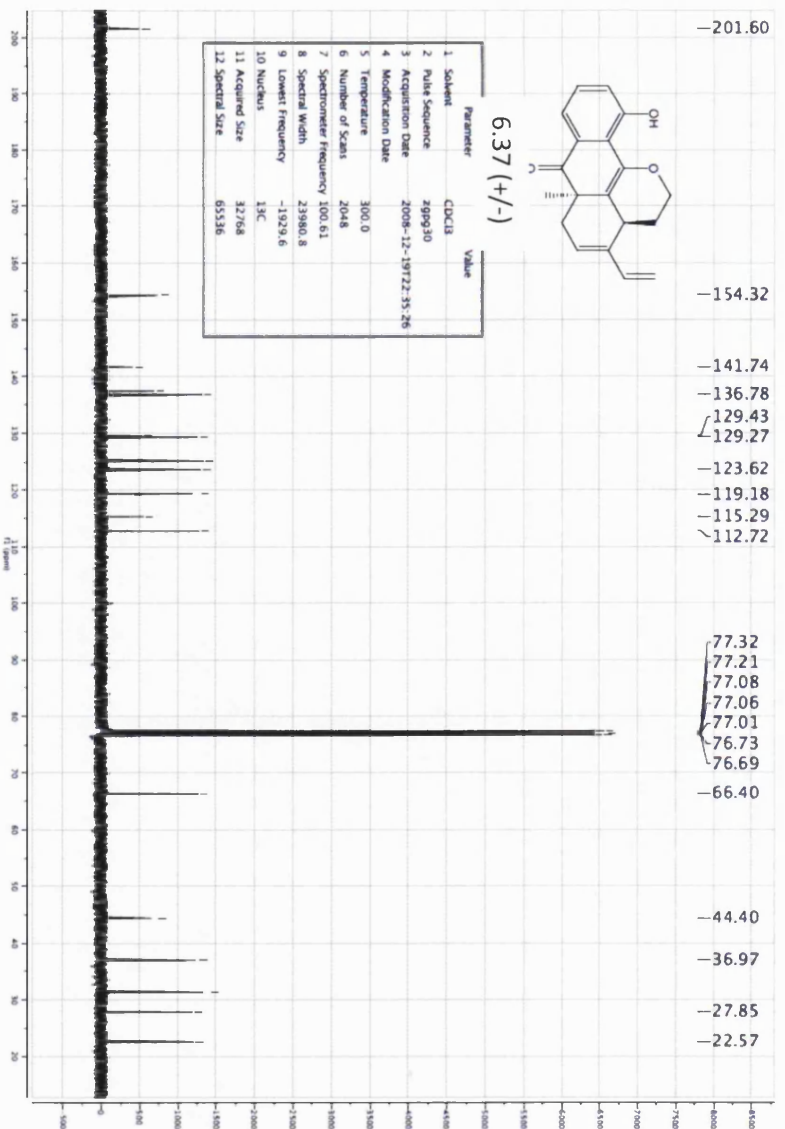
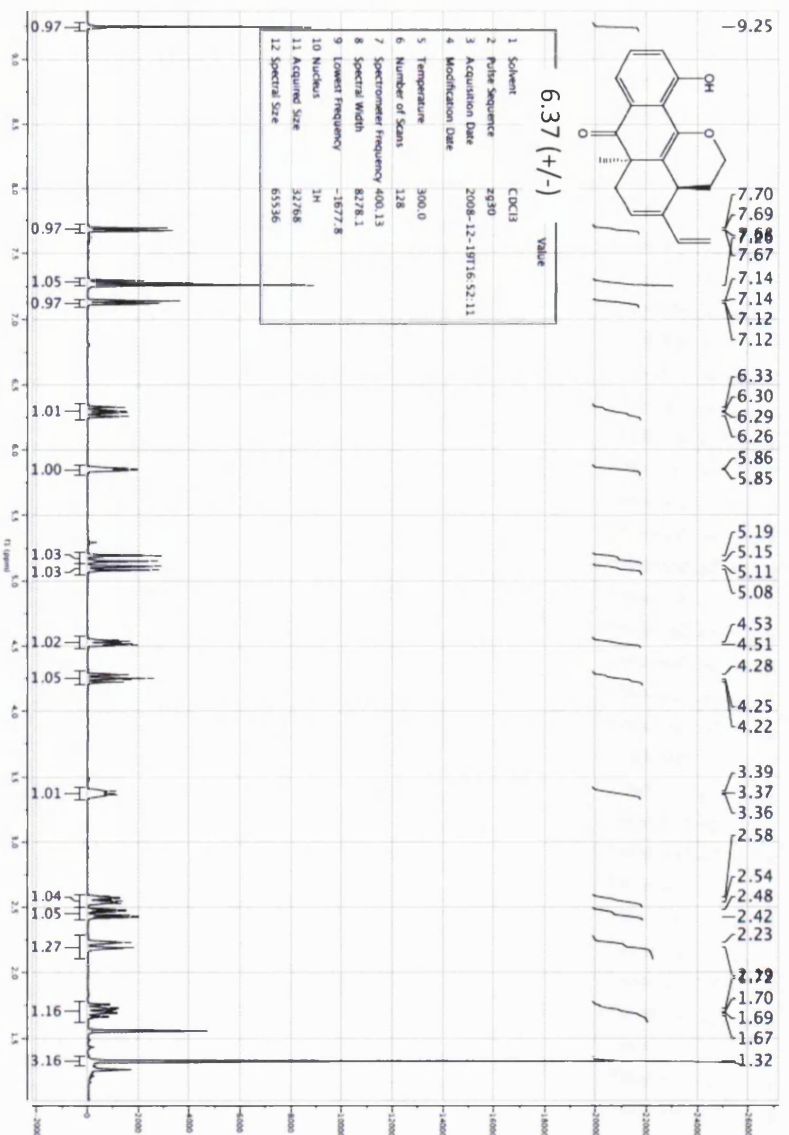


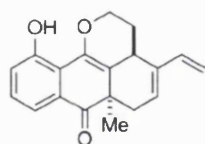


6.39 (+/-)

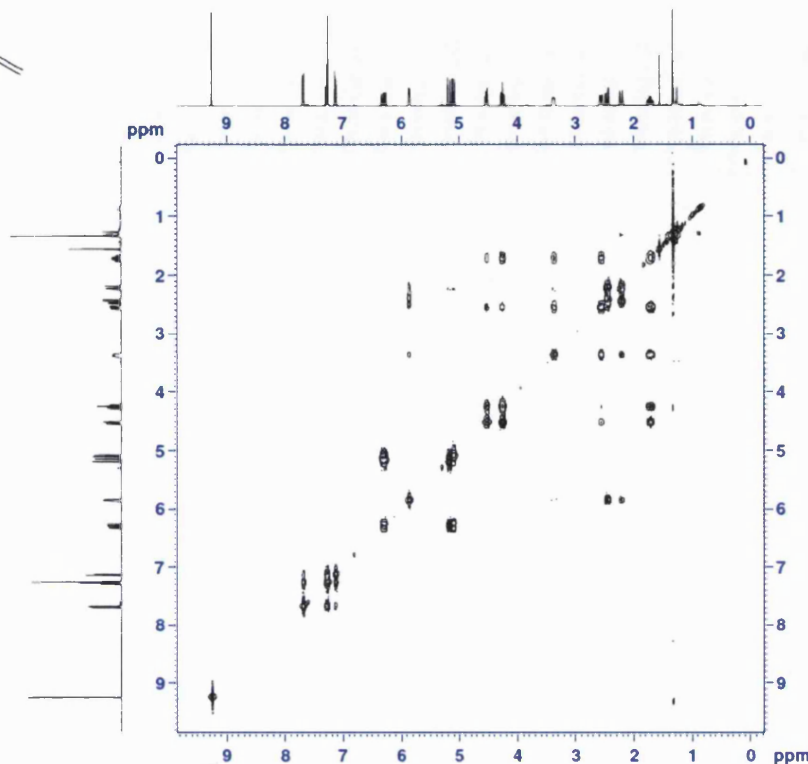








6.37 (+/-)



Current Data Parameters
NAME yb1-19-12-2008-60
EXPNO 11
PROCNO 1

F2 - Acquisition Parameters
DATA 20081219
TIME 20.41
INSTRUM spect
PROBHD 5 mm BBO BB-1H
PULPROG zgpg30
TD 2048
SOLVENT CDCl3
NS 8
DS 8
SWH 4032.250 Hz
FIDRES 1.968874 Hz
AQ 0.2140020 sec
RG 163.7
DM 124.000 umic
DE 8.00 umic
TE 300.0 K
D0 0.0000309 sec
D1 1.4240307 sec
d13 0.00000400 sec
D14 0.00010000 sec
SFO 400.1319441 MHz

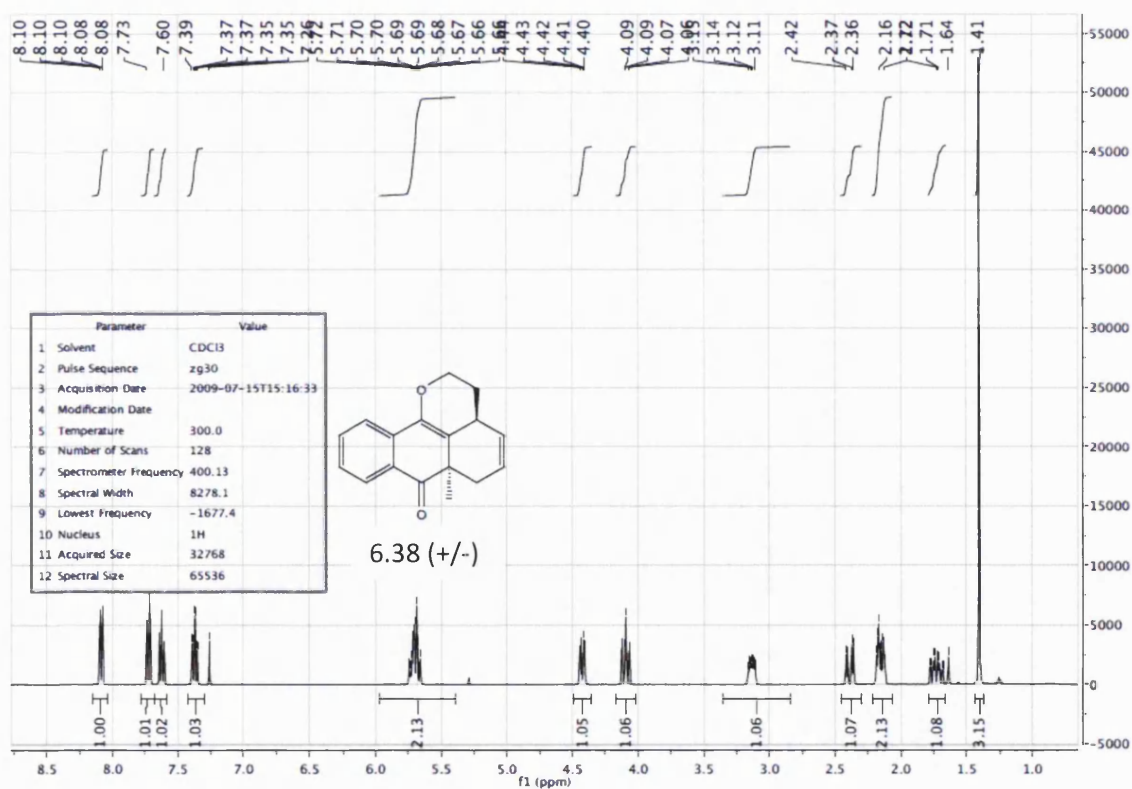
CHANNEL F1
NUC1 1H
P0 7.88 umic
P1 7.88 umic
PL1 0.00 dB
SFO1 400.1319441 MHz

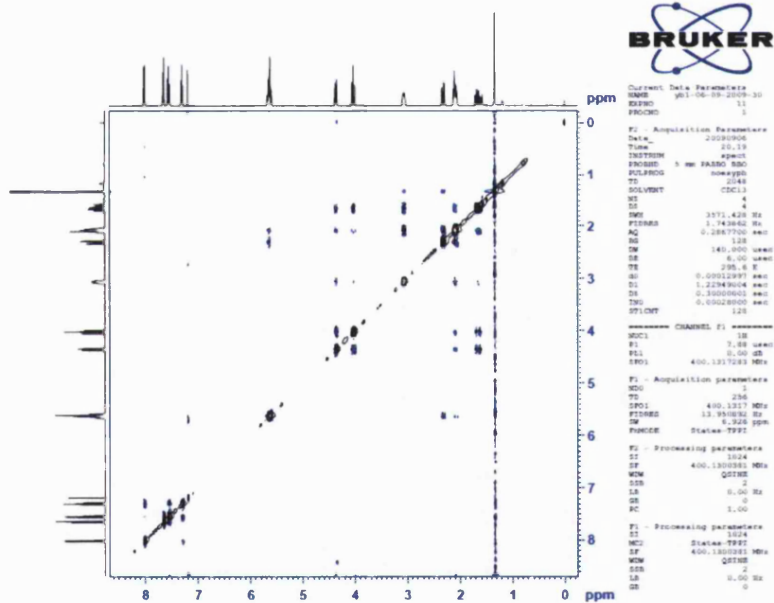
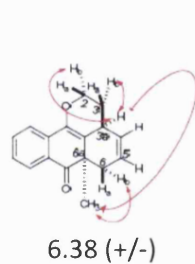
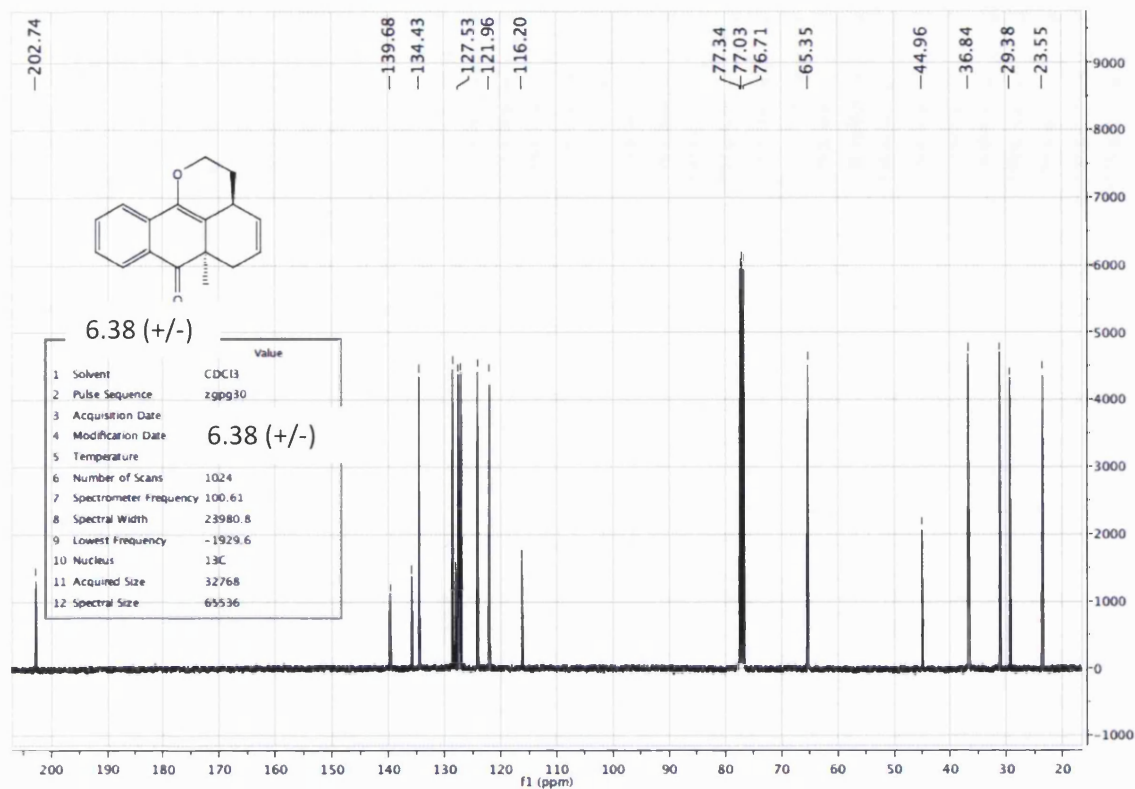
GRADIENT CHANNEL
GPMAX 8196.100
GPMIN 8196.100
GPF1 10.00 V
GPF2 10.00 V
GPA 1000.00 umic

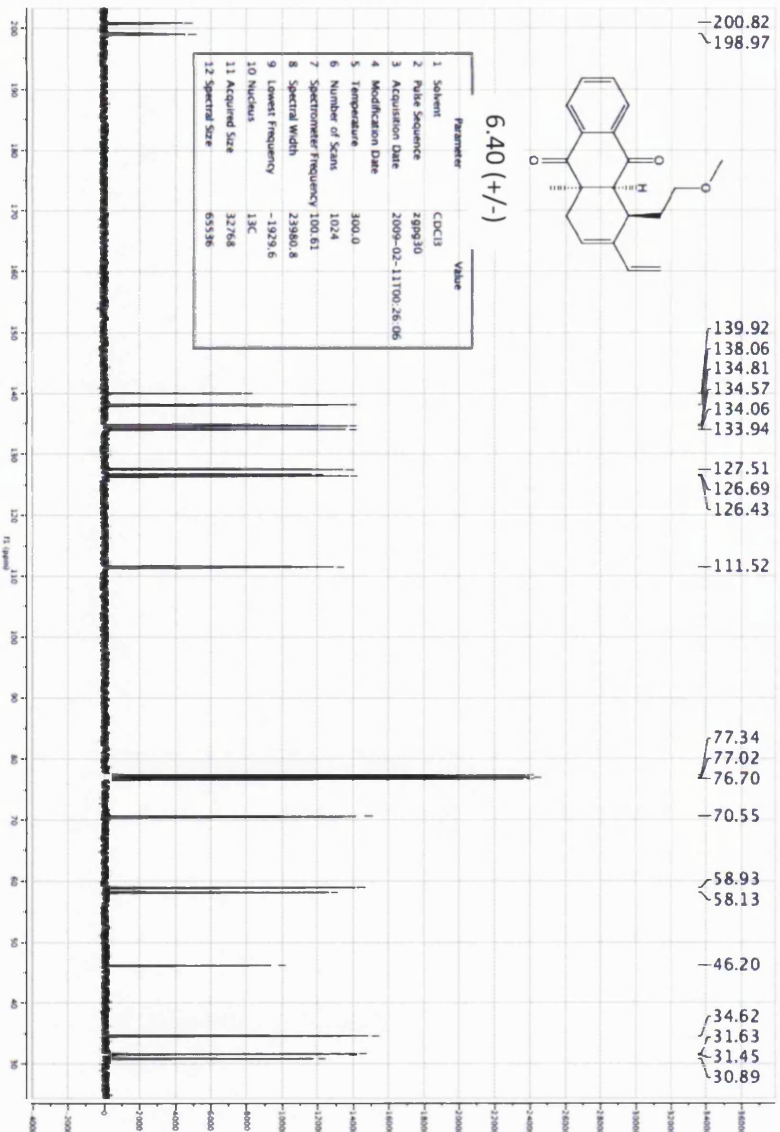
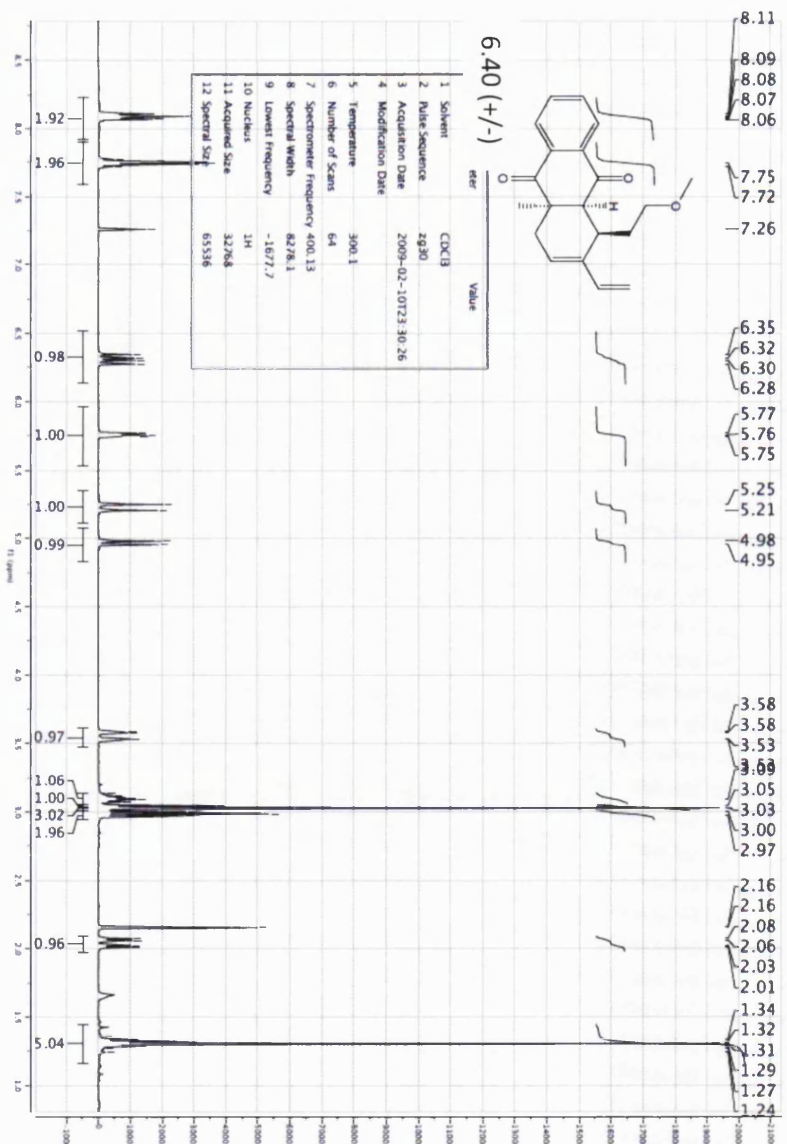
F1 - Acquisition Parameters
NS 8
DS 8
TD 128
SFO1 400.132 MHz
FIDRES 31.502016 Hz
DM 10.077 ppm
PULPROG zgpg30

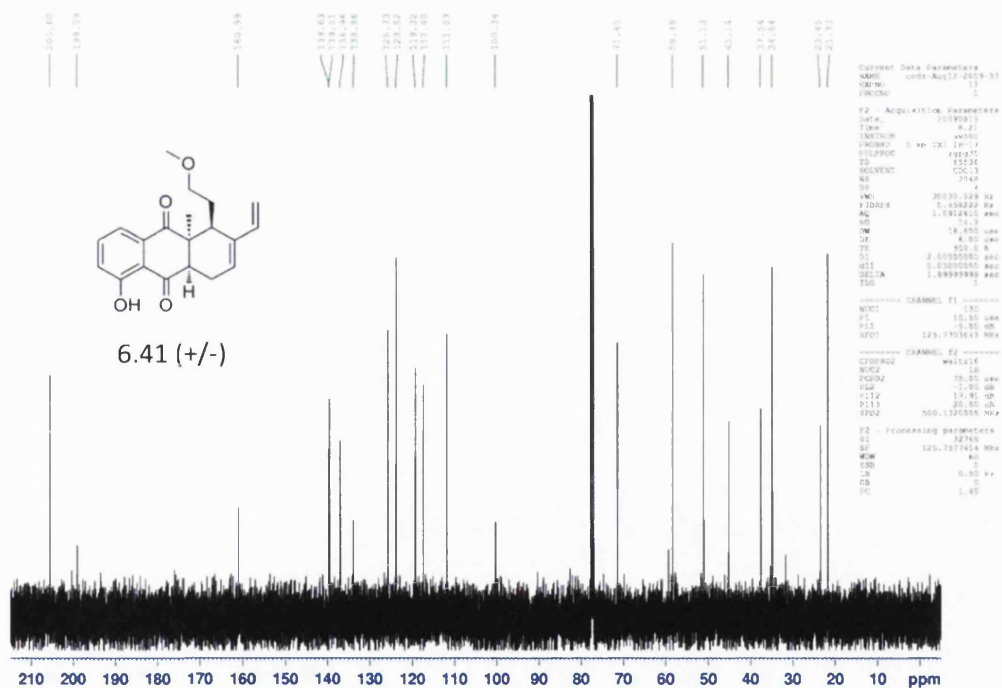
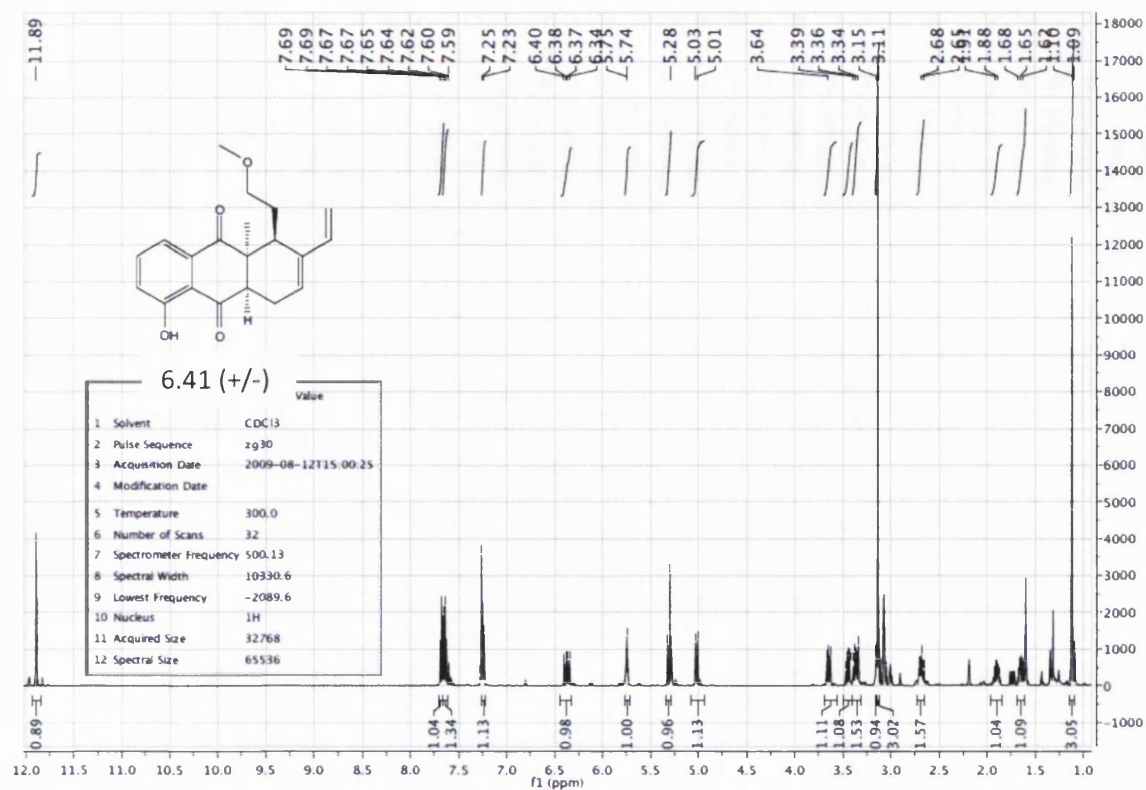
F2 - Processing Parameters
SI 1024
SF 400.130381 MHz
WDW EM
SSB 0
GB 0
PC 1.40

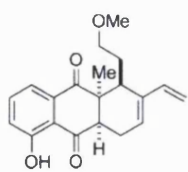
F1 - Processing Parameters
SI 1024
SF 400.130381 MHz
WDW EM
SSB 0
GB 0
PC 1.40



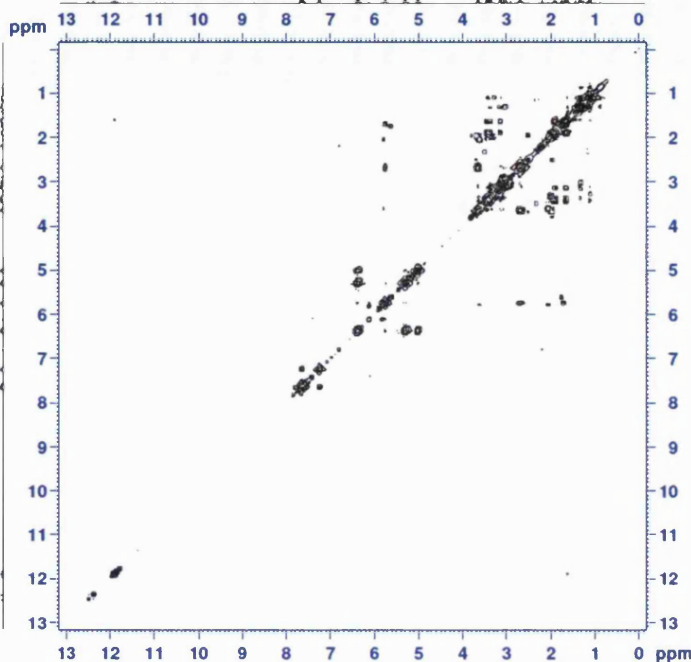








6.41 (+/-)



Current Data Parameters
NAME: 002-Aug17-2009-33
EXPNO: 12
PROCNO: 1

F2 - Acquisition Parameters
Data: 20090813
Time: 6.18
INSTRUM: zg30
PROBHD: 5 mm TXI 1H-13
PULPROG: zgpg30
TD: 65536
SOLVENT: CDCl3
NS: 4
DS: 4
SWH: 6444.647 Hz
FIDRES: 0.253208 Hz
AQ: 0.1537250 sec
RG: 327.68
DM: 75.000 umic
DE: 6.00 umic
TE: 300.2 K
D1: 0.0000300 sec
D11: 1.4648919 sec
d13: 0.0000040 sec
D14: 0.0001000 sec
D15: 0.0001000 sec
D16: 0.0001000 sec

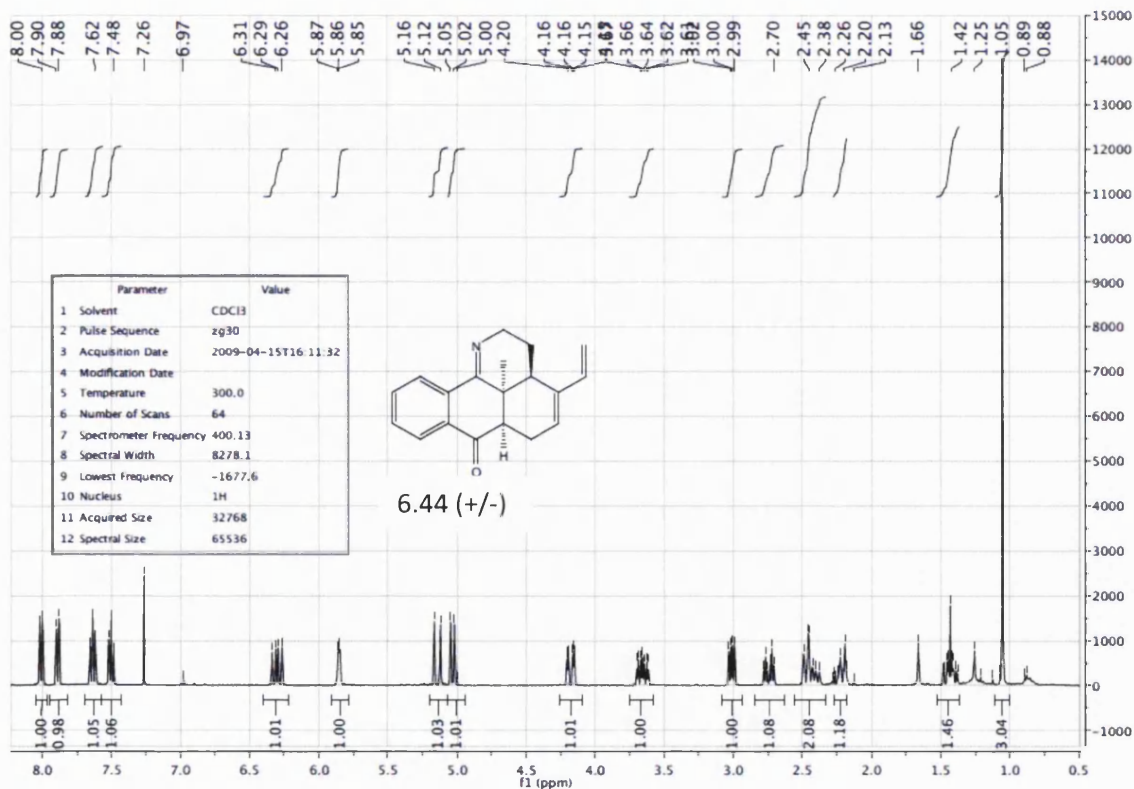
--- CHANNEL f1 ---
NUC1: 13C
P1: 8.50 umic
PL1: 0.00 dB
SFO1: 500.1332984 MHz

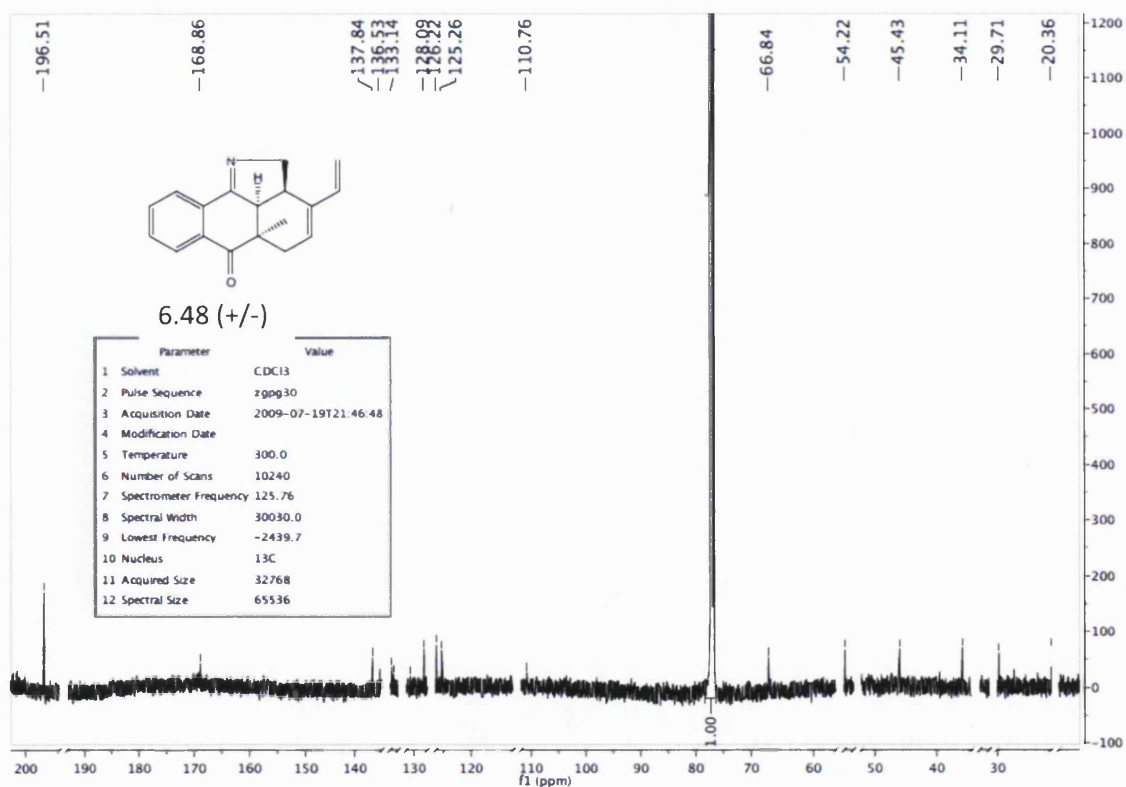
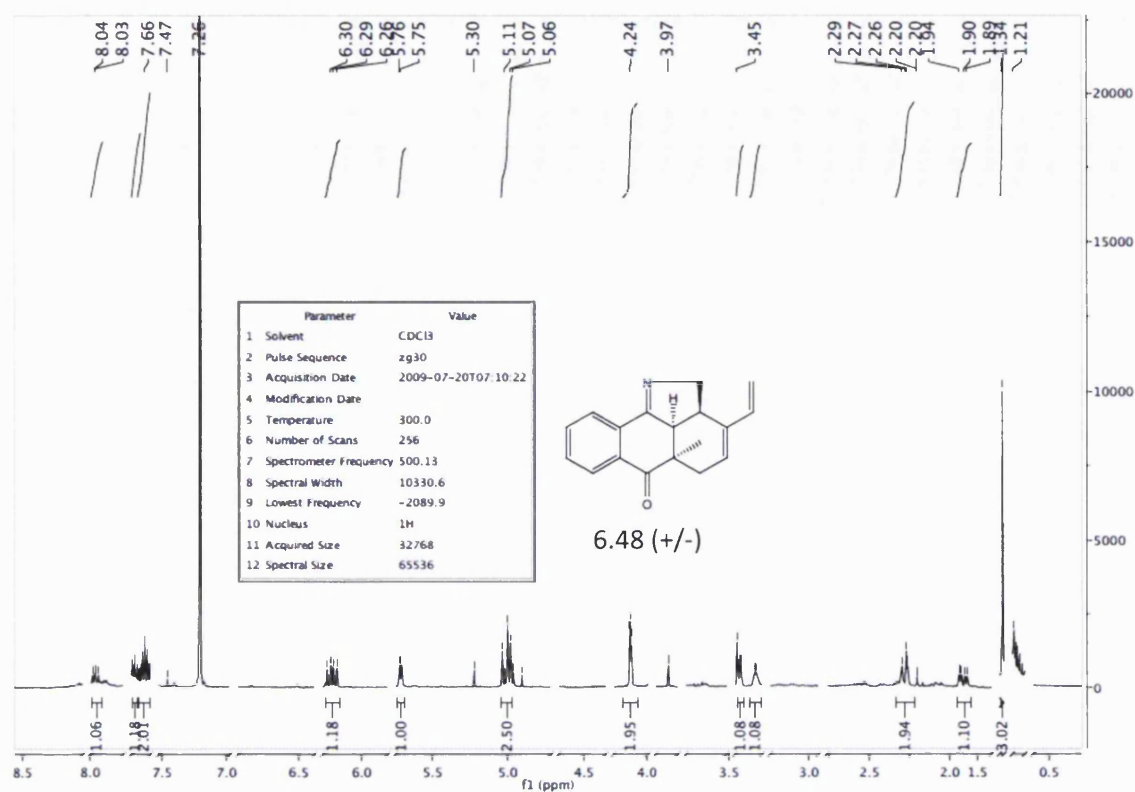
--- GRADIENT CHANNEL ---
CPHASEC: SINE.100
CPHASEG: SINE.100
CPS1: 16.00 V
CPS2: 16.00 V
P15: 1000.00 umic

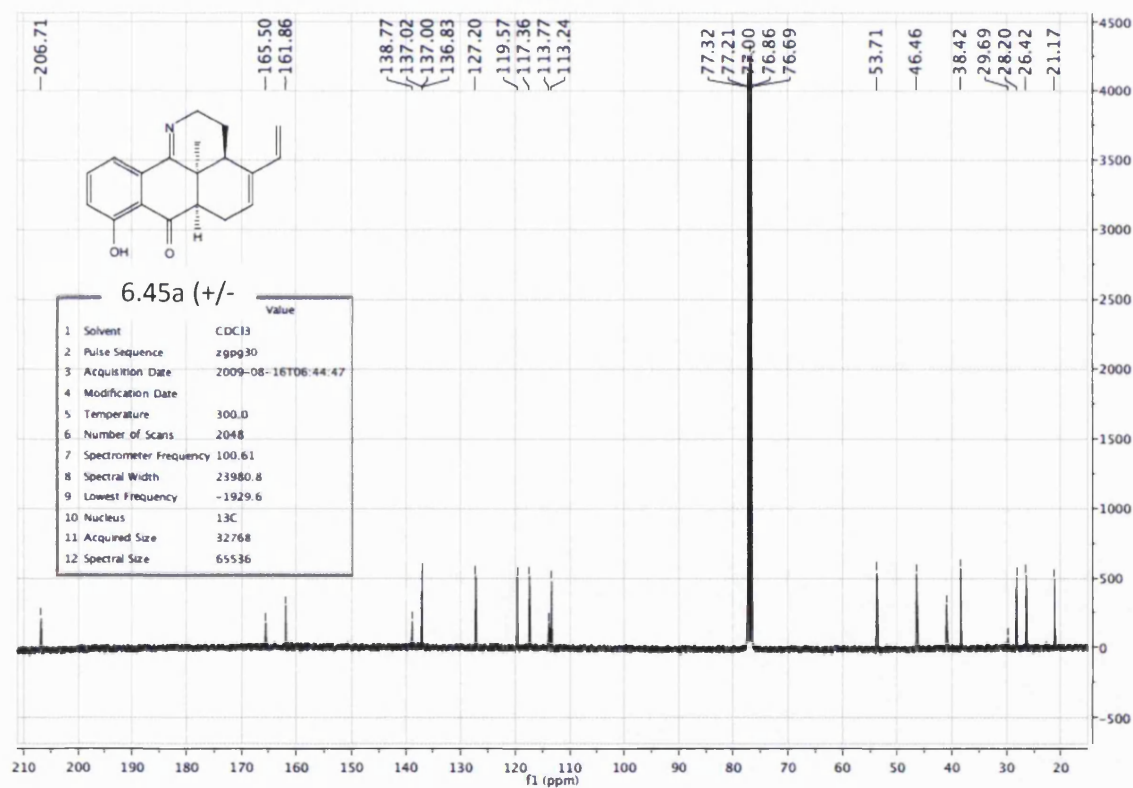
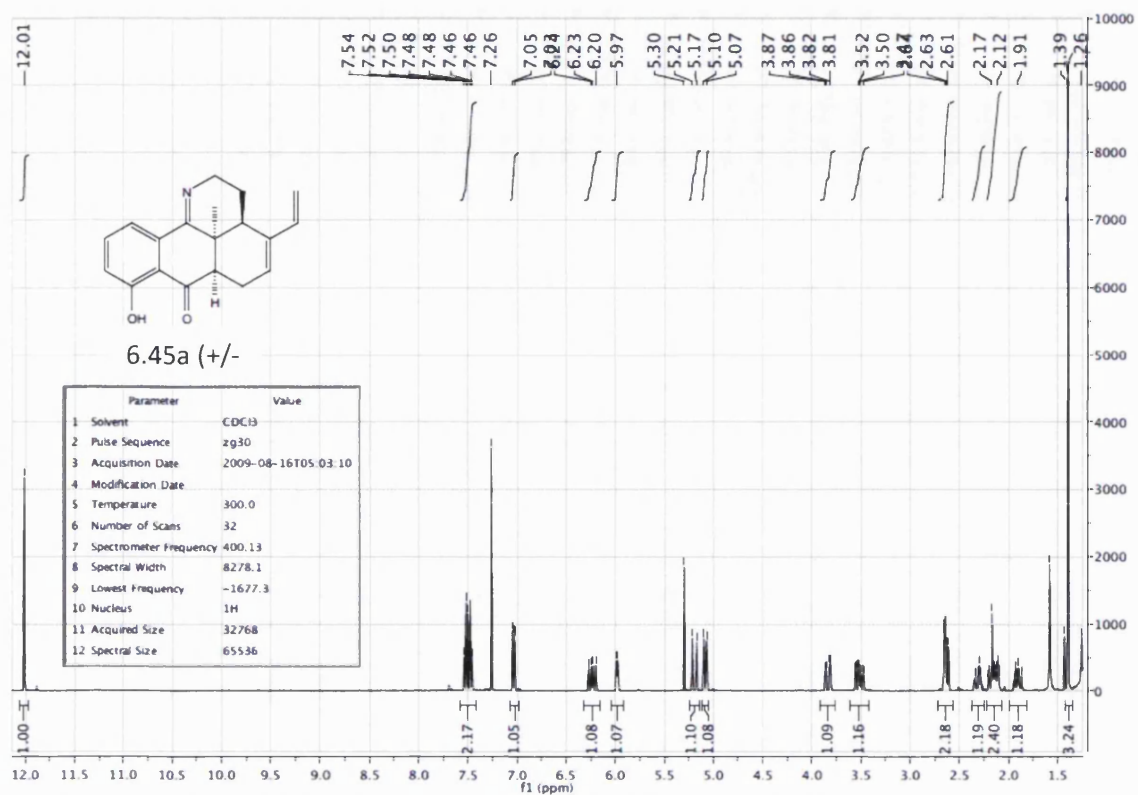
F1 - Acquisition parameters
RG: 1
DS: 4
SWH: 6444.647 Hz
FIDRES: 0.253208 Hz
DM: 75.000 umic
DE: 6.00 umic
TE: 300.2 K
D1: 0.0000300 sec
D11: 1.4648919 sec
d13: 0.0000040 sec
D14: 0.0001000 sec
D15: 0.0001000 sec
D16: 0.0001000 sec

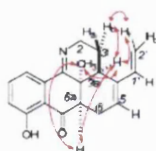
F2 - Processing parameters
SI: 32768
SF: 500.1300449 MHz
WDW: SINE
SSB: 0
LB: 0.00 Hz
GB: 0
PC: 1.40

F1 - Processing parameters
SI: 32768
SF: 500.1300449 MHz
WDW: SINE
SSB: 0
LB: 0.00 Hz
GB: 0

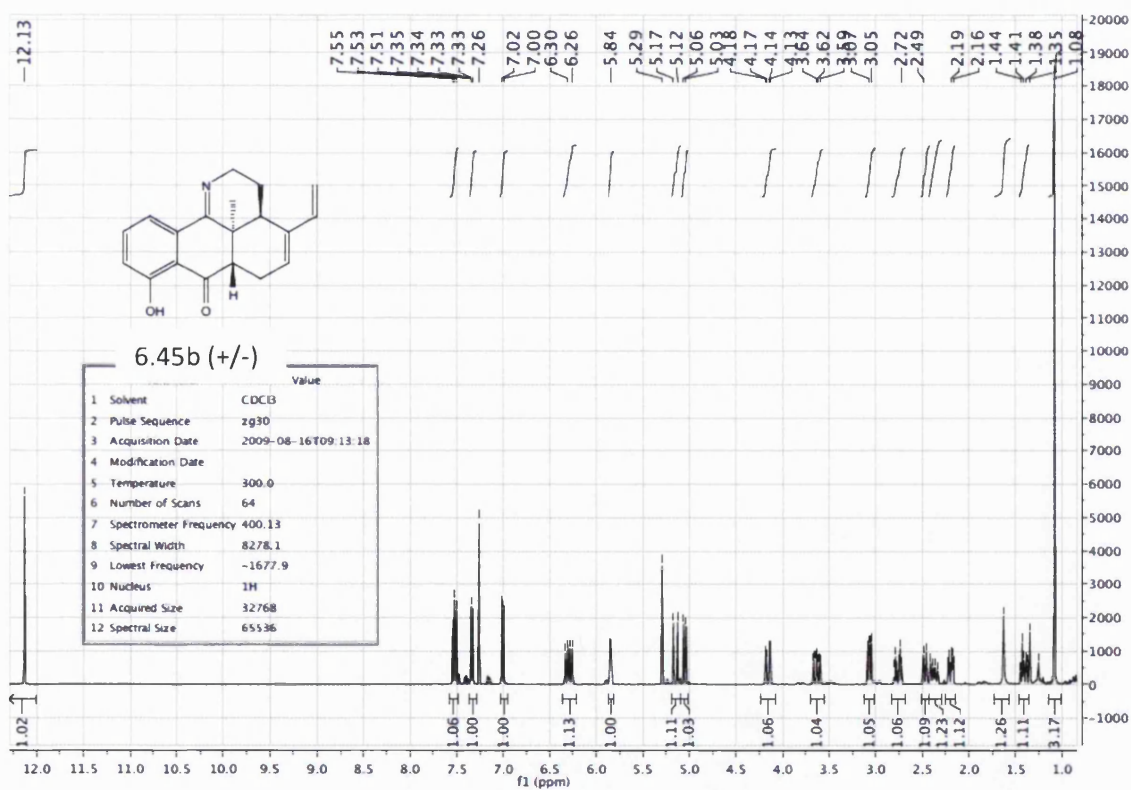
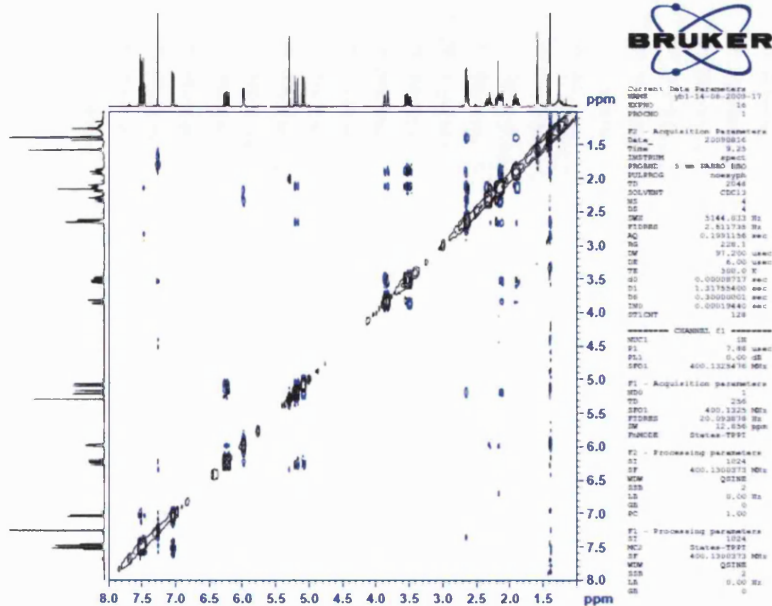


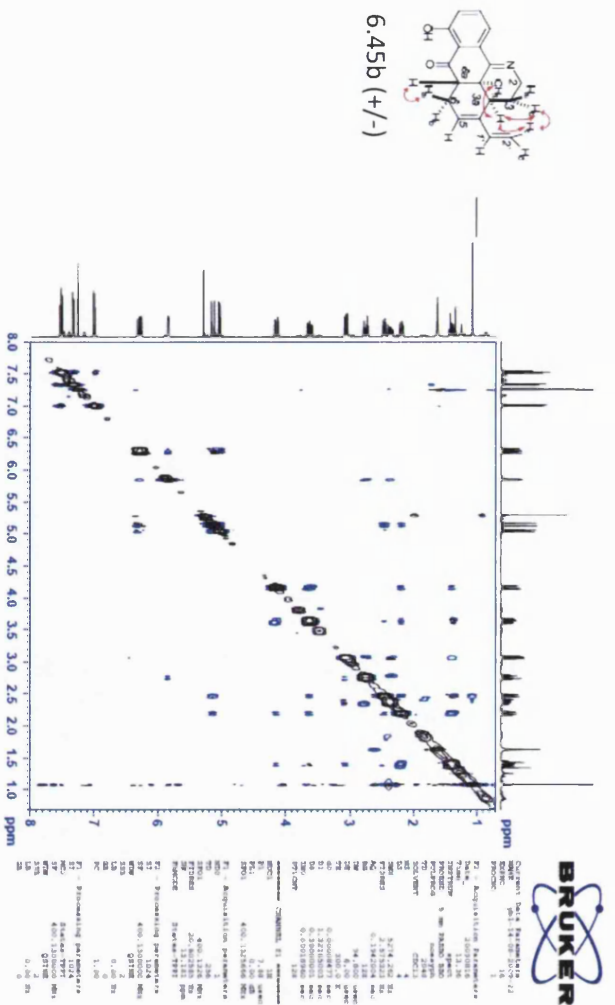
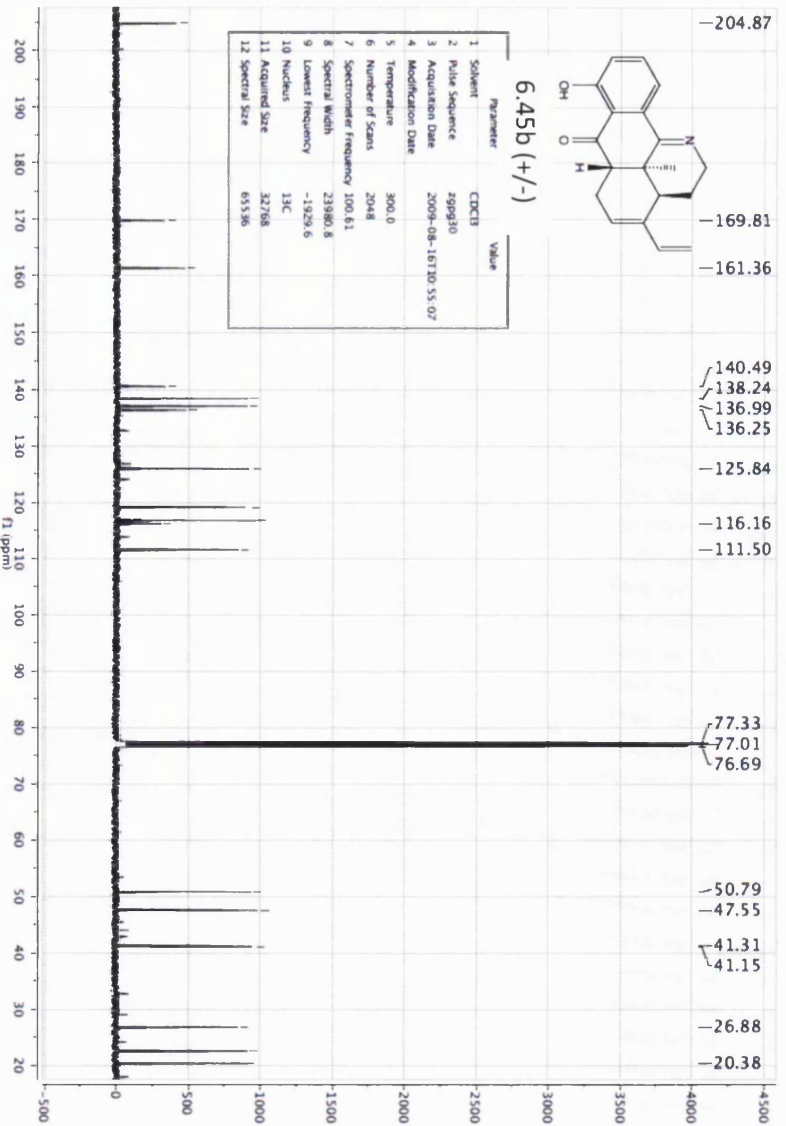


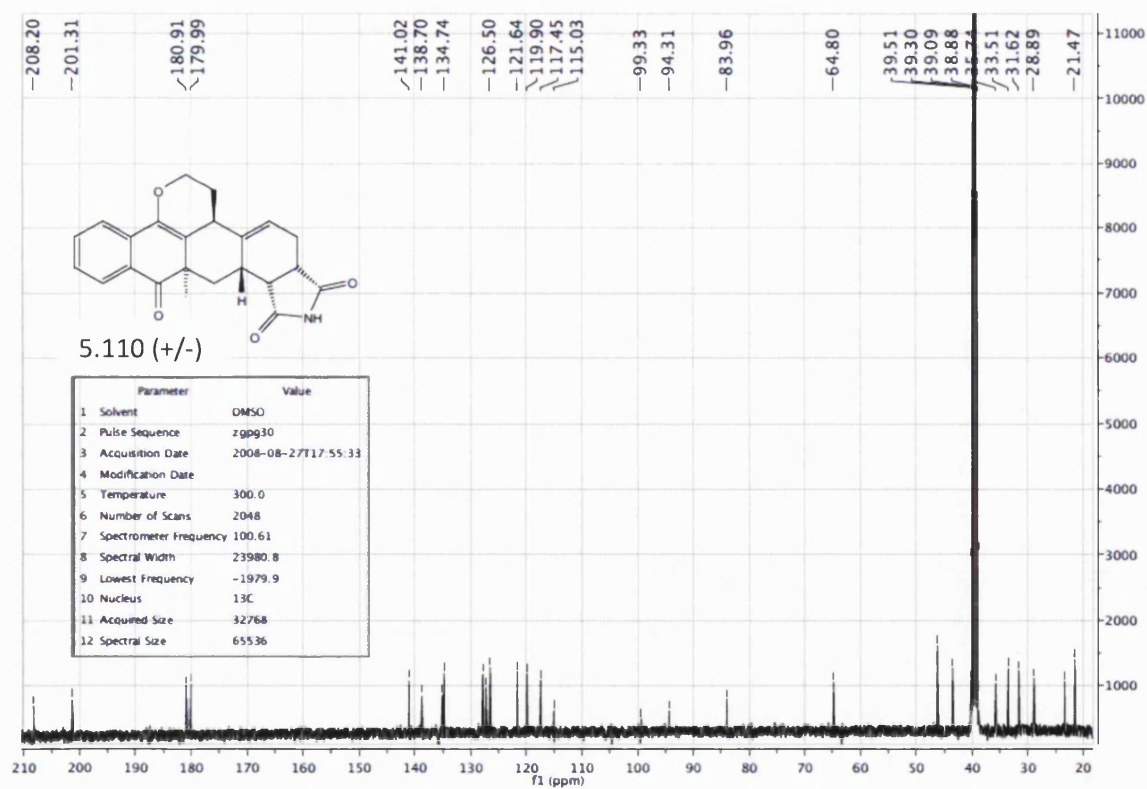
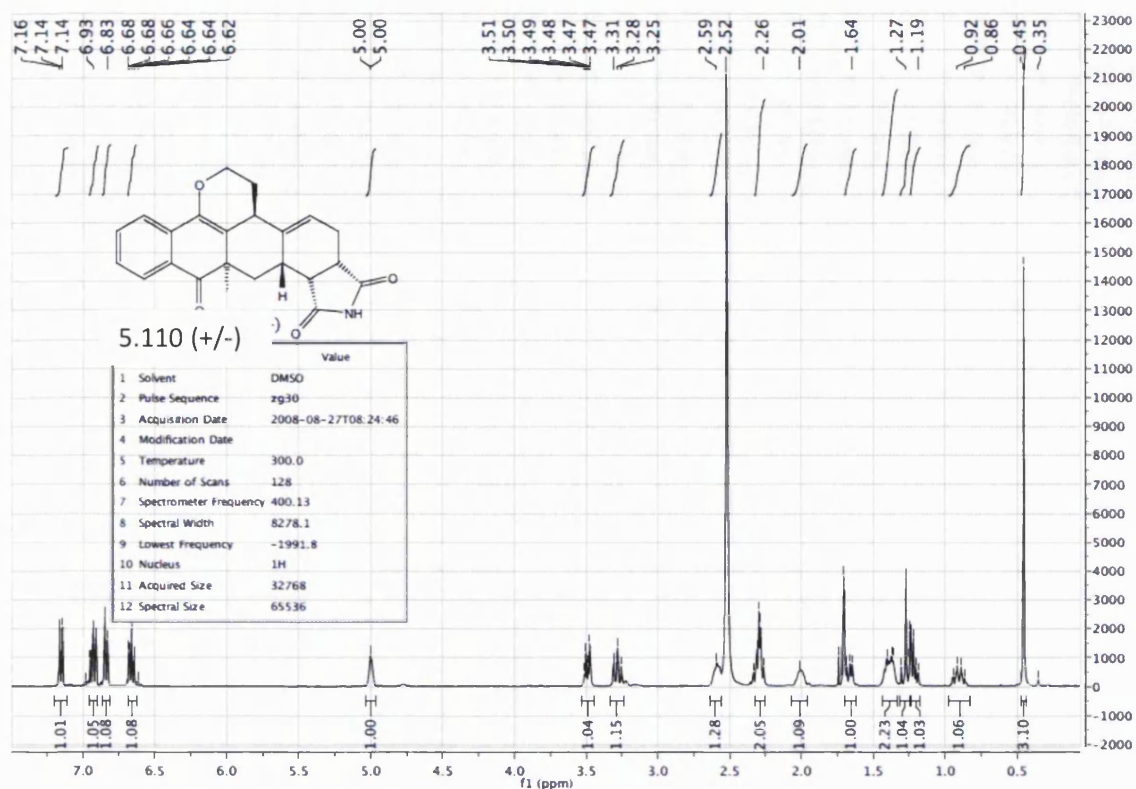


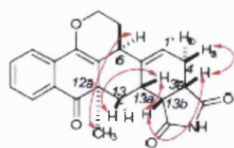


6.45a (+/-)









5.110 (+/-)

